State of Oregon
Oregon Department of Geology and Mineral Industries
Brad Avy, State Geologist

BULLETIN 108

GEOLOGY OF THE NORTH HALF OF THE LOWER CROOKED RIVER BASIN, CROOK, DESCHUTES, JEFFERSON, AND WHEELER COUNTIES, OREGON

by Jason D. McClaughry, Mark L. Ferns, and Caroline L. Gordon

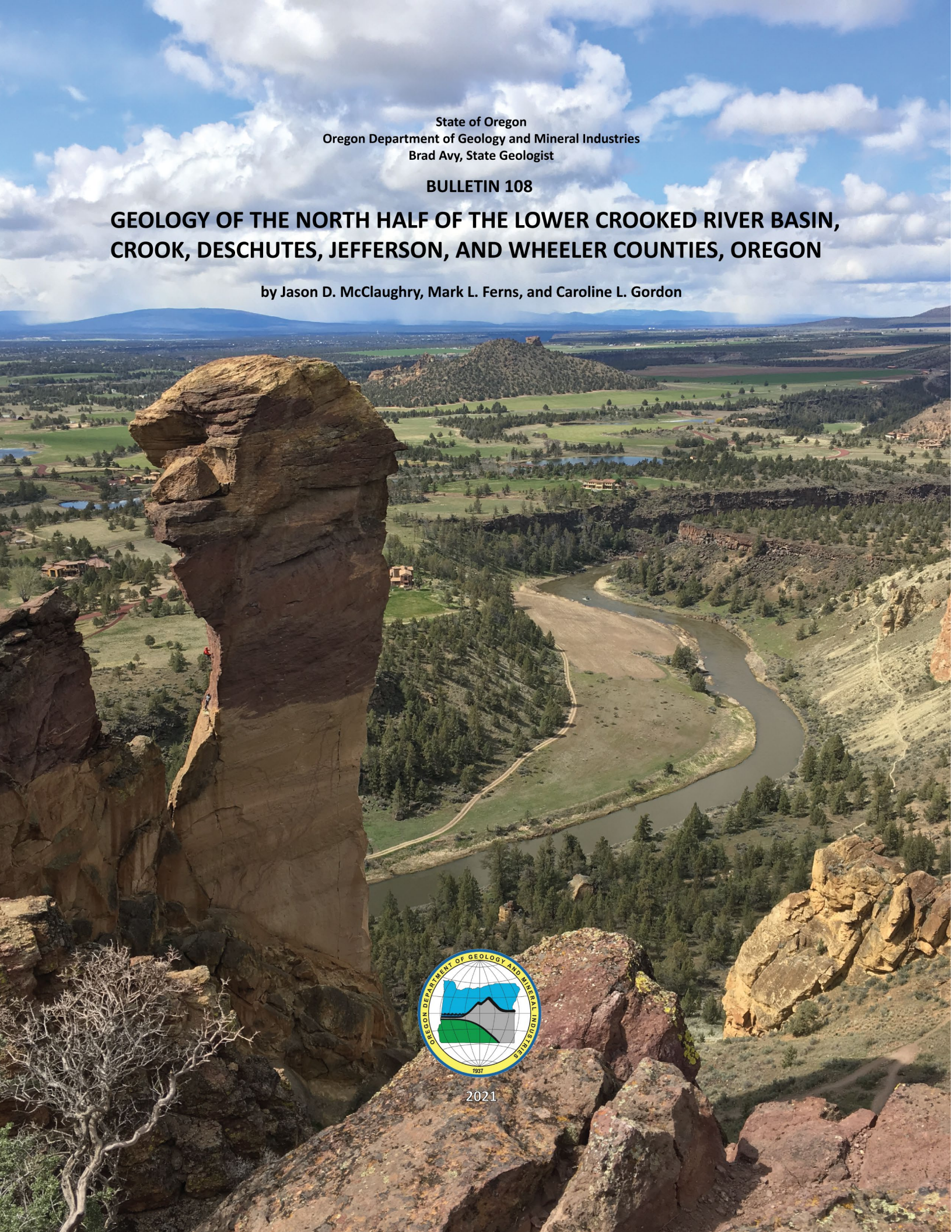

2021

State of Oregon
Oregon Department of Geology and Mineral Industries
Brad Avy, State Geologist

BULLETIN 108

GEOLOGY OF THE NORTH HALF OF THE LOWER CROOKED RIVER BASIN, CROOK, DESCHUTES, JEFFERSON, AND WHEELER COUNTIES, OREGON

by Jason D. McClaughry[1], Mark L. Ferns[2], and Caroline L. Gordon[3]

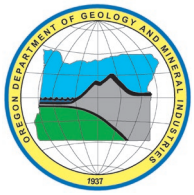

2021

[1] Oregon Department of Geology and Mineral Industries, Baker City Field Office, Baker County Courthouse, 1995 3rd Street, Ste. 130, Baker City, OR 97814; jason.mcclaughry@oregon.gov
[2] Retired, formerly at Oregon Department of Geology and Mineral Industries, Baker City Field Office, Baker County Courthouse, 1995 3rd Street, Ste. 130, Baker City, OR 97814
[3] Retired, formerly at U.S. Forest Service, Ochoco National Forest, 3160 NE 3rd Street, Prineville, OR 97754

NOTICE

WHAT'S IN THIS PUBLICATION?

This publication provides an updated and spatially accurate geologic framework for the north half of the lower Crooked River basin. Geologic data in the publication provide significant new details about the volcanic and structural geologic history of the area and the geologic conditions controlling the distribution of water resources, aggregate and other mineral and energy resources, and geologic hazards.

Cover photograph: Rock climbers scale the tuff of Smith Rock at Monkey Face at Smith Rock State Park. In the distance, the north-flowing Crooked River winds through a canyon lined by basalt lava flows from Newberry Volcano (44.370075, -121.142390). View is looking northwest to Coyote Butte.
Photo credit: Jason McClaughry, 2017.

Expires: 12/1/2021

Oregon Department of Geology and Mineral Industries Bulletin 108
Published in conformance with ORS 516.030.

For additional information:
Administrative Offices
800 NE Oregon Street, Suite 965
Portland, OR 97232
Telephone (971) 673-1555
Fax (971) 673-1562
https://www.oregon.gov/dogami

TABLE OF CONTENTS

LIST OF FIGURES

LIST OF TABLES

MAP PLATE

Geologic Map of the North Half of the Lower Crooked River Basin, Crook, Deschutes, Jefferson, and Wheeler Counties, Oregon, scale 1:63,360.

GEODATABASE

LCB2021_GeMS10.7.gdb

See the appendix for geodatabase description.
Geodatabase is Esri® version 10.7 format.

SHAPEFILES AND SPREADSHEETS

Shapefiles

Alteration Geochemistry: LCB2021_AlteredGeochemPoints.shp
Alteration Zones: LCB2021_AlteredZones.shp
Geochemistry: LCB2021_GeochemPoints.shp
Geochronology: LCB2021_GeochronPoints.shp
Magnetics: LCB2021_MagneticPoints.shp
Orientation Points: LCB2021_OrientationPoints.shp
Reference map: LCB2021_RefMap.shp
Volcanic Vents: LCB2021_VentPoints.shp
Wells: LCB2021_WellPoints.shp
Cross Section Lines: LCB2021_XSectionLines.shp

Spreadsheets (Microsoft® Excel®)

LCB2021_DATA.xlsx master file contains sheets:

Alteration Geochemistry: LCB2021_AlteredGeochemPoints
Geochemistry: LCB2021_GeochemPoints
Geochronology: LCB2021_GeochronPoints
Magnetics: LCB2021_MagneticPoints
Orientation Points: LCB2021_OrientationPoints
Wells: LCB2021_WellPoints
Volcanic Vents: LCB2021_VentPoints

"Deciphering the history of old volcanoes is like putting together a jigsaw puzzle without the cover picture to guide you, and with many of the pieces lost"

—Peter Lipman, U.S. Geological Survey

1.0 INTRODUCTION

The north half of the lower Crooked River basin encompasses an area of ~2,338 km^2 (903 mi^2) east of the Cascade Range in central Oregon (**Figure 1-1**; plate; Hydrologic Unit Code 8 [HUC8] subbasin 17070305 referred to herein simply as the lower Crooked River basin). Detailed field mapping, integrated with many detailed geologic datasets, has enabled us to reveal a long-lived and complex history of volcanism and sedimentation in this part of central Oregon.

The lower Crooked River basin has been a locus of magmatism for the past 47 million years, including the formation of two large-scale Paleogene rhyolite calderas, deposition of volcaniclastic sedimentary rocks and tuff, and eruption and emplacement of Neogene and Quaternary basaltic lava flows. The earliest magmatism in the lower Crooked River basin is recorded by 46.4 Ma high-MgO alkali-olivine basalt and ~44 to 39 Ma intermediate to silicic calc-alkaline volcanic and intrusive rocks that are part of the Eocene Clarno Formation. Clarno volcanism, focused in the Ochoco volcanic field in the eastern half of the lower Crooked River basin, peaked at 41.8 Ma with the eruption of the tuff of Steins Pillar and formation of the ~16 × 11 km (10 × 7 mi) Wildcat Mountain caldera. The Clarno Formation is overlain in the western half of the lower Crooked River basin by a bimodal assemblage of tholeiitic mafic lava flows and intrusions, rhyolitic tuffs, lava flows and domes, and volcaniclastic sedimentary rocks that are part of the late Eocene to Oligocene John Day Formation. John Day rocks in the lower Crooked River basin make up the lower Crooked volcanic field and include the Crooked River caldera, a large-scale ~41 × 27 km (25.5 × 17 mi) multicyclic caldera formed between 29.7 and 27.6 m.y.a. Sedimentary rocks of the early Miocene Simtustus Formation and ~17- to 16-Ma lava flows of the early Miocene Columbia River Basalt Group unconformably overlie Paleogene rocks in the lower Crooked River basin. In the western part of the basin these rocks infill the central depression of the Crooked River caldera, recording the earliest development of the Crooked River drainage. Late Miocene and Pliocene volcaniclastic sedimentary rocks, ash-flow tuff, and lava flows of the Deschutes Formation, cropping out across the western part of the lower Crooked River basin, record the onset of late High Cascades volcanism, early development of the central Oregon segment of the High Cascades intra-arc graben, and sedimentary and volcanic infilling of the Deschutes Basin on the west. Mafic Deschutes Formation lava flows mapped across the western part of the lower Crooked River basin erupted from vents in the Bowman volcanic field between 8.8 to 3.3 m.y.a. Intracanyon Deschutes Formation mafic lava flows, following channels incised into older rock, record the late Neogene development of ancestral Deschutes and Crooked River channels closely approximating present-day river courses. Pliocene and older rocks are overlain in the western part of the lower Crooked River basin by a broad plain of Quaternary basaltic lava flows erupted from Newberry Volcano between 720 and 400 k.y.a. Bedrock units are locally covered across the lower Crooked River basin by Late Pleistocene and Holocene surficial deposits.

The geology of the lower Crooked River basin, was mapped by the Oregon Department of Geology and Mineral Industries (DOGAMI), with the primary objective to provide an updated and spatially accurate geologic framework for the area (**Figure 1-1**; plate). Additional key objectives of the study include: 1) determining the geologic history of volcanic rocks in this part of central Oregon, east of the Cascade Range; 2) characterizing the stratigraphic framework and geologic conditions controlling the distribution of water resources; 3) mapping the distribution of potential aggregate sources and other mineral

resources; and 4) describing the nature of geologic hazards in the region. New detailed geologic mapping presented here also provides a basis for future geologic, geohydrologic, and geohazard studies in the lower Crooked River basin (**Figure 1-1**; plate).

The core products of this study are this report, accompanying geologic map and cross sections (plate), Esri ArcGIS™ geodatabase, and Microsoft Excel® spreadsheets tabulating point data. The geodatabase presents new geologic mapping in a digital format consistent with the U.S. Geological Survey (USGS) National Cooperative Geologic Mapping Program Geologic Map Schema (GeMS) (U.S. Geological Survey National Cooperative Geologic Mapping Program, 2020). It contains spatial information, including geologic polygons, contacts, structures, as well as data about each geologic unit such as age, lithology, and mineralogy. The geodatabase also includes point feature classes for geochemistry, geochronology, magnetic polarity, orientation points, volcanic vents, and well data. Digitization at scales of 1:24,000 or larger was accomplished using a combination of georeferenced 1:24,000-scale USGS digital raster images, imagery, and where available, high-resolution lidar topography and imagery. Surficial and bedrock geologic units contained in the geodatabase are depicted on the map plate at a scale of 1:63,360 in order to show contrasting bedrock lithology, structural relations, and surficial geology in the lower Crooked River basin. The map plate also includes six geologic cross sections constructed on the basis of the digital data included in the geodatabase. Details in the geodatabase and plottable map plate are referable to this report and accessible in digital appendices.

Geologic mapping in the lower Crooked River basin is a high priority of the Oregon Geologic Map Advisory Committee (OGMAC), supported in part by grants from the STATEMAP component of the USGS National Cooperative Geologic Mapping Program (05HQAG0037, 06HQAG0027, G20AC00202), and by the Oregon Water Resources Department (OWRD) through Interagency Agreement DOGAMI IAA# DASPS-2542-16/OWRD IAA 16 047 (2016). Additional funds were provided by the State of Oregon through the Oregon Department of Geology and Mineral Industries.

Figure 1-1. Location of the lower Crooked River basin and regional geographic features. Solid red line is the study area boundary. Green lines show the boundaries of hydrologic basins in the region.

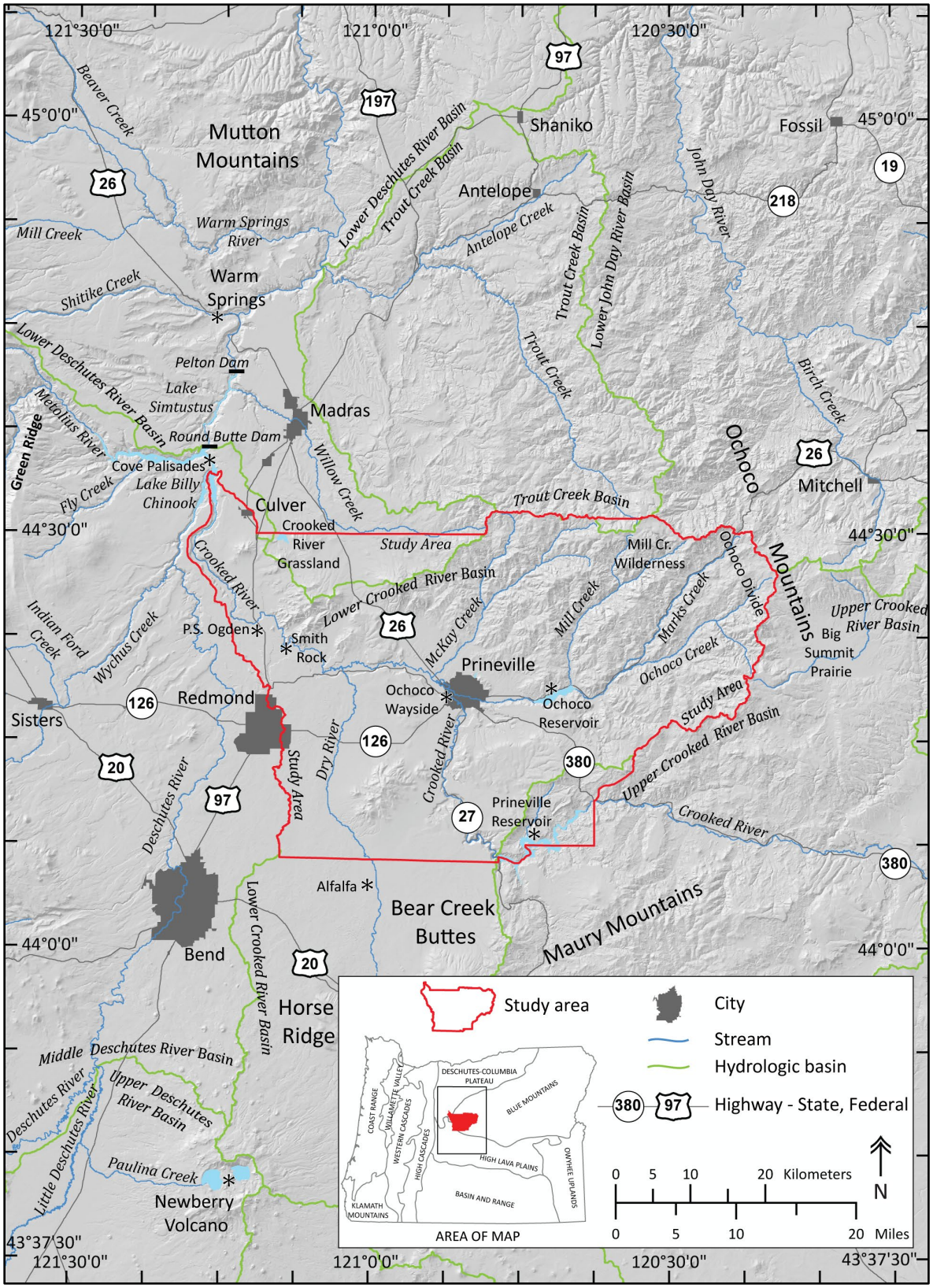

2.0 GEOGRAPHY

The lower Crooked River basin is located east of the Cascade Range in central Oregon, situated at the intersection of the High Lava Plains, Blue Mountains, and Deschutes-Columbia Plateau physiographic provinces (**Figure 1-1**; Dicken, 1965). The basin encompasses approximately 2,338 km^2 (903 mi^2) of the Crooked River drainage, reaching from Ochoco Divide on the east to the main stem Crooked River near Redmond on the west and from roughly the latitude of Prineville Reservoir on the south to the latitude of Lake Billy Chinook on the north (**Figure 1-1**; plate). The north-northwest-flowing Crooked River and its major tributaries, including McKay, Mill, Marks, and Ochoco creeks, drain the area. This part of central Oregon is rugged, transitioning from the forested uplands of the Ochoco Mountains on the east to more subdued broad plateaus and deep canyons of the High Desert and Crooked River grasslands on the west. Topographic relief in the lower Crooked River basin ranges from 1,779 m (5,841 ft) along Ochoco Divide on the northeast to 610 m (2,000 ft) at Lake Billy Chinook on the northwest. The lower Crooked River basin has a semi-arid local steppe to upland climate averaging ~27 cm (10.6 in) of precipitation annually (NOAA, 2020). The city of Prineville lies near the geographic center of the lower Crooked River basin.

Property ownership in the lower Crooked River basin is a mixture of privately held range and agricultural land and public lands managed by the United States and State of Oregon. Significant parcels of forested upland areas of the Ochoco Mountains are managed by the U.S. Forest Service (USFS), Ochoco National Forest. The Ochoco National Forest in the map area includes the Mill Creek Wilderness. The USFS also manages the Crooked River National Grassland, covering an extensive area north of Smith Rock and along the lower reaches of the Deschutes and Crooked rivers, in the northwest part of the map area (**Figure 1-1**; plate). The Bureau of Land Management (BLM), Prineville District manages sagebrush-, grass-, and Western juniper-covered high desert areas south and north of Prineville. Six Oregon State Parks are located within the lower Crooked River basin including Cove Palisades, Peter Skene Ogden, Smith Rock, Ochoco Wayside, Ochoco Lake, and Prineville Reservoir (**Figure 1-1**; Bishop and Smith, 1990; McClaughry and others, 2009a, b, c; McClaughry and Patton, 2017).

U.S. Highway 26 is the major transportation corridor in the lower Crooked River basin, connecting Ochoco Divide, Prineville, and the Crooked River National Grassland (**Figure 1-1**; plate). U.S. Highway 97 runs from south to north along the northwest part of the map area. Other main highways include Oregon State Routes 27, 126, 360, and 380 (**Figure 1-1**; plate). A number of other local roads provide access to the remainder of the map area. Lands administered by the USFS and BLM can be accessed by a number of paved or gravel roads and unimproved dirt tracks. Roadless parts of the map area can be accessed by a network of designated USFS, BLM, and State Park trails.

3.0 METHODOLOGY

The suite of Eocene to Pleistocene volcanic rocks exposed in the lower Crooked River basin is stratigraphically complex, reflecting the variable processes of deposition and reworking of volcanic and volcaniclastic units. Thus, reliable map correlations, even of similar appearing stratigraphic sequences, benefits greatly from the use of detailed geologic mapping, combined with numerous direct field observations. Conventional lithologic criteria, in combination with geochemical analyses, corroborating isotopic ages, and measurements of natural remanent magnetization were used to assign rocks and deposits to geologic map units (**Figure 3-1**; plate; appendix). Comparative visual analysis of unanalyzed rocks with analyzed rocks, in the context of stratigraphic position, allowed for wider correlation of map units.

Figure 3-1. Supporting geologic data. (a) Geochemical analyses. Black points are whole rock XRF analyses (*n* = 548); green points are ICP-MS analyses and fire assays of alteration zone samples (*n* = 29). (b) Green triangles are isotopic ages (*n* = 55). (c) Strike and dip symbols are orientation measurements (*n* = 74). (d) Red points are measurements of magnetic polarity (*n* = 88). (e) Red triangles are Bowman volcanic field vents (*n* = 17). (f) Yellow points are located wells (*n* = 1,585 wells). See the appendix and geodatabase for complete description of the data.

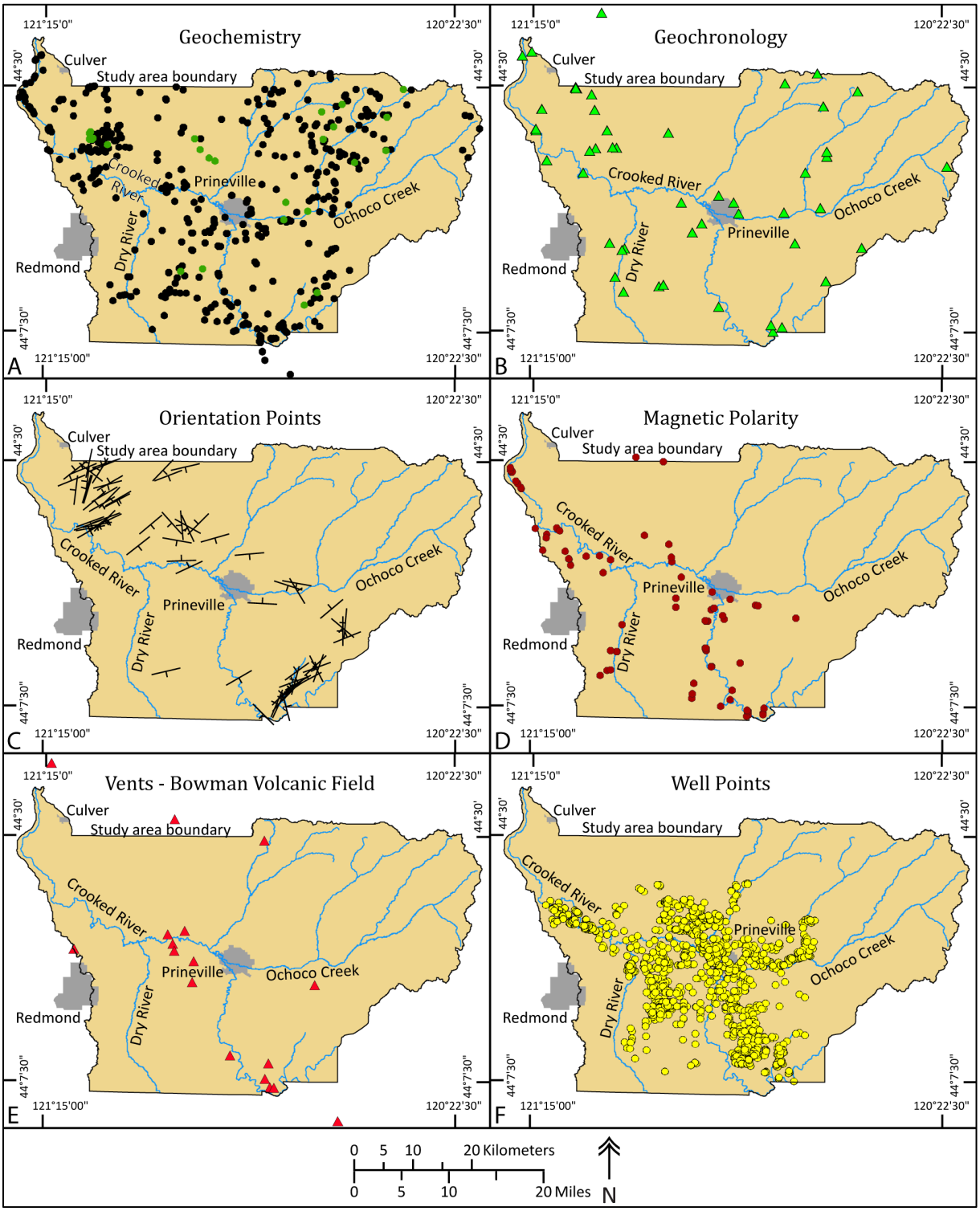

Mapping presented in this report was collected using standard USGS 1:24,000-scale topographic maps, USGS digital raster graphics of traditional topographic maps, 2005-2018 National Agriculture Imagery Program digital orthophotos, and 1-m lidar (8 pts/m^2) digital elevation models (DEMs). Fieldwork consisted of data collection along main highways and roads, forest roads, and trails, combined with numerous traverses mapping lithologic contacts and faults across private lands and lands managed by the USFS, BLM, and State of Oregon.

Geologic linework portrayed on the geologic map is based upon detailed observations at 1020 field stations visited by the authors between 2005 and 2014. Supplementary lithologic information was obtained from comparison of more than 400 rock samples collected from field sites. Lithologic map correlations also rely on 548 new and compiled X-ray fluorescence (XRF) whole rock geochemical analyses, 17 Inductive Coupled Mass Spectrometry (ICP-MS) and Inductive Coupled Atomic Emission Spectrometry (ICP-AES) geochemical analyses of rocks from hot-spring alteration zones, 12 fire assay analyses of alteration zones, 55 new and compiled $^{40}Ar/^{39}Ar$, K-Ar, and $^{206}Pb/^{238}U$ isotopic ages, petrographic analysis of 113 thin sections, 88 field measurements of natural remanent magnetization, and 74 field collected orientation measurements (**Figure 3-1**; plate; appendix). Surficial units within the project area were delineated on the basis of geomorphology as interpreted from a combination of field observations, 1-m lidar DEMs, 2005 to 2018 National Agriculture Imagery Program orthophotos, and USGS 7.5′ topographic maps.

In this report, volcanic rocks with fine-grained (<1 mm [0.04 in]; Mackenzie and others, 1997; Le Maitre and others, 2004), average crystal or particle size in the groundmass are characterized in the following manner:

- A coarse groundmass if the average crystal or particle size is <1 mm (0.04 in) and can be determined using the naked eye (>~0.5 mm [0.02 in]).
- A medium groundmass if crystals of average size cannot be determined by eye but can be distinguished by using a hand lens (>~0.05 mm [0.002 in]).
- A fine groundmass if crystals or grains of average size can be determined only by using a microscope (or by hand lens recognition of sparkle or sheen in reflected light, indicating the presence of crystalline groundmass).
- A glassy groundmass if the groundmass has (fresh), or originally had (altered), groundmass with the characteristics of glass (conchoidal fracture; sharp, transparent edges; vitreous luster; etc.).
- Mixtures of crystalline and glassy groundmass are described as intersertal; ratios of glass to crystalline materials may be indicated by textural terms including holocrystalline, hypocrystalline, hyalophitic, hyalopilitic, and holohyaline.
- Microphenocrysts are defined as crystals larger than the overall groundmass and <1 mm across (0.04 in).

Intrusive igneous rocks are described as being coarse grained if crystal diameters are >5 mm (0.2 in); as being medium grained if the range of crystal diameters is between 1 and 5 mm (0.04 in and 0.2 in); and fine grained if the range of crystal diameters is <1 mm (0.04 in) (Mackenzie and others, 1997; Le Maitre and others, 2004).

Grain size of clastic sedimentary rocks is described following the Wentworth (1922) scale. Hand samples of unconsolidated sediments and clastic sedimentary rocks were compared in the field and/or in the laboratory to graphical representations of the Wentworth scale to determine average representative grain size in various parts of a respective sedimentary geologic unit.

Whole-rock XRF geochemical data are essential for separating difficult-to-distinguish lavas and pyroclastic rocks into eruptive units in the volcanic-dominated terrain of central Oregon (**Figure 3-1a**;

plate; appendix). Many lavas are too fine grained and glassy to be adequately characterized by mineralogical criteria alone and texturally and mineralogically similar appearing units can have meaningfully different chemical signatures. Descriptive rock unit names for volcanic rocks are based in part on the online British Geological Survey classification schemes (Gillespie and Styles, 1999; Robertson, 1999; Hallsworth and Knox, 1999), and normalized major element analyses plotted on the total alkali ($Na_2O + K_2O$) versus silica (SiO_2) diagram (TAS) of Le Bas and others (1986), Le Bas and Streckeisen (1991), and Le Maitre and others (1989, 2004). Whole-rock geochemical samples were prepared and analyzed by XRF at the Washington State University GeoAnalytical Lab, Pullman, Washington, and at the Franklin and Marshall College Department of Geosciences, Lancaster, Pennsylvania (appendix). Analytical procedures for the Washington State University GeoAnalytical Lab are described by Johnson and others (1999) and are available online at https://environment.wsu.edu/facilities/geoanalytical-lab/technical-notes/; Analytical procedures for the Franklin and Marshall X-ray laboratory are described by Boyd and Mertzman (1987) and Mertzman (2000), and are available online at http://www.fandm.edu/earth-environment/laboratory-facilities/xrf-and-xrd-lab. Major element determinations are normalized to a 100-percent total on a volatile-free basis and recalibrated with total iron expressed as FeOTotal. Tuff samples analyzed were composed mainly of juvenile material; hydrothermal alteration zones, as well as accidental and accessory fragments were avoided to obtain the best approximation of magma composition. Rhyolites (e.g., tuffs, flows, domes) that exceed the highest SiO_2-rich position (>77.8 weight percent SiO_2) of the granite minimum in the SiO_2–$NaAlSi_3O_8$–$KAlSi_3O_8$ ternary system (Tuttle and Bowen, 1958) are considered to have been modified by secondary processes and are noted in the appendix (LCB2021_GeochemPoints.shp and Master excel file LCB2021_DATA, geochemistry spreadsheet, LCB2021_GeochemPoints.xls). High field strength elements (e.g., Hf, Zr, Nb, Ta, Ti, U, Th) are highly immobile and unaffected by post-eruptive alteration, thus these elements are used for correlation and trend display on variation diagrams. Further details of this process are described in the appendix under the heading *Geochemistry*.

The distribution of alteration zones in the lower Crooked River basin is defined on the basis of field mapping, published literature (Brooks, 1963; Waters, 1966; Waters and Vaughan, 1968a, b; Swinney and others, 1968; Swanson, 1969; Gray and Baxter, 1986; Thormahlen, 1984), and unpublished mineral resource reports archived by DOGAMI. The geodatabase contains a polygon overlay feature class of alteration zones (LCB2021_AltZones.shp) mapped in the lower Crooked River basin. Seventeen samples obtained from alteration zones in the lower Crooked River basin were analyzed at ALS Chemex (ALS) in Reno, Nevada by ICP-MS and ICP-AES methods using their ME-MS41 analytical package (**Figure 3-1a**; appendix). Further details of this process are described in the appendix under the heading *Alteration Geochemistry*.

Our mapping presents 15 new and previously published $^{40}Ar/^{39}Ar$ ages (Ferns and McClaughry, 2006a, 2007; McClaughry and Ferns, 2006a, b, 2007 d; McClaughry and others, 2009a, b, c, d; Dunbar and Perkins, 2015) (**Figure 3-1b**; plate; appendix). Samples for $^{40}Ar/^{39}Ar$ age determinations were prepared and analyzed at the College of Oceanic and Atmospheric Sciences, Oregon State University, Corvallis (OSU). The methodology for $^{40}Ar/^{39}Ar$ geochronology at OSU is summarized by Duncan and Keller (2004) and on the OSU laboratory website http://geochronology.coas.oregonstate.edu/. Two $^{40}Ar/^{39}Ar$ ages were determined by Dr. Matt Heizler at the New Mexico Geochronological Research Laboratory (NMGRL) administered by the New Mexico Bureau of Geology and Mineral Resources at the New Mexico Institute of Mining and Technology in Socorro, New Mexico. The general operational details for the NMGRL can be found at internet site http://geoinfo.nmt.edu/labs/argon/. The map also includes 10 new $^{206}Pb/^{238}U$ zircon ages determined for Eocene and Oligocene ash-flow tuffs and rhyolite domes. New $^{206}Pb/^{238}U$

zircon ages were prepared and analyzed by Dr. Joshua Schwartz at California State University, Northridge (CSUN), and at the University of California, Santa Barbara (UCSB). Chang and others (2006) described the sample preparation methods and data collection techniques employed for obtaining the igneous zircon ages. Three other $^{206}Pb/^{238}U$ zircon ages in the lower Crooked River basin were published by Seligman and others (2014). Twenty-four additional $^{40}Ar/^{39}Ar$ and K-Ar ages in the area come from published studies by Brown and others (1980), Evans and Brown (1981), Fiebelkorn and others (1982, 1983), Smith and Snee (1984), Smith (1986a, b), Smith and others (1987), Robinson and others (1990), Smith and others (1998). J. Donnelly-Nolan and M. Lanphere, written commun. (2008) provided two $^{40}Ar/^{39}Ar$ ages for basaltic lavas from Newberry Volcano and one $^{40}Ar/^{39}Ar$ age for a basalt lava flow in the upper part of the Deschutes Formation. Numerical ages assigned to dated units are described using standard conventions in reporting age in millions of years ago (mega-annum, abbreviated Ma) for units >1 m.y. old; for units <1 m.y. old, ages are reported in thousands of years ago (kilo-annum, abbreviated ka). Further details of this process are described in the appendix under the heading *Geochronology*.

Orientation measurements of geological planes (e.g., inclined bedding) were obtained in the field area by traditional compass and clinometer methods and compiled from data published by previous workers (**Figure 3-1c**; appendix). Further details of this process are described in the appendix under the heading *Orientation Points*.

The magnetic polarity of strongly magnetized lavas was determined at numerous outcrops in the lower Crooked River basin using a handheld digital fluxgate magnetometer (**Figure 3-1d**; appendix). Magnetic polarity reversals, commonly preserved by volcanic rocks and readily measured in the field, provide for 1) distinguishing between flow units with normal and reversed magnetic polarity; 2) a check on the permissible age of isotopically dated samples, when compared to the paleomagnetic time scale (Cande and Kent, 1992); and 3) another means to constrain possible depositional ages for some undated strata. Further details of this process are described in the appendix under the heading *Natural Remanent Magnetization*.

Seventeen late Miocene and Pliocene volcanic vents were identified in and adjacent to the lower Crooked River basin during the course of mapping individual lava flows in the Deschutes Formation (**Figure 3-1e**; plate; appendix). Volcanic vent locations are included in the geodatabase and are further described in the appendix under the heading *Volcanic Vents*.

Subsurface geology shown in the geologic cross sections incorporates lithologic interpretations from water-well drill records available through the Oregon Water Resources Department (OWRD) GRID system (**Figure 3-1e**; appendix). An attempt was made to locate water wells and other drill holes that have well logs archived by OWRD. Approximate locations were estimated using a combination of sources, including internal OWRD databases of located wells, Google Earth™, tax lot maps, street addresses, and aerial photographs. The accuracy of the locations ranges widely, from errors up to 0.8 km (0.5 mi) for wells located only by Township/Range/Section (2.6 km^2 [1 mi^2]) and plotted at the section centroid to a few tens of meters for wells located by address or tax lot number on a city lot with bearing and distance from a corner. For each well, the number of the well log is indicated in the database. This number can be combined with the first four letters of the county name (e.g., CROO 50194), to retrieve an image of the well log from the OWRD web site (http://apps.wrd.state.or.us/apps/gw/well_log/). A database of 1585 located water-well logs is provided in the appendix; many, but not all, of these located wells include interpreted subsurface geologic units. Further details of this process are described in the appendix under the heading *Well Points*.

New mapping was compiled with published and unpublished data and converted into digital format using Esri ArcGIS™ ArcMap™ GIS software. On-screen digitizing was performed through heads-up

digitizing using georeferenced 1:24,000-scale USGS digital raster images of traditional topographic maps, hillshade derivative of USGS 10-m DEMs, 1-m lidar DEMs, and 2005 to 2018 National Agriculture Imagery Program digital orthophotos. Digitization and the final digital Esri ArcGIS™ format geodatabase was completed at a minimum scale of 1:8,000, supported by 3D visualization of lidar topographic data in Quick Terrain Modeler™ (Duda and others, 2018, 2019). Colors given for hand-sample descriptions are from the Geological Society of America Rock-Color Chart Committee (1991). The geologic time scale used is the 2021 (v2021/05) version of the International Commission on Stratigraphy chronostratigraphic chart (https://stratigraphy.org/chart) revised from Gradstein and others (2004), Ogg and others (2008), and Cohen and others (2013).

Geographic map coordinates (decimal degree, datum = WGS84) are provided for outcrop photographs shown for report figures, allowing the interested reader to visit these sites in the field or to remotely visualize the area using Google Earth™. Coordinates can be entered into the "Fly to" box (e.g., 45.661323, -121.471230) in the search toolbar, and Google Earth™ will automatically locate and focus on the specified site.

4.0 PREVIOUS WORK

The 1:63,360-scale geologic map compiled for the north half of the lower Crooked River basin covers all or parts of thirty-five USGS 7.5-minute quadrangles (**Figure 4-1**). The index map shown in **Figure 4-2** graphically summarizes the sources of mapping reviewed for our geologic depiction and other sources reviewed during the preparation of this report. **Table 4-1** shows a list of some previous regional geologic investigations reviewed during the current geologic study of the lower Crooked River basin. Reports listed in **Table 4-1**, are organized in chronological order; those shown in bold are geologic maps that lie within the study area.

The geologic setting of the lower Crooked River basin has been relatively unevaluated until comparatively recent times. The first large scale reconnaissance geologic maps for the area were made by Hodge (1942) and Williams (1957). Later mapping efforts focused on groundwater studies (Robinson and Price, 1963) and mercury mineralization (Swinney and others, 1968; Waters, 1968; Waters and Vaughn, 1968a, b). Swanson (1969) produced a small-scale (1:250,000) map of the east half the Bend AMS sheet. Robinson and Stensland (1979) published a geologic map (1:62,500) of the Smith Rock area (**Figure 4-2**; **Table 4-1**). Subsequent investigations examined the geology and geothermal potential at Powell Buttes (Weidenheim, 1980; Brown and others, 1980) and produced 1:24,000-scale geologic maps of the Hensley Butte, Grizzly Mountain, and Steelhead Falls 7.5′ quadrangles (**Figure 4-2**; **Table 4-1**; Bingert, 1984; Thormahlen, 1984; Ferns and others, 1996). Obermiller (1987) and Smith and others (1998) mapped the geology of the Smith Rock area covering parts of both the Opal City and Gray Butte 7.5′ quadrangles (1:24,000) (**Figure 4-2**; **Table 4-1**). Gannett and others (2001) and Lite and Gannett (2002) produced a regional groundwater flow simulation and hydrogeologic framework of the upper Deschutes Basin. Sherrod and others (2004) published a 1:100:000-scale map of the Bend 30- × 60-minute quadrangle which covered the western part of the study area (**Figure 4-2**; **Table 4-1**).

The core part of this compilation is based upon detailed 1:24,000-scale geologic maps published by DOGAMI between 2005 and 2007, including the Hensley Butte, Salt Butte, Houston Lake, Prineville, Ochoco Reservoir, Powell Buttes, Stearns Butte, and Eagle Rock 7.5′ quadrangles (**Figure 4-2**; **Table 4-1**; plate; McClaughry and Ferns, 2006a, b, 2007a, b, c, d; Ferns and McClaughry, 2006a, b, 2007). Additional key contributions in the area were published by Smith and others (1998), McClaughry and others (2009a, b, c, d), Patridge (2010), and Seligman and others (2014) (**Table 4-1**). A hydrologic study provided to the

City of Prineville by Dunbar and Perkins (2015), examined subsurface geology beneath Prineville Airport (**Table 4-1**).

Figure 4-1. The lower Crooked River basin study area. The project area, outlined in black, encompasses ~2,338 km² (903 mi²) of the north half of the lower Crooked River basin and all or parts of thirty-five USGS 7.5′ quadrangles. Label abbreviations are as follows: C – Culver; CR – Crooked River; MC – Marks Creek; MK – McKay Creek; ML – Mill Creek; OC – Ochoco Creek; OD – Ochoco Divide; P – Prineville; PR – Prineville Reservoir; R – Redmond; SR – Smith Rock.

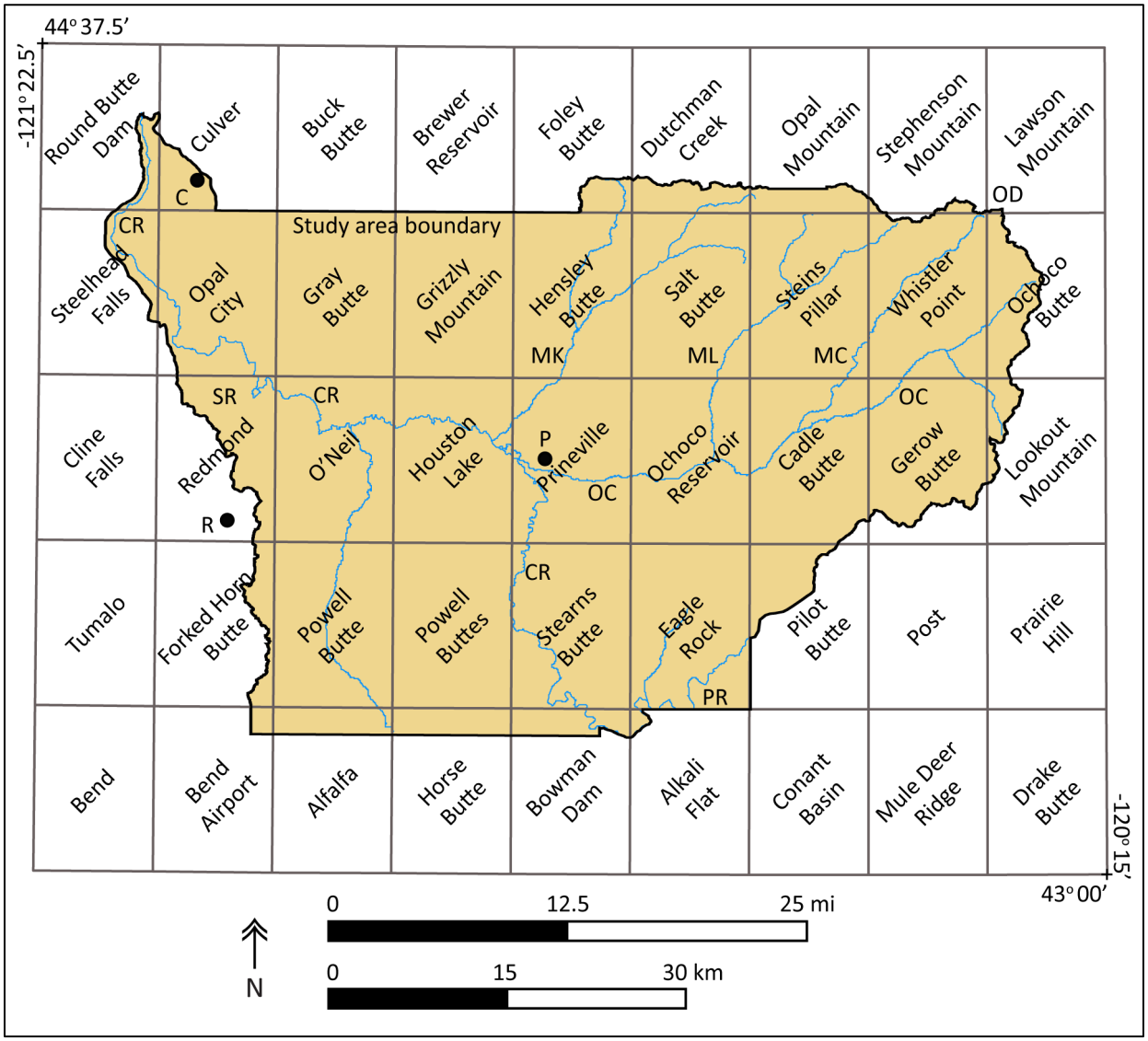

Figure 4-2. Index map of published geologic maps and university theses reviewed in preparation of the geologic map of the north half of the lower Crooked River basin. Red outline is the study area; dashed where the study area is modified from the outline of the lower Crooked River basin.

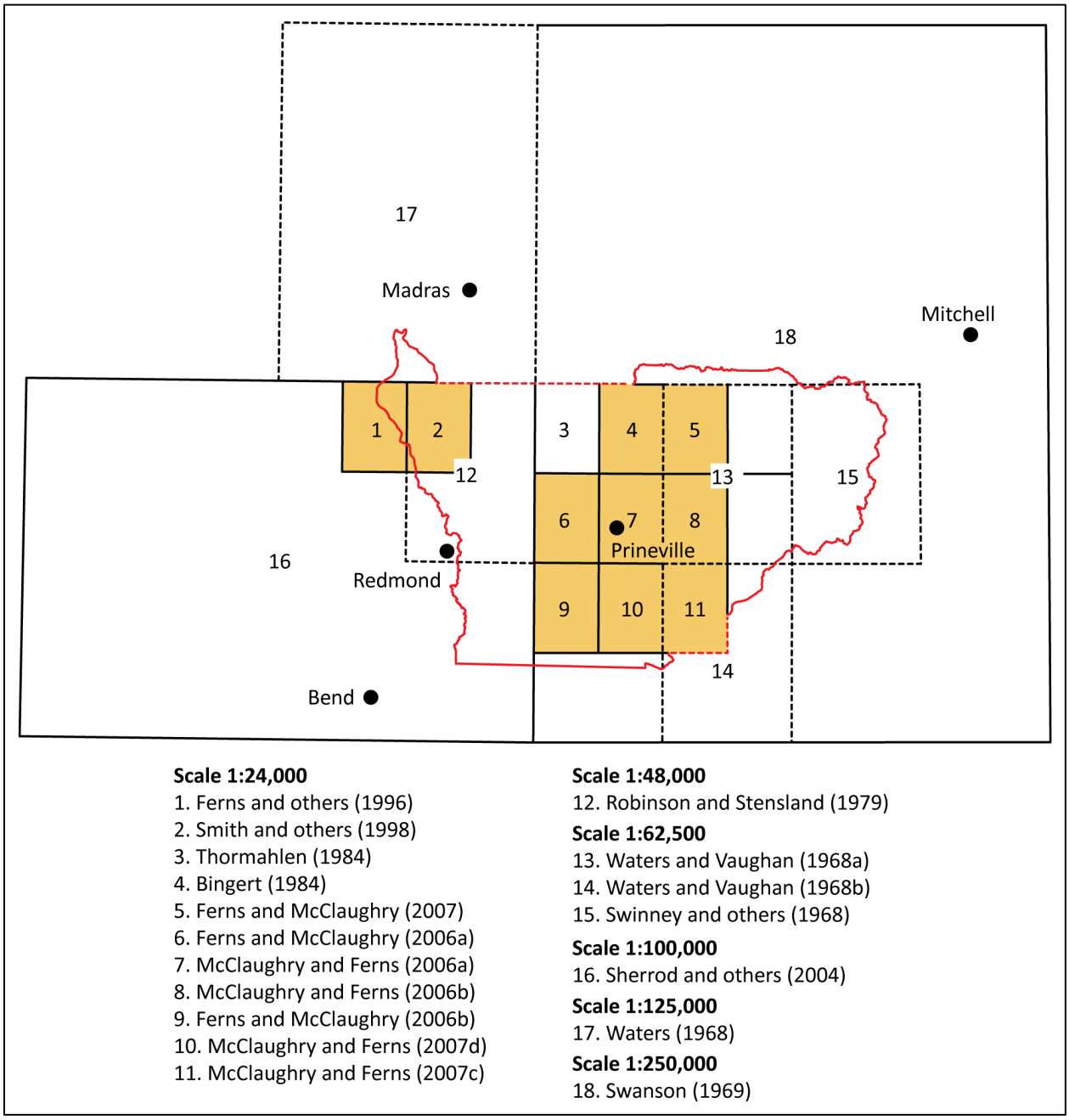

Scale 1:24,000
1. Ferns and others (1996)
2. Smith and others (1998)
3. Thormahlen (1984)
4. Bingert (1984)
5. Ferns and McClaughry (2007)
6. Ferns and McClaughry (2006a)
7. McClaughry and Ferns (2006a)
8. McClaughry and Ferns (2006b)
9. Ferns and McClaughry (2006b)
10. McClaughry and Ferns (2007d)
11. McClaughry and Ferns (2007c)

Scale 1:48,000
12. Robinson and Stensland (1979)

Scale 1:62,500
13. Waters and Vaughan (1968a)
14. Waters and Vaughan (1968b)
15. Swinney and others (1968)

Scale 1:100,000
16. Sherrod and others (2004)

Scale 1:125,000
17. Waters (1968)

Scale 1:250,000
18. Swanson (1969)

Table 4-1. Chronological listing of maps and reports reviewed for the lower Crooked River basin study. Maps shown in bold font are totally or partially within the study area.

Author	Year	Subject	Scale
Stearns	1931	Geology and water resources middle Deschutes River Basin	
Hodge	1942	Geology of north-central Oregon	
Williams	1957	Geologic map of the Bend quadrangle	**1:250,000**
Robinson and Price	1963	Ground water in the Prineville area	
Brooks	1963	Quicksilver in Oregon	
Waters	1966	Stein's Pillar area	
Waters	**1968**	**Reconnaissance geologic map of the Madras quadrangle**	**1:125,000**
Waters and Vaughan	**1968a**	**Reconnaissance geologic map of the Ochoco Reservoir quadrangle**	**1:62,500**
Waters and Vaughan	**1968b**	**Reconnaissance geologic map of the Eagle Rock quadrangle**	**1:62,500**
Swinney and others	**1968**	**Reconnaissance geologic map Lookout Mountain quadrangle**	**1:62,500**
Swanson	**1969**	**Reconnaissance geologic map of the east half of the Bend quadrangle**	**1:250,000**
Robinson and Stensland	**1979**	**Geologic map of the Smith Rock area**	**1:48,000**
Weidenheim	**1980**	**Geologic map of Powell Buttes**	**1:24,000**
Brown and others	1980	Geology and geothermal resource potential of Powell Buttes	
Robinson and Brem	1981	Geologic field trip between Kimberly and Bend	
Ashwill	1983	Gray Butte fossil floras	
Thormahlen	**1984**	**Geologic map of the NW 1/4 of the Prineville quadrangle**	**1:24,000**
Bingert	**1984**	**Geologic map of the NE 1/4 of the Prineville quadrangle**	**1:24,000**
Smith	1986a	Stratigraphy of Neogene rocks in the Deschutes Basin	
Smith	1986b	Stratigraphy of Neogene rocks in the Deschutes Basin	
Smith	1986c	Simtustus Formation	
Smith	1987	The Deschutes Formation	
Gray and Baxter	1986	Reinterpretation of the Gray Butte limestone and arenite	
Obermiller	**1987**	**Geologic map of the Smith Rock–Gray Butte area**	**1:24,000**
Walker and Robinson	1990	Paleogene rocks of the Blue Mountains	
Robinson and others	1990	Paleogene rocks of the Blue Mountains	
Smith	1991	Neogene continental volcaniclastic rocks, Deschutes basin	
Hooper and others	1993	Prineville Basalt	
Ferns and others	**1996**	**Geologic map of the Steelhead Falls 7.5' quadrangle**	**1:24,000**
Smith and others	1998	Tectonism, volcanism, and floristic change near Gray Butte	
Gannett and others	**2001**	**Ground-water hydrology of the upper Deschutes Basin**	
Lite and Gannett	2002	Geology of regional ground-water flow in the upper Deschutes Basin	
Sherrod and others	2002	Hydrogeology of the upper Deschutes Basin	
Gannett and Lite	2004	Regional groundwater flow in the upper Deschutes Basin	
Sherrod and others	**2004**	**Geologic map of the Bend quadrangle**	**1:100,000**
Ferns and McClaughry	**2006a**	**Geologic map of the Houston Lake 7.5' quadrangle**	**1:24,000**
Ferns and McClaughry	**2006b**	**Geologic map of the Powell Buttes 7.5' quadrangle**	**1:24,000**
McClaughry and Ferns	**2006a**	**Geologic map of the Prineville 7.5' quadrangle**	**1:24,000**
McClaughry and Ferns	**2006b**	**Geologic map of the Ochoco Reservoir 7.5' quadrangle**	**1:24,000**
McClaughry and Ferns	**2007c**	**Geologic map of the Eagle Rock 7.5' quadrangle**	**1:24,000**
McClaughry and Ferns	**2007d**	**Geologic map of the Stearns Butte 7.5' quadrangle**	**1:24,000**
Ferns and McClaughry	**2007**	**Geologic map of the Salt Butte and Hensley Butte 7.5' quadrangles**	**1:24,000**
McClaughry and others	2009a	Field trip guide to the Wildcat Mountain caldera	
McClaughry and others	2009b	Field trip guide to Neogene stratigraphy of the lower Crooked River basin	
McClaughry and others	2009c	Field trip guide to the Crooked River caldera	
McClaughry and others	2009d	Paleogene calderas of central and eastern Oregon	
Jensen and others	2009	Field guide to Newberry Volcano	
Patridge	2010	Petrogenesis of John Day Formation ash-flow tuffs near Prineville	
Dunbar and Perkins	2015	Hydrostratigraphy of the Prineville Municipal Airport wells	
Seligman and others	2014	Earliest caldera-forming eruptions of the Yellowstone plume	

5.0 GEOLOGIC AND TECTONIC SETTING

The lower Crooked River basin is located in the back-arc region of the central Oregon Cascade Range (**Figure 5-1**). The Cascade Range is a north-south-trending volcanic arc stretching for ~1,300 km (800 mi) between northern California and southern British Columbia. Volcanoes making up the range and their eroded remnants are the observable magmatic expression of oblique convergence since ~40 Ma along the Cascadia subduction zone, where the offshore Juan de Fuca tectonic plate is subducted beneath North America (**Figure 5-1**; Lux, 1982; Phillips and others, 1986; Verplanck and Duncan, 1987; Conrey and others, 2002; Sherrod, 2019). From Three Sisters (Oregon) north to Mount Adams (Washington state), the High Cascades occupy an ~30-km-wide (18.6 mi) structural graben formed by a northward propagating rift (**Figure 5-2**; Allen, 1966; Taylor, 1981; Williams and others, 1982; Smith and Taylor, 1983; Smith and others, 1987; Conrey and others, 2002; McClaughry and others, 2012, 2020a; Conrey and others, 2019). The High Cascades graben is segmented into three northward younging parts, including a southern segment between the Three Sisters and Mount Jefferson, a central segment between Mount Jefferson and Mount Hood, and a northern segment between Mount Hood and Mount Adams known as the Hood River graben (the respective segments are numbered 1 through 3 in **Figure 5-2**; Conrey and others, 2002; Conrey and others, 2019; McClaughry and others, 2020a). The segmented and structurally discontinuous High Cascades graben is time-transgressive, propagating northward from central Oregon (Green Ridge) to Mount Adams (Washington state) at an overall rate of 4 cm/yr (1.6 in/yr) since 5.3 Ma (**Figure 5-2**; Smith and others, 1987; Sherrod and Smith, 2000; Conrey and others, 2002). East of the Cascade Range, the lower Crooked River basin occupies the area between the southwest edge of the Blue Mountains uplift, the High Lava Plains, the Klamath–Blue Mountain gravity-anomaly lineament, and the junction of the Brothers and Sisters fault zones (Rogers, 1966; Fisher, 1967; Lawrence, 1976; Taylor, 1977; Riddihough and others, 1986; Walker and Robinson, 1990) (**Figure 5-2**).

5.1 Stratigraphic and structural synopsis

The following synopsis summarizes the distribution, composition, lithology, and age of map units and structural development of the lower Crooked River basin since the middle Eocene. This synopsis is divided on the basis of the broad periods of time used in the Explanation of Map Units starting on page 63 and shown in **Figure 5-3** and on the plate. Major geologic subdivisions in the lower Crooked River basin include: a) 46.4 to ~39 Ma Clarno Formation; b) 39.7 to ~22 Ma John Day Formation; c) ~22 to 16 Ma Simtustus Formation and ~16 Ma Columbia River Basalt Group (CRBG); d) 8.8 to 3.3 Ma Deschutes Formation; e) <1.2 Ma Quaternary volcanic rocks; and f) Late Pleistocene to Holocene surficial deposits (**Figure 5-3**).

Figure 5-1. Tectonic setting of the northwest United States and southwest Canada showing regional plate boundaries, the Cascadia subduction zone, and volcanoes of the Cascade Range. The surface projection of the Cascadia megathrust (red line) is defined by bathymetry where the abyssal plain meets the continental slope. The study area is shown by a red polygon in north-central Oregon. Modified after Nelson and others (2006).

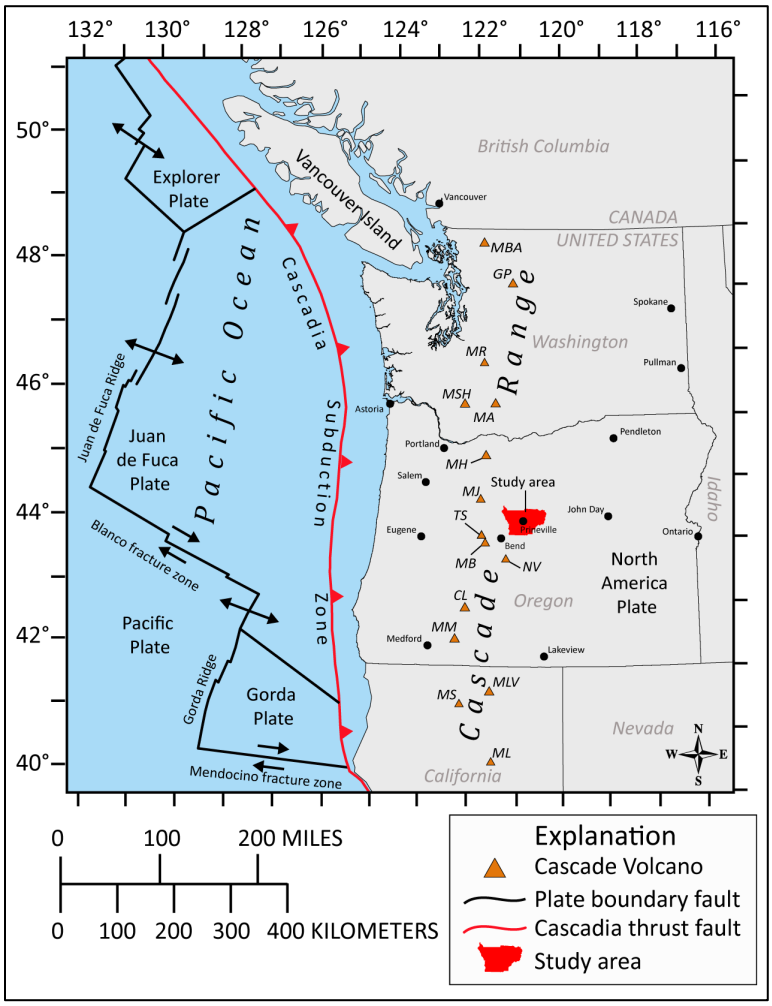

Figure 5-2. Map of the Cascade Range in the Pacific Northwest showing geographic locations, approximate extent of Western (tan) and High (purple) Cascades, and the spatial relations of some major structural features in Oregon (*following page*). Modified from McClaughry and others (2020a). Note that the names Western Cascades and High Cascades are not used in Washington or south of Mount Shasta in California. The study area is shown by a red polygon in central Oregon. The numerals 1, 2, and 3 refer to the three segments of the High Cascades graben from south to north: 1) southern segment, 2) central segment, and 3) Hood River graben. Labels: BV – Boring Volcanic Field; HRF – Hood River fault zone; HCF – Horse Creek fault zone; GCF – Gales Creek fault; GRF – Green Ridge fault zone; PB – Portland Basin; PHF – Portland Hills fault; MHFZ – Mount Hood fault zone; SV – Simcoe Mountains; TB – Tualatin Basin. Oregon physiographic provinces after Dicken (1965). Geologic provinces of Washington from the Washington Geological Survey (https://www.dnr.wa.gov/programs-and-services/geology/explore-popular-geology/geologic-provinces-washington).

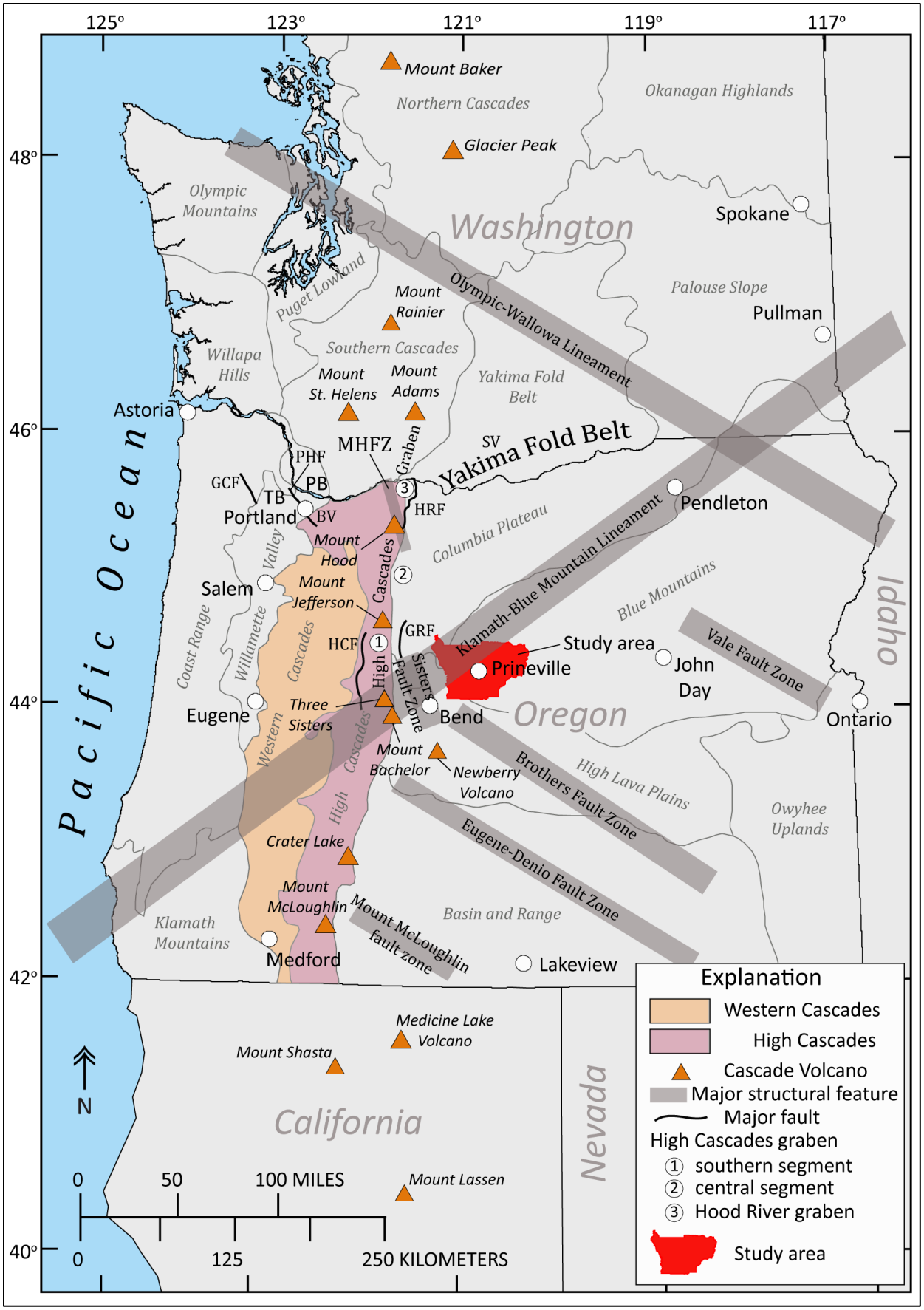
125°
123°
121°
119°
117°
48°
46°
44°
42°
40°
Mount Baker
Northern Cascades
Okanagan Highlands
Glacier Peak
Olympic Mountains
Washington
Spokane
Puget Lowland
Olympic-Wallowa Lineament
Palouse Slope
Mount Rainier
Pullman
Southern Cascades
Willapa Hills
Mount St. Helens
Mount Adams
Yakima Fold Belt
Astoria
MHFZ
Graben
SV
Yakima Fold Belt
PHF
GCF
PB
TB
Portland
BV
HRF
Pendleton
Columbia Plateau
Mount Hood
Cascades
Valley
Salem
Mount Jefferson
Klamath-Blue Mountain Lineament
Blue Mountains
Idaho
Coast Range
Willamette
Cascades
HCF
GRF
Study area
Vale Fault Zone
Prineville
John Day
High Cascades
Sisters Fault Zone
Eugene
Three Sisters
Bend
Oregon
Ontario
Western Cascades
Mount Bachelor
Newberry Volcano
Brothers Fault Zone
High Lava Plains
Owyhee Uplands
Crater Lake
Eugene-Denio Fault Zone
Mount McLoughlin
Basin and Range
Klamath Mountains
Mount McLoughlin fault zone
Medford
Lakeview
Medicine Lake Volcano
Mount Shasta
California
Nevada
N
0
50
100 MILES
0
125
250 KILOMETERS
Mount Lassen
Explanation
Western Cascades
High Cascades
Cascade Volcano
Major structural feature
Major fault
High Cascades graben
① southern segment
② central segment
③ Hood River graben
Study area

Figure 5-3. Outcrop areas of major geologic subdivisions mapped in the lower Crooked River basin, shown by red fill. (a) Eocene Clarno Formation. (b) Eocene and Oligocene John Day Formation. (c) Lower Miocene Simtustus Formation and Columbia River Basalt Group. (d) Deschutes Formation. (e) Quaternary volcanics. (f) Quaternary surficial deposits.

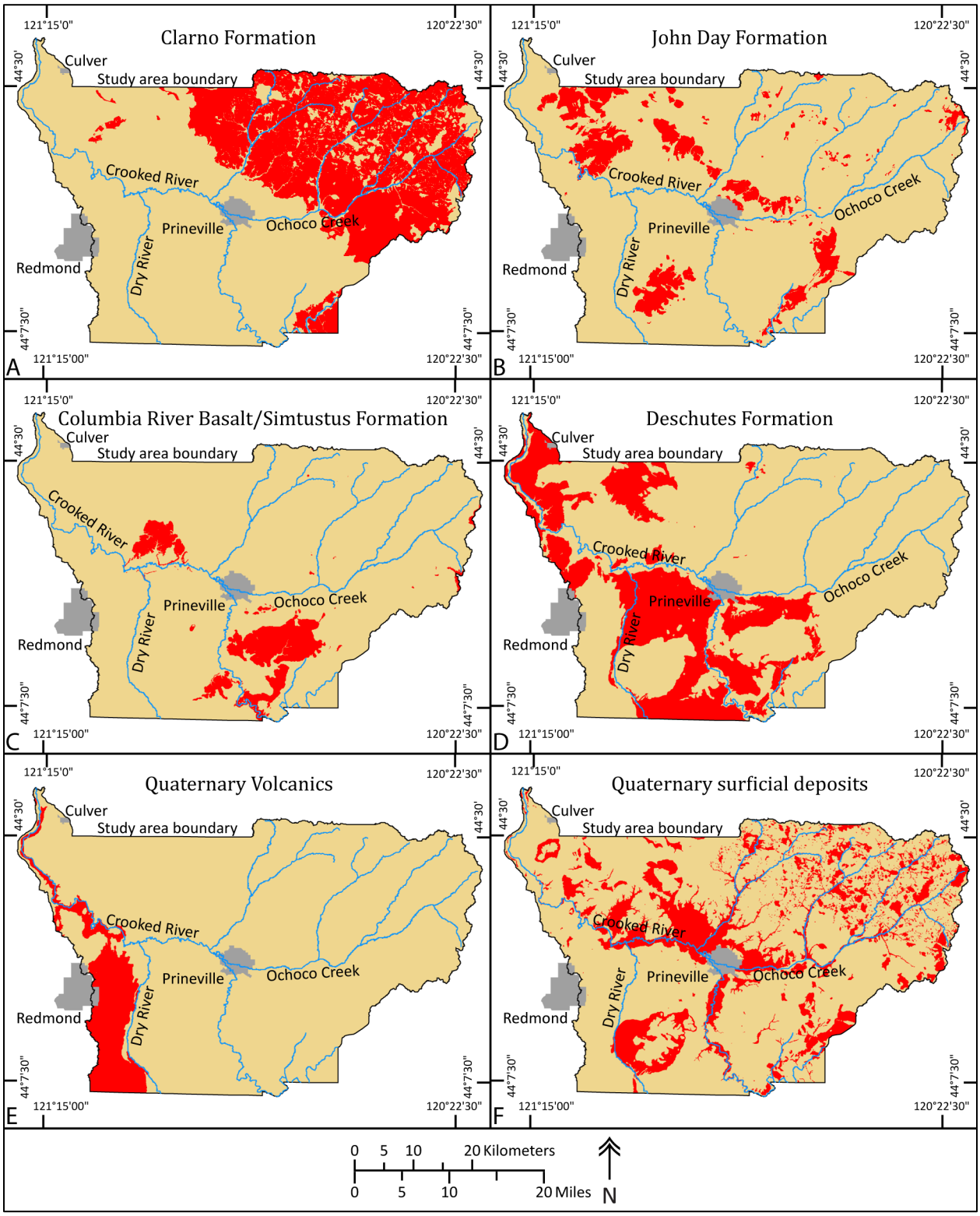

5.1.1 Lower Cenozoic Volcanic and Sedimentary Rocks

5.1.1.1 Clarno Formation

5.1.1.1.1 Distribution, composition, and lithology

Early Eocene high-magnesium alkali-olivine basalt and middle Eocene basaltic andesite, andesite, and dacite lavas, domes, and subvolcanic intrusions, breccia dikes, and rhyolite domes, lava flows, and tuff are the oldest rock units cropping out in the lower Crooked River basin. These rocks, exposed along the shores of Prineville Reservoir and covering ~1,115 km^2 (430 mi^2) of the eastern part of the lower Crooked River basin, are part of the Eocene Clarno Formation (**Figure 5-3a**, **Figure 5-4**; plate). Regionally, the Clarno Formation consists of Eocene non-marine alkaline to calc-alkaline volcanic rocks, intrusions, and volcanogenic sedimentary rocks ranging in age from ~54 to 39 Ma (Merriam, 1901a, b; Waters and others, 1951; Evernden and James, 1964; Waters and Vaughan, 1968a, b; Swanson and Robinson, 1968; Swanson, 1969; McKee, 1970; Enlows and Parker, 1972; Rogers and Novitsky-Evans, 1977, Manchester, 1981; Fiebelkorn and others, 1982, 1983; Vance, 1988; Walker, 1990; Walker and Robinson, 1990; White and Robinson, 1992; Bestland and others, 1999; Retallack and others, 2000; Appel, 2001; McClaughry and others, 2009a, d; 2014; Gaylord and others, 2015). A suite of older rocks, ranging in age from 53.6 to 45.26 Ma, are discontinuously exposed near the hamlets of Clarno and Mitchell (**Figure 5-4**; Bestland and others, 1999, 2002; Appel, 2001). This suite of older rocks marks the lower boundary of the Clarno Formation in north-central Oregon and is herein referred to as the early Clarno Formation. Mineral and chemical compositions of these older rocks are distinct from the ~44 to 40 Ma calc-alkaline magmatic pulse that characterizes the younger, main part of the Clarno Formation. The early Clarno rocks are coeval with and are more compositionally comparable to the calc-alkaline and alkaline rock suites of the Challis volcanic field of Idaho (~51 to 44 Ma; McIntyre and others, 1982; Moye and others, 1988). They are unlikely to be co-genetic with the main magmatic phase of the younger main part of the Clarno Formation (Walker and Robinson, 1990).

Early Eocene high-magnesium alkali-olivine basalt (**Tceb**) mapped along the shores of Prineville Reservoir are the oldest rocks found in the lower Crooked River basin (plate). Chemical composition of the basalt, characterized by high magnesium (MgO = 9.11 to 13.04 weight percent; *n* = 2 analyses) and high total alkali contents ($Na_2O + K_2O$ = 3.14 to 3.95 weight percent), minerology (olivine, clinopyroxene, orthopyroxene), and a 46.4 Ma isotopic age indicate an association with rocks forming the early part of the Clarno Formation at Clarno and Mitchell (**Figure 5-4**).

Variably exhumed, Eocene volcanic and intrusive rocks of the Clarno Formation, younger than 44 Ma mapped across the Ochoco Mountains in the eastern part of the lower Crooked River basin, are part of the Ochoco volcanic field (**Figure 5-3a**, **Figure 5-5**; plate; McClaughry and others, 2009a, d). Magmatism between ~43.9 and 41.5 Ma in the Ochoco volcanic field produced a flow-on-flow succession of basaltic andesite, andesite, and dacite lava flows, domes, and subvolcanic intrusions (**Tcau**, **Tcid**, **Tcev**, **Tcqb**, **Tchp**, **Tcih**, **Tcal**, **Tcdp**) (**Figure 5-5**; Ferns and McClaughry, 2007; McClaughry and others, 2009a, d). Volcanogenic sedimentary deposits common throughout much of the regional distribution of the Clarno Formation, are conspicuously rare (**Tces**, **Tcdf**) within the core of the Ochoco volcanic field, being restricted to isolated eruptive centers (e.g., Round Mountain; plate) and marginal depocenters (e.g., Gray Butte, Clarno, and the Painted Hills; **Figure 5-4**). The original extent of the Ochoco volcanic field is currently unknown, but it may be preserved from the Maury Mountains on the south to the Horse Heaven mining district on the north, forming a belt of coincident Eocene vents and quicksilver deposits (**Figure 5-4**; Waters and others, 1951; Brooks, 1963; Swanson, 1969).

Figure 5-4. Regional extent of the Eocene Clarno and Eocene-Oligocene John Day Formations and Eocene-Oligocene calderas in eastern Oregon. Tan shade is the mapped outcrop belt of the Clarno Formation. Green shade is the mapped outcrop belt of the John Day Formation. Red-dashed lines are the western, southern, and eastern facies of the John Day Formation as defined by Robinson and others (1990). Labels are as follows: A – Ashwood; C – Clarno; CO – Cougar Butte; CB – Cadle Butte; CR – Cougar Rock; CRC – Crooked River caldera; D – Dale; GB – Gray Butte; HB – Hampton Butte; HH – Horse Heaven; HR – Haystack Reservoir; JDF – John Day Formation; LB – Logan Butte; ML – Magone Lake; OD – Ochoco Divide; OR – Ochoco Reservoir; P – Pilot Butte; PB – Powell Buttes; PH – Painted Hills; PR – Prineville Reservoir; RM – Round Mountain; SM – Smith Rock; SR – Sheep Rock; SV – Susanville; TF – Teller Flat; TM – Tower Mountain; TMC – Tower Mountain caldera; W – Whitney; WMC – Wildcat Mountain caldera.

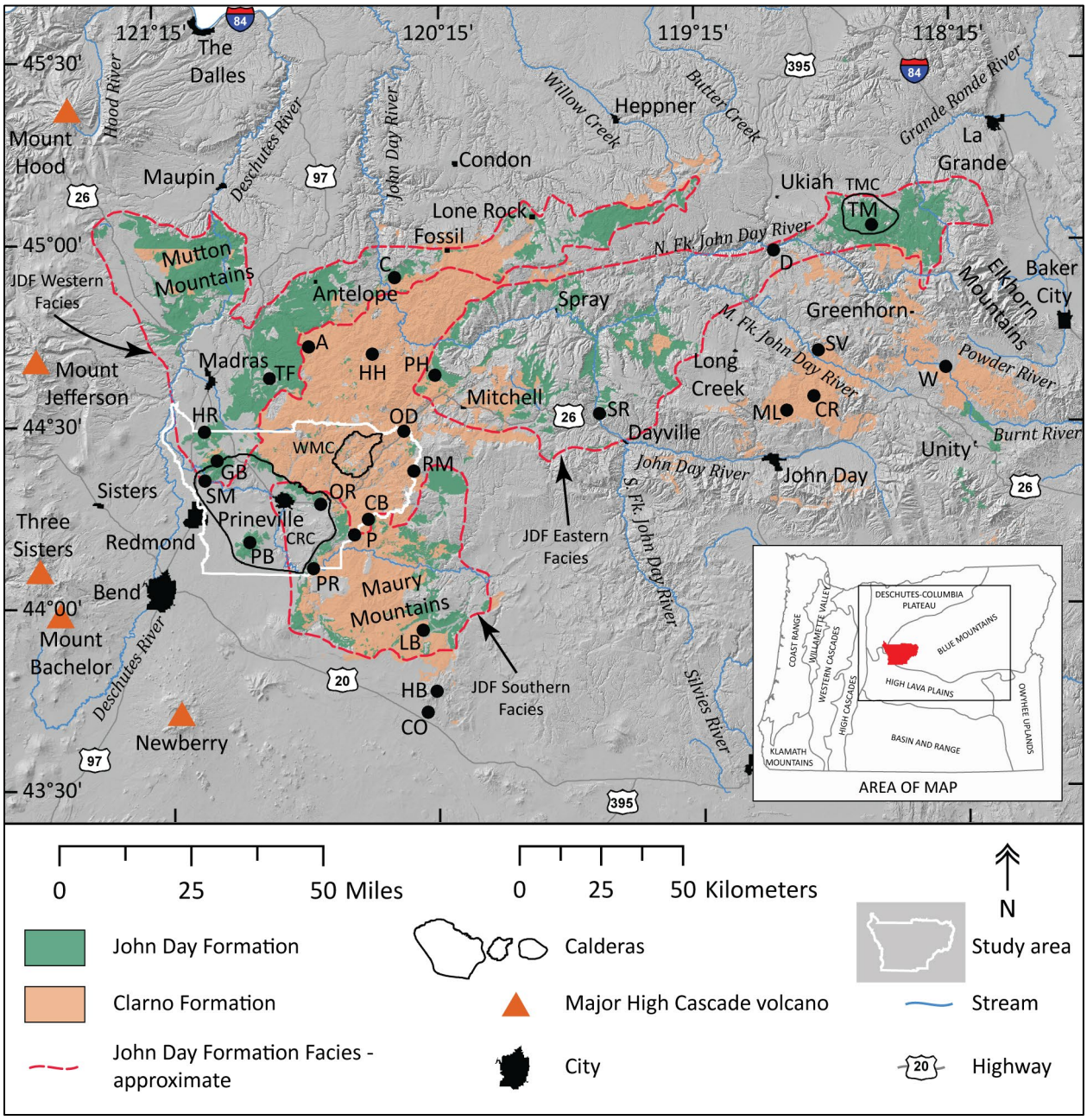

Figure 5-5. Simplified geologic map of the middle Eocene Wildcat Mountain caldera within the Ochoco volcanic field. Geology shown north of the lower Crooked River basin is from Stroh (1979) in OGDC-7, Franczyk and others (2020).

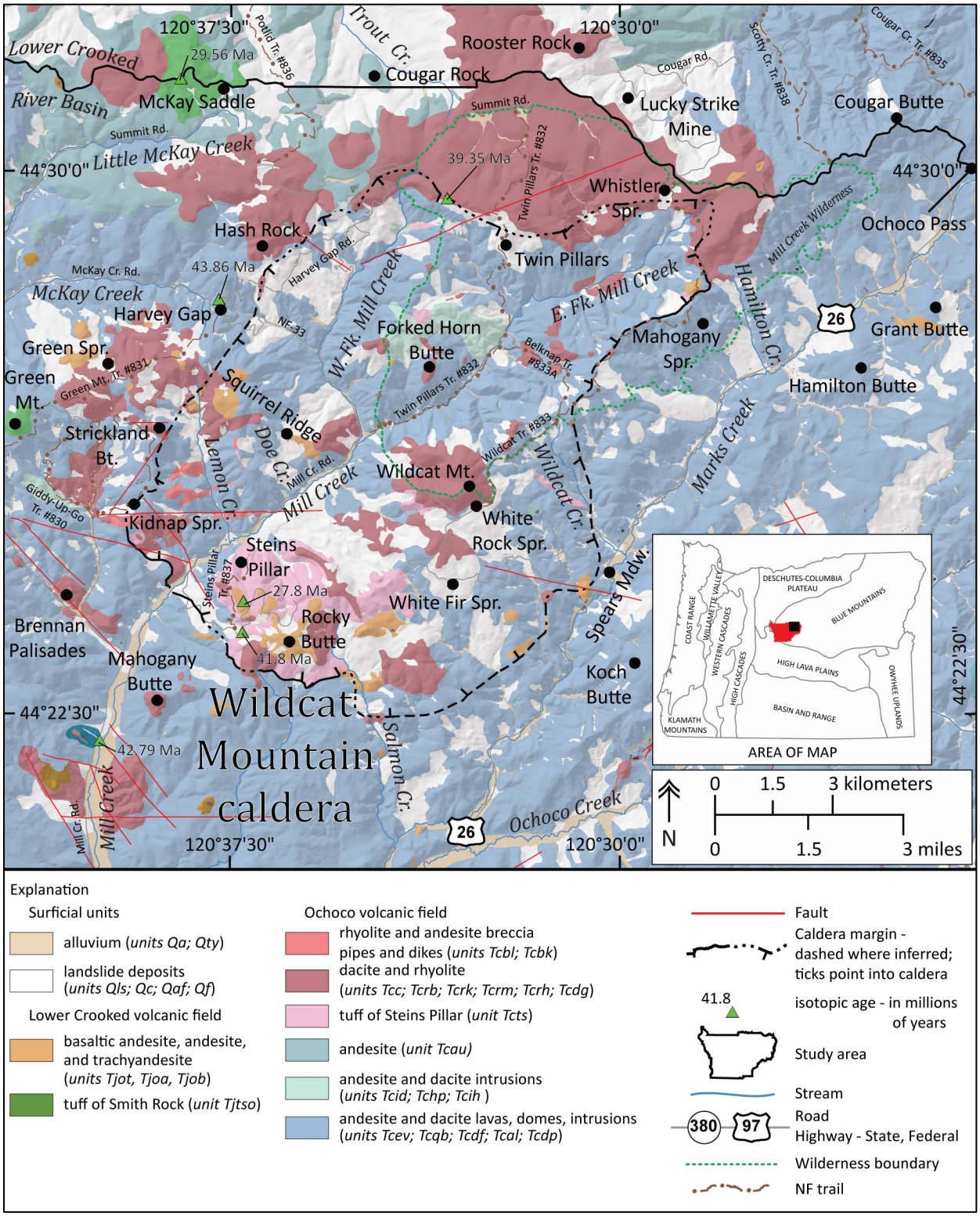

The Ochoco volcanic field is underlain by variably deformed Cretaceous and older(?) sedimentary rocks exposed between Ochoco Divide and Mitchell (**Figure 5-4**). It is flanked on the west, north, and east by Eocene to Oligocene depocenters that lie in an arcuate belt between Gray Butte, Clarno, and the Painted Hills (**Figure 5-4**). The depocenters preserve regionally segmented and stratigraphically discontinuous volcanic and sedimentary successions of the Clarno and John Day Formations (**Figure 5-4**; Walker, 1990; Robinson and others, 1990; Smith and others, 1998; Retallack and others, 2000; Bestland and others, 1999). The Horse Heaven mining district, characterized by a thick section of andesite, tuff, and a 42.1 ± 0.8 Ma mineralized (cinnabar) rhyolite flow and dome complex, lies between Clarno and the Wildcat Mountain caldera (**Figure 5-4**; Waters and others, 1951; Swanson and Robinson, 1968; Fiebelkorn and others, 1982, 1983). The younger Oligocene Crooked River caldera forms an embayment along the southwest part of the Ochoco Mountains, partially overlapping the Ochoco volcanic field (**Figure 5-4**; plate).

The middle Eocene Wildcat Mountain caldera, located ~19 km (12 mi) northeast of Prineville, is the major vent feature within the Ochoco volcanic field and is one of several large rhyolite eruptive centers that formed in eastern Oregon during the middle Eocene and Oligocene (**Figure 5-4, Figure 5-5**, **Figure 5-6**, **Figure 5-7**; plate; McClaughry and others, 2009a, d). Eruption of the tuff of Steins Pillar (**Tcts**) at 41.8 Ma resulted in the formation of the Wildcat Mountain caldera, an ~16 × 11 km (10 mi x 7 mi) roughly circular caldera that collapsed and filled with more than 90 km^3 (21.5 mi^3) of rhyolite ash-flow tuff (**Figure 5-5**, plate). Post-volcanic erosion has stripped away most of the intracaldera fill and outflow deposits, and part of the original topographic rim of the caldera, leaving a distinct depression with more than 800 m (2,625 ft) of vertical relief (**Figure 5-6**, **Figure 5-7**; plate).

The Wildcat Mountain caldera is characterized by a combination of thickly ponded silicic pumice-lithic ash-flow tuff, nearly vertical caldera-bounding faults, and rhyolite dome complexes that surround the structure (**Figure 5-5**, plate; Ferns and McClaughry, 2007; McClaughry and others, 2009a, d, 2014). Rhyolite and dacite lavas, domes, and intrusions (**Tcrb**, **Tcrk**, **Tcrm**, **Tcrh**, **Tcdg**) were emplaced along the ring-fracture zone of the Wildcat Mountain caldera and in central vent areas between ~41 and 39 Ma following the main subsidence phase (**Figure 5-5**, **Figure 5-7**; plate). Repeated injection of silicic magma within central areas of the caldera during this phase formed a prominent central resurgent dome that was accompanied by the emplacement of linear breccia pipes (**Tcbl**, **Tcbk**) and hydrothermal alteration along the ring-fracture (**Figure 5-5**, **Figure 5-6**, **Figure 5-7**; plate). This phase of magmatic and hydrothermal activity around the periphery of the Wildcat Mountain caldera produced mercury mineralization between Kidnap Spring and Strickland Butte that was explored by prospectors and mined to a limited extent between 1940 and 1942 (Brooks, 1963).

Silicic rocks erupted from the Wildcat Mountain caldera record the onset of widespread Paleogene ash-flow tuff eruptions in eastern Oregon and overlap the regional transition (~39.7 Ma) from dominantly calc-alkaline magmatism that characterizes the older Clarno Formation to the bimodal basalt and rhyolite volcanic assemblage associated with the younger John Day Formation.

Rocks of the Ochoco volcanic field and Wildcat Mountain caldera are broadly calc-alkaline, with compositions ranging from basalt (SiO_2 = 50.34 weight percent) to rhyolite (SiO_2 = 76.26 weight percent). The full range of silica is present, with all units in the study area having an average dacite composition (avg = 65.53 weight percent SiO_2; *n* = 82; **Figure 5-8a-b**; appendix). Mafic to intermediate rocks forming the main part of the Ochoco volcanic field are typically medium- to low-potassium (avg = 1.39 weight percent K_2O) basalt, basaltic andesite, andesite, and low-silica dacite with silica contents ranging between 50.34 and 66.73 weight percent SiO_2 (avg = 60.50 weight percent SiO_2; *n* = 46; **Figure 5-8c**; appendix). Plagioclase and clinopyroxene phenocrysts are present in most mafic to intermediate composition lava

flows, dikes, and domes in the Ochoco volcanic field. Olivine is present in mafic rocks, while orthopyroxene, resorbed quartz, and lesser biotite and hornblende are present in the intermediate composition rocks. Rocks are often glomeroporphyritic. Andesites commonly contain xenocrysts of plagioclase ± quartz ± clinopyroxene ± orthopyroxene (Suayah and Rogers, 1991).

Silicic rocks in the Ochoco volcanic field mapped around the Wildcat Mountain caldera are high-silica dacites and rhyolites with silica contents ranging between 66.81 and 76.26 weight percent SiO_2 (avg = 71.96 weight percent SiO_2; *n* = 36; **Figure 5-8a**; appendix). These rocks have characteristically low contents of incompatible high-field strength elements such as niobium (avg = 13 ppm Nb), zirconium (avg = 217 ppm Zr), and yttrium (avg = 28 ppm Y), and generally, have lower abundances of the light rare-earth elements lanthanum (avg = 31 ppm La) and cerium (avg = 60 ppm Ce) (**Figure 5-9a**, **Figure 5-10**; appendix). Plagioclase, sanidine, and clinopyroxene phenocrysts are present in silicic rocks. Chemical composition, inclusion of hydrous minerals (amphibole ± biotite), and a continuous range in magma compositions in rocks of the Ochoco volcanic field, is similar to rocks found in subduction-type settings (**Figure 5-9b**; appendix; Seligman and others, 2014). However, the location of the Ochoco volcanic field far behind the well-defined Eocene Western Cascades arc indicates a probable intraplate origin for these rocks (du Bray and John, 2011; Seligman and others, 2014).

Figure 5-6. Panoramic view across the Wildcat Mountain caldera (44.454086, -120.620466). The rhyolite of Hash Rock (Tcrh) forms the plateau around the north part of the caldera. Part of the remnant feeder conduit for this flow is at Twin Pillars. Wildcat Mountain, a post-subsidence rhyolite dome is on the east. The central part of the caldera is formed from a central resurgent dome that is marked by a series of post-subsidence intrusions such as the rhyolite plug at Forked Horn Butte. White dashed line shows the approximate trace of the caldera margin.

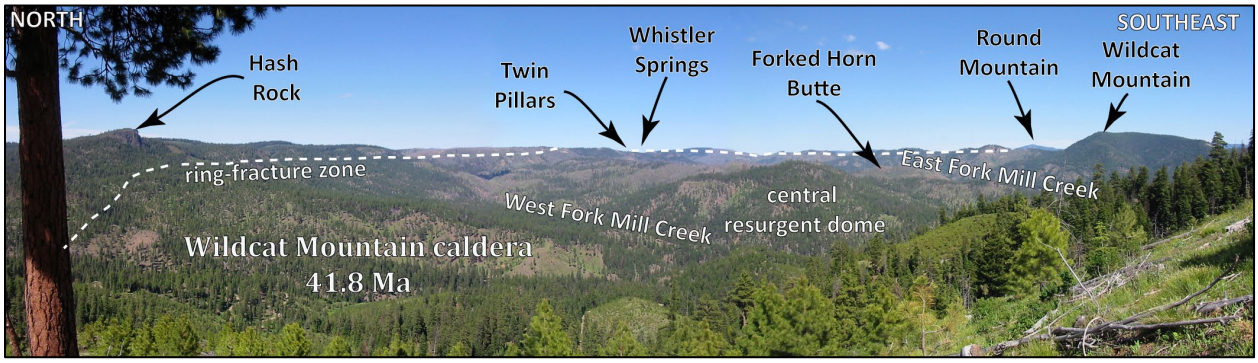

Figure 5-7. Stage development of the middle Eocene Wildcat Mountain caldera (*following page*). Black dashed line in frame 4 represents the current depth of erosion into the structure of the Wildcat Mountain caldera.

Formation of the Wildcat Mountain caldera

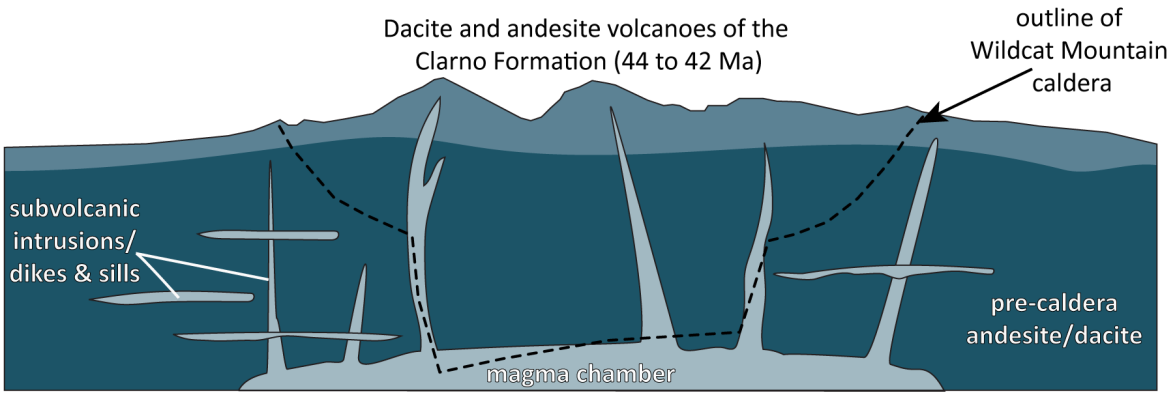

1. Pre-Wildcat Mountain caldera magma moves upward fracturing surrounding rocks.

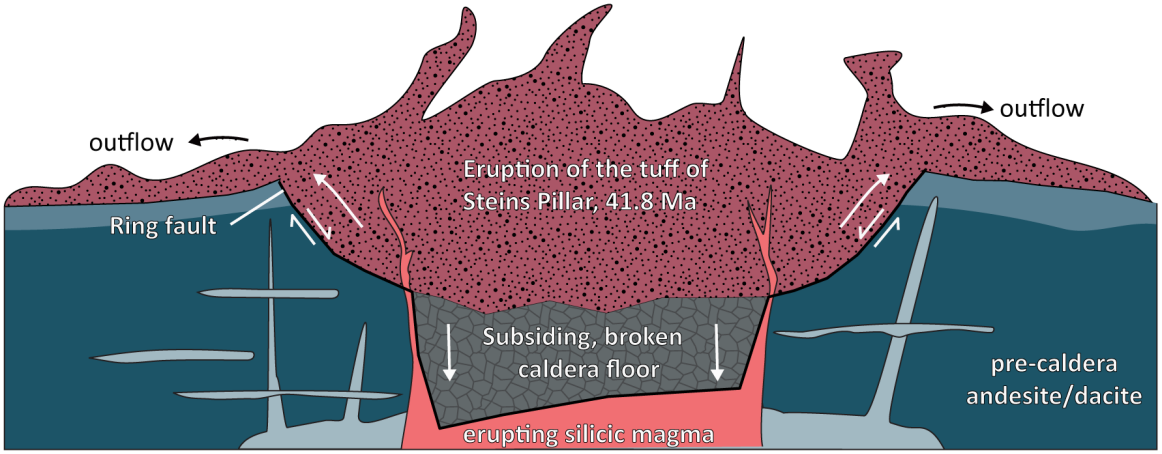

2. Initial caldera-forming eruption and Wildcat Mountain caldera subsidence.

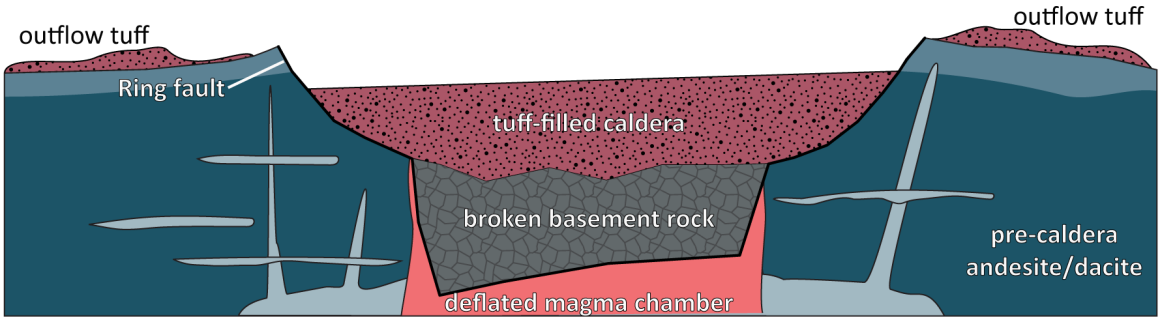

3. Wildcat Mountain caldera following caldera subsidence.

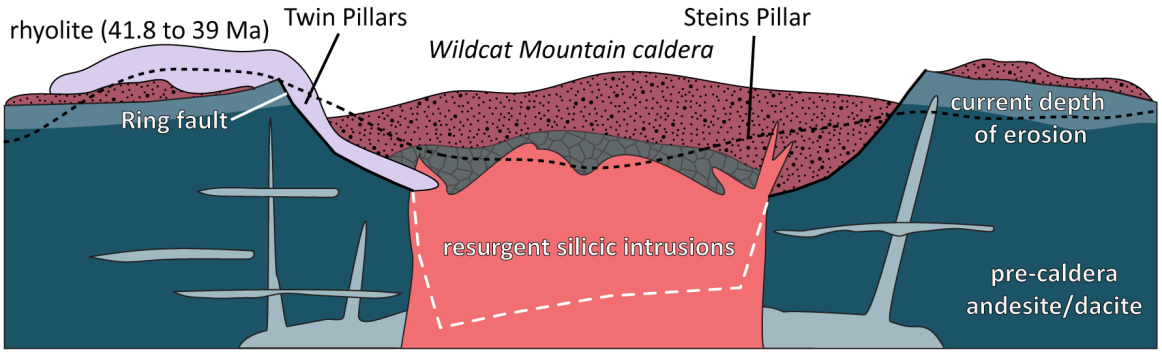

4. Post-caldera intrusion and resurgence.

Figure 5-8. Geochemical variation diagrams for the Ochoco and Lower Crooked volcanic fields (*n* = 228 analyses). (a) Total alkalis ($Na_2O + K_2O$) versus silica (SiO_2) (TAS) classification (normalized to 100 percent anhydrous). Fields and rock names are from Le Bas and others (1986) and Le Maitre and others (1989). Red-dashed line is the dividing line between alkaline, subalkaline/tholeiitic fields after Cox and others (1979). Data include 82 analyses from the Ochoco volcanic field and 146 analyses from the Lower Crooked volcanic field. Note the continuum of compositions for calc-alkaline rocks in the Ochoco volcanic field and bimodal composition of rocks in the Lower Crooked volcanic field. (b) Total iron/magnesium (FeOTotal/MgO) versus silica (SiO_2) diagram for mafic to intermediate rocks. Tholeiitic and calc-alkaline fields are from Miyashiro (1974). Data include 36 analyses from the Ochoco volcanic field and 46 analyses from the Lower Crooked volcanic field. (c) Potassium (K_2O) versus silica (SiO_2). Classification boundaries distinguishing low-, medium, and high-K rocks from Peccerillo and Taylor (1976).

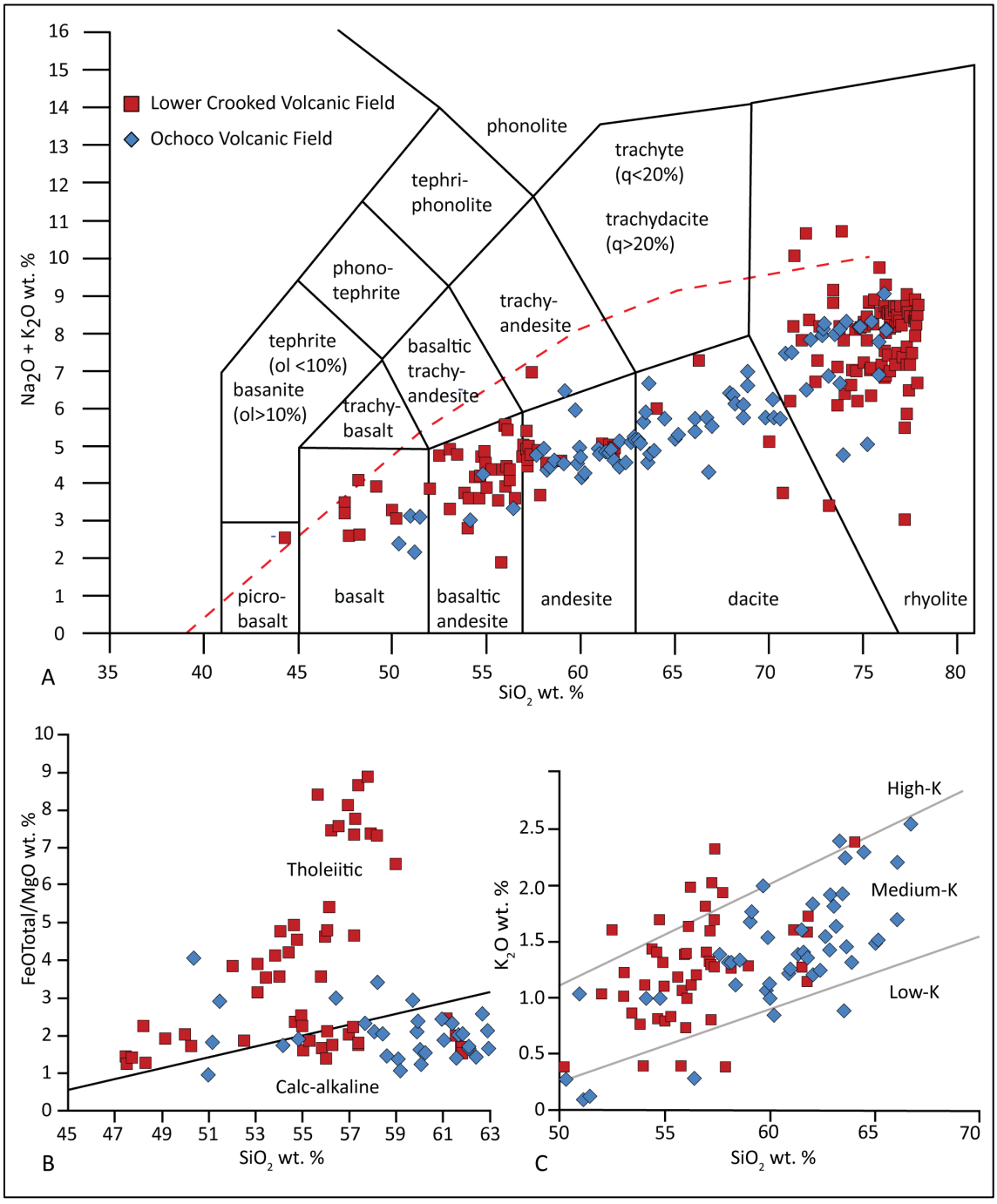

Figure 5-9. Trace element discrimination diagrams for silicic rocks in the Ochoco and Lower Crooked volcanic fields (*n* = 280 analyses). (a) Zirconium (Zr) versus niobium (Nb) variation diagram for silicic rocks (SiO_2 > 65 weight percent). (b) Rubidium (Rb) versus niobium plus yttrium (Nb+Y). Classification boundaries defining tectonic settings after Pearce and others (1984). Data in A and B include 49 analyses from the Ochoco volcanic field and 91 analyses from the Lower Crooked volcanic field.

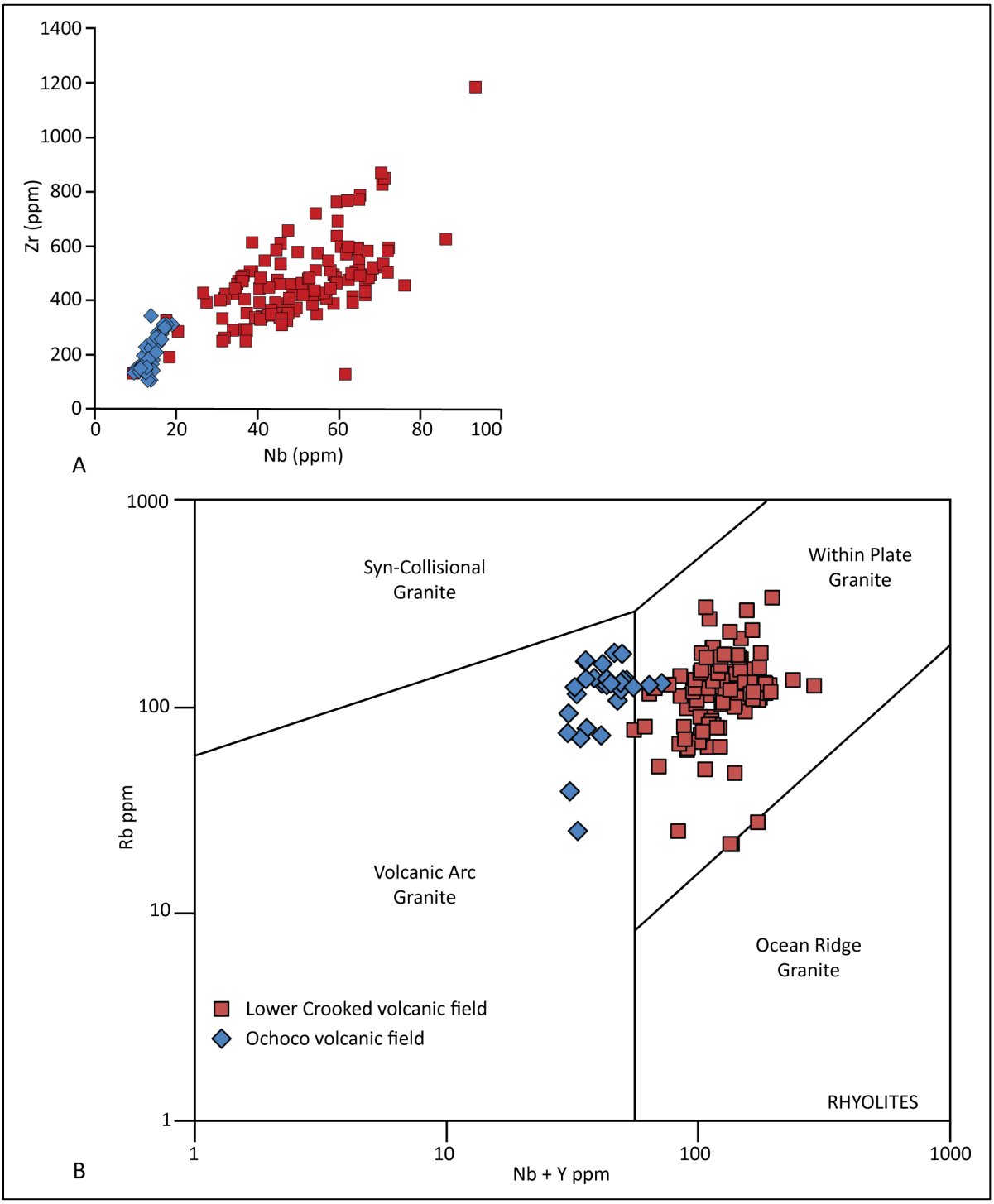

Figure 5-10. Trace element variation diagrams for silicic rocks in the Ochoco volcanic field (*n* = 34 analyses). (a) Zirconium (Zr) versus niobium (Nb). (b) Thorium (Th) versus niobium (Nb).

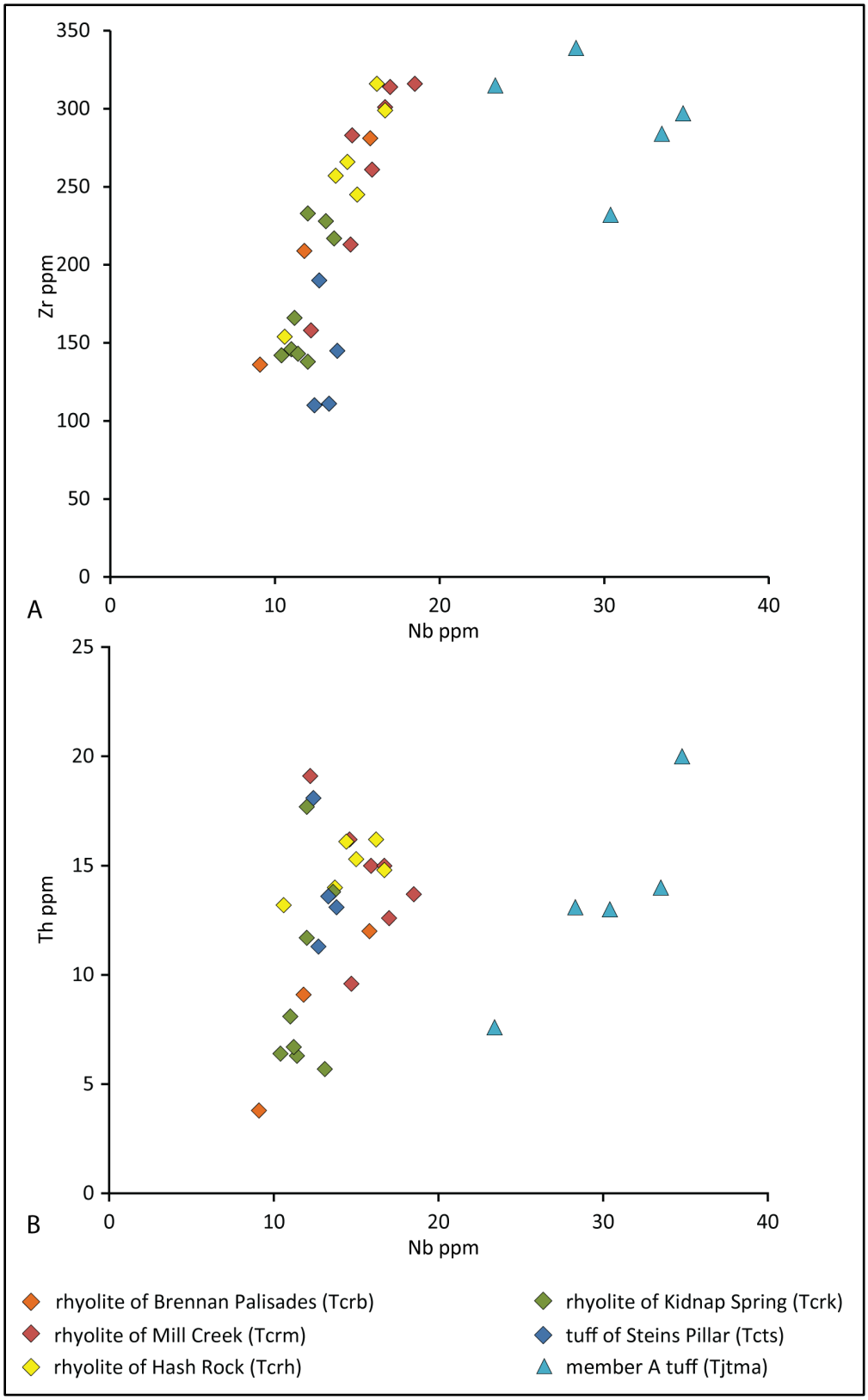

5.1.1.1.2 Age

A regional stratigraphy has not been developed for the Eocene Clarno Formation, but available isotopic ages, combined with geochemical compositions indicate two distinct parts to the formation across north-central Oregon (**Figure 5-11**). The suite of older, discontinuously exposed, alkaline to aluminous rocks, marking the lower boundary of the early Clarno Formation has returned $^{40}Ar/^{39}Ar$ ages ranging between 53.6 and 45.26 Ma (Bestland and others, 1999, 2002; Appel, 2001).

Appel (2001) reported a number of $^{40}Ar/^{39}Ar$ ages for early Clarno Formation intrusive bodies, cropping out near the community of Mitchell, ~62 km (39 mi) northeast of Prineville (**Figure 5-11**). These units include: 1) clinopyroxene-olivine-nepheline-bearing, mafic to ultramafic intrusions at Marshall Butte and Corporate Butte with respective $^{40}Ar/^{39}Ar$ isochron ages of 49.37 ± 0.49 Ma (whole rock; sample MB-3) and 46.19 ± 1.2 Ma (whole rock; sample MB-1) and 52.08 ± 3.9 Ma (whole rock; sample CB-1); 2) the clinopyroxene-olivine-bearing Hudspeth Mill intrusion with an $^{40}Ar/^{39}Ar$ isochron age of 45.26 ± 0.31 Ma (whole rock; sample HM-2); 3) Black Butte dacite with an $^{40}Ar/^{39}Ar$ plateau age of 48.97 ± 0.14 Ma (phlogopite; sample BB-1); 4) pyroxene-mica (phlogopite)-feldspar-bearing lamprophyre dikes with an $^{40}Ar/^{39}Ar$ plateau age of 48.67 ± 0.17 Ma (phlogopite; sample SR-1) at Spetch Rim and $^{40}Ar/^{39}Ar$ isochron age of 47.8 ± 0.24 Ma (phlogopite; sample MC-2) for the Mudcreek dike; and 5) the peraluminous high-silica biotite-quartz-plagioclase-garnet rhyolite Scott Butte dike with $^{40}Ar/^{39}Ar$ plateau ages of 50.93 ± 0.14 Ma (biotite; sample SB-1) and 50.97 ± 0.11 Ma (biotite; SB-2). Broadly similar ages are reported for the oldest early Clarno Formation rocks in the type area, near Clarno, ~74 km (46 mi) north-northeast of Prineville (**Figure 5-4**). In the Clarno Unit of the John Day Fossil Beds National Monument, the lower part of the early Clarno Formation consists of structurally domed debris-flow conglomerates, the 51.2 ± 0.5 Ma pyroxene-plagioclase andesite of Pine Creek ($^{40}Ar/^{39}Ar$ plateau; whole rock; sample 93603), and a 53.6 ± 0.3 Ma plagioclase-hornblende dacite dome ($^{40}Ar/^{39}Ar$ plateau; plagioclase; sample 93602) (Bestland and others, 1999, 2002) (**Figure 5-11**). These older rocks in the Clarno Unit are onlapped by less deformed debris-flow conglomerates, 43.4 Ma andesite lava flows, and red beds.

The early Clarno Formation in the lower Crooked River basin is defined by compositionally distinct high-magnesium alkali-olivine basalt lava flows exposed on the north shore of Prineville Reservoir (**Tceb**) (plate). These high-magnesium alkali-olivine basalt flows are compositionally similar to early Clarno Formation rocks cropping out near Mitchell and of similar age with an $^{40}Ar/^{39}Ar$ plateau age of 46.40 ± 0.12 Ma (groundmass; sample 03 LCJ 06) (**Figure 5-11**; **Table 5-1**). Walker and Robinson (1990) reported a K-Ar age of 53.7 ± 1.0 Ma for andesite from a locality near Cadle Butte (plagioclase; sample 648-628) in the southeast part of the map area, but the date is of uncertain quality, location, and stratigraphic position (plate; **Table 5-1**).

More widespread Clarno Formation exposures in north-central Oregon form a tightly constrained cluster of ages for intermediate calc-alkaline rocks that range between ~44 and 40 Ma (**Figure 5-11**; Urbanczyk, 1994; Bestland and others, 1999, 2002; Appel, 2001; Ferns and McClaughry, 2007; McClaughry and others, 2009a, d; Bromley, 2011). The Clarno Formation in its type area near the community of Clarno (Merriam, 1901a, b) consists of an aerially extensive assemblage of andesite flows intercalated with thick horizons of claystone, debris flow conglomerate, and lesser amounts of tuff and red beds (Bestland and others, 1999, 2002; Retallack and others, 2000). Bestland and others (2002) determined $^{40}Ar/^{39}Ar$ plateau ages of 43.8 ± 0.5 Ma for the basalt of Hancock Canyon (plagioclase; sample 91613) and 43.4 ± 0.4 Ma for the andesite of Horse Mountain (plagioclase; sample 93634) (**Figure 5-11**). A single tuff exposed near the middle of his "claystone of Red Hill" unit returned an $^{40}Ar/^{39}Ar$ plateau age of 42.7 ± 0.3 Ma (plagioclase; sample 93653). Plagioclase separates obtained from reworked tuffs at the Nut Beds site within the conglomerate of Hancock Canyon have returned an $^{40}Ar/^{39}Ar$ age of 43.76 ± 0.29

Ma (Manchester, 1990, 1994), while zircons from the same unit have fission track ages of 43.6 and 43.7 (± 10 percent) (Vance, 1988) (**Figure 5-11**).

Geologic mapping and $^{40}Ar/^{39}Ar$ total fusion ages of whole rock samples reported by Urbanczyk (1994) recognized broadly similar aged magmatic pulses in the eastern Clarno Formation at Magone Lake, Susanville, and Cougar Rock in northeast Oregon (**Figure 5-11**). Urbanczyk (1994) separated mapped Clarno units in these areas into a 43.5 to 36.7 Ma lower sequence of mildly alkaline basalts and andesites and a 37.6 to 33.6 Ma upper sequence of calc-alkaline basalts, andesites, and dacites. Total fusion $^{40}Ar/^{39}Ar$ ages from the lower sequence range from 43.5 ± 0.4 Ma on an andesite flow near the base (whole rock; sample KMU89-143) to 36.7 ± 0.2 Ma obtained on dacite near the top of the sequence (whole rock; sample SPL89-163). A basalt flow within the lower sequence has an $^{40}Ar/^{39}Ar$ age of 39.9 ± 0.5 Ma (whole rock; sample SPL89-5). The upper sequence includes several basaltic lava flows with $^{40}Ar/^{39}Ar$ ages of 37.6 ± 0.4 Ma (whole rock; sample SPL 89-74) and 35.3 ± 0.2 Ma (whole rock; sample KMU89-130). A dacite within the upper sequence yielded an $^{40}Ar/^{39}Ar$ age of 33.6 ± 0.3 Ma (whole rock; sample KMU89-31). $^{40}Ar/^{39}Ar$ ages reported by Bromley (2011) for samples of basaltic andesite lava flows obtained from the upper part of the Magone Lake section of Urbanczyk (1994) include 40.64 ± 0.31 (groundmass; sample K90-367) and 41.09 ± 0.42 Ma (groundmass; sample K90-328) (**Figure 5-11**). Additional dating of Clarno Formation basaltic andesite lava flows, intercalated with debris flow conglomerate near Whitney, provided similar ages to those reported by Urbanczyk (1994) and Bromley (2011), having whole rock $^{40}Ar/^{39}Ar$ plateau ages of 41.89 ± 0.5 (groundmass; sample DGB GM 2D2-13) and 40.08 ± 0.38 Ma (groundmass; sample DGB GM 2D4-13) (**Figure 5-11**; Gaylord and others, 2015; McClaughry and others, 2019).

Across the Ochoco Mountains, in the northeast part of the lower Crooked River basin, the Clarno Formation consists of middle to late Eocene basaltic andesite, andesite, and dacite lavas, domes, and subvolcanic intrusions, breccia dikes, and silicic tuff and rhyolite dome complexes forming the Ochoco volcanic field (McClaughry and others, 2009a, d). Isotopic ages obtained from rocks in the Ochoco volcanic field indicate magmatism progressed through several stages with early emplacement of andesitic to dacitic lavas and intrusions. $^{40}Ar/^{39}Ar$ plateau ages for the oldest rocks in the Ochoco volcanic field include 43.86 ± 0.89 Ma on porphyritic dacite (**Tcdp**) cropping out at Harvey Gap (plagioclase; sample 279 LCJ 06; Ferns and McClaughry, 2007), 42.79 ± 0.44 Ma for a hornblende-porphyritic andesite dike (**Tcid**) exposed along Mill Creek Road (plagioclase; sample 45 P 05; McClaughry and Ferns, 2006b), and 41.50 ± 0.48 Ma for the andesite of Little McKay Creek (**Tcau**) (plagioclase; sample 322 LCJ 06) (**Figure 5-11**; plate; **Table 5-1**). The tuff of Steins Pillar (**Tcts**), emplaced during the formation of the Wildcat Mountain caldera, has a $^{206}Pb/^{238}U$ zircon age of 41.8 ± 0.2 Ma (sample 152 LCJ 06). The post-caldera rhyolite of Hash Rock (**Tcrh**), overlying the tuff of Steins Pillar, has an $^{40}Ar/^{39}Ar$ plateau age 39.35 ± 0.30 Ma (plagioclase; sample 280 LCJ 06; McClaughry and others, 2009a, d) (**Figure 5-11**; plate; **Table 5-1**).

Figure 5-11. Regional stratigraphy and isotopic ages of the John Day and Clarno Formations (*following page*). Note that ages marked by an asterisk were determined by the K-Ar method. All other ages reported were determined by the $^{40}Ar/^{39}Ar$ or $^{206}Pb/^{238}U$ zircon method. Labels are as follows: KM – Kimberly Member; HV – Haystack Valley Member; BM – Balm Creek Member; JC – Johnson Creek Member.

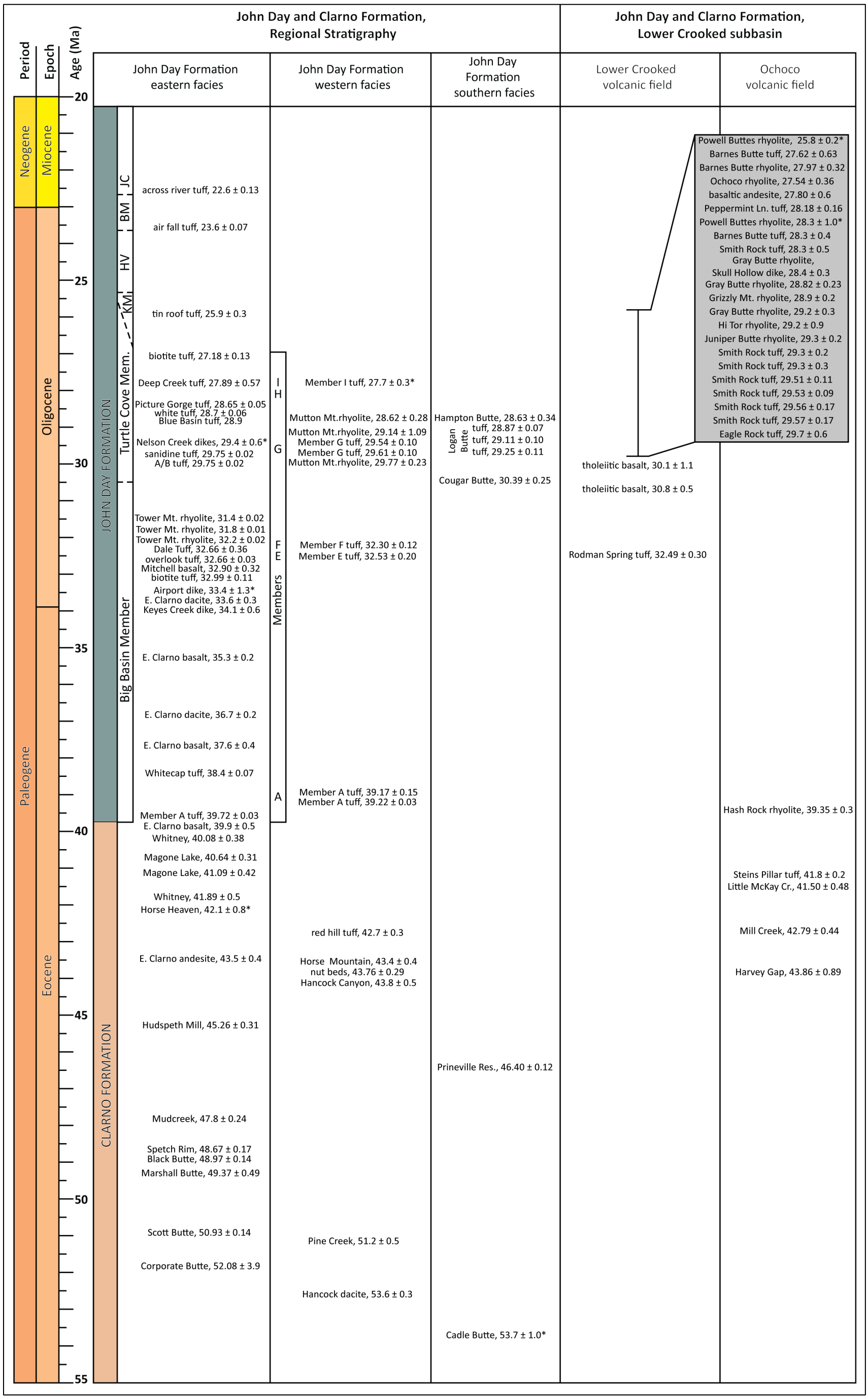
John Day and Clarno Formation, Regional Stratigraphy
John Day and Clarno Formation, Lower Crooked subbasin
Period
Epoch
Age (Ma)
Neogene
Miocene
Oligocene
Paleogene
Eocene
20
25
30
35
40
45
50
55
JOHN DAY FORMATION
CLARNO FORMATION
Big Basin Member
Turtle Cove Mem.
JC
BM
HV
KM
John Day Formation eastern facies
across river tuff, 22.6 ± 0.13
air fall tuff, 23.6 ± 0.07
tin roof tuff, 25.9 ± 0.3
biotite tuff, 27.18 ± 0.13
Deep Creek tuff, 27.89 ± 0.57
Picture Gorge tuff, 28.65 ± 0.05
white tuff, 28.7 ± 0.06
Blue Basin tuff, 28.9
Nelson Creek dikes, 29.4 ± 0.6*
sanidine tuff, 29.75 ± 0.02
A/B tuff, 29.75 ± 0.02
Tower Mt. rhyolite, 31.4 ± 0.02
Tower Mt. rhyolite, 31.8 ± 0.01
Tower Mt. rhyolite, 32.2 ± 0.02
Dale Tuff, 32.66 ± 0.36
overlook tuff, 32.66 ± 0.03
Mitchell basalt, 32.90 ± 0.32
biotite tuff, 32.99 ± 0.11
Airport dike, 33.4 ± 1.3*
E. Clarno dacite, 33.6 ± 0.3
Keyes Creek dike, 34.1 ± 0.6
E. Clarno basalt, 35.3 ± 0.2
E. Clarno dacite, 36.7 ± 0.2
E. Clarno basalt, 37.6 ± 0.4
Whitecap tuff, 38.4 ± 0.07
Member A tuff, 39.72 ± 0.03
E. Clarno basalt, 39.9 ± 0.5
Whitney, 40.08 ± 0.38
Magone Lake, 40.64 ± 0.31
Magone Lake, 41.09 ± 0.42
Whitney, 41.89 ± 0.5
Horse Heaven, 42.1 ± 0.8*
E. Clarno andesite, 43.5 ± 0.4
Hudspeth Mill, 45.26 ± 0.31
Mudcreek, 47.8 ± 0.24
Spetch Rim, 48.67 ± 0.17
Black Butte, 48.97 ± 0.14
Marshall Butte, 49.37 ± 0.49
Scott Butte, 50.93 ± 0.14
Corporate Butte, 52.08 ± 3.9
John Day Formation western facies
I
H
G
F
E
Members
A
Member I tuff, 27.7 ± 0.3*
Mutton Mt.rhyolite, 28.62 ± 0.28
Mutton Mt.rhyolite, 29.14 ± 1.09
Member G tuff, 29.54 ± 0.10
Member G tuff, 29.61 ± 0.10
Mutton Mt.rhyolite, 29.77 ± 0.23
Member F tuff, 32.30 ± 0.12
Member E tuff, 32.53 ± 0.20
Member A tuff, 39.17 ± 0.15
Member A tuff, 39.22 ± 0.03
red hill tuff, 42.7 ± 0.3
Horse Mountain, 43.4 ± 0.4
nut beds, 43.76 ± 0.29
Hancock Canyon, 43.8 ± 0.5
Pine Creek, 51.2 ± 0.5
Hancock dacite, 53.6 ± 0.3
John Day Formation southern facies
Hampton Butte, 28.63 ± 0.34
Logan Butte tuff, 28.87 ± 0.07
tuff, 29.11 ± 0.10
tuff, 29.25 ± 0.11
Cougar Butte, 30.39 ± 0.25
Prineville Res., 46.40 ± 0.12
Cadle Butte, 53.7 ± 1.0*
Lower Crooked volcanic field
tholeiitic basalt, 30.1 ± 1.1
tholeiitic basalt, 30.8 ± 0.5
Rodman Spring tuff, 32.49 ± 0.30
Ochoco volcanic field
Powell Buttes rhyolite, 25.8 ± 0.2*
Barnes Butte tuff, 27.62 ± 0.63
Barnes Butte rhyolite, 27.97 ± 0.32
Ochoco rhyolite, 27.54 ± 0.36
basaltic andesite, 27.80 ± 0.6
Peppermint Ln. tuff, 28.18 ± 0.16
Powell Buttes rhyolite, 28.3 ± 1.0*
Barnes Butte tuff, 28.3 ± 0.4
Smith Rock tuff, 28.3 ± 0.5
Gray Butte rhyolite,
Skull Hollow dike, 28.4 ± 0.3
Gray Butte rhyolite, 28.82 ± 0.23
Grizzly Mt. rhyolite, 28.9 ± 0.2
Gray Butte rhyolite, 29.2 ± 0.3
Hi Tor rhyolite, 29.2 ± 0.9
Juniper Butte rhyolite, 29.3 ± 0.2
Smith Rock tuff, 29.3 ± 0.2
Smith Rock tuff, 29.3 ± 0.3
Smith Rock tuff, 29.51 ± 0.11
Smith Rock tuff, 29.53 ± 0.09
Smith Rock tuff, 29.56 ± 0.17
Smith Rock tuff, 29.57 ± 0.17
Eagle Rock tuff, 29.7 ± 0.6
Hash Rock rhyolite, 39.35 ± 0.3
Steins Pillar tuff, 41.8 ± 0.2
Little McKay Cr., 41.50 ± 0.48
Mill Creek, 42.79 ± 0.44
Harvey Gap, 43.86 ± 0.89

Table 5-1. Summary of isotopic ages for the Clarno Formation in the lower Crooked River basin.

Map Unit	Age	Sample	Method	Material Analyzed	Source	UTM N (NAD 83)	UTM E (NAD 83)
Tcrh	39.35 ± 0.30 Ma	280 LCJ 06[1]	$^{40}Ar/^{39}Ar$	plagioclase	McClaughry and others (2009a, d)	4929638	694355
Tcts	41.80 ± 0.20 Ma	152 LCJ 06[2]	$^{206}Pb/^{238}U$	zircon	this study	4918369	689457
Tcau	41.50 ± 0.48 Ma	322 LCJ 07[1]	$^{40}Ar/^{39}Ar$	plagioclase	Ferns and McClaughry (2007)	4930554	681985
Tcid	42.79 ± 0.44 Ma	45 P 05[1]	$^{40}Ar/^{39}Ar$	plagioclase	McClaughry and Ferns (2006b)	4915506	685899
Tcdp	43.86 ± 0.89 Ma	279 LCJ 06[1]	$^{40}Ar/^{39}Ar$	plagioclase	Ferns and McClaughry (2007)	4926868	688595
Tceb	46.40 ± 0.12 Ma	03 LC 06[3]	$^{40}Ar/^{39}Ar$	whole rock	this study	4889216	682767
Tcdp?	53.7 ± 1.0 Ma	648-628	K-Ar	plagioclase	Walker and Robinson (1990)	4903097	695905

All ages reported at ±2σ.

[1]Ages determined at the College of Oceanic and Atmospheric Sciences, Oregon State University, Corvallis.

[2]Ages determined at California State University, Northridge.

[3]Ages determined at the New Mexico Geochronological Research Laboratory (NMGRL), Socorro.

5.1.1.2 John Day Formation

5.1.1.2.1 Distribution, composition, and lithology

The Clarno Formation is overlain in the western part of the lower Crooked River basin by mafic lava flows and intrusions, rhyolitic tuffs, lava flows and domes, and volcaniclastic sedimentary rocks that are part of the late Eocene to Oligocene John Day Formation (**Figure 5-4**, **Figure 5-11**; plate). Regionally, the John Day Formation consists of a dissected belt of volcanogenic sedimentary rocks, mafic lavas, rhyolite domes, and widespread rhyolite tuffs, covering more than 20,000 km^2 (7,722 mi^2) of central and eastern Oregon (**Figure 5-4**, **Figure 5-11**; Marsh, 1875; Peck, 1964; Swanson, 1969; Fisher and Rensberger, 1972; Robinson, 1975; Robinson and Stensland, 1979; Robinson and Brem, 1981; Robinson and others, 1984; Obermiller, 1987; Robinson and others, 1990; Smith and others, 1998). The regional stratigraphy of the John Day Formation was established by Peck (1964), Fisher and Rensberger (1972), Robinson and Brem (1981), and Robinson and others (1990). Robinson and Brem (1981) divided the formation into a western, southern, and eastern facies (**Figure 5-4**, **Figure 5-11**). The western facies is divided into members designated alphabetically from A to I (**Figure 5-4**, **Figure 5-11**; Peck, 1964; Robinson and Brem, 1981; Robinson and others, 1990). The eastern facies is divided into seven members that include from oldest to youngest the Big Basin, Turtle Cove, Kimberly, Haystack Valley, Balm Creek, Johnson Creek, and Rose Creek members (**Figure 5-4**, **Figure 5-11**; Fisher and Rensberger, 1972). The southern facies has not been formally divided into members (**Figure 5-4**, **Figure 5-11**).

The oldest part of the John Day Formation in the Lower Crooked Basin is the ~39.7 Ma Member A ash-flow tuff (**Tjtma**), cropping out northwest of Gray Butte and along Ochoco Divide (**Figure 5-12**; plate). This rhyolite tuff, erupted from a yet undiscovered volcanic center, is widespread across north-central Oregon, forming an important stratigraphic marker that regionally defines the base of the John Day Formation (**Figure 5-11**, **Figure 5-12**; plate; Swanson and Robinson, 1968; Robinson and others, 1990). Several other map units, including the tuff of North Unit canal (**Tjtn**), the 32.5 Ma tuff of Rodman Spring (**Tjtr**), and volcaniclastic sedimentary deposits (**Tjtt**) together form the older part of the John Day Formation in the lower Crooked River basin (**Figure 5-11**, **Figure 5-12**).

Early John Day Formation map units in the lower Crooked River basin are overlain by a bimodal assemblage of tholeiitic mafic lava flows, and rhyolite tuff, lava flow, and dome complexes. These rocks cover ~1,500 km^2 (580 mi^2) in the western part of the lower Crooked River basin, and collectively make up the Lower Crooked volcanic field (**Figure 5-4**, **Figure 5-8a**, **Figure 5-11**, **Figure 5-12**; plate; McClaughry and others, 2009c, d).

The oldest parts of the Lower Crooked volcanic field are defined by a series of iron- and titanium-rich tholeiitic basaltic andesite and andesite lava flows and intrusions (**Tjba**, **Tjia**) that were erupted from volcanic centers situated between Haystack and Prineville Reservoirs between ~34 and 29.6 Ma (**Figure 5-8b-c**, **Figure 5-11**, **Figure 5-12**; plate). Emplacement of tholeiitic lava flows in the lower part of the Lower Crooked volcanic field coincided with the eruption of several prominent ash-flows (**Tjte**, **Tjta**) at ~29.7 to 29.6 Ma (**Figure 5-12**). These ash-flow tuffs, cropping out as prominent sheets along the north shore of Prineville Reservoir, were erupted from now obscure vent sources. Chemical composition, age, and deposits thickness suggest these tuffs may signify the pre-cursor stages of formation of the Crooked River caldera.

Collapse along arcuate ring-fractures and eruption of several major ash-flow tuff units, including the tuff of Smith Rock (**Tjtsi**, **Tjtso**, **Tjtsn**), tuff of Peppermint Lane (**Tjtp**), and tuff of Barnes Butte (**Tjtb**) between 29.6 and 27.6 Ma produced the large-scale, multicyclic Crooked River caldera (**Figure 5-4**, **Figure 5-11**, **Figure 5-12**; **Figure 5-13**, **Figure 5-14**; plate; McClaughry and Ferns, 2006a, 2007a; McClaughry and others, 2009b, d). The Crooked River caldera forms a semi-elliptical 41 × 27 km (25.5 × 16.8 mi) caldera, whose partially eroded remains extend from Gray Butte on the northwest, along the western front of the Ochoco Mountains, and southeast to Prineville Reservoir (**Figure 5-12**, **Figure 5-13**; plate; McClaughry and Ferns, 2007a; McClaughry and others, 2009b, d). It is characterized by a combination of thickly ponded silicic pumice-lithic ash-flow tuff, nearly vertical caldera-bounding faults, rhyolite dome complexes that surround the structure, and a corresponding regional relative gravity low (**Figure 5-13**, **Figure 5-14**; plate).

The Crooked River caldera is coincident with a relatively undissected structural area juxtaposed between the Klamath-Blue Mountain gravity-anomaly lineament and junction of the Brothers and Sisters fault zones (**Figure 5-2**). Two major fault zones that parallel the northeast trend of the Klamath-Blue Mountain gravity-anomaly lineament bracket the caldera (**Figure 5-12**; plate). The Cyrus Springs fault zone (Smith and others, 1998) bounds the northwest margin while the Prineville Reservoir fault zone bounds the southeast margin. These lineaments define a circumferential, peripheral fault zone that mimics the arcuate structural margin of the caldera that encircles the intracaldera ash-flow tuff. This peripheral fault zone extends at least 10 km (6 mi) outside the main area of subsidence and is associated with numerous small rhyolite intrusions (**Figure 5-12**, **Figure 5-13**, **Figure 5-14**; plate).

Rocks of the Crooked River caldera straddle a stratigraphic discontinuity between the western and southern facies of the John Day Formation and are correlative with Members G and H (**Figure 5-4**). More than 580 km^3 (139 mi^3) of tuff was erupted during formation of the Crooked River caldera. Outflow units of the tuff of Smith Rock (**Tjtso**, **Tjtsn**) are exposed discontinuously around the periphery of the caldera and have been traced as John Day Formation Member G as far north as Antelope, 58 km (36 mi) northeast of Smith Rock State Park (**Figure 5-4**, **Figure 5-12**; plate).

The major initial subsidence phase of the caldera at 29.6 Ma was closely followed by the ring-fault controlled extrusion of large (20 to 80 km^2 [~7.7 to 31 mi^2]) fields of rhyolite lava flows, domes, and intrusions along the structural margin, with a major pulse at 29.3 Ma (**Figure 5-11**, **Figure 5-12**, **Figure 5-13**, **Figure 5-14**; plate). Late-stage rhyolite domes and lava flows erupted up until ~25.8 Ma (**Figure 5-11**, **Figure 5-12**; plate). Remnants of these rhyolite domes and lava flows are mapped at Powell Buttes (**Tjpq**, **Tjps**, **Tjpa**, **Tjpi**), Gray Butte (**Tjrg**), Grizzly Mountain (**Tjrgm**), Barnes Butte (**Tjrb**), Ochoco Reservoir (**Tjro**), and Pilot Butte (**Tjrpb**) (**Figure 5-12**, **Figure 5-13**, **Figure 5-14**; plate). The post-caldera rhyolite dome phase was accompanied by a second sequence of ash-flow tuff eruptions, which produced the tuff of Peppermint Lane (**Tjtp**) at 28.18 Ma and the tuff of Barnes Butte (**Tjtb**) at ~28 Ma from now obscure vent sources at Barnes Butte in the southeast part of the Crooked River caldera (**Figure 5-12**, **Figure 5-13**,

Figure 5-14; plate). It is not clear whether eruption of the tuff of Peppermint Lane (**Tjtp**) and tuff of Barnes Butte (**Tjtb**) resulted in the formation of a second collapse structure, as no topographic expression of a subsidiary caldera ring-structure is clearly defined. The post-caldera rhyolite phase was also accompanied by hot-spring systems that formed both within and around the periphery of the Crooked River caldera (**Figure 5-12**, **Figure 5-14**; plate). Hot-spring systems deposited massive quartz and calcite veins (± cinnabar) along ring-fractures and peripheral fault structures as well as finely laminated to massive mudstones, siliceous pool sinter, and sinter breccia along the caldera wall. Major volcanic activity in the field waned around 25.8 Ma with emplacement of quartz-phyric rhyolite at Powell Buttes (**Tjpq**) (**Figure 5-12**; plate).

Rocks of the Lower Crooked volcanic field and the Crooked River caldera are notably texturally, petrographically, and chemically distinct from those of the adjacent, ~10 to 13 m.y. older Ochoco volcanic field (**Figure 5-8, Figure 5-9**; plate; appendix; McClaughry and others, 2009c, d). Mafic to intermediate composition lava flows and intrusions, predating the formation of the Crooked River caldera within the Lower Crooked volcanic field, are tholeiitic picrobasalt, basalt, basaltic andesite, andesite, and trachyandesite (**Tjba, Tjia**) with silica contents ranging between 44.31 and 59.0 weight percent SiO_2 (avg = 53.85 weight percent SiO_2; *n* = 38).

The least evolved part of the pre-caldera mafic suite of rocks is defined by olivine-phyric, iron- and titanium-rich picrobasalt and basalt lava flows (**Tjba**) mapped between Gray Butte and the Cyrus Springs fault zone outside the northwest margin of the Crooked River caldera. These rocks are characterized by silica contents ranging between 44.31 and 52.52 weight percent SiO_2 (avg = 48.57 weight percent SiO_2; *n* = 9) and notably high contents for magnesium (MgO = 5.18 to 10.83 weight percent; avg = 7.17 weight percent MgO), iron (FeOTotal = 9.55 to 13.93 weight percent; avg = 12.06 weight percent FeOTotal), and titanium (1.67 to 2.88 weight percent TiO_2; avg = 2.22 weight percent TiO_2) (**Figure 5-8a-b**; appendix). Total alkalis (K_2O + Na_2O) range between 2.54 and 4.72 weight percent (avg = 3.43 weight percent K_2O + Na_2O). Picrobasalt and basalt lava flows (**Tjba**) cropping out north of Gray Butte contain olivine and plagioclase phenocrysts with interstitial to subophitic titaniferous clinopyroxene. Chemistry and petrography of the olivine-phyric lava flows is similar to those reported by Robinson (1969), Robinson and Brem (1981) and Robinson and others (1990) for alkali olivine basalt lava flows found in John Day Formation members E, F, and G north of the lower Crooked River basin.

More evolved pre-caldera basaltic andesite and andesite (**Tjba**) mapped along the periphery of the Crooked River caldera, north of Gray Butte, and at Prineville Reservoir are compositionally similar to icelandite with silica contents ranging between 53.08 and 59.0 weight percent SiO_2 (avg = 55.71 weight percent SiO_2; *n* = 21). Icelandite-type basaltic andesite and andesite lava flows contain similar iron (FeOTotal = 10.69 to 15.51 weight percent; avg = 13.39 weight percent FeOTotal) and titanium (1.71 to 3.31 weight percent TiO_2; avg = 2.31 weight percent TiO_2) contents to less evolved mafic rocks mapped north of Gray Butte but are distinguished by characteristically lower magnesium (MgO = 1.39 to 4.23 weight percent; avg = 2.68 weight percent MgO). Total alkalis (K_2O + Na_2O) range between 2.78 and 5.57 weight percent (avg = 4.36 weight percent K_2O + Na_2O). Samples of basaltic andesite and andesite are sparsely plagioclase-phyric with a groundmass of aligned plagioclase, microgranular clinopyroxene, cubic Fe-Ti oxides, and variably altered interstitial glass (Patridge, 2010). Phenocrysts of olivine are rare and are usually altered to iddingsite. Chemistry and petrography of the basaltic andesites and andesites indicate compositions similar to those reported by Robinson and Brem (1981) and Robinson and others (1990) for iron-rich trachyandesites in John Day Formation Member B.

A prominent multiphase intrusion composed of dikes and sills of black, aphyric basaltic andesite and andesite (**Tjia**) (SiO_2 = 52.02 to 57.78 weight percent; avg = 55.85 weight percent SiO_2; *n* = 7) is mapped

north of Gray Butte. Intrusive rocks have characteristically high iron (FeOTotal = 13.25 to 14.60 weight percent; avg = 14.11 weight percent FeOTotal) and titanium (1.61 to 3.81 weight percent TiO_2; avg = 2.44 weight percent TiO_2) contents and lower magnesium (MgO = 1.62 to 4.04 weight percent; avg = 2.51 weight percent MgO) similar to icelandite-type pre-caldera lava flows (**Tjba**). Seligman and others (2014) reported that pre-caldera mafic to intermediate basalts associated with the Crooked River caldera also have elevated high-field strength elements and high Nb/Yb and Th/Yb ratios relative to normal mid-ocean ridge basalts.

Rhyolitic tuffs and lava flows, domes, and intrusions mapped across the Lower Crooked volcanic field in association with the Crooked River caldera range from low-to high-silica peralkaline rhyolite with silica contents ranging between 70.79 and 77.76 weight percent (avg = 75.43 weight percent SiO_2; *n* = 122; **Figure 5-8a**; appendix). Rhyolites have characteristically elevated contents of incompatible large-ion lithophile elements such as barium (Ba = 153 to 1541 weight percent, avg = 863 ppm), high-field strength elements such as niobium (Nb = 27 to 93 ppm; avg = 55.2 ppm), zirconium (Zr = 131 to 1185 ppm; avg = 534 ppm), and yttrium (Y = 45 to 223 ppm; avg = 90 ppm), and the light rare-earth elements lanthanum (La = 36 to 95 ppm; avg = 61 ppm) and cerium (Ce = 67 to 228 ppm; avg = 134 ppm) (**Figure 5-9a-b**, **Figure 5-15**; appendix). Lower Crooked volcanic field silicic rocks are nearly aphyric, with sparse quartz and feldspar, contain no hydrous minerals, and have distinctly elevated Nb + Y concentrations, indicating an affinity with A-type rhyolites and a probable intraplate origin (**Figure 5-9b**; Patridge, 2010; Seligman and others, 2014). Major and minor trace element concentrations indicate that rhyolites of the Lower Crooked volcanic field are the products of at least two differently evolved magmatic sources (high-iron group and low-iron group) that evolved independently from one another and that were persistent in the area both before and after formation of the Crooked River caldera (Patridge, 2010). Seligman and others (2014) attributed the combined isotopic and trace-element compositional characteristics of both mafic and silicic rocks at the Crooked River caldera as being consistent with a deep, undepleted, sublithospheric mantle origin. The bimodal basalt-rhyolite character, trace-element concentrations, aphyric rock textures, mineral assemblages, and low $\delta^{18}O_{zircon}$ values of successive caldera-forming tuffs and post-caldera rhyolites, indicate that the Crooked River caldera formed as a voluminous low-$\delta^{18}O$ province similar to many middle Miocene to Quaternary rhyolites of the Yellowstone-Snake River Plain (Seligman and others, 2014). These characteristics, combined with regional geologic relations and geodynamic models, suggest that the Crooked River caldera formed through intraplate magmatism, possibly sourced from the initial appearance of the Yellowstone plume east of the ancestral Cascade arc in the Oligocene (Seligman and others, 2014).

Mafic to intermediate composition lava flows and domes erupted in the Ochoco Mountains following major caldera-forming phases of the Crooked River caldera, are basaltic andesite, andesite, trachyandesite, and low-silica dacite with silica contents ranging between 54.69 and 64.0 weight percent (avg = 58.08 weight percent SiO_2; *n* = 18) (**Figure 5-8a-b**; appendix). Post-caldera mafic to intermediate rocks also contain characteristically less iron (5.44 to 10.01 weight percent FeOTotal; avg = 7.36 weight percent FeOTotal) and titanium (0.8 to 1.65 weight percent TiO_2; avg = 1.20 weight percent TiO_2) than mafic units emplaced directly preceding formation of the Crooked River caldera.

Figure 5-12. Simplified geologic map of the Oligocene Crooked River caldera (*following page*).

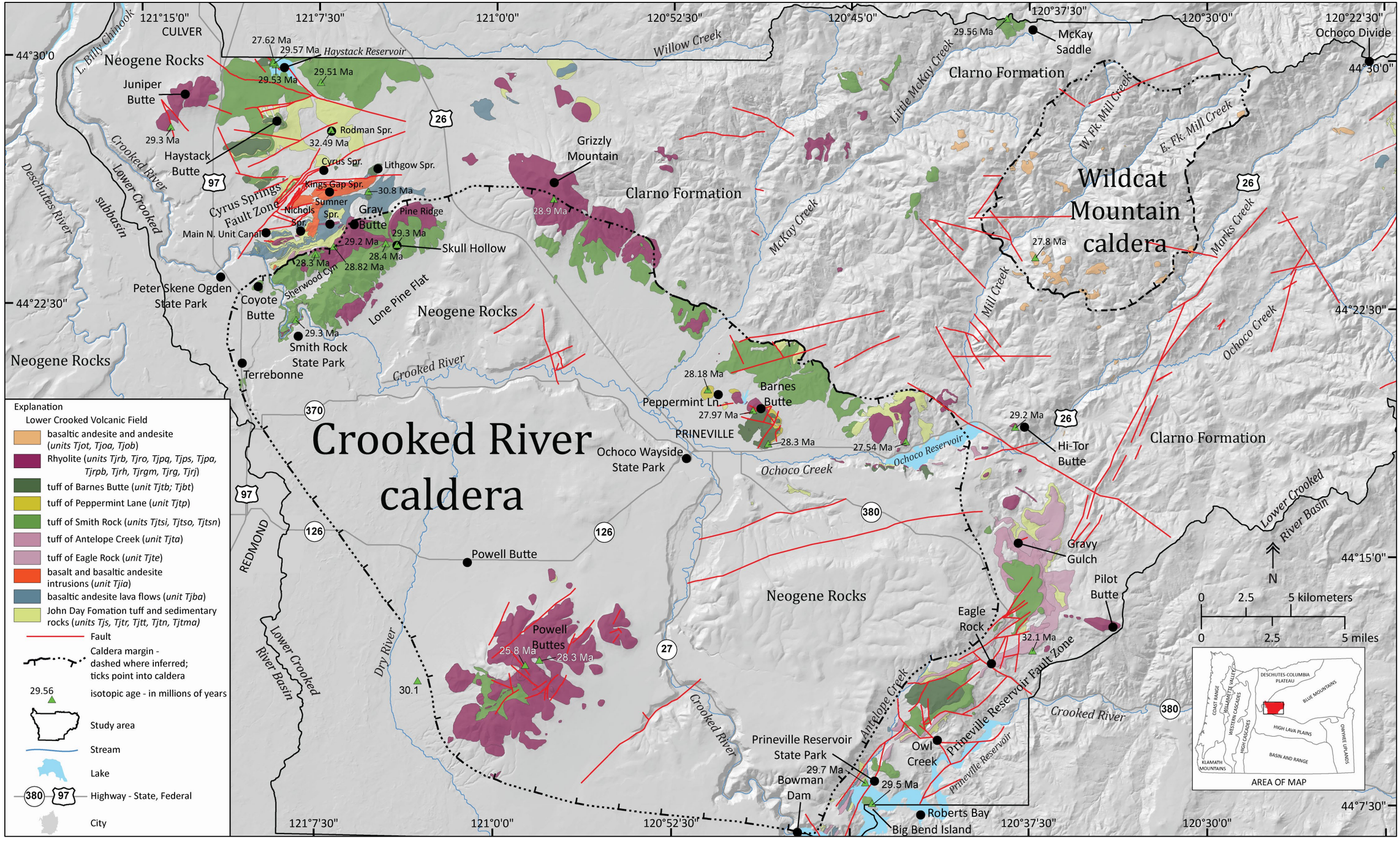
Crooked River caldera
Wildcat Mountain caldera
Neogene Rocks
Clarno Formation
Grizzly Mountain
Haystack Butte
Juniper Butte
Gray Butte
Pine Ridge
Skull Hollow
Lone Pine Flat
Coyote Butte
Smith Rock State Park
Peter Skene Ogden State Park
Terrebonne
Sherwood Cyn
Cyrus Springs Fault Zone
Rodman Spr.
Cyrus Spr.
Lithgow Spr.
Kings Gap Spr.
Sumner Spr.
Nichols Spr.
Main N. Unit Canal
Haystack Reservoir
Willow Creek
Little McKay Creek
McKay Creek
McKay Saddle
W. Fk. Mill Creek
E. Fk. Mill Creek
Mill Creek
Marks Creek
Ochoco Divide
Ochoco Creek
Ochoco Reservoir
Ochoco Wayside State Park
Hi-Tor Butte
Gravy Gulch
Pilot Butte
Eagle Rock
Barnes Butte
Peppermint Ln
PRINEVILLE
Powell Butte
Powell Buttes
Dry River
Crooked River
Antelope Creek
Prineville Reservoir Fault Zone
Prineville Reservoir
Prineville Reservoir State Park
Owl Creek
Bowman Dam
Roberts Bay
Big Bend Island
L. Billy Chinook
Deschutes River
Crooked River
Lower Crooked subbasin
Lower Crooked River Basin
REDMOND
121°15'0" CULVER
121°7'30"
121°0'0"
120°52'30"
120°45'0"
120°37'30"
120°30'0"
120°22'30"
44°30'0"
44°22'30"
44°15'0"
44°7'30"
26
97
370
126
380
27
27.62 Ma
29.57 Ma
29.53 Ma
29.51 Ma
29.3 Ma
32.49 Ma
30.8 Ma
28.9 Ma
29.3 Ma
29.2 Ma
28.4 Ma
28.3 Ma
28.82 Ma
29.3 Ma
28.18 Ma
27.97 Ma
28.3 Ma
27.54 Ma
29.56 Ma
27.8 Ma
29.2 Ma
32.1 Ma
25.8 Ma
28.3 Ma
30.1
29.7 Ma
29.5 Ma
Explanation
Lower Crooked Volcanic Field
basaltic andesite and andesite (units Tjot, Tjoa, Tjob)
Rhyolite (units Tjrb, Tjro, Tjpq, Tjps, Tjpa, Tjrpb, Tjrh, Tjrgm, Tjrg, Tjrj)
tuff of Barnes Butte (unit Tjtb; Tjbt)
tuff of Peppermint Lane (unit Tjtp)
tuff of Smith Rock (units Tjtsi, Tjtso, Tjtsn)
tuff of Antelope Creek (unit Tjta)
tuff of Eagle Rock (unit Tjte)
basalt and basaltic andesite intrusions (unit Tjia)
basaltic andesite lava flows (unit Tjba)
John Day Fomation tuff and sedimentary rocks (units Tjs, Tjtr, Tjtt, Tjtn, Tjtma)
Fault
Caldera margin - dashed where inferred; ticks point into caldera
isotopic age - in millions of years
Study area
Stream
Lake
Highway - State, Federal
City
Lower Crooked River Basin
N
0 2.5 5 kilometers
0 2.5 5 miles
DESCHUTES-COLUMBIA PLATEAU
BLUE MOUNTAINS
HIGH LAVA PLAINS
OWYHEE UPLANDS
BASIN AND RANGE
KLAMATH MOUNTAINS
HIGH CASCADES
WESTERN CASCADES
WILLAMETTE VALLEY
COAST RANGE
AREA OF MAP

Figure 5-13. Panorama showing topographic features of the Crooked River caldera. Rhyolite domes described in the text are labeled. View is from northwest to north to east from Stearns Butte (44.238099, -120.841495). Total view distance from northwest to east is ~48 km (30 mi).

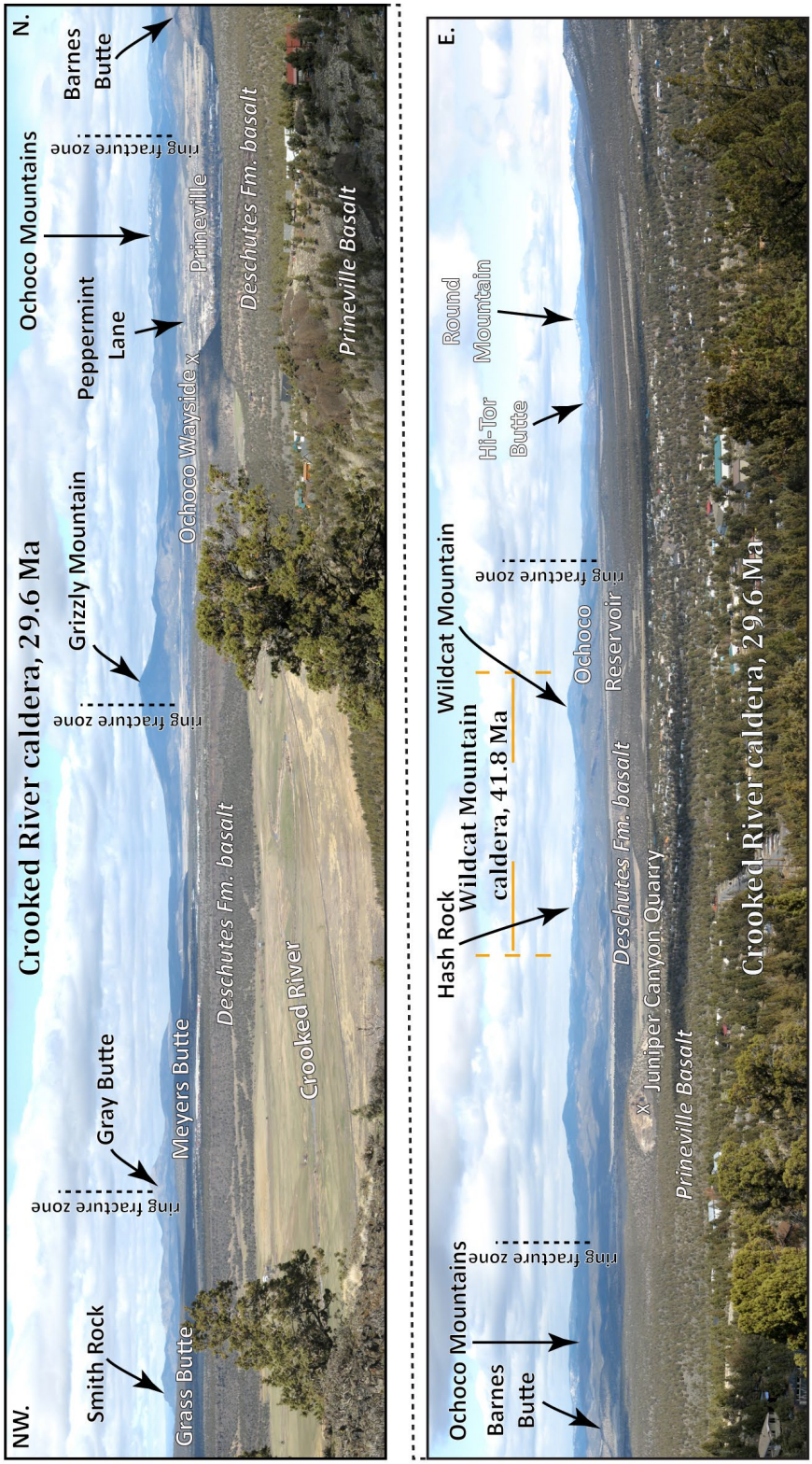

Figure 5-14. Stage development of the Oligocene Crooked River caldera.

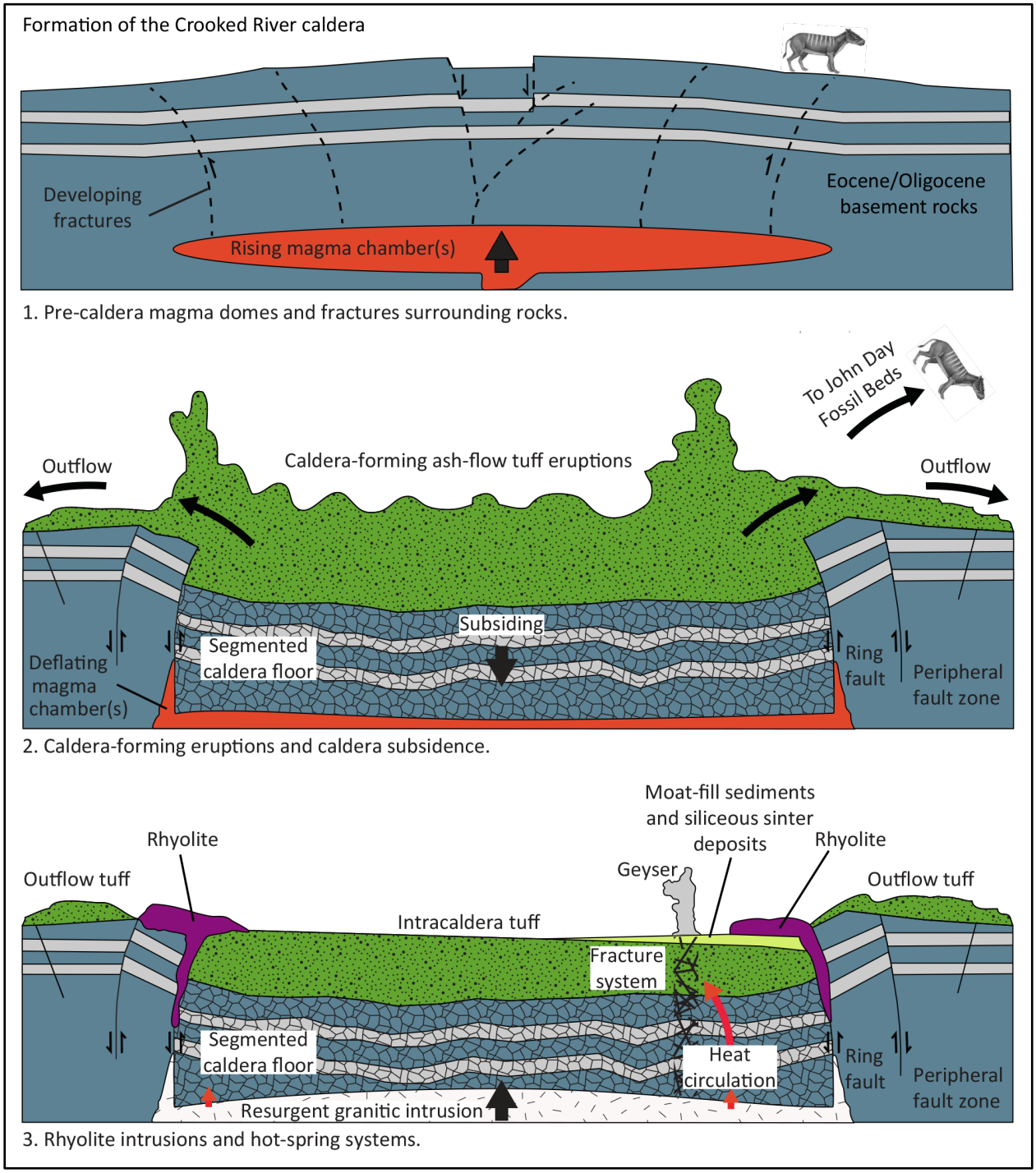

Figure 5-15. Trace element variation diagrams for silicic rocks in the Lower Crooked volcanic field (*n* = 122 analyses). (a) Zirconium (Zr) versus niobium (Nb). (b) Thorium (Th) versus niobium (Nb).

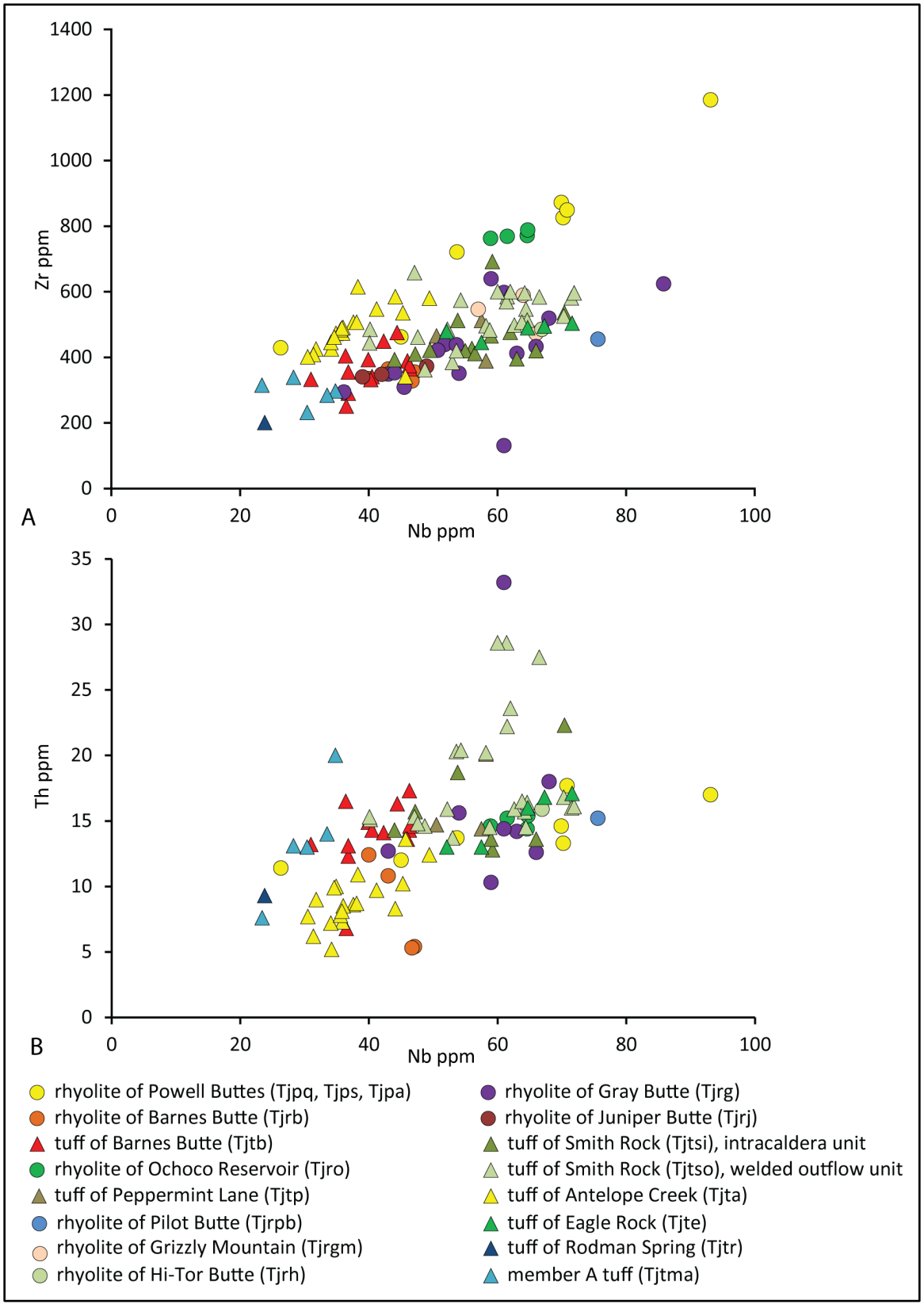

5.1.1.2.2 Age

Numerous $^{40}Ar/^{39}Ar$ and K-Ar ages have been obtained for prominent tuff marker beds in the John Day Formation, allowing for regional stratigraphic correlation (**Figure 5-11**). The base of the John Day Formation is generally defined by the regionally widespread Member A ash-flow tuff that has returned single-crystal $^{40}Ar/^{39}Ar$ ages of 39.72 ± 0.03 near the Painted Hills, 39.22 ± 0.03 near Clarno, and 39.17 ± 0.15 Ma (alkali feldspar; sample GSO95-140) near Ashwood (**Figure 5-4**, **Figure 5-11**; C.C. Swisher in Bestland and Retallack, 1994a, b; Smith and others, 1998; Retallack and others, 2000). Aerially extensive tuffs in the western facies, situated above the Member A ash-flow tuff, have a number of high-precision single crystal $^{40}Ar/^{39}Ar$ ages on alkali feldspar, including 38.2 ± 0.07 Ma for the Whitecap Knoll tuff and 33.6 ± 0.2 Ma for the Slanting Leaf beds near Clarno, 32.53 ± 0.20 Ma for Member E (sample GSO95-139), 32.30 ± 0.12 for Member F (sample GSO95-143), 29.54 ± 0.10 (sample GSO95-136) and 29.61 ± 0.10 (sample GSO95-134) for Member G, and 27.62 ± 0.63 for Member H (sample GSO95-134) (**Figure 5-4**, **Figure 5-11**; C.C. Swisher in Bestland and Retallack, 1994a; Smith and others, 1998). An ash-flow tuff, defined as Member I near the top of the formation in the western facies, has a K-Ar age of 27.7 ± 0.3 Ma (glass; sample PTR-71-6; Robinson and others, 1990). Rhyolite domes and lava flows, forming the Mutton Mountains northwest of Madras, have $^{40}Ar/^{39}Ar$ ages of 28.62 ± 0.28 (plateau; glass; sample AKJ MMR04), 29.14 ± 1.09 (isochron; plagioclase; sample AKJ MMR02), and 29.77 ± 0.23 Ma (plateau; plagioclase; sample AKJ MMD04), similar to those in Member G and mapped encircling the Crooked River caldera (**Figure 5-4**, **Figure 5-11**; Johnson, 2011).

Ash-flow and ash-fall tuffs forming prominent marker beds in the eastern facies are well exposed in the John Day Fossil Beds National Monument and have been used there to subdivide the formation into seven members (Graham, 2014). Members in the eastern facies include from oldest to youngest the Big Basin, Turtle Cove, Kimberly, Haystack Valley, Balm Creek, Johnson Creek, and Rose Creek members (**Figure 5-11**). High-precision $^{40}Ar/^{39}Ar$ age dates on tuffs in the eastern facies from the Painted Hills Unit of the John Day Fossil Beds National Monument include the 32.99 ± 0.11 Ma biotite tuff, 32.66 ± 0.03 Ma overlook tuff, 29.75 ± 0.02 Ma A/B tuff, 29.75 ± 0.02 Ma sanidine tuff, and the 28.65 ± 0.05 Ma Picture Gorge ignimbrite (**Figure 5-4**, **Figure 5-11**; C.C. Swisher in Retallack and others, 2000; Hunt and Stepleton, 2004; Albright III and others, 2008). Tuffs with high-precision $^{40}Ar/^{39}Ar$ ages in the Sheep Rock Unit of the John Day Fossil Beds National Monument include the 28.9 Ma Blue Basin tuff, 28.7 ± 0.06 Ma white tuff, 27.89 ± 0.57 Ma Deep Creek tuff, 27.18 ± 0.13 Ma biotite tuff, 25.9 ± 0.3 Ma tin roof tuff, and the 22.6 ± 0.13 Ma across the river tuff (**Figure 5-4**, **Figure 5-11**; C.C. Swisher in Hunt and Stepleton, 2004; Albright and others, 2008). Hunt and Stepleton (2004) provided an additional age of 23.6 ± 0.07 Ma obtained from an airfall tuff exposed at the contact between the Haystack Valley and overlying Balm Creek Member. The Rose Creek Member, mapped as the youngest part of the John Day Formation in the eastern facies, has an age of about ~18.8 to 18.2 Ma on the basis of its Hemingfordian mammalian fauna (Hunt and Stepleton, 2004).

Several additional high-resolution isotopic ages have been determined for rocks associated with the Tower Mountain caldera, forming the far eastern part of the eastern facies of the John Day Formation (**Figure 5-4**, **Figure 5-11**; McClaughry and others, 2009d; Brown, 2017). The Dale Tuff, erupted during formation of the Tower Mountain caldera, has returned an $^{40}Ar/^{39}Ar$ plateau age of 32.66 ± 0.36 Ma (feldspar) (Brown, 2017). U-Pb dating of zircons from three post-caldera rhyolites yielded ages of 32.167 ± 0.020 Ma (sample CH07a), 31.798 ± 0.012 Ma (sample TM5), and 31.426 ± 0.016 Ma (sample CH08a) (**Figure 5-11**; Brown, 2017).

Silicic rocks in the western part of the eastern facies of the John Day Formation are interbedded with tholeiitic basaltic andesite lava flows and are locally invaded by dike systems of comparable mafic

composition, near Mitchell (63 km [39 mi] east of Prineville) (**Figure 5-4**). Enlows and Parker (1972) and Taylor (1981) reported low-precision K-Ar ages of 29.4 ± 0.6 and 33.4 ± 1.3 Ma for the Mitchell area Nelson Creek and Airport dikes, while Appel (2001) obtained a more precise $^{40}Ar/^{39}Ar$ isochron age of 34.1 ± 0.6 Ma for the Keyes Creek segment of the Mitchell dike system (whole rock; sample BD-1) (**Figure 5-11**). Bromley (2011) reported an $^{40}Ar/^{39}Ar$ plateau age of 32.90 ± 0.32 Ma for tholeiitic basalt flows (groundmass; sample JDM-293) cropping out at the base of the John Day Formation near Mitchell (**Figure 5-11**).

The southern facies has received less attention than the more well studied western and eastern facies, but age data reported is similar to other parts of the John Day Formation (**Figure 5-4**, **Figure 5-11**). Robinson and others (1990) reported a K-Ar age of 32.1 ± 0.7 Ma (plagioclase; sample 648-625A) for their lower member tuff exposed east of Prineville Reservoir (**Figure 5-12**; see discussion under the tuff of Eagle Rock, unit **Tjte** below). Ages of 29.25 ± 0.11, 29.11 ± 0.10, and 28.87 ± 0.07 Ma were obtained for southern facies tuffs at Logan Butte (58 km [36 mi] southeast of Prineville), and are comparable to Member G in the western facies, and the Turtle Cove Member of the eastern facies (**Figure 5-4**, **Figure 5-11**; C.C. Swisher in Bestland, 1995). Rhyodacite to dacite volcanic centers at Hampton and Cougar buttes, south of the main John Day outcrop belt (74 km [46 mi] southeast of Prineville), have $^{40}Ar/^{39}Ar$ plateau ages of 30.39 ± 0.13 (plagioclase; sample HTB-0501) and 28.63 ± 0.17 Ma (plagioclase; sample HTB-0613) (**Figure 5-4**, **Figure 5-11**; Iademarco, 2009; Iademarco and Grunder, 2012).

The earliest part of the John Day Formation in the lower Crooked River basin is the 39.7 to 39.2 Ma Member A ash-flow tuff (**Tjtma**), mapped northwest of Gray Butte and along Ochoco Divide (**Figure 5-12**; plate). Several other units, including the tuff of North Unit canal (**Tjtn**), the tuff of Rodman Spring (**Tjtr**), and interbedded, discontinuous sedimentary intervals (**Tjtt**) form the older part of the John Day Formation in the lower Crooked River basin (**Figure 5-12**; plate). Smith and others (1998) reported a single crystal $^{40}Ar/^{39}Ar$ age of 32.49 ± 0.30 Ma (alkali feldspar; sample GSO95-130) for the tuff of Rodman Spring (**Tjtr**) (**Figure 5-12**; **Table 5-2**; plate).

Between ~34 and 29.6 Ma iron- and titanium-rich tholeiitic basaltic andesites and andesite flows and intrusions (**Tjob**, **Tjia**), were erupted from volcanic centers situated between Haystack and Prineville Reservoirs (**Figure 5-12**; plate). Northwest of Gray Butte, tholeiitic lavas (**Tjob**) set directly on older calc-alkaline lavas of the Clarno Formation (**Tcal**) and lie stratigraphically beneath the 32.49 Ma tuff of Rodman Spring (**Tjtr**) (**Figure 5-12**; plate). Fiebelkorn and others (1982, 1983) reported a K-Ar age of 30.8 ± 0.5 Ma for a multiphase tholeiitic andesite intrusion (**Tjia**) (whole rock; sample 10-6-78-2), mapped along the northwest margin of the Crooked River caldera north of Gray Butte (**Figure 5-12**; **Table 5-2**; plate; appendix). A basaltic andesite lava sampled in a geothermal test well drilled along the west flank of Powell Buttes yielded a comparable K-Ar age of 30.1 ± 1.1 Ma (whole rock; DOGMI-Bas81-2/UT-225) (**Figure 5-12**; **Table 5-2**; plate; appendix; Brown and others, 1980; Evans and Brown, 1981; Fiebelkorn and others, 1982, 1983).

Late eruptions of tholeiitic mafic lava flows in the Lower Crooked volcanic field coincided with the eruption of the tuff of Eagle Rock (**Tjte**) and the tuff of Antelope Creek (**Tjta**) at ~29.7 to 29.6 Ma. The older tuff of Eagle Rock has a $^{206}Pb/^{238}U$ zircon age of 29.7 ± 0.6 Ma (sample CR-8; Seligman and others, 2014) for a sample at Prineville Reservoir, which supplants an earlier K-Ar age of 32.1 Ma reported by Robinson and others (1990) (**Figure 5-12**; **Table 5-2**; plate). The tuff of Antelope Creek (**Tjta**) is undated, but has an age of ~29.6 Ma, as the unit is bracketed between the 29.7 Ma tuff of Eagle Rock (**Tjte**) and the 29.51 Ma Prineville Reservoir lobe of the tuff of Smith Rock (**Tjtso**) (**Figure 5-12**; plate).

Eruption of the tuff of Smith Rock (**Tjtsi**, **Tjtsn**, **Tjtso**) records the earliest development of the Crooked River caldera at 29.56 Ma (**Figure 5-12**; **Table 5-2**; plate). Outflow units of the tuff of Smith Rock (**Tjtso**)

are exposed discontinuously around the periphery of the caldera and have yielded indistinguishable high precision $^{40}Ar/^{39}Ar$ and $^{206}Pb/^{238}U$ zircon ages including: 1) the Prineville Reservoir lobe above Prineville Reservoir in the southern part of the map area has a $^{206}Pb/^{238}U$ zircon age of 29.5 ± 0.2 Ma (sample JM ER 13-4); 2) the McKay Saddle lobe cropping out in the Ochoco Mountains in the northeast part of the map area has an $^{40}Ar/^{39}Ar$ age of 29.56 ± 0.17 Ma (alkali feldspar; sample 448 LCJ 07; McClaughry and others, 2009b, d); and 3) the Haystack Reservoir lobe, equivalent to Member G of Peck (1964), Robinson (1975), and Smith and others (1998), cropping out along the north shore of Haystack Reservoir has $^{40}Ar/^{39}Ar$ ages of 29.53 ± 0.09 Ma (alkali feldspar; sample GSO95-133) and 29.57 ± 0.17 Ma (alkali feldspar; sample GSO95-132) (**Figure 5-12**; **Table 5-2**; plate). An outcrop of the Haystack Reservoir lobe east of Haystack Reservoir yielded an indistinguishable $^{206}Pb/^{238}U$ zircon age of 29.51 ± 0.11 Ma (sample HS-JM-04) (**Figure 5-12**; **Table 5-2**; plate). These dates are indistinguishable from geochemically similar John Day Formation Member G tuffs exposed north of the Crooked River caldera that have returned comparable $^{40}Ar/^{39}Ar$ ages of 29.61 west of Teller Flat and 29.54 Ma near Antelope (**Table 5-2**; Smith and others, 1998).

Isotopic ages obtained from the intracaldera unit of the tuff of Smith Rock (**Tjtsi**), infilling the Crooked River caldera, are comparable to outflow units with $^{206}Pb/^{238}U$ zircon ages of 29.3 ± 0.2 Ma (sample SRT-SKULL-1) for a sample obtained from Skull Hollow and an identical age of 29.3 ± 0.3 Ma (sample 24 LCJ 06) for tuff cropping out west of the Crooked River in Smith Rock State Park (**Figure 5-12**; **Table 5-2**; plate). Intracaldera tuff (**Tjtsi**) mapped near the top of the exposed section, southwest of Gray Butte, has a younger $^{206}Pb/^{238}U$ zircon age of 28.3 ± 0.5 Ma (sample 1 OCJ 14), similar to tuffs exposed in the central part of the caldera near Barnes Butte(**Tjtp**, **Tjtb**) (~28 Ma).

Subsidence phases and ash-flow tuff eruptions from the Crooked River caldera were accompanied by ring-fault controlled extrusion of fields of rhyolite lava flows, domes, and intrusions, now forming conspicuous high buttes around the periphery of the volcanic center (**Figure 5-12**, **Figure 5-13**; plate). $^{40}Ar/^{39}Ar$ and $^{206}Pb/^{238}U$ zircon ages obtained from rhyolites indicate a major pulse of silicic volcanism at the caldera between 29.3 and 27.54 Ma, following eruption of the tuff of Smith Rock (**Tjtsn**; **Tjtso**; **Tjtsn**); less precise K-Ar ages may extend the youngest age of this silicic volcanism to 25.8 Ma (**Figure 5-12**; **Table 5-2**; plate). $^{206}Pb/^{238}U$ zircon ages from rhyolites encircling the northwest and northeast part of the Cooked River caldera, include 29.3 ± 0.3 Ma at Juniper Butte (**Tjrj**) (sample JB-JM-01), 29.2 ± 0.3 Ma at Gray Butte (**Tjrg**) (sample GSO95-141R), 28.4 ± 0.3 Ma for a dike at Skull Hollow (**Tjrg**) (sample SR-RH-2), 28.9 ± 0.2 Ma at Grizzly Mountain (**Tjrgm**) (sample PAT GR2), and 29.2 ± 0.9 Ma at Hi-Tor Butte (**Tjrh**) (sample 2013CRC-10/1A.29VI.05; Seligman and others, 2014) (**Figure 5-12**; **Table 5-2**; plate). Rhyolites dated by $^{40}Ar/^{39}Ar$ geochronology have yielded ages of 28.82 ± 0.23 Ma at Gray Butte (**Tjrg**) (anorthoclase; sample GSO95-141; Smith and others, 1998), 27.54 ± 0.36 Ma at Ochoco Reservoir (**Tjro**) (plateau; whole rock; sample 1.15VII.05; McClaughry and Ferns, 2006b), and 27.97 ± 0.32 Ma at Barnes Butte (**Tjrb**) (plateau; whole rock; sample 4B.12VII.05; McClaughry and Ferns, 2006a) (**Figure 5-12**; **Table 5-2**; plate). Less precise K-Ar ages of 28.3 ± 1.0 Ma (unit **Tjpa**) (anorthoclase; sample PB-5/AH-34; Evans and Brown, 1981) and 25.8 ± 0.2 Ma (unit **Tjps**) (sanidine; sample 648-623B; Robinson and others, 1990) were reported for rhyolite domes forming parts of the Powell Buttes complex, along the southwest margin of the Crooked River caldera (**Figure 5-12**; **Table 5-2**; plate). Pilot Butte, a prominent dome complex outside the southeast margin of the caldera, is undated (plate).

Emplacement of rhyolites domes and flows around the Crooked River caldera was accompanied by additional rhyolitic ash-flow tuff eruptions. The tuff of Peppermint Lane (**Tjtp**) cropping out in the vicinity of Prineville has an $^{40}Ar/^{39}Ar$ plateau age of 28.18 ± 0.16 Ma (feldspar; sample 1.9II.06) (**Figure 5-12**; **Table 5-2**; plate). Zircons obtained from a sample of the tuff of Barnes Butte (**Tjtb**) at Barnes Butte yielded

a $^{206}Pb/^{238}U$ age of 28.3 ± 0.4 Ma (sample 6.12VII.05; Seligman and others, 2014) (**Figure 5-12**; **Table 5-2**; plate). The eruptive age for the tuff of Barnes Butte (**Tjtb**) may be closer to ~28 Ma as the unit overlies the 28.18 Ma tuff of Peppermint Lane (**Tjtp**) and is intruded by the 27.97 Ma rhyolite of Barnes Butte (**Tjrb**) (McClaughry and Ferns, 2006a). The tuff of Barnes Butte (**Tjtb**) is also considered in this report to include ash-flow tuff mapped capping mesas and cuestas between Gray Butte and Haystack Reservoir in the northwest part of the lower Crooked River basin. These outcrops were previously mapped and correlated with the ignimbrite defining the base of Member H tuff of the John Day Formation (Robinson and Stensland, 1979; Robinson and others, 1990; Smith and others, 1998). A sample obtained near the west end of Haystack Reservoir on this tuff yielded a slightly younger, but less precise $^{40}Ar/^{39}Ar$ plateau age of 27.62 ± 0.63 Ma (sanidine; sample GS095-134; Robinson and Stensland, 1979; Smith and others, 1998).

Rocks representing late John Day Formation volcanism in the lower Crooked River basin include basaltic andesite (**Tjob**), andesite (**Tjoa**) and trachyandesite (**Tjot**) cropping out in the Ochoco Mountains. A sample of basaltic andesite (**Tjob**) obtained from an outcrop between Rocky Point and Steins Pillar yielded an integrated $^{40}Ar/^{39}Ar$ age of 27.80 ± 0.6 Ma (whole rock; sample JM-SP13-4) (**Figure 5-12**; **Table 5-2**; plate).

Table 5-2. Summary of isotopic ages for the John Day Formation in the lower Crooked River basin.

Map Unit	Age	Sample	Method	Material Analyzed	Source	UTM N (NAD 83)	UTM E (NAD 83)
Tjps	25.8 ± 0.2 Ma	648-623Bb	K-Ar	sanidine	Robinson and others (1990)	4895497	661595
Tjpa	28.3 ± 1.0 Ma	PB-5/AH-34	K-Ar	anorthoclase	Evans and Brown (1981)	4895807	662385
Tjro	27.54 ± 0.36 Ma	1.15VII .05[1]	$^{40}Ar/^{39}Ar$	whole rock	McClaughry and Ferns (2006b)	4908651	682531
Tjob	27.80 ± 0.06 Ma	JM-SP13-4	$^{40}Ar/^{39}Ar$	whole rock	this study	4918974	689554
Tjrb	27.97 ± 0.32 Ma	4B.12VII.05[1]	$^{40}Ar/^{39}Ar$	whole rock	McClaughry and Ferns (2006a)	4910132	673924
Tjtp	28.18 ± 0.16 Ma	1.9II.06[1]	$^{40}Ar/^{39}Ar$	sanidine	this study	4911212	671357
Tjtb	27.62 ± 0.63 Ma	GS095-134[2]	$^{40}Ar/^{39}Ar$	alkali feldspar	Smith and others (1998)	4928877	646465
Tjtb	28.3 ± 0.4 Ma	6.12VII.05[3]	$^{206}Pb/^{238}U$	zircon	Seligman and others (2014)	4908296	674823
Tjrg (dike)	28.4 ± 0.6 Ma	SR-RH-2	$^{206}Pb/^{238}U$	zircon	this study	4918858	653065
Tjrgm	28.9 ± 0.2 Ma	PAT GR2[3]	$^{206}Pb/^{238}U$	zircon	this study	4921617	662405
Tjrh	29.2 ± 0.9 Ma	2013CRC-10/1A.29VI.05[4]	$^{206}Pb/^{238}U$	zircon	Seligman and others (2014)	4909654	688632
Tjrg	28.82 ± 0.23 Ma	GSO95-41[2]	$^{40}Ar/^{39}Ar$	alkali feldspar	Smith and others (1998)	4918587	650165
Tjrg	29.2 ± 0.3 Ma	GSO95-41R[3]	$^{206}Pb/^{238}U$	zircon	this study	4918587	650165
Tjrj	29.3 ± 0.2 Ma	JB-JM-01[3]	$^{206}Pb/^{238}U$	zircon	this study	4925003	640847
Tjtsi	28.3 ± 0.5 Ma	1 OCJ 14[3]	$^{206}Pb/^{238}U$	zircon	this study	4918140	649161
Tjtsi	29.3 ± 0.2 Ma	SRT-SKULL-1[3]	$^{206}Pb/^{238}U$	zircon	this study	4918805	653710
Tjtsi	29.3 ± 0.3 Ma	24 LCJ 06[3]	$^{206}Pb/^{238}U$	zircon	this study	4914422	648183
Tjtso	29.5 ± 0.2 Ma	JM ER 13-4[3]	$^{206}Pb/^{238}U$	zircon	this study	4888345	681250
Tjtso	29.56 ± 0.17 Ma	448 LCJ 07[1]	$^{40}Ar/^{39}Ar$	alkali feldspar	McClaughry and others (2009b, d)	4932488	687455
Tjtsn	29.53 ± 0.09 Ma	GSO-95-133[2]	$^{40}Ar/^{39}Ar$	alkali feldspar	Smith and others (1998)	4928677	646625
Tjtso	29.57 ± 0.17 Ma	GSO95-132[2]	$^{40}Ar/^{39}Ar$	alkali feldspar	Smith and others (1998)	4928767	646475
Tjtso	29.51 ± 0.11 Ma	HS-JM-04[2]	$^{206}Pb/^{238}U$	zircon	this study	4927762	649171
Member G	29.54 ± 0.10 Ma	GSO95-136[2*]	$^{40}Ar/^{39}Ar$	alkali feldspar	Smith and others (1998)	4968228	667794
Member G	29.61 ± 0.10 Ma	GSO95-144[2*]	$^{40}Ar/^{39}Ar$	alkali feldspar	Smith and others (1998)	4945697	661104
Tjte	29.7 ± 0.6 Ma	CR8/18 LC 06[4]	$^{206}Pb/^{238}U$	zircon	Seligman and others (2014)	4889338	680837
Tjte(?)	32.1 ± 0.7 Ma	648-625A	K-Ar	plagioclase	Robinson and others (1990)	4897167	689979
Tjba	30.1 ± 1.1 Ma	DOGMI-Bas81-2/UT-225	K-Ar	whole rock	Evans and Brown (1981)	4894397	655605
Tjba	30.8 ± 0.5 Ma	10-6-78-2	K-Ar	whole rock	Fiebelkorn and others (1982, 1983)	4921737	652015
Tjtr	32.49 ± 0.30 Ma	GS095-130[2]	$^{40}Ar/^{39}Ar$	alkali feldspar	Smith and others (1998)	4925107	649835

All ages reported at ±2σ.
[1]Ages determined at the College of Oceanic and Atmospheric Sciences, Oregon State University, Corvallis.
[2]Ages determined at the New Mexico Geochronological Research Laboratory (NMGRL), Socorro.
[3]Ages determined at California State University, Northridge and at the University of California, Santa Barbara.
[4]Ages determined at the University of California, Los Angeles.
* Reported age from outside map area.

5.1.2 Upper Cenozoic Volcanic and Sedimentary Rocks

5.1.2.1 Columbia River Basalt Group and Simtustus Formation

5.1.2.1.1 Distribution, composition, and lithology

Following the end of Lower Crooked volcanic field magmatism, the Crooked River caldera became a long-lived depocenter for the episodic emplacement of Neogene volcanic flows and sedimentary deposits (**Figure 5-16**; plate; McClaughry and others, 2009b). During the early Miocene, a sequence of tuffaceous siltstone and sandstone, diatomite, cobble conglomerate, and dacite tuff (SiO_2 = 66.47 to 70.08 weight percent; *n* = 3) mapped here as unit **Tmos** infilled topographic lows that developed within the basin structure of the Crooked River caldera (McClaughry and Ferns, 2007c; McClaughry and others, 2009b). These rocks (**Tmos**) overlie the John Day Formation and older units in the lower Crooked River basin and are locally interbedded with, or are overlain by tholeiitic lavas of the Prineville Basalt (**Tcpb**) of the CRBG (**Figure 5-16**; plate).

On the basis of lithologic texture and stratigraphic position, early Miocene tuffaceous sedimentary rocks (**Tmos**) mapped beneath and interbedded with the early Miocene Prineville Basalt (**Tcpb**) in the lower Crooked River basin are considered herein to be equivalent to the Simtustus Formation as defined by Smith (1986a, b, c). The Simtustus Formation at its type locality in the northern Deschutes Basin, consists of volcanogenic sandstone, mudstone, and tuff, intercalated with both the Prineville and Grande Ronde basalts. Sedimentary rocks of unit **Tmos** have been previously mapped in the lower Crooked River basin as part of the upper John Day Formation (Waters and Vaughan, 1968b; Swanson, 1969). However, these sedimentary rocks (**Tmos**) are texturally distinct from the bulk of the John Day Formation, are only weakly altered, and in the southern part of the basin overlie John Day rocks with an angular unconformity. An invasive relationship of Prineville Basalt down into unit **Tmos** sedimentary rocks, as shown by crude pillows, chilled rinds, and admixed baked siltstone, indicates that lava flows did not flow over older well-lithified units, but instead interacted with wet unconsolidated sediment (**Tmos**) of equivalent age, standing water, or some combination thereof. Maximum thickness of the Simtustus Formation (**Tmos**) in the lower Crooked River basin is ≤152 m (500 ft).

Lithologic texture and sedimentary structures (e.g., massive bedding, channel forms, rip-up fragments, and burrow traces) suggest the Simtustus Formation (**Tmos**) aggraded in the lower Crooked River basin by channel and flood plain deposition in low-gradient, mixed load, possibly highly sinuous streams. This fluvial aggradation may have resulted from an abundance of incoming sediment supplied by large-scale silicic pyroclastic eruptions of similar age in southeast Oregon (Ferns and others, 2017) and regional drainage disruption by emplacement of CRBG lava flows, including the Prineville Basalt (**Tcpb**) (Smith, 1986c). The mapped and paired distribution of tuffaceous sedimentary rocks of unit **Tmos** and the Prineville Basalt (**Tcpb**) mark the early Miocene south-to-north channel course of the ancestral Crooked River and link this ancestral drainage with the early Miocene aggrading fluvial system of the Deschutes River (**Figure 5-16**; plate).

The Simtustus Formation (**Tmos**) is also regionally correlative with the Mascall Formation of Merriam (1901a) and Merriam and others (1925), well exposed in the John Day Valley, 100 km (62 mi) northeast of Prineville. The Mascall Formation was defined by Merriam (1901a) in the John Day Valley and consists of tuffaceous sedimentary rocks deposited as alluvial floodplain and channel deposits (Bestland and others, 2008). The formation is conformable upon the ~17.14 Ma Picture Gorge Basalt of the CRBG (Bailey, 1989; Bestland and others, 2008; Cahoon and others, 2020). The 16.2 Ma Mascall Ignimbrite (K-Ar; Davenport, 1971), a unit now correlated with the 16.16 Ma unit 1 of the Dinner Creek Tuff ($^{40}Ar/^{39}Ar$;

Streck and others, 2015), crops out within the Mascall Formation in the type area near Picture Gorge. The Mascall Formation at Picture Gorge is overlain by the 7.1 Ma Rattlesnake Tuff (**Tmtr**), separated by a conspicuous angular unconformity (stop 4.2 in Ferns and others, 2017). Similarly, the Simtustus Formation cropping out along the Crooked River near Bowman Dam is overlain by Rattlesnake Tuff (**Tmtr**), there interbedded with Deschutes Formation lava flows (**Figure 5-16**; plate). The Simtustus and Mascall Formations thus share a similar structural and stratigraphic position relative to the CRBG and overlying upper Miocene units.

The CRBG is an extensive succession of tholeiitic basalt and basaltic andesite lava flows that cover more than 167,300 km^2 (64,595 mi^2) in parts of Washington, Oregon, and Idaho (**Figure 5-17**, **Figure 5-18**; Tolan and others, 1989; Reidel and others, 2013). Lava flows of the CRBG, mapped in the lower Crooked River basin, include the Prineville (**Tcpb**) and Picture Gorge (**Tcpg**) Basalts (**Figure 5-18**; Uppuluri, 1974; Smith, 1986a, b; Tolan and others, 1989; Bailey, 1989; Hooper and others, 1993). The ~16.1 Ma Prineville Basalt is a geographically restricted, but chemically distinctive CRBG unit that covers an area of ~11,440 km^2 (4,417 mi^2) in central and north-central Oregon (**Figure 5-17**). The estimated volume of the Prineville Basalt is ~590 km^3 (142 mi^3) (Reidel and others, 2013).

The Prineville Basalt (**Tcpb**) directly overlies the Simtustus Formation (**Tmos**) and forms a high plateau between Combs Flat and the Crooked River in the south part of the map area (**Figure 5-16**; plate). The Prineville Basalt (**Tcpb**) also crops out above Simtustus Formation (**Tmos**) sedimentary rocks between the Crooked River and Lone Pine Flat, northwest of the city of Prineville (**Figure 5-16**; plate). North of the map area the Prineville Basalt (**Tcpb**) is exposed along the Deschutes River. Prineville lava flows have been mapped north to Tygh Valley and Butler Canyon (~132 km [82 mi] north-northwest of the map area), into the valley of the Clackamas River (~160 km [99.5 mi] northwest of the map area), and down the canyon of the John Day River, nearly to its mouth at the Columbia River (~195 km [121 mi] northeast of the map area) (**Figure 5-17**; Hooper and others, 1993). The largest number of individual flows and thickest section of Prineville Basalt is in the Crooked River canyon, west of Bowman Dam (**Figure 5-16**; plate), where the succession attains a maximum composite thickness of 210 m (690 ft). No vents, as indicated by dikes, scoria, welded spatter, or tephra deposits have been found for the Prineville Basalt, but the thickness of the unit and number of individual lava flows exposed near Bowman Dam and Paquet Gulch, led Hooper and others (1993) to suggest those areas as the most probable eruptive sites for the unit.

The Prineville Basalt is a chemically distinctive stratigraphic marker in north-central Oregon, characterized by aphyric to sparsely plagioclase- and olivine-microporphyritic tholeiitic basalts and basaltic andesites with unusually high incompatible element concentrations of barium (Ba = 1,645 to 3,202) and phosphorous (P_2O_5 = 1.15 to 2.02 weight percent) (n = 53 samples [4 outside map area]) (**Figure 5-19**; appendix). On the basis of geochemistry, Hooper and others (1993) identified three chemical types for the Prineville Basalt; a Bowman Dam chemical type, a high-SiO_2 chemical type, and a high-TiO_2-P_2O_5 chemical type (**Figure 5-20a-d**; appendix). All three chemical types are present in the lower Crooked River basin. The Bowman Dam chemical type is the oldest and most voluminous of the three chemical types covering and area >11,000 km^2 (4,247 mi^2) (Hooper and others, 1993). Bowman Dam lava flows have a narrow basalt chemical composition (SiO_2 = 50.82 to 53.10 weight percent; n = 39 [2 outside map area]), with high contents of titanium (TiO_2 = 2.19 to 2.85 weight percent), phosphorous (P_2O_5 = 1.15 to 1.71 weight percent), and strontium (Sr = 365 to 586 ppm) (**Figure 5-20a-d**; appendix). The high-SiO_2 chemical type lava flows have a basaltic andesite composition (SiO_2 = 53.66 to 56.19 weight percent; n = 8 [2 outside map area]), with similar high contents of titanium (TiO_2 = 2.48 to 2.84 weight percent) and phosphorous (P_2O_5 = 1.21 to 1.54 weight percent) to the Bowman Dam chemical type (**Figure 5-20a-b**; appendix). These lava flows are distinguished from the Bowman Dam and high-TiO_2-

P_2O_5 chemical type flows on the basis of higher silica and less amounts of magnesium (MgO = 2.23 to 3.79 weight percent) and strontium (Sr = 281 to 428 ppm) (**Figure 5-20a-d**; appendix). The high-TiO_2-P_2O_5 chemical type lava flows have a basalt composition (SiO_2 = 50.83 to 51.67 weight percent; *n* = 5) marked by higher phosphorous (P_2O_5 = 1.57 to 2.02) and titanium (TiO_2 = 3.05 to 3.15 weight percent) (**Figure 5-20a-b**; appendix). Strontium (Sr = 396 to 414 ppm) content in the high-TiO_2–P_2O_5 chemical type is similar to the Bowman Dam chemical type (**Figure 5-20c-d**; appendix). The Prineville Basalt (**Tcpb**) is distinguished from overlying lava flows of the late Miocene Deschutes Formation and Quaternary Newberry lava flows on the basis of generally glassy rock texture with fewer recognizable crystals and notably high concentrations of phosphorous (P_2O_5) and barium (Ba) (**Figure 5-19**; appendix).

The ~17 to 16 Ma Picture Gorge Basalt (**Tcpg**) covers an area of >10,680 km^2 (4,123 mi^2) in northeast Oregon (**Figure 5-18**; Cahoon and others, 2020). The estimated volume of the Picture Gorge Basalt (**Tcpg**) is ~2,400 km^3 (576 mi^3) (Reidel and others, 2013). In the eastern part of the lower Crooked River basin, the Picture Gorge Basalt (**Tcpg**) is mapped as thin ridge-capping lava flows along Ochoco Divide north of Round Mountain and on top of Lookout Mountain (**Figure 5-16**; plate). Scattered outcrop remnants of the Picture Gorge Basalt (**Tcpg**) are also mapped discontinuously above the Mill Creek and McKay Creek drainages in the northern part of the lower Crooked River basin (**Figure 5-16**; plate). Picture Gorge lava flows (**Tcpg**) in the lower Crooked River basin are high-magnesium tholeiitic basalt (SiO_2 = 49.69 to 51.76 weight percent; FeOTotal = 9.97 to 10.88; MgO = 5.80 to 7.99 weight percent; *n* = 6) comparable to lavas cropping out in the type area of the Picture Gorge Basalt (Bailey, 1989; Cahoon and others, 2020) (**Figure 5-19**; appendix). The Picture Gorge Basalt (**Tcpg**) is distinguished from the Prineville Basalt (**Tcpb**) on the basis of lower amounts of phosphorous (P_2O_5 <0.5 weight percent) and barium (Ba <300 ppm) (**Figure 5-19**; appendix). Outcrops exposing the local stratigraphic relations between the Picture Gorge (**Tcpg**) and Prineville Basalts (**Tcpb**) have not been found.

Figure 5-16. Simplified geologic map of Neogene rocks in the lower Crooked River basin (*following page*). Geology shown west and north of the of the lower Crooked River basin is from Sherrod and others (2004) and Waters (1968) in OGDC-7, Franczyk and others (2020).

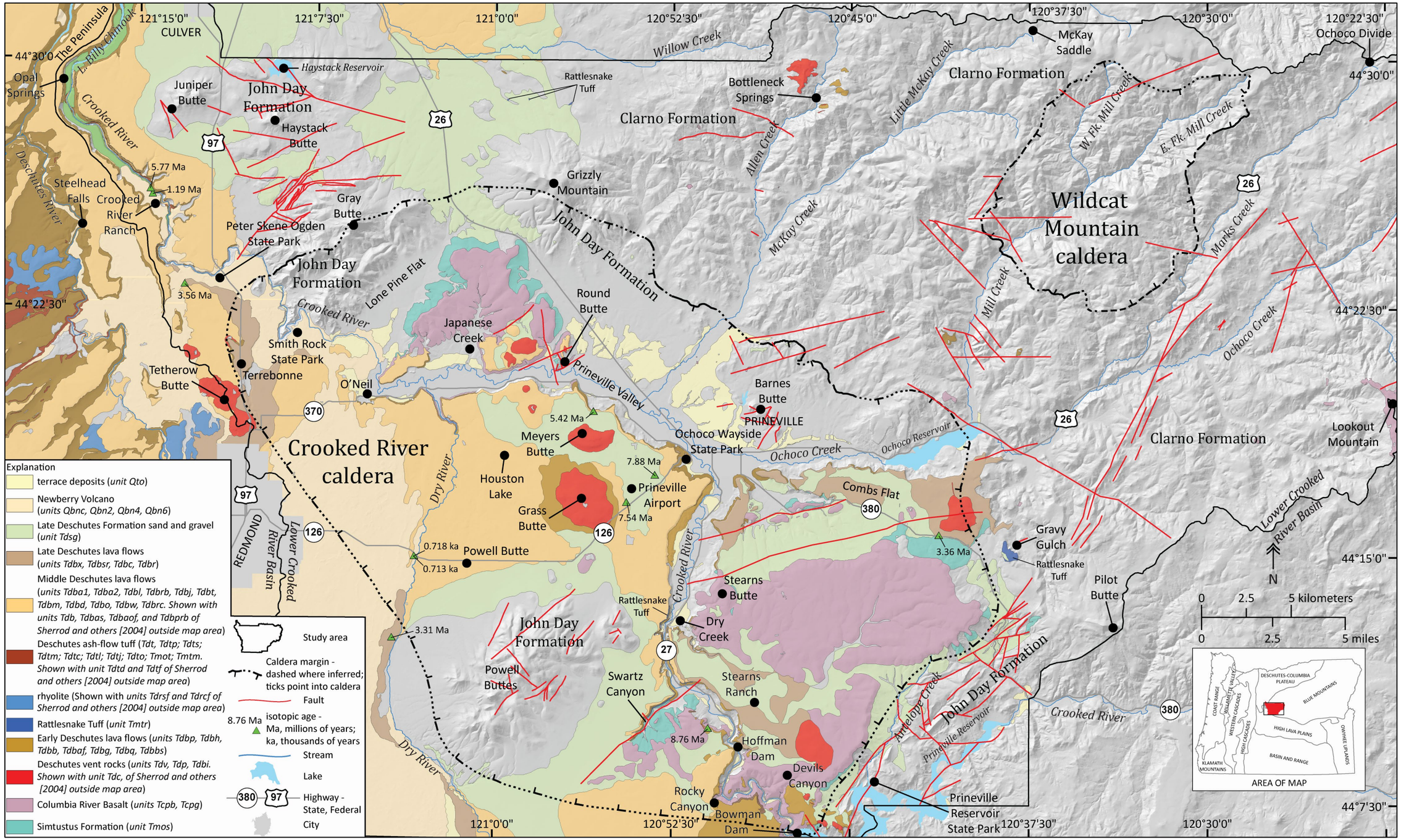
121°15'0"
121°7'30"
121°0'0"
120°52'30"
120°45'0"
120°37'30"
120°30'0"
120°22'30"
44°30'0"
44°22'30"
44°15'0"
44°7'30"
CULVER
Opal Springs
The Peninsula
L. Billy Chinook
Crooked River
Deschutes River
Juniper Butte
Haystack Reservoir
John Day Formation
Haystack Butte
Rattlesnake Tuff
Willow Creek
Bottleneck Springs
Clarno Formation
Little McKay Creek
McKay Saddle
Ochoco Divide
Allen Creek
W. Fk. Mill Creek
E. Fk. Mill Creek
Steelhead Falls
Crooked River Ranch
5.77 Ma
1.19 Ma
Gray Butte
Grizzly Mountain
Peter Skene Ogden State Park
John Day Formation
Lone Pine Flat
McKay Creek
Wildcat Mountain caldera
Marks Creek
3.56 Ma
Crooked River
Round Butte
Japanese Creek
Smith Rock State Park
Terrebonne
Tetherow Butte
O'Neil
Prineville Valley
Barnes Butte
PRINEVILLE
Mill Creek
Ochoco Creek
Lookout Mountain
5.42 Ma
Meyers Butte
Ochoco Wayside State Park
Ochoco Reservoir
Clarno Formation
Crooked River caldera
Houston Lake
Dry River
7.88 Ma
Prineville Airport
7.54 Ma
Grass Butte
Combs Flat
Gravy Gulch
Rattlesnake Tuff
3.36 Ma
Lower Crooked River Basin
REDMOND
Lower Crooked River Basin
0.718 ka
0.713 ka
Powell Butte
Stearns Butte
Rattlesnake Tuff
Crooked River
Pilot Butte
N
0 2.5 5 kilometers
0 2.5 5 miles
3.31 Ma
John Day Formation
Powell Buttes
Dry Creek
Swartz Canyon
Stearns Ranch
Antelope Creek
John Day Formation
Crooked River
Prineville Reservoir
8.76 Ma
Hoffman Dam
Devils Canyon
Rocky Canyon
Bowman Dam
Prineville Reservoir State Park
AREA OF MAP
DESCHUTES-COLUMBIA PLATEAU
BLUE MOUNTAINS
HIGH LAVA PLAINS
OWYHEE UPLANDS
BASIN AND RANGE
KLAMATH MOUNTAINS
HIGH CASCADES
WESTERN CASCADES
WILLAMETTE VALLEY
COAST RANGE
Explanation
terrace deposits (unit Qto)
Newberry Volcano (units Qbnc, Qbn2, Qbn4, Qbn6)
Late Deschutes Formation sand and gravel (unit Tdsg)
Late Deschutes lava flows (units Tdbx, Tdbsr, Tdbc, Tdbr)
Middle Deschutes lava flows (units Tdba1, Tdba2, Tdbl, Tdbrb, Tdbj, Tdbt, Tdbm, Tdbd, Tdbo, Tdbw, Tdbrc. Shown with units Tdb, Tdbas, Tdbaof, and Tdbprb of Sherrod and others [2004] outside map area)
Deschutes ash-flow tuff (Tdt, Tdtp; Tdts; Tdtm; Tdtc; Tdtl; Tdtj; Tdto; Tmot; Tmtm. Shown with unit Tdtd and Tdtf of Sherrod and others [2004] outside map area)
rhyolite (Shown with units Tdrsf and Tdrcf of Sherrod and others [2004] outside map area)
Rattlesnake Tuff (unit Tmtr)
Early Deschutes lava flows (units Tdbp, Tdbh, Tdbb, Tdbaf, Tdbg, Tdbq, Tdbbs)
Deschutes vent rocks (units Tdv, Tdp, Tdbi. Shown with unit Tdc, of Sherrod and others [2004] outside map area)
Columbia River Basalt (units Tcpb, Tcpg)
Simtustus Formation (unit Tmos)
Study area
Caldera margin - dashed where inferred; ticks point into caldera
Fault
8.76 Ma isotopic age - Ma, millions of years; ka, thousands of years
Stream
Lake
Highway - State, Federal
City

Figure 5-17. Sketch map showing the outcrop distribution of the CRBG (orange fill), including the Prineville Basalt (Tcpb) (lined pattern). The extent of the CRBG includes areas from which the lava flows have been eroded, in addition to areas where lava flows are concealed by younger units. Modified from Reidel and others (2013) and Ferns and McClaughry (2013). Label abbreviations are as follows: BC – Butler Canyon; CJD – Chief Joseph Dike Swarm; PDG – Picture Gorge Dike Swarm; SD – Steens Dike Swarm; ST – Steens Mountain.

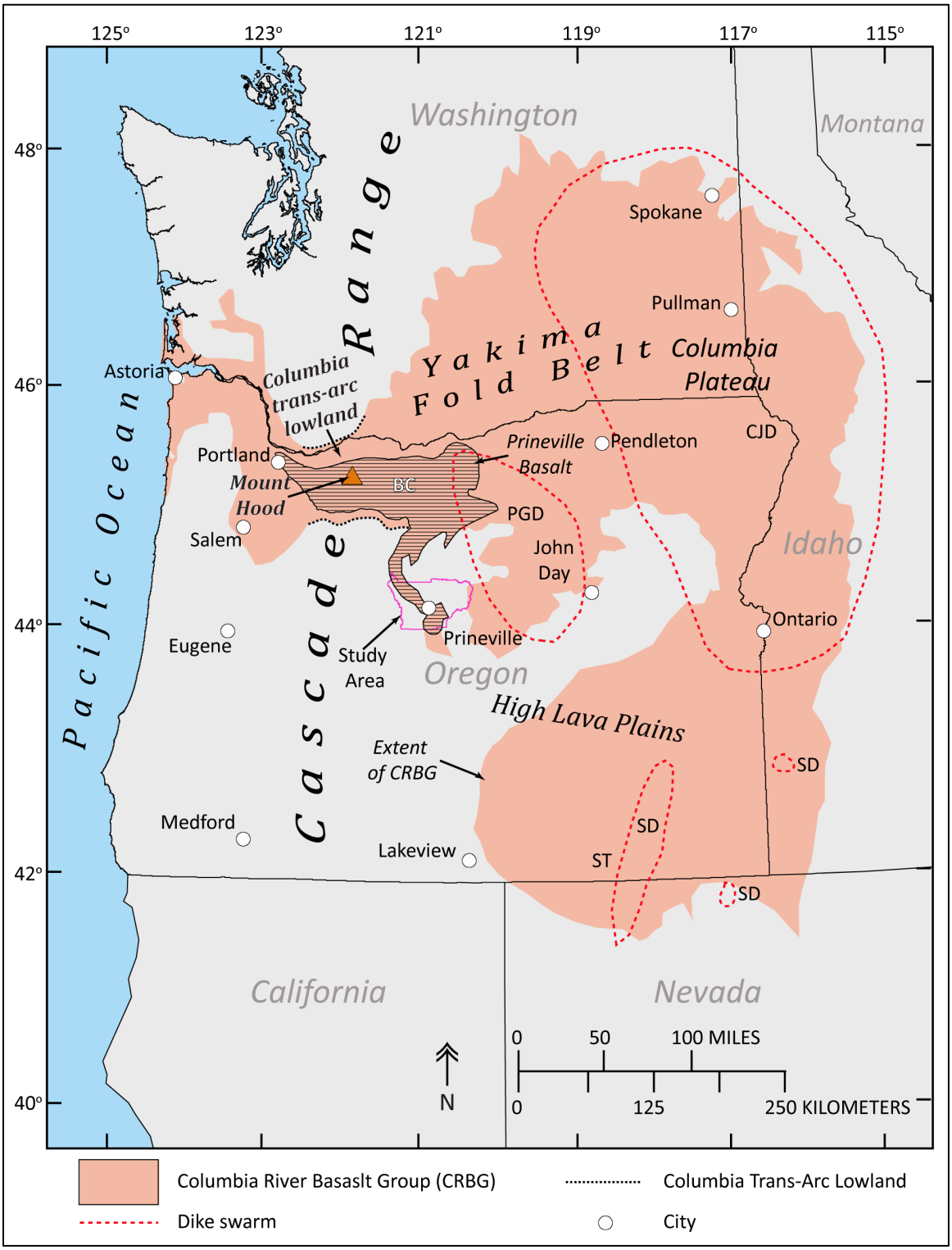

Figure 5-18. Chart showing the stratigraphy and nomenclature for the CRBG. Modified from Reidel and others (2002), with updated stratigraphy from Reidel and others (2013) and Reidel and Tolan (2013). Updated U/Pb ages from Kasbohm and Schoene (2018) are shown in parentheses, for example (15.895). Updated $^{40}Ar/^{39}Ar$ ages from Mahood and Benson (2017) are shown in square brackets, for example [16.54]. Selected $^{40}Ar/^{39}Ar$ ages for the Picture Gorge Basalt from Cahoon and others (2020) are shown in curly brackets, for example {16.22}. Age of the base of Steens in vertical brackets is from Moore and others (2018), for example |16.97|.

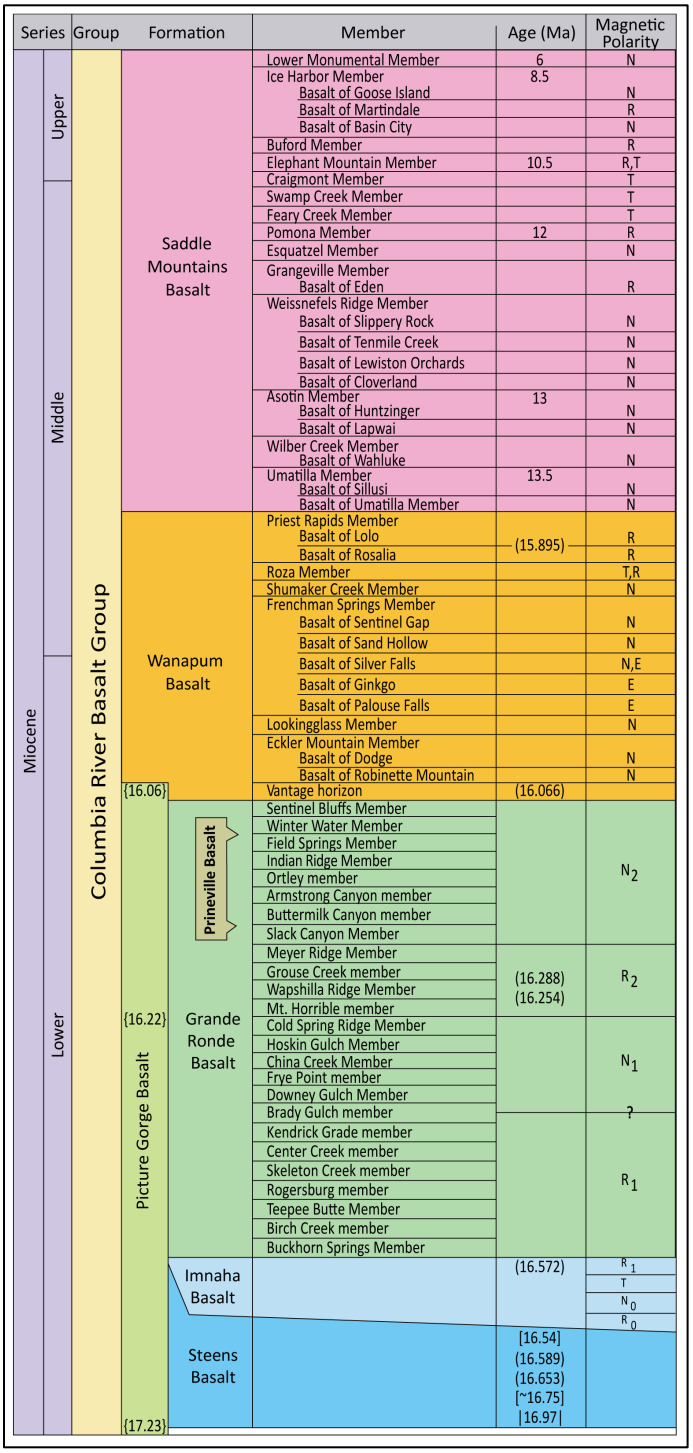

Figure 5-19. Geochemical variation diagrams for Neogene lava flows in the lower Crooked River basin (*n* = 236 analyses). (a) The Prineville Basalt (Tcpb) is distinguished by its unusually high concentrations of phosphorous (P_2O_5) and barium (Ba). (b) Total iron/magnesium (FeOTotal/MgO) versus silica (SiO_2) diagram discriminating basaltic lavas of Newberry Volcano, the Deschutes Formation, the Prineville Basalt (Tcpb), and Picture Gorge Basalt (Tcpg). Tholeiitic and calc-alkaline fields are from Miyashiro (1974).

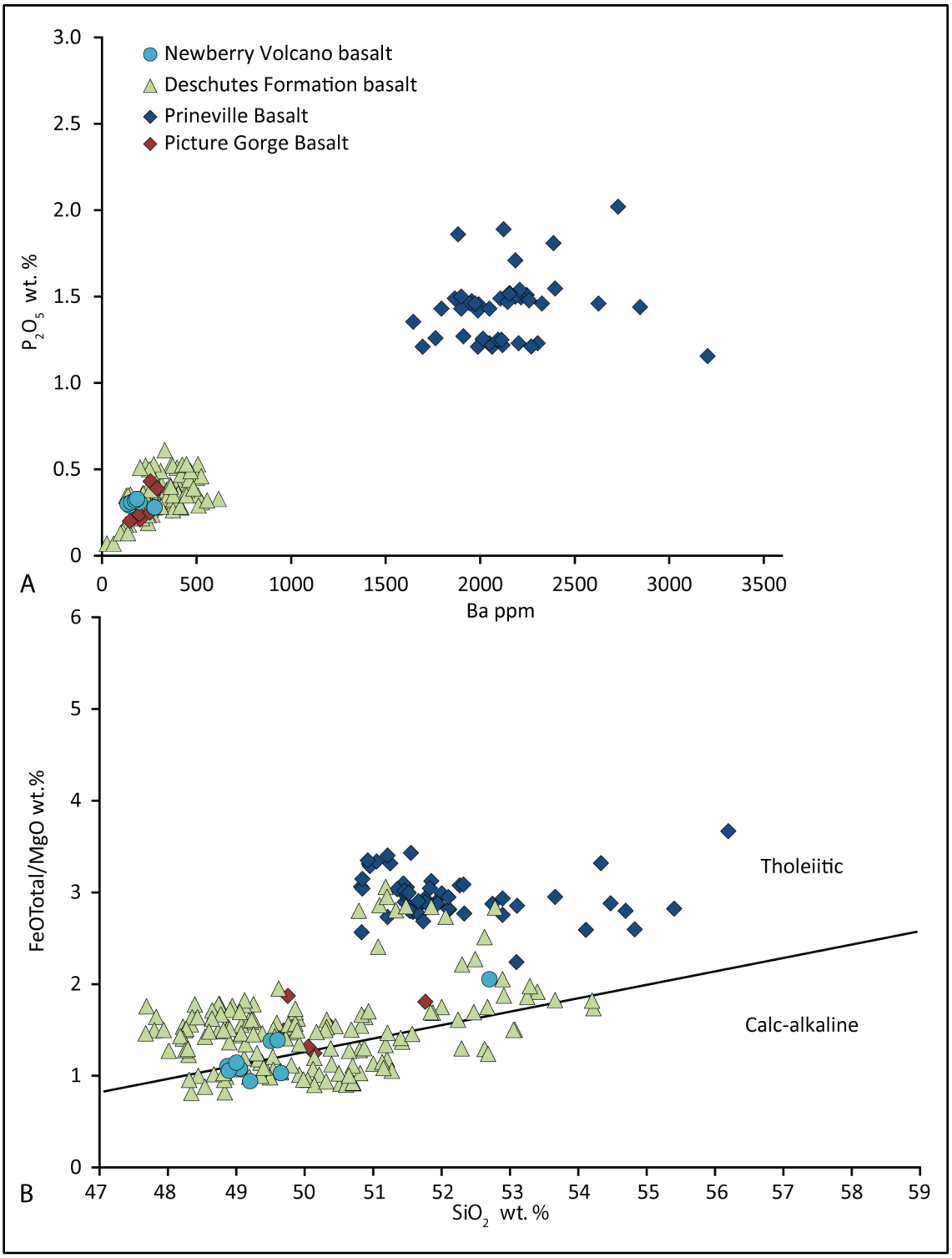

Figure 5-20. Geochemical variation diagrams for the Prineville Basalt (Tcpb) in the lower Crooked River basin (*n* = 52 analyses). (a) Titanium (TiO_2) versus phosphorous (P_2O_5). (b) Magnesium (MgO) versus silica (SiO_2). (c) Vanadium (V) versus strontium (Sr). (d) Zirconium (Zr) versus strontium (Sr).

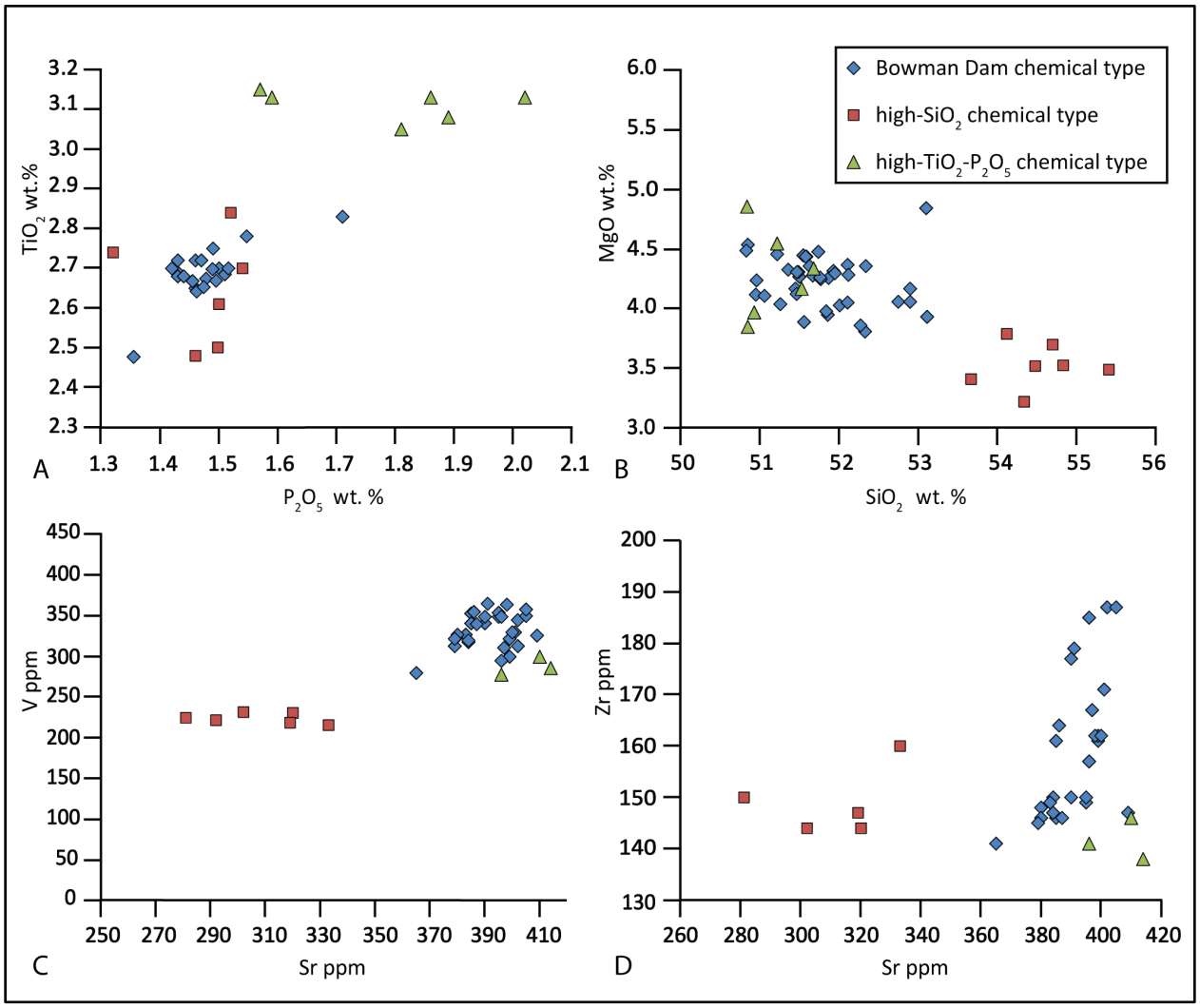

5.1.2.1.2 Age

Isotopic dating of CRBG lava flows has struggled with accuracy and precision issues, complicating the development of an unambiguous chronology for the timing and duration of CRBG volcanism (Baksi, 2013; Barry and others, 2013). Isotopic dating of basalt lava flows by K-Ar and $^{40}Ar/^{39}Ar$ techniques suggests main-phase eruptions of the Grande Ronde Basalt occurred over a 0.4 m.y. interval, between ~16.0 and 15.6 Ma (**Figure 5-18**). The eruption of younger Wanapum Basalt is considered to span a time period between ~15.6 and <15 Ma (**Figure 5-18**; Barry and others, 2010, 2013). Work by Kasbohm and Schoene (2018) has established a more accurate and precise age model for the CRBG, improving understanding of the eruption timing of Wanapum and Grande Ronde flows. Kasbohm and Schoene (2018) examined silicic tuff interbeds between basalt lava flows in central and eastern parts of the Columbia Plateau, dating them by U-Pb geochronology on single zircon crystals (**Figure 5-18**). High precision U-Pb zircon dates of interbedded tuffs indicate slightly older ages for CRBG units across the Columbia Plateau, including those present in the lower Crooked River basin. The upper age limit of the Grande Ronde Basalt is constrained

by a U-Pb date of 16.066 ± 0.04 Ma (zircon; sample CRB1533) for ash from the Vantage Horizon, which marks the top of the formation (**Figure 5-18**). The R2 magnetostratigraphic unit within the Grande Basalt has a U-Pb age of 16.254 ± 0.034 Ma (zircon; sample CRB1556), determined for ash between the Wapshilla Ridge and Meyers Ridge Members (**Figure 5-18**). U-Pb ages place an end to Grande Ronde volcanism at ~16 Ma.

The Prineville Basalt (**Tcpb**) was previously assigned a middle Miocene age on the basis of an $^{40}Ar/^{39}Ar$ age of 15.7 ± 0.1 Ma (whole rock; sample D12; appendix; Smith, 1986a, b) obtained on the lowest lava flow cropping out at Pelton Dam in the Deschutes Basin (Hooper and others, 1993) and interbedded relations with N2 and R2 flows of the Grande Ronde Basalt north of the Deschutes Basin. At the northern mapped extent of the Prineville Basalt (**Tcpb**) in Butler Canyon, two flows of the Prineville Basalt are interfingered with the N2 magnetostratigraphic unit of the Grande Ronde Basalt, lying above the R2-N2 boundary (**Figure 5-17**, **Figure 5-18**). An upper basaltic andesite lava flow of the Prineville Basalt (**Tcpb**) lies directly beneath the Winter Water Member in Butler Canyon, while a lower Bowman Dam chemical type flow is exposed beneath the Buttermilk Canyon member (Michael Sawlan, written commun., 2014). The Prineville Basalt (**Tcpb**) is thus assigned a more precise early Miocene age of ~16.1 Ma bracketed by U/Pb dates of 16.066 ± 0.04 Ma for ash from the overlying Vantage Horizon at the top of the Grande Ronde Basalt and 16.254 ± 0.034 Ma for ash between the underlying Wapshilla Ridge and Meyer Ridge Members of the R2 magnetostratigraphic unit (**Figure 5-18**; Kasbohm and Schoene, 2018). An early Miocene age is also inferred for the Simtustus Formation (**Tmos**) in the lower Crooked River basin on the basis of interdigitated contact relations with the ~16.1 Ma Prineville Basalt.

An early geochronological study of the Picture Gorge Basalt (**Tcpg**) in the Picture Gorge type area near Dayville, reported K-Ar ages ranging between 15.9 and 14.7 Ma, with uncertainties of as much as 0.8 m.y. (2σ) (Watkins and Baksi, 1974). West of Dayville, the Picture Gorge Basalt lies beneath the Mascall Formation, which there includes the regionally widespread 16.16 Ma unit 1 of the Dinner Creek Tuff ($^{40}Ar/^{39}Ar$; Streck and others, 2015; Mascall Ignimbrite, Davenport, 1971). As mapped regionally, the Picture Gorge Basalt is interpreted to interfinger with the Grande Ronde Basalt (Long and Duncan, 1982; Reidel and others, 1989a) along Butte Creek, northeast of Dayville. Cahoon and others (2020), applying modern $^{40}Ar/^{39}Ar$ dating methods to known or newly geochemically correlated localities cropping out in northeast Oregon, reported eleven high-precision groundmass plateau isochron ages for the Picture Gorge Basalt (**Tcpg**) ranging between 17.23 ± 0.04 and 16.06 ± 0.06 Ma (**Figure 5-18**). The range of ages indicates the Picture Gorge Basalt (**Tcpg**) erupted earlier and for a longer duration than other CRBG main-phase units (Cahoon and others, 2020).

5.1.2.2 Deschutes Formation

5.1.2.2.1 Distribution, composition, and lithology

The Deschutes Formation is a succession of late Miocene to early Pliocene volcaniclastic sedimentary rocks, ash-flow tuff, and lava flows distributed over an area of 4,970 km^2 (1,920 mi^2) of the Deschutes Basin on the east side of the Cascade Range, mapped between the Mutton Mountains, Ochoco Mountains, and Bear Creek Buttes (**Figure 5-21**; Russell, 1905; Stearns, 1931; Hodge, 1942; Stensland, 1970, Peterson and others, 1976; Robinson and Stensland, 1979; Farooqui and others, 1981; Taylor, 1983; Priest and others, 1983; Smith 1986a, 1987; Smith and others, 1987; Lite and Gannett, 2002; Sherrod and others, 2004; McClaughry and others, 2009b). These rocks record the late Miocene onset of late High Cascades volcanism, early development of the central Oregon segment of the High Cascades intra-arc graben, and late Miocene and early Pliocene sedimentary and volcanic infilling of the Deschutes Basin

(**Figure 5-2**, **Figure 5-21**). Four major depositional environments for the Deschutes Formation were recognized by Smith (1986a, 1987) including proximal volcanic rocks of the High Cascades arc, an arc-adjacent alluvial plain, the ancestral Deschutes River, and the inactive basin margin (**Figure 5-21**). Proximal High Cascade arc rocks in the Deschutes Formation consist predominantly of lava flows and tuffs, such as those exposed on Green Ridge east of the Metolius River. Strata emplaced in arc-adjacent alluvial plain depositional settings include Cascade-derived lava flows, intrabasinal rhyolite domes and flows, ash-flow and air-fall tuffs, and volcaniclastic sediment gravity flow deposits. Units deposited in ancestral Deschutes River settings include alluvial plain and sediment gravity flow deposits, ash-flow tuff, and intracanyon lava flows (**Figure 5-16**). Inactive basin margin deposits are comprised of alluvium derived from the Ochoco and Mutton Mountains, reworked fallout tephra from the Cascade Range, ash-flow tuff, and mafic lava flows erupted from vents in the western part of the lower Crooked River basin (**Figure 5-16**).

The thickest part of the Deschutes Formation in the Deschutes Basin is at Green Ridge in the Cascade Range, where a flow-on-flow succession of vent-proximal andesite to rhyodacite lava flows and andesite to rhyodacite ash-flow tuffs is as thick as 700 m (2,296 ft) (**Figure 5-21**). The Deschutes Formation thins to ~260 m (853 ft) east towards the center of the Deschutes River Basin, where it is dominated by volcaniclastic sedimentary rocks, ash-flow tuff, and fewer lava flows. To the north, these rocks onlap older John Day Formation units forming the Mutton Mountains (**Figure 5-21**). East and northeast of Madras, the Deschutes Formation is as thick as 75 m (246 ft) and is dominantly epiclastic material eroded from silicic John Day and Clarno formation rocks forming the Ochoco Mountains (**Figure 5-21**). The thickest accumulation of Deschutes Formation strata in the lower Crooked River basin trace the late Miocene and Pliocene course of the Crooked River from south to north. Composite sections of mafic lava flows, volcaniclastic sedimentary rocks, and tuff are as thick as 160 m (525 ft) in the Crooked River canyon south of Prineville (plate, cross section D-D′), as thick as 220 m (720 ft) beneath the Prineville Airport (plate, cross sections A-A′, B-B′, and C-C′), and thicker than 330 m (1,080 ft) between Peter Skene Ogden State Park and Lake Billy Chinook in the northwest part of the lower Crooked River basin (plate, cross section A-A′) (**Figure 5-16**, **Figure 5-21**).

At the Deschutes Formation type area along the Deschutes River west of Madras and at Cove Palisades in the northwest part of the lower Crooked River basin, the formation is chiefly a succession of volcaniclastic sedimentary rocks (**Tds**) and widespread ash-flow tuff deposits (**Tdt**, **Tdtp**, **Tdts**, **Tdtm**, **Tdtc**, **Tdtl**, **Tdtj**, **Tdto**), with fewer mafic to intermediate composition lava flows (**Tdbp**, **Tdbo**, **Tdbl**, **Tdba1**, **Tdba2,** **Tdbl**, **Tdbt**) (**Figure 5-16**, **Figure 5-21**; plate). Ash-flow tuff and volcaniclastic sedimentary deposits predominate in the lower part of the Deschutes Formation along the lower Crooked River. These units were emplaced during widespread explosive eruptions and pyroclastic activity during late High Cascades volcanism (Smith, 1986a, Pitcher, 2017; Pitcher and others, 2017). Rhyodacite and rhyolite units (e.g., rhyolite of Cline Buttes, rhyolite of Steelhead Falls) were emplaced west of present-day Redmond, contemporaneously with the earliest ash-flow tuff eruptions (**Figure 5-16**, **Figure 5-21**; Sherrod and others, 2004). The upper part of the Deschutes Formation, by contrast, lacks widespread pyroclastic flow deposits and is instead dominated by paleosols and less notable ash-fall deposits. Lava flows are increasingly abundant in the formation in the vicinity of major eruptive centers located near the Cascade Range crest on the west.

Rocks assigned to the Deschutes Formation in the northwest part of the lower Crooked River basin were chiefly deposited between 7.5 and 4 Ma across a broad active arc-adjacent plain that prograded eastward from principal volcanic source areas in the early High Cascade Range to an adjacent fluvial basin (Deschutes Basin; Smith 1986a, 1987, 1991; Smith and others, 1987). Influx of sediment, pyroclastic

material, and lavas onto the active arc-adjacent plain in the Deschutes Basin waned and ceased with faulting along Green Ridge at ~5.42 Ma and related subsidence of the central Oregon High Cascade axis into an intra-arc extensional graben. (**Figure 5-2**, **Figure 5-16**, **Figure 5-21**; Taylor, 1981; Smith and Taylor, 1983; Smith and others, 1987; Conrey and others, 2002).

Rocks mapped as part of the Deschutes Formation in the lower Crooked River basin, southeast of Smith Rock, were emplaced between ~8.8 and 3.3 Ma across inactive basin margin settings of the larger Deschutes Basin (**Figure 5-16**, **Figure 5-21**). Sedimentary (**Tdsg**, **Tds**) and pyroclastic rocks (**Tmot**, **Tmtm**) were deposited along the ancestral Crooked River and on low-gradient alluvial fans radiating outward from uplands composed of middle Miocene and older rocks (e.g., Prineville Basalt, Simtustus, John Day, and Clarno formations). At least 20 plains forming and intracanyon olivine-phyric basalt and basaltic andesite lava flows (**Tdbx**, **Tdbsr**, **Tdbc**, **Tdbr**, **Tdbrb**, **Tdbj**, **Tdbt**, **Tdbm**, **Tdbd**, **Tdbo**, **Tdbw**, **Tdbrc**, **Tdbp**, **Tdbh**, **Tdbb**, **Tdbaf**, **Tdbg**, **Tdbq**, **Tdbbs**) were erupted from as many as 17 intrabasinal shield volcanoes and cinder cones (**Tdv**, **Tdp**, **Tdbi**) scattered across the western part of the lower Crooked River basin. Collectively these mafic vents and corresponding lava flows define the Bowman volcanic field, mapped between Round Butte (Deschutes Basin) on the northwest and Alkali Butte on the southeast (**Figure 5-16**, **Figure 5-21**; plate). Basalt and basaltic andesite vents within the Bowman volcanic field spatially correspond with the structure of the Oligocene Crooked River caldera; vent distribution may have been, in part, controlled by pre-existing zones of structural weakness related to the caldera (**Figure 5-16**; plate). The northwest-southeast alignment of vents between Round Butte (Deschutes Basin) and Alkali Butte also parallels the north-northwest-striking Sisters fault zone, lying along the eastern edge of the High Cascades (**Figure 5-21**).

Bowman volcanic field mafic lava flows are distinctly olivine- to plagioclase-phyric and typically diktytaxitic. Vesicle sheets and/or cylinders are ubiquitous. Bowman volcanic field mafic lava flows in the lower Crooked River basin have a narrow range of silica content (SiO_2 = 47.67 to 53.65 weight percent, avg = 49.94 weight percent SiO_2; *n* = 158), but a wider variation in other oxides including aluminum (Al_2O_3 = 13.21 to 18.48 weight percent, avg = 16.3 weight percent Al_2O_3), titanium (TiO_2 = 0.7 to 2.91 weight percent, avg = 1.62 weight percent TiO_2), iron (FeOTotal = 8.13 to 14.65 weight percent, avg = 10.82 weight percent FeOTotal), magnesium (MgO = 4.4 to 10.32 weight percent, avg = 7.53 weight percent MgO), and potassium (K_2O = 0.15 to 1.16 weight percent, avg = 0.54 weight percent K_2O) (**Figure 5-22a-d**; appendix).

Basalt and basaltic andesite lava flows, erupted from vents of the Bowman volcanic field, entered the ancestral Crooked River at numerous points between Bowman Dam and O'Neil (**Figure 5-16**, **Figure 5-21**; plate). These lavas flowed downstream as channel-confined intracanyon flows through a narrow gorge incised into older rocks. Many of these channel-confined flows apparently emptied into a stagnant, low gradient basin at present-day Prineville (e.g., units **Tdbsr**, **Tdbc**, **Tdbm**, **Tdbrc**, **Tdbb**, **Tdbh**, **Tdbaf**) (**Figure 5-16**, **Figure 5-21**; plate). Farther-traveled flows, erupted in inactive basin margin settings south of Smith Rock, including the basalt of Pelton Dam (**Tdbp**), basalt of Opal Springs (**Tdbo**), and basalt of Tetherow Butte (**Tdbt**) are mapped north of Smith Rock into the Deschutes Basin (**Figure 5-16**, **Figure 5-21**; plate). These lava flow units (**Tdbp**, **Tdbo**, **Tdbt**) form key stratigraphic markers in the Deschutes Formation type area in the northwest part of the lower Crooked River basin, where they interfinger with arc-adjacent plain units (**Figure 5-21**). Late Miocene and early Pliocene lava flows, erupted in the Bowman volcanic field, thus record part of the Neogene development of the combined northward-flowing Deschutes-Crooked River drainage system (McClaughry and Ferns 2007b; McClaughry and others, 2009b).

Figure 5-21. Regional extent of the Deschutes Formation, Bowman volcanic field, and distribution of proximal High Cascades arc, arc-adjacent alluvial plain, ancestral Deschutes River, and inactive basin margin depositional settings. Depositional settings modified after Smith (1987, 1991).

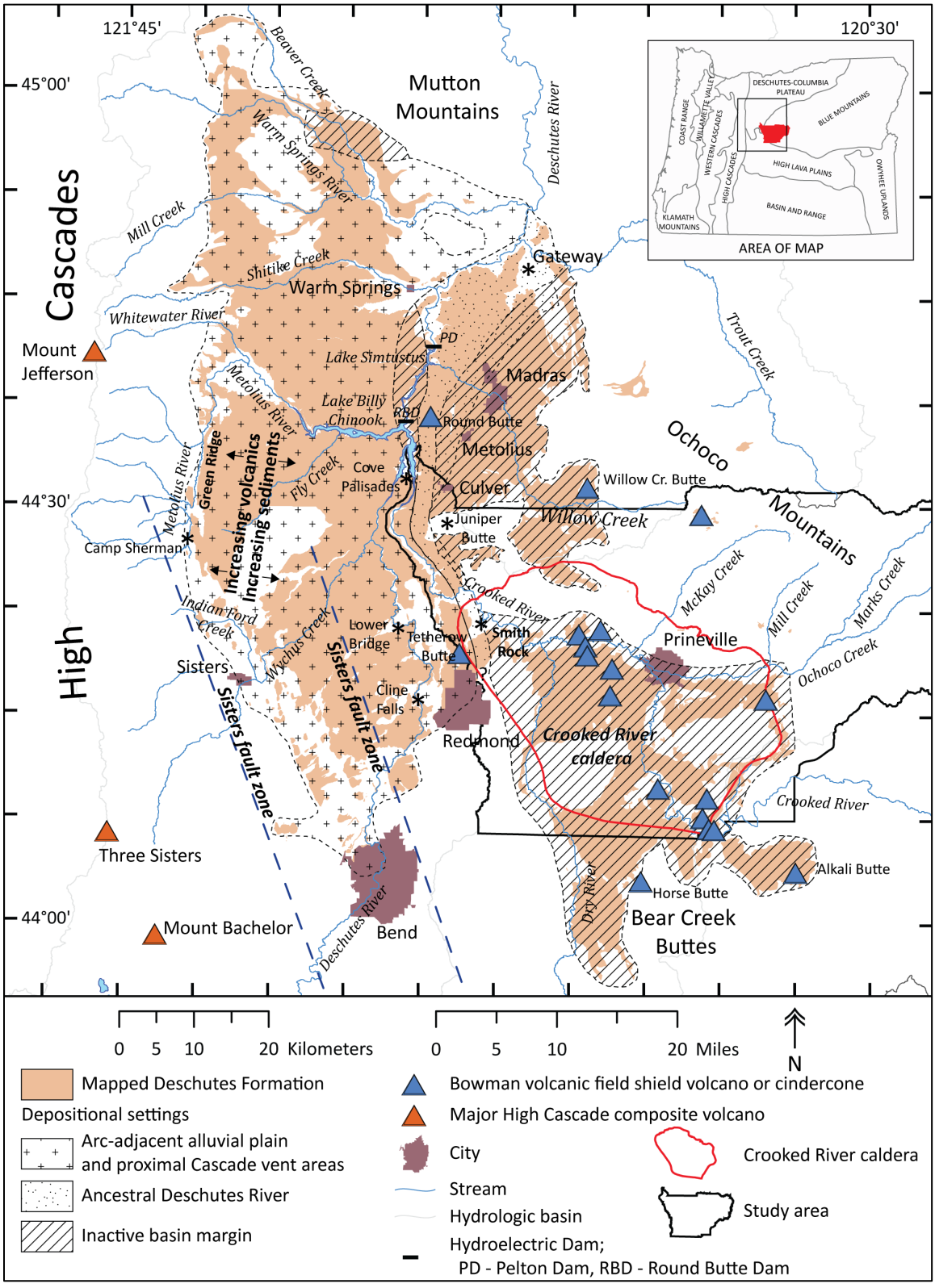

Figure 5-22. Geochemical variation diagrams for mafic lavas in the Deschutes Formation in the lower Crooked River basin (part 1 of 2) (*n* = 169 analyses). (a) Titanium (TiO_2) versus silica (SiO_2). (b) Magnesium (MgO) versus silica (SiO_2). *(next page)* **(c) Potassium (K_2O) versus silica (SiO_2). (d) Total iron (FeOTotal) versus silica (SiO_2).**

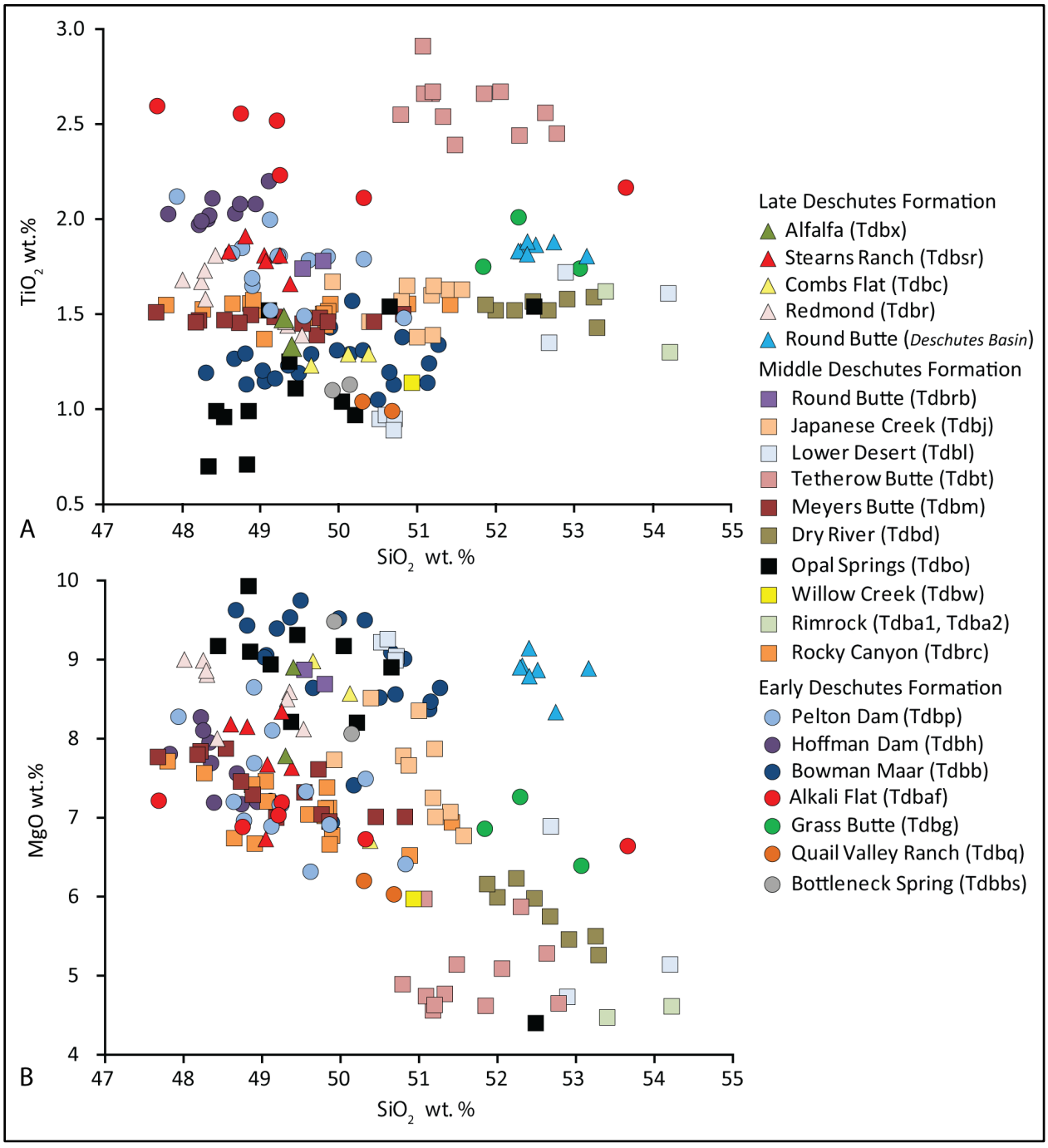

Figure 5-22, *continued*. **Geochemical variation diagrams for mafic lavas in the Deschutes Formation in the lower Crooked River basin (part 2 of 2) (n = 169 analyses). (a) Titanium (TiO_2) versus silica (SiO_2). (b) Magnesium (MgO) versus silica (SiO_2). (c) Potassium (K_2O) versus silica (SiO_2). (d) Total iron (FeOTotal) versus silica (SiO_2).**

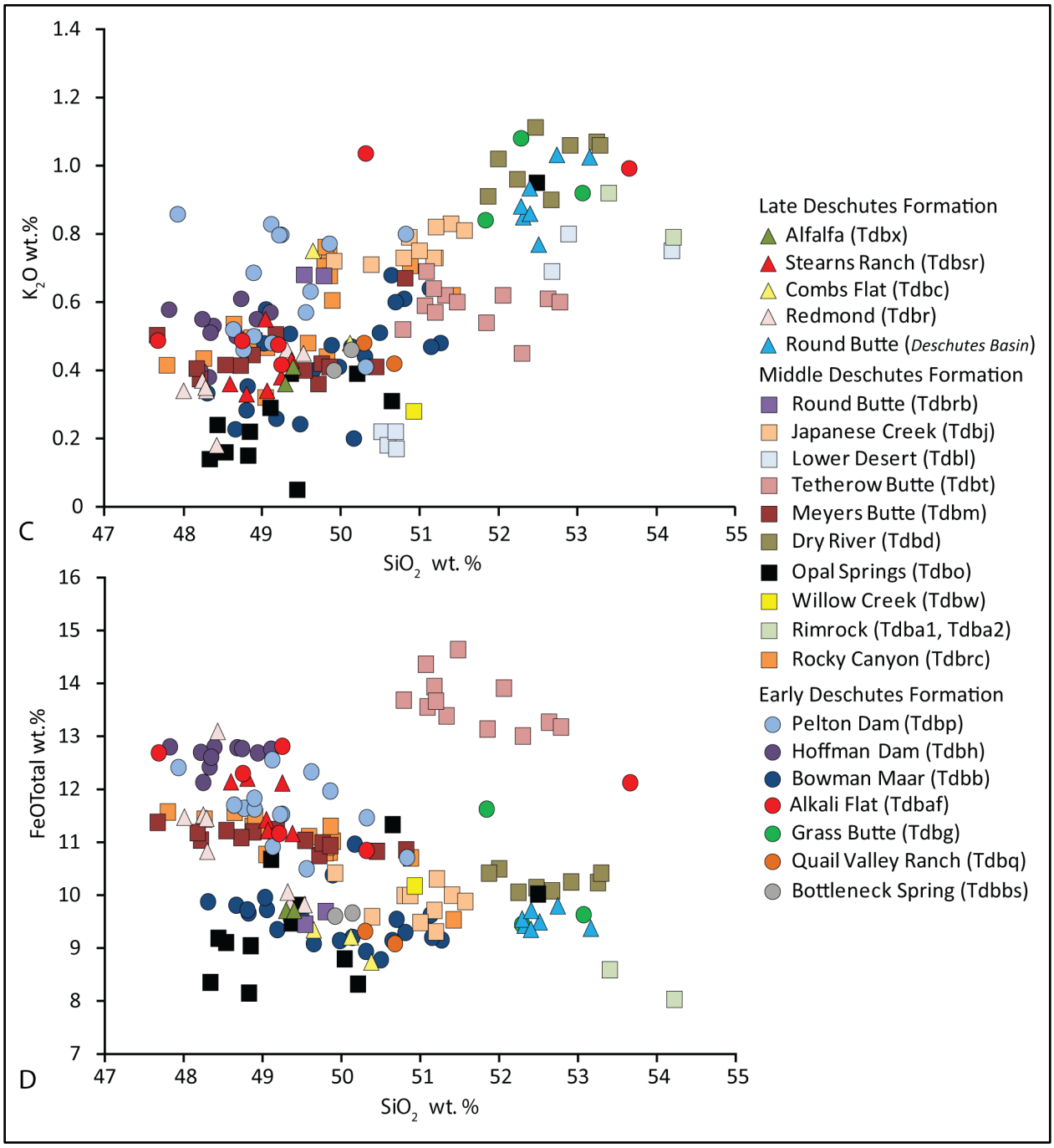

5.1.2.2.2 Age

Geochronology of the Deschutes Formation was outlined by Smith (1986a, b), and Smith and others (1987) in the Deschutes Basin type area at Green Ridge and along the Deschutes and Crooked rivers west of Madras (**Figure 5-21**). The oldest parts of the Deschutes Formation in the type area are defined by the basalt of Pelton Dam (**Tdbp**) cropping out along the Deschutes River and lower Willow Creek, and a basaltic andesite lava flow mapped near the exposed base of the Green Ridge section (**Figure 5-21**). A sample of the basalt of Pelton Dam (**Tdbp**), from an outcrop on lower Willow Creek yielded an $^{40}Ar/^{39}Ar$ plateau age of 7.42 ± 0.22 Ma (whole rock; sample J203; Smith, 1986a, b; Smith and others, 1987; recalibrated to 7.52 ± 0.45 Ma by Pitcher, 2017). The basaltic andesite cropping out at the base of Green Ridge yielded an $^{40}Ar/^{39}Ar$ plateau age of 7.27 ± 0.08 Ma (whole rock; sample RC808; Smith, 1986a, b; Smith and others, 1987) (**Figure 5-21**). The upper part of the Deschutes Formation, northeast of the confluence of the Metolius, Deschutes, and Crooked rivers, is bracketed by the Round Butte member, which has an $^{40}Ar/^{39}Ar$ plateau age of 3.97 ± 0.05 Ma (whole rock; sample D10; Smith, 1986a, b; Smith and others, 1987; recalibrated to 4.00 ± 0.10 Ma; Pitcher, 2017) (**Figure 5-21**). The stratigraphically highest basaltic andesite lava flow on Green Ridge has an $^{40}Ar/^{39}Ar$ plateau age of 5.27 ± 0.04 Ma (whole rock; sample RC89; Smith, 1986a, b; Smith and others, 1987; recalibrated to 5.34 ± 0.04 Ma by Pitcher, 2017) (**Figure 5-21**). Over most of the Deschutes Basin, the top of the Deschutes Formation is marked by ~5.4 to 5.3 m.y. old lavas, including the basalt of Lower Desert (**Tdbl**) (**Figure 5-16**; plate). A sample obtained from the Canadian Bench flow of the basalt of Lower Desert (**Tdbl**) on The Peninsula yielded an $^{40}Ar/^{39}Ar$ plateau age of 5.43 ± 0.05 Ma (whole rock; sample D9; Smith and others, 1986a, b; recalibrated to 5.47 ± 0.10 Ma by Pitcher, 2017) (**Table 5-3**; appendix). Ash-flow tuffs and related eruption-induced volcaniclastic sediments were deposited between 6.3 and 5.45 Ma (Smith, 1986a, b; Smith and others, 1987; Pitcher, 2017). Similar aged rhyodacite and rhyolite domes and flows were emplaced at Cline Buttes west of Redmond and southwest of Steelhead Falls along the Deschutes River (**Figure 5-16**). Sherrod and others (2004) obtained $^{40}Ar/^{39}Ar$ ages of 6.14 ± 0.06 Ma (plagioclase; sample S94-B78) for the rhyolite of Cline Buttes and 6.74 ± 0.20 Ma (plagioclase; sample S94-B100) for the rhyodacite southwest of Steelhead Falls.

Isotopic ages obtained from mafic lava flows within the Bowman volcanic field in the lower Crooked River basin indicate the Deschutes Formation there is as old as 8.76 Ma and as young as 3.31 Ma (**Figure 5-16**, **Figure 5-21**, **Figure 5-23**; **Table 5-3**; appendix). Lava flow packages in the Bowman volcanic field are informally divided here into the early, middle, and late Deschutes Formation on the basis of stratigraphic position relative to the 7.1 Ma Rattlesnake Tuff (**Figure 5-16**) and timing relations with the onset of faulting along Green Ridge in the Deschutes Basin around 5.42 Ma (**Figure 5-21**; Smith, 1986a, b; Smith and others, 1987; McClaughry and others, 2009c).

The oldest mapped unit forming part of the early Deschutes Formation in the lower Crooked River basin is the 8.76 ± 0.24 Ma basalt of Quail Valley Ranch (**Tdbq**) ($^{40}Ar/^{39}Ar$ plateau; whole rock; sample 276 LCJ 06), cropping out in the Crooked River canyon south of Prineville (**Figure 5-16**, **Figure 5-21**, **Figure 5-23**; **Table 5-3**; plate; appendix; McClaughry and Ferns, 2007d). Two other lavas, lying stratigraphically above the basalt of Quail Valley Ranch (**Tdbq**) in the Crooked River canyon have $^{40}Ar/^{39}Ar$ plateau ages, including the 7.88 ± 0.05 Ma basalt of Bowman Maar (**Tdbb**) (whole rock; sample CROO53726-545565) and the 7.54 ± 0.02 Ma basalt of Hoffman Dam (**Tdbh**) (whole rock; sample CROO53265-445) (**Figure 5-16**, **Figure 5-21**, **Figure 5-23**; **Table 5-3**; plate; appendix; Dunbar and Perkins, 2015). The 7.52 Ma basalt of Pelton Dam (**Tdbp**) is recognized in well CROO 50194 (sample PB411) west of Powell Buttes. The upper part of the early Deschutes Formation in the lower Crooked River basin is bracketed by the Rattlesnake Tuff (**Tmtr**), a prominent marker unit interbedded with the formation along the Crooked River

canyon, south of Prineville. The Rattlesnake Tuff (**Tmtr**) has $^{40}Ar/^{39}Ar$ ages of 7.05 ± 0.01 and 7.093 ± 0.015 Ma obtained for outcrops in the Harney Basin, ~160 km (100 mi) southeast of the lower Crooked River basin (Streck and Grunder, 1995; Jordan and others, 2004).

Continued mafic eruptions in the Bowman volcanic field, following deposition of the Rattlesnake Tuff (**Tmtr**), produced part of the middle Deschutes Formation. Lava flows were erupted from vents at Willow Creek Butte north of the map area, from vents south of Powell Buttes, as well as at Tetherow Butte near Terrebonne and Meyers and Round buttes located along the Crooked River west of Prineville (**Figure 5-16**, **Figure 5-21**; plate). Lava flows forming the middle part of the Deschutes Formation have yielded several $^{40}Ar/^{39}Ar$ plateau ages, including 6.30 ± 0.09 Ma for the basalt of Willow Creek (**Tdbw**) (whole rock; sample D13; Smith, 1986a, b), 5.43 ± 0.05 Ma for the Canadian Bench flow of the basalt of Lower Bridge (**Tdbm**) (whole rock; sample D9; Smith, 1986a, b; recalibrated to 5.47 ± 0.10 Ma by Pitcher), 5.42 ± 0.11 Ma for the basalt of Meyers Butte (**Tdbm**) (whole rock; sample 7.13VII.05; Ferns and McClaughry, 2006a), and 5.17 ± 0.03 Ma and 5.57 ± 0.20 Ma for the Agency Plains flow of the basalt of Tetherow Butte (**Tdbt**) (groundmass; Pitcher, 2017; Pitcher and others, 2017, 2021) (**Figure 5-16**, **Figure 5-23**; **Table 5-3**; plate; appendix).

Higher titanium upper flows of the basalt of Opal Springs (**Tdbo**) yielded an original $^{40}Ar/^{39}Ar$ plateau age of 6.31 ± 0.1 Ma (whole rock; sample D5; Smith, 1986a), subsequently revised to 5.77 ± 0.07 Ma (Smith, 1986b; Smith and others, 1987). A recalibrated age of 5.85 ± 0.14 Ma was reported for the basalt of Opal Springs (**Tdbo**) by Pitcher (2017) (**Figure 5-16**, **Figure 5-23**; **Table 5-3**; plate; appendix). High-precision single crystal $^{40}Ar/^{39}Ar$ ages (Pitcher, 2017; Pitcher and others, 2017) on stratigraphically bracketing tuffs, including the older 6.25 Ma Chinook tuff and younger 5.99 Ma Osborne Canyon ignimbrite member (**Tdto**) indicate the age of the basalt of Opal Springs (**Tdbo**) is more likely around 6 Ma.

A series of ash-flow tuffs cropping out along the lower Crooked River canyon above the ~6 Ma basalt of Opal Springs (**Tdbo**) and beneath the 5.47 Ma basalt of Lower Desert (**Tdbl**) have high-precision $^{40}Ar/^{39}Ar$ plateau ages on plagioclase reported by Pitcher (2017) and Pitcher and others (2017). Dated tuffs present in the map area include the 5.99 ± 0.02 Ma Osborne Canyon ignimbrite member (**Tdto**) (sample DB-061A), 5.98 ± 0.01 Ma Jackson Buttes ignimbrite member (**Tdtj**) (sample DB-198), 5.93 ± 0.02 Ma Lower Bridge ignimbrite member (**Tdtl**) (sample DB-077), 5.76 ± 0.02 Ma McKenzie Canyon ignimbrite member (**Tdtm**) (sample DB-043A), and the 5.68 ± 0.02 Ma Steelhead Falls ignimbrite member (**Tdts**) (sample DB-083) (Pitcher, 2017). Pitcher (2017) and Pitcher and others (2017) reported $^{40}Ar/^{39}Ar$ plateau ages on plagioclase for several other tuffs of similar stratigraphic position in the Deschutes Formation that are not present in the lower Crooked River basin, including the 6.25 ± 0.07 Ma (sample DB-187) Chinook tuff, 5.68 ± 0.01 Ma (sample DB-019) Fly Creek tuff, and 5.45 ± 0.04 Ma (sample DB-008) Six Creek tuff. Aubin (2000) reported $^{40}Ar/^{39}Ar$ ages of 5.56 ± 0.06 Ma for the Balanced Rocks tuff (recalibrated to 5.60 ± 0.12 Ma; Pitcher, 2017) and 5.38 ± 0.06 Ma for the Six Creek tuff outside the map area.

Late Pliocene lavas, exposed south and west of Powell Buttes, along the Crooked River, and underlying Combs Flat, define the late Deschutes Formation in the lower Crooked River basin (**Figure 5-16**). Ages from late Deschutes units include an $^{40}Ar/^{39}Ar$ plateau age of 3.56 ± 0.30 Ma for the basalt of Redmond (**Tdbr**) (whole rock; sample D3a; Smith, 1986a), and K-Ar ages of 3.36 ± 0.08 Ma for the basalt of Combs Flat (**Tdbc**) (whole rock; sample CF1; Smith, 1986a, b) and 3.31 ± 0.15 Ma for the basalt of Alfalfa (**Tdbx**) (K-Ar; whole rock; sample 00Ole-8 [389J]; J. Donnelly-Nolan and M. Lanphere, unpub. data, 2008) (**Figure 5-16**, **Figure 5-23**; **Table 5-3**; plate; appendix). Lavas erupted from the Stearns Ranch shield volcano (**Tdbsr**) about 3 Ma marked the end of eruptive activity during late Deschutes time. The lower Crooked

River basin then underwent an aggradational phase where dominantly fluvial sand and gravel (**Tdsg**) accumulated above the volcanic plateaus left by Deschutes Formation volcanism.

Table 5-3. Summary of isotopic ages for Neogene lava flows and tuffs in the lower Crooked River basin.

Map Unit	Age	Sample	Method	Material Analyzed	Source	UTM N (NAD 83)	UTM E (NAD 83)	Polarity (NRM)
Qbnc	~0.4 Ma	nd	$^{40}Ar/^{39}Ar$	whole rock	Jensen and others (2009)	nd	nd	N
Qbn4	0.713 ± 0.12 Ma	00OLe-5 (369J)	$^{40}Ar/^{39}Ar$	whole rock	J. Donnelly-Nolan and M. Lanphere, unpub.data (2008)	4901497	655205	N
Qbn4	0.718 ± 0.43 Ma	00OLe-5 (369J)	K/Ar	whole rock	J. Donnelly-Nolan and M. Lanphere, unpub.data (2008)	4901497	655205	N
Qbi	1.19 ± 0.08 Ma	D4	$^{40}Ar/^{39}Ar$	whole rock	Smith (1986a, b)	4921327	639994	R
Tdbx	3.31 ± 0.15 Ma	00OLe-8 (389J)	K/Ar	whole rock	J. Donnelly-Nolan and M. Lanphere, unpub.data (2008)	4896903	654090	N
Tdbc	3.36 ± 0.08 Ma	CF1	K/Ar	whole rock	Smith (1986a, b)	4903507	684535	R
Tdbr	3.56 ± 0.30 Ma	D3a	$^{40}Ar/^{39}Ar$	whole rock	Smith (1986a, b)	4916347	641934	R
Tdbt	5.17 ± 0.03 Ma	B-286[1]	$^{40}Ar/^{39}Ar$	groundmass	Pitcher and others (2021)	4957845	641980	N
Tdbt	5.57 ± 0.20 Ma	D7[2]	$^{40}Ar/^{39}Ar$	whole rock	Smith (1986a, b); Pitcher (2017); Pitcher and others (2017)	4934737	638824	N
Tdbm	5.42 ± 0.11 Ma	7.13VII.05[3]	$^{40}Ar/^{39}Ar$	whole rock	Ferns and McClaughry (2006a)	4909866	664996	R
Tdbl	5.47 ± 0.10 Ma	D9[4,#]	$^{40}Ar/^{39}Ar$	whole rock	Smith (1986a, b); Pitcher (2017); Pitcher and others (2017)	4933957	637244	N
Tdts	5.68 ± 0.02 Ma	DB-019	$^{40}Ar/^{39}Ar$	plagioclase	Pitcher (2017); Pitcher and others (2017)	4925159*	636912*	R
Tdtm	5.76 ± 0.02	DB-043A	$^{40}Ar/^{39}Ar$	plagioclase	Pitcher (2017); Pitcher and others (2017)	4918415*	640430*	R
Tdto	5.99 ± 0.02	DB-061A	$^{40}Ar/^{39}Ar$	plagioclase	Pitcher (2017); Pitcher and others (2017)	4925136*	636720*	R
Tdbo	5.85 ± 0.14 Ma	D5[5]	$^{40}Ar/^{39}Ar$	whole rock	Smith (1986a, b); Pitcher (2017); Pitcher and others (2017)	4921697	639804	N
Tdbw	6.30 ± 0.09 Ma	D13	$^{40}Ar/^{39}Ar$	whole rock	Smith (1986a, b)	4941689	650507	N
Tdbp	7.52 ± 0.45 Ma	J203[6]	$^{40}Ar/^{39}Ar$	whole rock	Smith (1986a, b); Pitcher (2017); Pitcher and others (2017)	4947634	642315	N
Tdbh	7.54 ± 0.02 Ma	CROO53265-445[3]	$^{40}Ar/^{39}Ar$	whole rock	Dunbar and Perkins (2015)	4904825	666986	N/R
Tdbb	7.88 ± 0.05 Ma	CROO53726-545565[3]	$^{40}Ar/^{39}Ar$	whole rock	Dunbar and Perkins (2015)	4906405	668543	N/R
Tdbq	8.76 ± 0.24 Ma	276 LCJ 06[3]	$^{40}Ar/^{39}Ar$	whole rock	McClaughry and Ferns (2007d)	4892328	671927	ID

All ages reported at ±2σ. Polarity – N, normal; R, reversed; ID, indeterminate. nd = no data.
[1]Age obtained from an outcrop near Warm Springs, north of the map area.
[2]Recalibrated age from Pitcher (2017) and Pitcher and others (2017) from original reported age of 5.31 ± 0.05 Ma reported by Smith (1986a, b).
[3]Ages determined at the College of Oceanic and Atmospheric Sciences, Oregon State University, Corvallis.
[4]Recalibrated age from Pitcher (2017) and Pitcher and others (2017) from original reported age of 5.43 ± 0.05 Ma reported by Smith (1986a, b).
[5]Recalibrated age from Pitcher (2017) and Pitcher and others (2017) from original reported age of 5.77 ± 0.07 Ma reported by Smith (1986a, b).
[6]Recalibrated age from Pitcher (2017) and Pitcher and others (2017) from original reported age of 7.42 ± 0.22 Ma reported by Smith (1986a, b).
*Approximate locations from original coordinates in Pitcher and others (2017).
[#]Basalt of Lower Desert (Tdbl) overlies the basalt of Tetherow Butte (Tdbt).

Figure 5-23. Correlation of Neogene basalt units with the paleomagnetic time scale of Cande and Kent (1992) *(following page)***. The Rattlesnake Tuff is included as it forms an important stratigraphic marker, interbedded with Neogene basalts in the Crooked River canyon south of Prineville. Patterns show natural magnetization: dark fill – normal polarity; white fill – reversed-polarity. Units in the left column are samples with radiometric age-date determinations (bars showing age and standard deviation are patterned similar to time scale); those in the right column have not been isotopically dated and are arranged on the basis of relative stratigraphic position. Upper case abbreviations following unit names indicate natural remanent magnetization determined by using a portable fluxgate magnetometer (N – normal polarity; R – reversed-polarity; ND – indeterminate or no data).**

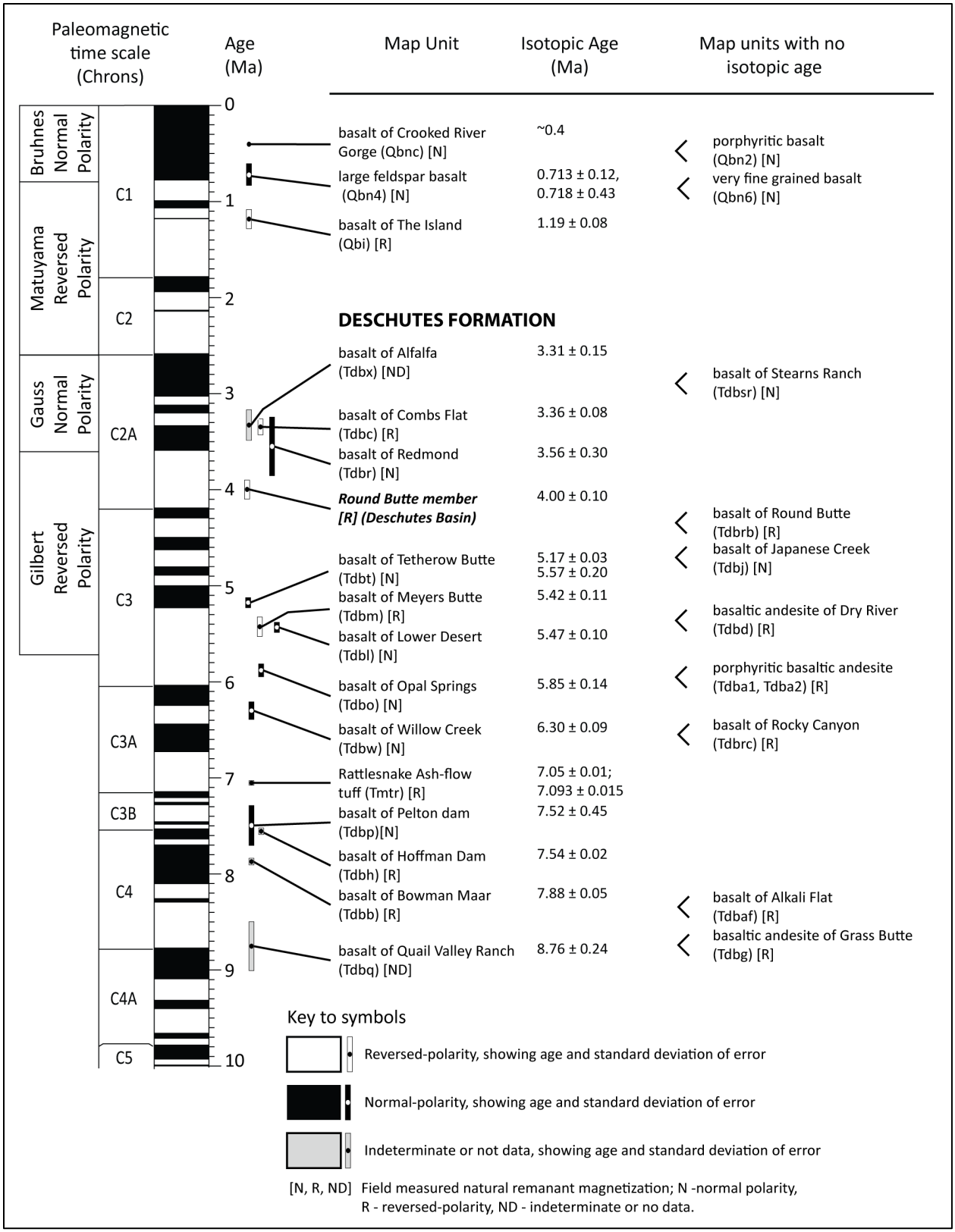
Paleomagnetic time scale (Chrons)
Age (Ma)
Map Unit
Isotopic Age (Ma)
Map units with no isotopic age
Bruhnes Normal Polarity
Matuyama Reversed Polarity
Gauss Normal Polarity
Gilbert Reversed Polarity
C1
C2
C2A
C3
C3A
C3B
C4
C4A
C5
0
1
2
3
4
5
6
7
8
9
10
basalt of Crooked River Gorge (Qbnc) [N]
~0.4
large feldspar basalt (Qbn4) [N]
0.713 ± 0.12, 0.718 ± 0.43
basalt of The Island (Qbi) [R]
1.19 ± 0.08
porphyritic basalt (Qbn2) [N]
very fine grained basalt (Qbn6) [N]
DESCHUTES FORMATION
basalt of Alfalfa (Tdbx) [ND]
3.31 ± 0.15
basalt of Stearns Ranch (Tdbsr) [N]
basalt of Combs Flat (Tdbc) [R]
3.36 ± 0.08
basalt of Redmond (Tdbr) [N]
3.56 ± 0.30
Round Butte member [R] (Deschutes Basin)
4.00 ± 0.10
basalt of Round Butte (Tdbrb) [R]
basalt of Tetherow Butte (Tdbt) [N]
5.17 ± 0.03
5.57 ± 0.20
basalt of Japanese Creek (Tdbj) [N]
basalt of Meyers Butte (Tdbm) [R]
5.42 ± 0.11
basaltic andesite of Dry River (Tdbd) [R]
basalt of Lower Desert (Tdbl) [N]
5.47 ± 0.10
basalt of Opal Springs (Tdbo) [N]
5.85 ± 0.14
porphyritic basaltic andesite (Tdba1, Tdba2) [R]
basalt of Willow Creek (Tdbw) [N]
6.30 ± 0.09
basalt of Rocky Canyon (Tdbrc) [R]
Rattlesnake Ash-flow tuff (Tmtr) [R]
7.05 ± 0.01; 7.093 ± 0.015
basalt of Pelton dam (Tdbp)[N]
7.52 ± 0.45
basalt of Hoffman Dam (Tdbh) [R]
7.54 ± 0.02
basalt of Bowman Maar (Tdbb) [R]
7.88 ± 0.05
basalt of Alkali Flat (Tdbaf) [R]
basalt of Quail Valley Ranch (Tdbq) [ND]
8.76 ± 0.24
basaltic andesite of Grass Butte (Tdbg) [R]
Key to symbols
Reversed-polarity, showing age and standard deviation of error
Normal-polarity, showing age and standard deviation of error
Indeterminate or not data, showing age and standard deviation of error
[N, R, ND] Field measured natural remanant magnetization; N -normal polarity, R - reversed-polarity, ND - indeterminate or no data.

5.1.2.3 Quaternary intracanyon basalt and basalt from Newberry Volcano

5.1.2.3.1 Distribution, composition, and lithology

The basalt of The Island (**Qbi**), now preserved as an intracanyon lava along the Crooked River in the northwest part of the map area, is the oldest of the Quaternary lavas preserved in the lower Crooked River basin (**Figure 5-16**; plate). This basalt flow sequence was erupted and flowed into the basin at 1.19 Ma. The vent area for the basalt of The Island (**Qbi**) is presumed to be located to the south, at or near Newberry Volcano, but lavas cannot be mapped further south than Crooked River Ranch (**Figure 5-16**; plate; Peterson and others, 1976; Smith, 1986a, b; Dill, 1992).

Younger Middle Pleistocene lavas (**Qbn6**, **Qbn4**, **Qbn2**, **Qbnc**), erupted from vents on the north flank of Newberry Volcano ~40 km (25 mi) south of the map area, cover a broad area along the western edge of the lower Crooked River basin (**Figure 1-1**, **Figure 5-16**; plate). Newberry units are applied naming and abbreviation conventions consistent with Sherrod and others (2004); the basalt of Crooked River Gorge, unit **Qbnc** follows the work of Jensen and others (2009). The oldest of the Newberry lavas in the western part of the lower Crooked River basin include the very fine grained basalt (**Qbn6**) and large feldspar basalt (**Qbn4**) of Sherrod and others (2004), erupted around 0.7 Ma and the porphyritic basalt (**Qbn2**) erupted between 0.7 and 0.4 Ma. These flows are capped by the basalt of Crooked River Gorge (**Qbnc**), erupted around 0.4 Ma (Jensen and others, 2009). The Crooked River Gorge lava (**Qbnc**) flowed northward from Newberry Volcano following an ancestral Deschutes River channel and forming a broad plain extending to Redmond and Smith Rock (**Figure 1-1**, **Figure 5-16**; plate; Sherrod and others, 2004). Between O'Neil and Smith Rock this lava flow inundated a broad, shallow channel cut into Oligocene rocks of the Crooked River caldera, near the paleo confluence of the Deschutes and Crooked Rivers (**Figure 5-16**; plate; Jensen and others, 2009). Downstream of Smith Rock, the basalt flow descended into the Crooked River canyon, nearly filling the steep-walled gorge and flowing at least another 8 km (5 mi) to Lake Billy Chinook (**Figure 5-16**; plate). The Crooked River has since incised a steep-walled canyon into the basalt of Crooked River Gorge (**Qbnc**) and a thick succession of older late Miocene lavas, tuffs, and sedimentary rocks of the Deschutes Formation (**Figure 5-16**; plate).

Upstream of O'Neil, Late to Middle Pleistocene fluviatile terrace deposits (**Qto**), composed of gravel and sand, accumulated at Forest Crossing and in the Prineville Valley, as westward flow of the Crooked River was impounded by intracanyon basalt dams (**Qbnc**) (**Figure 5-16**; plate). The crest of the lava dam was at an elevation of ~902 m (2,960 ft), while the highest remnant of the upper terrace deposit stands at an elevation of ~905 m (2,970 ft) near Barnes Butte (**Figure 5-16**; plate). Sand and gravel terraces intermixed with layers of silt and clay, were deposited upstream of O'Neil along the Crooked River, in the Prineville Valley, and along the channels of major tributaries including McKay and Ochoco Creeks (**Figure 5-16**; plate). Inundation of the drainage system by the basalt of Crooked River Gorge (**Qbnc**) at 0.4 Ma forced the Deschutes River west, where it established a new channel through the City of Redmond (**Figure 5-16**; plate). The Crooked River, which formerly joined the ancestral Deschutes upstream near Smith Rock State Park reestablished a channel along the northern edge of the basalt and cut a deep gorge downstream to Lake Billy Chinook following the paleo drainage of the pre-basalt Deschutes River (**Figure 5-16**; plate). The basalt impoundments elevated the base level for sediment deposition (**Qto**) in the Prineville Valley and may have resulted in the formation of temporary lakes (Robinson and Price, 1963; Sherrod and others, 2004).

5.1.2.3.2 Age

The reversed magnetic polarity basalt of The Island **(Qbi**) has an $^{40}Ar/^{39}Ar$ plateau age of 1.19 ± 0.08 Ma determined for a sample of the flow obtained near Crooked River Ranch (whole rock; sample D4; Smith, 1986a, b) (**Figure 5-23**; **Table 5-3**; plate; appendix). Lavas mapped as part of Newberry Volcano have normal magnetic polarity and are thus younger than 0.78 Ma (Champion and others, 2002, 2004). The oldest of the Newberry lavas in the western part of the lower Crooked River basin include the very fine grained basalt (**Qbn6**) and large feldspar basalt (**Qbn4**) (Sherrod and others, 2004). Unit **Qbn4** has an $^{40}Ar/^{39}Ar$ age of 0.713 ± 0.12 Ma (whole rock; sample 00OLe-5 [369J]) and a K-Ar age of 0.718 ± 0.43 Ma (whole rock; sample 00OLe-5 [369J]) (J. Donnelly-Nolan and M. Lanphere, unpub. data, 2008; **Figure 5-23**; **Table 5-3**; plate; appendix). Porphyritic basalt flows of unit **Qbn2** are undated but erupted between 0.713 and 0.4 Ma on the basis of stratigraphic position between units **Qbn4** and **Qbnc** (plate). The section capping basalt of Crooked River Gorge (**Qbnc**) has $^{40}Ar/^{39}Ar$ ages indicating eruption of the basalt around 0.4 Ma (M. Lanphere and A. Calvert, in Jensen and others, 2009).

5.1.2.4 Surficial deposits

5.1.2.4.1 Distribution, composition, and lithology

Steep slopes and valley bottoms have accumulated late Pleistocene and Holocene surficial units including stream alluvium (**Qa**, **Qty**, **Qto**), fan deposits (**Qaf**, **Qoaf**), landslide deposits (**Qls**), and colluvium (**Qc**) (plate). Human-modified ground and areas of significant construction, including railroad grades, dams and levees, road embankments, and mined land are mapped as unit **Qf**. Surficial units reflect late Pleistocene and younger landscape adjustments as major drainages have continued to incise into bedrock units. The largest accumulations of alluvium (**Qa**, **Qty**, **Qto**) are along the Crooked River, which meanders through the low-lying western part of the lower Crooked River basin (plate). Landslide deposits are common along the canyon walls of the Crooked River and along steep slopes in the Ochoco Mountains (**Qls**) (plate).

5.1.2.4.2 Age

Surficial deposits in the lower Crooked River basin chiefly range from Late Pleistocene to upper Holocene in age, but age constraints are few. Unit **Qto** terrace deposits mapped upstream of Smith Rock are inferred to have formed in the Middle Pleistocene around 0.4 Ma, on the basis of their spatial association with the 0.4 Ma basalt of Crooked River Gorge (**Qbnc**) (**Figure 5-16**; plate). Sands and gravels comprising the unit likely accumulated upstream of O'Neil and Smith Rock in response to damming of the northwest-flowing Crooked River by the basalt of Crooked River Gorge (**Qbnc**). Composite landslides (**Qls**) in the Ochoco Mountains typically form large complexes of varying age that are recurrently active (**Figure 5-5**; plate). Radiometric age-dates obtained from charcoal collected from auger holes in a small landslide along Doe Creek, active in 2000, in the Ochoco National Forest, revealed the most recent historic movement in the landslide complex was ~9240 BP (**Figure 5-5**; plate). The presence of undisturbed in-situ Mazama tephra recovered from one of the drill holes suggests that no landslide movement has occurred at this location since at least ~6850 BP (L. Chitwood to C. Gordon, written commun., 2001).

6.0 EXPLANATION OF MAP UNITS

The suite of volcanic, intrusive, and sedimentary rocks and surficial deposits preserved in the lower Crooked River basin have been divided into 105 map units, ranging in age from middle Eocene to Holocene. The Explanation of Map Units describes the basis for subdividing rocks into stratigraphic units on the geologic map shown on the plate. A time-rock chart graphically displaying age ranges and stratigraphic relations for the map units is shown in **Figure 6-1** and on the plate. Widely separated stratigraphic units, were grouped on the basis of multiple criteria including apparent stratigraphic position, lithology, geochemical composition, isotopic age, and magnetic polarity. Unit names follow established stratigraphic nomenclature where possible, whereas informal rock names are assigned to previously unnamed units. Informal unit names are based on composition or sites of good exposure. The Clarno, John Day, Simtustus, and Deschutes formations are formally named, but separate units within those formations are only informally named (Marsh, 1875; Merriam, 1901a; Russell, 1905; Farooqui and others, 1981; Smith, 1986c; Smith and others, 1987). Formal stratigraphic names have been established for the CRBG; those rocks are assigned to units following conventions established by Thayer (1957), Thayer and Brown (1966), Brown and Thayer (1966), Hooper and others (1993), Tolan and others (1989, 2009), and Reidel and others (2013).

Cascade Range volcanic rocks are subdivided here on the basis of conventions established by Peck (1964), Priest and others (1983), Priest (1990), and Conrey and others (1997). These time-stratigraphic intervals include: 1) an early Western Cascade episode at ~40 to 18 Ma; 2) a late Western Cascade episode at ~18 to 9 Ma; 3) an early High Cascade episode at ~9 to 4 Ma; and 4) a late High Cascade episode at ~4 Ma to present. Rocks of the late Miocene to early Pliocene Deschutes Formation correspond to volcanism during an early High Cascades episode.

Figure 6-1. Time-rock chart showing the 105 geologic units in the north half of the lower Crooked River basin identified by this study (*following page*).

TIME ROCK CHART

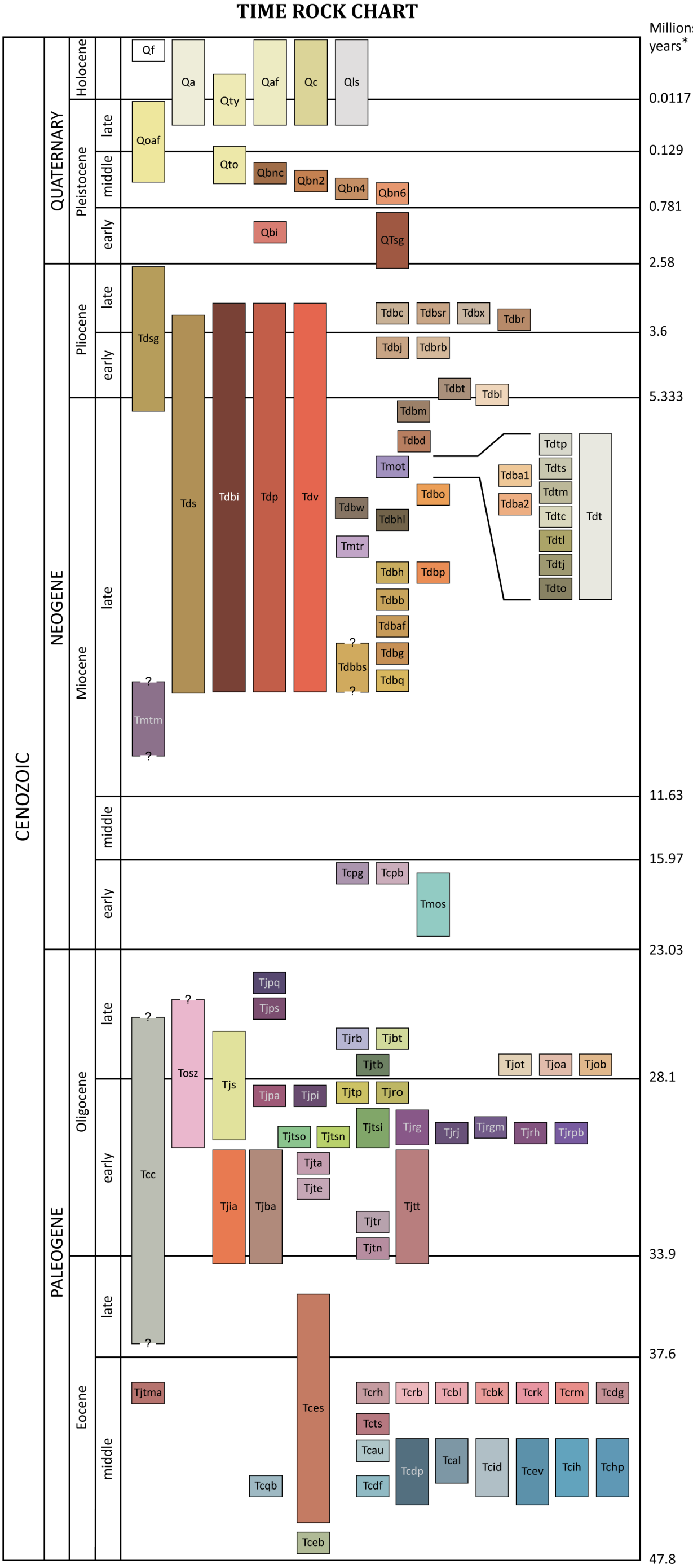

*The geologic time scale used is the 2020 (v2020/01) version of the International Stratigraphic Commission on chronographic chart (https://stratigraphy.org/chart) revised from Gradstein and others (2004), Ogg and others (2008), and Cohen and others (2013).

6.1 Overview of map units

UPPER CENOZOIC SURFICIAL DEPOSITS

Qf modern fill and construction material (upper Holocene)
Qa alluvium (Holocene and Upper Pleistocene)
Qty younger terrace deposits (Holocene and Upper Pleistocene)
Qaf alluvial fan deposits (Holocene and Upper Pleistocene)
Qc colluvium (Holocene and Upper Pleistocene)
Qls landslide deposits (Holocene and Upper Pleistocene)
Qoaf older alluvial fan deposits and colluvium (Upper and Middle Pleistocene)
Qto older terrace deposits (Upper and Middle Pleistocene)

Disconformity

UPPER CENOZOIC VOLCANIC AND SEDIMENTARY ROCKS

QUATERNARY BASALT FROM NEWBERRY VOLCANO

Qbnc basalt of Crooked River Gorge (Middle Pleistocene) ~0.4 Ma ($^{40}Ar/^{39}Ar$)
Qbn2 porphyritic basalt (Middle Pleistocene)
Qbn4 large-feldspar basalt (Middle Pleistocene) 0.713 ± 0.12 Ma ($^{40}Ar/^{39}Ar$); 0.718 ± 0.43 Ma (K-Ar)
Qbn6 very fine grained basalt (Middle Pleistocene)

QUATERNARY INTRACANYON BASALT

Qbi basalt of The Island (lower Pleistocene) 1.19 ± 0.08 Ma ($^{40}Ar/^{39}Ar$)

QUATERNARY OR UPPER PLIOCENE SEDIMENTARY ROCKS

QTsg sedimentary rocks (lower Pleistocene or upper Pliocene)

Disconformity

LOWER PLIOCENE AND UPPER MIOCENE VOLCANIC AND SEDIMENTARY ROCKS OF THE EARLY HIGH CASCADES

DESCHUTES FORMATION

Tdsg sand and gravel (Pliocene and upper Miocene)
Tds sedimentary rocks and tuff (Pliocene and upper Miocene)

BOWMAN VOLCANIC FIELD

Tdbx basalt of Alfalfa (upper Pliocene) 3.31 ± 0.15 Ma (K-Ar)
Tdbsr basalt of Stearns Ranch (upper Pliocene)
Tdbc basalt of Combs Flat (upper Pliocene) 3.36 ± 0.08 Ma (K-Ar)
Tdbr basalt of Redmond (upper Pliocene) 3.56 ± 0.30 Ma ($^{40}Ar/^{39}Ar$)
Tdbrb basalt of Round Butte (lower Pliocene)
Tdbj basalt of Japanese Creek (lower Pliocene)

Tdbt basalt of Tetherow Butte (lower Pliocene or upper Miocene) 5.17 ± 0.03 Ma ($^{40}Ar/^{39}Ar$; outside map area); 5.57 ± 0.20 Ma ($^{40}Ar/^{39}Ar$)

Tdbm basalt of Meyers Butte (upper Miocene) 5.42 ± 0.11 Ma ($^{40}Ar/^{39}Ar$)

Tdbd basaltic andesite of Dry River (upper Miocene)

Tdbo basalt of Opal Springs (upper Miocene) 5.85 ± 0.14 Ma ($^{40}Ar/^{39}Ar$)

Tdbw basalt of Willow Creek (upper Miocene) 6.30 ± 0.09 Ma ($^{40}Ar/^{39}Ar$)

Tdbrc basalt of Rocky Canyon (upper Miocene)

Tdbp basalt of Pelton Dam (upper Miocene) (cross sections A-A′ and B-B′ only) 7.52 Ma ± 0.45 Ma ($^{40}Ar/^{39}Ar$; outside map area)

Tdbh basalt of Hoffman Dam (upper Miocene) 7.54 ± 0.02 Ma ($^{40}Ar/^{39}Ar$)

Tdbb basalt of Bowman Maar (upper Miocene) 7.88 ± 0.05 Ma ($^{40}Ar/^{39}Ar$)

Tdbaf basalt of Alkali Flat (upper Miocene) (cross sections C-C′ and D-D′ only)

Tdbg basaltic andesite of Grass Butte (upper Miocene)

Tdbq basalt of Quail Valley Ranch (upper Miocene) 8.76 ± 0.24 Ma ($^{40}Ar/^{39}Ar$)

Tdbbs basalt of Bottleneck Spring (upper Miocene[?])

Tdv basalt vents (Pliocene and upper Miocene)

Tdp vent pyroclastic rocks (Pliocene and upper Miocene)

Tdbi basalt intrusions (Pliocene and upper Miocene)

DESCHUTES FORMATION LAVA FLOWS IN THE WESTERN PART OF THE LOWER CROOKED RIVER BASIN NOT ASSIGNED TO THE BOWMAN VOLCANIC FIELD

Tdbl basalt of Lower Desert (lower Pliocene or upper Miocene) 5.47 ± 0.10 Ma ($^{40}Ar/^{39}Ar$)

Porphyritic basaltic andesite lava flows subdivided into:

Tdba1 rimrock-forming basaltic andesite (upper Miocene)

Tdba2 olivine-augite and hypersthene-bearing basaltic andesite (upper Miocene)

DESCHUTES FORMATION ASH-FLOW TUFFS IN THE WESTERN PART OF THE LOWER CROOKED RIVER BASIN NOT ASSIGNED TO THE BOWMAN VOLCANIC FIELD

Tdt ash-flow tuff, undivided (upper Miocene)

Tdtp Peninsula ignimbrite member (upper Miocene)

Tdts Steelhead Falls ignimbrite member (upper Miocene) 5.68 ± 0.02 Ma ($^{40}Ar/^{39}Ar$)

Tdtm McKenzie Canyon ignimbrite member (upper Miocene) 5.76 ± 0.02 Ma ($^{40}Ar/^{39}Ar$)

Tdtc Cove ignimbrite member (upper Miocene)

Tdtl Lower Bridge ignimbrite member (upper Miocene) 5.93 ± 0.02 Ma ($^{40}Ar/^{39}Ar$; outside map area)

Tdtj Jackson Buttes ignimbrite member (upper Miocene) 5.98 ± 0.01 Ma ($^{40}Ar/^{39}Ar$; outside map area)

Tdto Osborne Canyon ignimbrite member (upper Miocene) 5.99 ± 0.02 Ma ($^{40}Ar/^{39}Ar$)

DESCHUTES FORMATION ASH-FLOW TUFFS IN THE EASTERN PART OF THE LOWER CROOKED RIVER BASIN NOT ASSIGNED TO THE BOWMAN VOLCANIC FIELD

Tmot pumice tuff (upper Miocene)

Tmtm tuff (upper Miocene[?])

LATE MIOCENE ASH-FLOW TUFFS IN THE LOWER CROOKED RIVER BASIN NOT ASSIGNED TO THE DESCHUTES FORMATION

Tmtr Rattlesnake Tuff (upper Miocene) 7.05 ± 0.01 ($^{40}Ar/^{39}Ar$; outside map area); 7.093 ± 0.015 Ma ($^{40}Ar/^{39}Ar$; outside map area)

Angular unconformity to disconformity

COLUMBIA RIVER BASALT GROUP

Tcpb Prineville Basalt (lower Miocene)

Tcpg Picture Gorge Basalt (lower Miocene)

Disconformity

SIMTUSTUS FORMATION

Tmos tuffaceous sedimentary rocks and tuff (lower Miocene)

Angular unconformity to disconformity

LOWER CENOZOIC VOLCANIC AND SEDIMENTARY ROCKS

JOHN DAY FORMATION

LOWER CROOKED VOLCANIC FIELD

Tjot trachyandesite (upper Oligocene)

Tjoa andesite (upper Oligocene)

Tjob basaltic andesite (upper Oligocene) 27.80 ± 0.06 Ma ($^{40}Ar/^{39}Ar$)

Tjs tuffaceous sedimentary rocks (Oligocene)

Crooked River caldera

Tjbt rhyolite breccia and dacite tuff (upper Oligocene)

Tjrb rhyolite of Barnes Butte (upper Oligocene) 27.97 ± 0.32 Ma ($^{40}Ar/^{39}Ar$)

Tjtb tuff of Barnes Butte (upper Oligocene) 27.62 ± 0.63 Ma ($^{40}Ar/^{39}Ar$); 28.3 ± 0.4 Ma ($^{206}Pb/^{238}U$ zircon)

Tjtp tuff of Peppermint Lane (lower Oligocene) 28.18 ± 0.16 Ma ($^{40}Ar/^{39}Ar$)

Tjro rhyolite of Ochoco Reservoir (lower Oligocene) 27.54 ± 0.36 Ma ($^{40}Ar/^{39}Ar$)* *stratigraphically discordant radiometric age

Rhyolite of Powell Buttes subdivided into:

Tjpq quartz- and sanidine-phyric rhyolite (upper Oligocene)

Tjps sanidine-phyric rhyolite (upper Oligocene) 25.8 ± 0.2 (K-Ar)

Tjpa aphyric rhyolite (lower Oligocene) 28.3 ± 1.0 (K-Ar)

Tjpi aphyric rhyolite dikes (lower Oligocene)

Tjrpb rhyolite of Pilot Butte (lower Oligocene)

Tjrgm rhyolite of Grizzly Mountain (lower Oligocene) 28.9 ± 0.2 Ma ($^{206}Pb/^{238}U$ zircon)

Tjrh rhyolite of Hi-Tor Butte (lower Oligocene) 29.2 ± 0.9 Ma ($^{206}Pb/^{238}U$ zircon)

Tjrg rhyolite of Gray Butte (lower Oligocene) 28.82 ± 0.23 Ma ($^{40}Ar/^{39}Ar$); 29.2 ± 0.3 Ma ($^{206}Pb/^{238}U$ zircon); 28.4 ± 0.3 Ma ($^{206}Pb/^{238}U$ zircon)

Tjrj rhyolite of Juniper Butte (lower Oligocene) 29.3 ± 0.2 Ma ($^{206}Pb/^{238}U$ zircon)

Disconformity to nonconformity

Tjtsi tuff of Smith Rock, intracaldera unit (lower Oligocene) 29.3 ± 0.3 Ma ($^{206}Pb/^{238}U$ zircon); 29.3 ± 0.2 Ma ($^{206}Pb/^{238}U$ zircon); 28.3 ± 0.5 ($^{206}Pb/^{238}U$ zircon)

Tjtso tuff of Smith Rock, welded outflow unit (lower Oligocene)
Haystack Reservoir lobe – 29.57 ± 0.17 Ma ($^{40}Ar/^{39}Ar$); 29.51 ± 0.11 Ma ($^{206}Pb/^{238}U$ zircon); McKay Saddle lobe – 29.56 ± 0.17 Ma ($^{40}Ar/^{39}Ar$)
Prineville Reservoir lobe – 29.5 ± 0.2 Ma ($^{206}Pb/^{238}U$ zircon)

Tjtsn tuff of Smith Rock, nonwelded outflow unit (lower Oligocene)
Haystack Reservoir lobe – 29.53 ± 0.09 ($^{40}Ar/^{39}Ar$)

Angular unconformity to disconformity

Tjta tuff of Antelope Creek (lower Oligocene)

Tjte tuff of Eagle Rock (lower Oligocene) 29.7 ± 0.6 Ma ($^{206}Pb/^{238}U$ zircon)

Tjba basalt, basaltic andesite, and andesite lava flows (lower Oligocene and upper Eocene) 30.1 ± 1.1 (K-Ar); 30.8 ± 0.5 Ma (K-Ar)

Tjia basaltic andesite and andesite intrusions (lower Oligocene and upper Eocene)

JOHN DAY FORMATION UNITS NOT ASSIGNED TO THE LOWER CROOKED VOLCANIC FIELD

Tjtr tuff of Rodman Spring (lower Oligocene) 32.49 ± 0.30 Ma ($^{40}Ar/^{39}Ar$)

Tjtt tuffaceous sedimentary rocks and tuff (lower Oligocene and upper Eocene)

Tjtn tuff of North Unit Canal (lower Oligocene or upper Eocene)

Tjtma Member A tuff (middle Eocene) 39.72 ± 0.03 ($^{40}Ar/^{39}Ar$; outside map area); 39.22 ± 0.03 ($^{40}Ar/^{39}Ar$; outside map area); 39.17 ± 0.15 Ma ($^{40}Ar/^{39}Ar$; outside map area)

Unconformity

CLARNO FORMATION

OCHOCO VOLCANIC FIELD

Tces volcaniclastic sedimentary rocks (upper and middle Eocene)

Wildcat Mountain caldera

Tcrb rhyolite of Brennan Palisades (middle Eocene)

Tcbl rhyolite breccia pipes and dikes (middle Eocene)

Tcbk andesite and dacite breccia pipes and dikes (middle Eocene)

Tcrk rhyolite of Kidnap Spring (middle Eocene)

Tcrm rhyolite of Mill Creek (middle Eocene)

Tcrh rhyolite of Hash Rock (middle Eocene) 39.35 ± 0.30 Ma ($^{40}Ar/^{39}Ar$)

Tcdg dacite of Green Mountain (middle Eocene)

Tcts tuff of Steins Pillar, intracaldera unit (middle Eocene) 41.8 ± 0.2 Ma ($^{206}Pb/^{238}U$ zircon)

Tcau andesite of Little McKay Creek (middle Eocene) 41.50 ± 0.48 Ma ($^{40}Ar/^{39}Ar$)

Tcid andesite and dacite intrusive rocks (middle Eocene) 42.79 ± 0.44 Ma ($^{40}Ar/^{39}Ar$)

Tcev vent deposits (middle Eocene)

Tcqb quartz-bearing basalt dikes (middle Eocene)

Tcdf breccia (middle Eocene)

Tchp plagioclase- and hornblende-phyric andesite and dacite (middle Eocene)

Tcih hornblende-phyric andesite (middle Eocene)

Tcal basalt, basaltic andesite, andesite, and dacite lava flows (middle Eocene)

Tcdp porphyritic andesite, dacite, and rhyolite lava flows, domes, and intrusions (middle Eocene) 43.86± 0.89 Ma ($^{40}Ar/^{39}Ar$)

Unconformity

ROCKS OF THE EARLY CLARNO FORMATION

Tceb alkali olivine basalt (lower Eocene) 46.40 ± 0.12 Ma ($^{40}Ar/^{39}Ar$)

OTHER ROCKS

Tosz sheared rock zone (Oligocene)

Tcc clay in alteration zones (Oligocene and/or Eocene [?])

6.2 Upper Cenozoic surficial deposits

Qf **modern fill and construction material (upper Holocene)**—Artificial or constructed fill deposits of poorly sorted and crudely layered mixed gravel, sand, clay, and other engineered fill (**Figure 6-2**; plate). Deposits mapped as modern fill and construction material (**Qf**) in the map area are associated with railroad grades, dams and levees, road embankments, causeways, culvert fills, and mined land. These deposits usually contain rounded to angular clasts ranging from small pebbles up to several meters across. The orientation of clasts is typically less uniform than is found in naturally occurring imbricated or bedding-parallel gravel. Older fills are likely uncompacted versus newer fills, which are likely engineered and reinforced using geotextiles or retaining structures. The thickness of fill-deposits may exceed 30 m (98 ft). Unit **Qf** is assigned a late Holocene age, ranging from the late 1800s to recent times (**Figure 6-1**; plate).

Figure 6-2. Surficial deposits mapped near Ochoco Dam. Red lines are geologic contacts. Dashed arrows indicate the direction of downslope movement within the Ochoco Reservoir landslide complex (Qls). The basemap is a 1-m lidar DEM. Map unit abbreviations are explained in Section 6.1, Overview of Map Units.

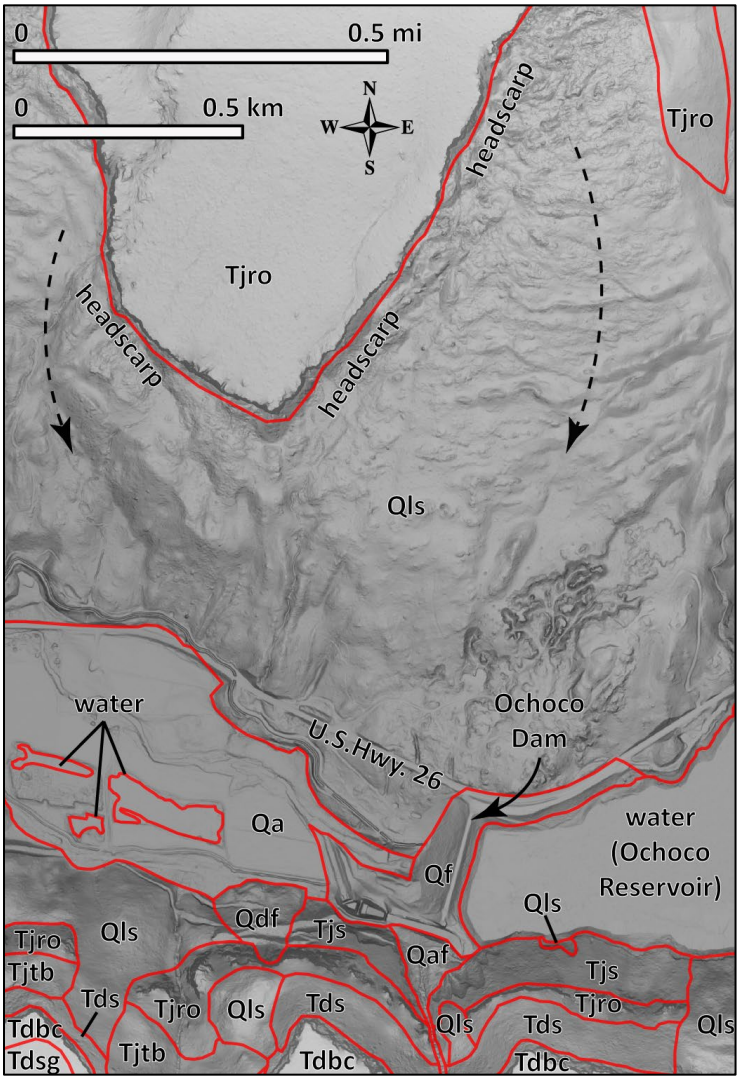

Qa **alluvium (Holocene and Upper Pleistocene)—**Unconsolidated, poorly- to moderately-stratified gravel, sand, and silt along streams, including the Crooked River, McKay Creek, Marks Creek, Ochoco Creek, Mill Creek and their tributaries (**Figure 6-2**; plate). The unit (**Qa**) includes overbank deposits consisting of sand, silt, and clay in terraces along the Crooked River. Along the upper reach of the Crooked River, downstream of Bowman Dam, alluvium consists mostly of angular cobble to boulder gravel, reworked from the toes of landslide, talus, and debris fan deposits. The unit (**Qa**) locally includes alluvial fan deposits too small to map separately at the mouths of small tributary streams. Alluvial deposits (**Qa**) may be up to 30 to 60 m (100 to 200 ft) thick in the vicinity of Prineville, but the base of this unit is difficult to distinguish from underlying Miocene and Pliocene sedimentary rocks using only well log information. Unit **Qa** is assigned a Late Pleistocene and Holocene age on the basis of stratigraphic position (**Figure 6-1**; plate).

Qty **younger terrace deposits (Holocene and Upper Pleistocene)—**Moderately dissected, unconsolidated deposits of gravel and sand, with subordinate amounts of silt and clay preserved in low terraces 3 to 5.5 m (10 to 18 ft) above the modern floodplain of the Crooked River between Bowman Dam on the south and Forrest Crossing on the north (plate). The unit **Qty** terrace is visible on 1-m lidar DEMs as a planar to very gently sloping, equal-elevation surface (tread) on both sides of the modern channel. Steeper descending slopes (risers) define the streamside edges of terraces. Individual terrace deposits may be up to 6 m (20 ft) thick. Unit **Qty** is assigned a Late Pleistocene and Holocene age on the basis of stratigraphic position (**Figure 6-1**; plate).

Qaf **alluvial fan deposits (Holocene and Upper Pleistocene)—**Unconsolidated, poorly sorted, poorly graded deposits of boulders, cobbles, pebbles, granules, sand, silt, and clay in upland drainages and as fan-shaped accumulations at the transition between low-gradient valley floodplains and steeper uplands (plate). Unit **Qaf** deposits are chiefly mapped at the mouths of steep drainages in the Ochoco Mountains and along the canyon walls of the Crooked River between Bowman Dam and Lake Billy Chinook (plate), where high-resolution lidar topographic data are available. Small fan deposits (**Qaf**) are also mapped at the mouths of small drainages incised into terrace deposits of unit **Qto**, west of Prineville. In major drainages, such as the Crooked River, alluvial fans have prograded onto Quaternary terraces (**Qto**, **Qty**) or floodplains (**Qa**), where fan toes have locally been beheaded by axial streams. In the lower Crooked River basin, mapped fans (**Qaf**) cover areas <0.04 hectares (0.1 acres) up to areas as large as 502 hectares (1,241 acres). The local thickness of alluvial fan deposits (**Qaf**) is up to 10 m (33 ft). Unit **Qaf** is assigned a Late Pleistocene and Holocene age on the basis of stratigraphic position (**Figure 6-1**; plate).

Qc **colluvium (Holocene and Upper Pleistocene)—**Unconsolidated mixtures of rock and soil deposited in rockfall and talus cones beneath steep slopes (plate). Colluvium is mapped on steep (>6 percent) debris-mantled slopes where the underlying bedrock is concealed and in swales and valleys where there is no well-defined alluvial floodplain. Thin, unmapped, veneers of colluvium are present in many areas on and beneath steep slopes; these deposits are often interbedded with debris flow deposits on alluvial fans (**Qaf**). Thickness of colluvial deposits is highly varied; maximum thickness is several meters. Unit **Qc** is assigned a Late Pleistocene and Holocene age on the basis of stratigraphic position (**Figure 6-1**; plate).

Qls **landslide deposits (Holocene and Upper Pleistocene)—**Unconsolidated, chaotically mixed masses of rock and soil deposited by landslides, including slumps, slides, earthflows, debris flows, and rock avalanches (**Figure 6-2**; plate). Unit **Qls** deposits consist of individual slide masses or form large complexes resulting from reactivation of older landslide terrain. Landslide terrain is characterized by sloping hummocky surfaces, closed depressions, springs and wet seeps, and locally, open ground fissures. Tilted trees and trees with bent trunks or disrupted fence lines may be common on the surface. Toes to more recent deposits retain convex-up, fan-shaped morphologies. Landslides are often traceable uphill to head scarps or failure surfaces. In deeper landslides, these head scarps commonly expose bedrock. Landslide deposits (**Qls**) mapped in the lower Crooked River basin cover areas <0.04 hectares (0.1 acres) up to large complexes as large as 1,971 hectares (4,881 acres). A majority of mapped landslide deposits (**Qls**) are simple rotational or shallow-seated earthflow-type features that occur along major drainages. Thickness of landslide deposits (**Qls**) is highly varied but may be more than several tens of meters in larger deposits. Landslide deposits (**Qls**) range in age from Late Pleistocene to those that have been recurrently active in the Holocene (**Figure 6-1**; plate). Large complexes mapped as Quaternary landslide deposits (**Qls**) typically include many discrete deposits of varying age that have not been differentiated. Landslide deposits (**Qls**) are typically referred to as clay, boulders, rock, or rock and clay in water well logs.

Qoaf **older alluvial fan deposits and colluvium (Upper and Middle Pleistocene)—**Unconsolidated, poorly sorted deposits of cobble- and boulder-dominated gravel, sand, and silt principally found in broad aprons fringing Oligocene rhyolite domes (e.g., Powell Buttes, Barnes Butte, Grizzly Mountain, Juniper Butte) and high standing exposures of the intracaldera unit of the tuff of Smith Rock (**Tjtsi**) (e.g., Lone Pine Flat, Coyote Butte) (plate). The unit also includes small fans scattered throughout the central and western part of the map area (plate). Deposits grade down slope from coarse, clay-rich boulder gravel to fine- to medium-grained gravel, sand, and silt. Locally, older alluvial fan deposits (**Qoaf**) include deeply incised, alluvium-filled channels formed during periods of high-water flow in ephemeral streams (e.g., Skull Hollow, Japanese Creek) (plate). The distal part of the large fan prograding south from Grizzly Mountain, northwest of Prineville is underlain by Upper and Middle Pleistocene terrace deposits (**Qto**). Local thickness of older alluvial fan deposits (**Qoaf**) is probably <20 m (66 ft). Unit **Qoaf** is assigned a Middle to Late Pleistocene age on the basis of deeply incised surface channels and stratigraphic position (**Figure 6-1**; plate). However, some areas mapped as older alluvial fan deposits and colluvium (**Qoaf**) are likely to have been active into the Holocene.

Qto **older terrace deposits (Upper and Middle Pleistocene)—**Unconsolidated to weakly consolidated, moderately to well sorted, massive to stratified deposits of gravel, sand, silt, and clay in terraces along the Crooked River between Prineville Reservoir and Peter Skene Ogden State Park (**Figure 6-3**, **Figure 6-4**, **Figure 5-16**; plate). Unit **Qto** is also mapped up Ochoco Creek to Ochoco Reservoir and along Dry River southwest of Powell Buttes (**Figure 5-16**; plate). Terrace deposits (**Qto**) are visible on 1-m lidar DEMs as a planar to very gently sloping, equal-elevation surface (tread). Steeper descending slopes (risers) define the streamside edges of terraces. Tread surfaces lie ~18 to 45 m (60 to 150 ft) above the current base level of the Crooked River. Unit **Qto** deposits mapped along the canyon wall of the Crooked River between Bowman Dam and Prineville are as thick as 20 m (65 ft), and consist predominantly of clast-supported, imbricated, well-rounded

boulder- to pebble-sized gravel. Gravel deposits are interbedded with planar stratified to cross stratified sand and silt and massive deposits of brown clay. Inset, sand-filled channel forms contain pebble clusters and outsized boulders. In the Prineville Valley, upper terrace deposits are in excess of 90 m thick (300 ft), forming a broad, gently sloping plain covering ~25 km^2 (9.6 mi^2) (plate). Lite and Gannett (2002) reported a laterally persistent succession of terrace deposits in the Prineville Valley consisting of ~30 m (100 ft) of sand with some gravel, ~45 m (150 ft) of fine-grained (mostly silt and fine sand), and a thin section (3 m [10 ft]) of coarse sand and gravel (**Figure 6-3b**). The surfaces of these terrace deposits reach a maximum elevation of ~1,036 m (3,400 ft) near the east end of Prineville Reservoir, descending along the Crooked River to ~953 m (3,126 ft) at Bowman Dam, ~890 m (2,920 ft) south of Prineville, ~890 m (2,920 ft) at Round Butte, and ~872 m (2,860 ft) near O'Neil (**Figure 5-16**; plate). Terraces along tributary drainages reach elevations of ~967 m (3,173 ft) at the east end of Ochoco Reservoir. Between O'Neil and Lone Pine Flat, **Qto** terrace deposits are banked against the basaltic andesite of Dry River (**Tdbd**) and partially onlap the basalt of Crooked River Gorge (**Qbnc**), whose upper surface is at an elevation of ~902 m (2,960 ft) near O'Neil (**Figure 5-16**, **Figure 6-4**; plate).

The mapped distribution of unit **Qto** upstream of the basalt of Crooked River Gorge (**Qbnc**), near O'Neil indicates their accumulation during the Middle to Late Pleistocene in response to damming of the Crooked River by unit **Qbnc** lava flows (**Figure 5-16**; plate; Sherrod and others, 2004). The crest of the lava dam was ~902 m (2,960 ft), while the highest remnant of the upper terrace deposit stands at an elevation of ~905 m (2,970 ft) near Barnes Butte (**Figure 5-16**; plate). Sand and gravel terraces intermixed with layers of silt and clay were deposited upstream of O'Neil along the Crooked River, in the Prineville Valley, and along the channels of major tributaries including McKay and Ochoco Creeks (**Figure 5-16**; plate). Unit **Qto** is assigned a late and Middle Pleistocene age on the basis of stratigraphic position, relative to the ~0.4 Ma basalt of Crooked River Gorge (**Qbnc**) (**Figure 6-1**; plate).

Figure 6-3. Terrace deposits (Qto). (a) Bench-forming terrace deposits (Qto) near Round Butte, (44.348794, -120.933855). View is looking north. (b) Cobble-rich terrace deposits (Qto) mapped along NE Jordan Lane in Prineville (44.306079, -120.833787). The arrow points to a 25-cm-long (9.8 in) hammer for scale in the bottom-center part of the photograph. Photo credits: Jason McClaughry, 2007.

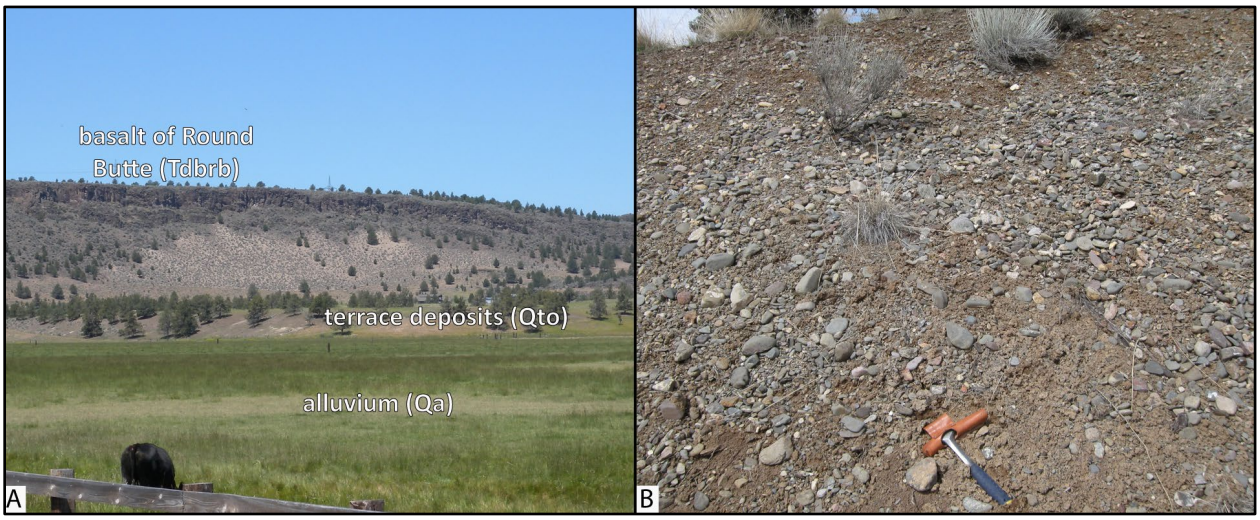

Figure 6-4. Terrace deposits (Qto) banked against the basaltic andesite of Dry River (Tdbd), west of O'Neil (44.335985, -121.088237). View is looking southwest. Photo credit: Jason McClaughry, 2007.

Disconformity

6.3 Upper Cenozoic volcanic and sedimentary rocks

6.3.1 Quaternary basalt from Newberry Volcano

Qbnc **basalt of Crooked River Gorge (Middle Pleistocene)—**High-alumina basalt lava flows (SiO_2 = 48.87 to 49.65 weight percent; Al_2O_3 = 16.35 to 18.67 weight percent; K_2O = 0.35 to 0.41 weight precent; *n* = 5 analyses) mapped across a broad plain in the western part of the lower Crooked River basin south of Smith Rock (**Figure 5-16**, **Figure 5-19**; **Table 6-1**; plate; appendix). Northwest of Smith Rock unit **Qbnc** is confined within the Crooked River Gorge as an intracanyon lava flow (**Figure 5-16**, **Figure 6-5**, **Figure 6-6**, **Figure 6-7**; plate). The upper surface of the lava flow (**Qbnc**) is irregular, capped by tumuli, residual depressions, and pressure ridges (**Figure 6-6b**). Plain-forming flows of unit **Qbnc** mapped south of Smith Rock range from 3 to 30 m (10 to 100 ft) thick, as determined on the basis of the interpretation of water well logs (**Figure 5-16**; plate). Deeply incised intracanyon outcrops of unit **Qbnc**, forming prominent vertical cliffs and benches from Peter Skene Ogden State Park downstream to Crooked River Ranch, range from ~60 m (200 ft) to >100 m (328 ft) thick (**Figure 5-16**; plate). Typical hand samples are medium light gray (N6) to dark gray (N3), vesicular, and aphyric to sparsely olivine-phyric, with ~1 percent (vol.) fresh iridescent, moderate yellow green (5GY 7/4) olivine phenocrysts ≤2 mm (0.1 in) across, distributed within a fine-grained, diktytaxitic, holocrystalline groundmass of plagioclase and intergranular olivine.

Unit **Qbnc** has normal magnetic polarity and is assigned a Middle Pleistocene age on the basis of $^{40}Ar/^{39}Ar$ ages which indicate eruption of the basalt at ~0.4 Ma (**Figure 5-23**, **Figure 6-1**; **Table 5-3**; plate; appendix; M. Lanphere and A. Calvert in Jensen and others, 2009). The basalt of Crooked River Gorge (**Qbnc**) was erupted from now buried vents on the north flank of Newberry Volcano, ~40 km (25 mi) south of the lower Crooked River basin (**Figure 1-1**). Equivalent to unit Qbn of Sherrod and others (2004).

Figure 6-5. Intracanyon basalt of Crooked River Gorge (Qbnc) at Peter Skene Ogden State Park. The basalt is here >100 m (328 ft) thick. View is looking west from the old U.S. Highway 97 bridge (44.392559, -121.193977). Photo credit: Jason McClaughry, 2008.

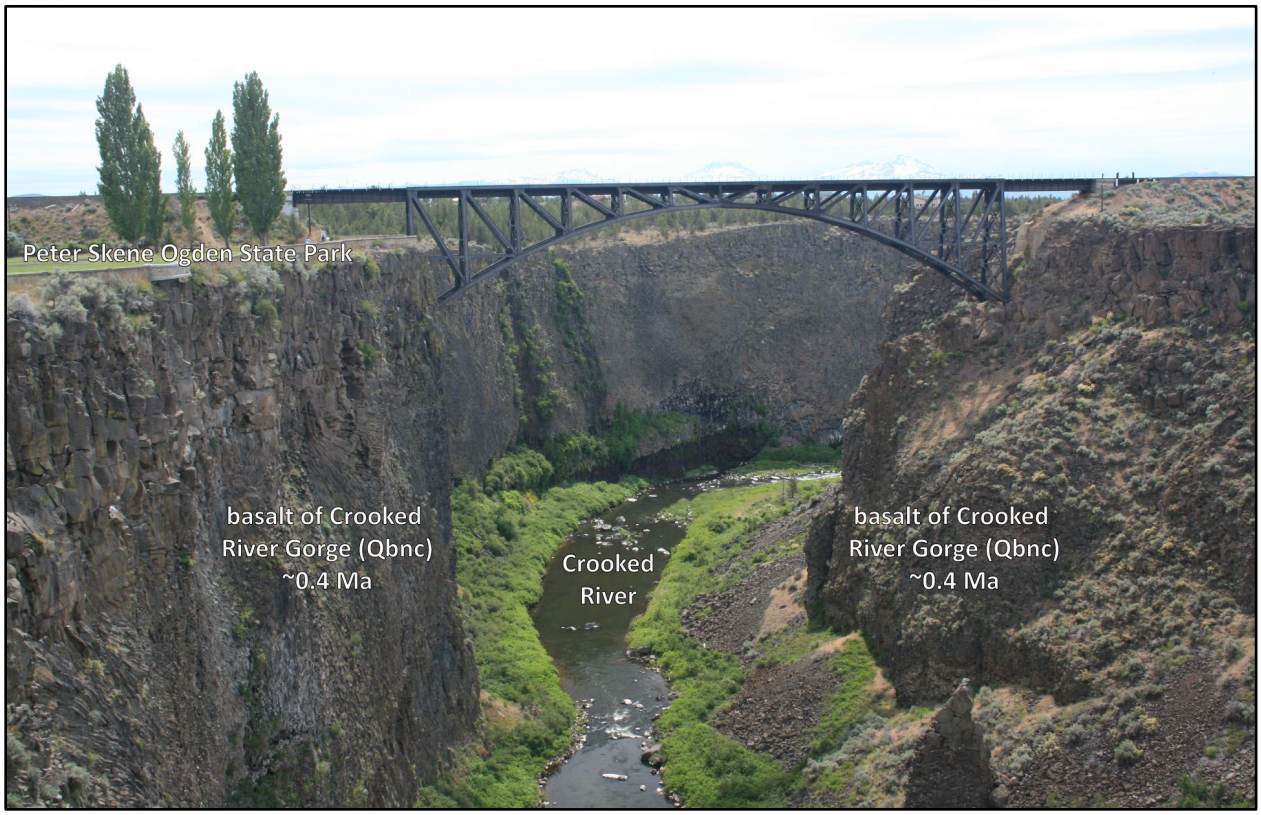

Figure 6-6. The basalt of Crooked River Gorge (Qbnc). (a) Intracanyon basalt of Crooked River Gorge (Qbnc) cropping out on the north side of the Crooked River near the U.S. Highway 97 bridge crossing (44.392871, -121.191975). CR – Crooked River. View is looking northeast. (b) The surface of the basalt of Crooked River Gorge (Qbnc) is capped by tumuli, residual depressions, and pressure ridges. The house is built on top of an elongate tumulus (44.362332, -121.158597). View is looking west. Photo credits: Jason McClaughry, 2008.

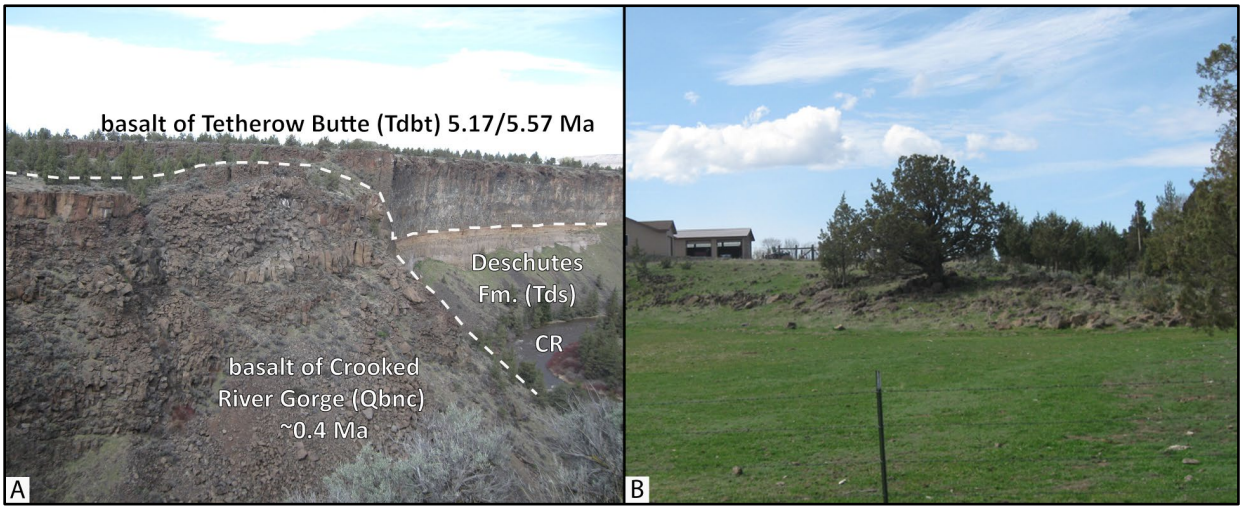

Figure 6-7. Aerial view of intracanyon lava flows (Qbnc, Qbi) filling the Crooked River Gorge downstream of Smith Rock. View is looking southeast. Photo credit: Jason McClaughry, 2011.

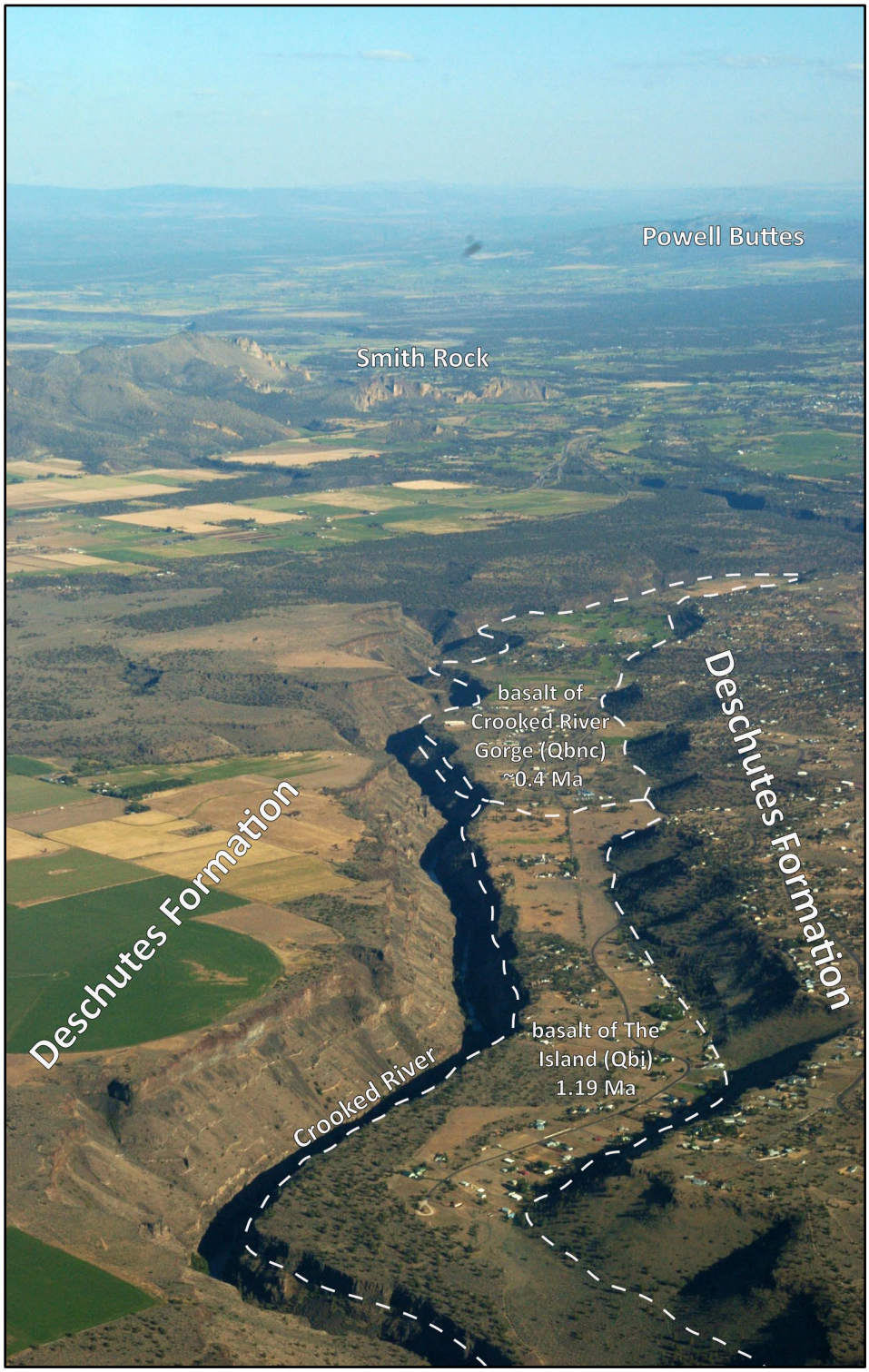

Table 6-1. Select geochemical analyses for Quaternary lava flows in the lower Crooked River basin.

Sample	SR-B-4[1]	RC95-173[2]	193J[3]	369J[3]	BBB-1[4]
Geographic Area	Smith Rock	Crooked River Ranch	Powell Butte Highway	Powell Butte Highway	Crooked River Gorge
Formation	Newberry Volcano	Newberry Volcano	Newberry Volcano	Newberry Volcano	nd
Map Unit	Qbnc	Qbnc	Qbn2	Qbn4	Qbi
UTM N (NAD 83)	4913895	4921114	4892568	4901497	4924720
UTM E (NAD 83)	648102	640039	651813	655205	636840
Age (Ma)	~0.4 Ma	~0.4 Ma	nd	0.713 Ma	1.19 Ma
Map Label	G277	G382	G66	G128	G428
Oxides, weight percent					
SiO_2	49.05	49.00	49.20	49.60	49.59
Al_2O_3	16.89	16.35	17.80	17.60	17.04
TiO_2	1.24	1.63	1.20	1.53	1.51
FeOTotal	9.67	10.20	8.85	9.96	9.32
MnO	0.16	0.18	0.15	0.17	0.16
CaO	10.72	9.55	9.58	10.26	9.64
MgO	8.95	8.92	9.38	7.17	8.69
K_2O	0.35	0.40	0.47	0.35	0.39
Na_2O	2.69	3.46	0.47	3.09	3.35
P_2O_5	0.28	0.33	0.47	0.30	0.31
LOI	nd	nd	0.47	nd	nd
Total_I	nd	nd	0.47	nd	nd
Trace Elements, parts per million					
Ni	177	159	nd	94	nd
Cr	302	298	nd	0	306
Sc	29	25	nd	174	27
V	176	217	nd	240	210
Ba	278	184	nd	134	232
Rb	3	3	nd	3	3
Sr	398	305	nd	323	358
Zr	113	133	nd	121	132
Y	21	31	nd	31	28
Nb	6	8	nd	7	9
Ga	13	18	nd	19	19
Cu	57	44	nd	67	50
Zn	78	75	nd	84	75
Pb	nd	nd	nd	0	1
La	nd	nd	nd	8	nd
Ce	nd	nd	nd	22	27
Th	nd	2	nd	0	nd
Nd	nd	nd	nd	0	nd
U	nd	nd	nd	nd	nd

Major element determinations have been normalized to a 100-percent total on a volatile-free basis and recalculated with total iron expressed as FeOTotal; nd - no data or element not analyzed; na - not applicable or no information. LOI, Loss on Ignition; Total_I, original analytical total. Data from: [1]Obermiller (1987); [2]R.M. Conrey, written commun. (2007); [3]J.M. Donnelly-Nolan, written commun. (2008); [4]Smith (1986a).

Qbn2 **porphyritic basalt (Middle Pleistocene)—**High-alumina basalt lava flow (SiO_2 = 49.20 weight percent; Al_2O_3 = 17.80 weight percent; K_2O = 0.47 weight precent; *n* = 1 analyses) mapped southwest of Powell Buttes in the western part of the lower Crooked River basin (**Figure 5-16**, **Figure 5-19**; **Table 6-1**; plate; appendix; J. Donnelly-Nolan, written commun., 2008). Unit **Qbn2** is as thick as 15 m (50 ft) west of Dry River (**Figure 5-16**; plate). Typical hand samples are medium light gray (N6) to dark gray (N3), vesicular, and olivine-phyric, with 1 to 3 percent (vol.) fresh iridescent moderate yellow green (5GY 7/4) olivine phenocrysts from 1 to 3 mm (0.04 to 0.1 in) across, distributed within a fine-grained, diktytaxitic, holocrystalline groundmass of plagioclase and intergranular olivine.

Unit **Qbn2** has normal magnetic polarity and is assigned a Middle Pleistocene age on the basis of stratigraphic position (**Figure 5-23**, **Figure 6-1**; plate; appendix; J. Donnelly-Nolan, written commun., 2008). Equivalent to the informally named porphyritic basalt, map unit Qbn2 of Sherrod and others (2004).

Qbn4 **large-feldspar basalt (Middle Pleistocene)—**High-alumina basalt lava flow (SiO_2 = 49.50 to 49.60 weight percent; Al_2O_3 = 17.40 to 17.60 weight percent; K_2O = 0.35 to 0.38 weight precent; *n* = 2 analyses) mapped as a narrow, north-south trending outcrop band west of Powell Buttes in the western part of the lower Crooked River basin (**Figure 5-16**, **Figure 5-19**; **Table 6-1**; plate; appendix; J. Donnelly-Nolan, written commun., 2008). The upper surface of the lava flow (**Qbn4**) is irregular, capped by tumuli, residual depressions, and pressure ridges. Vesicles are commonly lined by clear quartz and botryoidal masses of white to pink zeolite minerals. Unit **Qbn4** is as thick as 15 m (50 ft) west of Dry River (**Figure 5-16**; plate). Typical hand samples are medium light gray (N6) to dark gray (N3) and porphyritic, containing ≤2 percent (vol.), clear, lath-shaped to equant, euhedral plagioclase phenocrysts ≤7 mm (0.3 in) across and ≤3 percent (vol.) plagioclase microphenocrysts ≤1 mm (0.04 in), distributed within a fine-grained, diktytaxitic, holocrystalline groundmass of plagioclase and intergranular olivine.

Unit **Qbn4** has normal magnetic polarity and is assigned a Middle Pleistocene age on the basis of stratigraphic position, geomorphic setting, and isotopic ages of 0.713 ± 0.12 Ma ($^{40}Ar/^{39}Ar$; whole rock; sample 00OLe-5 [369J]) and 0.718 ± 0.43 Ma (K-Ar; whole rock; sample 00OLe-5 [369J]) (**Figure 5-16**, **Figure 5-23**, **Figure 6-1**; **Table 5-3**; plate; appendix; J. Donnelly-Nolan and M. Lanphere, unpub. data, 2008). Equivalent to the informally named large feldspar basalt, map unit Qbn4 of Sherrod and others (2004).

Qbn6 **very fine grained basalt (Middle Pleistocene)—**Basaltic andesite lava flow (SiO_2 = 52.70 weight percent; Al_2O_3 = 16.00 weight percent; K_2O = 0.77 weight precent; *n* = 1 analysis) mapped as a narrow, north-south trending outcrop belt west of Powell Buttes in the western part of the lower Crooked River basin (**Figure 5-16**, **Figure 5-19**; **Table 6-1**; plate; appendix; J. Donnelly-Nolan, written commun., 2008). The surface of the lava flow is very irregular. Thickness of unit **Qbn6** is unknown. Typical hand samples are dark gray (N3) to black (N2) and aphyric with a very fine-grained, diktytaxitic, holocrystalline groundmass of plagioclase and intergranular olivine.

Unit **Qbn6** has normal magnetic polarity and is assigned a Middle Pleistocene age on the basis of stratigraphic position and geomorphic setting (**Figure 5-23**, **Figure 6-1**; plate; appendix; J. Donnelly-Nolan, written commun., 2008). Equivalent to the informally named very fine grained basalt, map unit Qbn6 of Sherrod and others (2004).

6.3.2 Quaternary intracanyon basalt

Qbi **basalt of The Island (lower Pleistocene)—**Intracanyon high-alumina basalt lava flows (SiO_2 = 49.28 to 49.59 weight percent; Al_2O_3 = 16.99 to 17.04 weight percent; K_2O = 0.35 to 0.39 weight percent; *n* = 2 analyses) mapped in the Crooked River canyon west of Juniper Butte, from Crooked River Ranch to 4.5 km (2.8 mi) north of the contemporary confluence with the Deschutes River (**Figure 5-16**, **Figure 5-19**, **Figure 6-7**, **Figure 6-8**; **Table 6-1**; plate; appendix; J. Donnelly-Nolan, written commun., 2008). The unit is named for exposures on The Island, a prominent mesa in the vicinity of Cove Palisades State Park in the northwest corner of the lower Crooked River basin (**Figure 6-8**; plate; Ferns and others, 1996). Unit **Qbi** is as thick as 170 m (558 ft) and consists of a flow-on-flow succession of lava flows characterized by prominent columnar joint sets. Locally, the unit (**Qbi**) consists of a single cooling unit marked by thick upper and lower colonnades separated by a thick interior entablature. Pillow basalt and hyaloclastite breccia are intermittently exposed along the lava flow margins. Typical hand samples are medium light gray (N6) to dark gray (N3) and olivine-phyric, containing 1 to 3 percent (vol.) fresh iridescent, moderate yellow green (5GY 7/4) olivine microphenocrysts and phenocrysts ≤2 mm (0.08 in), distributed within a fine-grained, diktytaxitic, holocrystalline groundmass of plagioclase, intergranular olivine, and ophitic clinopyroxene.

The basalt of The Island (**Qbi**) has reversed magnetic polarity but is otherwise chemically and texturally indistinguishable from overlying, normal polarity Newberry lavas (**Qbnc**) and the underlying, normal polarity, basalt of Opal Springs (**Tdbo**) (**Figure 5-23**). The unit (**Qbi**) is assigned an early Pleistocene age on the basis of stratigraphic position and an $^{40}Ar/^{39}Ar$ age of 1.19 ± 0.08 Ma (whole rock; sample D4) obtained near Crooked River Ranch (**Figure 5-16**, **Figure 5-23**, **Figure 6-1**; **Table 5-3**; plate; appendix; Smith, 1986a, b).

The vent area for the basalt of The Island (**Qbi**) is presumed to be located to the south, at or near Newberry Volcano (e.g., Peterson and others, 1976; Smith, 1986a, b; 1986; Dill, 1992). However, these lava flows cannot be mapped further south than Crooked River Ranch (**Figure 5-16**; plate). The source of unit **Qbi** lava flows may therefore be: 1) buried by younger, normal polarity flows of Newberry Volcano upstream; or 2) alternatively, these flows were erupted from yet undiscovered source vents in the Crooked River canyon or areas north of the lower Crooked River basin (Sherrod and others, 2004). Ferns and others (1996) note that bench-forming flow surfaces on the basalt of The Island (**Qbi**) along the Crooked River canyon remain at a constant 730 m (2,400 ft) elevation along the length of their exposure (Dill, 1992; Ferns and others, 1996). The constant flow surface elevation would be consistent with lava flows backing up (south) into the Crooked River Gorge from vents north of the north of the lower Crooked River basin or from vents within the canyon itself (Sherrod and others, 2004). North-descending flow surfaces along the outcrop extent would be expected for lava flows traveling downstream from vents located to the south.

Figure 6-8. Upper Miocene Deschutes Formation and younger intracanyon basalt of The Island (Qbi) cropping out on The Island at Cove Palisades State Park. The view is looking west across the Crooked River arm of Lake Billy Chinook from SW Jordan Road (44.545583, -121.262195). Photo credit: Jason McClaughry, 2011.

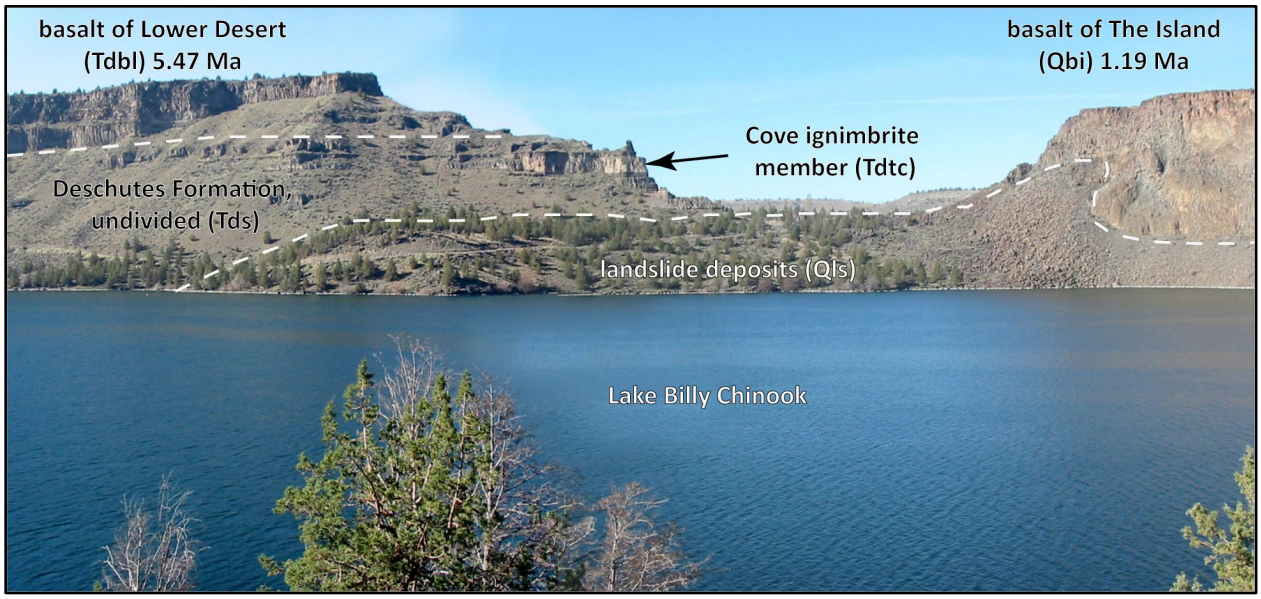

6.3.3 Quaternary or upper Pliocene sedimentary rocks

QTsg **sedimentary rocks (lower Pleistocene or upper Pliocene)—**Moderately cemented to poorly consolidated, moderate brown (5YR 3/4), massive, pebble-rich sandstone, medium dark gray (N4) to dark gray (N3), plane-parallel to trough cross-stratified sandstone, and well-sorted pebble to cobble conglomerate (**Figure 6-9**). Unit **QTsg** is mapped as an elevated terrace around the north and east slopes of Barnes Butte (plate). These rocks unconformably overlie the intracaldera unit of the tuff of Smith Rock (**Tjtsi**) and in turn are locally onlapped by Holocene landslide deposits (**Qls**) 1.6 km (1 mi) west of Ochoco Dam (plate). Unconsolidated fluviatile terrace deposits of unit **Qto** are inset into unit **QTsg** between McKay Creek and Prineville (plate). Thickness of unit **QTsg** is as thick as 55 m (180 ft), on the basis of water well logs. Unit **QTsg** is assigned a late Pliocene or early Pleistocene age on the basis of stratigraphic position (**Figure 6-1**; plate).

Figure 6-9. Planar to cross-stratified sandstone and pebbly sandstone (QTsg) cropping out east of Barnes Butte along NE Wainright Road (44.319699, -120.783414). Hammer for scale is 40 cm (15.7 in) long. Photo credit: Jason McClaughry, 2005.

Disconformity

6.3.4 Lower Pliocene and upper Miocene volcanic and sedimentary rocks of the early High Cascades

6.3.4.1 Deschutes Formation

Tdsg **sand and gravel (Pliocene and upper Miocene)—**Unconsolidated to partially consolidated fluviatile sand and gravel mapped mantling upper Miocene and Pliocene plateau-forming basalts of the Deschutes Formation and fringing Oligocene and older strata in the western part of the lower Crooked River basin (**Figure 5-16**, **Figure 6-10**; plate). Unit **Tdsg** is mapped up to an elevation of about 1,098 m (3,600 ft) on the southeast flanks of Powell Buttes, 1,189 m (3,900 ft) along Juniper Canyon, and up to a maximum elevation of ~1,128 m (3,700 ft) fringing Grizzly Mountain (**Figure 5-16**; plate). The sand component is generally fine to medium grained, well sorted, and consists of ~70 percent (vol.) angular to subround grains of clear feldspar, ~15 percent (vol.) amphibole, ~10 percent (vol.) pumice fragments, ~3 percent (vol.) quartz, and ~2 percent (vol.) magnetite. The gravel component is generally moderately sorted, consisting of subround to well-rounded, cobble-sized, locally imbricated (where partially cemented) clasts of basalt and rhyolite. Thickness of unit **Tdsg** is ≤25 m (82 ft). Unit **Tdsg** is assigned a late Miocene and Pliocene age on the basis of stratigraphic position (**Figure 5-16**, **Figure 6-1**, **Figure 6-10**; plate). Sand and gravel deposits (**Tdsg**) mantle basaltic lava flows as young as the 3.36 Ma basalt of Combs Flat (**Tdbc**), but elsewhere sit directly on lava flows of late Miocene age.

Tds **sedimentary rocks and tuff (Pliocene and upper Miocene)—**Chiefly partially consolidated volcaniclastic conglomerate, pebbly sandstone, tuffaceous sandstone, lapilli tuff, and matrix- to clast-supported boulder conglomerate and breccia (**Figure 5-16**, **Figure 6-11**, **Figure 6-12**, **Figure 6-13**; plate). Stratigraphic sections of unit **Tds** are laterally discontinuous, interfinger with Deschutes Formation lava flows and ash-flow tuff beds, and are commonly poorly exposed weathering to form soil-mantled hillslopes (**Figure 6-11**). Sedimentary beds are characterized by cut and fill channel-forms with erosional surfaces that bound discrete depositional successions (**Figure 6-13**; Smith, 1991). Well-exposed stratigraphic sections of unit **Tds** cropping out beneath Ochoco Wayside State Park are as thick as 60 m (200 ft); sections are as thick as 220 m (720 ft) in the northwest part of the mapped area (**Figure 5-16**; plate). Unit **Tds** is assigned a late Miocene and Pliocene age on the basis of stratigraphic position and isotopic ages from bracketing lava flows and ash-flow tuffs (**Figure 5-16**, **Figure 5-23**, **Figure 6-1**; **Table 5-3**; plate).

Figure 6-10. Examples of plateau mantling sand and gravel (Tdsg). (a) Clast-supported cobble gravel mapped above the basalt of Combs Flat (Tdbc) (44.284056, -120.782806). (b) Massive sand deposits exposed in a borrow pit east of Juniper Canyon (44.259111, -120.804892). Person for scale in both photographs is 1.9 m (6.2 ft) tall. Photo credits: Jason McClaughry, 2005.

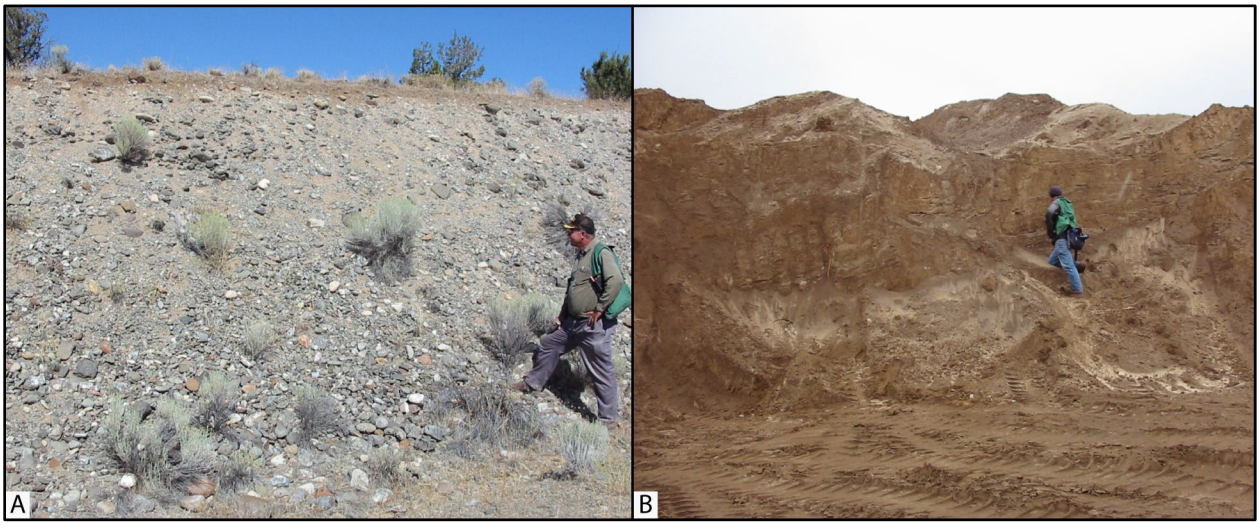

Figure 6-11. Deschutes Formation lavas overlying sedimentary rocks of unit Tds south of Prineville (44.285395, -120.827824). Small shield volcanoes (Tdv) that form Grass Butte and Meyers Butte are visible on the skyline. The X marks the location of a pillow delta forming the lower part of the basalt of Rocky Canyon (Tdbrc). View is looking west. Photo credit: Jason McClaughry, 2005.

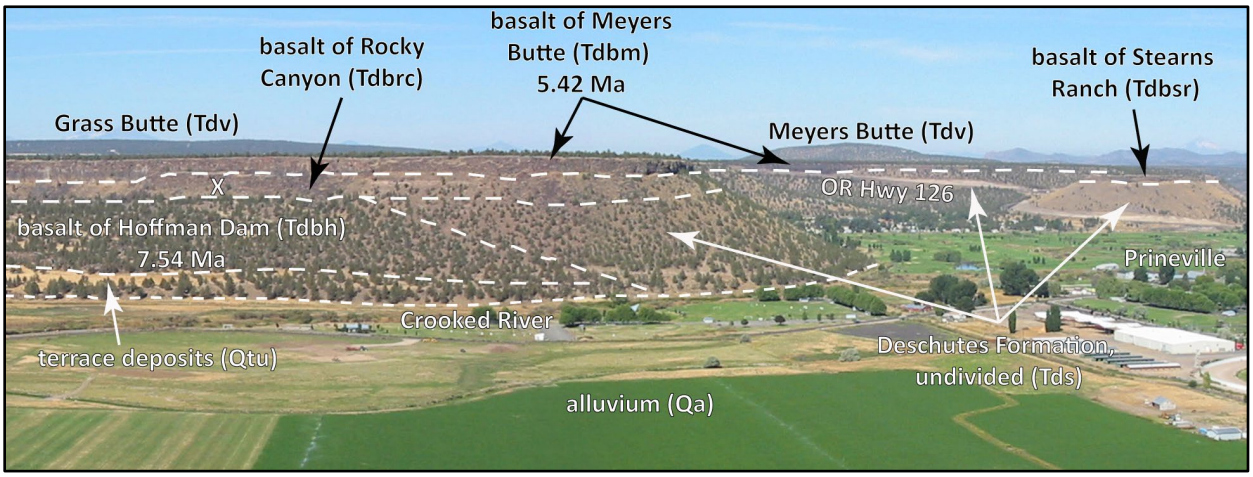

Figure 6-12. Outcrop of the 3.36 Ma basalt of Combs Flat (Tdbc) overlying clast-supported cobble conglomerate of unit Tds in the Deschutes Formation (44.280963, -120.771156). Dashed white line marks the contact. Person for scale is 1.8 m (5.8 ft) tall. Photo credit: Mark Ferns, 2005.

Figure 6-13. Examples of the Deschutes Formation (Tds) in the lower Crooked River basin. (a) The basalt of Rocky Canyon (Tdbrc) overlying massive tuffaceous sandstone and cross-stratified sandstone of unit Tds (44.276652, -120.858778). The upper part of unit Tds sandstone is here characterized by a 10 to 15 cm (3.9 to 5.9 in) thick, red-colored baked zone where it is in contact with the overlying lava flow. Dashed white line marks the contact. Arrow points to 40-cm-long (15.7 in) hammer for scale in the lower right part of the photograph. (b) Close-up photograph of the sedimentary unit outlined by the white rectangle in A. The sandstone is characterized by well-defined current-ripple cross laminae. The cross laminae are inclined to the left (south) in the photograph indicating local transport from north to south (right to left in the photograph). Orange pencil for scale is 17 cm (6.7 in) long. Photo credit: Jason McClaughry, 2005.

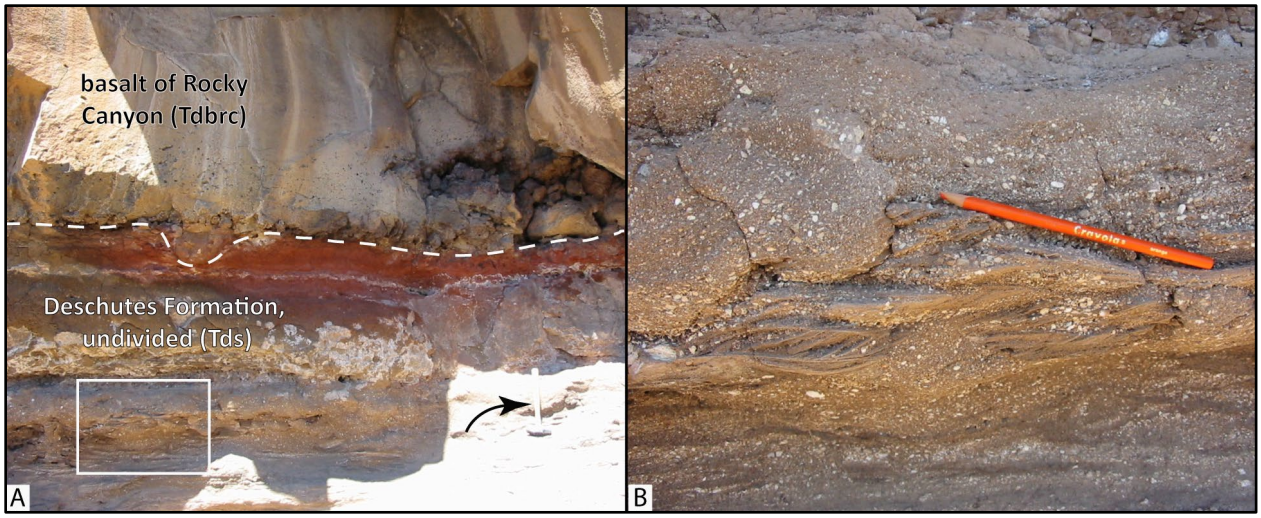

6.3.4.2 Bowman volcanic field

Tdbx **basalt of Alfalfa (upper Pliocene)—**High-alumina basalt lava flow (SiO_2 = 49.3 to 49.4 weight percent; Al_2O_3 = 16.60 to 17.50 weight percent; K_2O = 0.36 to 0.41 weight percent; *n* = 2 analyses) mapped along Dry River, west of Powell Buttes (**Figure 5-16**; **Figure 5-22**, **Table 6-2**; plate; appendix; J. Donnelly-Nolan, written commun., 2008). Unit **Tdbx** weathers to a boulder-covered surface mantled by thin deposits of sand. A slight hematite alteration of olivine and magnetite commonly occurs on weathered surfaces. Thickness of unit **Tdbx** is at least 15 m (50 ft) along Dry River (plate). Typical hand samples are medium light gray (N6) to dark gray (N3), vesicular, and olivine-phyric, containing ≤2 percent (vol.) moderate yellow green (5GY 7/4) olivine phenocrysts ≤2 mm (0.1 in) across and ≤3 percent (vol.) plagioclase and olivine microphenocrysts ≤1 mm (0.04 in), distributed within a fine-grained, locally diktytaxitic, holocrystalline groundmass of plagioclase and intergranular olivine.

The basalt of Alfalfa (**Tdbx**) has normal magnetic polarity and is assigned a late Pliocene age on the basis of stratigraphic position above the basaltic andesite of Dry River (**Tdbd**) and a K-Ar age of 3.31 ± 0.15 Ma (whole rock; sample 00Ole-8 [389J]) determined for a sample from an outcrop west of Powell Buttes (**Figure 5-16**, **Figure 5-23**, **Figure 6-1**; **Table 5-3**; plate; appendix; J. Donnelly-Nolan and M. Lanphere, unpub. data, 2008). Referred to as the basalt near Alfalfa (unit Qbn5) by Sherrod and others (2004).

Table 6-2. Select XRF geochemical analyses for lava flows in the late Deschutes Formation in the lower Crooked River basin.

Sample	196J[1]	66 LCJ 06[2]	136P05[2]	RC03-9[3]
Geographic Area	Dry River	Crooked River Ranch	Combs Flat	Redmond
Formation	Deschutes Formation	Deschutes Formation	Deschutes Formation	Deschutes Formation
Map Unit	Tdbx	Tdbsr	Tdbc	Tdbr
UTM N (NAD 83)	4893550	4894674	4906025	4911057
UTM E (NAD 83)	653554	670660	676122	646205
Age (Ma)	~3.31 Ma	nd	~3.36 Ma	~3.56 Ma
Map Label	G74	G91	G186	G242
Oxides, weight percent				
SiO_2	49.30	49.59	49.65	48.25
Al_2O_3	17.50	17.16	15.86	15.97
TiO_2	1.48	1.48	1.23	1.67
FeOTotal	9.70	11.10	9.33	11.51
MnO	0.17	0.20	0.17	0.20
CaO	10.21	9.59	11.47	9.83
MgO	7.78	7.04	8.98	8.99
K_2O	0.36	0.48	0.75	0.37
Na_2O	3.20	3.03	2.25	2.88
P_2O_5	0.30	0.34	0.31	0.33
LOI	nd	1.23	0.92	0.30
Total_I	nd	100.04	99.75	99.70
Trace Elements, parts per million				
Ni	79	102	168	192
Cr	nd	106	399	343
Sc	nd	29	32	36
V	nd	259	238	270
Ba	201	313	527	216
Rb	5	8	11	5
Sr	335	338	768	239
Zr	118	97	101	106
Y	27	31	23	34
Nb	9	6	8	5
Ga	nd	21	16	18
Cu	nd	97	65	77
Zn	76	87	67	96
Pb	nd	4	3	2
La	nd	11	18	5
Ce	nd	21	41	17
Th	nd	nd	2	nd
Nd	nd	1	nd	nd
U	nd	46	47	nd

Major element determinations have been normalized to a 100-percent total on a volatile-free basis and recalculated with total iron expressed as FeOTotal; nd - no data or element not analyzed; na - not applicable or no information. LOI, Loss on Ignition; Total_I, original analytical total. Data from: [1]J.M. Donnely-Nolan, written commun. (2008); [2]McClaughry and Ferns (2007d); [3]R.M. Conrey, written commun. (2007).

Tdbsr **basalt of Stearns Ranch (upper Pliocene)—**Basalt lava flow (SiO_2 = 48.60 to 49.38 weight percent; Al_2O_3 = 15.54 to 16.55 weight percent; K_2O = 0.33 to 0.55 weight percent; *n* = 6 analyses) mapped capping a northwest-southeast trending plateau south of Dry Creek, between Prineville Reservoir and the Crooked River (**Figure 5-16**, **Figure 5-22**, **Figure 6-14**; **Table 6-2**; plate; appendix). The lava flow also crops out as prominent rimrock along the east side of the Crooked River, north to Ochoco Wayside State Park (**Figure 5-16**, **Figure 6-11**, **Figure 6-15**; plate). Unit **Tdbsr** is made up of two texturally indistinguishable flow lobes defined by subtle chemical differences and geographic location (**Figure 5-22**; **Table 6-2**; appendix). An early-phase, farther traveled flow sequence, contains less aluminum (Al_2O_3 = 15.54 to 15.68 weight percent), strontium (Sr = 343 to 356 ppm), and niobium (Nb = 6.6 to 7.5 ppm), and higher iron (FeOTotal = 12.12 to 12.21 weight percent) and magnesium (MgO = 8.15 to 8.34 weight percent) (**Figure 5-22**; plate). A younger, near-vent phase contains relatively higher amounts of aluminum (Al_2O_3 = 16.29 to 16.55 weight percent), strontium (Sr = 529 to 705 ppm), and niobium (Nb = 10.3 to 11.7 ppm), and less iron (FeOTotal = 11.16 to 11.42 weight percent) and magnesium (MgO = 6.73 to 7.63 weight percent) (**Figure 5-22**; plate). Unit **Tdbsr** is characterized by a hummocky flow surface. Cliff-forming outcrops are massive or are marked by columnar-jointing and interlayered vesicular zones. Vesicles are commonly filled by either botryoidal-shaped masses of opaline quartz or white (N9) to pinkish gray (5YR 8/1), branch-shaped zeolite. Maximum thickness of unit **Tdbsr** is ~24 m (80 ft) west of Stearns Butte (**Figure 5-16**; plate). Typical hand samples are medium light gray (N6) to dark gray (N3), vesicular, and olivine-, clinopyroxene- and plagioclase-microphyric, containing ≤2 percent (vol.) moderate brown (5YR 3/4), subhedral, equant, iddingsite-rimmed olivine and clinopyroxene microphenocrysts ≤1 mm (0.04 in) across and anhedral plagioclase laths ≤1 mm (0.04 in) long, distributed within a fine- to medium-grained, diktytaxitic, holocrystalline groundmass of equigranular plagioclase laths and intergranular olivine. Microphenocrysts are enclosed in poikilophitic to subophitic orthopyroxene and clinopyroxene.

The basalt of Stearns Ranch (**Tdbsr**) has normal magnetic polarity and is assigned a late Pliocene age on the basis of stratigraphic position, inset into the 3.36 Ma basalt of Combs Flat (**Tdbc**) south of Prineville (**Figure 5-16**, **Figure 5-23**, **Figure 6-1**; plate). The Stearns Ranch lava flow (**Tdbsr**) was erupted from an extant vent complex located at the head of Devils Canyon in the southern part of the lower Crooked River basin. Lava flows flowed west-northwest down a paleochannel incised into the underlying Prineville Basalt (**Tcpb**) (**Figure 5-16**, **Figure 6-15**; plate).

Tdbc **basalt of Combs Flat (upper Pliocene)—**Basalt lava flow (SiO_2 = 49.65 to 50.38 weight percent; Al_2O_3 = 15.86 to 17.79 weight percent; K_2O = 0.41 to 0.75 weight percent; *n* = 3 analyses) mapped capping an east-west elongated plateau, southeast of the city of Prineville (**Figure 5-16**, **Figure 5-22**, **Figure 6-15**; **Table 6-2**; plate; appendix). Unit **Tdbc** is characterized by an irregular upper flow surface capped by tumuli, residual depressions, and pressure ridges. The lower parts of individual lava flow lobes are marked by flow breccia. The maximum thickness of unit **Tdbc** is ~30 m (100 ft) south of Ochoco Creek (**Figure 5-16**, plate). Typical hand samples are medium light gray (N6) to dark gray (N3), vesicular, and plagioclase- and olivine-phyric, containing ≤2 percent (vol.) clear, euhedral, lath-shaped plagioclase microphenocrysts ≤1 mm (0.04 in) across and ≤2 percent (vol.) moderate brown (5YR 3/4), subhedral, equant, iddingsite-rimmed olivine phenocrysts ≤2 mm (0.1 in) across, distributed within a holocrystalline groundmass of plagioclase, intergranular olivine, and ophitic to subophitic clinopyroxene.

The basalt of Combs Flat (**Tdbc**) has reversed magnetic polarity and is assigned a late Pliocene age on the basis of a K-Ar age of 3.36 ± 0.08 Ma (whole rock; sample CF1; Smith, 1986a, b) determined for a sample obtained at the east end of Combs Flat (**Figure 5-16**, **Figure 5-23**, **Figure 6-1**; **Table 5-3**; plate; appendix). Lava flows were erupted from an extant vent complex located at the east end of Combs Flat and flowed west down a paleochannel incised into an irregular surface of older strata (**Figure 5-16**, **Figure 6-15**; plate).

Figure 6-14. Deschutes Formation basaltic lava flows cropping out near Hoffman Dam, south of Prineville (44.150892, -120.821358). View is looking to the north-northwest. The 8.76 Ma basalt of Quail Valley Ranch (Tdbq) is the oldest Deschutes-age lava flow mapped in the lower Crooked River basin. Photo credit: Jason McClaughry, 2006.

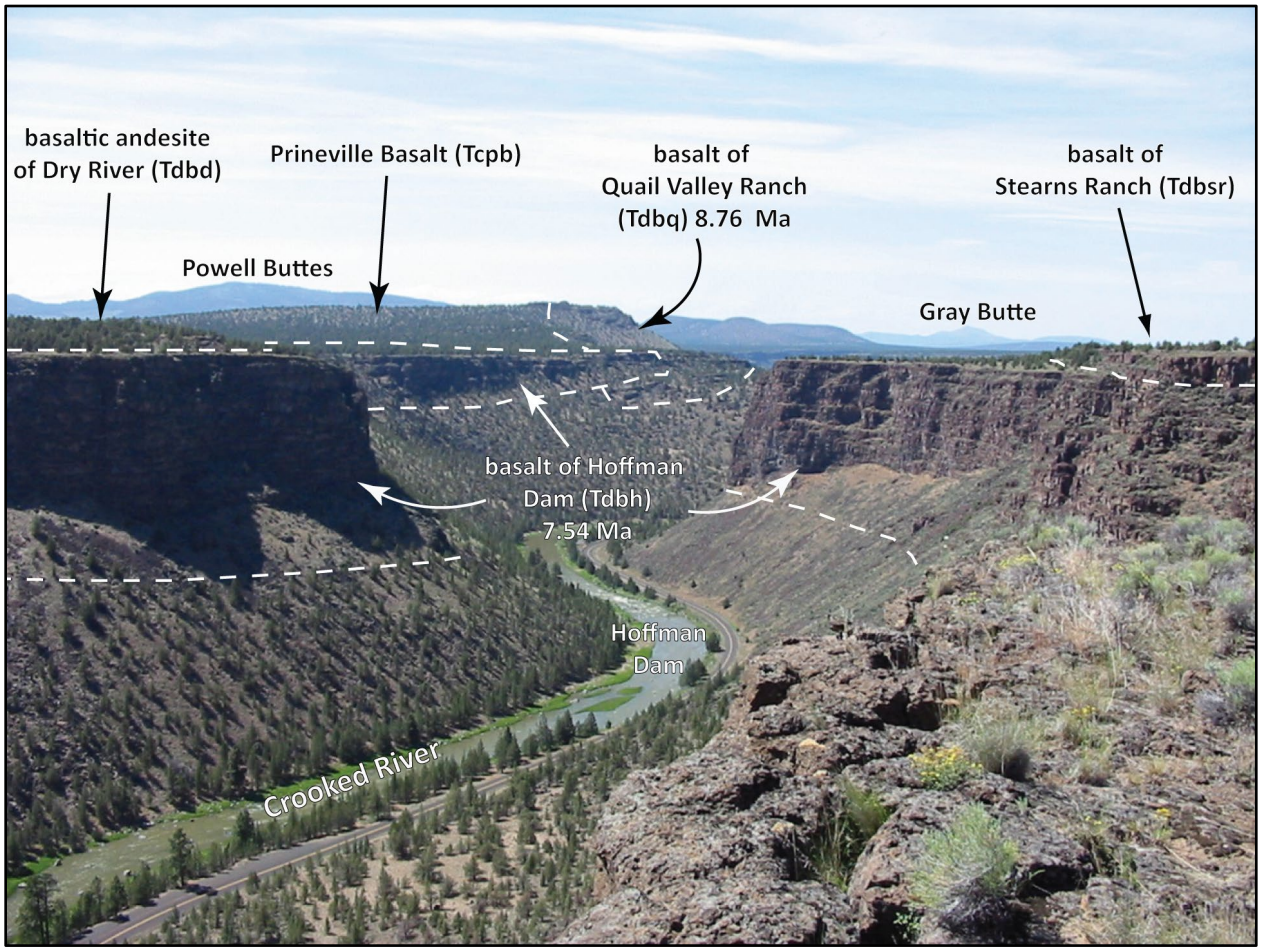

Figure 6-15. Topographically inverted Deschutes Formation lava flows trace the course of ancestral channels of the Crooked River. The high skyline on the east is underlain by Prineville Basalt (Tcpb). Photograph is looking southeast from Ochoco Wayside State Park (44.300434, -120.864134). Photo credit: Jason McClaughry, 2005.

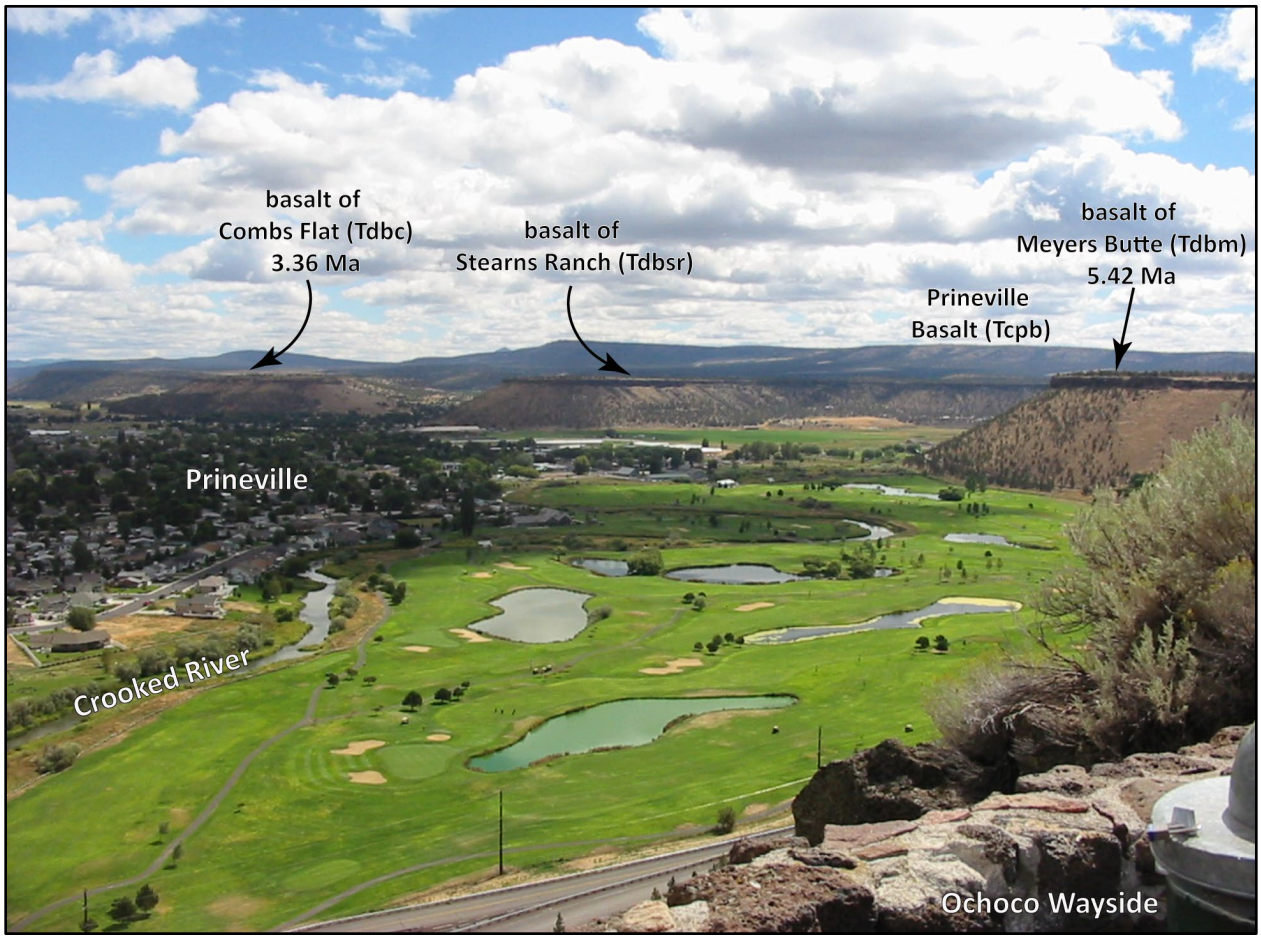

Tdbr **basalt of Redmond (upper Pliocene)—**Basalt lava flow (SiO_2 = 48.01 to 49.53 weight percent; Al_2O_3 = 15.97 to 17.13 weight percent; K_2O = 0.34 to 0.46 weight percent; *n* = 7 analyses) mapped across a broad plain between Redmond and Terrebonne, in the western part of the lower Crooked River basin (**Figure 5-16**, **Figure 5-22**, **Figure 6-16**; **Table 6-2**; plate; appendix). The lava flow (**Tdbr**) is also exposed along Dry River, west of Powell Buttes (plate). Unit **Tdbr** typically consists of one lava flow as thick as 8 to 15 m (26.2 to 49.2 ft). Typical hand samples are medium light gray (N6) to dark gray (N3) and vesicular, containing 5 to 10 percent (vol.) clear, euhedral, lath-shaped plagioclase and moderate yellow green (5GY 7/4) olivine phenocrysts ≤2 mm (0.1 in) across, distributed within a medium- to coarse-grained, diktytaxitic, holocrystalline groundmass.

The basalt of Redmond (**Tdbr**) has normal magnetic polarity and is assigned a late Pliocene age on the basis of stratigraphic position and an $^{40}Ar/^{39}Ar$ plateau age of 3.56 ± 0.30 Ma (whole rock; sample D3a; Smith, 1986a, b) determined for a sample obtained northwest of Terrebonne (**Figure 5-16**, **Figure 5-23**, **Figure 6-1**; **Table 5-3**; plate; appendix). The lava flow (**Tdbr)** underlies the 3.31 Ma basalt of Alfalfa (**Tdbx**) and overlies the basaltic andesite of Dry River (**Tdbd**) along Dry River, west of Powell Buttes (plate). Unit **Tdbr** is in part equivalent to the "Redmond flow" (unit Tmbr) of Robinson and Stensland (1979) who considered the lava equivalent to the Deschutes Formation; it is also equivalent to the basalt of Redmond (unit Tbr) of Sherrod and others (2004), who following the work of Smith (1986a), considered the lava to be a separate unit overlying the Deschutes Formation. We map the basalt of Redmond (**Tdbr**) here as part of the Deschutes Formation on the basis of composition, age, and stratigraphic relations with other Deschutes Formation lava flows (**Figure 6-1**; plate)

Figure 6-16. Columnar-jointed outcrop of the basalt of Redmond (Tbdr) along NE Smith Rock Way, east of Terrebonne (44.348644, -121.169747). Photo credit: Jason McClaughry, 2008.

Tdbrb **basalt of Round Butte (lower Pliocene)—**Basalt lava flow (SiO_2 = 49.54 to 49.80 weight percent; Al_2O_3 = 14.36 to 15.39 weight percent; K_2O = 0.68 weight percent; Sr = 717 to 795 ppm; *n* = 2 analyses) mapped capping Round Butte on the north side of the Crooked River, 9.5 km (6 mi) northwest of Prineville (**Figure 5-16**, **Figure 5-22**, **Figure 6-17**; **Table 6-3**; plate; appendix). The cliff-forming, butte-capping lava flow (**Tdbrb**) is columnar- to platy-jointed. Stretched vesicles are locally abundant near the exposed base of unit **Tdbrb**. Cliff faces are commonly segmented by tension cracks that have historically failed forming landslide deposits (**Qls**) that mantle the east slopes of Round Butte (plate). The maximum thickness of unit **Tdbrb** is 37 m (120 ft) (plate). Typical hand samples are medium light gray (N6) to dark gray (N3) and vesicular, containing sparse moderate yellow green (5GY 7/4) olivine phenocrysts ≤2 mm (0.1 in) across, distributed within a fine-grained, diktytaxitic, holocrystalline groundmass.

The basalt of Round Butte (**Tdbrb**) has reversed magnetic polarity and is assigned an early Pliocene age on the basis of stratigraphic position and geomorphic setting (**Figure 6-1**; plate; appendix). Round Butte lava flows (**Tdbrb**) were erupted from a series of N.20°W.-striking dikes and an eroded cinder cone forming the central part of Round Butte (**Figure 5-16**, **Figure 6-17a-b**; plate). The reader should note that Round Butte in the lower Crooked River basin discussed here is not to be confused with the larger, more widely known shield volcano that is the namesake of Round Butte Dam in Jefferson County, near the confluence of the Crooked and Deschutes Rivers (**Figure 5-21**).

Figure 6-17. Basalt of Round Butte (Tdbrb) in the lower Crooked River basin. (a) Basalt of Round Butte (Tdbrb) and vent complex exposed at Round Butte in the lower Crooked River basin (44.331051, -120.926945). View in the photograph is looking northwest across the Prineville Valley (44.348857, -120.951770). (b) Photograph of feeder dike, eroded cinder cone, and lavas flows on Round Butte. View is looking north. Photo credit: Jason McClaughry, 2008.

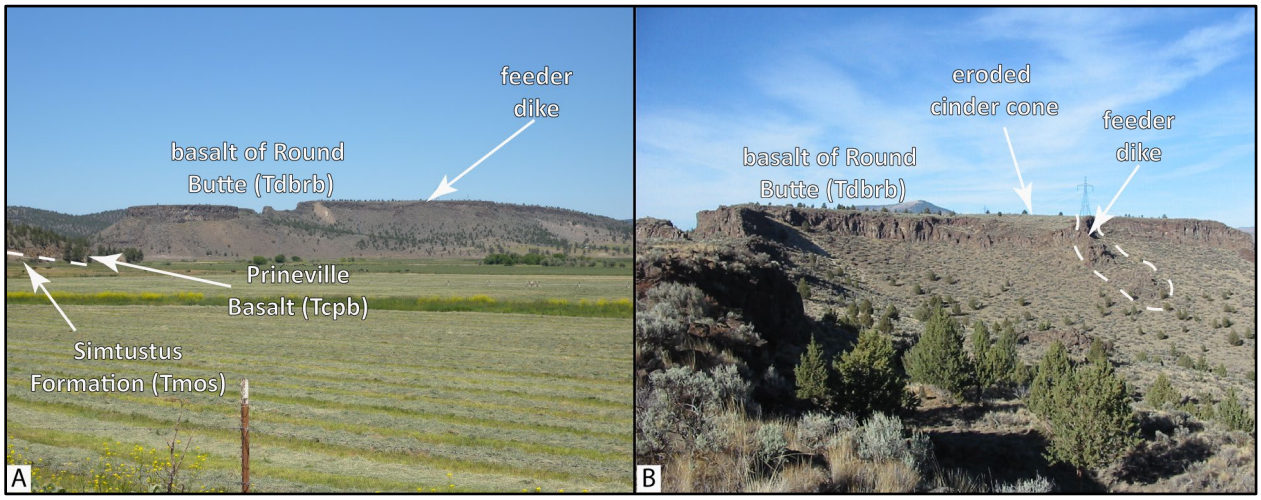

Table 6-3. Select XRF geochemical analyses for lava flows in the middle Deschutes Formation in the lower Crooked River basin.

Sample	517 LCJ 08	126 P 05[1]	SF-143b[2]	7.13VII.05[3]	RC03-40[4]	489 LCJ 08	03-PJ-05[1]	DP-1/CROO53265-210[5]	OC2c[2]	LITEA448460[6]	LITMR437478[6]	DT-184b[7]	7.31VIII.05[8]
Geographic Area	Round Butte	Japanese Creek	Crooked R. Gorge	Meyers Butte	Powell Butte Hwy.	Powell Butte Hwy.	Swartz Canyon	Prineville Airport	Crooked R. Gorge	Crooked R. Gorge	Powell Buttes	Willow Creek	Houston Lake
Formation	Deschutes	Deschutes	Deschutes	Deschutes	Deschutes	Deschutes	Deschutes	Deschutes	Deschutes	Deschutes	Deschutes	Deschutes	Deschutes
Map Unit	Tdbrb	Tdbj	Tdbt	Tdbm	Tdbd	Tdbd	Tdbd	Tdbd	Tdbo	Tdbo	Tdbo	Tdbw	Tdbrc
UTM N (NAD 83)	4912180	4912323	4926650	4909669	4909979	4896886	4889699	4904825	4921624	4917830	4893537	4929170	4904745
UTM E (NAD 83)	663380	660282	635804	665091	651823	654486	669475	666986	639863	639980	654769	661451	670709
Age (Ma)	nd	nd	~5.57 Ma	5.42 Ma	nd	nd	nd	nd	5.85 Ma	~5.85 Ma	~5.85 Ma	~6.3 Ma	nd
Map Label	G261	G265	G453	G227	G231	G100	G51	G163	G387	G323	G71	G499	G156
Oxides, weight percent													
SiO_2	49.80	50.87	52.06	49.86	52.24	53.29	53.25	52.47	49.11	50.21	48.44	50.93	51.42
Al_2O_3	15.39	15.84	13.66	17.06	16.39	16.42	16.15	16.20	15.84	17.58	17.55	17.92	16.82
TiO_2	1.78	1.65	2.67	1.46	1.52	1.43	1.59	1.57	1.52	0.97	0.99	1.14	1.55
FeOTotal	9.68	9.98	13.92	10.93	10.04	10.41	10.23	10.13	10.67	8.30	9.17	10.16	9.52
MnO	0.16	0.18	0.24	0.19	0.19	0.18	0.20	0.19	0.17	0.17	0.18	0.16	0.21
CaO	10.52	9.78	7.51	9.89	8.68	8.30	8.19	8.42	10.80	11.46	11.57	11.14	9.60
MgO	8.69	7.66	5.09	6.95	6.23	5.26	5.50	5.98	8.94	8.20	9.17	5.97	6.94
K_2O	0.68	0.79	0.62	0.41	0.96	1.06	1.07	1.11	0.29	0.39	0.24	0.28	0.62
Na_2O	2.78	2.79	3.69	2.93	3.43	3.24	3.36	3.58	2.51	2.59	2.51	2.70	2.96
P_2O_5	0.52	0.46	0.53	0.32	0.32	0.40	0.45	0.35	0.17	0.13	0.18	0.18	0.36
LOI	1.19	1.08	nd	1.02	1.86	1.58	1.15	0.28	nd	nd	0.01	0.36	0.83
Total_I	99.93	99.80	100.26	99.61	98.14	100.56	99.51	100.29	100.78	nd	nd	100.01	99.69
Trace Elements, parts per million													
Ni	149	133	38	113	90	70	64	76	nd	125	140	nd	90
Cr	342	255	nd	117	77	86	66	109	nd	209	198	nd	102
Sc	26	28	41	29	32	30	28	30	nd	35	42	nd	30
V	256	226	444	261	240	267	217	262	nd	250	238	nd	253
Ba	510	524	483	250	381	408	480	403	nd	137	125	nd	306
Rb	8.6	11	22	6	15	16	16	18	nd	6	1	nd	9
Sr	717	548	386	341	288	310	319	296	nd	268	230	nd	349
Zr	191	153	155	92	155	171	182	185	nd	73	70	nd	121
Y	28.2	34	38	30	40	45	45	42	nd	24	25	nd	34
Nb	9.1	12	nd	5	7	8	9	8	nd	5	4	nd	5.8
Ga	15.4	19	nd	20	19	19	21	18	nd	17	16	nd	21
Cu	41	54	nd	86	77	87	76	81	nd	94	85	nd	93
Zn	113	85	nd	85	96	107	93	92	nd	68	62	nd	90
Pb	1	2	nd	2	3	2	6	0	nd	5	0	nd	3
La	20	23	nd	11	16	17	18	13	nd	14	14	nd	12
Ce	55	48	nd	25	33	28	41	33	nd	5	20	nd	27
Th	1	2	nd	1	nd	1	2	3	nd	1	1	nd	1
Nd	0.5	1	nd	nd	nd	0	0	0	nd	nd	0	nd	0
U	39	43	nd	47	nd	0	0	0	nd	nd	nd	nd	0

Major element determinations have been normalized to a 100-percent total on a volatile-free basis and recalculated with total iron expressed as FeOTotal; nd - no data or element not analyzed; na - not applicable or no information. LOI, Loss on Ignition; Total_I, original analytical total. Data from: [1]Ferns and McClaughry (2006a); [2]Smith (1986a); [3]Ferns and McClaughry (2006b); [4]R.M. Conrey, written commun. (2007); [5]Dunbar and Perkins (2015); [6]Lite and Gannett (2002); [7]Thormahlen (1984); [8]McClaughry and Ferns (2006a).

Tdbj **basalt of Japanese Creek (lower Pliocene)—**Basalt lava flows (SiO_2 = 49.92 to 51.57 weight percent; Al_2O_3 = 15.26 to 16.15 weight percent; K_2O = 0.71 to 0.83 weight percent; Sr = 535 to 644 ppm; *n* = 10 analyses) mapped on both the north and south sides of the Crooked River, ~11 km (6.8 mi) northwest of Prineville (**Figure 5-16**, **Figure 5-22**, **Figure 6-18**; **Table 6-3**; plate; appendix). Unit **Tdbj** crops out as a flow-on-flow succession of lava flows characterized by columnar jointing (**Figure 6-18**). Upper flow surfaces are locally capped by tumuli and residual depressions. The maximum thickness of unit **Tdbj** is 52 m (170 ft) north of the Crooked River (**Figure 5-16**, **Figure 6-18**; plate). Subtle chemical differences in the succession suggest a lower part of the flow sequence with slightly lower contents of titanium (TiO_2 = 1.38 to 1.46 weight percent) and iron (FeOTotal = 9.29 to 9.58 weight percent) and higher contents of magnesium (MgO = 7.87 to 8.51 weight percent) and strontium (Sr = 644 ppm) (**Figure 5-22**; **Table 6-3**; appendix). The upper part of the flow succession has slightly higher contents of titanium (TiO_2 = 1.57 to 1.67 weight percent) and iron (FeOTotal = 9.70 to 10.41 weight percent) and lower contents of magnesium (MgO = 6.77 to 7.78 weight percent) and strontium (Sr = 535 to 548 ppm) (**Figure 5-22**; **Table 6-3**; appendix). Typical hand samples are medium light gray (N6) to dark gray (N3) and vesicular, containing ≤1 percent (vol.) moderate brown (5YR 3/4) subhedral, equant, iddingsite-rimmed olivine phenocrysts olivine microphenocrysts ≤1 mm (0.04 in), distributed within a fine-grained, diktytaxitic, holocrystalline groundmass of plagioclase and intergranular olivine.

The basalt of Japanese Creek (**Tdbj**) has normal magnetic polarity and is assigned an early Pliocene age on the basis of stratigraphic position above the 5.42 Ma basalt of Meyers Butte (**Tdbm**) (**Figure 6-1**; plate; appendix). Japanese Creek lava flows (**Tdbj**) were erupted from a 4-km-long (2.5 mi), N.20°W.-striking belt of extant cinder cone-capped vents and a series of N.20°W.-striking dikes (**Figure 5-16**, **Figure 6-18**; plate).

Figure 6-18. Flow-on-flow succession of the basalt of Japanese Creek (Tdbj) overlying the Prineville Basalt (Tcpb). The Prineville Basalt (Tcpb) and Japanese Creek lava flows (Tdbj) are crosscut by N.20°W.-striking dikes (center of photograph) and are capped by spatter vents. View looking northwest (44.345411, -120.989327). Photo credit: Jason McClaughry, 2005.

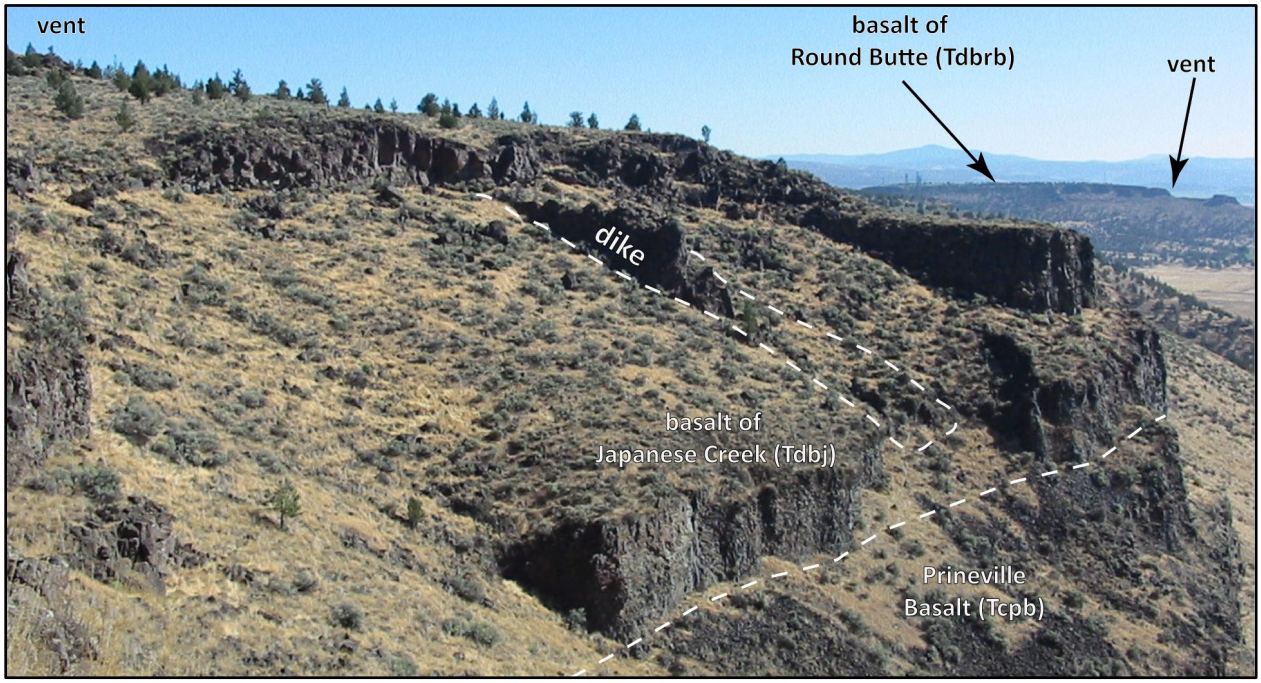

Tdbt **basalt of Tetherow Butte (lower Pliocene or upper Miocene)—**High-titanium basalt and basaltic andesite lava flows (SiO_2 = 50.79 to 52.78 weight percent; Al_2O_3 = 13.21 to 14.93 weight percent; TiO_2 = 2.39 to 2.91 weight percent; K_2O = 0.45 to 0.69 weight percent; Sr = 373 to 391 ppm; *n* = 12 analyses) mapped on both the east and west sides of the Crooked River canyon, north of Tetherow Butte (**Figure 5-16**, **Figure 5-22**, **Figure 6-6a**; **Table 6-3**; plate; appendix; Smith, 1986a, b). The maximum thickness of unit **Tdbt** is 30 m (100 ft) (plate). Typical hand samples are medium light gray (N6) to grayish black (N2) and aphyric to glomeroporphyritic, containing 1 to 2 percent (vol.) glomerocrysts of clear plagioclase and conspicuously zoned dusky green (5G 3/2) clinopyroxene ≤2 mm (0.1 in) across, distributed within a fine-grained, holohyaline groundmass of glass and Fe-Ti oxides. Olivine is rare.

The basalt of Tetherow Butte (**Tdbt**) has normal magnetic polarity and is assigned an early Pliocene or late Miocene age on the basis of an $^{40}Ar/^{39}Ar$ plateau age of 5.17 ± 0.03 Ma (groundmass; sample B-286; Pitcher and others, 2021) determined for a sample obtained north of the of the lower Crooked River basin, east of Warm Springs (**Figure 5-16**, **Figure 5-23**, **Figure 6-1**; **Table 5-3**; plate; appendix). The age published by Pitcher and others (2021) is younger than an $^{40}Ar/^{39}Ar$ plateau age of 5.31 ± 0.05 Ma (whole rock; sample D7) reported by Smith (1986a, b) and recalibrated to 5.57 ± 0.20 Ma by Pitcher (2017) for the Agency Plains flow of the basalt of Tetherow Butte (**Tdbt**). The younger 5.17 Ma date is a more likely age for the unit as the older dates of 5.31 and 5.57 Ma are incongruent with the normal magnetic polarity measured for the unit (**Tdbt**) and its correlation to the paleomagnetic time scale (**Figure 5-23**). Unit **Tdbt** was erupted from a 5-km-long (3.1 mi), N.35°W.-striking belt of extant cinder cone-capped vents forming Tetherow Butte along U.S. Highway 97 (**Figure 5-16**; plate; Smith, 1986a, b). The basalt of Tetherow Butte (**Tdbt**) includes both the Agency Plains and Crooked River basalt flows of Smith (1986a, b) and is correlative with to the Crooked River basalt flow (unit Tmbc) of Robinson and Stensland (1979). Equivalent to Tetherow Butte basalt flows (Tdbt) of Ferns and others (1996).

Tdbm **basalt of Meyers Butte (upper Miocene)—**High-alumina basalt lava flow (SiO_2 = 47.67 to 50.82 weight percent; Al_2O_3 = 16.43 to 17.36 weight percent; K_2O = 0.36 to 0.67 weight percent; Sr = 336 to 350 ppm; *n* = 13 analyses) mapped along the west side of the Crooked River canyon, between the mouth of Dry Creek and Meyers Butte (**Figure 5-16**, **Figure 5-22**, **Figure 6-11**, **Figure 6-15**, **Figure 6-19**; **Table 6-3**; plate; appendix; McClaughry and Ferns, 2006a; Ferns and McClaughry, 2006a). The basalt of Meyers Butte (**Tdbm**) crops out as rimrock-forming cliffs characterized by a massive outcrop habit or columnar jointing (**Figure 6-19**). Upper flow surfaces are capped by tumuli and residual depressions. Cliff exposures locally reveal partially collapsed lava tubes as wide as 2 m (6.5 ft) and vesicle cylinders as wide as 3 cm (1.2 in). The maximum thickness of unit **Tdbm** is 35 m (115 ft), north of Meyers Butte (plate). Typical hand samples are medium light gray (N6) to dark gray (N3), vesicular, and olivine-microporphyritic, containing ≤1 percent (vol.) moderate brown (5YR 3/4), anhedral to subhedral, subequant, iddingsite-rimmed olivine microphenocrysts ≤1 mm (0.4 in), distributed within a fine-grained, moderately trachytic, diktytaxitic, holocrystalline groundmass of equigranular plagioclase laths, intergranular olivine, and subophitic clinopyroxene.

The basalt of Meyers Butte (**Tdbm**) has reversed magnetic polarity and is assigned a late Miocene age on the basis of an $^{40}Ar/^{39}Ar$ plateau age of 5.42 ± 0.11 Ma determined for a sample obtained north of Meyers Butte (whole rock; sample 7.13VII.05; Ferns and McClaughry, 2006a) (**Figure 5-16**, **Figure 5-23**, **Figure 6-1**; **Table 5-3**; plate; appendix). The Meyers Butte lava flow

(**Tdbm**) was erupted from an extant vent forming Meyers Butte, west of Prineville (**Figure 5-16**, **Figure 6-20**; plate).

Figure 6-19. Deschutes Formation lava flows interbedded with the Rattlesnake Tuff (Tmtr) south of Prineville. Arrow shows the direction of flow of the Crooked Rivre. View is looking northwest (44.213481, -120.876729). Photo credit: Jason McClaughry, 2005.

Figure 6-20. Deschutes Formation mafic vents at Grass Butte and Meyers Butte and flanking lava flows. View is looking northeast from Powell Buttes (44.218561, -120.963675). Photo credit: Jason McClaughry, 2005.

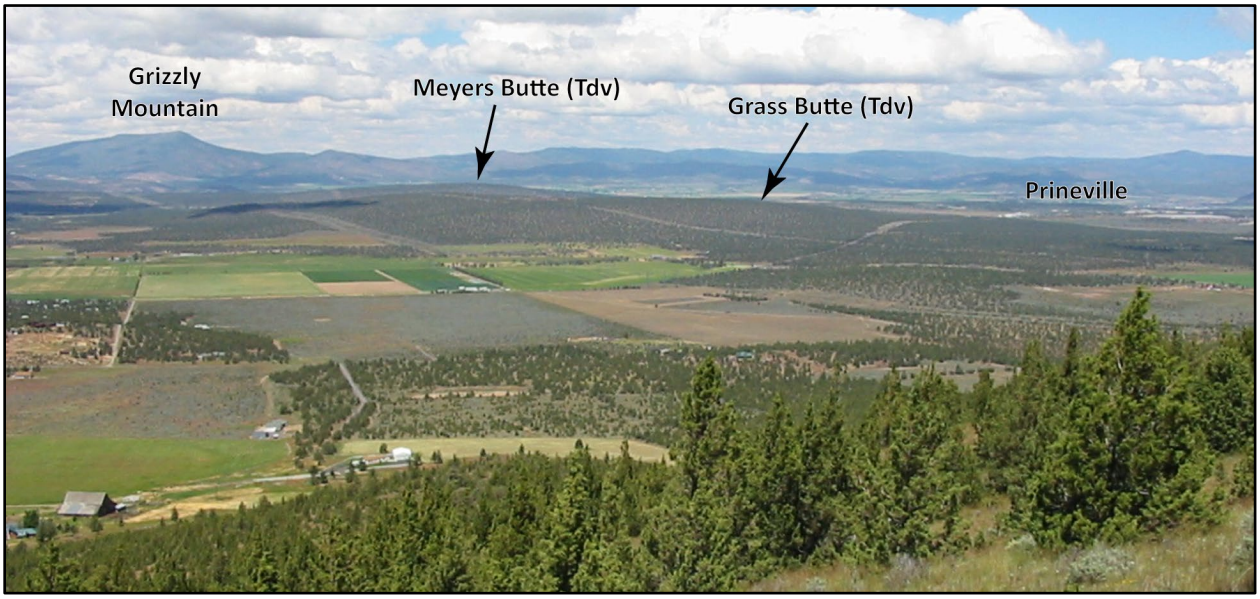

Tdbd **basaltic andesite of Dry River (upper Miocene)—**Basaltic andesite lava flow (SiO_2 = 51.87 to 53.29 weight percent; Al_2O_3 = 16.15 to 16.66 weight percent; K_2O = 0.9 to 1.07 weight percent; Sr = 284 to 334 ppm; *n* = 7 analyses) mapped across a broad plain in the southwestern part of the lower Crooked River basin (**Figure 5-16**, **Figure 5-22**, **Figure 6-14**, **Figure 6-21**; **Table 6-3**; plate; appendix). To the south of the map area, the basaltic andesite of Dry River (**Tdbd**) forms a broad hummocky flow surface reaching nearly to Alfalfa and Horse Butte (**Figure 1-1**, **Figure 5-21**). North into the lower Crooked River basin, lava flow lobes of the basaltic andesite of Dry River (**Tdbd**) bifurcate and are mapped around both the west and east sides of Powell Buttes (**Figure 6-21**; plate). West of Powell Buttes, unit **Tdbd** flows formed an extensive surface reaching as far north and west as Smith Rock (**Figure 5-16**, plate). East of Powell Buttes, unit **Tdbd** mantled an eroded surface of the early Miocene Prineville Basalt (**Tcpb**) and descended into the Crooked River canyon, reaching as far north as the east slope of Grass Butte (**Figure 5-16**, plate, cross section B-B′). The basaltic andesite of Dry River (**Tdbd**) crops out as distinct rimrock-forming cliffs characterized by columnar jointing, with blocky columns >1 m (3.3 ft) across. Upper flow surfaces are capped by tumuli and residual depressions. Vesicles are often filled by either botryoidal-shaped masses of opaline quartz or white (N9) to pinkish gray (5YR 8/1), branch-shaped zeolite. The maximum thickness of unit **Tdbd** is 25 m (80 ft) (plate). Typical hand samples are medium light gray (N6) to dark gray (N3), containing ≤2 percent (vol.) clear, euhedral, blocky to lath-shaped plagioclase phenocrysts ≤2 mm (0.1 in) and ≤2 percent (vol.) moderate yellow green (5GY 7/4), anhedral to subhedral, equant olivine phenocrysts ≤1.5 mm (0.06 in) across, distributed within a hypocrystalline groundmass of inequigranular, trachytic plagioclase laths, intergranular olivine, subophitic clinopyroxene, and intersertal glass.

The basaltic andesite of Dry River (**Tdbd**) has reversed magnetic polarity and is assigned a late Miocene age on the basis of stratigraphic position (**Figure 5-23**, **Figure 6-1**; appendix). Sherrod and others (2004) considered their basalt of Dry River (unit Tbdr) to be similar in age to the 3.56 Ma basalt of Redmond (**Tdbr**), but were unable to resolve the precise stratigraphic relations between the two units. Our geologic mapping indicates the basalt of Redmond (**Tdbr**) overlies the basaltic andesite of Dry River along the Powell Buttes Highway; similar age and stratigraphic relations can be observed 0.8 km (0.5 mi) south of Smith Rock, where the basalt of Redmond (**Tdbr**) is inset into the basaltic andesite of Dry River (**Tdbd**) and is therefore younger (plate). The Dry River flow unit (**Tdbm**) has also been geochemically recognized from well cuttings obtained from a depth of 64 m (201 ft) in water well CROO 53265 (map no. G163) on the eastern flank of Grass Butte. In the well, unit **Tdbd** sits stratigraphically below the basalt of 5.42 Ma Meyers Butte (**Tdbm**) and above the 7.54 Ma basalt of Hoffman Dam (**Tdbh**) (plate; appendix). Southwest of Powell Buttes, the basaltic andesite of Dry River (**Tdbd**) overlies flows geochemically correlated to the ~6 Ma basalt of Opal Springs (**Tdbo**). The basalt of Opal Springs (**Tdbo**) does not crop out southwest of Powell Buttes, but geochemistry of well cuttings recovered from water wells DESC 9317 (map nos. G16 and G17), CROO 51563 (map no. G71), CROO 50194 (map no. G76), and CROO 2960 (map nos. G140 and G141; north of the community of Powell Butte) identify the unit in the subsurface. Mapped surface and subsurface stratigraphic relations therefore constrain the age of the basaltic andesite of Dry River between 5.42 and ~6 Ma (**Figure 5-23**, **Figure 6-1**; appendix).

Vents for the basaltic andesite of Dry River (**Tdbd**) are unknown, but are inferred to be located south of the map area on the basis of a hummocky flow surface that can be traced on air-photos south at least to Horse Butte (~5.6 km [3.5 mi] south of the map area) (**Figure 1-1**, **Figure 5-21**). Unit **Tdbd** is equivalent to the basalt of Dry River (unit Tbdr) of Sherrod and others (2004).

Figure 6-21. The Prineville Basalt (Tcpb) and overlying intracanyon lava flows of the Deschutes Formation in the Crooked River canyon south of Prineville (44.127540, -120.825840). The Prineville Basalt (Tcpb) reaches a maximum composite thickness of 210 m (690 ft) in this area. View is looking northwest toward the mouth of Rocky Canyon. The Oligocene Powell Buttes rhyolite dome complex and the snow-capped High Cascades are visible on the horizon. White arrow shows the direction of flow for the Crooked River. Photo credit: Jason McClaughry, 2006.

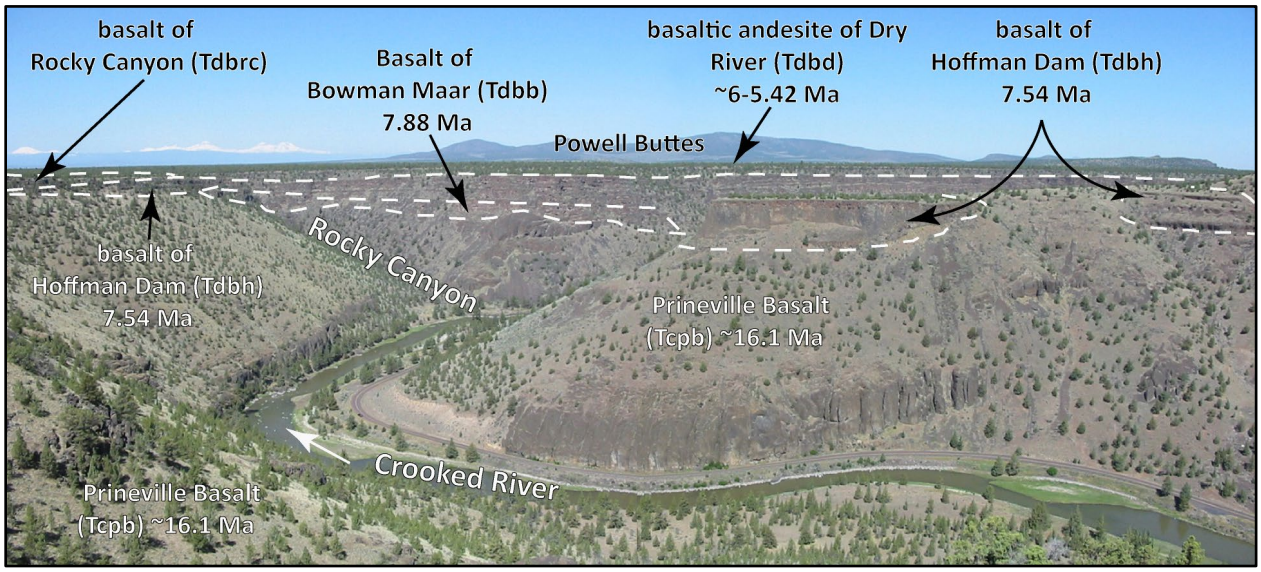

Tdbo **basalt of Opal Springs (upper Miocene)—**High-alumina basalt lava flows (SiO_2 = 48.34 to 52.49 weight percent; Al_2O_3 = 15.84 to 18.48 weight percent; K_2O = 0.05 to 0.95 weight percent; Sr = 143 to 330 ppm; *n* = 12 analyses) mapped along the floor of the Crooked River canyon from 3.2 km (2 mi) downstream of Peter Skene Ogden State Park, north to Opal Springs (**Figure 5-16**, **Figure 5-22**; **Table 6-3**; plate; appendix). Unit **Tdbo** consists of two to four lava flows, as thick as 40 m (131 ft), separated in places by paleosols and ash-flow tuff (Smith, 1986a, b). The type area at Crooked River Ranch, as defined by Smith (1986a), includes higher titanium and iron basalt and basaltic andesite (SiO_2 = 49.11 to 52.49 weight percent; TiO_2 = 1.52 to 1.54 weight percent; FeOTotal = 10.01 to 11.33 weight percent; *n* = 3 analyses) near the top of the sequence (map nos. G386, G387, and G388) (**Figure 5-16**, **Figure 5-22**; **Table 6-3**; plate; appendix). Flows in unit **Tdbo** exposed downstream of the type area along the Crooked River (map nos. G423 and G465) and cuttings recovered from water well JEFF 837 (map no. G323) are basalt (SiO_2 = 49.45 to 50.21 weight percent; *n* = 3) with lower amounts of titanium (TiO_2 = 0.97 to 1.11 weight percent) and potassium (K_2O = 0.05 to 0.39 weight percent) (**Figure 5-16**, **Figure 5-22**; **Table 6-3**; plate; appendix; Smith, 1986a; Ferns and others, 1996; Lite and Gannett, 2002). Large springs enter the Crooked River from many different levels within this flow sequence.

The basalt of Opal Springs (**Tdbo**) is only exposed in the Crooked River canyon downstream of Peter Skene Ogden State Park, but the low titanium and potassium (SiO_2 = 48.34 to 49.37 weight percent; TiO_2 = 0.7 to 1.25; K_2O = 0.14 to 0.39 weight percent; *n* = 6) part of the sequence have been identified in water well cuttings collected north and west of Powell Buttes. These samples were recovered from depth intervals of 38 to 59 m (125 to 192 ft) and 74 to 100 m (244 to 327 ft) in water well DESC 9317 (map nos. G16 and G17), from depth interval 144 to 146 m (473 to 478 ft) in water well CROO 51563 (map no. G71), from depth interval 101 m (332 ft) of water well CROO 50194 (map no. G76), and the 85 m (279 ft) and 115 to 122 m (377 to 400 ft) depth intervals

of water well CROO 2960 (map nos. G140 and G141; north of the community of Powell Butte; plate; appendix; Lite and Gannett, 2002). Typical hand samples are medium light gray (N6) to dark gray (N3), containing ≤1 percent (vol.) moderate yellow green (5GY 7/4), subhedral, equant olivine phenocrysts ≤2 mm (0.1 in) across, distributed within a fine-grained, diktytaxitic, holocrystalline groundmass.

The basalt of Opal Springs (**Tdbo**) has normal magnetic polarity and is assigned a late Miocene age on the basis of stratigraphic position and isotopic age (**Figure 5-23**). Higher titanium upper lava flows of the basalt of Opal Springs (**Tdbo**) yielded an original $^{40}Ar/^{39}Ar$ age of 6.31 ± 0.1 Ma (whole rock; sample D5; Smith, 1986a), subsequently revised to 5.77 ± 0.07 Ma (Smith, 1986b; Smith and others, 1987) (**Figure 5-16**, **Figure 5-23**, **Figure 6-1**; **Table 5-3**; plate; appendix). Pitcher (2017) recalibrated the 5.77 Ma age of Smith (1986b) to 5.85 ± 0.14 Ma. High-precision, single crystal $^{40}Ar/^{39}Ar$ ages on stratigraphically bracketing tuffs, including the younger 5.99 Ma Osborne Canyon ignimbrite member (**Tdto**) and older 6.25 Ma Chinook tuff, indicate the isotopic age reported is too young (Pitcher, 2017; Pitcher and others, 2017). Thus, the age of the basalt of Opal Springs (**Tdbo**) is ~6 Ma. Unit **Tdbo** is equivalent to the Opal Springs basalt member of Smith (1986a, b), Ferns and others (1996), and Sherrod and others (2004). Based on the high-alumina character of the unit, Smith (1986a, b) suggested a source area in the High Cascades, but an overall lack of exposure prohibits correlation of the lavas further to the west. Geochemical correlations with well cuttings west of Powell Buttes indicate the presence of the unit in the subsurface along the western edge of the lower Crooked River basin and toward yet unknown vents located south of the map area (plate).

Tdbw **basalt of Willow Creek (upper Miocene)—**High-alumina basalt lava flow (SiO_2 = 50.93 weight percent; Al_2O_3 = 17.92 weight percent; K_2O = 0.28 weight percent; *n* = 1 analysis) mapped in the northern part of the lower Crooked River basin at the head of McMeen Creek and Willow Creek (**Figure 5-16**, **Figure 5-22**; **Table 6-3**; plate; appendix; Thormahlen, 1984). The maximum thickness of unit **Tdbw** is as much as 60 m (200 ft) along Willow Creek. Typical hand samples are medium light gray (N6) to dark gray (N3) and plagioclase and pyroxene porphyritic, containing ≤1 percent (vol.) plagioclase, clinopyroxene, and olivine microphenocrysts ≤2 mm (0.1 in) across, distributed within a medium-grained, diktytaxitic, holocrystalline groundmass (Thormahlen, 1984). Accessory magnetite accounts for ~5 percent (vol.) of the rock.

The basalt of Willow Creek (**Tdbw**) has normal magnetic polarity and is assigned a late Miocene age on the basis of stratigraphic position and an $^{40}Ar/^{39}Ar$ plateau age of 6.30 ± 0.09 Ma determined for a sample from Willow Creek, ~2.4 km (1.5 mi) southeast of Madras (whole rock; sample D13; Smith, 1986a, b) (**Figure 1-1**, **Figure 5-23**, **Figure 6-1**; **Table 5-3**; plate; appendix). The basalt of Willow Creek (**Tdbw**) was erupted from an extant vent located ~1.6 km (1 mi) north of the lower Crooked River basin and flowed west and north along the Willow Creek drainage (**Figure 5-21**; Peck, 1964; Swanson, 1969; Robinson, 1975; Thormahlen, 1984).

Tdbrc **basalt of Rocky Canyon (upper Miocene)—**High-alumina basalt lava flow (SiO_2 = 47.79 to 51.42 weight percent; Al_2O_3 = 16.71 to 17.48 weight percent; K_2O = 0.32 to 0.76 weight percent; Sr = 308 to 363 ppm; *n* = 16 analyses) mapped beneath the basalt of Meyers Butte (**Tdbm**) and above the Rattlesnake Tuff (**Tmtr**) along the Crooked River canyon, between Rocky Canyon on the south and Prineville on the north (**Figure 5-16**, **Figure 5-22**, **Figure 6-11**, **Figure 6-21**; **Table 6-3**; plate; appendix; McClaughry and Ferns, 2006a; Ferns and McClaughry, 2006a, b). Unit **Tdbrc** typically crops out as cliffs characterized by columnar jointing. A 1- to 2-m-thick (3.3 to 6.6 ft) vesicular zone occurs at the upper surface of the flow. Vesicle cylinders up to 0.75 m (2.5 ft) in length are common. West of the Crooked River and 3.7 km (2.3 mi) east of Prineville Airport, cliff-forming outcrops of unit **Tdbrc** overlie a ≥20-m-thick (65.5 ft) section of basaltic pillow mounds and palagonite breccia containing subangular, black (N1) glassy basalt blocks and bombs (**Figure 5-16**, **Figure 6-11**; plate). Basaltic pillows are surrounded by a pale yellowish orange (10YR 8/6) palagonite matrix. Elongated pillow lobes form well-developed, steeply dipping foreset beds striking N.80°E. and dipping 40°NE. The maximum thickness of unit **Tdbrc** is ~65 m (210 ft) (plate). Typical hand samples are medium light gray (N6) to dark gray (N3), containing ≤1 percent (vol.) clear, euhedral, blocky plagioclase phenocrysts ≤2 mm (0.1 in) across and moderate brown (5YR 3/4) subhedral, equant, seriate iddingsite-rimmed olivine microphenocrysts ≤1 mm (0.04 in), distributed in a fine-grained, diktytaxitic, hypocrystalline groundmass of equigranular plagioclase, intergranular olivine, subophitic clinopyroxene, and sparse intersertal glass.

The basalt of Rocky Canyon (**Tdbrc**) has reversed magnetic polarity and is assigned a late Miocene age on the basis of stratigraphic position beneath the 5.42 Ma basalt of Meyers Butte (**Tdbm**) and above the 7.05 Ma Rattlesnake Tuff (**Tmtr**) (**Figure 5-23**, **Figure 6-1**; plate; appendix). Vents for the basalt of Rocky Canyon (**Tdbrc**) are unknown, but are inferred to be located south of the map area on the basis of mapped flow distribution and geochemically similar basalt that is exposed ~3.5 km (2.2 mi) southwest of Horse Butte (outside map area) (**Figure 1-1**, **Figure 5-21**). Potential eruptive sites include a vent at Horse Butte (unit QTvb of Swanson, 1969) and vents mapped in the area between Bear Creek Buttes, Horse Butte, and Pine Mountain (**Figure 1-1**, **Figure 5-21**; unit QTp of Walker and others, 1967).

Tdbp **basalt of Pelton Dam (upper Miocene) (cross section only)—**High-alumina basalt lava flows (SiO_2 = 47.93 to 50.83 weight percent; Al_2O_3 = 15.45 to 16.94 weight percent; K_2O = 0.45 to 0.85; weight percent; Sr = 314 to 421 ppm; *n* = 14 analyses) exposed near the base of the Deschutes Formation at Lake Simtustus (Deschutes River) and Pelton Dam, north of the lower Crooked River basin (**Figure 1-1**, **Figure 5-21**, **Figure 6-22**; **Table 6-4**; appendix). In the lower Crooked River basin, the basalt of Pelton Dam (**Tdbp**) is only recognized in the subsurface from well cuttings. North of the map area, along the Deschutes River canyon, the basalt of Pelton Dam forms a prominent bench between Round Butte Dam and Pelton Dam (**Figure 6-22**). Mapping in that area by Jay (1982) recognized 4 to 8 individual lava flows within the Pelton Dam unit, ranging from 25 to 40 m (82 to 131 ft) thick. Individual lava flows there are separated by weathered flow tops and local occurrences of thin <1 m (~3.3 ft) sedimentary interbeds (Jay, 1982). Pelton Dam lava flows are also exposed east of the Deschutes River, along Clark Drive near Gateway ("Clark Drive Basalt" of Hayman, 1983). Geochemical analyses, obtained by Jay (1982) from Pelton Dam lava flows in the Willow Creek area (**Figure 1-1**, **Figure 5-21**; north of the lower Crooked River basin), indicate a sequence of basalt lava flows (SiO_2 = 47.94 to 50.32 weight percent) containing about 14.18 to 16.29 weight percent Al_2O_3, 1.69 to 2.12 weight percent TiO_2, and 0.41 to 0.86 weight percent K_2O (appendix; Jay, 1982; Smith, 1986a, b). Samples obtained from a depth of 127 m (415 ft) in the JEFF 50287 well (map nos. G468, G469, and G470) near Opal Springs and the 74 to 100 m (244 to 327 ft) depth interval of the DESC 9317 well (map nos. G17 and G18) and the 125 m (411 ft) depth interval of the CROO 50194 well (map no. G77) near Powell Buttes have comparable geochemical values to those reported by Jay (1982) for the basalt of Pelton Dam (**Tdbp**) with 48.64 to 50.83 weight percent SiO_2, 16.15 to 16.94 weight percent Al_2O_3, 1.48 to 1.85 weight percent TiO_2, and 0.46 to 0.8 weight percent K_2O (plate; appendix; Lite and Gannett, 2002). Rocks of Pelton Dam (**Tdbp**) geochemical composition in water well DESC 9317 and CROO 50194 lie directly beneath flows geochemically correlated with the ~6 Ma basalt of Opal Springs (**Tdbo**) (**Figure 5-22**; **Table 6-4**; plate; appendix). Typical hand samples are grayish black (N2), vesicular, and microporphyritic to porphyritic, containing 5 to 10 percent (vol.) clear, subhedral to euhedral, blocky to prismatic plagioclase ≤3 mm (0.1 in) across and 3 to 5 percent (vol.) moderate brown (5YR 3/4), subhedral, equant, iddingsite-rimmed olivine ≤2 mm (0.1 in) across, distributed in a medium- to coarse-grained, equigranular, diktytaxitic, hypocrystalline groundmass composed of plagioclase, intergranular olivine, intergranular clinopyroxene, and glass.

The basalt of Pelton Dam (**Tdbp**) has normal magnetic polarity and is assigned a late Miocene age on the basis of stratigraphic position and an $^{40}Ar/^{39}Ar$ age of 7.42 ± 0.22 Ma for a sample obtained along Willow Creek northwest of Madras (whole rock; sample J203; Smith and Snee, 1984; Smith, 1986a, b; age recalibrated to 7.52 ± 0.45 Ma by Pitcher, 2017) (**Figure 1-1**, **Figure 5-21**, **Figure 5-23**, **Figure 6-1**; plate; appendix). The source of the basalt of Pelton Dam (**Tdbp**) is unknown, but Smith (1986a, b) suggested a source southeast of the Deschutes Basin on the basis of low aluminum contents (Al_2O_3 < 15.7 weight percent) relative to similar-aged High Cascades-derived flows, which generally have higher aluminum contents (Al_2O_3 > 16.7 weight percent). Recognition of lava flows with a basalt of Pelton Dam (**Tdbp**) geochemical signature in water well DESC 9317 extends the known extent of the unit south, at least to the west slope of Powell Buttes (plate). Source vents therefore must lie south of the lower Crooked River basin. The basalt of Pelton Dam is equivalent to the Pelton basalt member of Jay (1982), the "Clark Drive Basalt" of Hayman (1983), and the Pelton basalt member of Smith (1986a, b).

Figure 6-22. Basalt of Pelton Dam (Tdbp) at Lake Simtustus north of map area, downstream of Pelton Dam. The basalt of Pelton Dam (Tdbp) here directly overlies the Simtustus Formation (Tmos) and the Prineville Basalt (Tcpb). View is looking northwest from the overlook on NW Pelton Dam Road (44.669783, -121.240524). Photo credit: Jason McClaughry, 2013.

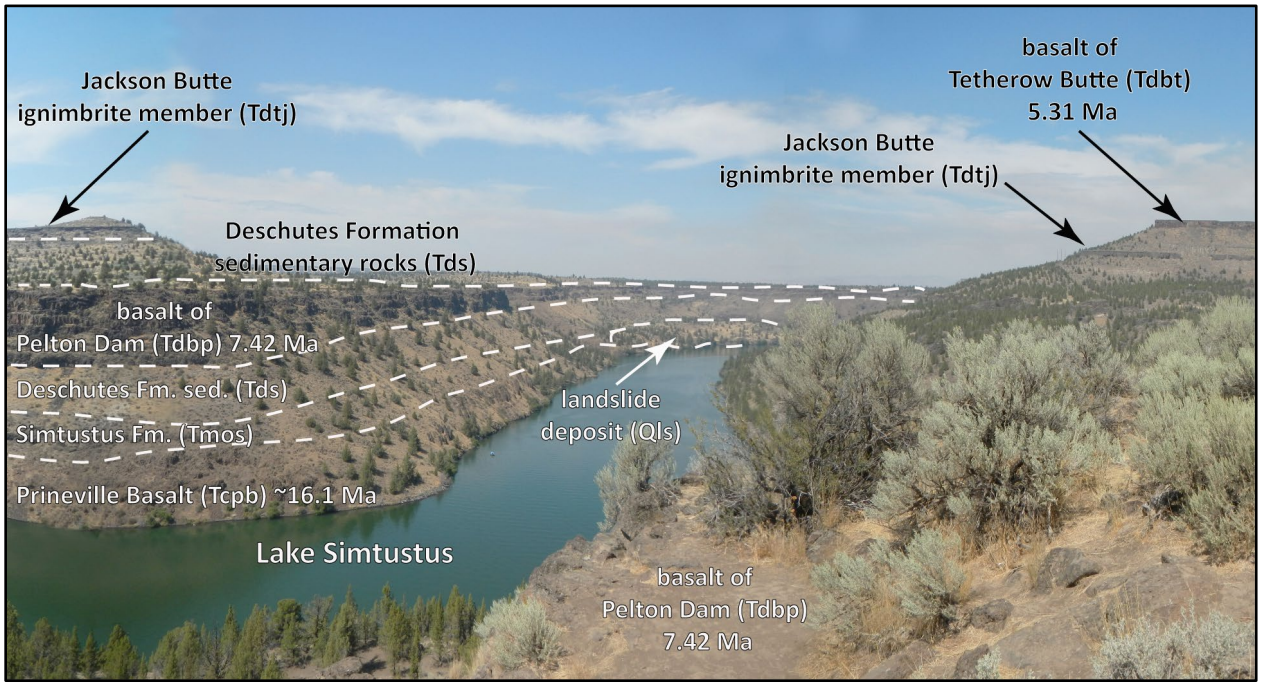

Table 6-4. Select XRF geochemical analyses for lava flows in the early Deschutes Formation in the lower Crooked River basin.

Sample	LITOPAL585[1]	RMCOS14 15[1]	RCWOG24 4327[1]	1.31VIII.05[2]	46 LCJ 06[2]	CROO5396 5-650[3]	114 P 05[4]	276 LCJ 06[2]	111 LCJ 06[5]
Geographic Area	Steelhead Falls	Steelhead Falls	Powell Butte	Stearns Butte	Devils Canyon	Prineville Airport	Grass Butte	Swartz Canyon	Bottleneck Spring
Formation	Deschutes	Deschutes	Deschutes	Deschutes	Deschutes	Deschutes	Deschutes	Deschutes	Deschutes
Map Unit	Tdbp	Tdbp	Tdbp	Tdbh	Tdbb	Tdbaf	Tdbg	Tdbq	Tdbbs
UTM N (NAD 83)	4927500	4927697	4887987	4902297	4888461	4904827	4902870	4892328	4929199
UTM E (NAD 83)	635270	635175	658525	669784	676499	667607	663200	671927	676538
Age (Ma)	~7.52 Ma	~7.52 Ma	~7.52 Ma	~7.54	~7.88	nd	nd	8.76 Ma	nd
Map Label	G469	G468	G17	G135	G29	G174	G145	G63	G500
Oxides, weight percent									
SiO_2	48.9	48.64	48.77	49.11	50.81	53.66	53.07	50.30	50.14
Al_2O_3	16.15	16.30	16.34	15.28	16.14	15.80	15.60	18.05	17.04
TiO_2	1.65	1.82	1.85	2.20	1.38	2.17	1.74	1.04	1.13
FeOTotal	11.63	11.70	11.64	12.76	9.28	12.12	9.62	9.30	9.65
MnO	0.2	0.20	0.20	0.22	0.17	0.19	0.16	0.18	0.16
CaO	9.89	10.01	10.19	9.37	9.69	6.38	9.48	11.36	10.76
MgO	7.69	7.20	6.96	7.21	9.01	6.64	6.39	6.20	8.06
K_2O	0.5	0.52	0.46	0.57	0.61	0.99	0.92	0.48	0.46
Na_2O	2.99	3.08	3.15	2.77	2.50	1.74	2.70	2.80	2.42
P_2O_5	0.41	0.53	0.44	0.52	0.42	0.30	0.33	0.28	0.18
LOI	1.47	0.20	0.19	0.84	1.27	nd	1.40	1.07	0.54
Total_I	nd	nd	nd	99.62	100.08	100.12	99.77	100.28	100.35
Trace Elements, parts per million									
Ni	142	137	80	117	179	32	107	65	128
Cr	297	237	173	198	385	56	242	151	409
Sc	32	36	33	34	29	29	23	38	36
V	283	293	308	345	225	285	223	278	240
Ba	339	342	356	374	379	193	617	360	141
Rb	4	7	4	9	8	17.9	10	4	5
Sr	314	349	314	330	574	590	1040	343	553
Zr	93	126	119	115	124	137	146	85	100
Y	28	34	32	38	26	36.6	29	28	21
Nb	6.6	9.4	8.6	6.9	10.0	13.7	9.1	7.9	4.8
Ga	19	20	17	21	17	20.3	20	16	17
Cu	56	125	82	99	58	37	47	58	34
Zn	91	115	100	106	84	115	93	77	84
Pb	2	0	1	3	4	<1	7	5	4
La	nd	19	19	14	13	11	24	13	13
Ce	20	35	15	31	35	24	51	20	21
Th	2	4	1	2	2	18.8	1	3	1
Nd	nd	0	0	nd	1	1.3	1	0	1
U	nd	nd	nd	52	41	49	38	0	45

Major element determinations have been normalized to a 100-percent total on a volatile-free basis and recalculated with total iron expressed as FeOTotal; nd - no data or element not analyzed; na - not applicable or no information. LOI, Loss on Ignition; Total_I, original analytical total. Data from: [1] Lite and Gannett; (2002); [2]McClaughry and Ferns (2006a); [3]Dunbar and Perkins (2015); [4]Ferns and McClaughry (2006a); [5]Ferns and McClaughry (2007).

Tdbh **basalt of Hoffman Dam (upper Miocene)—**Flow-on-flow succession of basalt lava flows (SiO_2 = 47.82 to 49.11 weight percent; Al_2O_3 = 15.28 to 16.07 weight percent; K_2O = 0.38 to 0.61 weight percent; Sr = 313 to 352 ppm; *n* = 10 analyses) mapped along the Crooked River between Bowman Dam and O'Neil (**Figure 5-16**, **Figure 5-22**, **Figure 6-14**, **Figure 6-19**, **Figure 6-21**, **Figure 6-23**; **Table 6-4**; plate; appendix). Unit **Tdbh** crops out as plateau-capping lava flows south of Rocky Canyon, forming a broad hummocky flow surface extending south of the lower Crooked River basin (**Figure 5-16**; plate). North of Rocky Canyon the basalt crops out as a thick, compound lava flow succession confined within the Crooked River canyon (**Figure 5-16**, **Figure 6-14**, **Figure 6-19**, **Figure 6-21**, **Figure 6-23**; plate). Intracanyon lava flows are mapped at least as far north as Prineville where they underlie the 5.42 Ma basalt of Meyers Butte (**Tdbm**) and the basalt of Rocky Canyon (**Tdbrc**) (**Figure 5-16**; plate). Unit **Tdbh** has also been geochemically identified in the subsurface from cuttings obtained from several water wells drilled at the Prineville Airport, east of Grass Butte (**Figure 5-16**; plate, cross sections A-A′ and B-B′; CROO 53724, map no. G211; CROO 53726, map nos. G194, G195, G196, and G198; CROO 53727, map no. G204; CROO 53878, map nos. G190 and G191; CROO 53965, map no. G170; CROO 53969, map nos. G182 and G183). Cliff-forming outcrops in the Crooked River canyon have columnar-jointing; well-developed columns in the basalt are oriented perpendicular to the contact along paleocanyon margins. Intracanyon exposures of unit **Tdbh** along the Crooked River, near Hoffman Dam, reach a maximum thickness of 180 m (590 ft) (**Figure 5-16**, **Figure 6-14**; plate). Typical hand samples are vesicular, medium light gray (N6) to dark gray (N3), and sparsely porphyritic, containing ≤1 percent (vol.) clear, subhedral, blocky to prismatic, seriate plagioclase phenocrysts ≤2 mm (0.1 in) and ≤1 percent (vol.) moderate brown (5YR 3/4), anhedral to subhedral, subequant, seriate, iddingsite-rimmed olivine phenocrysts ≤3.5 mm (0.1 in), enclosed in a medium-grained, diktytaxitic, hypocrystalline to hyalopilitic and variably trachytic groundmass of equigranular plagioclase, intergranular to hyalophitic olivine, poikilophitic to subophitic clinopyroxene, and intersertal glass. Intergranular olivine crystals have been pervasively altered to moderate brown (5YR 3/4) iddingsite.

The basalt of Hoffman Dam (**Tdbh**) has reversed magnetic polarity and is assigned a late Miocene age on the basis of stratigraphic position and an $^{40}Ar/^{39}Ar$ plateau age of 7.54 ± 0.02 Ma (whole rock; sample CROO53265-445; Dunbar and Perkins, 2015) obtained from geochemically correlated cuttings retrieved from a depth interval of 136 m (445 ft) in water well CROO 53265, drilled 0.8 km (0.5 mi) southwest of the Prineville Airport (**Figure 5-16**, **Figure 5-23**, **Figure 6-1**; **Table 5-3**; plate, map no. G164; appendix). South of Prineville, along the Crooked River, the basalt of Hoffman Dam (**Tdbh**) lies stratigraphically above the 8.76 Ma basalt of Quail Valley Ranch (**Tdbq**) and below the 7.05 Ma Rattlesnake Tuff (**Tmtr**) (**Figure 6-14**, **Figure 6-19**; plate). Vents for the basalt of Hoffman Dam (**Tdbh**) are unknown, but are inferred to be located south of the lower Crooked River basin on the basis of a muted hummocky flow surface that can be traced on air-photos south at least to Horse Butte (5.6 km [~3.5 mi] south of the map area; **Figure 1-1**, **Figure 5-21**). Distribution of the lava flows (**Tdbh**) indicates that they flowed north away from their source vents forming a broad lobe. Lava flows (**Tdbh**) emptied into the Crooked River canyon near Rocky Canyon and flowed downstream confined within a channel nearly identical to the modern river course (**Figure 5-16**; plate). Hoffman Dam lava flows (**Tdbh**) are geochemically comparable and of similar isotopic age to higher titanium lava flow lobes (flows six and seven, ~2.00 to 2.12 weight percent TiO_2) occurring near the top of the Pelton Dam basalt (**Tdbp**) section of Jay (1982) on Willow Creek near Madras. The two units are differentiated on the basis of

magnetic polarity, but isotopic ages indicate eruption during a time of several magnetic reversals. The basalt of Hoffman Dam and basalt of Pelton Dam (**Tdbp**), thus represent compositionally similar flow lobes of like age that erupted south of the lower Crooked River basin at ~7.5 Ma.

Figure 6-23. Intracanyon lava flows of the 7.54 Ma basalt of Hoffman Dam (Tdbh) against paleocanyon walls composed of Prineville Basalt (Tcpb). View is looking north (44.140835, -120.825027). Photo credit: Jason McClaughry, 2006.

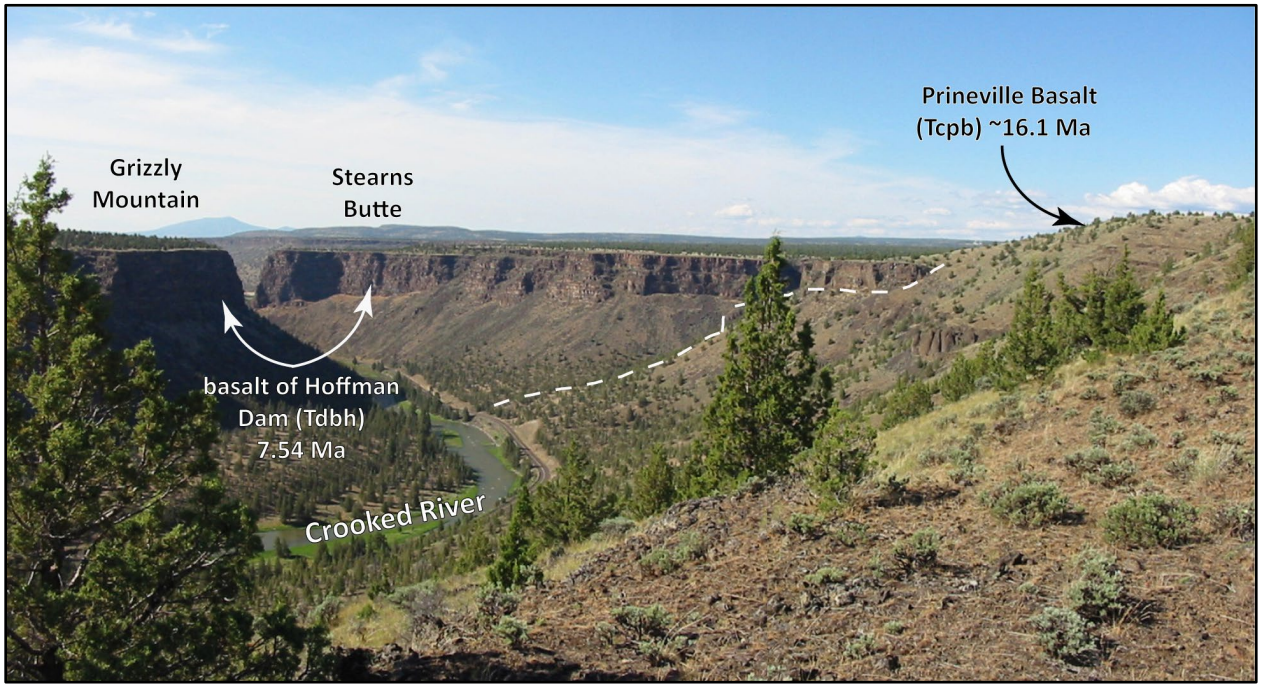

Tdbb **basalt of Bowman Maar (upper Miocene)—**High-alumina basalt lava flows (SiO_2 = 48.31 to 51.27 weight percent; Al_2O_3 = 15.76 to 17.34 weight percent; K_2O = 0.20 to 0.68 weight percent; Sr = 274 to 595 ppm; *n* = 22 analyses) mapped as plateau-capping and intracanyon lava flows along the Crooked River between Bowman Dam, Rocky Canyon, and Stearns Dam (**Figure 5-16**, **Figure 5-22**, **Figure 6-14**, **Figure 6-19**, **Figure 6-21**, **Figure 6-23**, **Figure 6-24**; **Table 6-4**; plate; appendix). Intracanyon lava flows extend at least as far north as the Prineville Airport, where the unit has been identified in the subsurface from cuttings obtained from several water wells drilled at that location (**Figure 5-16**; plate, cross sections A-A′ and B-B′; CROO 53265, map no. G164; CROO 3200, map no. G142). Cliff-forming outcrops in the Crooked River canyon have columnar-jointing; well-developed columns in the basalt are oriented perpendicular to the contact along paleocanyon margins. A welded 'a'ā flow surface is present in outcrops near Devils Canyon (**Figure 5-16**; plate). Intracanyon exposures of unit **Tdbb** along the Crooked River, near Hoffman Dam, reach a maximum thickness of 80 m (262 ft) (**Figure 5-16**; plate). Typical hand samples are medium light gray (N6) to dark gray (N3), vesicular, and sparsely microporphyritic to porphyritic, containing ≤1 percent (vol.) moderate brown (5YR 3/4), anhedral to subhedral, subequant, seriate iddingsitized olivine microphenocrysts and phenocrysts ≤2 mm (0.1 in), and ≤1 percent (vol.) clear plagioclase microphenocrysts ≤1 mm (0.04 in), enclosed in a fine- to medium-grained, diktytaxitic, holocrystalline groundmass of equigranular plagioclase, intergranular olivine, and

poikilophitic to subophitic clinopyroxene. Intergranular olivine crystals have been pervasively altered to moderate brown (5YR 3/4) iddingsite.

The basalt of Bowman Maar (**Tdbb**) has reversed magnetic polarity and is assigned a late Miocene age on the basis of stratigraphic position and an $^{40}Ar/^{39}Ar$ plateau age of 7.88 ± 0.05 Ma (whole rock; sample CROO53726-545565; Dunbar and Perkins, 2015) obtained from geochemically correlated cuttings retrieved from a depth interval of 166 m (545 ft) in water well CROO 53726, drilled 1.3 km (0.8 mi) northeast of the Prineville Airport (**Figure 5-16**, **Figure 5-23**, **Figure 6-1**; **Table 5-3**; plate, map no. G197; appendix). Along the Crooked River south of Prineville, the basalt of Bowman Maar (**Tdbb**) lies stratigraphically beneath the 7.54 Ma basalt of Hoffman Dam (**Tdbh**) and is inset into the 8.76 Ma basalt of Quail Valley Ranch (**Tdbq**) (**Figure 6-19**). The basalt of Bowman Maar (**Tdbb**) was erupted from a 3.2-km-long (2 mi), N.50°W.-striking belt of extant cinder cone-capped vents and a series of N.10°W.- to N.70°W.-striking dikes (**Figure 5-16**, **Figure 6-24**; plate). The vent area includes the now dissected Bowman Maar, exposed 1.6 km (1 mi) east-northeast of Bowman Dam (**Figure 6-24**, **Figure 6-25**). Distribution of the lava flows indicates they flowed north away from their source vents and descended into the Crooked River canyon near present-day Rocky Canyon; downstream lava flows were confined within a channel nearly identical to the modern river course (**Figure 5-16**; plate).

Figure 6-24. The basalt of Bowman Maar (Tdbb) and Bowman Maar vent complex on the north shore of Prineville Reservoir near Bowman Dam. Bowman Maar is a late Miocene hydrovolcanic eruptive center that formed above structurally deformed Oligocene rocks that predate eruption of the Crooked River caldera and the early Miocene Prineville Basalt (Tcpb). Lava flows erupted from the maar unconformably overlie the older, deformed Oligocene and Miocene and strata. View is looking north from Powder House State Park (44.103347, -120.781185). Photo credit: Jason McClaughry, 2006.

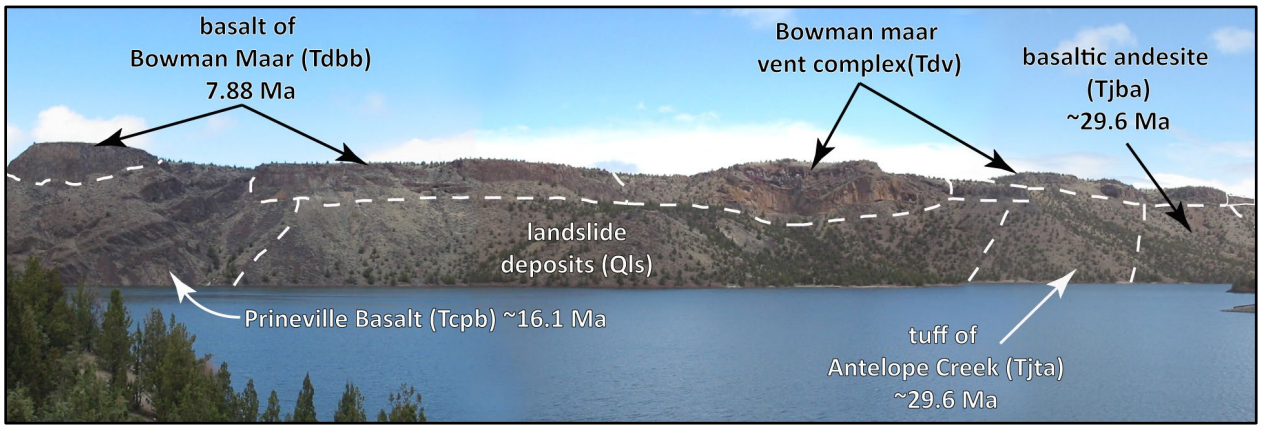

Figure 6-25. Bowman Maar. (a) Bowman Maar, a Deschutes Formation mafic vent complex mapped near Bowman Dam, is filled by a thick section of internally dipping lapilli tuff and an overlying crater-filling basaltic lava (Tdbb) (44.116742, -120.770893). En echelon basalt dikes locally intersect the maar complex. (b) Stratified, inward-dipping lapilli tuff filling Bowman Maar. (c) Stratified, inward-dipping lapilli tuff crosscut by more massive, chaotically mixed tuff breccias. These deposits may indicate pulsing eruptive activity or central vent collapse. Arrow points to 19 cm (7.5 in) tall yellow notebook for scale in the lower part of the photograph. (d) The lapilli tuff contains occasional, pebble- to cobble-sized, well-rounded (stream-worn) clasts, incorporated during hydromagmatic eruptions. The cobble is Prineville Basalt (Tcpb). Pencil for scale is 15 cm (5.9 in) long. Outcrop photos in B, C, and D are located at 44.115967, -120.769952. Photo credits: Jason McClaughry, 2006.

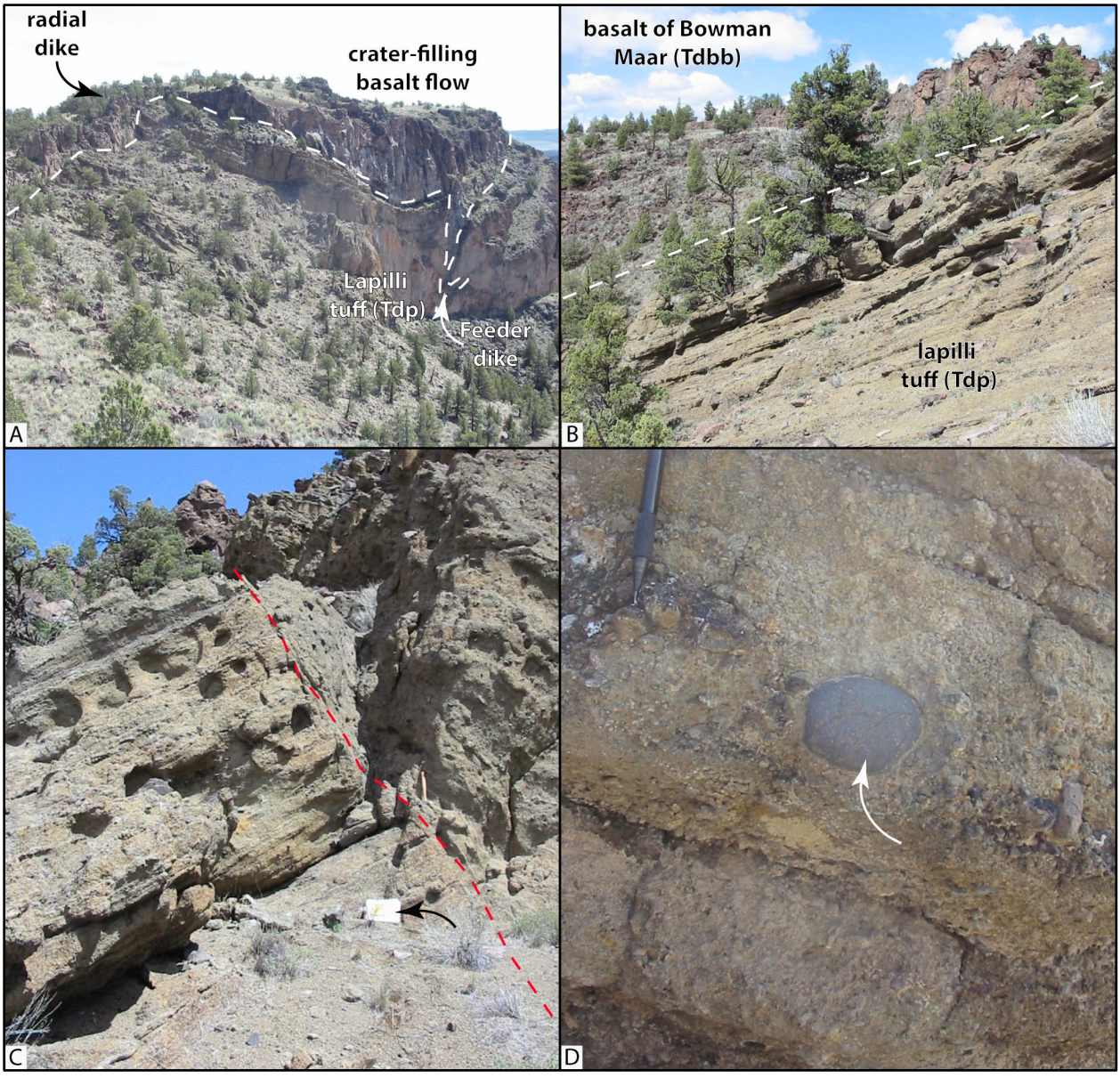

Tdbaf **basalt of Alkali Flat (upper Miocene) (cross section only)—**High-titanium basalt (SiO_2 = 47.68 to 49.21 weight percent; Al_2O_3 = 15.94 to 16.94 weight percent; TiO_2 = 2.51 to 2.59 weight percent; K_2O = 0.47 to 0.48 weight percent; Sr = 275 to 287 ppm; *n* = 3 analyses) and basaltic andesite (SiO_2 = 53.65 weight percent; Al_2O_3 = 15.8 weight percent; TiO_2 = 2.16 weight percent; K_2O = 0.99; weight percent; Sr = 590 ppm; *n* = 1 analysis) lava flows recognized in well cuttings from the 192 to 198 m (630 to 650 ft) depth interval of water well CROO 53965 at Prineville Airport (**Figure 5-16**, **Figure 5-22**; **Table 6-4**; plate, cross section B-B′, map nos. G171, G172, G173, and G174; appendix; Dunbar and Perkins, 2015). The Alkali Flat flow (**Tdbaf**) encountered at this interval in the CROO 53965 well sits directly below cuttings correlated to the basalt of Bowman Maar (**Tdbb**) and above the Prineville Basalt (**Tcpb**). It is stratigraphically and geochemically comparable to high-titanium basalt (SiO_2 = 49.25 to 50.31 weight percent; Al_2O_3= 15.63 to 15.71 weight percent; TiO_2 = 2.11 to 2.23 weight percent; K_2O = 0.41 to 1.03 weight percent; *n* = 2 analyses) underlying Alkali Flat and forming the rimrock on the southern side of Prineville Reservoir, ~4 km (2.5 mi) southeast of Bowman Dam (south of map area) (Smith, 1986a, b) (**Figure 5-21**). The maximum thickness of unit **Tdbaf**, south of Prineville Reservoir, is ≤60 m (200 ft). Typical hand samples are medium light gray (N6) to grayish black (N2), containing sparse olivine microphenocrysts, distributed within a fine-grained, diktytaxitic, holocrystalline groundmass.

The basalt of Alkali Flat (**Tdbaf**) has reversed magnetic polarity and is assigned a late Miocene age on the basis of stratigraphic position beneath the 7.88 Ma basalt of Bowman Maar (**Tdbb**) (**Figure 5-23**, **Figure 6-1**; plate; Smith, 1986a). Unit **Tdbaf** was erupted from an extant vent forming Alkali Butte, 14 km (8.7 mi) east-southeast of Bowman Dam (south of the map area) (**Figure 5-21**). Alkali Flat lava flows (**Tdbaf**) have not been found cropping out in the modern Crooked River canyon between Prineville and Bowman Dam (plate).

Tdbg **basaltic andesite of Grass Butte (upper Miocene)—**High-titanium and strontium basaltic andesite lava flow (SiO_2 = 53.07 weight percent; Al_2O_3 = 15.6 weight percent; TiO_2 = 1.74 weight percent; K_2O = 0.92 weight percent; Sr = 1,044 ppm; *n* = 1 analysis) forming Grass Butte, southwest of Prineville (**Figure 5-16**, **Figure 5-22**, **Figure 6-20**; **Table 6-4**; plate; appendix). Lava flows (**Tdbg**) were erupted from the extant cinder cone-capped vent forming Grass Butte (**Figure 5-16**, **Figure 5-21**, **Figure 6-20**; plate). Cinders (**Tdv**) and dikes (**Tdbi**) capping Grass Butte have an identical high-titanium and strontium basaltic andesite (SiO_2 = 51.84 to 53.05 weight percent; Al_2O_3 = 14.54 to 15.76 weight percent; TiO_2 = 1.75 to 2.01 weight percent; K_2O = 0.84 to 1.16; weight percent; Sr = 951 to 1144 ppm; *n* = 4 analyses) composition to the flanking lava flow (**Tdbg**) (**Figure 5-22**). Unit **Tdbg** generally weathers to a non-distinct surface of boulders mantled by sand and gravel of unit **Tdsg** (**Figure 5-16**). Thickness of unit **Tdbg** is >30 m (100 ft) (plate). Typical hand samples are medium light gray (N6) to dark gray (N3), containing >5 percent (vol.) moderate brown (5YR 3/4), anhedral to subhedral, subequant, seriate, iddingsitized olivine microphenocrysts and phenocrysts ≤2 mm (0.1 in), distributed in a fine-grained, diktytaxitic, holocrystalline groundmass of equigranular plagioclase and intergranular olivine.

The basaltic andesite of Grass Butte (**Tdbg**) has reversed magnetic polarity and is assigned a late Miocene age on the basis of stratigraphic position above the ~16.1 Ma Prineville Basalt (**Tcpb**) and below the 5.42 Ma basalt of Meyers Butte (**Tdbm**) (**Figure 5-23**, **Figure 6-1**; plate).

Tdbq **basalt of Quail Valley Ranch (upper Miocene)—**High-alumina basalt lava flow (SiO_2 = 50.30 to 50.68 weight percent; Al_2O_3 = 18.05 to 18.18 weight percent; K_2O = 0.42 to 0.48 weight percent; Sr = 340 to 343 ppm; *n* = 2 analyses) mapped against the Prineville Basalt (**Tcpb**) on the west side of the Crooked River canyon between the mouth of Swartz Canyon and Hoffman Dam (**Figure 5-16**, **Figure 5-22**; **Table 6-4**; plate; appendix). Unit **Tdbq** is characterized by columnar jointing and has an irregular surface capped by tumuli, residual depressions, and pressure ridges. The maximum thickness of unit **Tdbq** is 66 m (225 ft) (plate). Typical hand samples are medium light gray (N6) to dark gray (N3), containing >10 percent (vol.) plagioclase-olivine-pyroxene glomerocrysts ≤1 cm (0.4 in) across, 1 to 2 percent (vol.) clear, subhedral to euhedral, prismatic plagioclase phenocrysts ≤2 mm (0.1 in), moderate yellow green (5GY 7/4), subhedral, equant olivine phenocrysts ≤2 mm (0.1 in), and dusky green (5G 3/2), anhedral clinopyroxene ≤0.5 mm (0.02 in) across, distributed within a fine-grained, diktytaxitic, holocrystalline groundmass of equigranular plagioclase, intergranular olivine, and clinopyroxene. The relatively abundant and large glomerocrysts in the flow are a diagnostic field characteristics.

The basalt of Quail Valley Ranch (**Tdbq**) is the oldest Deschutes Formation lava flow mapped in the Crooked River canyon, south of Prineville. Unit **Tdbq** is assigned a late Miocene age on the basis of stratigraphic position and an $^{40}Ar/^{39}Ar$ plateau age of 8.76 ± 0.24 Ma (whole rock; sample 276 LCJ 06; McClaughry and Ferns, 2007d) (**Figure 5-23**, **Figure 6-1**; **Table 5-3**; plate; appendix). The basalt of Quail Valley Ranch (**Tdbq**) was erupted from several similar composition basalt dikes mapped along the west side of the Crooked River south of Swartz Canyon (**Figure 5-21**; plate).

Tdbbs **basalt of Bottleneck Spring (upper Miocene[?])—**High-alumina basalt lava flow (SiO_2 = 49.92 to 50.14 weight percent; Al_2O_3 = 16.34 to 17.04 weight percent; K_2O = 0.40 to 0.46 weight percent; Sr = 553 ppm; *n* = 2 analyses) mapped forming a prominent plateau west of Allen Creek (**Figure 5-16**, **Figure 5-22**; **Table 6-4**; plate; appendix). The typically grayish red (10R 4/2) weathering lava flow (**Tdbbs**) unconformably overlies a deeply eroded surface of Eocene and Oligocene rocks. Platy or columnar jointing is common (**Figure 6-26**). Locally, the basalt (**Tdbbs**) has well-developed vertical flow banding, flow folding, and irregular flattened vesicles. The unit locally includes a gravel composed of well-rounded boulders and cobbles. The maximum thickness of unit **Tdbbs** is 30 m (100 ft) (plate). Landslide deposits (**Qls**) are common along the mapped distribution of unit **Tdbbs** (**Figure 6-26**; plate). Typical hand samples are medium light gray (N6) to grayish black (N2), containing euhedral to subhedral phenocrysts of olivine, plagioclase, and pyroxene phenocrysts up to 2 to 4 mm (0.1 to 0.2 in) across, distributed within a fine-grained, holocrystalline, locally trachytic groundmass of equigranular plagioclase and intergranular olivine.

The basalt of Bottleneck Spring (**Tdbbs**) is assigned a late Miocene (?) age on the basis of stratigraphic position (**Figure 6-1**; plate). East-west-striking dikes (**Tdbi**), scoriaceous breccia, welded spatter, and fluidal and breadcrust bombs cropping out on top of and south of the plateau-forming exposure west of Allen Creek suggest that area is the eroded remnant of the vent source for the basalt (**Figure 5-21**; plate).

Figure 6-26. Basalt columns derived from the basalt of Bottleneck Spring (44.482966, -120.614327). The basalt complex here is deeply eroded and flanked by prominent landslide deposits. Photo credit: Jason McClaughry, 2006.

Tdv **basalt vents (Pliocene and upper Miocene)—**Basalt lava flows forming well-preserved to deeply-eroded, low-profile shield volcanoes in the Bowman volcanic field (**Figure 5-16**, **Figure 6-17**, **Figure 6-18**, **Figure 6-20**, **Figure 6-25**, **Figure 6-27**; plate). Unit (**Tdv**) includes shield volcanoes at Bowman Dam, Stearns Ranch, Grass Butte, Meyers Butte, Combs Flat, Japanese Creek, Round Butte, and Bottleneck Spring (**Figure 5-16**; plate). Many of the vents (**Tdv**) are capped by cinder cones of unit **Tdp** and host dikes of unit **Tdbi** (**Figure 6-27**). Deeply eroded vents (**Tdv**) are now marked only by feeder dikes (**Tdbi**) and the remains of scoria and cinder mounds (**Tdp**) (**Figure 6-27a-b**). Although the age of any single vent within the map unit likely spans a much briefer time, unit **Tdv** is assigned a late Miocene and Pliocene age on the basis of stratigraphic position and correlation with isotopically dated lava flows (**Figure 6-1**; plate).

Tdp **vent pyroclastic rocks (Pliocene and upper Miocene)—**Unconsolidated, massive to stratified, moderately- to well-sorted, dusky red (5R 3/4) and grayish black (N2) cinders, scoriaceous breccia, welded spatter, and fluidal and breadcrust bombs forming cinder cones associated with basalt vents (**Tdv**) (**Figure 5-16**, **Figure 6-27**; plate). Bedded lapilli tuff and palagonitic breccia occurs at some vents, most notably Bowman Maar in the south part of the map area (**Figure 6-25**; McClaughry and others, 2009b). Unit **Tdp** is assigned a late Miocene and Pliocene age on the basis of stratigraphic position and correlation with isotopically dated lava flows (**Figure 6-1**; plate).

Figure 6-27. Deschutes Formation mafic vent complexes. (a) Bedded scoria, fluidal bombs, and welded spatter (Tdp) exposed in the rock pit at the summit of Grass Butte (44.275683, -120.934991). Automobile for scale is 2 m (6.6 ft) tall. (b) N. 60° W.-striking basaltic andesite feeder dikes crosscut the bedded deposits in the upper part of the summit cinder cone (Tdbi) shown in A (44.276255, -120.935875). Person for scale is 1.9 m (6.2 ft) tall. Photo credits: Jason McClaughry, 2005.

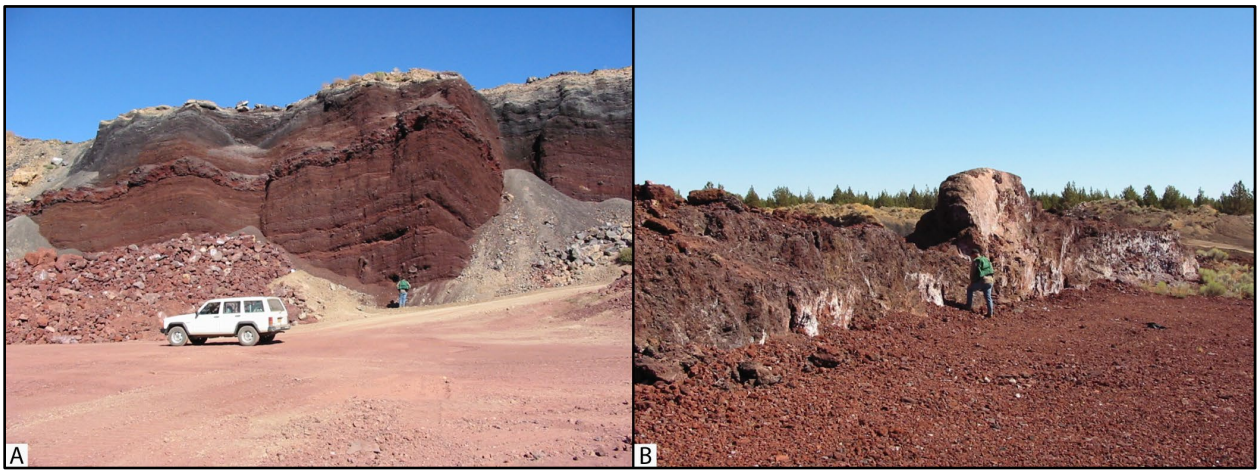

Tdbi **basalt intrusions (Pliocene and upper Miocene)—**Erosionally resistant, vertically-oriented, medium light gray (N6) to dark gray (N3) basalt and basaltic andesite dikes that were feeders for lava flows of the Deschutes Formation in the lower Crooked River basin (**Figure 5-16**, **Figure 6-17**, **Figure 6-18**, **Figure 6-25a**, **Figure 6-27b**; plate). Dikes (**Tdbi**) typically display irregular edges, vesicles stretched parallel to the dike margins, and locally contain mafic to silicic xenoliths. Dikes (**Tdbi**) are often capped by a low-lying shield of stacked lava flows, welded spatter, and scoria (**Figure 6-17**, **Figure 6-18**, **Figure 6-25a**, **Figure 6-27a**). Unit **Tdbi** is assigned a late Miocene and Pliocene age on the basis of stratigraphic position and correlation with isotopically dated lava flows (**Figure 6-1**; plate).

6.3.4.3 Deschutes Formation lava flows in the western part of the lower Crooked River basin not assigned to the Bowman volcanic field

Tdbl **basalt of Lower Desert (lower Pliocene or upper Miocene)—**High-alumina basalt and basaltic andesite lava flows (SiO_2 = 50.52 to 50.71 weight percent; Al_2O_3 = 16.95 to 17.39 weight percent; K_2O = 0.17 to 0.22 weight percent; *n* = 4 analyses) mapped beneath the basalt of Tetherow Butte (**Tdbt**) on the east side of the Crooked River canyon near Opal Springs and along the west side of the Crooked River canyon on The Peninsula (**Figure 5-16**, **Figure 5-22**, **Figure 6-8**; **Table 6-5**; plate; appendix; Conrey, 1985; Smith, 1986a, b; Ferns and others, 1996). The basalt of Lower Desert (**Tdbl**) contains relatively higher amounts of aluminum (Al_2O_3 > 16.95 weight percent) and lower contents of titanium (TiO_2 < 0.95 weight percent) and iron (FeOTotal < 8.46 weight percent) relative to the basalt of Tetherow Butte (**Tdbt**), indicating a different source area (**Figure 5-22**). Unit **Tdbl** includes the Canadian Bench and Fly Lake basalt flows as defined by Smith (1986a, b) and Dill (1992). The composite thickness of unit **Tdbl** is 49 m (160 ft) on The Peninsula (**Figure 5-16**; plate). Typical hand samples are medium light gray (N6) to dark gray (N3), containing olivine phenocrysts ≤3 mm (0.1 in) across, distributed within a fine-grained, holocrystalline groundmass of plagioclase and ophitic or intergranular pyroxene.

The basalt of Lower Desert (**Tdbl**) has normal magnetic polarity and is assigned a late Miocene age on the basis of an $^{40}Ar/^{39}Ar$ age of 5.43 ± 0.05 Ma obtained from the Canadian Bench flow on The Peninsula (whole rock; sample D9; Smith, 1986a, b; recalibrated to 5.47 ± 0.10 Ma by Pitcher, 2017) (**Figure 5-16**, **Figure 5-23**, **Figure 6-1**; **Table 5-3**; plate; appendix). The isotopic age reported for the basalt of Lower Desert (**Tdbl**) is incongruent with the magnetic polarity measured for the unit and its correlation to the currently accepted paleomagnetic time scale (**Figure 5-23**). The unit could therefore be as young as about 5.2 Ma. The basalt of Lower Desert (**Tdbl**) was likely erupted from High Cascade vents west of Green Ridge (**Figure 5-21**; Conrey, 1985; Smith, 1986a, b, 1991). Equivalent to the Lower Desert basalt member of Smith (1986a) and diktytaxitic olivine basalt flows (unit Tdb) of Ferns and others (1996).

Porphyritic basaltic andesite lava flows (upper Miocene)—Porphyritic basaltic andesite lava flows mapped at different stratigraphic levels in the Deschutes Formation (plate). Equivalent to the porphyritic basaltic andesite flows of Ferns and others (1996). Subdivided on the basis of stratigraphic position into the following two units:

Tdba1 **rimrock-forming basaltic andesite (upper Miocene)—**Basaltic andesite lava flows (SiO_2 = 53.40 weight percent; Al_2O_3 = 18.59 weight percent; K_2O = 0.92 weight percent; *n* = 1 analysis) mapped along the lower reaches of the Crooked River canyon in the northwest part of the lower Crooked River basin (**Figure 5-16**, **Figure 5-22**; **Table 6-5**; plate; appendix). A wider selection of samples obtained from this unit outside the map area, includes both low- and high-titanium basaltic andesite chemical compositions with ~1.4 to 1.7 weight percent TiO_2 and >2.0 weight percent TiO_2 at ~53 to 54 weight percent SiO_2 (**Figure 5-22**; **Table 6-5**; Smith, 1986a, b; Ferns and others, 1996). Unit **Tdba1** includes both lava flows overlying the Peninsula ignimbrite member (**Tdtp**) and lava flows mapped between the Peninsula (**Tdtp**) and the Steelhead Falls (**Tdts**) ignimbrite members (plate). These lava flows (**Tdba1**) interfinger with diktytaxitic olivine-phyric Lower Desert basalt (**Tdbl**) to the west in the Akawa Butte 7.5′ quadrangle. The composite thickness of unit **Tdba1** is ~37 m (120 ft) (plate). Typical hand samples are medium dark gray (N4) to grayish black (N2), containing glomerocrysts and sparse augite and olivine phenocrysts ≤2 mm (0.1 in) across, distributed within a fine-grained hypocrystalline groundmass.

Unit **Tdba1** has reversed magnetic polarity and is assigned a late Miocene age on the basis of stratigraphic position beneath the ~5.2 Ma basalt of Tetherow Butte (**Tdbt**) and above the 5.68 Ma Steelhead Falls ignimbrite member (**Tdts**) (**Figure 6-1**; plate).

Table 6-5. Select XRF geochemical analyses for lava flows and tuffs in the Deschutes Formation not assigned to the Bowman volcanic field in the lower Crooked River basin.

Sample	SF-142[1]	SF-134[1]	SF-135[1]	SF-140[1]	7.15IX.05[2]	156 P 05[3]	3C.13IX.05[4]
Geographic Area	Opal Springs	Opal Springs	Opal Springs	Opal Springs	Combs Flat	Crooked River/Dry Creek	Polly Creek
Formation	Deschutes	Deschutes	Deschutes	Deschutes	Deschutes	na	Deschutes
Map Unit	Tdbl	Tdbl	Tdba1	Tdba2	Tmot	Tmtr	Tmtm
UTM N (NAD 83)	4926799	4925309	4924058	4927127	4905774	4897672	4913957
UTM E (NAD 83)	635666	636418	637415	635429	676651	669540	688745
Age (Ma)	~5.47 Ma	~5.47 Ma	nd	nd	nd	~7.1	nd
Map Label	G451	G433	G420	G460	G185	G110	G276
Oxides, weight percent							
SiO_2	50.60	50.52	53.40	54.22	61.64	75.29	79.70
Al_2O_3	17.10	16.95	18.59	18.54	18.56	12.26	11.65
TiO_2	0.97	0.95	1.62	1.30	1.21	0.22	0.21
FeOTotal	8.37	8.46	8.57	8.01	1.64	1.81	0.44
MnO	0.17	0.17	nd	nd	0.15	0.10	0.02
CaO	10.90	11.0	8.44	8.52	8.29	1.14	0.43
MgO	9.26	9.22	4.47	4.61	4.09	0.63	0.15
K_2O	0.18	0.22	0.92	0.79	1.37	5.20	4.06
Na_2O	2.28	2.35	3.98	4.01	2.82	3.25	3.28
P_2O_5	0.17	0.16	nd	nd	0.22	0.09	0.05
LOI	nd	nd	nd	nd	5.12	3.53	1.94
Total_I	100.08	99.25	100.57	99.78	100.15	100.08	100.12
Trace Elements, parts per million							
Ni	nd	nd	nd	nd	43	0	0
Cr	nd	nd	nd	nd	87	4	0
Sc	nd	nd	nd	nd	25	6	9
V	nd	nd	nd	nd	181	19	7
Ba	nd	nd	nd	nd	391	665	831
Rb	nd	nd	nd	nd	26	89	90
Sr	nd	nd	nd	nd	489	60	42
Zr	nd	nd	nd	nd	135	270	322
Y	nd	nd	nd	nd	23	85	37
Nb	nd	nd	nd	nd	9	30	18
Ga	nd	nd	nd	nd	18	17	17
Cu	nd	nd	nd	nd	37	6	0
Zn	nd	nd	nd	nd	77	105	42
Pb	nd	nd	nd	nd	4	16	1
La	nd	nd	nd	nd	19	39	51
Ce	nd	nd	nd	nd	43	95	107
Th	nd	nd	nd	nd	3	8	9
Nd	nd	nd	nd	nd	nd	nd	nd
U	nd	nd	nd	nd	2	3	3

Major element determinations have been normalized to a 100-percent total on a volatile-free basis and recalculated with total iron expressed as FeOTotal; nd - no data or element not analyzed; na - not applicable or no information. LOI, Loss on Ignition; Total_I, original analytical total. Data from: [1]Smith (1986a); [2]McClaughry and Ferns (2006a); [3]Ferns and McClaughry (2006a); [4]McClaughry and Ferns (2006b).

Tdba2 olivine-augite and hypersthene-bearing basaltic andesite (upper Miocene)—Basaltic andesite lava flows (SiO_2 = 54.22 weight percent; Al_2O_3 = 18.54 weight percent; K_2O = 0.79 weight percent; *n* = 1 analysis) mapped along the lower reaches of the Crooked River canyon, near Opal Springs, in the northwest part of the lower Crooked River basin (**Figure 5-16**, **Figure 5-22**; **Table 6-5**; plate; appendix; Smith, 1986a, b; Ferns and others, 1996). Unit **Tdba2** is comprised of lava flows mapped beneath the Steelhead Falls ignimbrite member (**Tdts**) and above the Lower Bridge ignimbrite member (**Tdtl**). The composite thickness unit **Tdba2** is ~25 m (80 ft). Typical hand samples are medium dark gray (N4) to grayish black (N2), containing phenocrysts of olivine, augite, and hypersthene ≤2 mm (0.1 in) across, distributed within a fine-grained holohyaline groundmass.

Unit **Tdba2** has reversed magnetic polarity and is assigned a late Miocene age on the basis of stratigraphic position beneath between the 5.68 Ma Steelhead Falls ignimbrite member (**Tdtm**) and above the 5.93 Ma Lower Bridge ignimbrite member (**Tdtl**) (**Figure 6-1**; plate).

6.3.4.4 Deschutes Formation ash-flow tuffs in the western part of the lower Crooked River basin not assigned to the Bowman volcanic field

Tdt ash-flow tuff, undivided (upper Miocene)—Welded and nonwelded, pumiceous ash-flow tuff mapped along the Crooked River between Osborne Canyon and Lake Billy Chinook in the northwest part of the lower Crooked River basin (**Figure 5-16**; plate). Each ash-flow tuff is a single cooling unit that may consist of multiple pyroclastic flow and pumice fall deposits. The tuffs are irregularly distributed and highly variable in thickness, owing to channeling and erosion by succeeding ash-flows, debris flows, and hyperconcentrated flood flows (plate). Unit **Tdt** delineates prominent exposures of unnamed or uncorrelated ash-flow tuffs exposed along canyon walls of the Crooked River. It also includes a channel filling, welded vitric ash-flow tuff exposed at Alder Spring that lies between the Steelhead Falls (**Tdts**) and Peninsula (**Tdtp**) ignimbrite members.

The tuffs (**Tdt**) are assigned a late Miocene age on the basis of stratigraphic position beneath the ~5.2 Ma basalt of Tetherow Butte (**Tdbt**) and above the ~6 Ma basalt of Opal Springs (**Tdbo**) and isotopic ages reported by Pitcher (2017) and Pitcher and others (2017) (**Figure 6-1**; plate). All mapped tuffs have reversed magnetic polarity. Locally divided into the following informal members by Smith (1986a, b):

Tdtp Peninsula ignimbrite member (upper Miocene)—Brownish gray (5YR 4/1) to greenish gray (5GY 6/1), nonwelded to partially welded, lithic ash-flow tuff mapped along the Crooked River canyon southwest of Juniper Butte (**Figure 5-16**; plate). The tuff (**Tdtp**) is characterized by large, black (N1) aphyric bombs as much as 15 cm (5.9 in) across and sparsely phyric, medium gray (N5) rhyolite and black (N1) dacite pumice lapilli with plagioclase and clinopyroxene phenocrysts. Samples of black lapilli have a dacitic chemical composition with ~65 to 66 weight percent SiO_2 and 0.74 to 0.91 weight percent TiO_2. Black bombs have an andesitic chemical composition with ~61 percent SiO_2 (Smith, 1986a, b; appendix). The unit ranges from 1 to 12 m (3.3 to 39.5 ft) thick and thickens to the west (plate).

The Peninsula ignimbrite member (**Tdtp**) has reversed magnetic polarity and is assigned a late Miocene age on the basis of stratigraphic position beneath the ~5.2 Ma basalt of Tetherow Butte (**Tdbt**) and above the 5.68 Ma Steelhead Falls ignimbrite member (**Tdts**) (**Figure 6-1**; plate). Equivalent to the Peninsula ignimbrite member of Smith (1986a) and unit Tdtp of Ferns and others (1996).

Tdts **Steelhead Falls ignimbrite member (upper Miocene)—**Pinkish gray (5YR 8/1), white (N9), and pale yellowish brown (10YR 6/2), nonwelded to partially welded, vitric ash-flow tuff mapped along the Crooked River canyon, southwest of Juniper Butte (**Figure 5-16**; plate). Unit **Tdts** is characterized by abundant rhyodacite pumice lapilli and is often reversely graded (Smith, 1986a, b). Samples of pumice lapilli have a rhyodacite chemical composition with ~70 weight percent SiO_2 and ~0.52 weight percent TiO_2 (appendix; Smith, 1986a, b). The tuff (**Tdts**) ranges from 2 to 35 m (6.5 to 114.5 ft) in thickness and is underlain by a cogenetic, white pumice lapillistone as thick as 1.5 m (4.9 ft) (plate).

The Steelhead Falls ignimbrite member (**Tdts**) has reversed magnetic polarity and is assigned a late Miocene age on the basis of stratigraphic position and a single crystal $^{40}Ar/^{39}Ar$ plateau age of 5.68 ± 0.02 Ma reported by Pitcher and others (2017)(**Figure 6-1**; plate). Equivalent to the Steelhead Falls ignimbrite member of Smith (1986a) and unit Tdts of Ferns and others (1996).

Tdtm **McKenzie Canyon ignimbrite member (upper Miocene)—**Welded, sparsely porphyritic, lithic ash-flow tuff mapped along the Crooked River canyon between Peter Skene Ogden State Park and The Peninsula (**Figure 5-16**; plate). Unit **Tdtm** consists of a single cooling unit comprised of 1 to 5 discreet ash-flow tuffs, each separated by a nonwelded white (N9) basal ash-fall tuff. The maximum thickness of unit **Tdtm** in the map area is ~12 m (40 ft) (plate). Individual ash-flow tuffs are commonly welded and display reverse grading of pumice lapilli. Lower ash-flow tuffs are white (N9) and rich in white (N9) rhyolitic pumice, whereas the uppermost moderate orange pink (10R 7/4) tuff is welded, crudely columnar-jointed, and contains collapsed banded white (N9) and black (N1) pumice. Typical hand samples are moderate reddish orange (10R 6/6) to dark yellowish orange (10YR 6/6), containing 2 to 5 percent (vol.) microphenocrysts of feldspar and less than about 1 percent (vol.) hypersthene and augite (Sherrod and others, 2004). Olivine is rare but does occur in black pumice lapilli from the upper part of the unit (Stensland, 1970; Cannon, 1985). The tuffs are characterized by a diverse assemblage of pumice lapilli composed of white (N9) rhyodacite (SiO_2 = 70.5 to 72.2 weight percent; TiO_2 = 0.26 to 0.32 weight percent), black (N1) andesite (SiO_2 = 59.8 to 61.2 weight percent, TiO_2 = 1.41 to 1.53 weight percent), and banded pumice of mixed composition (SiO_2 = 64.0 weight percent, TiO_2 = 1.04 weight percent) (Cannon, 1985; Smith, 1986a, b; appendix). The banded pumice is diagnostic of the unit.

The McKenzie Canyon ignimbrite member (**Tdtm**) has reversed magnetic polarity and is assigned a late Miocene age on the basis of stratigraphic position beneath the 5.68 Ma Steelhead Falls ignimbrite member (**Tdts**) and above the 5.93 Ma Lower Bridge ignimbrite member (**Tdtl**) (**Figure 6-1**; plate). A single crystal $^{40}Ar/^{39}Ar$ plateau age of 5.76 ± 0.02 Ma was reported for this unit by Pitcher and others (2017). The unit thickens to more than 10 m (32.8 ft) to the southwest, toward a presumed buried vent southwest of Sisters (**Figure 5-21**). Equivalent to the McKenzie Canyon tuff of Cannon (1985), the McKenzie Canyon ignimbrite member of Smith (1986a), and unit Tdtm of Ferns and others (1996).

Tdtc **Cove ignimbrite member (upper Miocene)—**White (N9), nonwelded ash-flow tuff mapped on both the east and west canyon walls of the Crooked River at Cove Palisades State Park (**Figure 5-16**; plate). Unit **Tdtc** forms the prow of The Ship, a prominent landmark on the northern end of The Peninsula (**Figure 5-16**, **Figure 6-8**; plate). The tuff (**Tdtc**) is generally <12 m (40 ft) thick (plate). Unit **Tdtc** contains scattered white (N9) to light gray (N7) pumice lapilli up to 2 cm (0.8 in) across; both the pumice and tuff matrix contain abundant plagioclase crystals (Smith, 1986a, b). Pumice lapilli typically have a rhyodacite chemical composition (SiO_2 = 70.15 to 70.99 weight percent; TiO_2 = 0.41 to 0.55 weight percent) (Smith, 1986a, b; appendix).

The Cove ignimbrite member (**Tdtc**) has reversed magnetic polarity and is assigned a late Miocene age on the basis of stratigraphic position beneath the 5.76 Ma McKenzie Canyon ignimbrite member (**Tdtm**) and above the 5.93 Ma Lower Bridge ignimbrite member (**Tdtl**) (**Figure 6-1**; plate). Equivalent to the Cove ignimbrite member of Smith (1986a).

Tdtl **Lower Bridge ignimbrite member (upper Miocene)—**Nonwelded to weakly sintered, friable, slightly porphyritic, pumice-vitric ash-flow tuff mapped along the Crooked River canyon between Peter Skene Ogden State Park and Lake Billy Chinook in the northwest part of the lower Crooked River basin (**Figure 5-16**; plate). Unit **Tdtl** consists of two ash-flow tuffs that form a single cooling unit, 12 to 15 m (40 to 50 ft) thick (plate). The basal part of unit **Tdtl** includes a distinctive accretionary-lapilli ash-fall tuff deposit (Cannon, 1985). Unit **Tdtl** contains 10 to 15 percent (vol.) white and gray pumice lapilli and 1 to 5 percent (vol.) volcanic lithic clasts ≤2 cm (0.8 in) (Sherrod and others, 2004). White (N9) lapilli have a rhyodacite chemical composition (SiO_2 = 70.1 to 71.5 weight percent; TiO_2 = 0.4 to 0.64 weight percent) (Smith, 1986a, b; appendix). Medium gray (N5) lapilli are dacitic (SiO_2 = 66 to 68.7 weight percent; TiO_2 = 0.54 to 0.85 weight percent) (Cannon, 1985, Ferns and others, 1996; appendix). Typical hand samples are pinkish gray (5YR 8/1) to white (N9), containing 10 to 15 percent (vol.) plagioclase microphenocrysts and 5 to 7 percent (vol.) ferromagnesian minerals (augite, hypersthene, pargasitic amphibole) (Cannon, 1985). Trace amounts of biotite are also present (Stensland, 1970; Smith 1986a).

The Lower Bridge ignimbrite member (**Tdtl**) has reversed magnetic polarity and is assigned a late Miocene age on the basis of stratigraphic position between the 5.76 Ma McKenzie Canyon ignimbrite member (**Tdtm**) and above the 5.98 Ma Jackson Buttes ignimbrite member (**Tdtj**) (**Figure 6-1**; plate). A single crystal $^{40}Ar/^{39}Ar$ plateau age of 5.93 ± 0.02 Ma was reported for this unit by Pitcher and others (2017). The unit thickens to more than 15 m (49.2 ft) to the southwest, toward a buried vent area presumably located southwest of Sisters (**Figure 5-21**). Equivalent to the Lower Bridge tuff of Cannon (1985), the Lower Bridge ignimbrite member of Smith (1986a), and unit Tdtl of Ferns and others (1996).

Tdtj **Jackson Buttes ignimbrite member (upper Miocene)—**Light gray (N7), pinkish gray (5YR 8/1), to very pale orange (10YR 8/2), nonwelded to welded ash-flow tuff mapped along the east side of the Crooked River in the northern part of Cove Palisades State Park (**Figure 5-16**; plate). Unit **Tdtj** is named for exposures at Jackson Buttes on the Warm

Springs Indian Reservation where the tuff is as thick as 23 m (75.5 ft). White (N9) to light gray (N7) pumice lapilli in the tuff range from 1 to 6 cm (0.4 to 2.4 in) across and increase in diameter upward (Smith, 1986a, b).

The Jackson Buttes ignimbrite member (**Tdtj**) has reversed magnetic polarity and is assigned a late Miocene age on the basis of stratigraphic position beneath the 5.93 Ma Lower Bridge ignimbrite member (**Tdtl**) and above the 5.99 Ma Osborne Canyon ignimbrite member (**Tdto**) (**Figure 6-1**; plate). A single crystal $^{40}Ar/^{39}Ar$ plateau age of 5.98 ± 0.01 Ma was reported for this unit by Pitcher and others (2017). Equivalent to the Jackson Buttes ignimbrite member of Smith (1986a).

Tdto **Osborne Canyon ignimbrite member (upper Miocene)—**Pinkish gray (5YR 8/1), very pale orange (10YR 8/2), and white (N9), nonwelded vitric ash-flow tuff exposed along the Crooked River canyon between Osborne Canyon and Lake Billy Chinook in the northwest part of the lower Crooked River basin (**Figure 5-16**; plate). Unit **Tdto** consists of two ash-flow tuffs that form a single cooling unit. Thickness of unit **Tdto** ranges between 9 and 40 m thick (29.5 to 131.2 ft), thickening and thinning across channels carved into older units (plate). Weathering of unit **Tdto** has formed distinctive hoodoo landforms in the Crooked River canyon. The tuff (**Tdto**) is characterized by fumarolically-altered grayish orange (10YR 7/4) pumice lapilli and bombs as well as reverse grading of pumice lapilli. Pumice lapilli include white (N9) rhyolitic pumice (SiO_2 = 72.48 to 74.93 weight percent; TiO_2 = 0.26 to 0.27 weight percent) sampled from outcrops in the Crooked River canyon and black andesitic pumice (SiO_2 = 62.8 weight percent; TiO_2 = 1.18 weight percent) (Cannon, 1985; appendix) from lapilli recovered from a 15-m-thick (49.2 ft) orange ignimbrite at the 122 m (400 ft) depth interval of geothermal gradient well CROO 2463 (map no. G84), 6 km (3.8 mi) southwest of Powell Butte (Smith, 1986a, b).

The Osborne Canyon ignimbrite member (**Tdto**) has reversed magnetic polarity and is assigned a late Miocene age on the basis of stratigraphic position beneath the 5.98 Ma Jackson Buttes ignimbrite member (**Tdtj**) and above the ~6 Ma basalt of Opal Springs (**Tdbo**) (**Figure 6-1**; plate). A single crystal $^{40}Ar/^{39}Ar$ plateau age of 5.99 ± 0.02 Ma was reported for this unit by Pitcher and others (2017). Ferns and others (1996) named the tuff for exposures on the Crooked River near the mouth of Osborne Canyon (**Figure 5-16**; plate). Equivalent to unit O of Cannon (1985), the Hollywood ignimbrite member of Smith (1986a, b), and the Osborne Canyon member (unit Tdto) of Ferns and others (1996).

6.3.4.5 Deschutes Formation ash-flow tuffs in the eastern part of the lower Crooked River basin not assigned to the Bowman volcanic field

Tmot **pumice tuff (upper Miocene)—**White (N9) to light brownish gray (5YR 6/1), nonwelded, pumice-lithic-crystal andesitic tuff (SiO_2 = 61.64 weight percent; TiO_2 = 1.21 weight percent; *n* = 1 analysis) exposed on the south side of Combs Flat (**Figure 5-16**, **Figure 6-28**; **Table 6-5**; plate; appendix). The tuff (**Tmot**) is ~1.5 m (4.9 ft) thick and consists of two gradational flow-units. The basal flow unit is ~36 cm (14.2 in) thick and consists of white (N9), massive to faintly stratified tuff, containing andesite lithics and clusters of pumice. The upper unit consists of a base of ~10 cm (4 in) of plane-parallel stratified, normally graded pumice tuff that grades upward into ~1 m (3.3 ft) of clast-supported and coarse-tail normally graded pumice tuff. The upper part of the unit (**Tmot**) is >75 percent (vol.) pumice fragments with a maximum pumice size of ~2 cm (0.8 in)

long. The matrix is composed of ash to fine- to medium-grained sand composed of ~45 percent (vol.) clear feldspar, ~25 percent (vol.) euhedral to subhedral amphibole and pyroxene, ~20 percent subround pumice fragments, ~10 percent (vol.) pale yellowish orange (10YR 8/6) Fe-rich biotite and accessory bi-pyramidal magnetite.

The unit is assigned a late Miocene age on the basis of stratigraphic position directly below the 3.36 Ma basalt of Combs Flat (**Tdbc**) (**Figure 6-1**; plate). Mineralogy of unit **Tmot** is similar to that described for the 5.93 Ma Lower Bridge ignimbrite member, one of the most widespread ignimbrite members in the Deschutes Basin (**Tdtl**) (e.g., plagioclase, augite, hypersthene, and rare hornblende and biotite; Cannon, 1985; Smith, 1986a).

Figure 6-28. Pumice tuff (Tmot) exposed above the John Day Formation (Tjs) at the west end of Combs Flat (44.283899, -120.786342). Arrow points to 19 cm (7.5 in) tall yellow notebook. Photo credit: Jason McClaughry, 2005.

Tmtm **tuff (upper Miocene[?])—**White (N9), massive to platy, crystal-ash rhyolite tuff (SiO_2 = 79.70 weight percent; Ba = 831 ppm; Zr = 322 ppm; *n* = 1 analysis) that conformably overlies conglomerate of unit Tds east of Mill Creek, ~5 km (3 mi) northeast of Ochoco Reservoir (**Figure 5-16**; **Table 6-5**; plate; appendix). The crystal fraction consists mostly of clear feldspar and less than 2 percent (vol.) amphibole and/or pyroxene. The tuff is ≤4 m thick (~13 ft). Unit **Tmtm** is assigned a late Miocene (?) age on the basis of stratigraphic position, contact relations, and overall lack of alteration.

6.3.5 Late Miocene ash-flow tuffs in the lower Crooked River basin not assigned to the Deschutes Formation

Tmtr **Rattlesnake Tuff (upper Miocene)—**Vitric-pumice-lithic rhyolitic ash-flow tuff (SiO_2 = 75.29 to 76.47 weight percent; Zr = 270 to 309 ppm; Nb = 27.3 to 30.7 ppm; *n* = 5 analyses) mapped as a conspicuous ledge-forming marker bed in the walls of the Crooked River canyon between Swartz Canyon and the mouth of Dry Creek (**Figure 5-16**, **Figure 6-19**; **Table 6-5**; plate; appendix; Ferns and McClaughry, 2006b; McClaughry and Ferns, 2006a). The Rattlesnake Tuff (**Tmtr**) also crops out in isolated exposures ~5 km (3.1 mi) northwest of Grizzly Mountain, and near Gravy Gulch at the east end of Combs Flat (**Figure 5-16**, **Figure 6-29**; plate). Unit **Tmtr** consists of a single, nonwelded to partially welded cooling unit as thick as 7 to 15 m (23 to 49 ft) (**Figure 6-19**). The tuff (**Tmtr**) is typically matrix-supported and massively bedded, but coarse-tail grading of both pumice and lithics occurs locally. Devitrified, moderately flattened, black (N1), medium gray (N5), white (N9), and banded pumice ≤7 cm (2.8 in) long are found in outcrops in the Crooked River canyon and Gravy Gulch (**Figure 6-29**), while the maximum pumice size in exposures north of Grizzly Mountain is ~2 cm (1 in) across (Smith, 1986a, b) (**Figure 5-16**; plate). Pumices are commonly aligned parallel to bedding. Lithics consist of angular, moderate reddish brown (10R 4/6), feldspar-phyric rhyolite and dusky brown (5YR 2/2) andesite fragments up to 1 cm (0.5 in) across. Typical hand samples of the Rattlesnake Tuff (**Tmtr**) are very pale orange (10YR 8/2), to very light gray (N7), to medium gray (N5), and light brownish gray (5YR 6/1), and aphyric to very sparsely porphyritic. Phenocryst content is ≤1 percent (vol.) for the bulk tuff. The tuff (**Tmtr**) contains microphenocrysts and phenocrysts ≤2 mm (0.1 in) of clear, subhedral to euhedral anorthoclase and sanidine, clear, subhedral plagioclase, clear, subhedral quartz, and dusky green (5G 3/2), anhedral clinopyroxene (ferrohedenbergite), distributed within a vitric groundmass. The original vitroclastic texture of the tuff (**Tmtr**) is retained but is locally overprinted by very fine elongated crystals forming axiolitic structures.

The Rattlesnake Tuff (**Tmtr**) has reversed magnetic polarity (Parker, 1974; Streck, 1994) and is assigned a late Miocene age on the basis of stratigraphic position and $^{40}Ar/^{39}Ar$ ages of 7.05 ± 0.01 (sanidine from pumice; sample HP-91-12; Streck, 1994; Streck and Grunder, 1995) and 7.093 ± 0.015 Ma (sanidine; sample HP-91-12; Jordan and others, 2004) (**Figure 5-23**)**.** Capehart Lake in the western Harney Basin, ~160 km (100 mi) southeast of the lower Crooked River basin, is the probable source area for the Rattlesnake Tuff (**Tmtr**) (Streck 1994, Streck and Grunder, 1995).

Figure 6-29. Rattlesnake Tuff (Tmtr) mapped at the head of Gravy Gulch in the southeast part of the map area (44.249992, -120.638139). Hammer head for scale is 12 cm (4.7 in) wide. Photo credit: Jason McClaughry, 2006.

Angular unconformity to disconformity

6.3.6 Columbia River Basalt Group

Tcpb **Prineville Basalt (lower Miocene)—**High-titanium basalt, basaltic andesite, trachybasalt, and basaltic trachyandesite lava flows (SiO_2 = 50.82 to 56.19 weight percent; Al_2O_3 = 12.94 to 15.67 weight percent; TiO_2 = and 2.19 to 3.15; weight percent; *n* = 53 analyses [4 outside map area]), distinguished by unusually high incompatible element concentrations of barium (Ba = 1,645 to 3,202) and phosphorous (P_2O_5 1.15 to 2.02 weight percent) (**Figure 5-16**, **Figure 5-18**, **Figure 5-19**, **Figure 5-20**; **Table 6-6**; plate; appendix). On the basis of geochemistry, Hooper and others (1993) identified three chemical types for the Prineville Basalt; a Bowman Dam chemical type, a high-SiO_2 chemical type, and a high-TiO_2-P_2O_5 chemical type (see Stratigraphic Synopsis section 5.1.2.1.1; **Figure 5-20**; **Table 6-6**). All three chemical types are present in the lower Crooked River basin.

The Prineville Basalt (**Tcpb**) directly overlies the Simtustus Formation (**Tmos**) and forms a high plateau between Combs Flat and the Crooked River (**Figure 5-16**; plate). Unit (**Tcpb**) also crops out above the Simtustus Formation (**Tmos**) between the Crooked River and Lone Pine Flat, northwest of Prineville (**Figure 5-16**; plate). Prineville Basalt lava flows (**Tcpb**) are typically hackly to columnar jointed (**Figure 6-30**). Pillow structures and palagonite breccia are common along the base of some lava flows, particularly where lavas conformably overlie the Simtustus Formation (**Tmos**) (**Figure 6-30**, **Figure 6-31**, **Figure 6-32**). Common along this contact is the occurrence of pillows with chilled rinds, that are totally enclosed within or admixed with the underlying baked tuffaceous sedimentary rocks (**Tmos**) (**Figure 6-32**). Typical hand samples are medium dark gray (N4) to grayish black (N2), and aphyric to very sparsely microporphyritic, containing <1 percent (vol.) plagioclase microphenocrysts ≤1 mm (0.04 in), distributed within a very fine-grained, hypocrystalline to hyalopilitic groundmass composed of microlites of trachytic plagioclase and intergranular clinopyroxene. Olivine, Fe-Ti oxides, and apatite needles area associated with the augite.

The Prineville Basalt (**Tcpb**) includes rocks with both normal- and reversed-polarity magnetization (Hooper and others, 1993). The lower two Bowman Dam type lava flows have reversed magnetic polarity while the capping Bowman Dam type lava flow has normal magnetic polarity. The Prineville Basalt (**Tcpb**) was previously assigned a middle Miocene age on the basis of an $^{40}Ar/^{39}Ar$ age of 15.7 ± 0.1 Ma obtained at Pelton Dam (whole rock; sample D12; appendix; Smith, 1986a, b). At the northern mapped extent of the Prineville Basalt in Butler Canyon, two flows of the Prineville Basalt (**Tcpb**) are interfingered with the N2 magnetostratigraphic unit of the Grande Ronde Basalt (**Figure 5-17**). The upper basaltic andesite lava flow lies directly beneath the ~ 16 Ma Winter Water Member, while a lower Bowman Dam chemical type lava flow is exposed beneath the <16.25 Ma Buttermilk Canyon member (Michael Sawlan, written commun., 2014). The Prineville Basalt (**Tcpb**) is thus assigned a more precise early Miocene age of ~16.1 Ma (**Figure 5-18**). Unit **Tcpb** is equivalent to the Prineville Basalt as defined by Uppuluri (1974), Smith (1986a, b), Tolan and others (1989), and Hooper and others (1993).

Table 6-6. Select XRF geochemical analyses for lava flows in the Columbia River Basalt Group in the lower Crooked River basin.

Sample	PD4[1]	02-PJ-05[2]	04-P-05[2]	100P05[2]	1.13VII.05[3]	4.13VII.05[3]	2.14VII.05[4]	132P05[4]	3.13VII.05[2]	1.14VII.05[4]	2.28VII.05[5]	PRH89-13[6]	282 LCJ 06
Geographic Area	Bowman Dam	Swartz Canyon	Swartz Canyon	Swartz Canyon	Houston Lake	Prineville	Prineville	Prineville	Prineville	Prineville	Prineville	Prineville	Ochoco Divide
Formation	Prineville	Prineville	Prineville	Prineville	Prineville	Prineville	Prineville	Prineville	Prineville	Prineville	Prineville	Prineville	Picture Gorge
Unit	Tcpb	Tcpb	Tcpb	Tcpb	Tcpb	Tcpb	Tcpb	Tcpb	Tcpb	Tcpb	Tcpb	Tcpb	Tcpg
UTM N (NAD 83)	4886727	4889875	4891175	4892697	4915320	4912675	4904291	4905752	4912215	4904662	4911189	4911367	4923835
UTM E (NAD 83)	677081	667419	667730	669057	662696	663659	676628	677205	663230	676116	685087	660245	713139
Age (Ma)	~16.1 Ma	~16.1 Ma	~16.1 Ma	~16.1 Ma	~16.1 Ma	~16.1 Ma	~16.1 Ma	~16.1 Ma	~16.1 Ma	~16.1 Ma	~16.1 Ma	~16.1 Ma	nd
Chemical Type	Bowman Dam	Bowman Dam	Bowman Dam	Bowman Dam	high-SiO_2	high-SiO_2	high-SiO_2	high-SiO_2	high-TiO_2-P_2O_5	high-TiO_2-P_2O_5	high-TiO_2-P_2O_5	high-TiO_2-P_2O_5	na
Map Label	G5	G54	G59	G65	G293	G266	G150	G184	G257	G152	G239	G245	G415
Oxides, weight percent													
SiO_2	51.25	52.10	51.92	51.86	53.66	56.19	54.69	55.40	51.52	51.21	51.67	50.84	50.37
Al_2O_3	14.58	13.78	13.74	14.04	14.74	14.96	13.90	14.00	13.57	13.33	13.5	13.75	15.72
TiO_2	2.78	2.69	2.70	2.72	2.84	2.70	2.61	2.48	3.05	3.13	3.08	3.13	1.33
FeOTotal	13.41	12.32	12.51	12.18	10.07	8.18	10.36	9.85	12.5	12.43	11.97	12.12	10.88
MnO	0.24	0.25	0.25	0.25	0.21	0.15	0.24	0.23	0.24	0.26	0.25	0.23	0.2
CaO	7.90	8.07	8.14	8.12	8.40	7.02	6.82	6.47	8.01	8.4	8.45	8.79	10.83
MgO	4.04	4.37	4.32	4.26	3.41	2.23	3.70	3.49	4.17	4.55	4.34	3.85	7.06
K_2O	1.90	1.87	1.88	2.00	1.96	3.14	2.84	3.08	1.92	1.68	1.93	1.67	0.69
Na_2O	2.67	3.13	3.12	3.14	3.21	3.87	3.35	3.54	3.22	3.15	2.94	3.61	2.71
P_2O_5	1.23	1.43	1.42	1.43	1.52	1.54	1.50	1.46	1.81	1.86	1.89	2.02	0.21
LOI	nd	1.80	2.07	3.50	1.98	2.02	2.34	1.20	2.26	1.84	1.89	nd	0.96
Total_I	100.45	99.57	99.62	100.36	99.34	99.61	99.97	99.57	99.47	99.86	99.79	nd	nd
Trace Elements, parts per million													
Ni	39	15	14	13	7	12	8	9	18	17	15	17	65
Cr	nd	19	20	18	22	12	16	17	20	22	22	13	177
Sc	37	33	34	33	37	30	30	25	33	35	39	45	37
V	345	311	300	322	337	216	231	219	278	286	300	318	310
Ba	2202	1695	1763	1900	1973	2387	2112	2185	2728	2845	2625	3202	201
Rb	52	42.7	41.9	45.0	45.2	38.9	40.8	44.2	39.1	31.3	37.7	29	9.4
Sr	402	397	399	399	428	333	320	319	396	414	410	413	260
Zr	187	167	161	162	182	160	144	147	141	138	146	131	104
Y	43	51.8	51.2	51.8	58.3	52.4	50.6	50.4	52.5	53.6	53.0	53	30.1
Nb	nd	8.5	8.5	8.9	8.7	8.7	8.6	8.0	7.8	7.5	8.1	9	6.2
Ga	nd	19.7	19.9	20.2	21.0	20.7	18.9	20.2	19.7	19.7	19.2	19	19.3
Cu	nd	45	43	36	37	49	48	40	47	51	46	38	172
Zn	nd	121	118	117	144	109	117	103	116	119	129	129	83
Pb	nd	6	5	5	6	6	6	5	3	3	2	5	3
La	nd	27	27	30	29	29	29	28	28	28	23	31	9
Ce	nd	59	60	64	65	64	63	60	61	60	50	25	13
Th	nd	5.1	5.8	5.3	4.6	5.2	4.2	5.3	3.3	4.8	4.1	4	1.9
U	nd	1	4	2	3	3	1	2	1	3	2	nd	nd

Major element determinations have been normalized to a 100-percent total on a volatile-free basis and recalculated with total iron expressed as FeOTotal; nd - no data or element not analyzed. Magnetic polarity determined using portable fluxgate magnetometer. Data from: [1]Smith (1986a); [2]Ferns and McClaughry (2006b); [3]Ferns and McClaughry (2006a); [4]McClaughry and Ferns (2006a); [5]McClaughry and Ferns (2006b); [6]Hooper and others (1993).

Figure 6-30. Lava flows of the ~16.1 Ma Prineville Basalt (Tcpb) exposed at Bowman Dam. A basal pillow delta is exposed at the base of this section along the right dam abutment (44.110161, -120.785755). Arrow points to automobile for scale. Photo credit: Jason McClaughry, 2006.

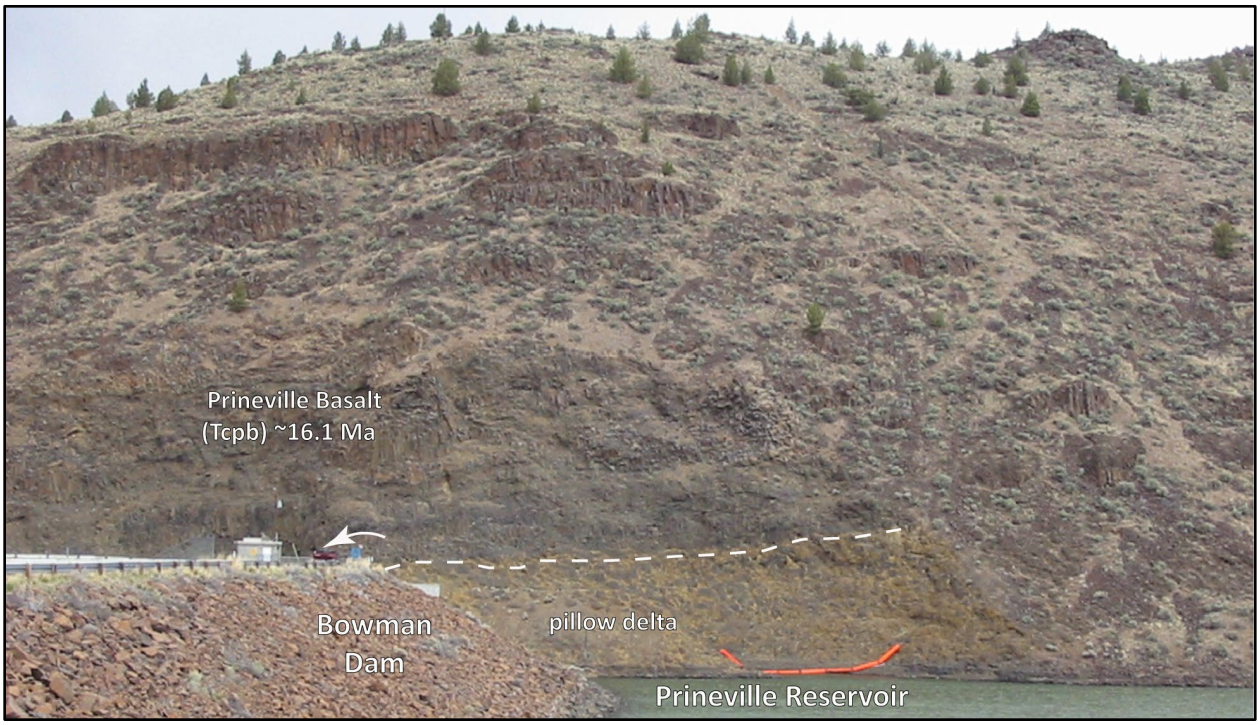

Figure 6-31. Pillow basalt near the base of a Prineville Basalt (Tcpb) lava flow along SE Juniper Canyon Road (44.236521, -120.803890). Hammer for scale is 40 cm (15.7 in) long. Photo credit: Jason McClaughry, 2006.

Figure 6-32. Pillow basalt lobes of Prineville Basalt (Tcpb) encased in tuffaceous sedimentary rocks of the Simtustus Formation (Tmos) on Combs Flat (44.274268, -120.707767). Person for scale is 1.9 m (6.2 ft) tall. Photo credit: Jason McClaughry, 2005.

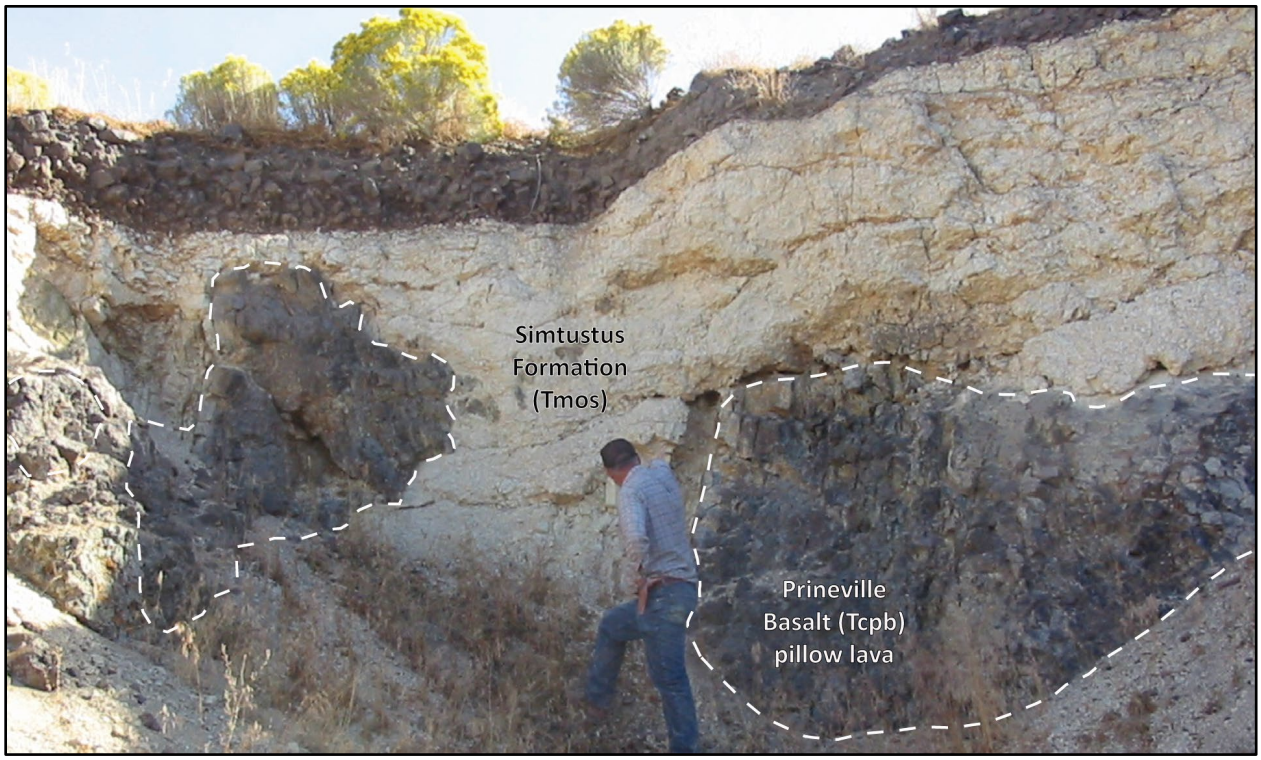

Tcpg **Picture Gorge Basalt (lower Miocene)—**Basalt lava flows (SiO_2 = 50.37 weight percent; Al_2O_3 = 15.72 weight percent; K_2O = and 0.69; weight percent; Sr = 260 ppm; *n* = 1 analysis) mapped along the eastern edge of the map area at Walton Lake and at Lookout Mountain (**Figure 5-16**, **Figure 5-18, Figure 5-19**; **Table 6-6**; plate; appendix). The unit includes four additional areas of probable Picture Gorge Basalt (SiO_2 = 49.69 to 51.76 weight percent; Al_2O_3 = 15.74 to 17.49 weight percent; K_2O = and 0.26 to 0.86; weight percent; Sr = 290 to 384 ppm; *n* = 5 analyses) mapped discontinuously above the Mill Creek and McKay Creek drainages in the northern part of the lower Crooked River basin (**Figure 5-16**, **Figure 5-19**; **Table 6-6**; plate; appendix). These areas represent the remnants of multiple deeply eroded lava flows, which are commonly associated with underlying gravel deposits. The Picture Gorge Basalt is distinguished geochemically from the Prineville Basalt on the basis of lower amounts of phosphorous (<0.5 weight percent P_2O_5) and barium (<300 ppm Ba)(**Figure 5-19a**). Typical hand samples are medium dark gray (N4) to grayish black (N2), containing olivine, plagioclase, and pyroxene microphenocrysts and phenocrysts ≤3 mm (0.1 in) across, distributed within a hypocrystalline groundmass of equigranular plagioclase, subophitic clinopyroxene, and Fe-Ti oxides.

Unit **Tcpg** is assigned an early Miocene age on the basis of stratigraphic position and isotopic ages (**Figure 5-18**). West of Dayville, the Picture Gorge Basalt lies beneath the Mascall Formation, which there includes the regionally widespread 16.16 Ma unit 1 of the Dinner Creek Tuff ($^{40}Ar/^{39}Ar$; Streck and others, 2015; Mascall Ignimbrite, Davenport, 1971). Cahoon and others (2020), applying modern $^{40}Ar/^{39}Ar$ dating methods to known or newly geochemically correlated localities cropping out in northeast Oregon, reported eleven high-precision groundmass plateau

isochron ages for the Picture Gorge Basalt ranging between 17.23 ± 0.04 and 16.06 ± 0.06 Ma (**Figure 5-18**). Outcrops exposing the local stratigraphic relations between the Picture Gorge Basalt and Prineville Basalt in the lower Crooked River basin have not been found.

Disconformity

6.3.7 Simtustus Formation

Tmos **Tuffaceous sedimentary rocks and tuff (lower Miocene)—**Moderately indurated sedimentary rocks and tuff exposed beneath and locally interbedded with the Prineville Basalt (**Tcpb**) (**Figure 5-16**, **Figure 6-32**, **Figure 6-33**; plate). Sedimentary deposits (**Tmos**) include light brownish gray (5YR 6/1) to yellowish gray (5Y 8/1) and white (N9) tuffaceous siltstone and sandstone, white (N9) to dark gray (N3), massive to plane-parallel stratified volcaniclastic sandstone, white (N9) diatomite, black (N1), well-sorted, clast-supported cobble conglomerate, and matrix-supported, cobble to boulder conglomerate (**Figure 6-33**). Sedimentary structures include massive bedding, channel forms, rip-up fragments, and burrow traces. White (N9) to medium gray (N5) tuff beds are locally present within unit **Tmos**, including a dacite tuff (SiO_2 = 66.47 weight percent; TiO_2 = 1.09 weight percent; Zr = 181 ppm; Nb = 11.7 ppm; *n* = 1 analysis) cropping out along the Crooked River (**Figure 6-33a**) and recovered from beneath the Prineville Airport, and a dacite tuff (SiO_2 = 70.08 weight percent; TiO_2 = 0.89 weight percent; Zr = 296 ppm; Nb = 14.8 ppm; *n* = 1 analysis) mapped west of Eagle Rock (**Figure 5-12**, **Figure 6-33a**; **Table 6-7**; McClaughry and Ferns, 2007c). Sedimentary units are marked by baked horizons or totally enclose basalt pillows with quenched rinds, where they are directly overlain by the Prineville Basalt (**Tcpb**) (**Figure 6-32**). Maximum thickness of unit (**Tmos**) in the lower Crooked River basin is ≤152 m (500 ft) (plate).

Early Miocene sedimentary rocks (**Tmos**) mapped beneath and interbedded with the early Miocene Prineville Basalt (**Tcpb**) in the lower Crooked River basin are considered herein to be correlative with the Simtustus Formation of Smith (1986a, b, c). Sedimentary rocks of unit **Tmos** have been previously mapped in the lower Crooked River basin as part of the upper John Day Formation (Waters and Vaughan, 1968b; Swanson, 1969). However, these sedimentary rocks (**Tmos**) are texturally distinct from the bulk of the John Day Formation, are only weakly altered, and in the southern part of the basin overlie John Day rocks with an angular unconformity. Thus, an early Miocene age is assigned to unit **Tmos** on the basis of contact relations with the ~16.1 Ma Prineville Basalt and dissimilarity with older strata of the John Day Formation (plate).

Figure 6-33. Tuff in the Simtustus Formation (Tmos). (a) Simtustus Formation (Tmos) tuff cropping out along the Crooked River Highway (44.170446, -120.837696). The outcrop here is mantled by fluvial terrace deposits (Qto). Photo credit: Jason McClaughry, 2009. (b) Simtustus Formation (Tmos) tuffaceous sedimentary rocks and tuff exposed below the Prineville Basalt (Tcpb) at the head of O'Neil Creek (44.204866, -120.674818). The section contains interbedded massive siltstone, sandstone, and 1- to 2-m-thick (3.3- to 6.5 ft) intervals of conglomerate. Photo credit: Jason McClaughry, 2006.

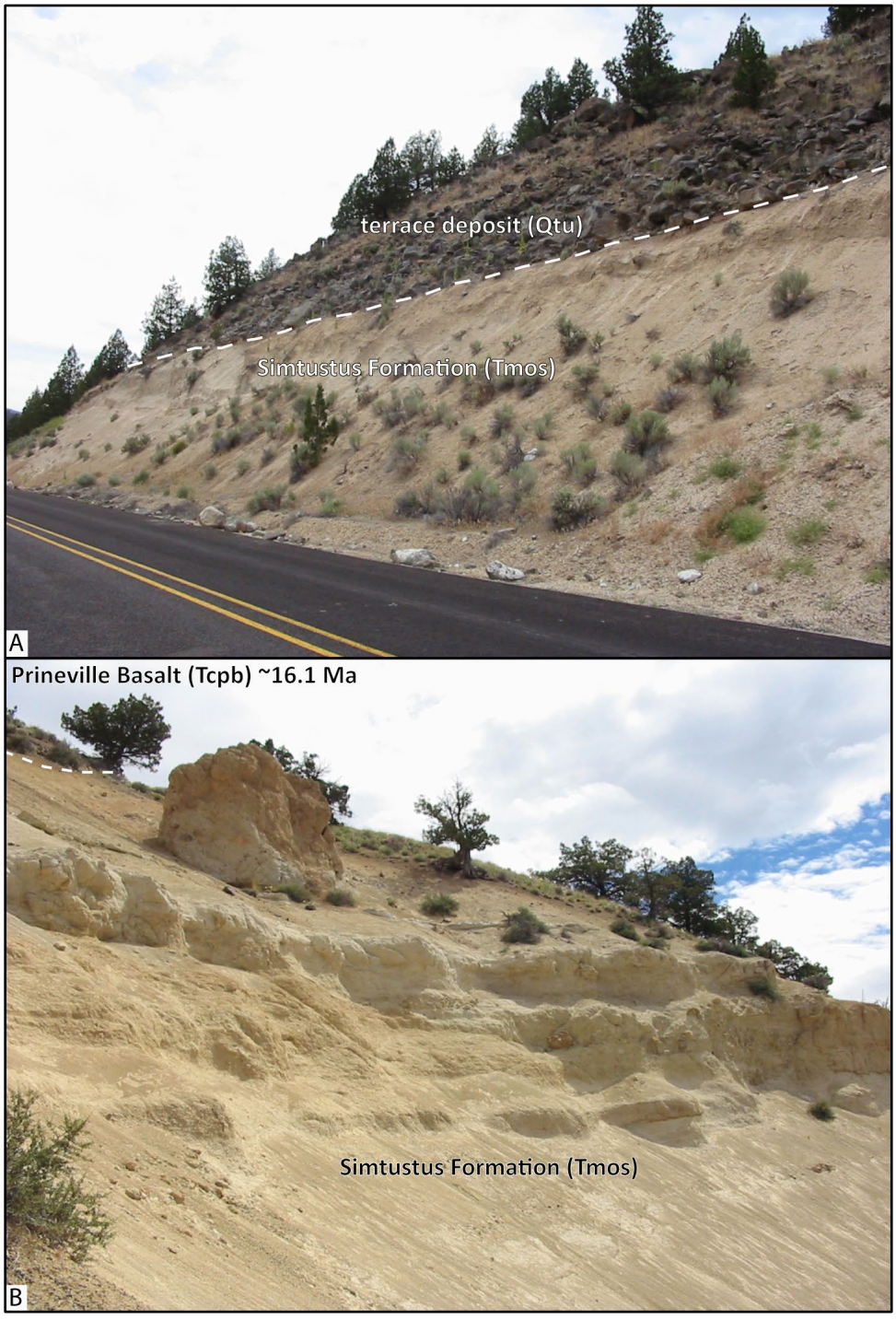

Table 6-7. Select XRF geochemical analyses for Simtustus Formation volcanic rocks in the lower Crooked River basin.

Sample	SIM-CR-15	72 LCJ 06[1]	CROO53726-695[2]	CROO53726-675[2]
Geographic Area	Crooked River	Eagle Rock	Prineville Airport	Prineville Airport
Formation	Simtustus	Simtustus	Simtustus	Simtustus
Map Unit	Tmos	Tmos	Tmos	Tmos
UTM N (NAD 83)	4893078	4897257	4906405	4906405
UTM E (NAD 83)	672924	685825	668543	668543
Age (Ma)	nd	nd	nd	nd
Map Label	G67	G106	G199	G200
Oxides, weight percent				
SiO_2	66.48	70.08	70.90	63.89
Al_2O_3	15.08	16.47	13.39	17.74
TiO_2	1.10	0.89	0.95	1.08
FeOTotal	6.87	4.73	5.51	8.08
MnO	0.09	0.06	0.11	0.11
CaO	3.67	2.07	2.45	3.00
MgO	2.44	1.11	1.47	3.78
K_2O	1.96	2.67	3.39	1.19
Na_2O	2.03	1.84	1.70	0.94
P_2O_5	0.27	0.09	0.13	0.19
LOI	12.02	10.18	9.12	18.02
Total_I	100.21	100.41	99.77	99.93
Trace Elements, parts per million				
Ni	8	5	8	25
Cr	26	12	19	15
Sc	18	14	13	12
V	81	72	114	517
Ba	520	588	351	392
Rb	43.5	56.5	67.6	41.3
Sr	257	152	183	195
Zr	181	296	223	180
Y	41.9	29.1	44.6	53.3
Nb	11.7	14.8	19.0	14.4
Ga	20	17.8	23.1	23.5
Cu	31	14	20	72
Zn	103	78	111	116
Pb	<1	13	<1	<1
La	25	25	29	30
Ce	48	62	53	67
Th	14.6	6.1	15.2	17.1
Nd	1	2	0.5	<0.5
U	14	8	17	24

Major element determinations have been normalized to a 100-percent total on a volatile-free basis and recalculated with total iron expressed as FeOTotal; nd - no data or element not analyzed. Data from: [1]McClaughry and Ferns (2007c); [2]Dunbar and Perkins (2015).

Angular unconformity to disconformity

6.4 Lower Cenozoic volcanic and sedimentary rocks

6.4.1 John Day Formation

6.4.1.1 Lower Crooked volcanic field

Tjot **trachyandesite (upper Oligocene)—**High-strontium trachyandesite (SiO_2 = 57.41 weight percent; K_2O = 2.32 weight percent; Na_2O = and 4.63 weight percent; Sr = 2,520 ppm; *n* = 1 analysis) mapped at the head of Deer Creek in the north-central part of the lower Crooked River basin (**Figure 5-12**, **Figure 6-34**; **Table 6-8**; plate; appendix). Unit **Tjot** crops out as a blocky jointed, dome-like feature (**Figure 6-34**), and is flanked by gravel with clasts of similar composition. Typical hand samples are light gray (N7) and aphyric to very sparsely porphyritic, containing ≤1 percent (vol.) plagioclase phenocrysts and glomerocrysts ≤2 mm (0.1 in) long, distributed within a fine- to medium-grained vesicular, holocrystalline groundmass. Unit **Tjot** is assigned a late Oligocene age on the basis of similar stratigraphic position to units **Tjoa** and **Tjob** (**Figure 6-1**; plate).

Figure 6-34. Outcrop of trachyandesite (Tjot) cropping out east of the upper part of Allen Creek (44.494165, -120.743245). Arrow points to 19 cm (7.5 in) tall yellow notebook for scale in the lower-center part of the photograph. Photo credit: Jason McClaughry, 2006.

Table 6-8. Select XRF geochemical analyses for the John Day Formation in the lower Crooked River basin *(continued on next pages)*.

Sample	253 LCJ 06[1]	360 LCJ 07	JM-SP13-4	9.13X.05[2]	PAT BB1[3]	PAT OR2A[3]	350 LCJ 07	1.9II.06[2]	1.15VII.05[4]	3B.30VI.05[5]	7.29VI.05[5]	08-PJ-05[5]
Geographic Area	Deer Creek	Steins Pillar	Steins Pillar	Prineville	Barnes Butte	Ochoco Reservoir	Haystack Reservoir	Peppermint Lane	Ochoco Reservoir	Powell Buttes	Powell Buttes	Powell Buttes
Formation	John Day	John Day	John Day	John Day	John Day	John Day	John Day	John Day	John Day	John Day	John Day	John Day
Map Unit	Tjot	Tjoa	Tjob	Tjbt	Tjrb	Tjtb	Tjtb	Tjtp	Tjro	Tjpq	Tjps	Tjpa
UTM N (NAD 83)	4929248	4918477	4919172	4913263	4910549	4907089	4929057	4911212	4908651	4894939	4894446	4897320
UTM E (NAD 83)	679413	692361	689459	676401	674005	680948	647082	671357	682531	661288	662225	663815
Age (Ma)	nd	nd	27.8 Ma	nd	~27.97 Ma	~28 Ma	~27.6 Ma	28.18 Ma	27.54 Ma	nd	~25.8 Ma	~28.3 Ma
Map Label	G497	G332	G348	G270	G235	G212	G48X	G240	G221	G92	G88	G107
Oxides, weight percent												
SiO_2	57.41	56.29	54.69	66.30	78.05	78.18	76.20	75.47	75.98	77.50	75.25	79.34
Al_2O_3	16.48	16.64	16.54	13.36	11.27	11.61	12.36	12.65	11.95	8.23	11.67	11.56
TiO_2	1.65	1.18	1.52	1.01	0.16	0.15	0.24	0.31	0.28	0.30	0.29	0.14
FeOTotal	5.52	8.19	10.01	8.78	1.80	1.15	2.29	2.67	2.86	6.70	3.83	0.95
MnO	0.08	0.14	0.29	0.13	0.02	0.01	0.03	0.05	0.05	0.11	0.04	0.01
CaO	7.95	8.15	8.08	2.19	0.14	0.17	1.66	1.83	0.19	0.50	0.30	0.09
MgO	3.08	4.71	4.23	0.53	0.09	0.08	0.38	0.60	0.09	0.11	0.14	0.05
K_2O	2.32	1.11	0.81	3.65	5.98	4.95	5.84	4.71	4.56	4.32	4.70	4.33
Na_2O	4.63	3.26	3.39	3.63	2.47	3.64	0.96	1.63	3.98	2.16	3.74	3.49
P_2O_5	0.87	0.33	0.44	0.42	0.02	0.06	0.04	0.08	0.05	0.06	0.05	0.04
LOI	0.62	2.12	2.27	1.53	nd	nd	7.00	7.45	0.44	2.02	1.67	0.70
Total_I	99.60	99.86	100.24	99.92	96.85	97.73	nd	100.05	99.69	99.94	100.27	100.11
Trace Elements, parts per million												
Ni	25	48	66	9	7	0	0	0	4	7	6	2
Cr	17	70	84	5	4	2	1	0	0	0	0	0
Sc	12	22	20	25	1	2	3	5	3	2	1	1
V	147	201	214	43	14	4	8	24	9	21	10	8
Ba	825	261	303	836	503	520	437	957	765	233	516	963
Rb	13	30	32	87	135	124	137	96	118	109	112	115
Sr	2520	434	410	167	13	11	50	76	29	22	17	10
Zr	205	215	227	610	335	341	393	512	771	872	826	462
Y	12	27	31	86	67	69	89	96	111	87	106	63
Nb	23.6	15.7	20.3	45.2	40.0	40.5	39.9	57.5	64.6	69.9	70.2	45.0
Ga	21	20	21	22	21	23	24	20	25	25	29	23
Cu	64	112	139	9	5	4	4	12	3	7	5	0
Zn	94	94	114	131	99	93	138	118	128	217	155	43
Pb	6	3	13	8	11	12	15	12	11	16	11	3
La	22	19	29	66	54	54	59	60	87	82	68	30
Ce	99	40	48	140	103	111	127	157	186	173	155	68
Th	2	4	5	11	12	15	17	14	14	15	13	12
Nd	0	0	0	0	0	0	0	0	0	0	0	0
U	2	0	0	4	4	5	5	6	5	3	2	5

Major element determinations have been normalized to a 100-percent total on a volatile-free basis and recalculated with total iron expressed as FeOTotal; nd - no data or element not analyzed; na - not applicable or no information. LOI, Loss on Ignition; Total_I, original analytical total. Data from: [1]Ferns and McClaughry (2007); [2]McClaughry and Ferns (2006a); [3]Patridge (2010); [4]McClaughry and Ferns (2006b); [5]Ferns and McClaughry (2006a).

Table 6-8, *continued***. Select XRF geochemical analyses for the John Day Formation in the lower Crooked River basin (part 2 of 3).**

Sample	25-P-05[5]	520 LCJ 08[6]	PAT GR 1[3]	1A.29VII.05[4]	GSO95-41	95-BE-31	24 LCJ 06[6]	SRT-SKULL-1	1 OCJ 14	HS-JM-04	394 LCJ 07	448 LCJ 07
Geographic Area	Powell Buttes	Pilot Butte	Grizzly Mountain	Hi-Tor Butte	Gray Butte	Juniper Butte	Smith Rock	Skull Hollow	Gray Butte	Haystack Reservoir	Haystack Reservoir	McKay Saddle
Formation	John Day	John Day	John Day	John Day	John Day	John Day	John Day	John Day	John Day	John Day	John Day	John Day
Map Unit	Tjpi	Tjrpb	Tjrgm	Tjrh	Tjrg	Tjrj	Tjtsi	Tjtsi	Tjtsi	Tjtso	Tjtso	Tjtso
UTM N (NAD 83)	4894204	4899157	4921617	4909654	4918587	4926355	4914422	4918805	4918140	4927762	4928678	4932488
UTM E (NAD 83)	660894	691805	662405	688632	650165	641551	648183	653710	649161	649171	646517	687455
Age (Ma)	nd	nd	28.9 Ma	29.2 Ma	nd	~29.3 Ma	29.3 Ma	29.3 Ma	28.3 Ma	29.57 Ma	29.51 Ma	29.56 Ma
Map Label	G80	G125	G385	G226	G335	G445	G283	G341	G325	G471	G482	G516
Oxides, weight percent												
SiO_2	75.58	78.44	77.87	76.78	77.01	78.60	76.88	80.92	76.88	78.24	78.11	76.34
Al_2O_3	12.95	11.81	11.99	12.24	12.45	10.92	12.09	9.65	11.51	11.32	10.84	13.04
TiO_2	0.28	0.16	0.22	0.19	0.21	0.13	0.24	0.18	0.21	0.13	0.15	0.24
FeOTotal	2.04	0.93	1.35	2.00	1.58	1.63	2.49	2.09	2.28	1.31	1.92	1.13
MnO	0.01	0.01	0.01	0.04	0.02	0.01	0.05	0.07	0.04	0.03	0.03	0.02
CaO	0.69	0.13	0.18	0.40	0.28	0.12	0.48	0.18	0.39	0.66	0.10	0.50
MgO	0.14	0.09	0.02	0.12	0.07	0.16	0.23	0.15	0.34	0.08	0.11	0.13
K_2O	4.53	4.22	4.36	4.66	4.29	5.01	4.25	6.69	6.79	4.54	8.40	4.11
Na_2O	3.72	4.16	3.93	3.51	4.03	3.41	3.22	0.03	1.50	3.59	0.33	4.43
P_2O_5	0.05	0.05	0.06	0.05	0.06	0.03	0.07	0.04	0.05	0.09	0.02	0.05
LOI	1.18	0.81	0.00	2.82	1.30	nd	2.10	1.60	3.14	1.70	2.00	0.92
Total_I	99.81	99.72	97.92	100.08	99.51	nd	99.58	100.10	nd	99.95	nd	99.73
Trace Elements, parts per million												
Ni	3	1	1	0	8	9	2	4	6	8	0	0
Cr	0	7	2	1	16	0	0	37	12	7	1	1
Sc	3	7	3	2	0	0	3	0	0	0	0	3
V	13	12	0	7	9	4	9	34	12	9	17	14
Ba	908	975	994	1001	999	309	1035	756	890	488	111	1120
Rb	117	133	128	128	149	172	134	233	184	160	180	131
Sr	63	18	40	35	28	14	43	39	15	25	8	47
Zr	429	455	546	485	624	373	512	410	536	569	420	596
Y	38	86	86	91	75	99	114	86	107	61	90	113
Nb	26.3	75.6	57.0	66.9	85.8	49.0	53.8	47.2	70.4	61.4	53.6	71.9
Ga	18	21	25	25	34	30	22	25	31	32	30	26
Cu	2	2	2	2	11	2	0	3	15	17	5	0
Zn	58	50	115	146	148	111	180	80	164	102	124	168
Pb	8	1	14	12	14	14	7	1	17	17	28	8
La	41	96	71	81	57	81	59	65	69	58	60	68
Ce	94	200	146	172	228	130	139	148	155	113	108	172
Th	11	15	16	16	33	15	19	14	22	29	20	16
Nd	0	0	0	0	0	0	0	0	0	0	0	0
U	4	3	3	5	4	0	5	2	1	2	5	5

Major element determinations have been normalized to a 100-percent total on a volatile-free basis and recalculated with total iron expressed as FeOTotal; nd - no data or element not analyzed; na - not applicable or no information. LOI, Loss on Ignition; Total_I, original analytical total. Data from: [1]Ferns and McClaughry (2007); [2]McClaughry and Ferns (2006a); [3]Patridge (2010); [4]McClaughry and Ferns (2006b); [5]Ferns and McClaughry (2006a); [6]McClaughry and others (2009a, c).

Table 6-8, *continued***. Select XRF geochemical analyses for the John Day Formation in the lower Crooked River basin (part 3 of 3).**

Sample	JM ER 13-4	PH95 376[6]	PAT PR28[3]	17 LC 06[7]	18 LC 06[7]	16 LC 06[7]	SR-B-10[8]	RC95-74[9]	484 LCJ 08	11 LCJ 06[7]	430 LCJ 07
Geographic Area	Prineville Reservoir	Antelope	Prineville Reservoir	Prineville Reservoir	Prineville Reservoir	Prineville Reservoir	Lithgow Spring	Gray Butte	Rodman Spring	Prineville Reservoir	Ochoco Divide
Formation	John Day	John Day	John Day	John Day	John Day	John Day	John Day	John Day	John Day	John Day	John Day
Map Unit	Tjtso	Member G	Tjtsn	Tjta	Tjte	Tjba	Tjba	Tjia	Tjtr	Tjtt	Tjtma
UTM N (NAD 83)	4888345	4969518	4888345	4889827	4889331	4889365	4922582	4920872	4925107	4893363	4926007
UTM E (NAD 83)	681250	669334	681287	680715	680777	680227	651958	648010	649855	685309	710631
Age (Ma)	29.5 Ma	29.54 Ma	~29.5 Ma	~29.6 Ma	29.7 Ma	~29.6 Ma	~30 Ma	nd	32.49 Ma	nd	~39.7 Ma
Map Label	G25	na	G26	G52	G45	G47	G403	G372	G431	G69	G441
Oxides, weight percent											
SiO_2	76.48	75.21	74.45	75.28	78.97	56.15	48.23	52.02	79.31	77.77	73.17
Al_2O_3	12.11	12.81	13.35	11.66	10.96	14.36	15.22	13.51	11.79	12.39	13.10
TiO_2	0.17	0.32	0.39	0.30	0.18	2.03	2.88	3.81	0.23	0.21	0.68
FeOTotal	2.50	2.20	3.28	3.70	2.06	12.37	13.66	14.08	1.82	0.90	3.97
MnO	0.04	0.03	0.03	0.03	0.02	0.27	0.23	0.22	0.03	0.02	0.02
CaO	0.39	0.77	0.62	0.84	0.29	6.17	8.88	8.24	2.56	2.27	2.17
MgO	0.12	0.57	0.80	0.31	0.15	2.29	6.10	3.68	0.73	0.26	0.53
K_2O	4.11	6.01	1.80	5.25	3.87	1.63	1.01	1.03	2.14	3.42	2.69
Na_2O	4.01	2.05	5.20	2.55	3.42	3.79	3.08	2.82	1.31	2.68	3.44
P_2O_5	0.06	0.03	0.07	0.07	0.07	0.94	0.70	0.56	0.08	0.07	0.24
LOI	1.25	6.84	0.00	2.58	1.59	2.70	nd	nd	8.36	11.85	2.66
Total_I	99.74	nd	91.61	99.63	99.85	99.53	99.83	nd	100.29	100.43	100.20
Trace Elements, parts per million											
Ni	7	16	0	9	7	4	66	0	1	2	10
Cr	9	4	7	4	0	7	95	40	5	0	8
Sc	0	4	7	6	2	30	29	34	5	3	10
V	12	8	27	28	13	148	243	330	30	15	53
Ba	1032	221	153	915	960	374	321	386	1320	683	762
Rb	128	192	48	108	118	46	18	25	50	71	78
Sr	50	28	26	145	43	291	404	256	418	96	245
Zr	584	582	380	535	490	243	276	212	201	350	315
Y	223	103	95	86	120	61	41	42	83	53	32
Nb	66.5	56.0	45.1	45.3	64.7	20.9	26.0	23.0	23.8	44.1	23.4
Ga	31	28	21	23	24	25	23	27	17	21	15
Cu	18	7	8	0	0	4	42	20	13	0	10
Zn	122	110	118	158	131	120	135	138	98	79	43
Pb	15	17	12	27	2	2	0	7	13	10	5
La	95	nd	62	44	68	29	0	0	38	54	35
Ce	226	nd	130	100	148	59	0	0	85	107	79
Th	28	20	14	10	16	3	0	3	9	11	8
Nd	0	nd	0	0	0	0	0	0	0	0	0
U	2	nd	7	3	5	0	0	0	3	5	3

Major element determinations have been normalized to a 100-percent total on a volatile-free basis and recalculated with total iron expressed as FeOTotal; nd - no data or element not analyzed; na - not applicable or no information. LOI, Loss on Ignition; Total_I, original analytical total. Data from: [1]Ferns and McClaughry (2007); [2]McClaughry and Ferns (2006a); [3]Patridge (2010); [4]McClaughry and Ferns (2006b); [5]Ferns and McClaughry (2006a); [6]McClaughry and others (2009a, c); [7]McClaughry and Ferns (2007c); [8]Obermiller (1987); [9]Smith and others (1998). Sample PH95 376 is outside the map area.

Tjoa **andesite (upper Oligocene)—**Andesite and dacite lava flows and domes (SiO_2 = 61.6 to 64.06 weight percent; Al_2O_3 = 16.36 to 17.19 weight percent; K_2O = 1.14 to 2.38 weight percent; Sr = 288 to 414 ppm; *n* = 6 analyses) mapped unconformably across the southern part of the Wildcat Mountain caldera (**Figure 5-12**, **Figure 6-35**; **Table 6-8**; plate; appendix; Ferns and McClaughry, 2007). Platy to blocky columnar jointing characterizes outcrops of unit **Tjoa**, with vesicle-rich zones occurring along the outer margins of mapped lava flows and domes. Quarry exposures along U.S. Highway 26, at the mouth of Sears Creek, have wildly radiating and flaring columns, vesicles filled by banded agate, and 1- to 2-cm-thick (0.4 to 0.8 in) quartz veins striking N.75°W. and dipping 8°SW. (**Figure 6-36**). Unit **Tjoa** typically weathers to form slopes armored by platy rock fragments and subround boulders. Locally, a conglomerate composed of clasts of the tuff of Steins Pillar (**Tcts**), is exposed at the base of unit (**Tjoa**). Typical hand samples are medium bluish gray (5B 5/1) to black (N1) and porphyritic, containing 5 to 10 percent (vol.) microphenocrysts of clear, subhedral to anhedral, lath-shaped to blocky, etched and embayed, variably perthitic, seriate, plagioclase ≤2 mm (0.1 in) across, dusky green (5G 3/2), subhedral clinopyroxene ≤2 mm (0.1 in) across, and ≤1 percent (vol.) plagioclase-clinopyroxene glomerocrysts up to 4 mm (0.2 in), distributed within a hypocrystalline groundmass.

Unit **Tjoa** is assigned a late Oligocene age on the basis of stratigraphic position above the 41.8 Ma tuff of Steins Pillar (**Tcts**); these rocks are inferred to be comparable in stratigraphic position to 27.8 Ma basaltic andesite flows and intrusions of unit **Tjob** (**Figure 6-1**; plate).

Figure 6-35. Columnar-jointed glassy, porphyritic andesite (Tjoa) cropping out east of Mahogany Butte in the northeast part of the map area (44.377025, -120.627874). Arrow points to 40 cm (15.7 in) long hammer for scale. Photo credit: Jason McClaughry, 2007.

Figure 6-36. Sears Creek quarry along U.S. Highway 26, northeast of Prineville (44.401958, -120.512693). The quarry has exposed a porphyritic andesite intrusion (Tjoa), marked by wildly radiating and flaring columns, vesicles filled by banded agate, and quartz veins. Photo credit: Jason McClaughry, 2007.

Tjob **basaltic andesite (upper Oligocene)—**Basaltic andesite lavas and domes (SiO_2 = 54.69 to 57.38 weight percent; Al_2O_3 = 16.39 to 17.79 weight percent; K_2O = 0.73 to 1.4 weight percent; Sr = 310 to 627 ppm; *n* = 11 analyses) mapped unconformably across the southern part of the Wildcat Mountain caldera in the northeast part of the lower Crooked River basin (**Figure 5-12**, **Figure 6-37**; **Table 6-8**; plate; appendix; Ferns and McClaughry, 2007). Unit **Tjob** includes both feeder intrusions and geochemically equivalent lava flows. Feeder vents for basaltic andesite lavas form prominent domes and dike structures along Marks Creek and Salmon Creek (**Figure 5-12**, **Figure 6-37a**). Basaltic andesite dikes and domes are vesicular along their margins, typically strongly vertically flow-foliated, and have columnar jointing. Columns are pseudohexagonal and range from 0.2 to 0.5 m (0.7 to 1.6 ft) across. Basaltic andesite lava flows, cropping out as muted knobs and ridges, form relatively thin (<15 m [49 ft]) flow units, unconformable across and inset into older Eocene deposits. Columnar jointing characterizes lava flows, with pseudohexagonal columns ranging in width from 0.5 to 0.75 m (1.6 to 2.5 ft) across (**Figure 6-37b**). Blocky to subround boulders, intermixed with red-oxidized soils mark the weathered surface of basaltic andesite lava flows. Typical hand samples are medium gray (N5) to black (N1) and aphyric to sparsely porphyritic, containing ≤2 percent (vol.) seriate, subhedral to anhedral, etched and embayed, quartz xenocrysts ≤3.5 mm (0.1 in) across, distributed within a very fine-grained holocrystalline groundmass composed of equigranular plagioclase microlites, intergranular pyroxene, and Fe-Ti oxides. Xenocrysts are typically rimmed by 0.1 mm (0.004 in) thick

aggregates of clinopyroxene and orthopyroxene. Plagioclase is commonly poikilophitic, enclosing blocky clinopyroxene.

Unit **Tjob** is assigned a late Oligocene age on the basis of unconformable stratigraphic position above the 41.8 Ma tuff of Steins Pillar (**Tcts**) and an integrated $^{40}Ar/^{39}Ar$ age of 27.80 ± 0.6 Ma obtained for a sample between Rocky Point and Steins Pillar (whole rock; sample JM-SP13-4) (**Figure 5-11**, **Figure 5-12**, **Figure 6-1**; **Table 5-2**; plate; appendix).

Figure 6-37. Upper Oligocene andesitic lava flows and domes. (a) High-standing basaltic andesite intrusion (Tjob) in the headwaters area of Salmon Creek. View is looking east from USFS Road 500 (44.396215, -120.592386). (b) Columnar-jointed basaltic andesite (Tjob) cropping out along Salmon Creek (44.382544, -120.576849). Photo credits: Jason McClaughry, 2007.

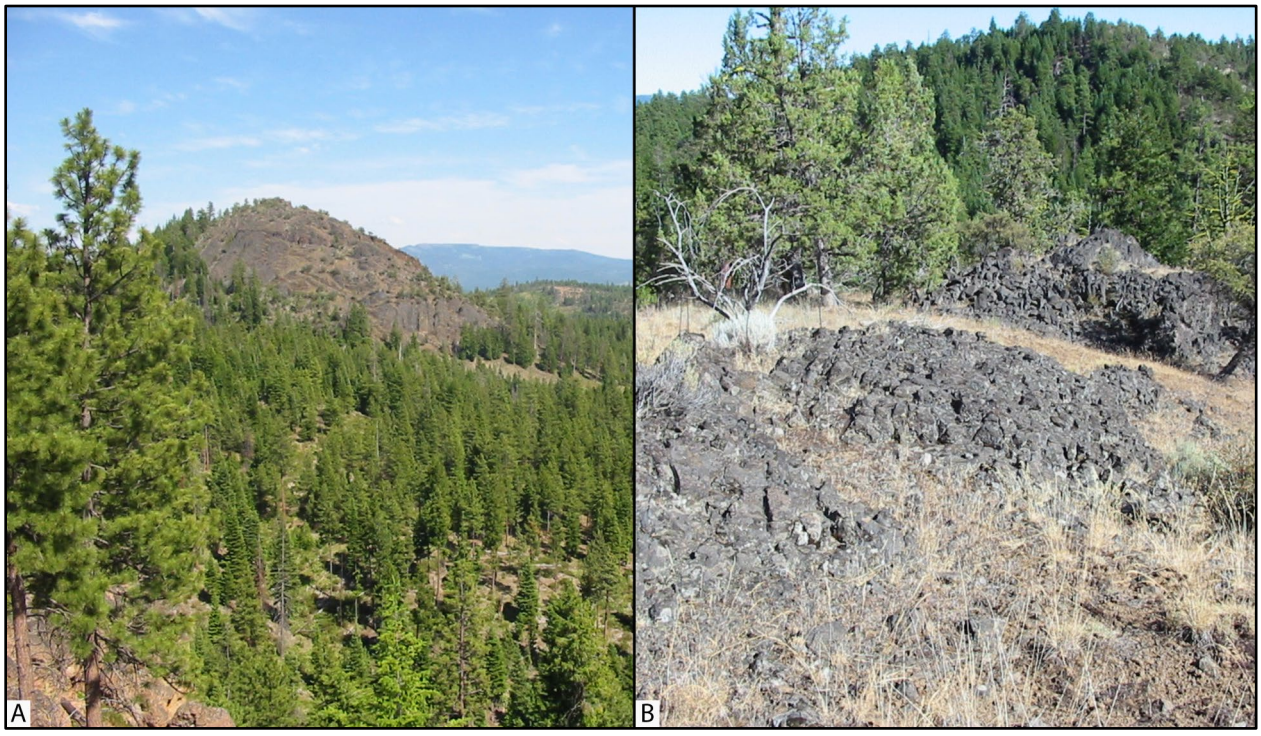

Tjs **tuffaceous sedimentary rocks (Oligocene)—**Light greenish gray (5GY 8/1), pale red (SR 6/2), very pale orange (10YR 8/2), to grayish orange (10YR 7/4), massive to stratified, indurated claystone, tuffaceous siltstone, and sandstone overlying the tuff of Smith Rock (**Tjtsi**) along the south rim of Combs Flat and in more subdued outcrops north of Powell Buttes (**Figure 5-12**; plate). The unit includes sedimentary interbeds exposed between outflow tuff deposits of the tuff of Smith Rock (**Tjtso**, **Tjtsn**) and the overlying the tuff of Barnes Butte (**Tjtb**) south of Haystack Reservoir. Unit **Tjs** is commonly thinly bedded, with sedimentary beds as thick as thick as 15 cm (6 in). Outcrops of indurated siltstone and fine-grained sandstone typically weather to angular chips and popcorn-weathered surfaces, due to the presence of expansive bentonitic clay. Partially opalized limb casts, petrified wood, and fragmental fossil imprints of *Metasequoia occidentalis* occur locally within unit **Tjs**. Unit **Tjs** is assigned an Oligocene age on the basis of stratigraphic position above basaltic andesite lavas of unit **Tjba** and below sedimentary strata of unit **Tmos** (**Figure 6-1**; plate)

6.4.1.1.1 Crooked River caldera

Tjbt **rhyolite breccia and dacite tuff (upper Oligocene)—**Silicified rhyolite breccia and welded tuff mapped along the northeastern margin of the Crooked River caldera, north of Prineville (**Figure 5-12**; plate). The breccia is grayish red purple (5RP 4/2) to moderate brown (5YR 3/4), welded, clast-supported and consists of angular to subround clasts of rhyolite, expanded pumice, and coarse-grained, alkali-feldspar-dominated granitic lithics up to 11 cm (4.3 in) across. Many clasts display bleached halos. The matrix component (~15 percent vol.) is crystalline, porphyritic, and apparently welded. Bulbous masses of aphyric rhyolite are exposed beneath the breccia; angular coarse-grained granitic rock fragments are commonly mixed with the eroding breccia float. A distinct, massive to perlitic, porphyritic vitrophyre crops out with the breccia. The breccia is overlain by a moderate brown (5YR 4/4) to medium gray (N5), strongly welded dacite pumice tuff (SiO_2 = 66.01 weight percent; Zr = 610 ppm; Nb = 45.2 ppm; *n* = 1 analysis), with flattened pumices up to 30 cm (12 in) long and pebble-sized angular rhyolite lithic clasts. The deposit is internally marked by 10 to 20 cm (4 to 8 in) thick shear zones and folded fiamme. The unit is assigned a late Oligocene age on the basis of stratigraphic position (**Figure 6-1**; plate). Mapped contact relations between the breccia, welded tuff, and intracaldera unit of the tuff of Smith Rock (**Tjtsi**) indicate emplacement of the unit following formation of the Crooked River caldera.

Tjrb **rhyolite of Barnes Butte (upper Oligocene)—**High-silica rhyolite dome complex mapped along the summit and northern margin of Barnes Butte (**Figure 5-12**, **Figure 5-15**, **Figure 6-38**; **Table 6-8**; plate; appendix). The rhyolite is typically altered, with very high silica content (SiO_2 = 81.82 to 82.68 weight percent; *n* = 3 analyses); a single unaltered sample from unit **Tjrb** has a SiO_2 content of 78.05 weight percent. Compared to other rhyolite domes associated with the Crooked River caldera, the rhyolite of Barnes Butte (**Tjrb**) displays lower levels of barium (Ba = 503 ppm), zirconium (Zr = 328 to 364; *n* = 4 analyses) and niobium (Nb = 40.0 to 47.1 ppm; *n* = 4 analyses) (**Figure 5-15**; **Table 6-8**; appendix). Outcrops within the dome complex are either massive or flow-banded, marked by 0.5- to 1.5-m thick (1.6- to 4.9- ft), vertically oriented, perlitic bands (**Figure 6-39**). The rhyolite of Barnes Butte (**Tjrb**) intrudes the tuff of Barnes Butte (**Tjtb**); the contact aureole between the rhyolite (**Tjrb**) and the tuff (**Tjtb**) is locally marked by silicified zones containing visible cinnabar (**Figure 6-38**). The main alteration zone occurs along a N.75°W.-striking fault zone, which was the site of the Barnes Butte mercury prospect (**Figure 6-38**; Brooks, 1963). Unit **Tjrb** includes rhyolite plugs that project through the intracaldera unit of the tuff of Smith Rock (**Tjtsi**) northwest of Barnes Butte Reservoir (**Figure 5-12**; plate). Typical hand samples of the rhyolite (**Tjrb**) are light gray (N7) to light bluish gray (5B 7/1) and sparsely porphyritic, containing ≤ 1 percent (vol.) clear to chalky white (N9), albite-twinned sanidine phenocrysts ≤2 mm (0.1 in) across, distributed within a devitrified, heavily silicified and recrystallized groundmass composed of quartz, feldspar, and abundant Fe-Ti oxides. Feldspars have overgrowth textures as well as embayed edges. Orthopyroxene, zircon, and apatite appear in minor amounts.

The rhyolite of Barnes Butte (**Tjrb**) is assigned a late Oligocene age on the basis of stratigraphic position and an $^{40}Ar/^{39}Ar$ plateau age of 27.97 ± 0.32 Ma (whole rock; sample 4B.12VII.05) (**Figure 5-11**, **Figure 5-12**, **Figure 6-1**; **Table 5-2**; plate; appendix; McClaughry and Ferns, 2006a).

Figure 6-38. Barnes Butte looking east from Ochoco Wayside (44.300427, -120.864236). The south end of the butte is underlain by the welded tuff of Barnes Butte (Tjtb), which has a $^{206}Pb/^{238}U$ zircon age of 28.3 ± 0.4 Ma. The rhyolite of Barnes Butte (Tjrb), which has an $^{40}Ar/^{39}Ar$ age of 27.97 ± 0.32 Ma, intrudes the tuff along the northern edge of the butte. The contact is marked by heavily silicified and mineralized tuff, and was the site of the ~ 1940s Barnes Butte mercury prospect. Photo credit: Jason McClaughry, 2013.

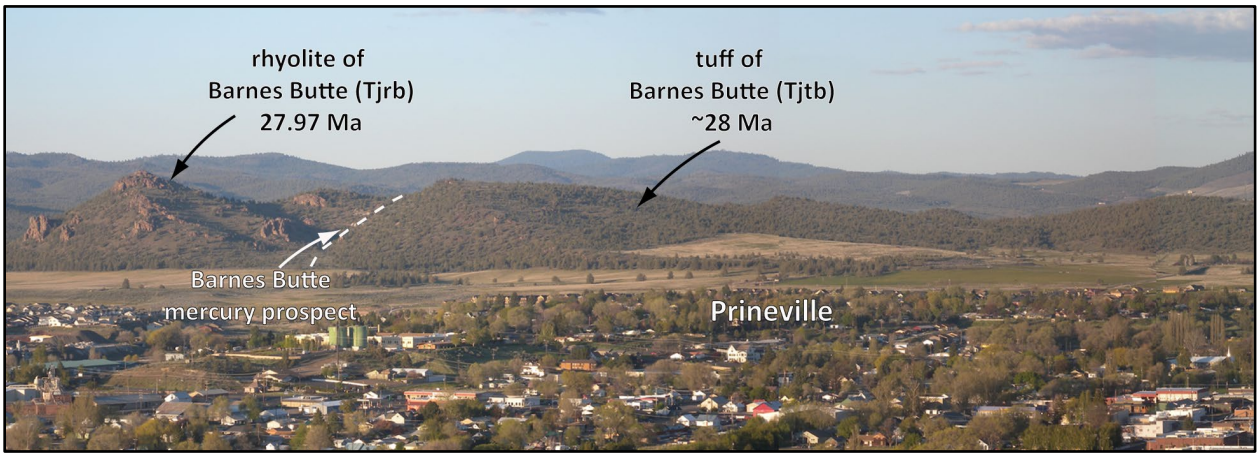

Figure 6-39. Vertically foliated rhyolite intrusion (Tjrb) underlying the northern part of Barnes Butte (44.323468, -120.818519). This outcrop has returned an $^{40}Ar/^{39}Ar$ plateau age of 27.97 ± 0.32 Ma. Person for scale sitting in the lower right side of the photograph is 1 m (3 ft) high. Photo credit: Jason McClaughry, 2005.

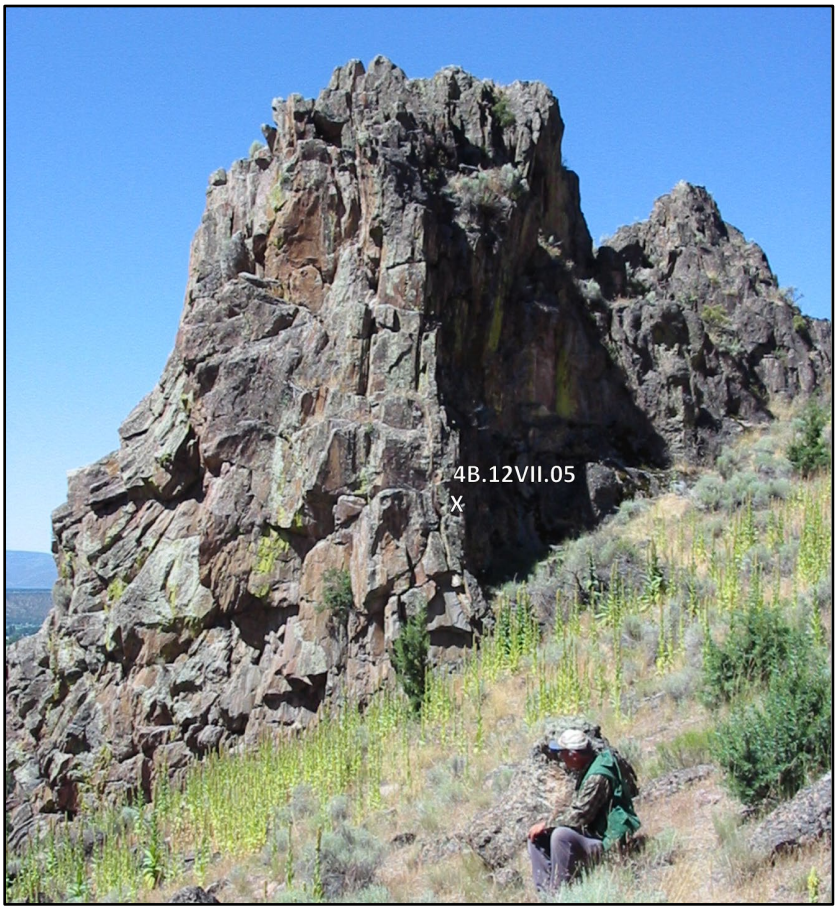

Tjtb **tuff of Barnes Butte (upper Oligocene)—**Rhyolite ash-flow tuff mapped across the southern part of Barnes Butte and in cliff-forming exposures along the southern margin of Ochoco Reservoir (**Figure 5-12**, **Figure 5-15**, **Figure 6-38**, **Figure 6-40**; **Table 6-8**; plate; appendix). The tuff of Barnes Butte (**Tjtb**) is a strongly vapor-phase altered unit, with very high silica content in some samples (SiO_2 = 81.43 to 83.9 weight percent; *n* = 3 analyses); less altered samples from unit **Tjtb** from the Barnes Butte area have silica contents ranging between 77.92 and 78.27 weight percent SiO_2 (*n* = 3 analyses) (**Figure 5-15**; **Table 6-8**; appendix). Zirconium contents for all samples from the Barnes Butte area range between 251 and 375 ppm Zr, while barium ranges between 410 and 620 ppm Ba and niobium ranges between 36.5 and 46.4 ppm Nb (*n* = 7 analyses) (**Figure 5-15**; **Table 6-8**; appendix). The tuff of Barnes Butte (**Tjtb**) is also considered in this report to include ash-flow tuff mapped capping mesas and cuestas between Gray Butte and Haystack Reservoir (**Figure 5-12**). These outcrops were previously mapped and correlated with the ignimbrite defining the base of the Member H tuff of the John Day Formation (Robinson and Stensland, 1979; Robinson and others, 1990; Smith and others, 1998). Similar stratigraphic position, mineralogy, like geochemistry, and comparable isotopic ages between the Barnes Butte and Haystack Reservoir outcrop areas suggest a permissible correlation (plate). Like the Barnes Butte type area, Member H tuff near Haystack Reservoir is strongly vapor-phase altered, with very high silica content in some samples (SiO_2 = 80.27 to 82.99 weight percent; *n* = 4). Less altered tuff samples from Haystack Reservoir have silica contents ranging between 76.20 to 77.99 weight percent SiO_2 (*n* = 3 analyses) and barium contents between 266 and 437 ppm, sharing similar contents of zirconium and niobium (Zr = 332 to 475 ppm; Nb = 31 to 44.4 ppm; all samples; *n* = 7 analyses) to tuff cropping out on Barnes Butte and along the south side of Ochoco Reservoir (**Figure 5-12**, **Figure 5-15**; **Table 6-8**; appendix).

The tuff of Barnes Butte (**Tjtb**) crops out in the Barnes Butte, Ochoco Reservoir, and Haystack Reservoir areas as conspicuous very pale orange (10YR 8/2) cliffs and ledges, characterized by blocky to columnar jointing (**Figure 5-12**, **Figure 6-40**). Lithophysae are abundant and characteristic features of the unit (**Tjtb**). Deeply weathered tuff (**Tjtb**) forms hoodoos and is associated with land-surfaces mantled by angular rock fragments and chips. Subround pumice to strongly welded pumice fiamme up to 7 cm (2.8 in) across make up ~5 percent (vol.) of the unit (**Tjtb**). Lithics make up ≤1 percent (vol.) of the unit (**Tjtb**) and include angular to subrounded, moderate brown (5YR 3/4) aphyric rhyolite ≤2.5 cm (1 in) across. A glassy, dark greenish gray (5G 4/1) perlitic vitrophyre is locally present at the base of the tuff. Maximum thickness of unit **Tjtb** is ~60 m (197 ft) on Barnes Butte, while at Haystack Reservoir tuff thickness ranges between 5 and 20 m (16.4 to 65.6 ft). Typical hand samples of the tuff (**Tjtb**) in the Barnes Butte and Haystack Reservoir areas are grayish orange pink (5YR 7/2) to very pale orange (10YR 8/2) and sparsely porphyritic, containing ≤1 percent (vol.) clear to chalky white (N9) quartz, sanidine, and plagioclase phenocrysts ≤2 mm (0.1 in) across, distributed within a fine-grained, devitrified, vitric groundmass with bands of spherulitic quartz.

The tuff of Barnes Butte (**Tjtb**) is assigned a late Oligocene age on the basis of stratigraphic position and a $^{206}Pb/^{238}U$ zircon age of 28.3 ± 0.4 Ma obtained for a sample on Barnes Butte (sample 6.12VII.05; Seligman and others, 2014) (**Figure 5-12**, **Figure 6-1**; **Table 5-2**; plate; appendix). The eruptive age for the tuff may be closer to ~28 Ma as unit **Tjtb** overlies the 28.18 Ma tuff of Peppermint Lane (**Tjtp**) and is intruded by a 27.97 Ma rhyolite dome (**Tjrb**) at Barnes Butte (**Figure 6-1**; **Table 5-2**; plate; appendix; McClaughry and Ferns, 2006a). A sample obtained near the west end of Haystack Reservoir, on the previously defined Member H tuff, yielded a

slightly younger, but less precise $^{40}Ar/^{39}Ar$ plateau age of 27.62 ± 0.63 Ma (sanidine; sample GS095-134; Smith and others, 1998) (**Figure 5-11**, **Figure 5-12**; **Table 5-2**; plate; appendix). Unit **Tjtb** is notably similar in chemical composition to the rhyolite dome complex (**Tjrb**) forming the north end of Barnes Butte, indicating that area as the probable vent site for the tuff (**Figure 5-12**; plate).

Figure 6-40. Blocky-jointed, welded, pumice-lithic-tuff (Tjtb) cropping out across the southern part of Barnes Butte (44.305854, -120.815838). This outcrop has returned a $^{206}Pb/^{238}U$ zircon age of 28.3 ± 0.4 Ma. Arrow points to 25 cm (9.8 in) long hammer for scale in the center of photograph. Photo credit: Jason McClaughry, 2013.

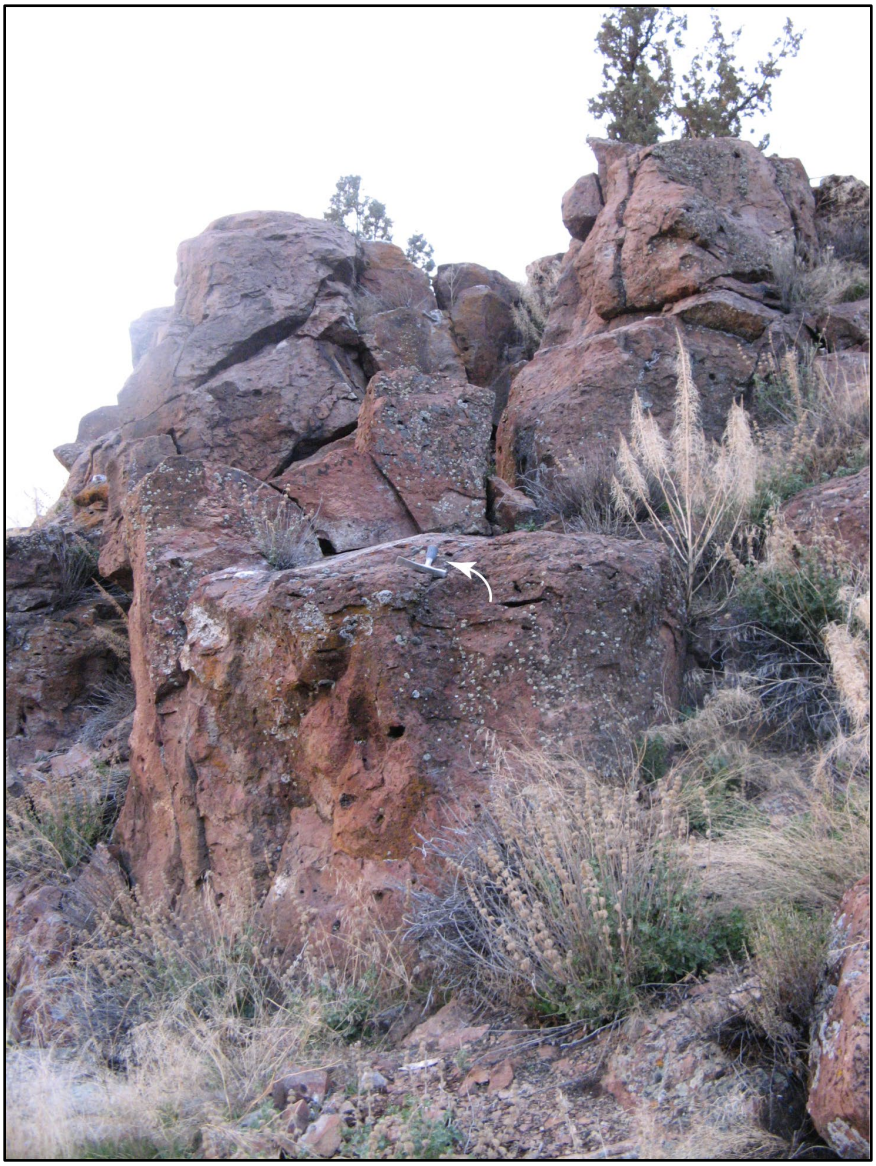

Tjtp **tuff of Peppermint Lane (lower Oligocene)—**Rhyolite pumice-lithic-crystal tuff and lapilli tuff (SiO_2 = 75.47 to 77.37 weight percent; Ba = 718 to 1054 ppm; Zr = 389 to 512 ppm; Nb = 50.5 to 58.2 ppm; *n* = 3 analyses) mapped along the south side of Barnes Butte and along Peppermint Lane, just north of Prineville (**Figure 5-12**, **Figure 5-15**, **Figure 6-41**; **Table 6-8**; plate; appendix). Outcrops of the tuff (**Tjtp**) are typically massive, with areas of platy jointing (**Figure 6-41a**). Weathering of the unit has formed rounded, low elevation hills, with surfaces mantled by angular rock chips. Well-rounded to partially flattened, clay-altered pumices and pumice lapilli ≤6 cm (2.4 in) across are abundant (**Figure 6-41b**). Lithics include moderate brown (5YR 4/4) to grayish black (N2), angular to subround mafic rocks and very pale orange (10YR 8/2) silicic rocks ≤10 cm (3.9 in) across. Thickness of unit **Tjtp** is unknown. Typical hand samples are yellowish gray (5Y 8/1; 5Y 7/2) to light greenish gray (5GY 8/1) and sparsely porphyritic, containing <3 percent (vol.) blocky sanidine and plagioclase microphenocrysts and phenocrysts <2 mm (0.1 in) across, distributed within a groundmass of clay-altered, devitrified, cuspate glass shards. Sanidine phenocrysts commonly have secondary grain overgrowths.

The tuff of Peppermint Lane (**Tjtp**) is assigned an early Oligocene age on the basis of stratigraphic position and an $^{40}Ar/^{39}Ar$ plateau age of 28.18 ± 0.16 Ma (feldspar; sample 1.9II.06) (**Figure 5-11**, **Figure 5-12**, **Figure 6-1**; **Table 5-2**; plate; appendix). The unit is intruded by the 27.97 Ma rhyolite of Barnes Butte (**Tjrb**) and is overlain by the ~ 28 Ma tuff of Barnes Butte (**Tjtb**).

Figure 6-41. The tuff of Peppermint Lane. (a) The tuff of Peppermint Lane (Tjtp) is exposed northwest of Barnes Butte (44.333862, -120.850772). The tuff here has an $^{40}Ar/^{39}Ar$ age of 28.18 ± 0.16 Ma. Person for scale is 1.9 m (6.2 ft) tall. (b) The tuff is nonwelded and sparsely porphyritic, containing abundant pumice and accretionary lapilli. Hammer head for scale is 12 cm (4.7 in) wide. Photo credits: Jason McClaughry, 2006.

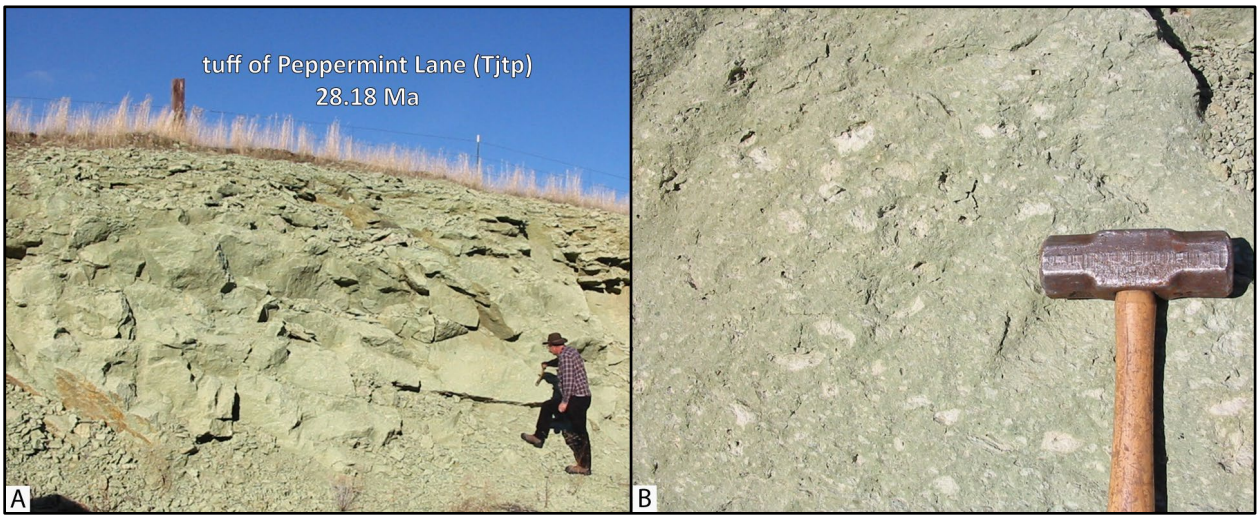

Tjro **rhyolite of Ochoco Reservoir (lower Oligocene)—**Rhyolite lava flow (SiO_2 = 73.44 to 75.98 weight percent; Ba = 735 to 904 ppm; Zr = 763 to 788 ppm; Nb = 58.9 to 64.7 ppm; *n* = 4 analyses) mapped overlying tuffaceous sedimentary rocks of unit **Tjs** at Ochoco Reservoir (**Figure 5-12**, **Figure 5-15**, **Figure 6-42**; **Table 6-8**; plate; appendix). Mapped distribution of the unit indicates a south-dipping (~N. 85° E., 17° SE.), relatively flat-topped, tabular flow body with a relatively consistent thickness of ~45 m (148 ft) (**Figure 6-42**; plate). Unit **Tjro** crops out as precipitous cliffs and ledges with platy to columnar jointing; contorted flow banding is common (**Figure 6-43**). The

upper surface of the lava flow (**Tjro**) is vertically flow-foliated and marked by convex flow-ridges (coulees). The lower part of the flow (**Tjro**) is marked by basal flow breccia. Pockets of multicolored agate and jasper and cavities filled with drusy quartz are locally found within the rhyolite. The weathered unit (**Tjro**) has surfaces mantled by angular rock fragments and chips and moderate brown (5YR 3/4) soils. Landslide complexes, originating from cliff-forming head scarps within the rhyolite flow, are extensive along the north shore of Ochoco Reservoir (**Figure 5-12**, **Figure 6-2**, **Figure 6-42**; plate). Typical hand samples of the rhyolite are medium gray (N5) to grayish red purple (5RP 4/2) and grayish blue (5PB 5/2) and sparsely porphyritic, containing ≤3 percent (vol.) clear sanidine phenocrysts ≤5 mm (0.2 in) and ≤1 percent (vol.) clinopyroxene microphenocrysts ≤1 mm (0.04 in), distributed within a devitrified hypohyalline, microcrystalline groundmass composed of alkali feldspar, cryptocrystalline quartz, and scattered Fe-Ti oxides. Original flow banding is defined by recrystallized zones and lenses of devitrified glass. Spherulitic and axiolitic overgrowth textures are common.

Unit **Tjro** is assigned an early Oligocene age on the basis of stratigraphic position and an $^{40}Ar/^{39}Ar$ plateau age of 27.54 ± 0.36 Ma (whole rock; sample 1.15VII.05; McClaughry and Ferns, 2006b) (**Figure 5-11**, **Figure 5-12**, **Figure 6-1**; **Table 5-2**; plate; appendix). The analyzed isotopic age, however, is discordant with its stratigraphic position beneath the ~28 Ma tuff of Barnes Butte (**Tjtb**). The plateau age reported for sample 1.15VII.05 contains 73.5 percent of the gas release; the overall plateau pattern does indicate possible ^{39}Ar recoil during irradiation (appendix). The plateau, total fusion, and isochron ages are indistinguishable.

Figure 6-42. Cliff-forming outcrops of the rhyolite of Ochoco Reservoir (Tjro) north of Ochoco Reservoir. A sample of the rhyolite from these cliffs has an $^{40}Ar/^{39}Ar$ age of 27.54 ± 0.36 Ma. The rhyolite directly overlies sedimentary rocks of unit Tjs and older andesite lava flows (Tcal) of the Clarno Formation. Landslide deposits (Qls) flank the rhyolite along its southern margin. View is looking west from Hi-Tor Butte (44.316316, -120.637519). Photo credit: Jason McClaughry, 2005.

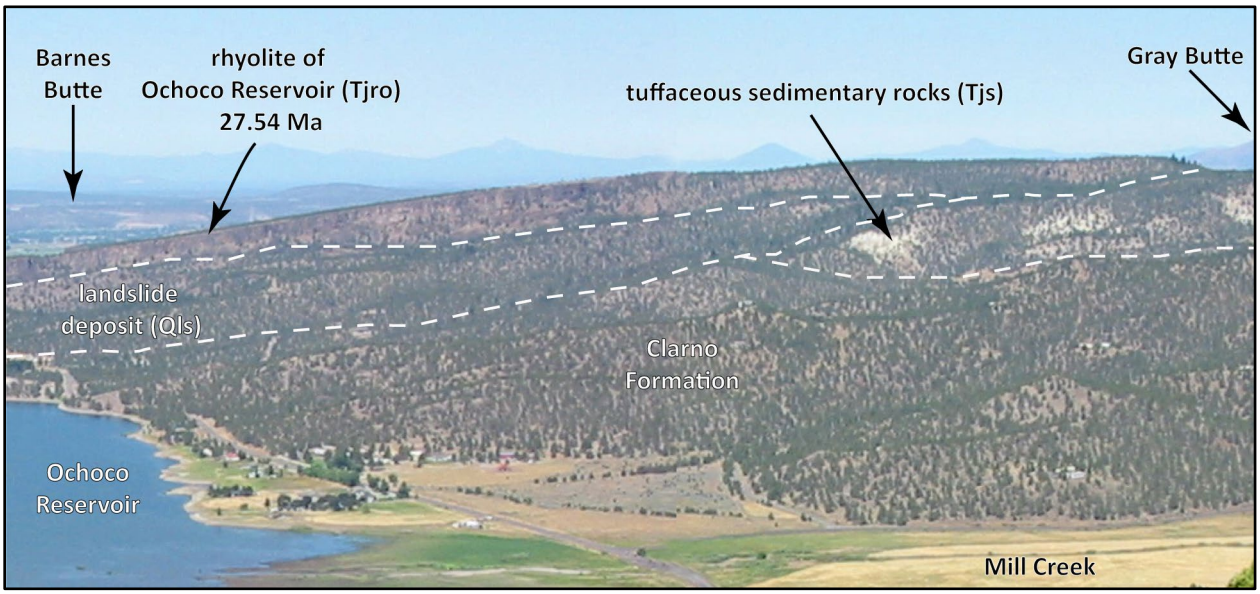

Figure 6-43. Outcrop of the rhyolite of Ochoco Reservoir (Tjro) displaying well-developed flow banding and flow folds north of Ochoco Reservoir (44.308808, -120.729345). Yellow notebook for scale is 19 cm (7.5 in) tall. Photo credit: Jason McClaughry, 2005.

rhyolite of Powell Buttes—Rhyolite mapped forming a post-caldera dome and flow field covering ~40 km^2 (15.5 mi^2) at Powell Buttes, along the southwest margin of the Crooked River caldera (**Figure 5-12**, **Figure 6-44**; plate; appendix). Subdivided into:

Tjpq **quartz- and sanidine-phyric rhyolite (upper Oligocene)—**Rhyolite (SiO_2 = 76.77 to 77.50 weight percent; Ba = 233 to 250 ppm; Zr = 872 to 1185 ppm; Nb = 69.9 to 93.1 ppm; *n* = 2 analyses) mapped across the summit and south flank of Powell Buttes (**Figure 5-12**, **Figure 5-15**; **Table 6-8**; plate; appendix). Unit **Tjpq** is typically poorly exposed as low-lying blocky jointed outcrops weathering to a surface armored by subrounded boulders. Typical hand samples of the rhyolite are medium gray (N5) to grayish red purple (5RP/2) and distinctly porphyritic, containing 5 to 10 percent (vol.) clear- to pale yellowish brown (10YR 6/2), seriate, pseudohexagonal quartz phenocrysts ≤3 mm (0.1 in) and ≤5 percent (vol.) clear, subhedral, lath-shaped, microcline-twinned alkali feldspar 1 to 6 mm (0.04 to 0.2 in) across, distributed within a devitrified, spherulitic groundmass. Pleochroic, grayish green (10GY 5/2) sodic-pyroxenes (aegirine-augite) occur as vapor-phase microphenocrysts within vesicles and along cracks in groundmass spherulites (**Figure 6-45**).

Quartz- and sanidine-pyric rhyolite (**Tjpq**) is assigned a late Oligocene age on the basis of stratigraphic position (**Figure 6-1**; plate). The unit (**Tjpq**) is considered to be the youngest rhyolite phase of the Powell Buttes complex. Conspicuous sodic-pyroxenes in samples of unit **Tjpq** suggest a peralkaline chemical affinity (**Figure 6-45**).

Tjps **sanidine-phyric rhyolite (upper Oligocene)—**Rhyolite lava flows and domes (SiO_2 = 75.25 to 76.70 weight percent; Ba = 408 to 516 ppm; Zr = 721 to 849 ppm; Nb = 53.7 to 70.8 ppm; *n* = 4 analyses) mapped across the summit and eastern flank of Powell Buttes (**Figure 5-12**, **Figure 5-15**; **Table 6-8**; plate; appendix). Outcrops of the rhyolite are typically massive or platy jointed. Weathered parts of the unit are characterized by a surface armored by platy rock fragments. The upper part of unit **Tjps** is locally marked by pumiceous zones and vertically oriented flow-banding. Typical hand samples of the rhyolite are light gray (N7) to pale purple (SP 6/2) and distinctly porphyritic, containing 5 to 10 percent (vol.) clear, blocky to lath-shaped, seriate sanidine phenocrysts ≤5 mm (0.2 in) across, distributed within a devitrified, spherulitic groundmass. The rock includes ≤1 percent (vol.) corroded, pleochroic, grayish green (10GY 5/2) sodic-pyroxenes (aegirine-augite) ≤1 mm (0.04 in) across. Spherulites in the groundmass are composed of radiating acicular needles of grayish green (10GY 5/2) sodic-pyroxene and sanidine. Fe-Ti oxides are abundant.

Sanidine-phyric rhyolite (**Tjps**) is assigned a late Oligocene age on the basis of stratigraphic position and a K-Ar age of 25.8 ± 0.2 Ma obtained from an outcrop at the summit of Powell Buttes (sanidine; sample 648-623b; Robinson and others, 1990) (**Figure 5-11**, **Figure 5-12**, **Figure 6-1**; **Table 5-2**; plate; appendix).

Figure 6-44. Powell Buttes rhyolite complex. (a) The central part of the Powell Buttes dome complex is intruded by a number rhyolite dikes. View is looking southeast (44.197787, -120.997195 W). (b) Vertically flow banded rhyolite dike forming the Rooster Combs (44.183659, -120.985650). Arrow points to person for scale. (c) Close-up photograph of rhyolite dike shown in B (44.182801, -120.987507). Arrow points to 19 cm (7.5 in) tall yellow notebook for scale. Photo credits: Jason McClaughry, 2005.

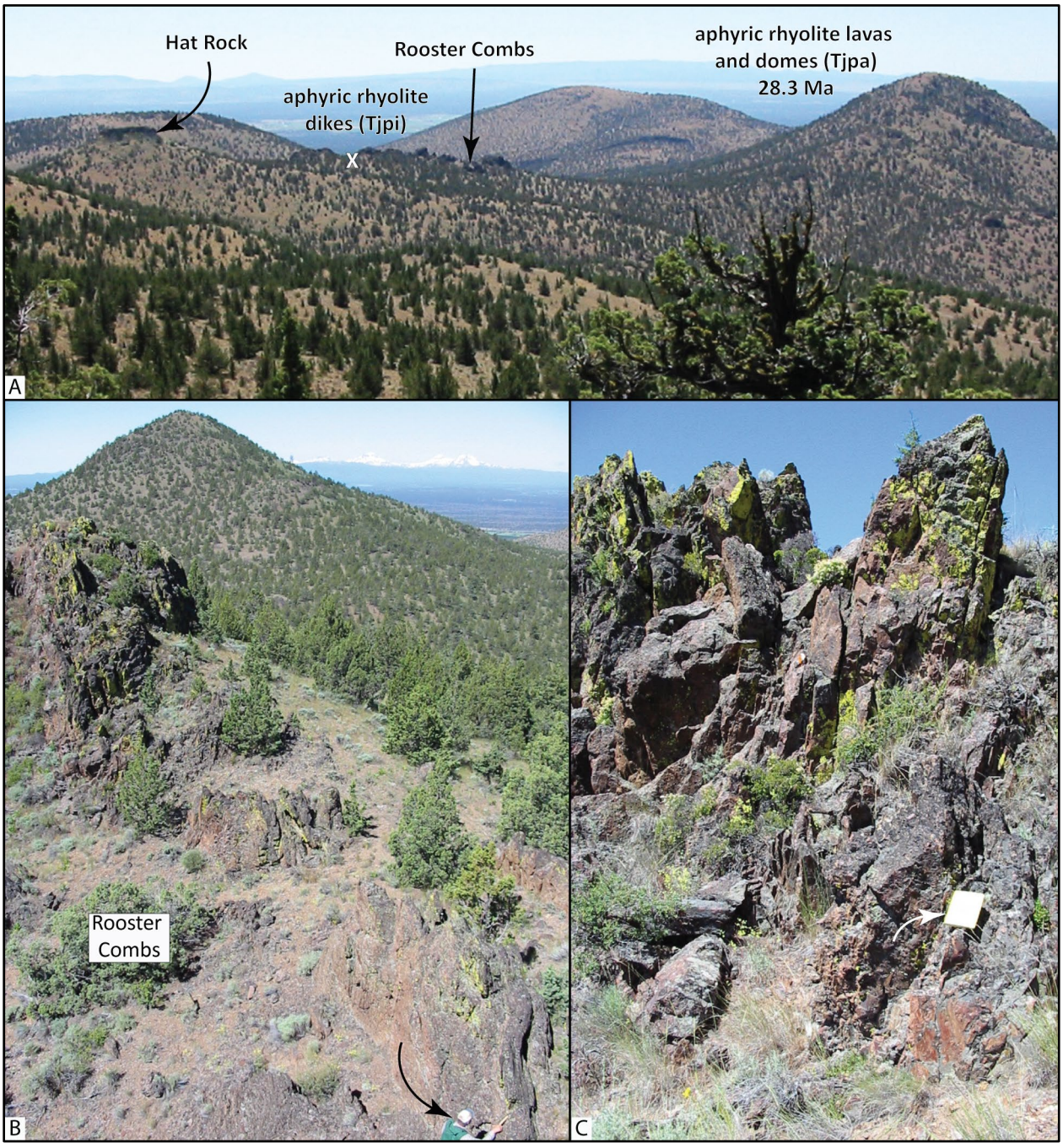

Figure 6-45. Photomicrograph of rhyolite from Powell Buttes. Small corroded, blue-green sodic-pyroxene (aegirine-augite) phenocrysts are sparsely distributed in quartz-sanidine-phyric (Tjpq) and sanidine-phyric (Tjps) rhyolites on Powell Buttes. Phenocrysts are typically set in a devitrified, spherulitic groundmass. Scale bar is 2.5 mm (0.2 in) across. Photo credit: Jason McClaughry, 2006.

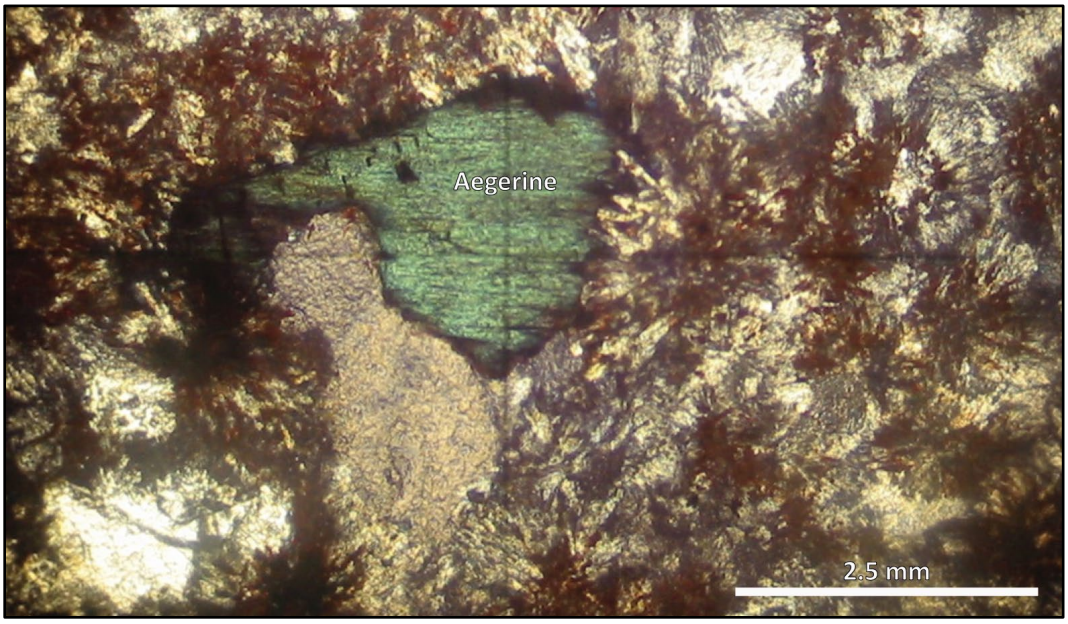

Tjpa **aphyric rhyolite (lower Oligocene)—**Rhyolite lava flows and domes (SiO_2 = 70.07 to 77.12 weight percent; Ba = 963 ppm; Zr = 462 ppm; Nb = 45.0 ppm; *n* = 11 analyses) forming the main part of the Powell Buttes rhyolite complex (**Figure 5-12**, **Figure 5-15**, **Figure 6-44a**, **Figure 6-46**; **Table 6-8**; plate; appendix). Outcrops are typically massive to flow banded, weathering to ledges and surfaces armored by platy fragments (**Figure 6-46b**). The bases and margins of individual flows and domes are defined by vesiculated zones and flow breccia. Flow tops are commonly marked by pumiceous breccia and perlitic vitrophyre. Unit **Tjpa** includes some lava flows referred to as dacite by Weidenheim (1980). Typical hand samples of the rhyolite are grayish blue (5PB 5/2) to pale purple (SP 6/2) and aphyric, with a completely devitrified and recrystallized spherulitic groundmass. Groundmass spherulites are composed of radiating acicular needles of grayish green (10GY 5/2) sodic-pyroxene and sanidine. The groundmass also contains abundant Fe-Ti oxides and high birefringence and high relief zircons. Miarolitic cavities are commonly lined with quartz crystals.

Aphyric rhyolite (**Tjpa**) is assigned an early Oligocene age on the basis of stratigraphic position and a K-Ar age of 28.3 ± 1.0 (whole rock; sample PB-5/AH-34; Evans and Brown, 1981; Robinson and others, 1990) (**Figure 5-11**, **Figure 5-12**, **Figure 6-1**; **Table 5-2**; plate; appendix).

Tjpi **aphyric rhyolite dikes (lower Oligocene)—** Rhyolite dikes (SiO_2 = 75.58 weight percent; Ba = 908 ppm; Zr = 429 ppm; Nb = 26.3 to 45.0 ppm; *n* = 1 analysis) mapped at Hat Rock and the Rooster Combs, just south of the summit of Powell Buttes (**Figure 5-12**, **Figure 5-15**, **Figure 6-44a-c**; **Table 6-8**; plate; appendix). The dikes (**Tjpi**) strike N.55°E. and are typically vertically flow banded. Well-developed vesicular zones parallel the vertical flow banding. Dikes (**Tjpi**) are often pumiceous near upper surfaces and show perlitic textures along contacts with the hosting tuff (**Tjtsi**). Typical hand samples are grayish blue (5PB 5/2) to pale purple (SP 6/2) and aphyric, with

a completely devitrified and recrystallized spherulitic groundmass. Unit **Tjpi** is assigned an early Oligocene age on the basis of stratigraphic association with aphyric rhyolite of unit **Tjpa** (**Figure 6-1**; plate).

Figure 6-46. Powell Buttes rhyolite complex. (a) Flows and domes of aphyric rhyolite (Tjpa). View is looking north towards Gray Butte from the top of Powell Buttes (44.165007, -121.999854). (b) Flow-banding in rhyolite on Powell Buttes (44.178014, -121.002690). Scale bar is 20 cm wide (7.9 in). Photo credit: Jason McClaughry, 2005.

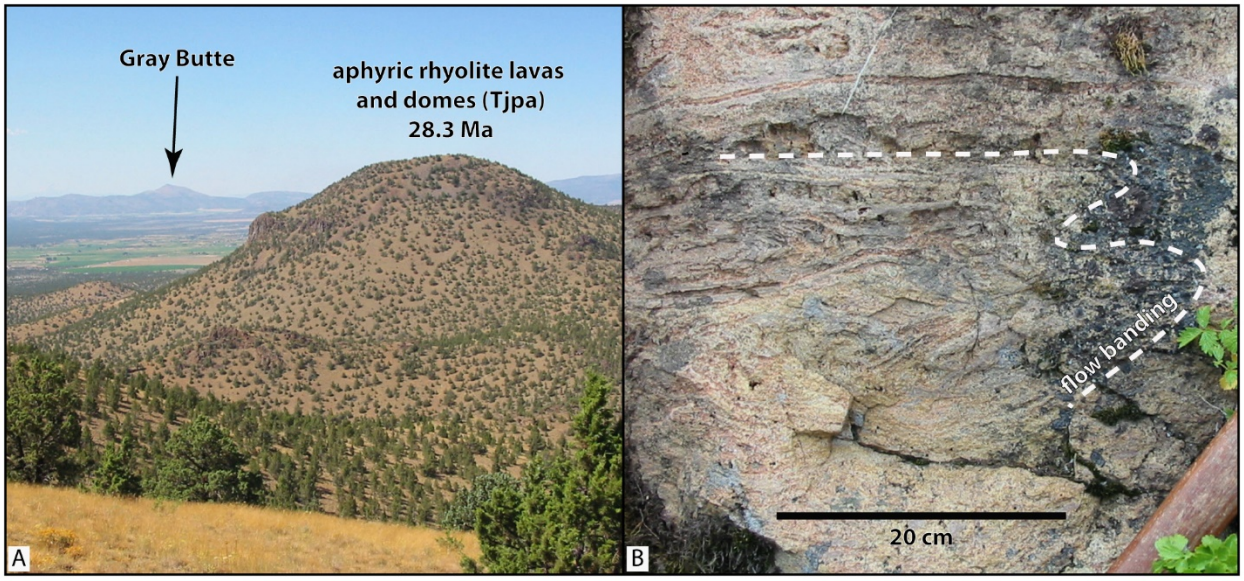

Tjrpb **rhyolite of Pilot Butte (lower Oligocene)—**Rhyolite (SiO_2 = 78.44 weight percent; Ba = 975 ppm; Zr = 455 ppm; Nb = 75.6 ppm; *n* = 1 analysis) mapped in a narrow, west-northwest striking ridge east of Gravy Gulch, along the southeastern margin of the Crooked River caldera (**Figure 5-12**, **Figure 5-15**; **Table 6-8**; plate; appendix). Outcrops of unit **Tjrpb** are typically massive to spherulitic and strongly flow banded. Zones of lithophysae are locally abundant (**Figure 6-47**). The unit (**Tjrpb**) typically weathers to fields of subround boulders. In the vicinity of Lawson Creek and Gravy Gulch (**Figure 5-12**; plate), the rhyolite consists of a composite section of breccia and rhyolite; a base of interbedded, tightly packed, perlite cobble breccia, massive pumiceous tuff, and ash-rich breccia grades upward into massive to perlitic rhyolite with flattened lithophysal cavities. The rhyolite intrudes units as young as the 29.5 Ma outflow unit of the tuff of Smith Rock (**Tjtso**) south of Gravy Gulch (**Figure 5-12**; plate). Where the contact between the rhyolite of Pilot Butte (**Tjrpb**) and outflow unit of the tuff of Smith Rock (**Tjtso**) crops out, the overlying tuff is hydrothermally altered and is marked by abundant quartz-filled lithophysal cavities. This location was also the site of several unnamed 1950s uranium prospects (John Breese, oral commun., 2008). Typical hand samples of the rhyolite are grayish blue (5PB 5/2), pale purple (SP 6/2), and white (N9) and sparsely porphyritic, containing ≤2 percent (vol.) clear, blocky to lath-shaped, seriate sanidine microphenocrysts and phenocrysts ≤2 mm (0.1 in) across, distributed within a devitrified groundmass. The rhyolite of Pilot Butte (**Tjrpb**) is assigned an early Oligocene age on the basis of stratigraphic position (**Figure 6-1**; plate).

Figure 6-47. Lithophysal rhyolite on the northwest flank of Pilot Butte (44.218163, -120.583420). GPS unit for scale is 12 cm (4.7 in) long. Photo credit: Jason McClaughry, 2007.

Tjrgm **rhyolite of Grizzly Mountain (lower Oligocene)—**Rhyolite (SiO_2 = 72.61 to 77.87 weight percent; Ba = 988 to 1128 ppm; Zr = 473 to 589 ppm; Nb = 57.0 to 66.0 ppm; *n* = 7 analyses) mapped as a N.55°W.-striking, post-caldera rhyolite dome and flow field covering ~20 km^2 (7.7 mi^2) along the northeast margin of the Crooked River caldera (**Figure 5-12**, **Figure 5-15**, **Figure 6-48, Figure 6-49**, **Table 6-8**; plate; appendix; Thormahlen, 1984; Patridge, 2010). The Grizzly Mountain rhyolite complex (**Tjrgm**) extends from just northwest of the summit of Grizzly Mountain to McKay Creek on the southeast, where it intrudes the intracaldera unit of the tuff of Smith Rock (**Tjtsi**) along the caldera margin (**Figure 5-12**; plate). Thormahlen (1984) separated the rhyolite into upper and lower suites. The upper suite consists of light gray (N7) to pale purple (SP 6/2), massive to columnar-jointed, sanidine-phyric rhyolite with small lens-shaped vugs filled with recrystallized material (**Figure 6-49**). Flow banding and lithophysal cavities are characteristic of the upper suite, near the summit of Grizzly Mountain (**Figure 6-49b**). Individual lava flows in the upper suite range between 10 and 30 m (32.8 and 98.4 ft) thick and commonly have flow breccia and grayish black (N2) vitrophyre with pitchy luster at the base. The lower rhyolite suite consists of locally vesicular and flow-banded aphyric rhyolite that is commonly altered to yellowish gray (5Y 7/2) with vesicles filled by chalky white (N9) opal and quartz. Typical hand samples of the upper rhyolite are light gray (N7) to pale purple (SP 6/2) and aphyric to porphyritic, containing

3 to 5 percent (vol.) sanidine, quartz, anorthoclase, and sparse sodic-oligoclase microphenocrysts and phenocrysts ≤2 mm (0.1 in) across, distributed within a devitrified, recrystallized spherulitic groundmass. Lower lava flows are nearly aphyric in hand sample, with relict phenocrysts of sodic-oligoclase enclosed in a devitrified groundmass now composed of fined-grained mosaics of quartz and anorthoclase.

The rhyolite of Grizzly Mountain (**Tjrgm**) is assigned an early Oligocene age on the basis of stratigraphic position and a $^{206}Pb/^{238}U$ zircon age of 28.9 ± 0.2 Ma obtained from a sample near the summit of Grizzly Mountain (sample PAT GR2) (**Figure 5-11**, **Figure 5-12**, **Figure 6-1**; **Table 5-2**; plate; appendix). Zircons from sample PAT GR2 are subhedral and 100 to 200 µm in length. Analysis of twenty zircons gave $^{206}Pb/^{238}U$ dates ranging from 32.8 ± 1.0 to 28.0 ± 0.7 Ma. Statistical deconvolution shows a prominent peak at 28.9 ± 0.2 Ma and a lesser peak at 31.8 ± 0.6 Ma (appendix).

Figure 6-48. Grizzly Mountain, an Oligocene rhyolite dome and flow field along the margin of the Crooked River caldera, rises over the Prineville Valley. View is looking north from Ochoco Wayside State Park (44.300335, -120.864183). Photo credit: Carrie Gordon, 2008.

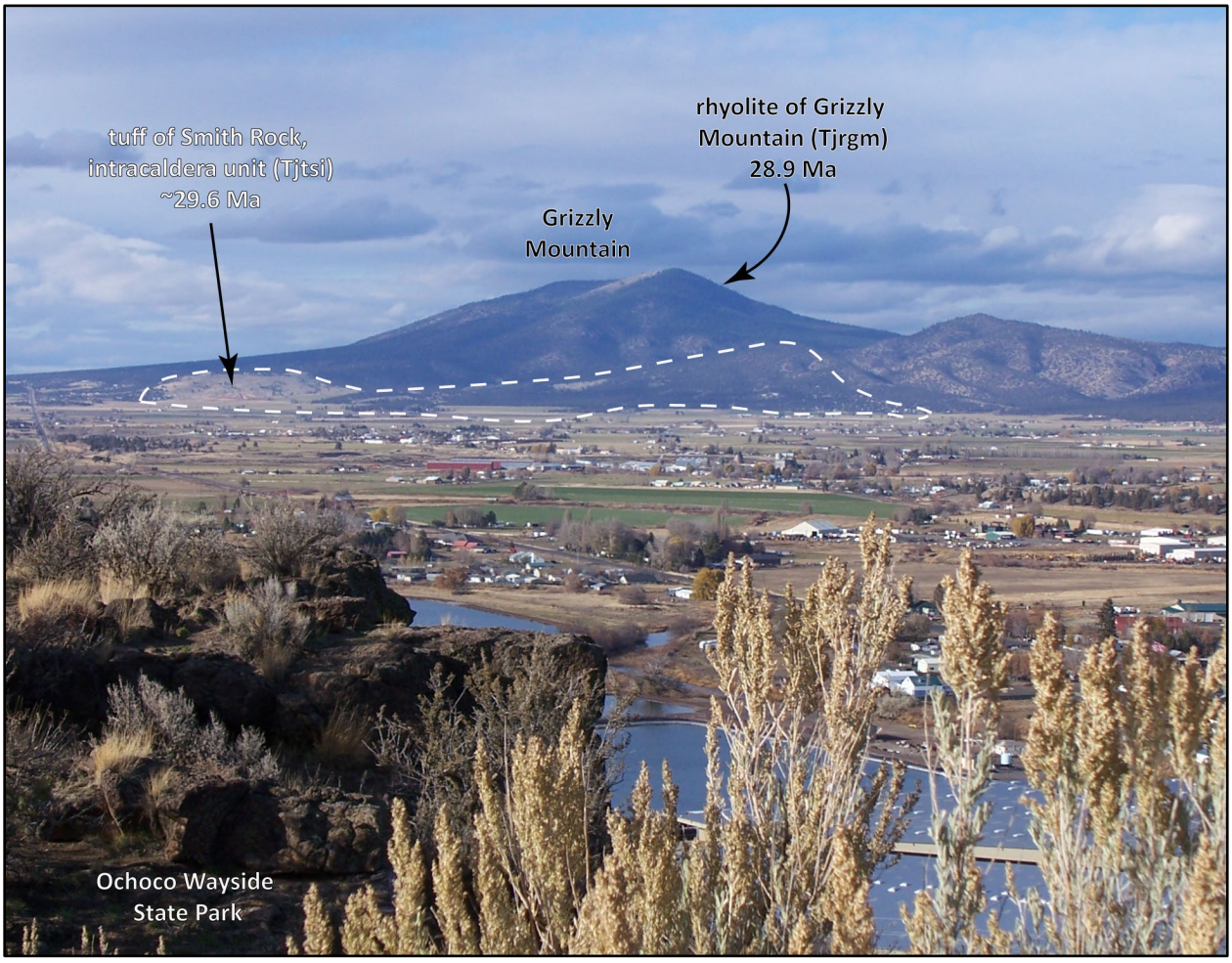

Figure 6-49. Grizzly Mountain rhyolite complex. (a) Blocky, flow-banded rhyolite near the summit of Grizzly Mountain (44.429573, -120.960046). Nearby outcrops of the rhyolite returned a $^{206}Pb/^{238}U$ zircon age of 28.9 ± 0.2 Ma. Smith Rock and Gray Butte are visible in the distance to the east, near the northwest margin of the Crooked River caldera. (b) Flow banded rhyolite near the outcrop in A. Hammer for scale is 40 cm (15.7 in) long. Photo credits: Jason McClaughry, 2008.

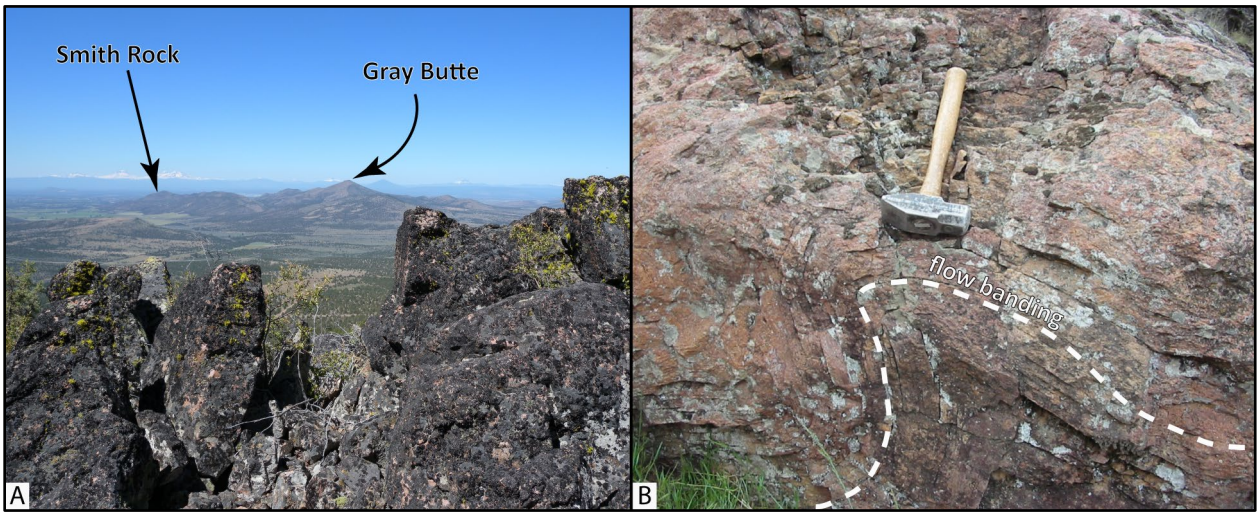

Tjrh **rhyolite of Hi-Tor Butte (lower Oligocene)—**Rhyolite (SiO_2 = 76.78 weight percent; Ba = 1,001; Zr = 485; Nb = 66.9 ppm; *n* = 1 analysis) mapped at Hi-Tor Butte, near the east end of Ochoco Reservoir (**Figure 5-12**, **Figure 5-15**, **Figure 6-50**, **Table 6-8**; plate; appendix). Outcrops of the rhyolite (**Tjrh**) are massive or have platy or columnar jointing. Flow banding and spherulitic zones are common. The base of the rhyolite (**Tjrh**) is composed of relatively fresh-appearing grayish black (N2) obsidian (**Figure 6-50**). Where deeply weathered, unit **Tjrh** is marked by a surface of angular rock fragments and moderate brown (5YR 4/4) soils. Typical hand samples of the rhyolite are light gray (N7), pale purple (SP 6/2), and grayish black (N2) and sparsely microporphyritic, containing <1 percent (vol.) sanidine microphenocrysts, distributed within a devitrified, holohyaline groundmass with spherulitic overgrowths. A micro flow-banded texture is defined in the groundmass by alternating recrystallized zones and lenses of devitrified glass.

The rhyolite of Hi-Tor Butte (**Tjrh**) is assigned an early Oligocene age on the basis of stratigraphic position and a $^{206}Pb/^{238}U$ zircon age of 29.2 ± 0.9 Ma obtained for a sample on Hi-Tor Butte (sample 2013CRC-10; Seligman and others, 2014) (**Figure 5-11**, **Figure 5-12**, **Figure 6-1**; **Table 5-2**; plate; appendix).

Figure 6-50. Obsidian forming part of the rhyolite of Hi-Tor Butte (Tjrh) (44.316067, -120.638716). This outcrop returned a $^{206}Pb/^{238}U$ zircon age of 29.2 ± 0.9 Ma. Hammer for scale is 40 cm (15.7 in) long. Photo credit: Jason McClaughry, 2005.

Tjrg **rhyolite of Gray Butte (lower Oligocene)—**Rhyolite (SiO_2 = 76.83 to 77.83 weight percent; Ba = 867 to 999; Zr = 309 to 624 ppm; Nb = 43.0 to 85.8 ppm; *n* = 7 analyses) mapped along the northwest margin of the Crooked River caldera (**Figure 5-12**, **Figure 5-15**, **Figure 6-49**, **Figure 6-51**, **Figure 6-52**, **Table 6-8**; plate; appendix). The rhyolite of Gray Butte forms a N.60°E.-striking complex of lava flows and domes covering ~65 km² (25 mi²), between the head of Sherwood Canyon on the southwest and across Pine Ridge nearly to U.S. Highway 26 on the northeast (**Figure 5-12**, **Figure 6-51**; plate). The unit includes geochemically similar, linear, vertically foliated low-silica rhyolite dikes (SiO_2 = 71.35 to 73.78 weight percent; Ba = 1,007 to 1,310 ppm; Zr = 598 to 692 ppm; Nb = 59.0 to 61.0 ppm; *n* = 3 analyses) and high-silica rhyolite (SiO_2 = 79.69 to 79.77 weight percent; Ba = 891 to 935 ppm; Zr = 421 to 438 ppm; Nb = 50.7 to 53.6 ppm; *n* = 2 analyses) intruding the tuff of Smith Rock (**Tjtsi**) at Smith Rock State Park and Skull Hollow and rhyolite dikes and sills (SiO_2 = 74.66 weight percent; Ba = 1,248 ppm; Zr = 131 ppm; Nb = 61 ppm; *n* = 1 analysis) intruding early Oligocene strata near Nichols Spring (**Figure 5-12**, **Figure 6-53**). Rhyolite dikes are locally intermingled with the tuff and are characterized by anastomosing contacts (Patridge, 2010). Vesicular zones along some dike contacts suggest their emplacement prior to complete degassing of unit **Tjtsi**.

Outcrops within the main rhyolite body at Gray Butte are massive or have platy jointing (**Figure 6-54**). Subvertical to vertical planar or contorted flow banding is common (**Figure 6-54**). Black (N1), perlitic vitrophyre is locally exposed along intrusive margins or at the base of lava flows. Typical hand samples of the rhyolite on Gray Butte are medium bluish gray (5B 5/1) to light

brownish gray (5YR 6/1) and aphyric to sparsely microporphyritic, containing ~5 percent (vol.) plagioclase, anorthoclase, Fe-rich clinopyroxene, and rarely quartz microphenocrysts distributed within a devitrified to recrystallized, spherulitic groundmass. Miarolitic cavities are commonly lined with quartz crystals. Rhyolite dikes are typically light gray (N7) and sparsely sanidine- and quartz-phyric where fresh and pale brown (5YR 5/2) to white (N9), with disseminated pyrite, where silicified. Typical hand samples from dikes contain phenocrysts of oligoclase, sanidine, and altered pyroxene and olivine, as well as glomerocrysts of feldspar, biotite, altered pyroxene and iron oxides in a felted microlitic to sometimes-spherulitic groundmass of feldspar and quartz (Patridge, 2010).

The rhyolite of Gray Butte (**Tjrg**) is assigned an early Oligocene age on the basis of stratigraphic position and isotopic ages. Smith and others (1998) reported an $^{40}Ar/^{39}Ar$ age of 28.82 ± 0.23 Ma for the rhyolite (anorthoclase; sample GSO 95-41), while a more recent $^{206}Pb/^{238}U$ zircon age obtained from a sample from the same outcrop indicates a slightly older emplacement age of 29.2 ± 0.3 Ma (sample GSO 95-41R) (**Figure 5-11**, **Figure 5-12**, **Figure 6-1**; **Table 5-2**; plate; appendix). Zircons from sample GSO 95-41R are small (<100 µm in length), subhedral, and in some cases have distinct core domains. Analysis of 20 zircons gave $^{206}Pb/^{238}U$ dates ranging from 28.5 ± 0.6 to 36.5 ± 1.0 Ma. Statistical deconvolution assuming three populations gives peak populations at 35.7 ± 0.6, 32.9 ± 0.3 and 29.2 ± 0.3 Ma (appendix). The latter date is statistically identical to a SHRIMP-RG date of 29.6 ± 0.8 obtained from the same sample. An additional sample obtained from a N.70°W.-striking dike, intruding the tuff of Smith Rock (**Tjtsi**) near Skull Hollow, returned a younger $^{206}Pb/^{238}U$ zircon age of 28.4 ± 0.3 Ma (sample SR RH2) (**Figure 5-11**, **Figure 5-12**; **Table 5-2**; plate; appendix). Zircons from sample SR RH2 are small (<100 µm in length) and subhedral. Cathodoluminescence imaging reveals oscillatory zoned zircons with little evidence for older core domains. Analysis of 20 zircons gave $^{206}Pb/^{238}U$ dates ranging from 31.0 ± 0.7 to 28.0 ± 0.7 Ma. Unmixing of zircon dates yields two populations at 30.0 ± 0.3 Ma and 28.4 ± 0.3 Ma (appendix).

Previous workers interpreted the rhyolite of Gray Butte (**Tjrg**) as a lava flow conformably bedded beneath the tuff of Smith Rock (**Tjtsi**) (Robinson and Stensland, 1979; Obermiller, 1987; Smith and others, 1998; Sherrod and others, 2004). On the basis of field evidence and map patterns, we interpret the rhyolite of Gray Butte as a ring-fracture rhyolite dome complex that post-dates initial collapse of the Crooked River caldera and deposition of the lower part of the tuff of Smith Rock (**Tjtsi**). An intrusive relationship between the rhyolite of Gray Butte and the tuff of Smith Rock (**Tjtsi**) is suggested by: 1) mapped nonconformable, subvertical to nearly vertical contact relations between the rhyolite and the tuff (**Figure 6-51**, **Figure 6-52**; plate); 2) the rhyolite has a relatively fresh appearance, whereas the tuff of Smith Rock (**Tjtsi**) is locally altered and heavily silicified along the contact between it and the rhyolite; and 3) the prevalence of east-west-striking rhyolite dikes geochemically similar to the rhyolite of Gray Butte that parallel the caldera margin. A range of ages for samples in the rhyolite of Gray Butte indicates several episodes of emplacement, consistent with a formation as a composite intrusion or dome complex (**Figure 5-12**; **Table 5-2**).

Figure 6-51. Precipitous, spire-forming outcrops of the tuff of Smith Rock (Tjtsi) along the northwest margin of the Crooked River caldera. The tuff is here intruded by a number of rhyolite dikes and domes, including the rhyolite of Gray Butte (Tjrg). View is looking north from an overlook at Smith Rock State Park (44.370043, -121.140811). The X in the center of the photograph marks the collection site of sample 1 OCJ 14 in the upper part of the tuff, which returned a $^{206}Pb/^{238}U$ zircon age of 28.3 ± 0.5 Ma. The Y near the right of the photograph marks the location of a thick rheomorphic zone in the lower part of the tuff (see Figure 6-57). Photo credit: Jason McClaughry, 2006.

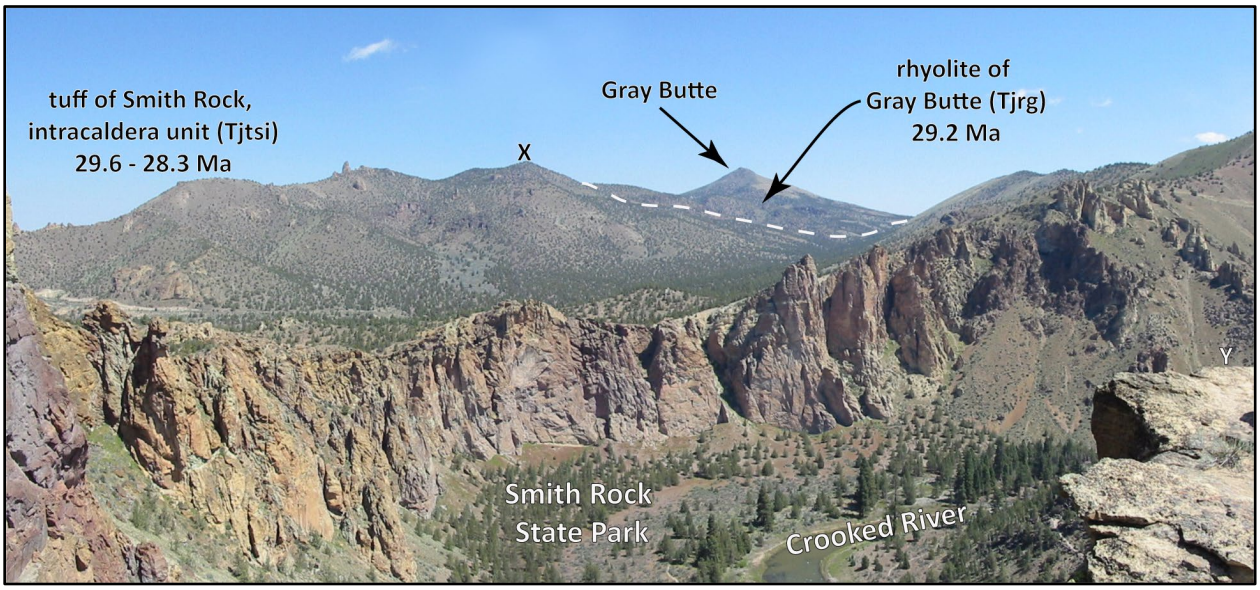

Figure 6-52. The rhyolite of Gray Butte (Tjrg) intruding the intracaldera unit of the tuff of Smith Rock (Tjtsi) along the northwest margin of the Crooked River caldera. Dashed white line marks the contact between the two units. The tuff of Smith Rock is commonly altered and heavily silicified along this contact. View is looking southwest from the summit of Gray Butte (44.416108, -121.101251). Photo credit: Jason McClaughry, 2007.

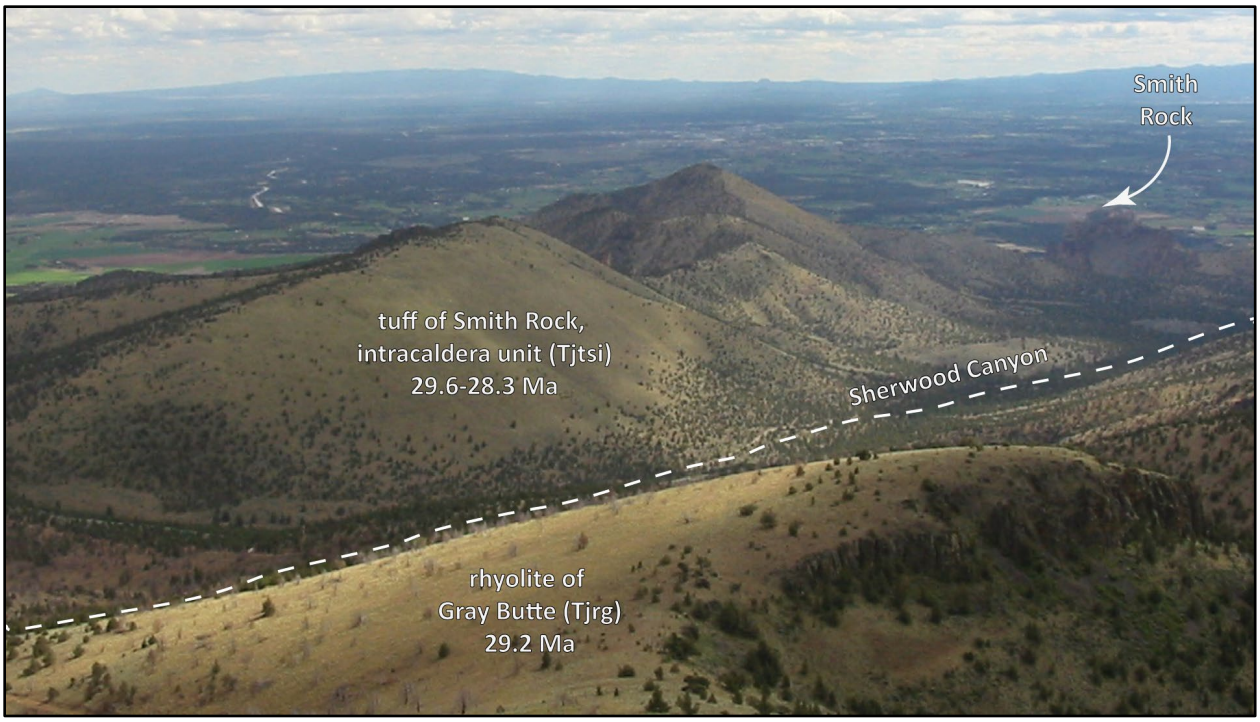

Figure 6-53. Intracaldera unit of the tuff of Smith Rock (Tjtsi) intruded by rhyolite dikes (Tjrg) at Smith Rock State Park. Quaternary basalt from Newberry Volcano (Qbnc) is inset into the incised Paleogene surface (44.367120, -121.137683). The X in the center right of the photograph is the site for sample 24 LCJ 06, which returned a $^{206}Pb/^{238}U$ zircon age of 29.3 ± 0.3 Ma. Photo credit: Jason McClaughry, 2006.

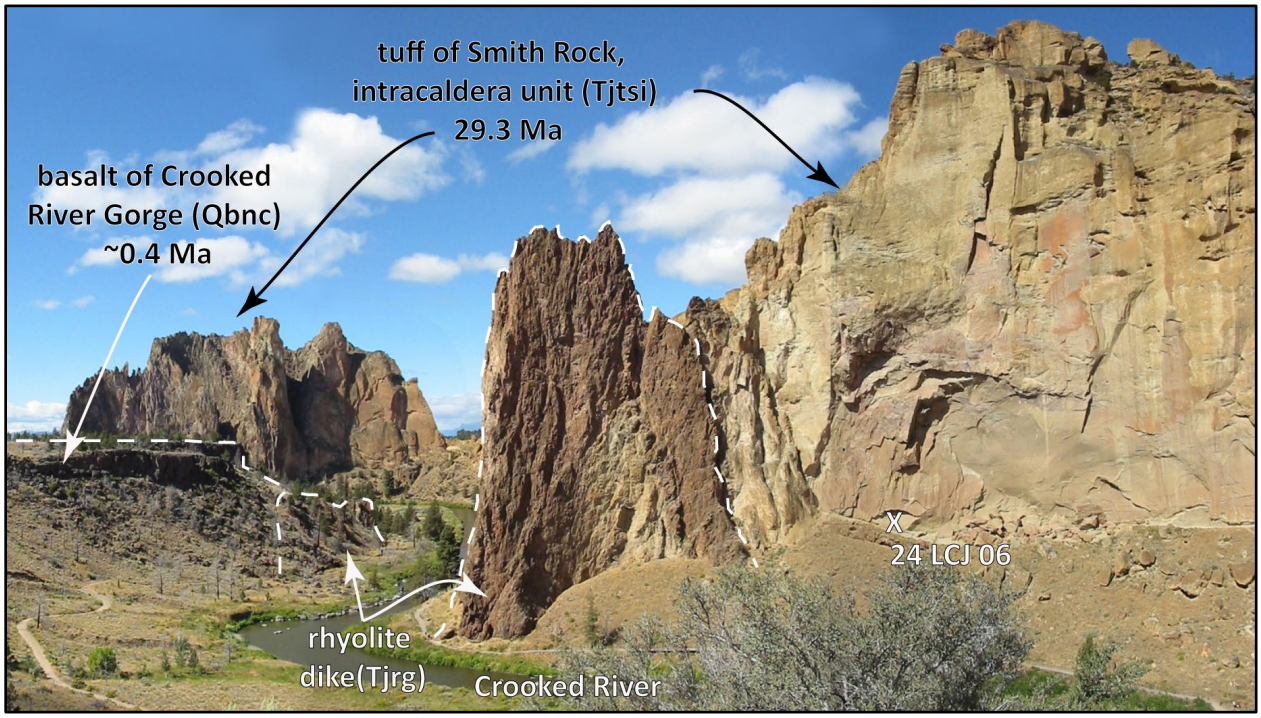

Figure 6-54. Flow banded rhyolite (Tjrg) on the south flank of Gray Butte (44.411047, -121.099410). Hammer for scale is 40 cm (15.7 in) long. Photo credit: Jason McClaughry, 2007.

Tjrj **rhyolite of Juniper Butte (lower Oligocene)—**Rhyolite dome complex (SiO_2 = 78.6 to 79.5 weight percent; Ba = 302 to 383 ppm; Zr = 334 to 373 ppm; Nb = 39 to 49 ppm; *n* = 4 analyses) mapped at Juniper Butte outside the northwest margin of the Crooked River caldera (**Figure 5-12**, **Figure 5-15**, **Table 6-8**; plate; appendix). The core to the rhyolite dome complex is composed of stony rhyolite marked by prominent vertical joint sets and distinct flow banding. Typical hand samples of the rhyolite are medium gray (N6) to pale red purple (5RP 6/2) and sparsely porphyritic, containing 3 to 5 percent (vol.) quartz, plagioclase, and sanidine phenocrysts ≤3 mm (0.1 in) across, distributed within a devitrified to completely recrystallized spherulitic groundmass.

The rhyolite of Juniper Butte (**Tjrj**) is assigned an early Oligocene age on the basis of stratigraphic position and a $^{206}Pb/^{238}U$ zircon age of 29.3 ± 0.2 Ma obtained for a sample on Juniper Butte (sample JB-JM-01) (**Figure 5-11**, **Figure 5-12**, **Figure 6-1**; **Table 5-2**; plate; appendix). Zircons from sample JB-JM-01 are subhedral, ranging from 100 to 200 µm in length. No obvious cores were observed in cathodoluminescence imaging. Analysis of 24 zircons yielded dates ranging from 35.8 ± 0.9 to 28.5 ± 0.7 Ma, and deconvoluted peak populations at 32.1 ± 0.8 and 29.3 ± 0.2 Ma (appendix).

Disconformity to nonconformity

Tjtsi **tuff of Smith Rock, intracaldera unit (lower Oligocene)—**Chiefly thickly-ponded, pumice-lithic and pumice-lapilli-lithic rhyolite ash-flow tuff (SiO_2 = 76.25 to 77.63 weight percent; Ba = 872 to 1121 ppm; Zr = 393 to 692 ppm; Nb = 44.0 to 66.0 ppm; *n* = 13 analyses) mapped in an arcuate outcrop belt along the margin of the Crooked River caldera, from the type area at Smith Rock State Park to Ochoco Reservoir (**Figure 5-12**, **Figure 5-15**; **Table 6-8**; plate; appendix). Also mapped as a roof pendant of tuff across the upper summit of Powell Buttes (**Figure 5-12**; plate). At Smith Rock State Park, the intracaldera tuff unit (**Tjtsi**) weathers to tan to yellowish gray (5Y 7/2), dusky yellow (5Y 6/4), pale olive (10Y 6/2), and pale red (10R 6/2) spires up to 200 m (656 ft) tall (**Figure 6-51**, **Figure 6-55**; McClaughry and Patton, 2017). Dense compaction and widespread propylitic alteration of the intracaldera tuff (**Tjtsi**) at Smith Rock State Park have made the unit more resistant to erosion, relative to caldera wall rocks, leading to the development of the inverted topography in this area (**Figure 5-12**; plate). Along the northeast margin and in central parts of the Crooked River caldera, correlative tuff deposits are less obvious, eroding to form rounded, low-elevation hills. Intracaldera tuff (**Tjtsi**) in the Crooked River caldera is everywhere else covered by younger geologic units (**Figure 5-12**, **Figure 5-16**; plate).

Bedding features within the intracaldera tuff (**Tjtsi**) are generally indistinct, but horizontal to gently dipping (<5°) lithic-rich breccia deposits and associated fine-grained ash horizons are intercalated with the pumice-rich tuff in exposures along the Crooked River at Smith Rock State Park and in Skull Hollow (**Figure 5-12**, **Figure 6-55a**; plate). Lithic-rich layers within the tuff (**Tjtsi**) are laterally discontinuous, 0.5 to 2 m (1.6 to 6.6 ft) thick, and are both clast- and matrix-supported. Lithics consist of angular to subangular green, altered basaltic andesite and andesite, tuff, silicified rhyolite similar in chemical composition to cross-cutting rhyolite intrusions, granitic fragments, and petrified wood. Rare clasts of limestone, some bearing Permian fusulinids (Thompson and Wheeler, 1942), also occur as xenoliths within the tuff, suggesting that the tuff of Smith Rock (**Tjtsi**) erupted through a Paleozoic limestone basement (**Figure 6-55b**). The average clast size in the lithic-rich lenses ranges from 2 to 6 cm ([0.8 to 2.4 in] long axes). The maximum

observed clast size in Smith Rock State Park is 28 cm (11 in); clasts up to 72 cm (28 in) across were found in lithic-rich deposits exposed in Skull Hollow (**Figure 5-12**; plate). Locally, petrified wood fragments exceed 1 m (3.3 ft) across. Clasts are not apparently shattered at the observed horizons. Pods of outsized clasts are prevalent. Locally, lithic-rich deposits are conformably interbedded with 10- to 12-cm-thick (3.9- to 4.7- in), fine-grained ash-rich beds. Internal contacts between the pumice-rich tuff, lithic-rich deposits, and fine-grained ash horizons are non-gradational. Pumice fragments are up to 60 cm (23.6 in) across, are typically round to flattened, and are crystal poor, with very sparse phenocrysts of sanidine. Crystals, pumice, and lithic fragments are enclosed in a matrix of devitrified and recrystallized, non-fused, lenticular to cuspate glass shards and devitrified ash. The overall volume of both pumice and lithics appears to decrease upward within the intracaldera unit of the tuff of Smith Rock (**Tjtsi**). The intracaldera unit (**Tjtsi**) is locally altered to clay, zeolite (clinoptolite), and hematite and contains cross cutting zeolite veinlets and vugs, cavities, and veinlets filled by calcite. The tuff (**Tjtsi**) is commonly heavily silicified along contacts with rhyolite dome complexes and intrusive dikes (**Figure 6-53**).

Figure 6-55. Intracaldera unit of the tuff of Smith Rock (Tjtsi) at Smith Rock State Park. (a) Close-up outcrop view of the intracaldera unit of the tuff of Smith Rock (Tjtsi) (44.368356, -121.139913). Hammer for scale is 40 cm (15.7 in) long. (b) Rare clasts of limestone, some bearing Permian fusulinids, occur as xenoliths within the tuff. Pencil for scale. Photo credits: Jason McClaughry, 2006, 2008.

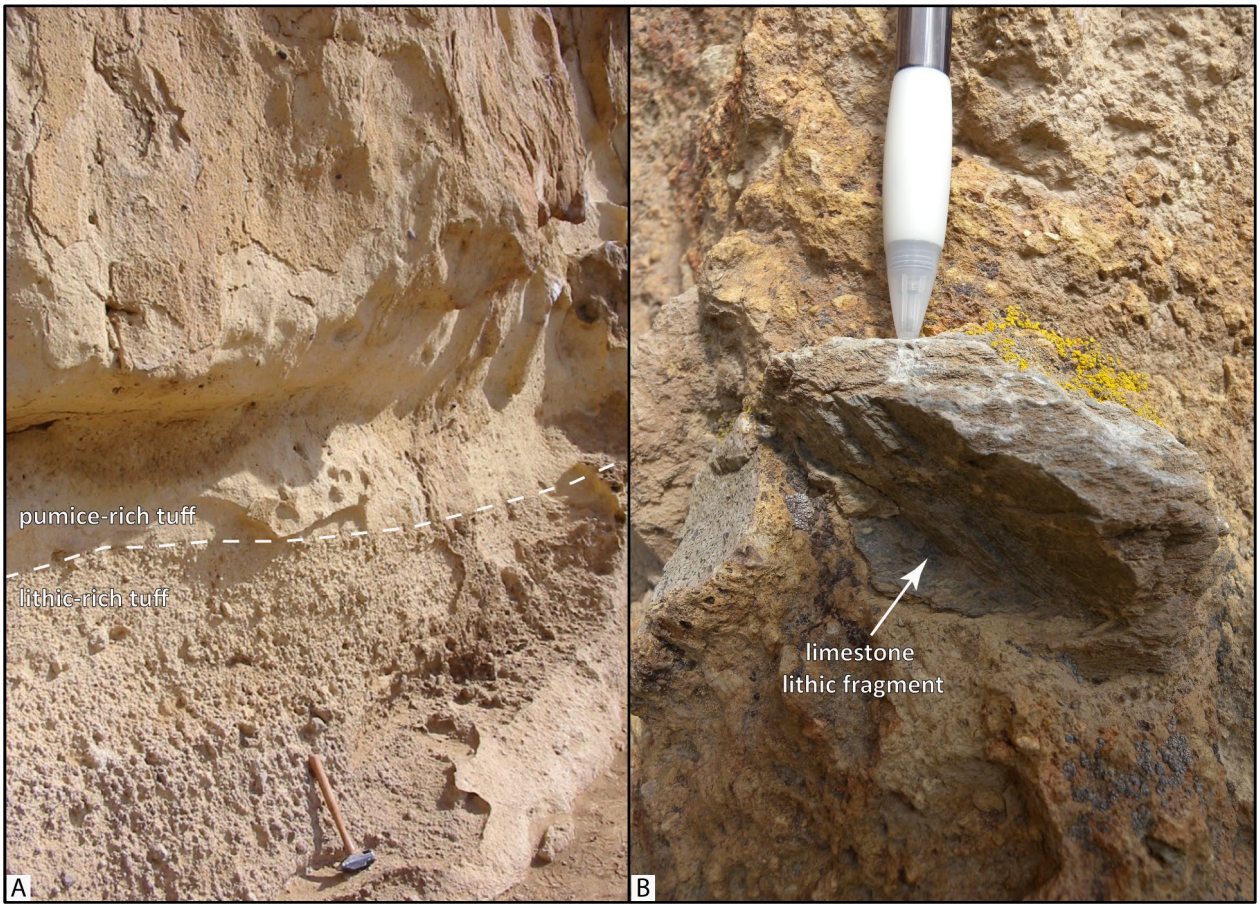

Rheomorphic zones in the intracaldera unit of the tuff of Smith Rock (**Tjtsi**) are best exposed along Staender Ridge, north of the Burma Road Trail in Smith Rock State Park (**Figure 5-12**, **Figure 6-57**; plate). The tuff here is characterized by a variety of rheomorphic textures, including strongly welded fiamme, complex flow bands and flow folds, ramp structures, and elongated vesicles (**Figure 6-57b**). Intense alteration is locally present in rheomorphic zones, marked by quartz-calcite-filled lithophysal cavities and secondary silica filling stockwork veinlets following closely spaced fractures. Rheomorphic caldera-fill along Staender Ridge is locally overlain by an irregular wavy erosional (?) contact suggesting a hiatus (?) or pulsating character in pyroclastic eruptions. Thickness of the rheomorphic zone along Staender Ridge is ~152 m (500 ft).

Typical hand samples of the tuff range from yellowish gray (5Y 7/2), to dusky yellow (5Y 6/4) and pale olive (10Y 6/2) and are crystal poor, containing ≤1 percent (vol.) sanidine phenocrysts ≤2 mm (0.1 in) across, distributed within a groundmass of clay-altered, devitrified ash and cuspate glass shards. Sanidine crystals commonly have secondary granophyric overgrowths that both rim and vein phenocrysts.

The intracaldera tuff (**Tjtsi**) is typically in complex, high angle to vertical contact with variably deformed and locally pervasively sheared country rocks; the tuff itself is not sheared along these contacts (**Figure 6-56**). The intracaldera unit (**Tjtsi**) is ringed and intruded by large (20 to 80 km^2 [7.7 to 30.9 mi^2]) fields of rhyolite dome complexes emplaced along the structural margins of the Crooked River caldera between ~29.3 and 25.8 Ma (**Figure 5-12**; **Table 5-2**; plate). Lithologic descriptions obtained from water-well logs within the Crooked River caldera indicate that unit **Tjtsi** thickens to hundreds of meters immediately away from contacts with both country rock and rhyolite domes (plate, cross sections A-A′, B-B′, E-E′, and F-F′). The intracaldera unit of the tuff of Smith Rock (**Tjtsi**) has a maximum exposed thickness of at least 500 m (1,640 ft) at Smith Rock State Park, where the tuff crops out between elevations of 820 m (2,690 ft) and 1,285 m (4,215 ft). The tuff (**Tjtsi**) is also identified in water well drill logs (e.g., well log DESC 55742) near Coyote Butte west of Smith Rock State Park at an elevation ~668 m (2,190 ft) (**Figure 5-12**; plate; appendix). In the vicinity of Barnes Butte, the tuff (**Tjtsi**) crops out in low-lying hills up to an elevation of 1,070 m (3,510 ft), and is identified in water well drill records to a depth elevation <640 m (2,100 ft) (e.g., wells CROO 426, CROO 492, CROO 590, CROO 967, CROO 969, CROO 1046, CROO 1229, CROO 2463, CROO 3016, CROO 50170, CROO 51032, CROO 51879, CROO 52398; **Figure 5-12**; plate; appendix). The base of the intracaldera tuff unit (**Tjtsi**) is nowhere exposed, but a minimum estimate of the bulk ash-flow tuff volume can be calculated. If not repeated by faults at Smith Rock, the intracaldera tuff (**Tjtsi**) unit has a minimum composite thickness of more than 600 m (1,968 ft). This minimum thickness combined with a caldera area of ~700 km^2 (270 mi^2) equals a minimum bulk volume of ~580 km^3 (139 mi^3) for the intracaldera tuff (**Tjtsi**). This minimum volume estimate does not account for outflow tuff deposits mapped outside the caldera ring fault.

The intracaldera unit of the tuff of Smith Rock (**Tjtsi**) is assigned an early Oligocene age on the basis of stratigraphic position and several isotopic ages. A sample obtained from outcrops at Smith Rock State Park yielded a $^{206}Pb/^{238}U$ zircon age of 29.3 ± 0.3 Ma (sample 24 LCJ 06) (**Figure 5-11**, **Figure 5-12**, **Figure 6-1**, **Figure 6-53**; **Table 5-2**; plate; appendix; stop 1-2 of McClaughry and others, 2009d). Zircons from sample 24 LCJ 06 yielded small (<100 µm in length), euhedral zircons. Cathodoluminescence imaging shows little obvious evidence for older cores. Analysis of 21 zircons from sample 24 LCJ 06 yielded dates ranging from 35.8 ± 0.9 to 28.4 ± 0.6 Ma. Statistical deconvolution yields peak populations at 34.3 ± 0.4, 31.3 ± 0.3, and 29.3 ± 0.3 Ma (appendix). A

second sample of intracaldera tuff (**Tjtsi**) obtained from Skull Hollow (SRT-SKULL-1), southeast of Gray Butte, has a $^{206}Pb/^{238}U$ zircon age of 29.3 ± 0.2 Ma (**Figure 5-11**, **Figure 5-12**; **Table 5-2**; plate; appendix). Zircons from sample SRT-SKULL-1 yielded euhedral zircons, ranging between 100 and 200 µm in length. Cathodoluminescence imaging shows minor evidence for distinct core domains. Analysis of 30 zircons from sample SRT-SKULL-1, yielded over dispersed data with $^{206}Pb/^{238}U$ dates ranging from 35.3 ± 0.9 to 28.3 ± 0.7 Ma. Statistical deconvolution of the data, assuming three populations, yields peaks nearly identical to sample 24 LCJ 06 at 34.3 ± 0.4, 31.3 ± 0.3 and 29.3 ± 0.2 Ma (appendix). An additional sample (1 OCJ 14) collected ~2.5 km (1.6 mi) southwest of Gray Butte, near the top of the exposed section of unit **Tjtsi** has a younger $^{206}Pb/^{238}U$ zircon age of 28.3 ± 0.5 (**Figure 5-11**, **Figure 6-51**; appendix). Zircons from sample 1 OCJ 14 are short (<100 µm in length) and stubby. Cathodoluminescence imaging shows little obvious evidence for older cores. Analysis of 16 zircons yielded dates ranging from 35.0 ± 1.0 to 28.1 ± 0.7 Ma. Statistical deconvolution shows a prominent peak at 30.6 ± 0.3 Ma with minor peaks at 28.3 ± 0.5 Ma (three zircons) and 33.9 ± 0.5 Ma (five zircons) (appendix). Ages for intracaldera-filling tuff at Smith Rock State Park and Skull Hollow are comparable to outflow units with numerous ages around ~ 29.5 Ma, while ages of intracaldera fill near the top of the exposed section share similar ages with tuffs exposed in the central part of the caldera near Barnes Butte (~28.3 Ma).

Figure 6-56. Roadcut excavation revealing part of the caldera-bounding ring fault along the northeast margin of the Crooked River caldera (44.358673, -120.821403). The intracaldera unit of the tuff of Smith Rock (Tjtsi) is separated from older Eocene andesite (Tcal) by a complex, high-angle contact. The tuff is not faulted and onlaps the andesite. The country rock is pervasively cut by a series of regularly spaced shear zones that parallel the caldera margin. Ticks point into the caldera. Person for scale is 1.8 m (5.9 ft) tall. Photo credit: Mark Ferns, 2006.

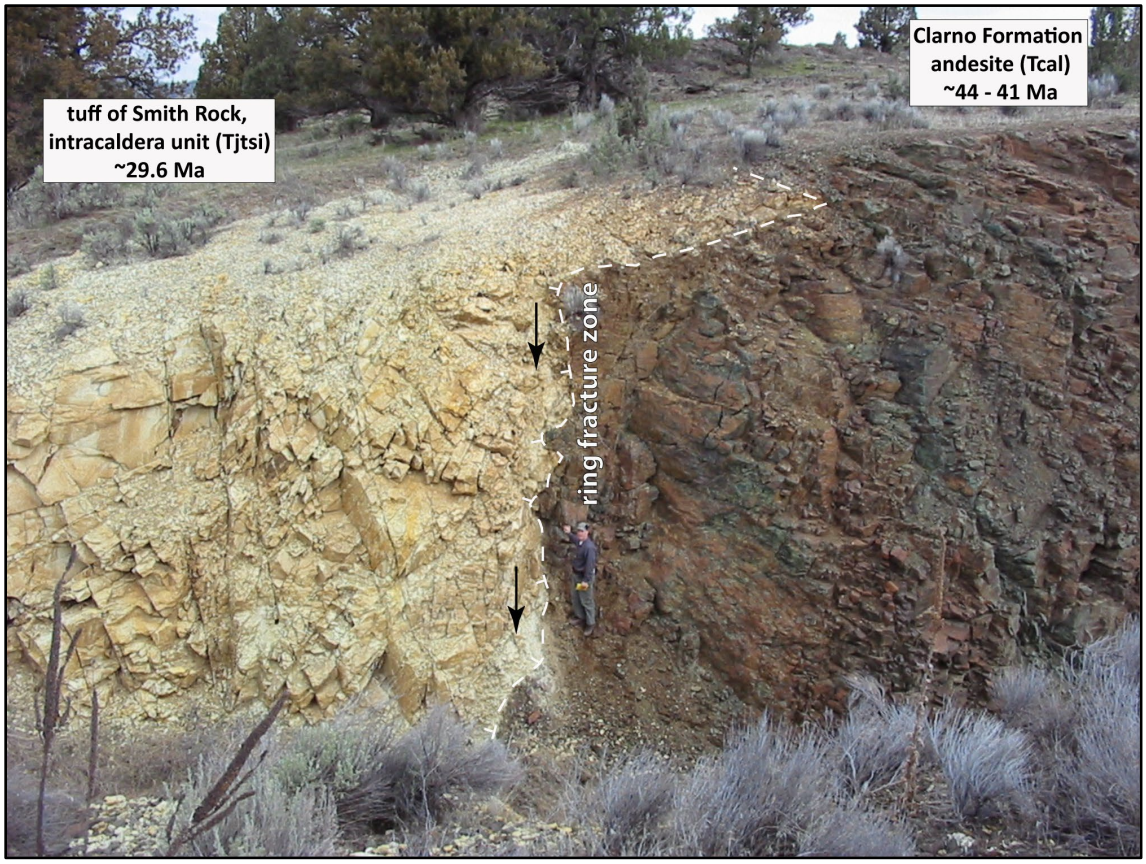

Figure 6-57. Rheomorphic zones in the intracaldera unit of the tuff of Smith Rock (Tjtsi) in Smith Rock State Park.(a) Strongly welded to rheomorphic ash-flow tuff (Tjtsi) along Staender Ridge, north of the Burma Road Trail (44.372867, -121.130587. The X in A is the approximate location of rheomorphic tuff shown in B. (b) Rheomorphic zones are defined by stretched and folded fiamme and lithophysal cavities filled by quartz and calcite (44.373833, -121.131803). Quarter for scale near the center of the photograph is 2.5 cm (1 in) in diameter. Photo credits: Jason McClaughry, 2014.

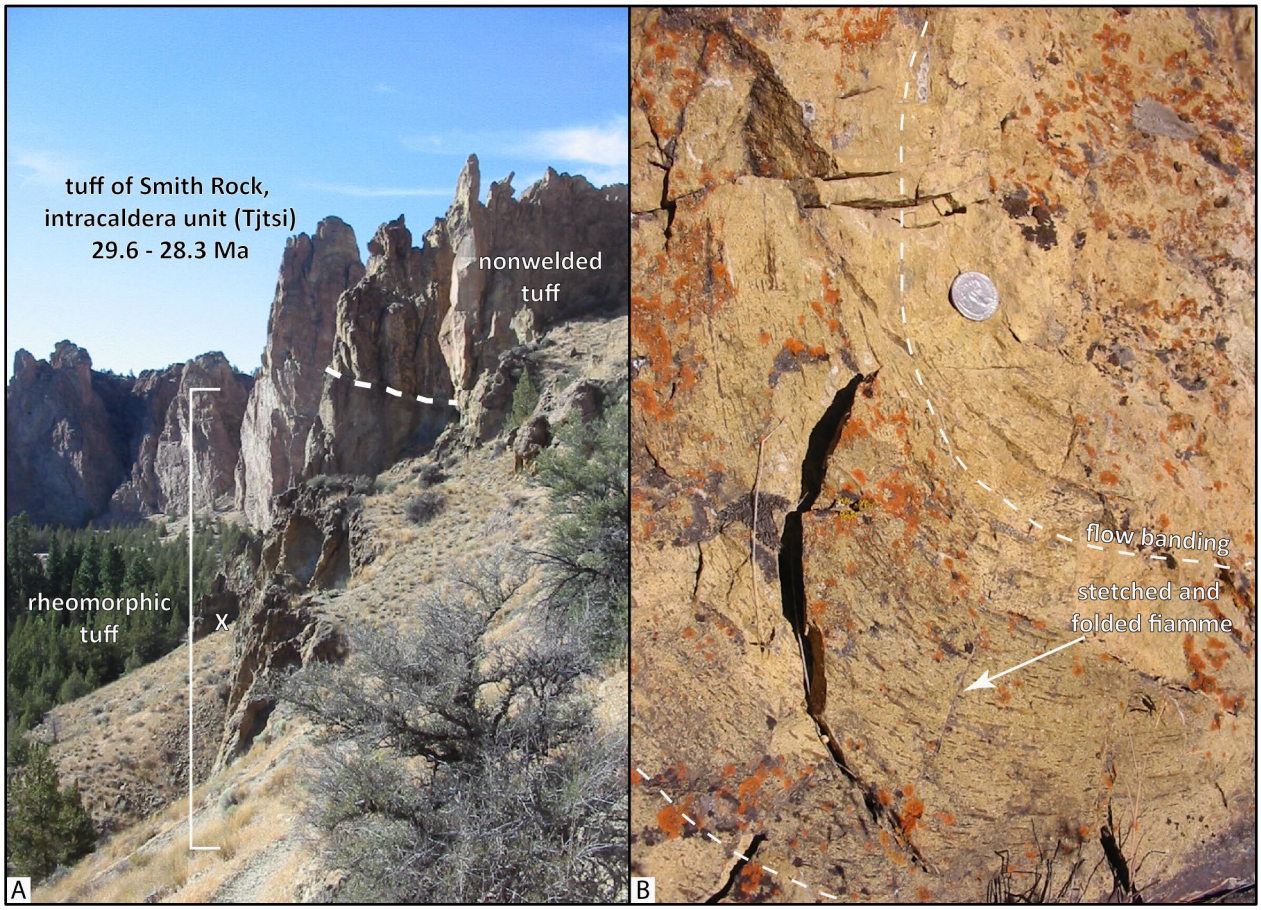

Tjtso **tuff of Smith Rock, welded outflow unit (lower Oligocene)**—Strongly welded to rheomorphic, very sparsely sanidine-phyric, pumice-lithic rhyolite tuff mapped around the periphery of the Crooked River caldera (**Figure 5-12**; plate). These rocks are chemically similar to the intracaldera unit (**Tjtsi**) and encircling rhyolite dome complexes (**Figure 5-12**, **Figure 5-15**; **Table 6-8**; plate, cross sections; appendix). Tuff units (**Tjtso**) are described geographically from northwest to northeast to southeast around the caldera and are referred to respectively as the Haystack Reservoir, McKay Saddle, and Prineville Reservoir lobes (**Figure 5-12**; plate). At Haystack Reservoir and at Prineville Reservoir, welded tuff is interbedded with and overlies nonwelded surge deposits and pyroclastic flow deposits (**Tjtsn**). Isotopic ages of ~29.6 Ma for unit **Tjtso** are indistinguishable from chemically and texturally similar John Day Formation, 29.54 Ma Member G ash-flow tuff, mapped to the north of the lower Crooked River basin near Antelope (**Figure 5-11**, **Figure 5-12**, **Figure 5-4**; **Table 5-2**; Smith and others, 1998).

Haystack Reservoir lobe—Rhyolite ash-flow tuff (SiO_2 = 77.39 to 77.8 weight percent; Zr = 420 to 600 ppm; Nb = 40.1 to 64.2 ppm; *n* = 11 analyses) mapped at Haystack Reservoir in the northwest part of the map area (**Figure 5-12**, **Figure 5-15**; **Figure 6-58**, **Figure 6-59**; **Table 6-8**; plate; appendix). The Haystack Reservoir outflow lobe (**Tjtso**) consists of strongly welded to rheomorphic, vitric-lithic-crystal rhyolite tuff (**Figure 6-60**, **Figure 6-61**). Outcrops are typically massive to columnar-jointed, locally weathering to pale reddish brown (10R 5/4) to dark yellowish orange (10YR 6/6). Strongly welded zones within the tuff (**Tjtso**) are marked by stretched and recrystallized pumice fiamme up to 25 cm (9.8 in) long that give the unit a strong eutaxitic fabric (**Figure 6-61**). Fiamme are locally fresh and relatively unaltered (**Figure 6-61a**); more commonly, fiamme are completely devitrified to axiolitically arranged crystals and rimmed with axiolites composed of quartz (**Figure 6-61b**). Rheomorphic zones are characterized by flow bands, flow folds, ramp structures, and elongated vesicles. Less strongly welded zones within the tuff (**Tjtso**) contain abundant, angular, light brownish gray (5YR /1), aphyric flow-banded rhyolite lithic fragments and subround, light brownish gray (5YR /1) pumices. Vitric float, locally found downslope from welded tuff exposures, suggests a vitrophyre may occur near the base of the unit (**Tjtso**)(Patridge, 2010). The tuff (**Tjtso**) is altered in places with ubiquitous secondary vapor phase minerals and quartz-infilling of lithophysal cavities (**Figure 6-60**). Composite thickness of the welded tuff (**Tjtso**) is up to 30 m (246 ft) on the east side of Haystack Reservoir, thickening to ~100 m (320 ft) along strike to the west (**Figure 5-12**, plate). Welded tuff (**Tjtso**) overlies nonwelded, plane-bedded and cross-bedded to massive, pumice- and accretionary-lapilli bearing ash-flow tuffs (**Tjtsn**) at Haystack Reservoir (**Figure 5-12**, **Figure 6-58**, **Figure 6-59**; plate).

Typical hand samples of the tuff are light brownish gray (5YR /1), grayish orange pink (5YR 7/2), very pale orange (10YR 8/2), and light gray (N7) and very sparsely porphyritic, containing 1 to 5 percent (vol.) broken to blocky sanidine, plagioclase, and quartz phenocrysts ≤2 mm (0.1 in) across, distributed within an eutaxitic groundmass of devitrified and clay-altered glass shards (**Figure 6-61**). Plagioclase, sanidine, and quartz phenocrysts typically have embayed and resorbed edges; phenocryst cores are commonly altered to white, chalky clay (Patridge, 2010). Spherulitic and axiolitic secondary grain overgrowth textures are common.

Outcrops east of U.S. Highway 97 were previously mapped as rhyolite by Robinson and Stensland (1979; unit Tjr) and Smith and others (1998; unit Tjrg) and were considered to form part of the Juniper rhyolite dome complex (**Figure 5-12**; plate). Herein, the outcrops between U.S. Highway 97 and Haystack Reservoir are reinterpreted as rheomorphic tuff (**Tjtso**) on the basis of a strongly welded, eutaxitic fabric, defined by 1 to 8 cm long (0.4 to 3.1 in), fresh-appearing obsidian fiamme, lithic fragments, and broken crystal fragments (**Figure 6-61**).

The Haystack Reservoir lobe of the tuff of Smith Rock (**Tjtso**) is assigned an early Oligocene age on the basis of stratigraphic position and an $^{40}Ar/^{39}Ar$ age of 29.57 ± 0.17 Ma (sanidine; sample GS095-132; Smith and others, 1998) and a $^{206}Pb/^{238}U$ zircon age of 29.51 ± 0.11 Ma (sample HS-JM-04) (**Figure 5-11**, **Figure 5-12**, **Figure 6-1**, **Table 5-2**; plate; appendix).

Figure 6-58. Haystack Reservoir lobe of the tuff of Smith Rock (Tjtsn, Tjtso) cropping out near the fishing pier at Haystack Reservoir. The lower yellowish gray (5Y 7/2) unit is a nonwelded pumice-crystal tuff (Tjtsn) with an $^{40}Ar/^{39}Ar$ age of 29.53 ± 0.09 Ma. The upper pale reddish brown (10R 5/4) unit is a strongly welded tuff (Tjtso) with an $^{40}Ar/^{39}Ar$ age of 29.57 ± 0.17 Ma. Photo credit: Jason McClaughry, 2008.

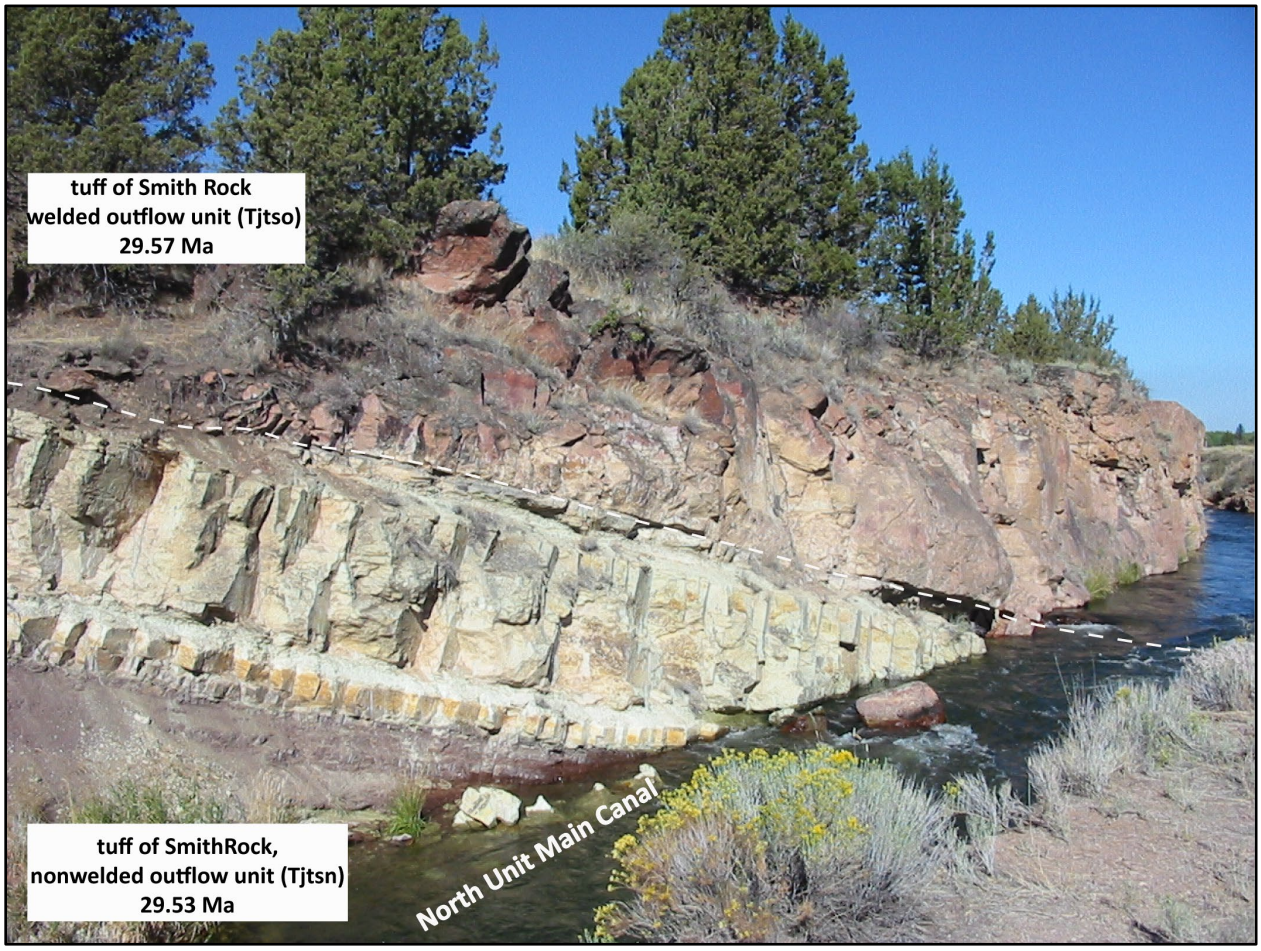

Figure 6-59. North-dipping ash-flow tuff units at Haystack Reservoir. The lower yellowish gray (5Y 7/2) unit is nonwelded pumice-crystal tuff (Tjtsn). The middle, pale reddish brown (10R 5/4) unit is a strongly welded tuff (Tjtso). The upper part of the section is capped by very pale orange (10YR 8/2), strongly welded tuff of Barnes Butte (Tjtb). View is looking east from the fishing pier at Haystack Reservoir (44.496662, -121.155535). Photo credit: Jason McClaughry, 2008.

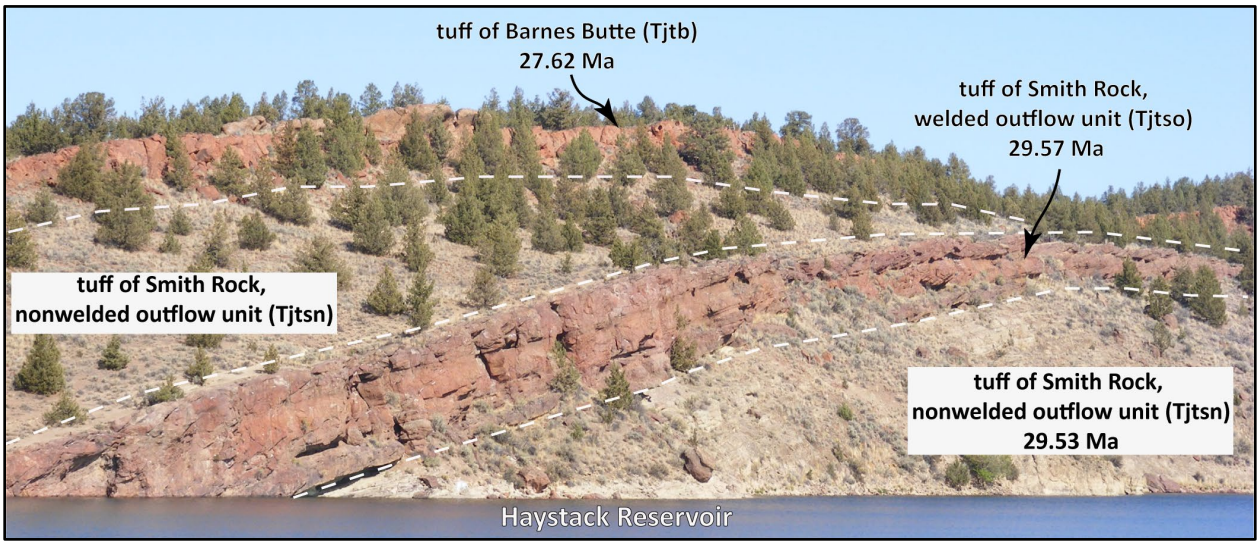

Figure 6-60. Welded outflow unit of the tuff of Smith Rock (Tjtso) exposed southeast of Haystack Reservoir (44.480233, -121.117394). The tuff forms distinct rimrock outcrops in the vicinity of Haystack Reservoir where it is typically characterized by abundant lithophysal cavities. Arrow points to 38 cm (15 in) long hammer for scale. This outcrop has a $^{206}Pb/^{238}U$ zircon age of 29.51 ± 0.11 Ma. Photo credit: Jason McClaughry, 2014.

Figure 6-61. Hand samples of the outflow unit of the tuff of Smith Rock (Tjtso). (a) Strongly welded ash-flow tuff (Tjtso), west of Haystack Reservoir. Outcrops here contain relatively fresh-appearing, glassy fiamme (44.489970, -121.170525). Penny for scale has a diameter of 1.5 cm (0.6 in). (b) Correlative with outcrops at the fishing pier along the western edge of Haystack Reservoir, contain stretched fiamme that are completely devitrified to axiolitically-arranged crystals (44.495882, -121.157012). Hammer head for scale is 12 cm (4.7 in) wide. Photo credits: Jason McClaughry, 2014.

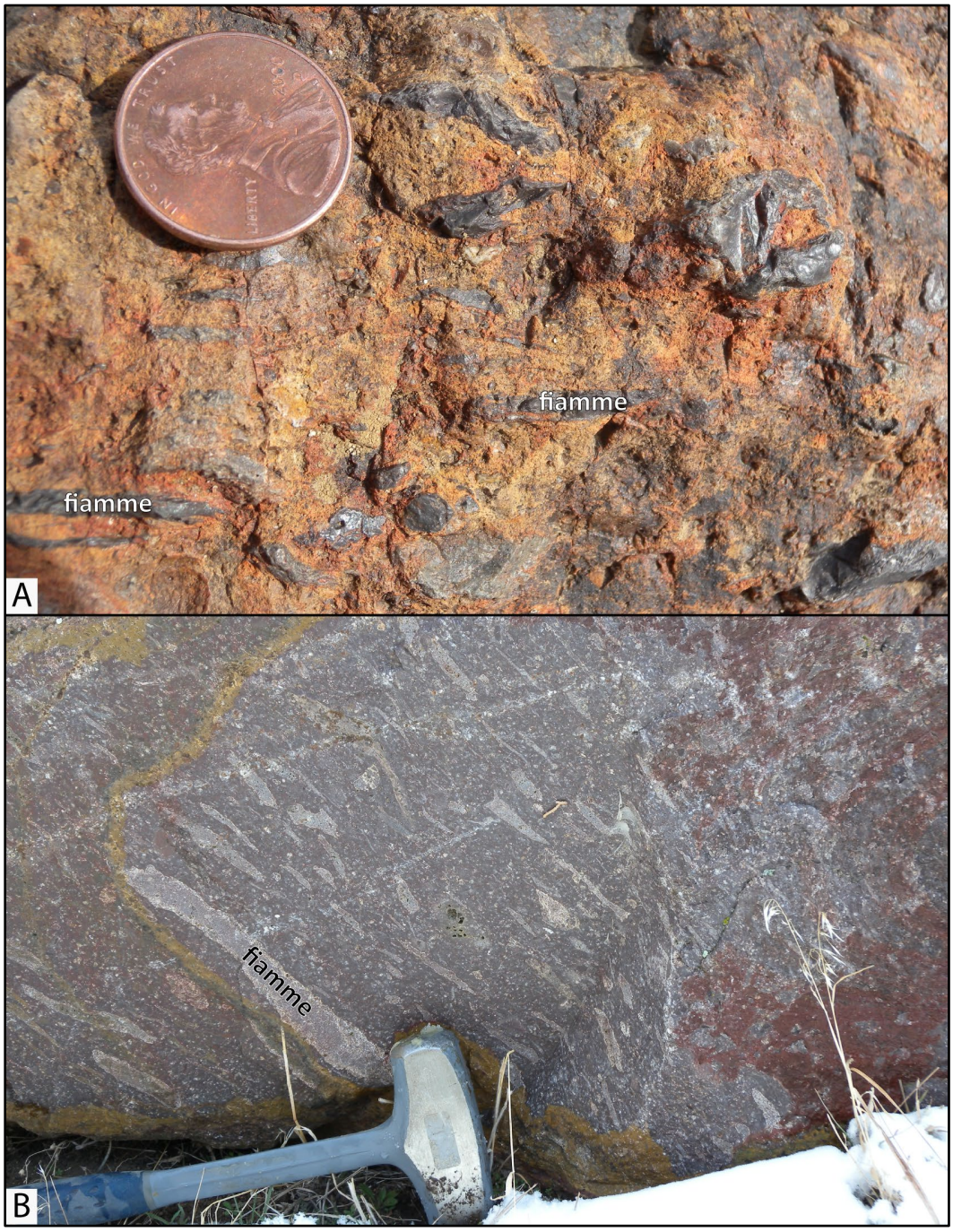

McKay Saddle lobe—Rhyolite ash-flow tuff (SiO_2 = 75.07 to 76.89 weight percent; Zr = 483 to 658; Nb = 40.2 to 71.9 ppm; *n* = 10 analyses) mapped at McKay Saddle and Green Mountain in the north central part of the map area (**Figure 5-12**, **Figure 5-15**; **Table 6-8**; plate; appendix). The McKay Saddle lobe (**Tjtso**) consists of at least four distinct flow units that reach a composite thickness of ~120 m (~400 ft) at McKay Saddle (**Figure 5-12**, plate). The base of the section mapped between Green Mountain and McKay Saddle consists of ~67 m (~220 ft) of pale purple (5P 6/2) to pale brown (5YR 5/2) and medium gray (N5), strongly welded, vitric-pumice-lithic-crystal tuff (**Figure 6-62a**). Outcrops are typically massive to platy and columnar jointed, locally weathering to precipitous cliffs and spires. Weathered surfaces are mantled by angular rock fragments and pale brown (5YR 5/2) soils. The lower tuff contains medium gray (N5), rounded pumice fragments and stretched to flattened fiamme up to 1 cm (0.4 in) across, and angular lithics of basalt, rhyolite, and devitrified, sanidine-plagioclase-phyric obsidian. The base of the McKay Saddle lobe (**Tjtso**) contains abundant lithophysal cavities up to 10 cm (3.9 in) across and locally is marked by a grayish black (N2), sparsely feldspar-phyric, lithophysae-bearing vitrophyre and vitrophyre breccia. Most lithophysae are filled by secondary quartz and zeolite. Typical hand samples from the lower part of the McKay Saddle lobe (**Tjtso**) are medium light gray (N6) to medium dark gray (N4), containing 1 to 5 percent seriate, broken, subhedral to anhedral, etched and embayed plagioclase, sanidine, oligoclase, and rare quartz and orthopyroxene microphenocrysts and phenocrysts ≤2 mm (0.1 in) across, distributed within a groundmass of devitrified glass shards. Bands of spherulitic and axiolitic feldspar and quartz, and secondary grain overgrowth textures are common.

The lower welded, vitric-pumice-lithic-crystal tuff in the McKay Saddle lobe (**Tjtso**) grades upward at McKay Saddle into ~18 m (~60 ft) of very fresh appearing medium light gray (N6) partially welded, obsidian tuff (**Figure 6-62b-c**). Outcrops are massive. Typical hand samples contain subrounded to flattened, black (N1), perlitic, opaque to partially translucent sanidine-plagioclase-phyric obsidian fragments up to 6 cm (2.4 in) across. Obsidian fragments are accompanied by ~2 percent (vol.) seriate, broken, subhedral to anhedral, etched and embayed, plagioclase, sanidine, oligoclase, and rare quartz and orthopyroxene microphenocrysts and phenocrysts ≤2 mm (0.1 in) across, and sparse pumice, basalt, and rhyolite lithic fragments up to 2 cm (0.8 in) across, contained within a groundmass of cuspate, non-fused glass shards. (**Figure 6-62b-c**).

Obsidian-rich tuff grades upward in the McKay Saddle lobe (**Tjtso**) into ~12 m (~40 ft) of moderately welded, lithic-crystal tuff. Good outcrops of the tuff are rare; the horizon is typically poorly exposed as a surface armored by boulders and angular, platy fragments. Typical hand samples are light gray (N7) to medium light gray (N6), containing a variety of banded obsidian, rhyolite, and andesite lithic fragments up to 2 cm (0.8 in) across and ~2 percent (vol.) seriate, broken, subhedral to anhedral, etched and embayed, plagioclase, sanidine, oligoclase, and rare quartz and orthopyroxene microphenocrysts and phenocrysts ≤2 mm (0.1 in) across, contained within a completely devitrified groundmass of flattened and contorted glass shards. Bands of spherulitic and axiolitic feldspar and quartz and secondary grain overgrowth textures are common.

The McKay Saddle lobe (**Tjtso**) is capped by a yellowish gray (5Y 7/2), nonwelded crystal-rich tuff. Outcrops of the upper tuff are rare; the horizon typically weathers to angular, platy fragments. Typical hand samples are distinctly porphyritic, containing ~5 to 7 percent (vol.) clear, subhedral to anhedral, blocky and lath-shaped, seriate, broken plagioclase, sanidine, and

oligoclase ≤2 mm (0.1 in) across, ≤1 percent (vol.) clear quartz ≤1 mm (0.04 in) across, and ≤1 percent (vol.) orthopyroxene ≤1 mm (0.04 in) across, distributed within a groundmass of completely devitrified glass shards.

The McKay Saddle lobe of the tuff of Smith Rock (**Tjtso**) is assigned an early Oligocene age on the basis of stratigraphic position and an $^{40}Ar/^{39}Ar$ age of 29.56 ± 0.17 Ma obtained from the upper crystal-rich tuff (sanidine; sample 448 LCJ 07) (**Figure 5-11**, **Figure 5-12**, **Figure 6-1**; **Table 5-2**; plate; appendix).

Figure 6-62. McKay Saddle lobe of the tuff of Smith Rock (Tjtso). (a) Strongly welded pumice-lithic-crystal tuff exposed on the summit of Green Mountain (44.441110, -120.695207). The tuff here forms prominent spires and contains abundant lithophysal cavities up to 2 cm (0.8 in) across. Arrow points to 40 cm (15 in) long hammer for scale in the center of photograph. (b) Partially welded obsidian tuff west of McKay Saddle (44.515640, -120.640685). Hammer head for scale is 12 cm (4.7 in) wide. (c) Photomicrograph of obsidian tuff, composed of opaque to translucent sanidine-plagioclase-phyric obsidian fragments, cuspate, non-fused glass shards, and sparse blocky sanidine phenocrysts. Scale bar is 1 cm (0.4 in) wide. Photo credits: Jason McClaughry, 2006,2007.

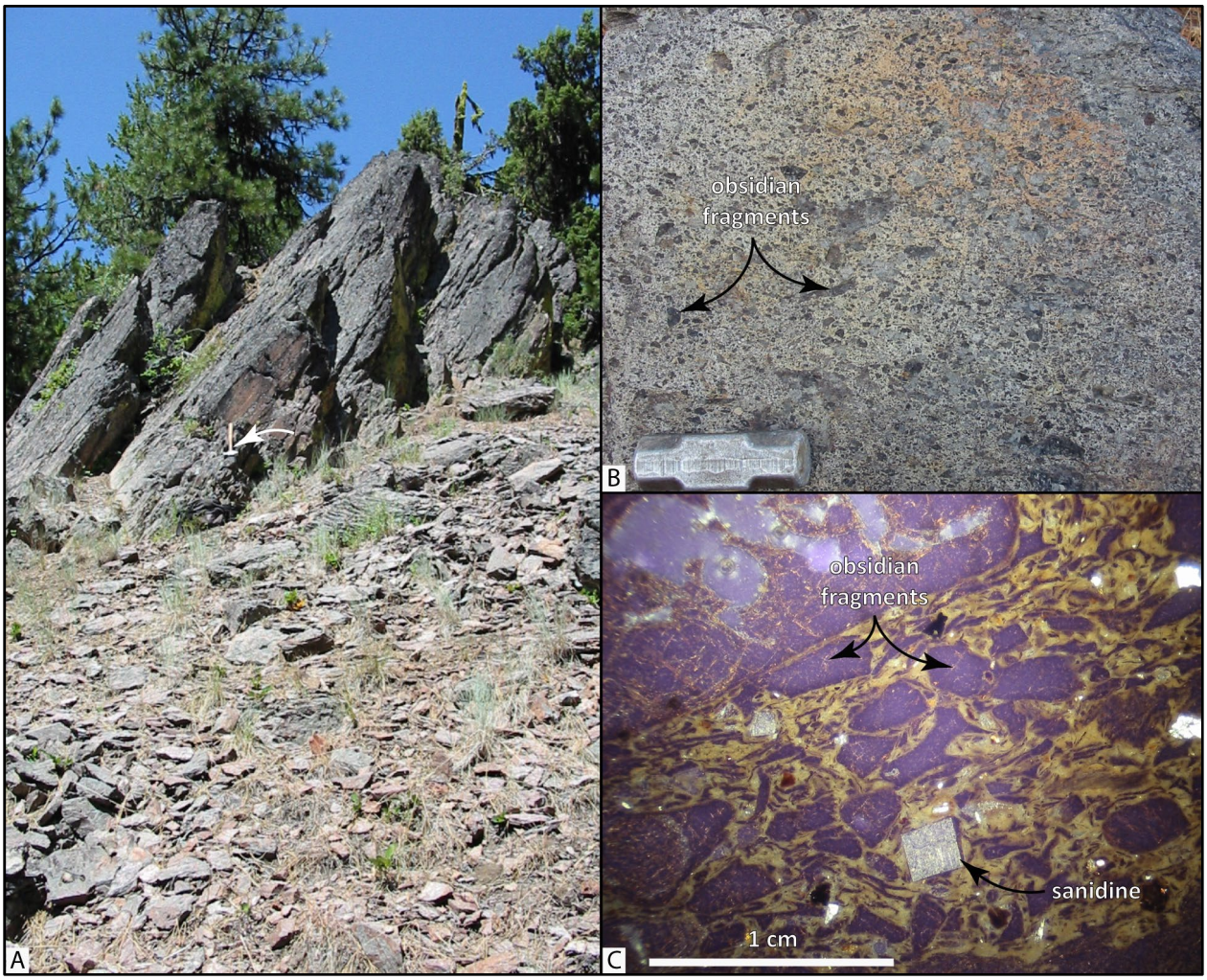

***Prineville Reservoir lobe*—**Rhyolite ash-flow tuff (SiO_2 = 76.48 to 77.87 weight percent; Ba = 539 to 1032; Zr = 362 to 584 ppm; Nb = 48.7 to 66.5 ppm; *n* = 4 analyses) mapped capping Big Bend Island at Prineville Reservoir and other ridges in Prineville Reservoir State Park (**Figure 5-12**, **Figure 5-15**, **Figure 6-63**, **Figure 6-64**; **Table 6-8**; plate; appendix). The Prineville Reservoir outflow lobe (**Tjtso**) consists of strongly welded to rheomorphic, vitric-lithic-crystal rhyolite tuff. Outcrops are typically massive to platy and columnar-jointed, locally weathering to precipitous cliffs, spires, and caverns (**Figure 6-63**). Weathered surfaces are typically mantled by angular rock fragments and moderate brown (5YR 4/4) soils. Strongly welded zones within the tuff (**Tjtso**) are marked by stretched and recrystallized pumice fiamme up to 15 cm (5.9 in) long that give the unit a strong eutaxitic fabric (Patridge, 2010). Fiamme are typically completely devitrified to axiolitically-arranged crystals and rimmed with axiolites composed of quartz. Rheomorphic zones, present near the base of the tuff (**Tjtso**), are characterized by flow bands, flow folds, ramp structures, and elongated vesicles (**Figure 6-63**). Rheomorphic zones grade downward into lithophysal horizons that contain contorted vertical flow-foliations (**Figure 6-63**). Locally, a glassy, perlitic vitrophyre is exposed at the base of the welded tuff (**Tjtso**). Less strongly welded zones within the tuff contain abundant, angular, pale brown (5YR 5/2), aphyric flow-banded rhyolite lithic fragments and subround, brown-colored pumices. The tuff (**Tjtso**) is altered in places with ubiquitous secondary vapor phase minerals and quartz-infilling of lithophysal cavities. Welded tuff (**Tjtso**) overlies nonwelded, plane-bedded and cross-bedded to massive, pumice- and accretionary-lapilli bearing ash-flow tuffs (**Tjtsn**) at Big Bend Island (**Figure 5-12**, **Figure 6-63**). The Prineville Reservoir lobe (**Tjtso**) has a variable thickness that may exceed 100 m (328 ft) (plate).

Typical hand samples of the tuff are pale purple (5P 6/2), pale red purple (SRP 6/2), and pale yellowish orange (10 YR 8/6) and sparsely porphyritic, containing 1 to 5 percent (vol.) broken to blocky sanidine, plagioclase, and quartz phenocrysts ≤2 mm (0.1 in) across, distributed within an eutaxitic groundmass of devitrified and clay-altered glass shards (**Figure 6-61**). Plagioclase, sanidine, and quartz phenocrysts typically have embayed and resorbed edges; phenocryst cores are commonly altered to white, chalky clay (Patridge, 2010). Spherulitic and axiolitic secondary grain overgrowth textures are common.

The Prineville Reservoir lobe of the tuff of Smith Rock (**Tjtso**) is assigned an early Oligocene age on the basis of stratigraphic position and a $^{206}Pb/^{238}U$ zircon age of 29.5 ± 0.2 Ma obtained for a sample on Big Bend Island (sample JM ER 1-4) (**Figure 5-11**, **Figure 5-12**, **Figure 6-1**, **Figure 6-63**; **Table 5-2**; plate; appendix). Zircons from sample JM ER 1-4 are small (<100 μm in length) and stubby, with well-developed crystal faces. Cathodoluminescence imaging reveals commonly dark, embayed cores surrounded by lighter rims. Analysis of twenty zircons gave $^{206}Pb/^{238}U$ dates ranging from 36.5 ± 0.9 to 27.9 ± 0.6 Ma. Deconvolution of the dates yields peak populations at 33.48 ± 0.29 and 29.5 ± 0.2 Ma (appendix). The 29.5 Ma Prineville Reservoir lobe of the tuff of Smith Rock (**Tjtso**, **Tjtsn**) is separated from ~29.7 Ma basaltic andesite lava flows (**Tjba**), the tuff of Antelope Creek (**Tjta**), the tuff of Eagle Rock (**Tjte**), and tuffaceous sedimentary rocks (**Tjtt**) with angular unconformity along Prineville Reservoir (**Figure 5-12**, **Figure 6-64**, **Figure 6-65**; plate). At Prineville Reservoir, these older ~29.7 Ma beds (**Tjba**, **Tjta**, **Tjte** , **Tjtt**) strike N.25°E. to N.56°E., and dip 30° to 55°NW., while the overlying 29.5 Ma tuff of Smith Rock outflow unit (**Tjtsn**) strikes N.51°E. and dips 4°NW at Prineville State Park and strikes N.19°W. and dip 2°SW. on Big Bend Island (**Figure 5-12**, plate). This angular unconformity is interpreted to have formed with initial collapse of the Crooked River caldera at ~29.5 Ma on the basis of: 1) the <20 k.yr. difference in

age between the deformed and tilted 29.7 Ma tuff of Eagle Rock (**Tjte**) and syn-caldera 29.5 Ma outflow tuff of Smith Rock (**Tjtso**); and 2) the discontinuous exposure and local thinning and thickening of unit **Tjtso** across tilted rocks, indicating ponding in areas of low relief during emplacement (**Figure 6-63**).

Figure 6-63. Prineville Reservoir lobe of the tuff of Smith Rock (Tjtso) northwest of Prineville Reservoir. (a) Columnar-jointed, rheomorphic welded tuff (Tjtso) (44.181442, -120.665629). (b) Outflow tuff here includes rheomorphic and lithophysal zones. Photo credits: Jason McClaughry, 2006.

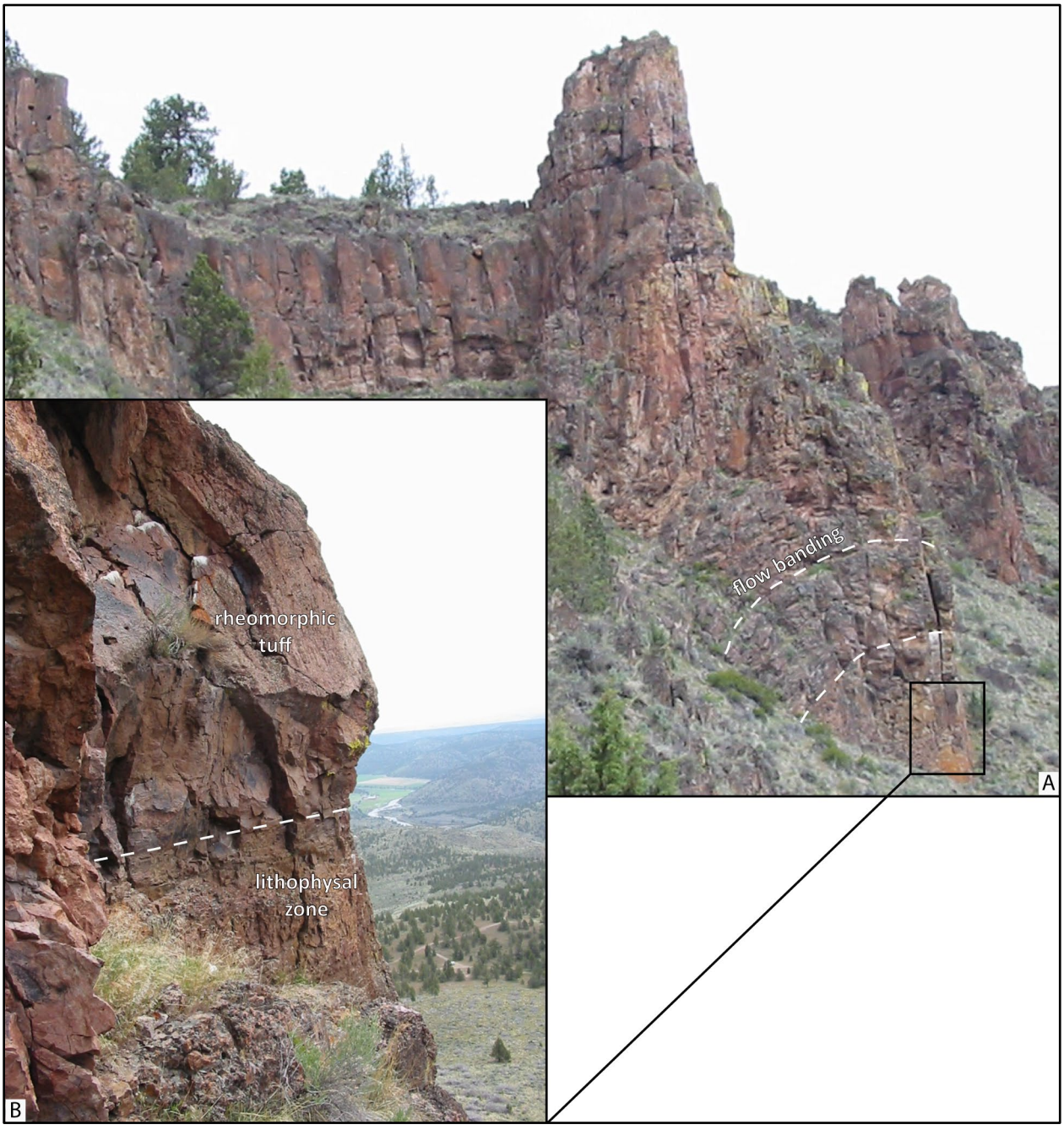

Figure 6-64. Prineville Reservoir lobe of the tuff of Smith Rock (Tjtso). (a) Welded and nonwelded (Tjtsn) outflow unit of the 29.5 Ma tuff of Smith Rock (Tjtso) unconformably overlying a northwest dipping section of 29.7 Ma ash-flow tuffs (Tjta, Tjte) at Prineville Reservoir along the southern margin of the Crooked River caldera. The locations marked with an X and Y are the collection sites for tuff $^{206}Pb/^{238}U$ zircon ages. The north-dipping tuff of Eagle Rock (Tjte) has a $^{206}Pb/^{238}U$ zircon age of 29.7 ± 0.6 Ma (sample CR-8; X), while relatively flat lying, strongly welded outflow unit of the tuff of Smith Rock (Tjtso) capping Big Bend Island has a $^{206}Pb/^{238}U$ zircon age of 29.5 ± 0.2 Ma (sample JM-ER 1-4; Y). View is looking northeast (44.121816, -120.752099). (b) Nonwelded outflow unit of the tuff of Smith Rock (Tjtsn) exposed on Big Bend Island (44.123119, -120.730009). Person for scale in the left side of photograph. (c) Bedded, varicolored, nonwelded tuff (Tjtsn) exposed on the east side of Big Bend Island (44.125534, -120.733410). These deposits are correlative with to the 29.53 Ma, nonwelded outflow unit of the tuff of Smith Rock (Tjtsn) mapped beneath welded outflow tuff at Haystack Reservoir along the northwest margin of the Crooked River caldera. Photo credits: Jason McClaughry, 2009.

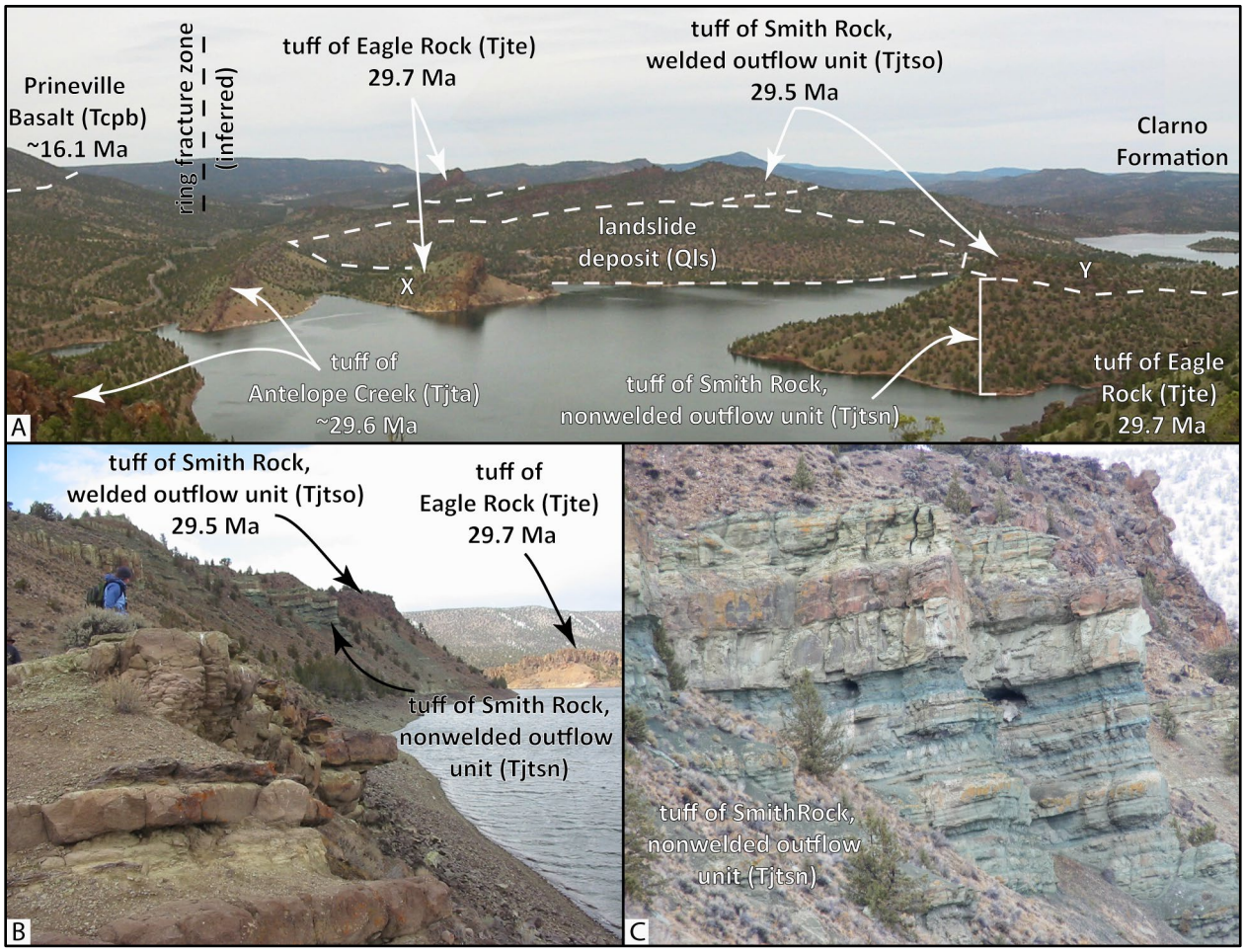

Figure 6-65. Northwest-dipping early Oligocene strata exposed near the Prineville Reservoir county boat ramp (44.132985, -120.747462). The section includes two thick rhyolitic tuffs (Tjta, Tjte) interbedded with tholeiitic basaltic andesite (Tjba) and volcaniclastic sedimentary rocks (Tjtt). Dashed white lines are approximate contacts between units. Schematic strike and dip symbol shows the structural orientation of early Oligocene strata. The X in the right of the photograph marks the collection location of sample CR-8, which returned a $^{206}Pb/^{238}U$ zircon age of 29.7 ± 0.6 Ma. Photo credit: Jason McClaughry, 2006.

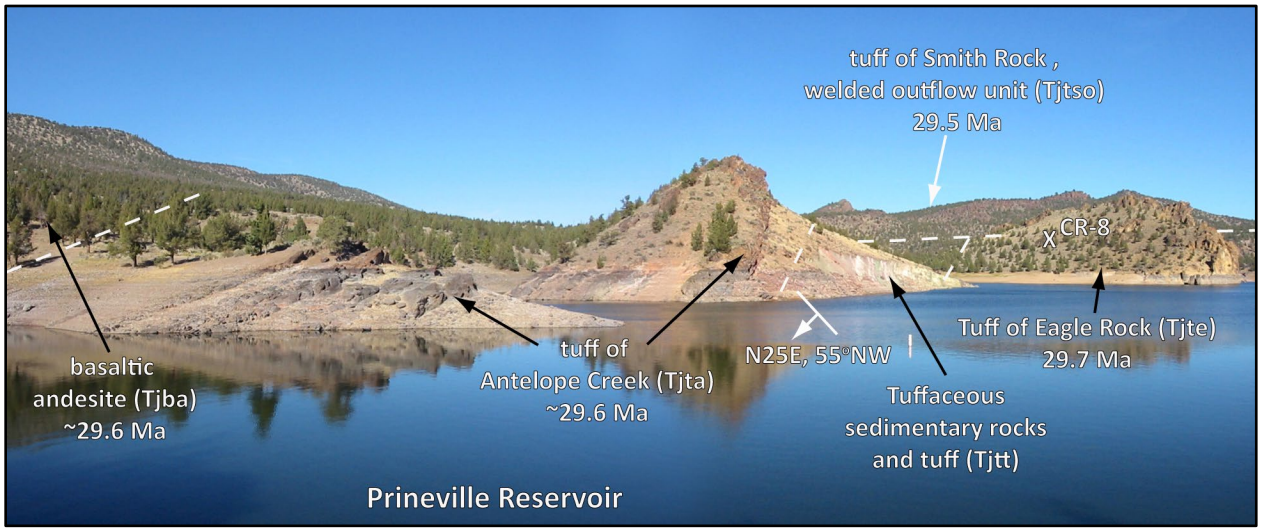

Tjtsn **tuff of Smith Rock, nonwelded outflow unit (lower Oligocene)—**Nonwelded, plane-bedded and cross-bedded to massive, pumice- and accretionary-lapilli bearing rhyolite ash-flow tuffs (SiO_2 = 71.16 to 75.1 weight percent; Zr = 289 to 393 ppm; Nb = 17.1 to 45.1 ppm; *n* = 5 analyses) mapped beneath the welded outflow unit of the tuff of Smith Rock (**Tjtso**) northwest of Gray Butte (Haystack Reservoir lobe) and at Prineville Reservoir (Prineville Reservoir lobe) (**Figure 5-12**, **Figure 5-15**, **Figure 6-64**, **Figure 6-66**; **Table 6-8**; plate; appendix). Unit **Tjtsn** is typically poorly exposed, except along roadcuts and reservoir banks. The tuffs (**Tjtsn**) contain abundant clay-altered pumice and rounded accretionary lapilli and less common angular fragments of spherulitic, devitrified glass and flow-banded rhyolite (**Figure 6-66a-b**; Patridge, 2010). Pale red (10R 6/2) oxidized material is present in the matrix of most tuffs. Plane-parallel bedding, cross bedding, pinch and swell structures, and grading are common within discrete tuff beds (**Figure 6-64c**). Individual beds of cross-bedded and plane-bedded tuff typically range from 10 to 30 cm (3.9 to 11.8 in) thick; more massive lapilli tuffs range from 1 to 3 m (3.3 to 9.8 ft) in thickness (**Figure 6-64c**, **Figure 6-66**). Composite thickness of the unit (**Tjtsn**) is as much as 61 m (200 ft) (plate). Typical hand samples of the nonwelded tuffs are yellowish gray (5Y 7/2), grayish green (5G 5/2), and pale brown (5YR 5/2) and porphyritic, containing 3 to 5 percent (vol.) clear to white (N9), broken to blocky, sanidine and quartz phenocrysts ≤2 mm (0.1 in) across and ≤1 percent (vol.) microphenocrysts of dusky yellow green (5GY 5/2), chlorite-altered pyroxene, distributed within a clay-altered (chlorite) groundmass of devitrified glass shards. Phenocrysts of sanidine and quartz are zoned, with embayed and resorbed edges (Patridge, 2010).

The nonwelded outflow unit of the tuff of Smith Rock (**Tjtsn**) is assigned an early Oligocene age on the basis of stratigraphic position and an $^{40}Ar/^{39}Ar$ plateau age of 29.53 ± 0.09 Ma obtained from an outcrop at Haystack Reservoir (sanidine; sample GSO 95-133; Smith and others, 1998) (**Figure 5-11**, **Figure 5-12**, **Figure 6-1**, **Figure 6-66**; **Table 5-2**; plate; appendix). On the basis of

sedimentary structures, grading, and prevalence of accretionary lapilli (**Figure 6-66b**), the tuffs are interpreted as hydromagmatic pyroclastic surge deposits and pulsating pyroclastic flows associated with overlying strongly welded outflow units (**Tjtso**). The distribution of the welded outflow tuff (**Tjtso**), combined with flow directions determined by surge cross-beds in unit **Tjtsn**, indicate a Crooked River caldera source vent.

Figure 6-66. Nonwelded outflow unit of the tuff of Smith Rock (Tjtsn) at the Haystack Reservoir fishing pier. (a) Nonwelded, massive to plane-bedded and cross-bedded pumice- and accretionary-lapilli bearing tuff (44.496267, -121.156291). Arrow points to 38 cm (15 in) long hammer for scale. (b) Accretionary lapilli within surge deposits in the outcrop in A. Pencil for scale. Photo credits: Jason McClaughry, 2008. A sample from this outcrop returned an $^{40}Ar/^{39}Ar$ age of 29.53 ± 0.09 Ma (sample GSO 95-133).

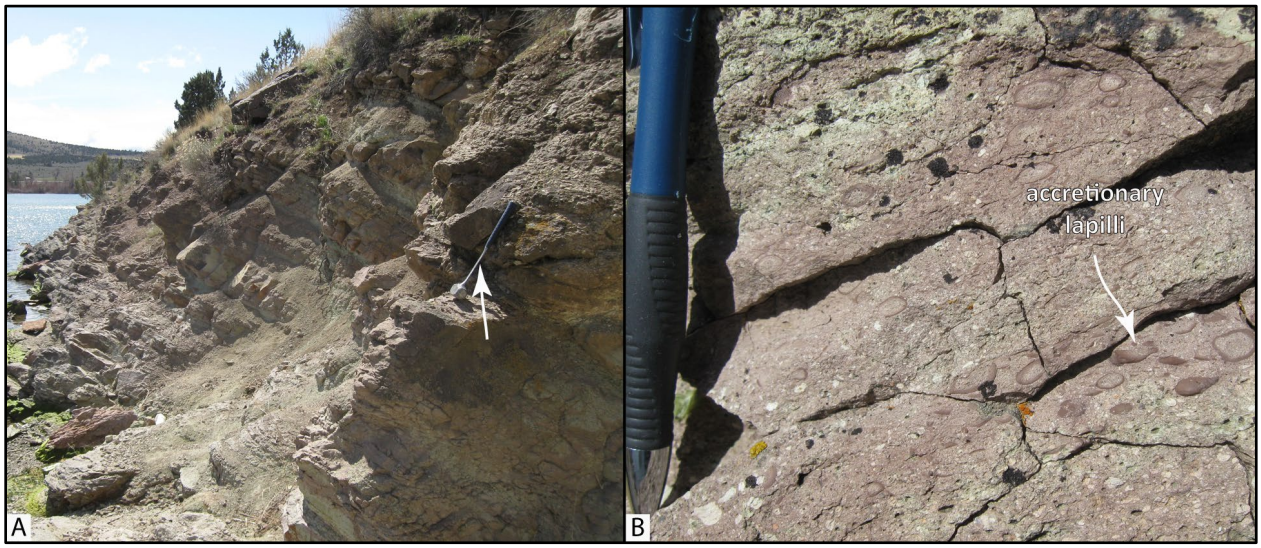

Angular unconformity to disconformity

Tjta **tuff of Antelope Creek (lower Oligocene)—**Rhyolite ash-flow tuff (SiO_2 = 73.71 to 77.92 weight percent; Zr = 340 to 615 ppm; Nb = 30.5 to 49.4 ppm; *n* = 21 analyses) mapped in a northwest-dipping stratigraphic section along the southeastern margin of the Crooked River caldera (**Figure 5-12**, **Figure 5-15**, **Figure 6-64a**, **Figure 6-65**; **Table 6-8**; plate; appendix). The tuff (**Tjta**) also caps a southeast-dipping stratigraphic section along the northwest margin of the Crooked River caldera, west of Gray Butte (**Figure 6-67**). Unit **Tjta** typically crops out as cliffs and hoodoos. The base of the tuff is strongly welded and locally displays rheomorphic features marked by contorted flow foliations and lithophysal cavities. Pumices and phenocrysts are sparse. Where present, pumices are banded, up to 2 cm (0.8 in) across, and are generally flattened, forming distinct fiamme. The tuff also contains a variety of lithic fragments, including obsidian, basalt, and andesite. Thickness of unit **Tjta** is as much as 73 m (240 ft) (plate). Typical hand samples of the tuff are pale red (10R 6/2), pale yellowish brown (10YR 6/2), and medium light gray (N6) and sparsely porphyritic, containing ≤3 percent (vol.) clear to chalky white (N9), blocky sanidine and plagioclase phenocrysts ≤2 mm (0.1 in) across, distributed within a clay-altered, eutaxitic groundmass of devitrified glass shards. Spherulitic and axiolitic overgrowth textures are common.

The tuff of Antelope Creek (**Tjta**) is assigned an early Oligocene age of ~29.6 Ma on the basis of stratigraphic position above the 29.7 Ma tuff of Eagle Rock (**Tjte**) and below the 29.5 Ma Prineville Reservoir lobe of the outflow unit of the tuff of Smith Rock (**Tjtso**) (**Figure 5-12**, **Figure 6-1**, **Figure 6-64a**, **Figure 6-65**; plate).

Figure 6-67. Southeast dipping section of early Oligocene strata. View is looking east from the old U.S Highway 97 bridge at Peter Skene Ogden State Park (44.391062, -121.190691). The intracaldera unit of the tuff of Smith Rock (Tjtsi) is inset into and onlaps the older deformed pre-Crooked River caldera strata. Gray Butte in the distance is a 29.2 Ma rhyolite intrusion that crosscuts the lower part of the tuff of Smith Rock (Tjtsi). White dashed line is the lower contact of the tuff of Antelope Creek (Tjta). Dashed black line demarcates the structural margin of the caldera. Arrows indicate the relative motion of the downthrown block within the caldera ring-fracture. Ticks point into the caldera. Schematic strike and dip symbol shows the structural orientation of early Oligocene strata. Photo credit: Jason McClaughry, 2008.

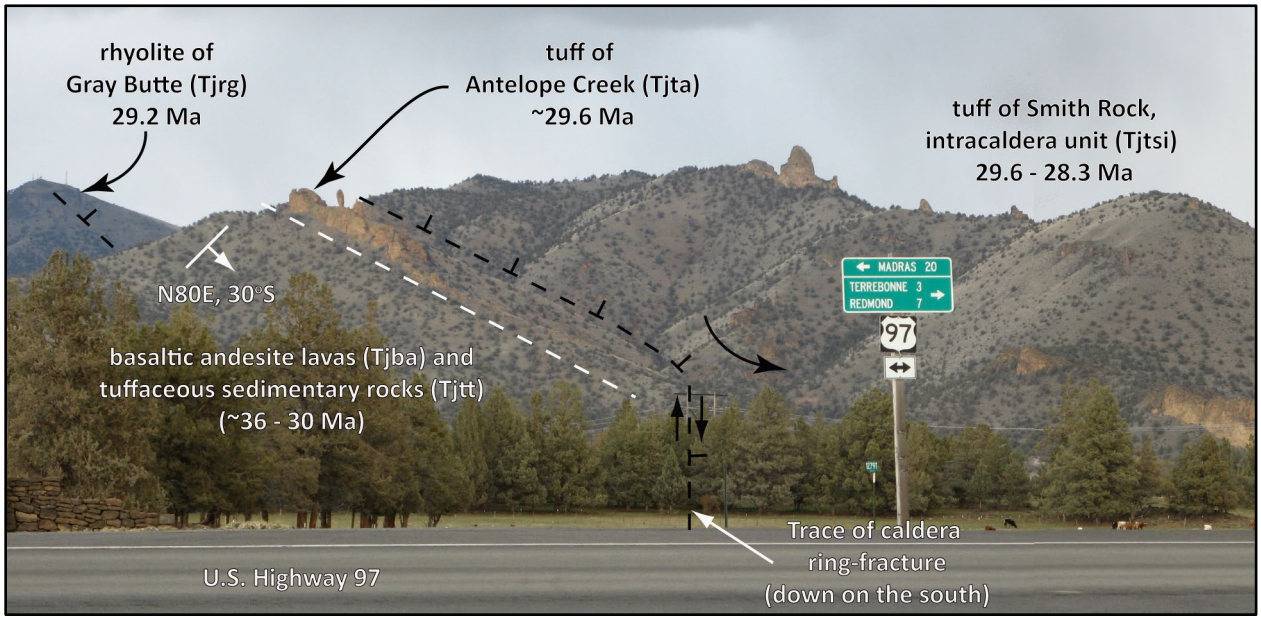

Tjte **tuff of Eagle Rock (lower Oligocene)—**Rhyolite ash-flow tuff (SiO_2 = 76.28 to 77.83 weight percent; Zr = 445 to 504 ppm; Nb = 52.1 to 71.6 ppm; *n* = 5 analyses) mapped along Prineville Reservoir (**Figure 5-12**, **Figure 5-15**, **Figure 6-64a**, **Figure 6-65**; **Table 6-8**; plate; appendix). Unit **Tjte** commonly crops out as precipitous cliffs and spires, often with columnar jointing (**Figure 6-68**). Strongly welded zones within the tuff are marked by stretched pumice fiamme up to 4 cm (1.6 in) long. Rheomorphic zones are characterized by flow bands, flow folds, ramp structures, and elongated vesicles (**Figure 6-69**). Less strongly welded zones within the tuff (**Tjte**) contain abundant, angular, dusky brown (5YR 2/2), aphyric lithic fragments and subround, pale brown (5YR 5/2) pumices. The lower part of the tuff is characterized by open lithophysal cavities and zones of vertically inclined platy joints. Secondary vapor phase minerals and disc-shaped, yellow to white pumices altered to zeolite are ubiquitous. East of Eagle Rock, in the southeast part of the map area, outcrops reveal fractures filled by silicified breccia (**Figure 5-12**). Thickness of unit **Tjte** is up to 75 m (246 ft), apparently thickening along strike to the west (plate). Typical hand samples of the tuff are pale red (10R 6/2), very pale orange (10YR 8/2), and medium light gray (N6) and very sparsely porphyritic, containing ≤1 percent (vol.) white (N9), blocky sanidine phenocrysts

≤2 mm (0.1 in) across, distributed within a clay-altered, eutaxitic groundmass of devitrified glass shards. Spherulitic and axiolitic overgrowth textures are common.

The tuff of Eagle Rock (**Tjte**) is assigned an early Oligocene age on the basis of stratigraphic position and a $^{206}Pb/^{238}U$ zircon age of 29.7 ± 0.6 Ma obtained for a sample on the north shore of Prineville Reservoir, north of Big Bend Island (sample CR-8; Seligman and others, 2014) (**Figure 5-11**, **Figure 5-12**, **Figure 6-1**, **Figure 6-64a**; **Table 5-2**; plate; appendix). An older K-Ar age of 32.1 ± 0.7 Ma (plagioclase) was reported, apparently for this tuff by Robinson and others (1990), but the date is of uncertain quality and location (**Figure 5-11**, **Table 5-2**; plate; appendix).

Figure 6-68. View looking north to cliff-forming exposures of the tuff of Eagle Rock (Tjte) overlying tuffaceous, volcaniclastic sedimentary rocks of the John Day (Tjtt) and Clarno (Tces) formations in the headwaters area of Owl Creek in the south part of the map area (44.164517, -120.681792). Photo credit: Jason McClaughry, 2006.

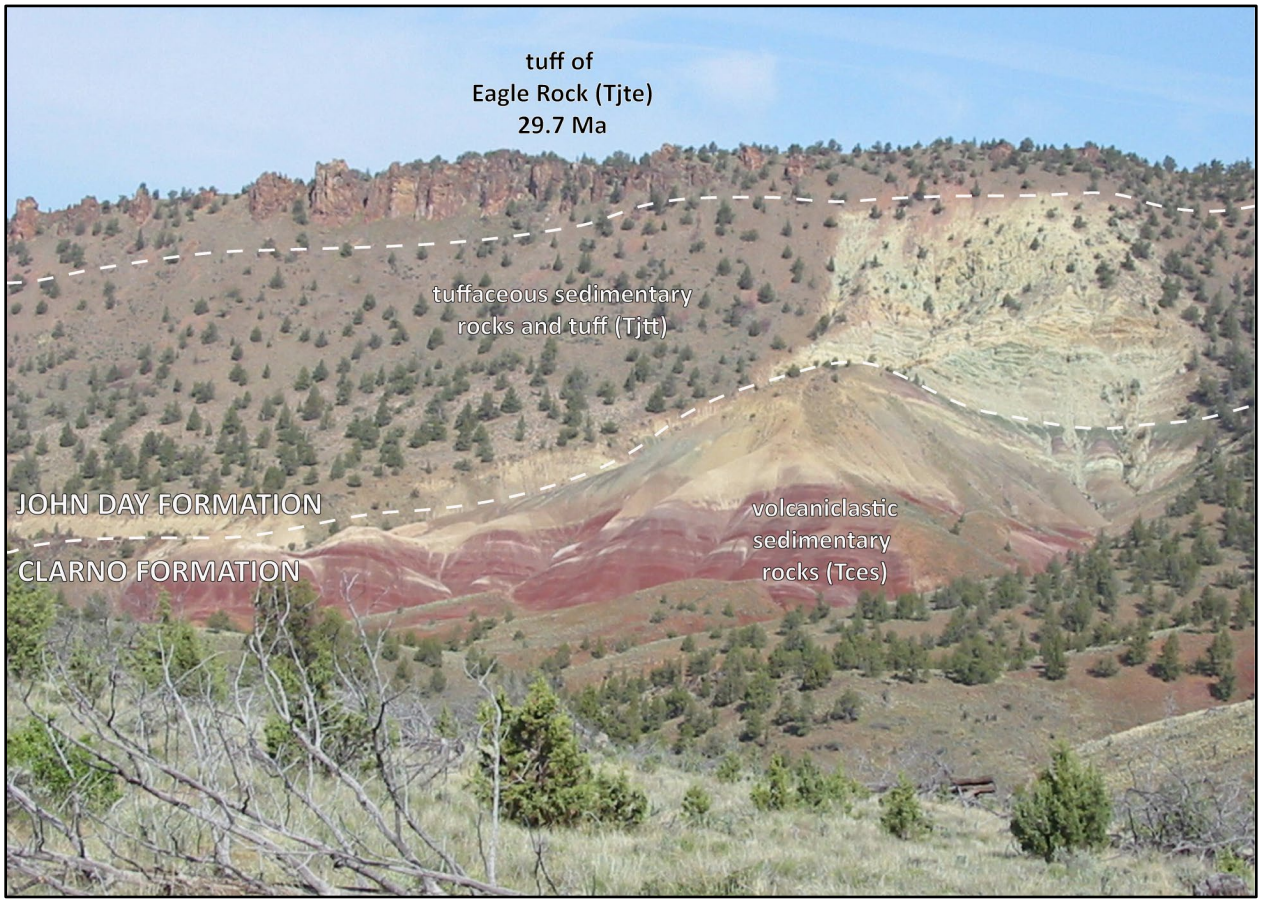

Figure 6-69. Spire forming outcrop of the tuff of Eagle Rock (Tjte) at Eagle Rock along the Paulina Highway (OR Highway 380) (44.195483, -120.650003). The tuff of Eagle Rock typically is characterized by rheomorphic textures including flow bands, flow folds, ramp structures, and elongated vesicles. Photo credit: Jason McClaughry, 2008.

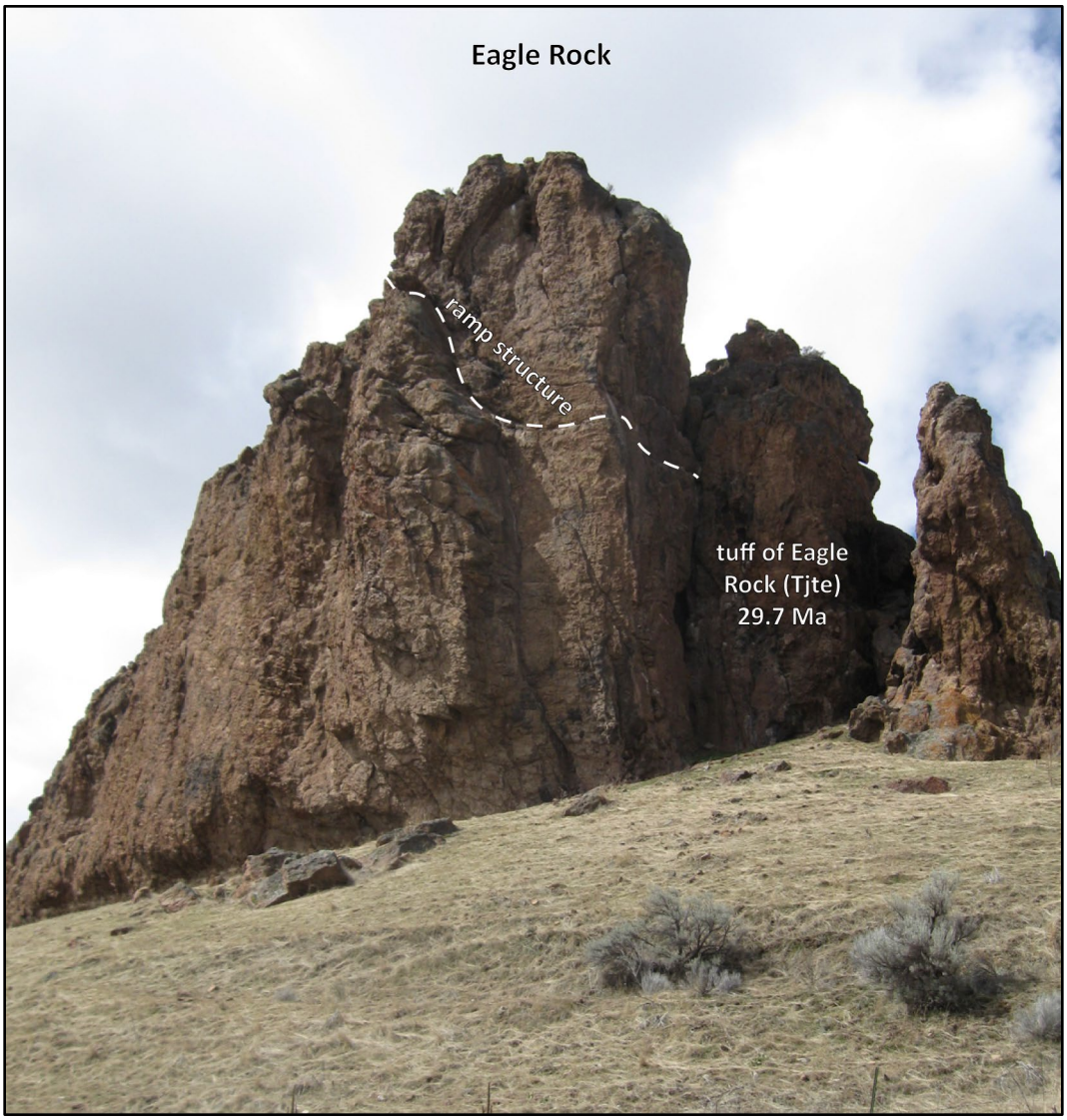

Tjba **basalt, basaltic andesite, and andesite lava flows (lower Oligocene and upper Eocene)—**Chiefly iron- and titanium-rich tholeiitic basaltic andesite and andesite lava flows (SiO_2 = 53.08 to 59.0 weight percent; TiO_2 = 1.71 to 3.31 weight percent; FeOTotal = 10.69 to 15.51 weight percent; *n* = 21 analyses) mapped along both the northwest and southeast margins of the Crooked River caldera (**Figure 5-12**, **Figure 6-70**; **Table 6-8**; plate; appendix). North and west of Gray Butte, unit **Tjba** includes a very poorly exposed series of tholeiitic picrobasalt and basalt lava flows (SiO_2 = 44.31 to 52.52 weight percent; TiO_2 = 1.67 to 2.88 weight percent; FeOTotal = 9.55 to 13.93 weight percent; *n* = 9 analyses) (**Figure 5-12**, **Figure 6-67**, **Figure 6-70**; **Table 6-8**; plate; appendix). Lava flows in unit **Tjba** are typically preserved in flow-on-flow successions, characterized by thin (1 to 3 m [3.3 to 9.8 ft]) individual flow lobes separated by vesicular flow tops and locally by dark reddish brown (10R 3/4) brecciated flow bases. Weathered outcrops have closely spaced fractures and are associated with talus cones of platy to blocky rubble and dark reddish brown (10R 3/4) and light olive brown (5Y 5/6) soils (**Figure 6-70**). At the Prineville Reservoir County boat ramp, outcrops have pervasive shear fabrics and secondary hydrothermal alteration features including zeolite-filled vesicles, calcite-filled fractures, and hydrothermal breccia cemented by quartz and calcite. Typical hand samples of basaltic andesite and andesite lava flows are dark gray (N3) to medium light gray (N6) and aphyric to sparsely porphyritic, containing ≤2 percent (vol.) lath-shaped plagioclase phenocrysts ≤2 mm (0.1 in) across, distributed within a very fine-grained hypocrystalline groundmass composed of plagioclase, microgranular clinopyroxene, rare iddingsite-altered olivine, cubic Fe-Ti oxides, and variably altered interstitial glass. Typical hand samples of picrobasalt and basalt are dark gray (N3) and contain sparse olivine and plagioclase microphenocrysts in a hypocrystalline groundmass composed of interstitial to subophitic titaniferous clinopyroxene and variably altered glass.

Unit **Tjba** is assigned a late Eocene(?) and early Oligocene age on the basis of stratigraphic position, interbedded with more precisely dated ash-flow tuff units (**Figure 6-1**, **Figure 6-65**; **Table 5-2**; plate; appendix). Along the western end of Prineville Reservoir tholeiitic lavas lie stratigraphically above the 29.7 Ma tuff of Eagle Rock (**Tjte**) and below the 29.5 Ma outflow unit of the tuff of Smith Rock (**Tjtso**) (**Figure 5-12**, **Figure 6-65**). Northwest of Gray Butte, similar composition lavas lie stratigraphically beneath the 32.49 Ma tuff of Rodman Spring (**Tjtr**) and sit directly on older calc-alkaline lavas of the Clarno Formation. Tholeiitic basaltic andesite and andesite lava flows (**Tjba**) cropping out between Lithgow Spring and Pine Ridge, along the northwest margin of the Crooked River caldera, have a K-Ar age of 30.8 ± 0.5 Ma (whole rock; sample 10-6-78-2) (Fiebelkorn and others, 1982, 1983) (**Figure 5-12**; plate). A compositionally similar tholeiitic basaltic andesite and andesite lava flow encountered in a geothermal test well, drilled just west of Powell Buttes, returned a K-Ar age of 30.1 ± 1.1 Ma (whole rock; DOGMI-Bas81-2/UT-225) (**Figure 5-11**, **Figure 5-12**; **Table 5-2**; plate; appendix; Brown and others, 1980; Evans and Brown, 1981; Fiebelkorn and others, 1982, 1983).

Figure 6-70. Tholeiitic basaltic andesite (Tjba) exposed above the tuff of Eagle Rock (Tjte) at the Prineville Reservoir County Boat Ramp along the southeast margin of the Crooked River caldera (44.132909, -120.749924). Arrow points to 40 cm (15.7 in) long hammer for scale. Similar composition lavas are also exposed northwest of Gray Butte, along the northwest margin of the caldera. Photo credit: Jason McClaughry, 2006.

Tjia **basaltic andesite and andesite intrusions (lower Oligocene and upper Eocene)—**Iron-and titanium-rich tholeiitic, aphyric basalt, basaltic andesite, and andesite dikes and sills (SiO_2 = 48.3 to 57.78 weight percent; TiO_2 = 1.61 to 3.81 weight percent; FeOTotal = 10.87 to 14.6 weight percent; *n* = 8 analyses) mapped north of Gray Butte (**Figure 5-12**; **Table 6-8**; plate; appendix). The unit (**Tjia**) includes dikes and sills up to 250 m (820 ft) wide, characterized by columnar jointing. Dikes of basalt and diabase contain olivine and subophitic to ophitic titaniferous clinopyroxene. Unit **Tjia** is assigned a late Eocene and early Oligocene age on the basis of stratigraphic association with similar composition lava flows of unit **Tjba** (**Figure 5-11**, **Figure 5-12**, **Figure 6-1**; **Table 5-2**; plate; appendix).

6.4.1.2 John Day Formation units not assigned to the lower Crooked volcanic field

Tjtr **tuff of Rodman Spring (lower Oligocene)—**Airfall tuff, nonwelded ash-flow tuff, and bedded lapillistone mapped near Rodman Spring and along North Unit Canal in the northwest part of the map area (**Figure 5-12**, **Figure 6-71**; **Table 6-8**; plate; appendix; Smith and others, 1998). The exposed bedded interval consists of ~3 to 4 m (9.8 to 13.1 ft) of pyroclastic-fall deposits, overlain by as much as 6 m (19.7 ft) of reworked tuff. Nonwelded rhyolite ash-flow tuff (**Tjtr**) (SiO_2 = 79.31 weight percent; Zr = 201 ppm; Nb = 23.8 ppm; *n* = 1 analysis), best exposed along North Unit Canal, is ~7 m (~30 ft) thick. It directly overlies airfall tuff deposits and thins abruptly to the east (**Figure 5-12**, **Figure 5-15**; **Table 6-8**; plate; appendix). Unit **Tjtr** is pervasively altered to clay and zeolite. Typical hand samples of the nonwelded ash-flow tuff (**Tjtr**) are white (N9) to pale greenish yellow (10Y 8/2) and distinctly porphyritic, containing 5 to 10 percent (vol.) slightly smoky, bipyramidal quartz, plagioclase, and chatoyant sanidine microphenocrysts and phenocrysts ≤2 mm (0.1 in) across, distributed within a eutaxitic groundmass of devitrified glass shards. The tuff also contains conspicuous pinkish gray (5YR 8/1) to orange pink (10R 7/4), variably altered perlite fragments. The perlite fragments are as much as 1 mm (0.04 in) across in the air-fall deposits and up to 5 cm (2 in) in diameter in the ash-flow tuff.

The tuff of Rodman Spring (**Tjtr**) is assigned an early Oligocene age on the basis of stratigraphic position and an $^{40}Ar/^{39}Ar$ age of 32.49 ± 0.30 Ma (sanidine; sample GS095-130) reported by Smith and others (1998) (**Figure 5-11**, **Figure 5-12**, **Figure 6-1**; **Table 5-2**; plate; appendix). The tuff of Rodman Spring (**Tjtr**) is considered to be equivalent to a tuff exposed near the base of member F of the John Day Formation near Teller Flat, ~25 km (15.5 mi) northeast of the map area (**Figure 5-12**). The member F tuff near Teller Flat has yielded a comparable $^{40}Ar/^{39}Ar$ age of 32.31 ± 0.07 Ma and also contains distinctive pinkish gray (5YR 8/1) perlite fragments (**Figure 5-11**; Smith and others, 1998). Microprobe analyses on feldspars from a bedded tuff exposed near the base of member F near Teller Flat are identical to analyses of feldspars of the tuff or Rodman Spring (**Tjtr**) (Smith and others, 1998).

Figure 6-71. Nonwelded ash-flow tuff and bedded lapillistone of the tuff of Rodman Spring (Tjtr) cropping out near Rodman Spring (44.463640, -121.116441). The tuff at this outcrop has an $^{40}Ar/^{39}Ar$ age of 32.49 ± 0.3 Ma. Scale bar is 1 m (3.3 ft) tall. Photo credit: Jason McClaughry, 2014.

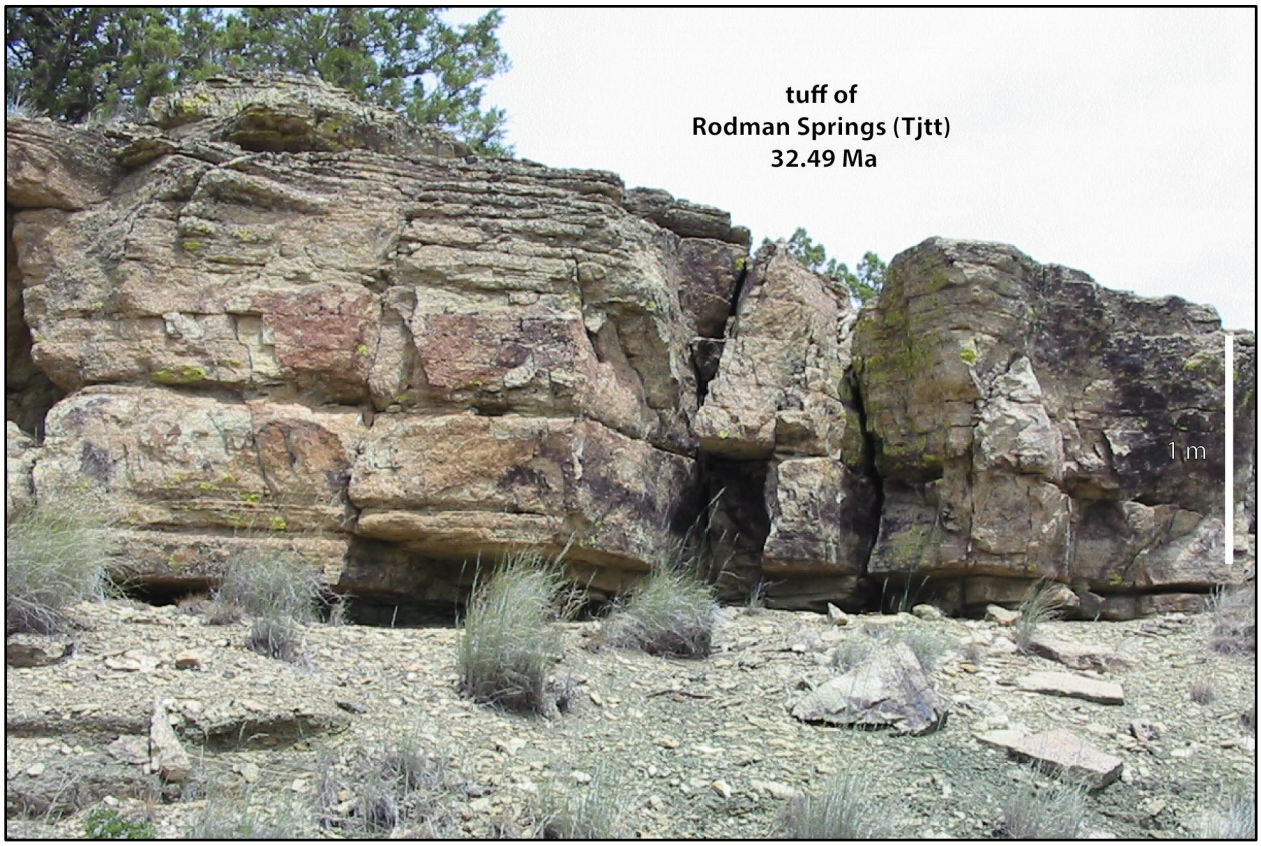

Tjtt **tuffaceous sedimentary rocks and tuff (lower Oligocene and upper Eocene)—**Tuffaceous sedimentary rocks and tuff locally mapped beneath the tuff of Antelope Creek (**Tjta**) at Prineville Reservoir and interbedded with lava flows of unit **Tjba** between Gray Butte and North Unit Canal (**Figure 5-12**, **Figure 6-65**, **Figure 6-67**, **Figure 6-68**; plate). The unit is best exposed along the north shore of Prineville Reservoir, where it forms precipitous cliffs near Owl Creek (**Figure 5-12**, **Figure 6-68**; plate). Outcrops typically consist of yellowish gray (5Y 7/2), grayish green (5G 5/2), pale greenish yellow (10Y 8/2), and pale brown (5YR 5/2), 0.5- to 1-m-thick (1.6- to 3.3- ft) beds of massive, fine- to medium-grained, nonwelded tuff, zeolite-cemented stratified tuffaceous lithic sandstone and siltstone, lenses of pebble breccia, and massive beds of pumice-rich conglomerate that unconformably overlie rocks of the Clarno Formation (**Figure 6-68**; plate). The unit includes thin (1 m [3.3 ft] thick) zones of dark gray (N3) welded tuff marked by flattened pumice clasts and thin (<1 cm [0.4 in] thick) layers of vitric sandstone. Near the head of Owl Creek, north of Prineville Reservoir (**Figure 5-12**; plate), the volcaniclastic section is capped by a very pale orange (10YR 8/2), ~10 m (32.8 m) thick, massive, nonwelded rhyolite pumice tuff (SiO_2 = 77.69 weight percent; Zr = 350; Nb = 44.1 ppm; *n* = 1 analysis) (**Figure 5-15**; **Table 6-8**; plate; appendix). Feathered pumice fragments are up to 5 cm (2 in) across. Angular black (N1) obsidian fragments are abundant.

The stratigraphic section of unit **Tjtt** mapped west of Gray Butte is deeply weathered (**Figure 5-12**, **Figure 6-67**; plate). It consists mainly of dark reddish brown (10R 3/) to pale reddish brown (10R 5/4), tuffaceous sandstone and mudstone, and pale greenish yellow (10Y 8/2) and white (N9), finely laminated lacustrine tuff, siltstone, shale, and accretionary-lapilli bearing basaltic andesite tuff. Sandstone contains pumice lapilli, quartz and feldspar crystals, and fragments of devitrified rhyolite, basalt, and basaltic andesite (compositionally similar to lavas of **Tjba**). Laminated lacustrine tuffs, as thick as 80 m (262 ft), are exposed at the exit to the North Unit Canal tunnel, northeast of Coyote Butte (**Figure 5-12**, **Figure 6-67**; plate). Shales are locally carbonaceous and contain abundant leaf-impressions. Zeolite is prevalent as a secondary alteration component.

Unit **Tjtt** is assigned a late Eocene or early Oligocene age on the basis of stratigraphic position and fossil assemblages (**Figure 6-1**; plate). At Prineville Reservoir unit **Tjtt** unconformably overlies the Clarno Formation and underlies the ~29.6 Ma tuff of Antelope Creek (**Tjta**) (**Figure 5-12**, **Figure 6-65**, **Figure 6-68**; plate). North of Gray Butte, unit **Tjtt** is interbedded with the 32.4 Ma tuff of Rodman Spring (**Tjtr**) and underlies the tuff of Antelope Creek (**Tjta**) (**Figure 5-12**, **Figure 6-67**; plate). Unit **Tjtt** sedimentary rocks mapped west of Gray Butte host some of the well-known Gray Butte fossil floras, including the Nichols Spring, Canal, and Trail Crossing floras (Ashwill, 1983). These floras are considered by Ashwill (1983) and Smith and others (1998) to be consistent with a late Eocene to early Oligocene age for the host strata. The unit is correlative with sedimentary rocks of members B, E, and F of the John Day Formation as defined by Robinson and Stensland (1979) and Robinson and others (1990).

Tjtn **tuff of North Unit Canal (lower Oligocene or upper Eocene)—**Pale greenish yellow (10Y 8/2), partially welded and highly altered rhyolitic ash-flow tuff interbedded with sedimentary rocks of unit **Tjtt** east of North Unit Canal in the northwest part of the map area (**Figure 5-12**; plate). The tuff (**Tjtn**) is 5 to 10 m (16.4 to 32.8 ft) thick and contains 1 to 3 percent (vol.) crystals of quartz, plagioclase, and altered anorthoclase. The tuff also contains 5 to 10 percent (vol.) dark gray (N3) volcanic lithic fragments as much as 2 cm (0.8 in) in diameter and white (N9) to pale greenish yellow (10Y 8/2) fibrous pumice lapilli as much as 8 cm (3 in) long. The tuff of North Unit Canal (**Tjtn**) is assigned an early Oligocene or late Eocene age on the basis of stratigraphic position (**Figure 6-1**; plate).

Tjtma **Member A tuff (middle Eocene)—**Regionally widespread rhyolite ash-flow tuff (SiO_2 = 73.17 to 75.1 weight percent; Zr = 219 to 319 ppm; Nb = 23.4 to 34.8 ppm; *n* = 5 analyses [4 outside map area]) mapped at Nichols Spring near Gray Butte, Willow Creek, and at Ochoco Divide (**Figure 5-12**, **Figure 5-15**; **Table 6-8**; plate; appendix; P.E. Hammond, written commun., 2008). The Member A tuff (**Tjtma**) mapped near Nichols Spring (**Figure 5-12**; plate) consists of at least three separate units. The upper part of unit **Tjtma** consists of 3 to 5 m (9.8 to 16.4 ft) of white (N9), bedded and massive tuff and lapilli tuff that forms a conspicuous marker bed. Typical hand samples of the tuff (**Tjtma**) contain ~5 percent (vol.) plagioclase crystals, rare quartz crystals, 2 to 5 percent (vol.) volcanic lithic fragments as much as 1 cm (0.4 in) in diameter, and rare accretionary lapilli as much as 5 mm (0.2 in) in diameter. The middle part of Member A (**Tjtma**) near Nichols Spring consists of at least 15 m (49.2 ft) of highly silicified, pale yellowish orange (10YR 8/6) to white (N9), nonwelded to slightly welded, devitrified rhyolitic tuff. Outcrops locally contain stratiform layers of lithophysal cavities. Typical hand samples contain 1 to 2 percent (vol.)

crystals of quartz and highly altered plagioclase and alkali feldspar. The lowermost exposed part of Member A (**Tjtma**) near Nichols Spring consists of at least 10 m (32.8 ft) of intensely altered, pale yellowish orange (10YR 8/6) to white (N9), nonwelded to strongly welded tuff. Outcrops typically contain pumice lapilli replaced by pale brown (5YR 5/2) Fe-hydroxides and secondary silica veinlets filling closely spaced fractures. Typical hand samples contain 5 to 10 percent (vol.) crystals, mainly quartz with lesser, highly altered anorthoclase and plagioclase. The unit contains small metasedimentary rock fragments visible in thin section. Although intense alteration precludes mineralogical analyses, this tuff is arguably correlated with the basal tuff in the Member A type section near Ashwood (**Figure 5-4**; Swanson and Robinson, 1968; Robinson and others, 1990).

Along Ochoco Divide, in the east part of the map area, Member A (**Tjtma**) consists of grayish red purple (5RP/2), pale purple (SP 6/2), to very pale orange (10YR 8/2), strongly welded, feldspar-phyric, stony lithic tuff (**Figure 5-12**; plate). The tuff has a eutaxitic texture defined by stretched flattened pumice fiamme up to several cm long. Much of the tuff exposed at this locality has altered to clay and was mapped separately as unit Tjc by Swinney and others (1968).

The Member A tuff (**Tjtma**) is assigned a middle Eocene age on the basis of stratigraphic position and single crystal $^{40}Ar/^{39}Ar$ ages (feldspar) of 39.72 ± 0.03 (Painted Hills), 39.22 ± 0.03 (near Clarno), and 39.17 ± 0.15 Ma (near Ashwood) (**Figure 5-4**, **Figure 5-11**, **Figure 6-1**; C.C. Swisher in Bestland and Retallack, 1994a, b; Smith and others, 1998; Retallack and others, 2000).

Unconformity

6.4.2 Clarno Formation

6.4.2.1 Ochoco volcanic field

Tces **volcaniclastic sedimentary rocks (upper and middle Eocene)—**Very pale orange (10YR 8/2), moderate red (5R 4/6), very dark red (5R 2/6), grayish brown (5YR 3/2), and pale greenish yellow (10Y 8/2) volcaniclastic sedimentary rocks exposed along the north shore of Prineville Reservoir and northwest of Gray Butte (**Figure 6-68**, plate). North of Prineville Reservoir, unit **Tces** consists of massive to thinly bedded, 0.2- to 0.6-m-thick (0.7- to 2- ft) beds of volcanic sandstone, siltstone, and claystone, weathering to form badland topography (**Figure 6-68**). The unit includes interbedded fine-grained tuffaceous sandstone beds and matrix-supported conglomerate at the mouth of Owl Creek and at the east end of Prineville Reservoir (**Figure 5-12; plate**). Sandstone is dominantly composed of euhedral plagioclase crystals as long as 2 mm (0.1 in) and rounded volcanic rock fragments, all of which have been largely converted to clay.

Stratigraphically correlative sedimentary rocks mapped east of North Unit canal and just north of Nichols Spring, northwest of Gray Butte, include grayish brown (5YR 3/2) and pale greenish yellow (10Y 8/2), well-cemented volcanic sandstone, siltstone, and shale interbedded with rhyolite ash-flow tuff (**Tjtma**) and porphyritic basalt to andesite lava flows (**Tcal**) (**Figure 5-12**; plate). Sandstone is comprised almost entirely of rhyolite and basaltic andesite grains. Unit **Tces** includes fossiliferous siltstone and shale and a laterally persistent rhyolite- and basaltic andesite-clast conglomerate, at least 4 m thick (13 ft). The Kings Gap and Sumner Spring floras of Ashwill (1983) are part of this unit (**Figure 5-12**).

Unit **Tces** is assigned a middle and late Eocene age on the basis of stratigraphic position and fossil assemblages (**Figure 6-1**; plate). Sedimentary rocks of unit **Tces** overlie 46.4 Ma alkali olivine basalt (**Tceb**) lava flows and porphyritic dacite (**Tcdp**) at Prineville Reservoir (plate). These rocks (**Tces**) are interbedded with the 39.7 to 39.2 Ma John Day Member A tuff (**Tjtma**) and older Clarno Formation lavas (**Tcal**) north of Gray Butte (plate). Strata herein assigned to unit **Tces** at Prineville Reservoir (**Figure 6-68**) were considered by Robinson and others (1990) to be equivalent to the Big Basin Member of the John Day Formation (Fisher and Rensberger, 1972), while similar rocks exposed northwest of Gray Butte were considered to be part of Member A of the John Day Formation by Smith and others (1998).

6.4.2.1.1 Wildcat Mountain caldera

Tcrb **rhyolite of Brennan Palisades (middle Eocene)—**Rhyolite (SiO_2 = 72.83 weight percent; Zr = 281 ppm; Nb = 15.8 ppm; *n* = 1 analysis) mapped at Brennan Palisades (**Figure 5-5**, **Figure 5-10**, **Figure 6-72a**; **Table 6-9**; plate; appendix). Layering or flow banding, defined by alternating vesicle-rich and vesicle-poor bands, is a common feature of the rhyolite (**Tcrb**) (**Figure 6-72b**). The bands are typically 2 to 5 cm thick (0.8 to 2 in) and laterally continuous over tens of meters. Locally, bands are preserved as well-developed kink folds and are separated by coarse breccia layers and lensoidal, boudin-like bands up to 30 cm (11.8 in) thick (**Figure 6-72b**). At Brennan Palisades, the layering dips at a low angle to the west, with the dip angle steepening to the east-southeast. Unit **Tcrb** weathers to hoodoos and balanced rocks; weathered outcrops are typically

mantled by a dark yellowish brown (10YR 4/2), grus-like soil (**Figure 6-72a**). The rhyolite (**Tcrb**) intrudes early to middle Eocene andesite and dacite (**Tcal**) at Brennan Palisades; near the junction of Mill and Schoolhouse Creeks the rhyolite (**Tcrb**) intrudes the intracaldera unit of the tuff of Steins Pillar (**Tcts**) (**Figure 5-5**; plate). Intrusive margins are locally defined by a relatively fresh-appearing greenish black (5G 2/1) vitrophyre. Typical hand samples are grayish blue (5PB 5/2), medium gray (N5), to grayish orange (10YR 6/2) and distinctly porphyritic, containing 5 to 7 percent (vol.) clear to chalky white (N9), subhedral to euhedral, blocky alkali feldspar phenocrysts ≤3 mm (0.1 in) across, distributed within a very fine-grained, devitrified hypocrystalline groundmass. The rhyolite of Brennan Palisades (**Tcrb**) is assigned a middle Eocene age on the basis of stratigraphic position (**Figure 6-1**; plate).

Figure 6-72. Rhyolite of Brennan Palisades (Tcrb). (a) Feldspar-phyric compound rhyolite intrusion (Tcrb) cropping out at Brennan Palisades and along Schoolhouse Creek (44.400670, -120.677753). (b) The rhyolite is characterized by alternating vesicle-rich and massive, vesicle-poor bands (44.400977, -120.677683). Yellow notebook for scale is 19 cm (7.5 in) tall. Photo credits: Jason McClaughry, 2006.

Table 6-9. Select XRF geochemical analyses for the Clarno Formation in the lower Crooked River basin *(continued on next page)*.

Sample	308 LCJ 07	296 LCJ 06	167 LCJ 06[1]	149 LC 06	280 LCJ 06[2]	269 LCJ 06[2]	101 LCJ 06[1]	151 LCJ 06[2]	152 LCJ 06[2]	126 LCJ 06	271 LCJ 06
Geographic Area	Brennan Palisades	Belknap Creek	Kidnap Spring	Wildcat Mtn.	Hash Rock	Twin Pillars	Green Mtn.	Steins Pillar	Steins Pillar	Forked Horn Butte	Twin Pillars
Formation	Clarno	Clarno	Clarno	Clarno	Clarno	Clarno	Clarno	Clarno	Clarno	Clarno	Clarno
Map Unit	Tcrb	Tcbk	Tcrk	Tcrm	Tcrh	Tcrh	Tcdg	Tcts	Tcts	Tcts	Tcts
UTM N (NAD 83)	4919077	4925768	4921104	4922348	4929638	4928503	4923803	4919232	4918369	4926508	4929216
UTM E (NAD 83)	685235	697595	686827	695085	694355	695885	685407	688054	689457	693767	695320
Age (Ma)	nd	nd	nd	nd	39.35 Ma	nd	nd	nd	41.8 Ma	nd	nd
Map Label	G346	G438	G379	G397	G502	G477	G414	G349	G331	G446	G495
Oxides, weight percent											
SiO_2	72.83	66.81	71.21	76.11	74.68	73.96	68.66	75.08	73.79	75.85	70.30
Al_2O_3	14.29	13.53	15.30	13.25	13.75	13.81	16.13	13.53	14.26	13.56	15.83
TiO_2	0.41	0.96	0.45	0.13	0.20	0.30	0.54	0.23	0.23	0.20	0.56
FeOTotal	2.72	7.14	2.73	1.96	2.21	2.11	3.62	2.19	2.56	1.36	4.39
MnO	0.05	0.07	0.06	0.02	0.02	0.04	0.06	0.02	0.04	0.01	0.04
CaO	1.51	5.52	2.39	0.40	0.94	1.29	3.53	2.87	1.66	1.68	2.40
MgO	0.12	1.50	0.26	0.00	0.00	0.11	0.72	1.00	0.77	0.40	0.64
K_2O	3.70	1.86	3.51	5.16	3.90	3.91	2.12	4.31	5.24	6.46	3.49
Na_2O	4.26	2.43	3.98	2.92	4.27	4.39	4.47	0.72	1.43	0.43	2.26
P_2O_5	0.10	0.17	0.10	0.04	0.03	0.07	0.14	0.04	0.02	0.04	0.10
LOI	1.21	1.46	2.48	1.65	1.16	1.13	2.02	8.68	6.65	7.03	8.20
Total_I	99.88	100.31	99.83	99.88	100.14	100.11	100.08	100.33	nd	100.13	100.31
Trace Elements, parts per million											
Ni	1	52	12	1	2	1	10	3	8	5	21
Cr	3	267	13	1	0	2	14	13	43	9	51
Sc	6	22	8	3	6	5	11	7	4	4	10
V	25	124	50	12	9	16	52	26	31	18	57
Ba	772	685	918	1010	950	935	715	657	1183	774	839
Rb	131	40	117	185	129	139	61	126	131	170	163
Sr	127	224	168	31	88	93	370	289	307	228	168
Zr	281	136	233	158	299	266	202	111	190	110	145
Y	26	22	21	34	27	24	23	19	32	23	28
Nb	15.8	9.1	12.0	12.2	16.7	14.4	11.3	13.3	12.7	12.4	13.8
Ga	17	13	17	16	16	17	17	13	19	14	16
Cu	10	27	21	2	1	5	27	5	11	3	31
Zn	58	71	47	52	51	44	53	35	60	28	51
Pb	10	2	8	9	10	10	9	6	24	4	10
La	31	19	35	42	37	35	26	23	42	28	29
Ce	60	24	63	79	75	71	54	40	97	49	58
Th	12	4	12	4	15	16	6	14	11	18	13
Nd	4	0	4	0	4	5	2	3	2	3	4
U	1	1	3	nd	nd	nd	5	nd	3	nd	11

Major element determinations have been normalized to a 100-percent total on a volatile-free basis and recalculated with total iron expressed as FeOTotal; nd - no data or element not analyzed. Data from [1]Ferns and McClaughry (2007); [2]McClaughry and others (2009a, d).

Table 6-9, *continued***. Select XRF geochemical analyses for the Clarno Formation in the lower Crooked River basin.**

Sample	119 LCJ 06[2]	03 LCJ 06[3]	45 P 05[4]	125 LCJ 06[2]	59 LC 06[5]	89 LCJ 06[5]	143 LC 06[5]	106P05[4]	279 LCJ 06[5]	03 LC 06[3]
Geographic Area	Jesse Spring	Prineville Reservoir	Mill Creek	Forked Horn Butte	Old Dry Creek	Schoolhouse Creek	Bottleneck Spring	Ochoco Reservoir	Harvey Gap	Prineville Reservoir
Formation	Clarno	Clarno	Clarno	Clarno	Clarno	Clarno	Clarno	Clarno	Clarno	Early Clarno
Map Unit	Tcau	Tcid	Tcid	Tchp	Tcal	Tcal	Tcdp (xenolith)	Tcdp	Tcdp	Tceb
UTM N (NAD 83)	4929863	4894178	4915506	4926162	4918498	4919684	4927098	4908847	4926162	4889216
UTM E (NAD 83)	691952	689246	685899	694099	682195	687142	677285	686355	694099	682767
Age (Ma)	41.5 Ma	nd	42.79 Ma	nd	nd	nd	nd	nd	43.86 Ma	46.4 Ma
Map Label	G503	G78	G296	G443	G334	G355	G459	G223	G454	G43
Oxides, weight percent										
SiO_2	57.12	60.02	65.76	67.91	59.42	62.51	73.81	64.50	58.21	50.95
Al_2O_3	16.40	16.32	15.60	16.11	15.89	17.16	14.15	16.33	17.83	12.48
TiO_2	1.47	1.05	0.68	0.61	1.13	0.82	0.35	0.87	0.82	0.83
FeOTotal	8.96	6.54	4.94	4.52	8.42	5.64	1.66	5.46	6.58	8.56
MnO	0.21	0.17	0.07	0.17	0.17	0.11	0.01	0.16	0.11	0.17
CaO	7.41	6.91	4.87	3.83	6.47	5.94	1.59	5.17	7.64	9.35
MgO	3.45	3.98	2.18	0.56	3.17	2.39	0.24	1.56	4.02	13.04
K_2O	1.37	1.12	2.19	2.12	1.51	1.42	3.90	2.29	1.32	2.29
Na_2O	3.35	3.58	3.52	3.98	3.41	3.80	4.22	3.45	3.28	1.66
P_2O_5	0.27	0.32	0.18	0.20	0.42	0.21	0.08	0.22	0.18	0.67
LOI	1.24	2.74	2.57	3.41	1.84	1.71	1.78	2.62	1.59	3.48
Total_I	100.26	99.85	99.55	100.18	99.92	100.29	100.12	99.48	99.74	99.59
Trace Elements, parts per million										
Ni	26	40	20	20	43	15	3	26	73	261
Cr	46	95	39	33	49	27	10	25	91	773
Sc	25	18	13	11	20	16	6	15	20	27
V	207	155	89	71	145	122	28	120	136	262
Ba	346	371	528	512	450	521	907	517	341	395
Rb	53	35	87	62	38	40	104	79	44	82
Sr	346	758	357	302	347	406	124	324	383	455
Zr	164	168	153	233	269	187	347	196	148	125
Y	29	20	14	24	31	22	24	28	21	32
Nb	12.5	13.1	9.6	14.1	20.3	10.8	13.2	13.2	9.2	8.7
Ga	19	22	18	17	19	18	17	18	17	12
Cu	54	68	28	27	63	36	18	31	54	87
Zn	88	80	55	69	94	67	23	63	66	75
Pb	5	5	4	9	6	7	15	6	4	nd
La	16	20	21	31	25	21	28	24	16	26
Ce	34	47	47	55	52	38	69	52	31	62
Th	4	2	6	5	4	4	15	7	5	2
Nd	2	0	2	3	1	2	2	3	1	2
U	29	1	12	10	24	17	nd	16	23	45

Major element determinations have been normalized to a 100-percent total on a volatile-free basis and recalculated with total iron expressed as FeOTotal; nd - no data or element not analyzed. Data from [1]Ferns and McClaughry (2007); [2]McClaughry and others (2009a, d); [3]McClaughry and Ferns (2007c); [4]McClaughry and Ferns (2006b); [5]Ferns and McClaughry (2007).

Tcbl **rhyolite breccia pipes and dikes (middle Eocene)—**Rhyolite breccia forming east-west-striking dikes mapped between Squirrel Ridge and Kidnap Spring, along the western edge of the Wildcat Mountain caldera (**Figure 5-5**, **Figure 6-73a**; plate). Outcrops typically form high-standing ridges and hoodoos weathering to slopes mantled by moderate red (5R 4/6) colored rock chips (**Figure 6-73a**). The breccia is clast-supported and contains a monolithologic assemblage of bleached white (N9) angular, vesicular, aphyric to sanidine-phyric rhyolite clasts with centimeter-scale dark yellowish orange (10YR 6/6) alteration halos (**Figure 6-73b**). Clasts have a maximum diameter of 30 cm (11.8 in) and average 2 to 4 cm (0.78 to 1.58 in) across. The matrix is moderate red (5R 4/6), fine grained, and is the altered equivalent of the clasts (**Figure 6-73b**). Unit **Tcbl** displays pervasive sulfide alteration and minor quartz veining. The breccia (**Tcbl**) is petrographically characterized by devitrified, altered sanidine-phyric rhyolite fragments that appear to be dissolved along their margins. Rhyolite breccia dikes are spatially coincident with andesite and dacite breccia dikes of unit **Tcbk** and intrude early to middle Eocene andesite (**Tcal**) (**Figure 5-5**; plate). Unit **Tcbl** is assigned a middle Eocene age on the basis of stratigraphic position (**Figure 5-5**, **Figure 6-1**; plate).

Figure 6-73. Rhyolite breccia pipes and dikes (Tcbl). (a) East-west-striking, hoodoo-weathering outcrop of rhyolite breccia (Tcbl) between Squirrel Ridge and Kidnap Spring, along the southwestern edge of the Wildcat Mountain caldera (44.425640, -120.644509). (b) The breccia (Tcbl) is typically bleached, moderate red (5R 4/6), monolithologic, and clast-supported, containing angular clasts of aphyric to sanidine-phyric rhyolite. Pencil for scale is 14 cm (5.5 in) long. Photo credits: Jason McClaughry, 2006.

Tcbk **andesite and dacite breccia pipes and dikes (middle Eocene)—**Andesite and dacite breccia forming east-west-striking dikes mapped near the mouth of Lemon Creek and along Belknap Creek within the Wildcat Mountain caldera (**Figure 5-5**, **Figure 6-74a**; plate). Outcrops are characterized by anastomosing breccia zones that enclose more coherent andesite and dacite blocks. Unit **Tcbk** typically forms erosionally-resistant, spire-like outcrops weathering to dark gray (N3) and moderate brown-oxidized (5YR 3/4) soils (**Figure 6-74a**). The breccia (**Tcbk**) is matrix- to clast-supported and contains an assemblage of yellowish gray (5Y 7/2), angular, moderately trachytic and aphyric andesite and dacite clasts up to 5 cm (2 in) in diameter (**Figure 6-74b**). Clast margins are typically smooth to moderately serrated; the boundaries between clasts and matrix are sharp. Jigsaw and crackle breccia textures are locally pervasive. Clasts are encased in a grayish blue (5PB 5/2) to dusky blue (5PB 3/2) silicified matrix of poorly sorted, sand-sized grains, angular crystal fragments of white (N9) alkali-feldspar, plagioclase, and pyroxene, and devitrified ash and/or glass. Crystals in the matrix are variably altered to sericite and chlorite(?); alteration is overall more prevalent in the matrix than clasts. Andesite and dacite breccia dikes (**Tcbk**) are spatially coincident with rhyolitic breccia dikes of unit **Tcbl** and intrude early to middle Eocene andesite (**Tcal**) and the middle Eocene rhyolite of Kidnap Spring (**Tcrk**) and rhyolite of Mill Creek (**Tcrm**) (**Figure 5-5**, **Figure 6-74a**; plate). Unit **Tcbk** is assigned a middle Eocene age on the basis of stratigraphic position (**Figure 5-5**, **Figure 6-1**; plate).

Figure 6-74. Andesite and dacite breccia pipes and dikes (Tcbk). (a) East-west-striking breccia dike (Tcbk) intruding sanidine-phyric rhyolite along the eastern edge of the Wildcat Mountain caldera near Belknap Creek (44.453831, -120.520595). (b) Breccia is typically blue (5PB 5/2) to dusky blue (5PB 3/2), and clast- to matrix-supported, containing angular clasts of andesite and dacite encased in a silicified matrix (44.420127, -120.655469). Increments on the photo scale are in centimeters. Photo credits: Jason McClaughry, 2007.

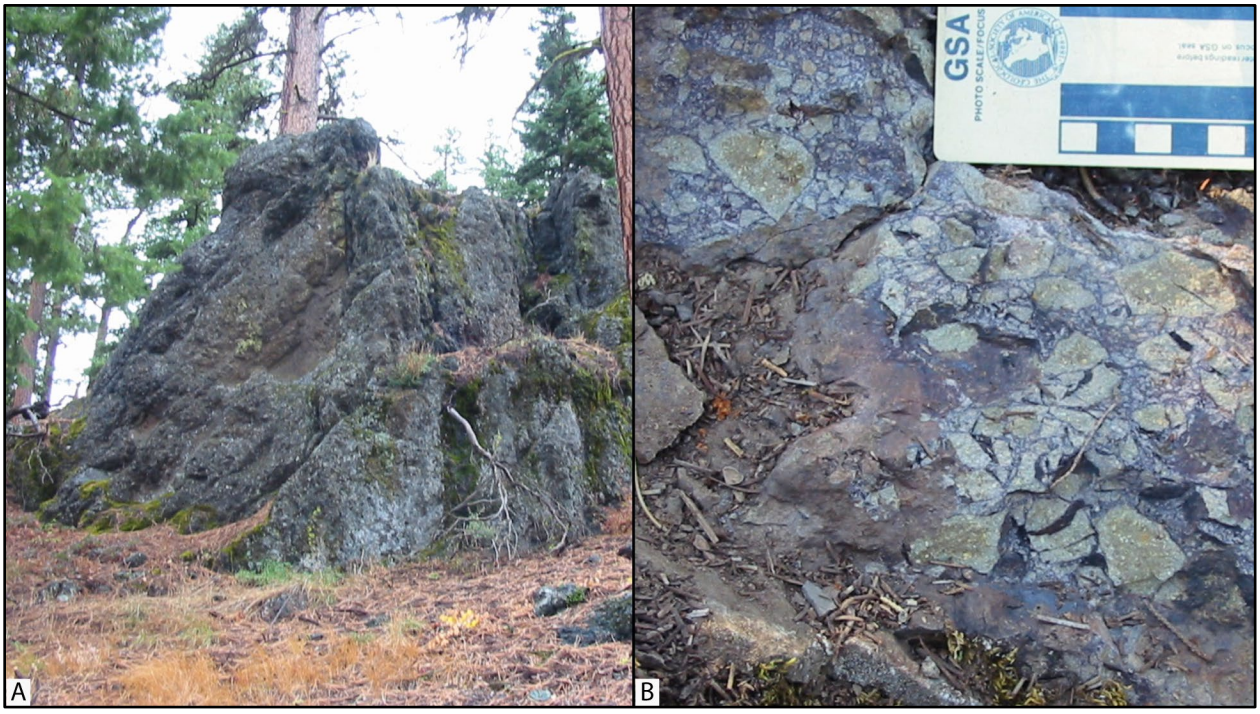

Tcrk **rhyolite of Kidnap Spring (middle Eocene)—**Rhyolite intrusions (SiO_2 = 68.64 to 76.25 weight percent; Zr = 138 to 233 ppm; Nb = 10.4 to 13.6 ppm; *n* = 8 analyses) mapped across the Wildcat Mountain caldera (**Figure 5-5**, **Figure 5-10**, **Figure 6-75a**; **Table 6-9**; plate; appendix; Ferns and McClaughry, 2007). Unit **Tcrk** typically crops out as low-lying, muted outcrops or high-standing ribs or spines up to 10 m (32.8 ft) high (**Figure 6-75a**). Vertical flow foliation and devitrified, clast-supported rhyolite autobreccia is characteristic of unit **Tcrk**. Weathered outcrops are mantled by dusky brown (5YR 2/2), coarse-grained sandy soils. Coarse-grained, crystalline granitic xenoliths up to 15 cm (0.49 ft) across are common (**Figure 6-75b**). Typical hand samples are grayish blue (5PB 5/2) to dark gray (N3) and porphyritic, containing 10 to 20 percent (vol.) subhedral to anhedral, etched and embayed phenocrysts of sanidine, hornblende, and quartz up to 5 mm (0.2 in) across, within a devitrified, hypocrystalline groundmass of plagioclase microlites, devitrified glass, spherulites, and Fe-Ti oxides. Both hornblende phenocrysts and the cores of sanidine crystals have been altered to sericite. The rhyolite of Kidnap Spring (**Tcrk**) is assigned a middle Eocene age on the basis of stratigraphic position, intruding the 41.8 Ma tuff of Steins Pillar (**Tcts**) (**Figure 5-5**, **Figure 6-1**; plate).

Figure 6-75. Rhyolite of Kidnap Spring (Tcrk). (a) Sanidine- and hornblende-phyric and glomeroporphyritic rhyolite of Kidnap Spring (Tcrk) exposed northwest of Forked Horn Butte (44.460056, -120.562311). (b) The rhyolite locally contains granitic xenoliths up to 15 cm (5.9 in) across (44.424515, -120.679674). Increments on the photo scale are in centimeters. Photo credits: Jason McClaughry, 2006, 2007.

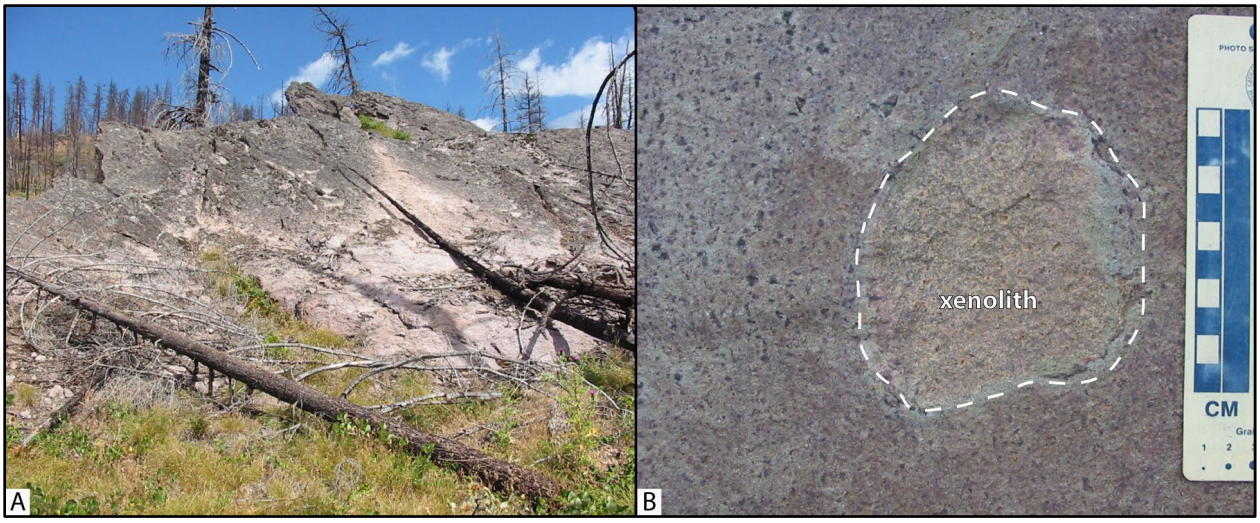

Tcrm **rhyolite of Mill Creek (middle Eocene)—**Rhyolite and high-silica dacite lava flows, domes, and shallow intrusions (SiO_2 = 68.87 to 76.26 weight percent; Zr = 158 to 316 ppm; Nb = 12.2 to 18.5 ppm; *n* = 7 analyses) mapped as a northeast trending outcrop belt along the eastern edge of the Wildcat Mountain caldera (**Figure 5-5**, **Figure 5-10**, **Figure 6-76a**; **Table 6-9**; plate; appendix; McClaughry and Ferns, 2006b; Ferns and McClaughry, 2007). Unit **Tcrm** typically crops out as cliffs and hoodoos. Columnar jointing, subhorizontal to vertical flow banding, complex flow folding, and vesicle bands are characteristic of the unit (**Tcrm**). Weathered surfaces are mantled by light brownish gray (5YR 6/1) to brownish gray (5YR 4/1) rock plates and angular chips (**Figure 6-76a**). Flow, dome, and intrusive margins are characterized by zones of relatively fresh greenish black (5GY 2/1) vitrophyre, black (N1) perlite, spherulites, and agate-filled lithophysal cavities

(**Figure 6-76b**). Where the rhyolite (**Tcrm**) is coincident with the margin of the Wildcat Mountain caldera, it is bleached white (N9), silicified, and displays propylitic alteration (epidote and chlorite) (**Figure 5-5**; plate). Unit **Tcrm** includes a chemically and petrographically similar, aphyric to sanidine-phyric, compound rhyolite dike mapped along Salmon Creek, along the southern edge of the Wildcat Mountain caldera (**Figure 5-5**, **Figure 6-77**). The dike complex along Salmon Creek strikes N.80°E., is vertically flow foliated, and is columnar jointed, with horizontal, pseudohexagonal columns perpendicular to the vertical foliation. Typical hand samples of the rhyolite are light brownish gray (5YR 6/1) to brownish gray (5YR 4/1) and aphyric to sparsely porphyritic, containing ≤2 percent (vol.) phenocrysts of clear to chalky white (N9), subhedral, blocky sanidine ≤2 mm (0.1 in) across, distributed in a devitrified, hypohyaline groundmass with bands of spherulites. The rhyolite of Mill Creek (**Tcrm**) is assigned a middle Eocene age on the basis of stratigraphic position, intruding and unconformably overlying the 41.8 Ma tuff of Steins Pillar (**Tcts**) (**Figure 5-5**, **Figure 6-1**; plate).

Figure 6-76. Rhyolite of Mill Creek (Tcrm). (a) Spire-forming, aphyric to sparsely sanidine-phyric, flow-banded rhyolite (Tcrm) cropping out along Mill Creek Road (44.352206, -120.671399). (b) The rhyolite is locally characterized by zones of lithophysal cavities and spherulites (44.355624, -120.679846). Hammer for scale is 40 cm (15.7 in) long. Photo credits: Jason McClaughry, 2005.

Figure 6-77. Sanidine-phyric rhyolite dike (Tcrm) exposed along Salmon Creek at the southern end of the Wildcat Mountain caldera (44.374863, -120.580156).

Tcrh **rhyolite of Hash Rock (middle Eocene)—**Rhyolite lava flow (SiO_2 = 72.97 to 74.85 weight percent; Zr = 245 to 316 ppm; Nb = 13.7 to 16.7 ppm; *n* = 4 analyses) mapped as a nearly continuous rim and plateau around the northern margin of the Wildcat Mountain caldera (**Figure 5-5**, **Figure 5-10**, **Figure 6-78**, **Figure 6-79a**; **Table 6-9**; plate; appendix). The northern part of the lava flow (**Tcrh**) extends outward from the caldera north to Rooster Rock (**Figure 5-5**). The relatively planiform rhyolite (**Tcrh**) presently covers an area of ~50 km^2 (20 mi^2) and ranges in thickness from 180 m (600 ft) near Hash Rock and Rooster Rock to over 305 m (1,000 ft) at the viewpoint west of Whistler Spring (**Figure 5-5**; plate). Unit **Tcrh** crops out as cliffs and hoodoos marked by columnar jointing, subhorizontal to vertical flow banding, complex flow folding, and vesicle bands (**Figure 6-78a-b**). Weathering of the rhyolite has formed surfaces mantled by moderate brown (5YR 3/4) rock plates and angular chips. Flow margins are characterized by zones of relatively fresh-appearing greenish black (5GY 2/1) vitrophyre, black (N1) perlite, lithophysal cavities, and poorly sorted autobreccia. Lithophysal cavities are commonly cored by lenticular- and butterfly-shaped fillings of banded moderate brown (5YR 4/4) and white (N9) agate, bubble agate, and opaline quartz. Where the rhyolite is coincident with the margin of the Wildcat caldera, it is bleached white (N9), silicified, and displays propylitic alteration (epidote and chlorite) (**Figure 5-5**; plate). An occurrence of cinnabar is present near the base of the lava at Whistler Spring and related intrusions at Strickland Butte (**Figure 5-5**; plate). Typical hand samples are medium light gray (N6) to pale purple (SP 6/2) and aphyric to sparsely porphyritic, containing 2 to 5 percent (vol.) clear to chalky white (N9) phenocrysts of lath-shaped plagioclase and blocky sanidine ≤3 mm (0.1 in) across, distributed in a devitrified to recrystallized, hypohyaline groundmass.

The Hash Rock lava flow (**Tcrh**) erupted from chemically and petrographically similar fissure-conduits now preserved south of Hash Rock and at Twin Pillars (**Figure 5-5**, **Figure 6-79b**; plate). The Twin Pillars feeder consists of strongly vertically flow banded, pale purple (SP 6/2), plagioclase- and sanidine-phyric rhyolite that forms distinct vertical east-west-striking dike sheets, with a composite width of ~260 m (850 ft) (**Figure 6-79b**; plate). A sample obtained from the intrusion at Twin Pillars shows geochemical traits identical to that of the plateau-capping rhyolite flow (SiO_2 = 74.12 weight percent; Zr = 245 to 266 ppm; Nb = 14.4 ppm; *n* = 1 analysis) (**Table 6-9**; plate; appendix). A dike mapped south of Hash Rock consists of an ~160 m (500 ft) wide, moderate brown (5YR 4/4) to white (N9) weathering, aphyric to sparsely plagioclase-phyric rhyolite cored by fresh appearing, flow-banded greenish black (5GY 2/1) vitrophyre and numerous lithophysae up to 3 cm (1.2 in) across (**Figure 5-5**; plate). Lithophysae are filled by radiating fibrous masses of white (N9) mordenite (zeolite).

The rhyolite of Hash Rock (**Tcrh**) is assigned a middle Eocene age on the basis of stratigraphic position and an $^{40}Ar/^{39}Ar$ plateau age of 39.35 ± 0.30 Ma obtained from a sample on the plateau above the east fork of Mill Creek (plagioclase; sample 280 LCJ 06) (**Figure 5-5**, **Figure 5-11**, **Figure 6-1**; **Table 5-1**; plate; appendix). Northwest of Twin Pillars, the rhyolite (**Tcrh**) directly overlies the 41.8 Ma tuff of Steins Pillar (**Tcts**) (**Figure 5-5**; plate). The rhyolite of Hash Rock (**Tcrh**) is chemically similar to the rhyolite of Mill Creek (**Tcrm**), but is differentiated on the basis of texture, petrography, and distribution (**Figure 5-5**, **Figure 5-10**; **Table 6-9**; plate; appendix).

Figure 6-78. Rhyolite of Hash Rock (Tcrh). (a) Rhyolite (Tcrh) cropping out above the intracaldera unit of the tuff of Steins Pillar (Tcts) in the headwaters area of the West Fork Mill Creek (44.493872, -120.555462). This outcrop has returned an $^{40}Ar/^{39}Ar$ age of 39.35 ± 0.30 Ma. Arrow points to 40 cm (15.7 in) long hammer for scale. (b) Tightly folded flow banding typical of the rhyolite of Hash rock (Tcrh). Scale bar is 10 cm (3.9 cm) tall. Photo credits: Jason McClaughry, 2006.

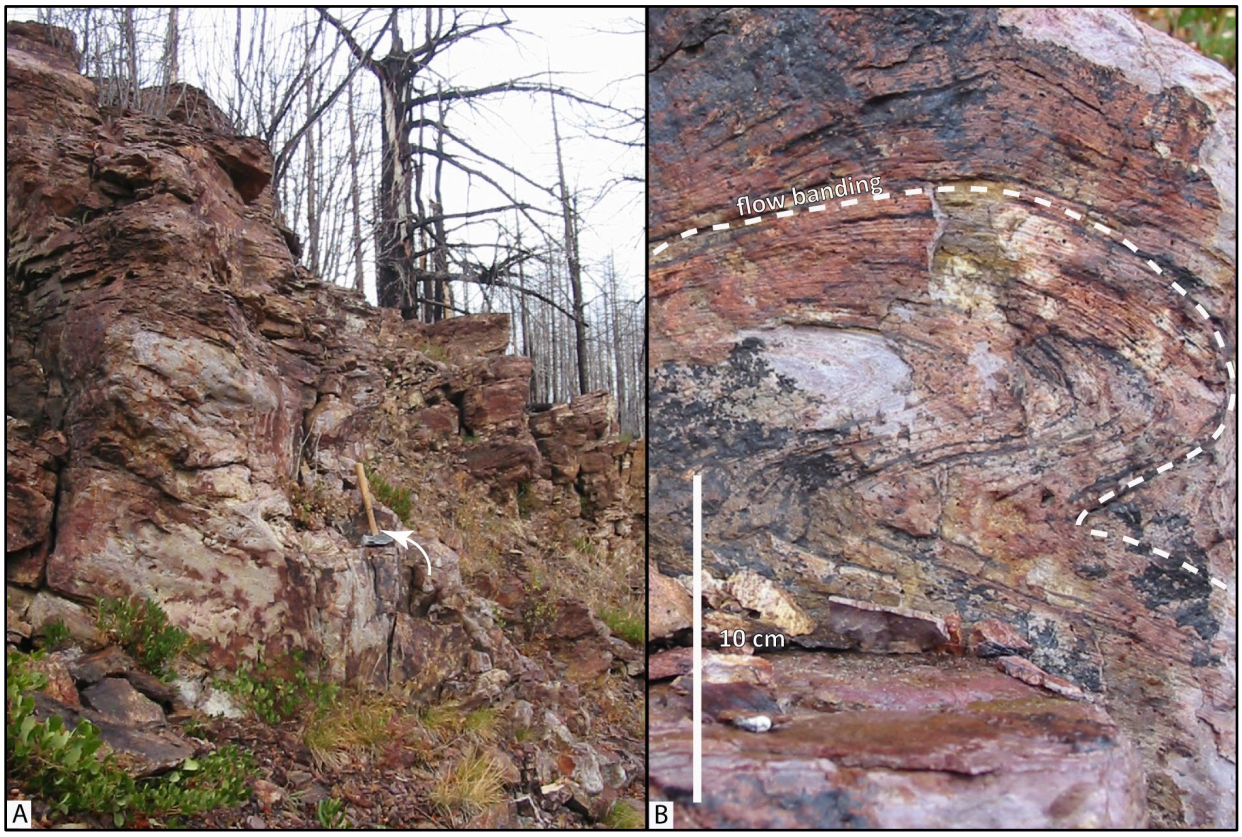

Figure 6-79. Twin Pillars. (a) View east across the Wildcat Mountain caldera toward Twin Pillars and Wildcat Mountain (44.495265, -120.573316). Twin Pillars is an east-west-striking compound rhyolite feeder dike for the rhyolite of Hash Rock (Tcrh) which underlies the viewpoint. Wildcat Mountain is a rhyolite dome residing along the southeastern edge of the Wildcat Mountain caldera. (b) View northwest to Twin Pillars in the headwaters area of Mill Creek (44.464010, -120.530277). Photo credits: Jason McClaughry, 2007, 2009.

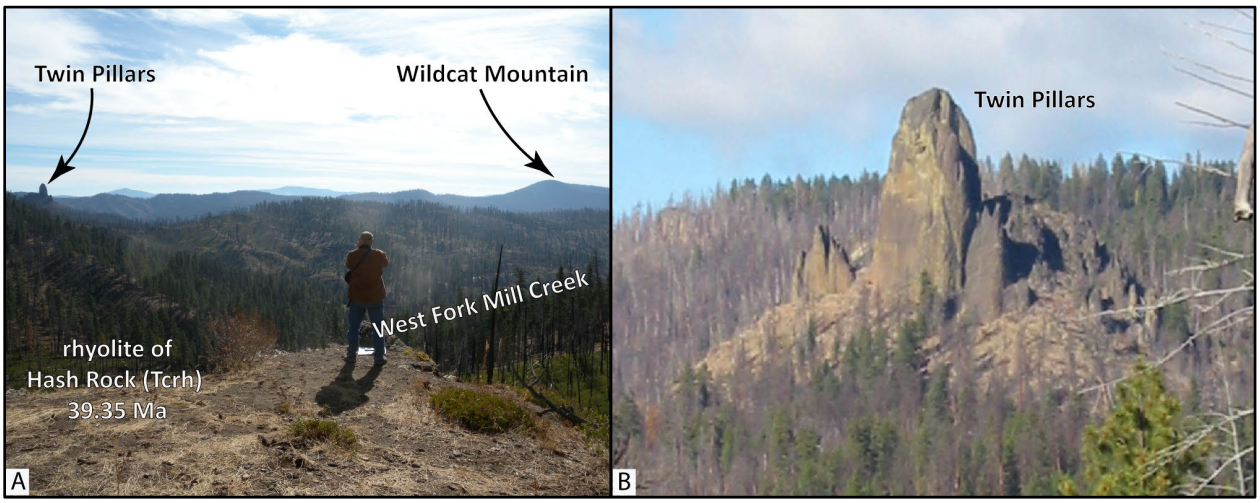

Tcdg **dacite of Green Mountain (middle Eocene)—**Dacite intrusion (SiO_2 = 68.91 weight percent; Zr = 202 ppm; Nb = 11.3 ppm; *n* = 1 analysis) mapped east of Green Mountain along the western edge of the Wildcat Mountain caldera (**Figure 5-5**, **Figure 5-10**, **Figure 6-78**, **Table 6-9**; plate; appendix). Outcrops of the dacite (**Tcdg**) have well-developed columnar jointing and subvertical to vertical foliation (**Figure 6-80**). Columns are up to 1 m (3.3 ft) across and have an internal platy fabric. Typical hand samples are grayish blue (5PB 5/2) and sparsely porphyritic, containing 2 to 5 percent (vol.) phenocrysts of clear to chalky white (N9), subhedral, seriate plagioclase, alkali-feldspar, and clinopyroxene ≤3 mm (0.1 in) across, and sparse biotite distributed in an equigranular holocrystalline groundmass of feldspar and intergranular opaque Fe-Ti oxides. Unit **Tcdg** is assigned a middle Eocene age on the basis of stratigraphic position (**Figure 5-5**, **Figure 6-1**; plate). The unit intrudes ~42 Ma aphyric (**Tcal**) and porphyritic (**Tcdp**) andesite and dacite along near vertical contacts south of Green Spring (**Figure 5-5**; plate).

Figure 6-80. Columnar-jointed, plagioclase-phyric dacite (Tcdg) cropping out along the Green Mountain Trail, east of Green Mountain (44.443966, -120.670460). Photo credit: Jason McClaughry, 2006.

Tcts **tuff of Steins Pillar, intracaldera unit (middle Eocene)—**Compound cooling unit of rhyolite ash-flow tuff (SiO_2 = 70.3 to 75.85 weight percent; Zr = 110 to 190 ppm; Nb = 12.4 to 13.8 ppm; *n* = 4 analyses) mapped within the Wildcat Mountain caldera (**Figure 5-5**, **Figure 5-10**, **Figure 6-81**, **Table 6-9**; plate; appendix). The tuff (**Tcts**) is mapped most extensively in the southern part of the caldera, but small outcrops are found north of Forked Horn Butte and Twin Pillars (**Figure 5-5**; plate). A minimum thickness for the tuff of 425 m (~1,400 ft) is estimated between the exposed base at Steins Pillar and Rocky Butte (**Figure 5-5**, **Figure 6-81**; plate)

The base of the tuff (**Tcts**) is exposed at Steins Pillar, one of a series of north-northwest-striking spires of strongly welded intracaldera ash-flow tuff (**Figure 5-5**, **Figure 6-82**; plate). Steins Pillar is ~106 m (350 ft) tall and consists of a compound cooling unit of pinkish gray (5YR 8/1) to yellowish gray (5Y 8/1), massive to flow banded, variably spherulitic, lithophysal, rheomorphic tuff. The spire-forming tuff is propylitically altered with secondary quartz and small calcite veins; thin breccia veins are locally pervasive.

The rheomorphic intracaldera tuff (**Tcts**) exposed at Steins Pillar, is succeeded upward by at least 305 m (1,000 ft) of yellowish gray (5Y 8/1) to pale red (10R 6/2), massive, poorly-sorted, nonwelded to weakly welded, locally propylitically altered and zeolitized, lithic- and pumice-rich tuff (**Figure 6-83**, **Figure 6-84**). Diffuse layering in the tuff is defined by alternating layers of lithics and pumices (**Figure 6-83b**). Lithics consist of medium gray (N5), aphyric to vesicular andesite rock fragments and brownish gray (5YR 4/1), flow-banded, aphyric rhyolite. Andesite lithics are composed of an equigranular plagioclase and pyroxene groundmass, are angular, and have a maximum size of 10 cm (3.9 in) across; these clasts average 2 to 5 cm (0.8 to 2 in) across. Rhyolite lithics are spherulitic, flow banded, angular, and reach a maximum size of 37 cm (14.6 in) across; rhyolite clasts average 10 to 15 cm (4 to 6 in) across. Pumices are very pale orange (10YR 8/2) to pale olive (10Y 6/2), banded, average 2 to 4 cm (0.8 to 1.6 in) in length, are moderately flattened, and are generally aligned in outcrop. Lithics and pumices are encased in a matrix of sparsely scattered, clear to white (N9), anhedral, sanidine crystals, sparse hornblende needles, and devitrified glass and ash. The tuff (**Tcts**) is locally intruded by rhyolite dikes near Rocky Butte (**Figure 6-83c**).

The intracaldera tuff (**Tcts**) is capped northwest of Twin Pillars by a heterogeneous assemblage of yellowish gray (5Y 8/1), very pale orange (10YR 8/2), to white (N9) bedded pumice tuff and interlayered stratified and graded lithic- and pumice-rich breccia and tuffaceous sandstone (**Figure 5-5**, **Figure 6-85**; plate). The pumice tuff (**Tcts**) north of Twin Pillars is poorly sorted and nonwelded, with ~20 percent (vol.) fresh, clear, feathered pumice fragments, ~10 percent (vol.) angular obsidian lithic fragments, and ~70 percent (vol.) crystal-rich ash matrix composed of sanidine and sparse hornblende needles. Intracaldera tuff (**Tcts**) locally overlies clast-supported megabreccia, composed of broken caldera-floor and wall rocks (**Tcal**) (**Figure 6-86**).

The tuff of Steins Pillar (**Tcts**) is assigned a middle Eocene age on the basis of stratigraphic position directly beneath the 39.35 Ma rhyolite of Hash Rock (**Tcrh**) and a $^{206}Pb/^{238}U$ zircon age of 41.8 ± 0.2 Ma for a sample collected southeast of Steins Pillar (sample 152 LCJ 06) (**Figure 5-5**, **Figure 5-11, Figure 6-1**, **Figure 6-83**; **Table 5-1**; plate; appendix). Zircons obtained from sample 152 LCJ 06 are subhedral, and small with typical lengths <100 µm. Cathodoluminescence images of these zircons show evidence for chemically distinct cores and rims. Cores display oscillatory and sector zoning and commonly display rounded and embayed textures where they are overgrown by rims with strong oscillatory zoning (appendix). Core and rim analysis of 25 zircons yielded thirty-three spot analyses with $^{206}Pb/^{238}U$ dates ranging from 53.0 to 39.8 Ma (appendix).

Statistical deconvolution of the data assuming three populations yields peaks at 50.1 ± 0.7, 45.8 ± 0.3 and 41.8 ± 0.2 Ma (appendix). The tuff of Steins Pillar (**Tcts**) was erupted from a series of fissures along the southern margin of the caldera including at least one vertical N.50°W.-striking, pumice-lithic tuff dike cropping out at the head of Wildcat Creek (**Figure 5-5**; plate). Outflow units, equivalent to the tuff of Steins Pillar (**Tcts**), are completely absent in the vicinity of Wildcat Mountain caldera and have not yet been identified elsewhere in the region.

Figure 6-81. View north across the southwest part of the Wildcat Mountain caldera (44.409397, -120.654502). Dashed white line shows the approximate location of the caldera margin; ticks point into the interior of the caldera. Dashed black line is the unconformable lower contact of the tuff of Steins Pillar (Tcts) over older andesite and dacite lava flows (Tcal). The X shows the location of the Steins Pillar viewpoint area shown in Figure 6-82. Photo credit: Jason McClaughry, 2006.

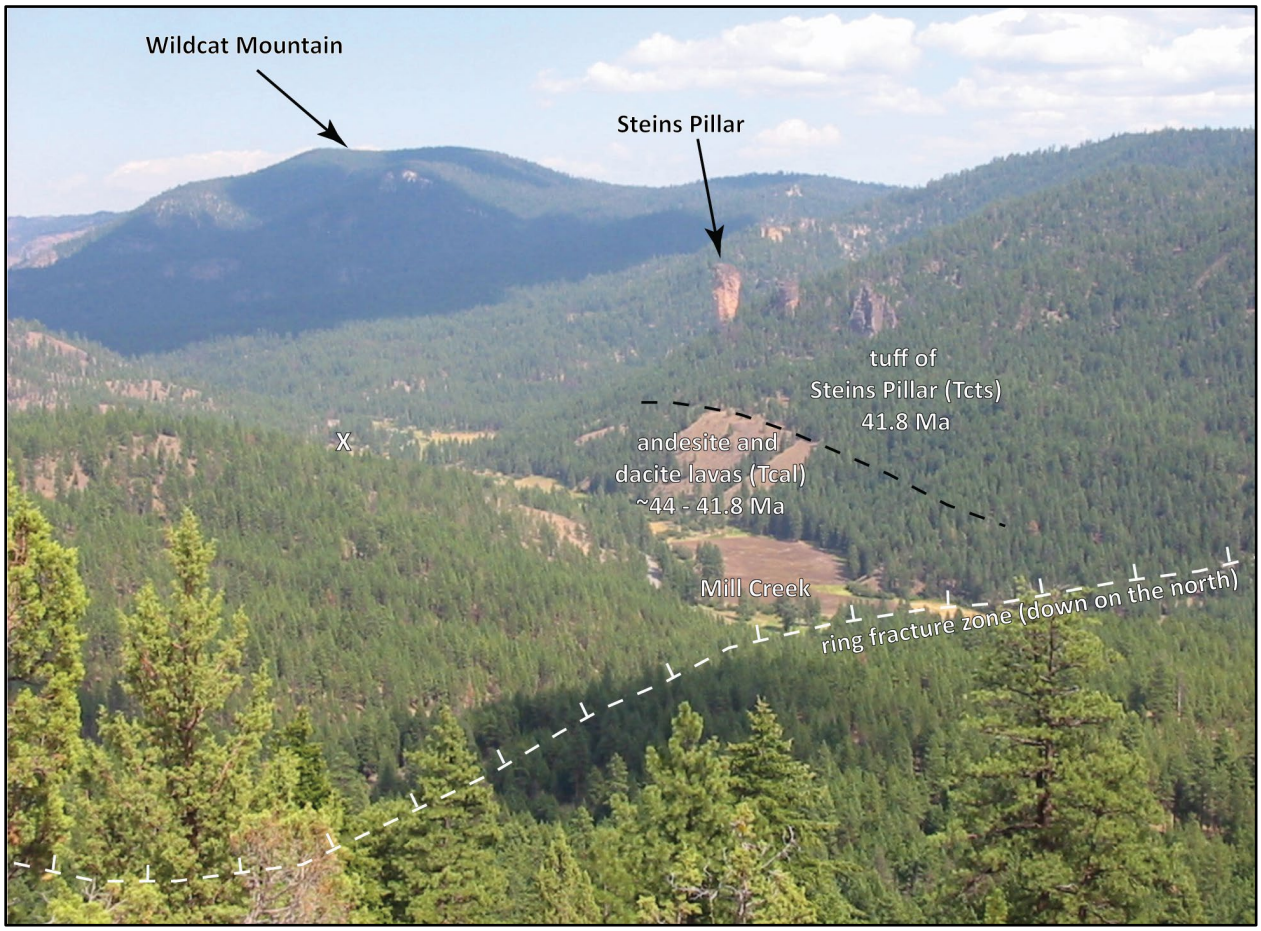

Figure 6-82. Steins Pillar viewed from the parking area along USFS Road 33 (44.417057, -120.618693). Steins Pillar is ~106 m (350 ft) tall and is composed of a compound cooling unit of strongly welded to rheomorphic, propylitically altered intracaldera ash-flow tuff (Tcts). Photo credit: Carrie Gordon, 2009.

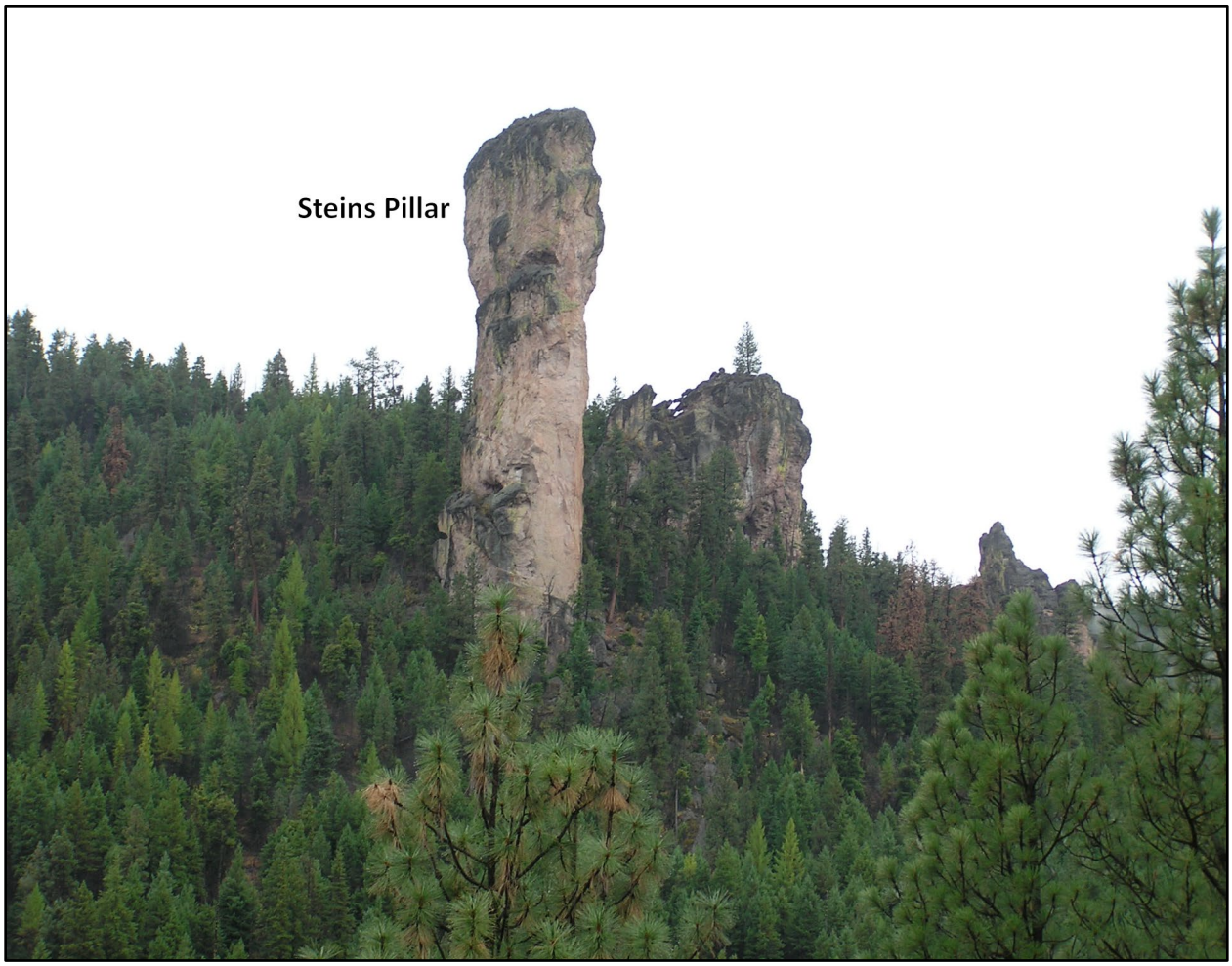

Figure 6-83. Nonwelded tuff of Steins Pillar (Tcts) and rhyolite dike. (a) The tuff of Steins Pillar (Tcts) exposed along USFS Road 500 (44.396854, -120.621664). This outcrop returned a $^{206}Pb/^{238}U$ zircon age of 41.8 ± 0.20 Ma (sample 152 LCJ 06). Person for scale is 1.6 m (5.2 ft) tall. (b) The upper part of the tuff of Steins Pillar (Tcts) consists of massive, poorly sorted, nonwelded to weakly welded, lithic- and pumice-rich tuff. Same location as in A. Increments on the photo scale are in centimeters. (c) The tuff of Steins Pillar (Tcts) is locally intruded by vertically foliated rhyolite dikes (44.397826, -120.620678). Kneeling person for scale is 1 m (3.3 ft) high. Photo credits: Jason McClaughry, 2009.

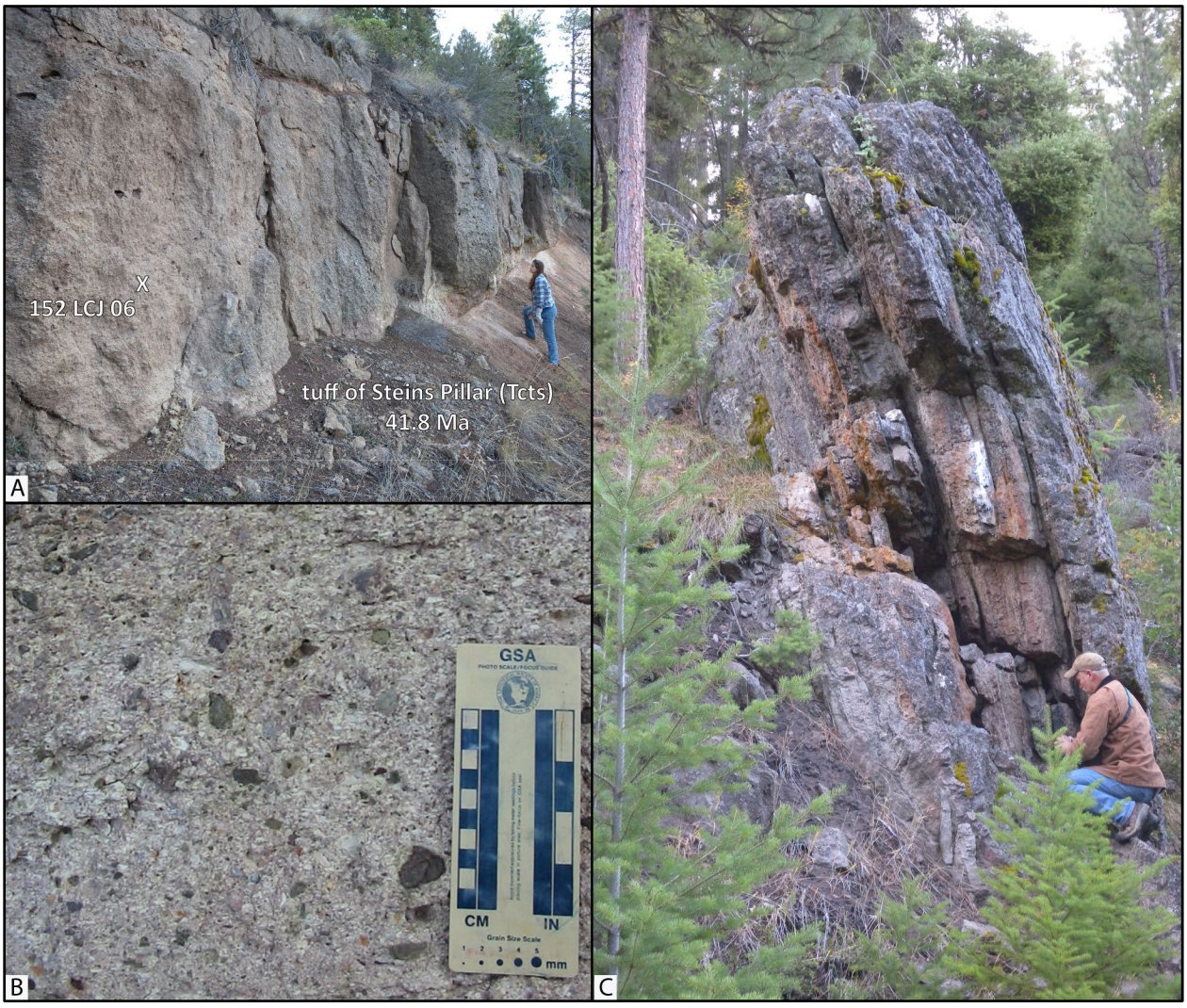

Figure 6-84. Nonwelded, lithic-rich tuff of Steins Pillar (Tcts). (a) Lithic-rich tuff of Steins Pillar (Tcts) cropping out along Wildcat Mountain Trail #833, north of Mahogany Spring (44.471807, -120.478798). The tuff sits directly against older early to middle Eocene andesite (Tcal) forming the eastern wall of the Wildcat Mountain caldera. Hammer for scale is 40 cm (15.7 in) long. (b) Close-up view of the lithic-rich tuff in A. Pencil for scale is 15 cm (5.9 in) long. Photo credits: Jason McClaughry, 2007.

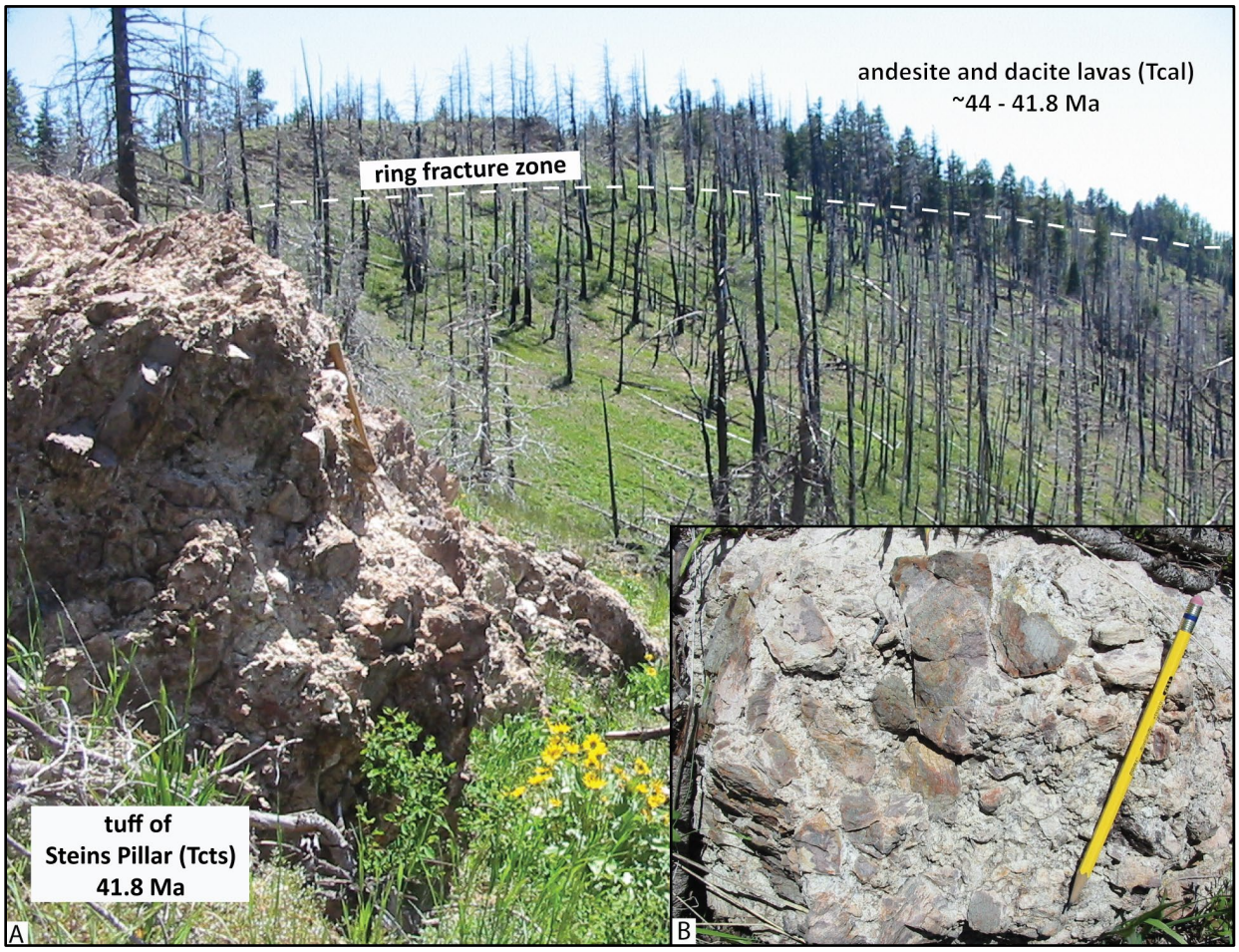

Figure 6-85. Nonwelded, bedded tuff of Steins Pillar (Tcts). (a) Upper part of the tuff of the Steins Pillar (Tcts) exposed along the northern rim of the Wildcat Mountain caldera, northwest of Twin Pillars (44.489868, -120.543593). The tuff here underlies the 39.35 Ma rhyolite of Hash Rock (Tcrh). (b) The upper part of the unit is composed of well-stratified pumice tuff and tuff breccia. Photo credits: Jason McClaughry, 2006.

Figure 6-86. Clast-supported megabreccia cropping out at the base of the tuff of Steins Pillar (Tcts) in the headwaters of West Fork Mill Creek (44.488007, -120.564001). Hammer for scale is 40 cm (15.7 in) long. Photo credit: Jason McClaughry, 2008.

Tcau **andesite of Little McKay Creek (middle Eocene)—**Andesite lava flows (SiO_2 = 57.64 to 61.01 weight percent; TiO_2 = 0.88 to 1.48 weight percent; FeOTotal = 6.07 to 8.13 weight percent; *n* = 6 analyses) mapped in the headwaters area of Little McKay Creek, along the northwest rim of the Wildcat Mountain caldera (**Figure 5-5**, **Figure 6-87**, **Table 6-9**; plate; appendix). Outcrops are typically columnar or platy jointed and weather to form rounded slopes armored by angular rock fragments and chips (**Figure 6-87**). Where deeply weathered, outcrops are commonly covered by dusky brown (5YR 2/2) soils. Andesite lava flows (**Tcau)** disconformably overlie and are inset into a variably dissected surface of porphyritic (**Tcdp**) and aphyric (**Tcal**) andesite and dacite (plate). Large landslide deposits (**Qls**) are commonly preserved downslope of the basal contact of unit **Tcau** (plate). Typical hand samples are dark gray (N3) to grayish black (N2) and aphyric to sparsely porphyritic, containing ≤2 percent (vol.) plagioclase phenocrysts ≤2 mm (0.1 in) across, distributed within a fine-grained holocrystalline groundmass.

The andesite of Little McKay Creek (**Tcau**) is assigned a middle Eocene age on the basis of stratigraphic position and an $^{40}Ar/^{39}Ar$ plateau age of 41.50 ± 0.48 Ma and a total fusion age of 42.42 ± 0.48 Ma (plagioclase; Sample 322 LCJ 06; Ferns and McClaughry, 2007) (**Figure 5-5**, **Figure 5-11, Figure 6-1**; **Table 5-1**; plate; appendix). The andesite (**Tcau**) sits directly on an irregular eroded surface of 43.86 Ma porphyritic dacite (**Tcdp**) and crops out below the 39.35 Ma rhyolite of Hash Rock (plate). Field relations demonstrating the stratigraphic position of the andesite relative to the 41.8 Ma tuff of Steins Pillar (**Tcts**) have not been found, although the unit appears to be offset by the ring-fracture zone of the Wildcat Mountain caldera (plate).

Figure 6-87. Andesite of Little McKay Creek (Tcau) exposed in a roadcut along Little McKay Road, west of McKay Saddle (44.507977, -120.645081). Automobile for scale. Photo credit: Jason McClaughry, 2007.

Tcid **andesite and dacite intrusive rocks (middle Eocene)—**Andesite and dacite dikes and intrusions (SiO_2 = 60.02 to 66.73 weight percent; TiO_2 = 0.63 to 1.05 weight percent; FeOTotal = 4.47 to 6.54 weight percent; *n* = 8 analyses) mapped in a northwest-striking belt between Mill Creek on the southeast and Allen Creek on the northwest (**Figure 5-5**, **Table 6-9**; plate; appendix). These intrusions form part of the basement to the Wildcat Mountain caldera, and mark the locations of feeder conduits for some of the andesite and dacite lavas (**Tcal**) of similar composition exposed across this part of the Ochoco Mountains (**Figure 6-88**). Outcrops are typically massive to platy jointed and are characterized by strong vertical foliation and folded flow bands (**Figure 6-88**). Granitic xenoliths up to 8 cm (3.1 in) across are common. Dikes (**Tcid**) generally strike N.35°W. to N.50°W, weathering to form high-standing ribs or spines. Secondary white (N9) calcite or very pale blue (5B 8/2) to white (N9) opaline quartz veinlets are common. The unit also includes a dark gray (N3), N.70°E.-striking, aphyric to clinopyroxene-microphyric andesite dike that intrudes sedimentary rocks (**Tces**) and porphyritic dacite (**Tcdp**) on the east end of Prineville Reservoir (**Figure 6-89**). The dike has distinct columnar jointing with wildly flaring pseudohexagonal columns up to 0.5 m (1.6 ft) across. Typical hand samples from dikes exposed between Mill Creek and Willow Creek (**Figure 6-88**) are light gray (N7), dark gray (N3), and grayish black (N2) and porphyritic, containing 5 to 10 percent (vol.) phenocrysts of hornblende up to 5 mm (0.2 in) across and microphenocrysts of plagioclase, hornblende, and clinopyroxene, distributed within a fine-grained, equigranular, pilotaxitic groundmass of euhedral plagioclase and amphibole microlites. Occasional hand samples contain 3 to 5 percent (vol.) etched and embayed quartz and plagioclase xenocrysts up to 2 mm (0.1 in) across. Typical hand samples from the dike mapped on the east end of Prineville Reservoir (**Figure 6-89**) are grayish black (N2) and

sparsely porphyritic, containing ≤1 percent (vol.) subhedral to euhedral phenocrysts of clinopyroxene and glomerocrysts of clinopyroxene and plagioclase up to 5 mm (0.2 in) across, enclosed in a holocrystalline groundmass of equigranular, trachytic plagioclase, and intersertal, moderate yellowish brown (10YR 5/4) devitrified glass.

Unit **Tcid** is assigned a middle Eocene age on the basis of stratigraphic position and an $^{40}Ar/^{39}Ar$ plateau age of 42.79 ± 0.44 Ma obtained from the Mill Creek dike (hornblende; sample 45 P 05; McClaughry and Ferns, 2006b; stop 1 of McClaughry and others 2009a) (**Figure 5-5**, **Figure 5-11, Figure 6-1**; **Table 5-1**; plate; appendix).

Figure 6-88. Hornblende- and plagioclase-phyric dacite dike (Tcid) cutting tuff breccia (Tcev) along Mill Creek Road (44.368961, -120.666720). This dike has an $^{40}Ar/^{39}Ar$ plateau age of 42.79 ± 0.44 Ma (sample 45 P 05). Person for scale is 1.9 m (6.2 ft) tall. Photo credit: Jason McClaughry, 2005.

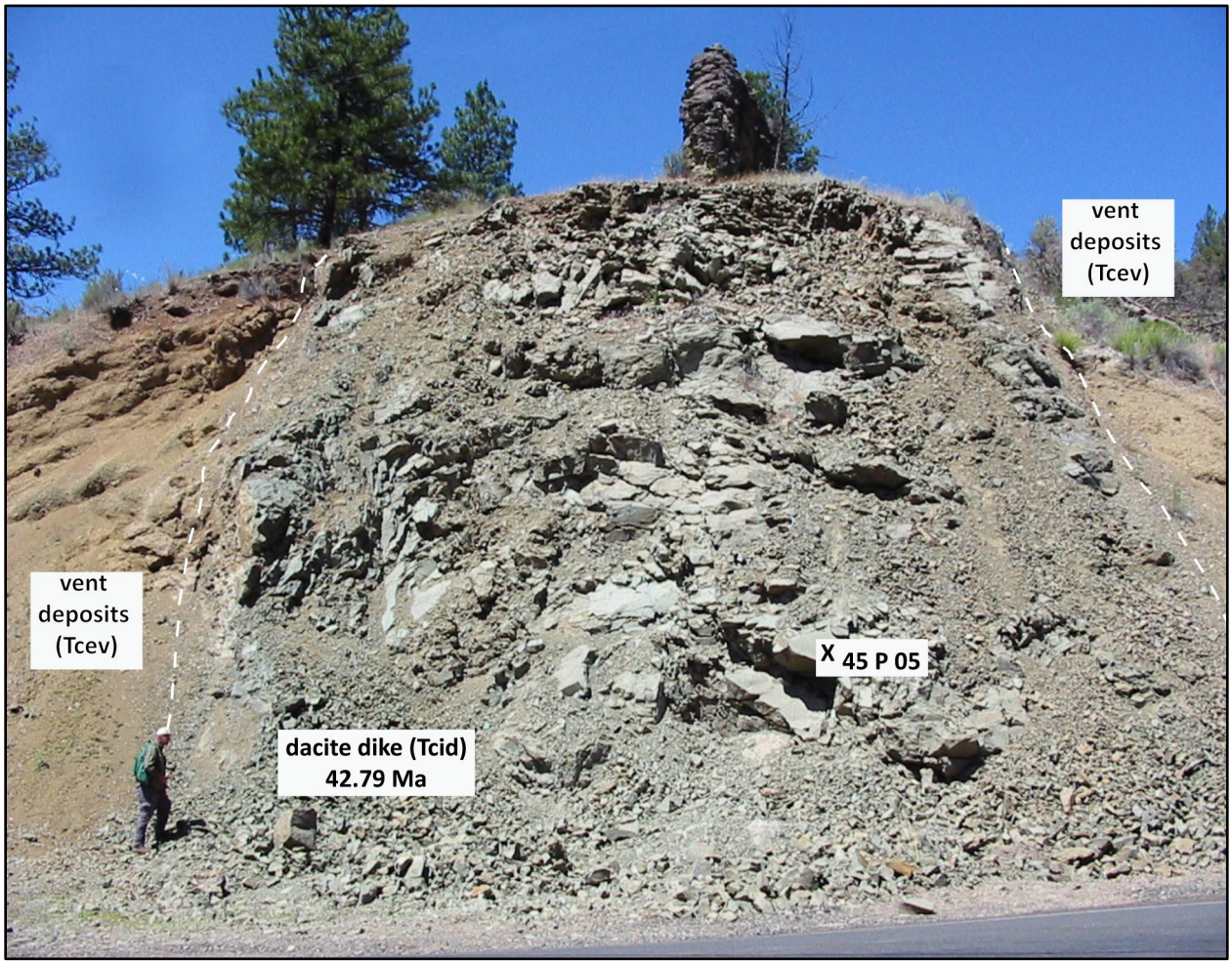

Figure 6-89. Columnar-jointed andesite dike (Tcid) cutting porphyritic dacite (Tcdp) and volcaniclastic sedimentary rocks (Tces) of the Clarno Formation at the east end of Prineville Reservoir (44.176422, -120.632228). Photo credit: Jason McClaughry, 2006.

Tcev **vent deposits (middle Eocene)—**Chiefly small, isolated exposures of vent deposits of varying age mapped at Prineville Reservoir, Ochoco Reservoir, and along Mill Creek (plate). Vent deposits at Prineville Reservoir consist of grayish red (10R 4/2) weathering welded scoria and fluidal volcanic bombs draped by medium gray (N5), aphyric spatter locally exposed beneath claystone of unit **Tces** (**Figure 6-90**). Deposits mapped near the west end of Ochoco Reservoir consist of moderate yellowish brown (10YR 5/4), distinctly bedded volcanogenic sandstone and massive, matrix-supported conglomerate. Vent deposits exposed along Mill Creek Road consist of moderate yellowish brown (10YR 5/4), clast-supported, crudely stratified, pebble-dominated breccia with angular, mafic volcanic clasts (**Figure 6-88**). Angular to subround, vesicular, outsized mafic volcanic blocks and bombs up to 20 cm (7.9 in) across are common. Exposures along Mill Creek include bedded grayish red (10R 4/2) scoria, pale red (10R 6/2) lapilli tuff, and white (N9) pumice tuff. The Mill Creek section is intruded by dacite and rhyolite dikes of unit **Tcid** and unit **Tcrm** (**Figure 6-88**; plate). The unit is assigned a middle Eocene age on the basis of stratigraphic position; vent deposits at Mill Creek are intruded by a 42.8 Ma dacite dike of unit **Tcid** (**Figure 6-1**; plate).

Figure 6-90. Welded scoria and spatter (Tcev) mapped beneath claystone of unit Tces in the headwaters of Owl Creek (44.165539, -120.684843). Hammer for scale is 40 cm (15.7 in) long. Photo credit: Jason McClaughry, 2006.

Tcqb **quartz-bearing basalt dikes (middle Eocene)—**Quartz-bearing basalt dikes mapped at O'Neil Butte and west of Lookout Mountain, in the eastern part of the map area (plate). At O'Neil Butte, the dikes intrude breccia of unit **Tcdf**. Unit **Tcdf** is mapped on the basis of work by Swinney and others (1968) and is assigned a middle Eocene age on the basis of stratigraphic position (**Figure 6-1**; plate).

Tcdf **breccia (middle Eocene)—**Matrix- to clast-supported, poorly-sorted, cobble-boulder breccia and conglomerate mapped on the flanks of Round Mountain and O'Neil Butte in the eastern part of the map area (**Figure 6-91**; plate). Unit **Tcdf** disconformably overlies porphyritic, hornblende-phyric andesite and dacite (**Tchp**). Outcrops typically weather to form steep-sided, narrow ridges and hoodoos as tall as 45 to 60 m (150 to 200 ft) (**Figure 6-91**). Where deeply weathered, outcrops are commonly covered by a mantle of moderate brown (5YR 3/4) clay soil and coarse-grained sand. Unit **Tcdf** breccia contains subangular to rounded clasts of medium gray (N5) hornblende- and feldspar-phyric andesite and dacite derived from underlying unit **Tchp**. Clasts average 15 to 30 cm (5.9 to 11.8 in) in diameter; near the top of the deposit clasts typically exceed 1.5 to 3 m (4.92 to 9.84 ft) in diameter (**Figure 6-91b**). Crackle breccia is locally present in clasts. Clasts are contained within by a poorly sorted, pale yellowish brown (10YR 6/2) matrix that is the crushed equivalent of the larger fragments. The percentage of matrix and average block size both increase upward in the deposit. Unit **Tcdf** is overlain at Round Mountain by glassy basaltic andesite lavas of unit **Tjob** and is assigned a middle Eocene age on the basis of stratigraphic position (**Figure 6-1**; plate).

Figure 6-91. Round Mountain breccia (Tcdf). (a) View looking south toward Round Mountain from the headwaters area of Scissors Creek, in the eastern part of the map area (44.404088, -120.358350). The northern flank of the mountain is underlain by a poorly sorted breccia (Tcdf) that weathers to hoodoos and precipitous spires. (b) Poorly sorted, clast- to matrix-supported boulder rich breccia (Tcdf) exposed on the north flank of Round Mountain (44.402349, -120.352285). Notebook for scale is 19 cm (7.5 in) tall. Photo credits: Jason McClaughry, 2007.

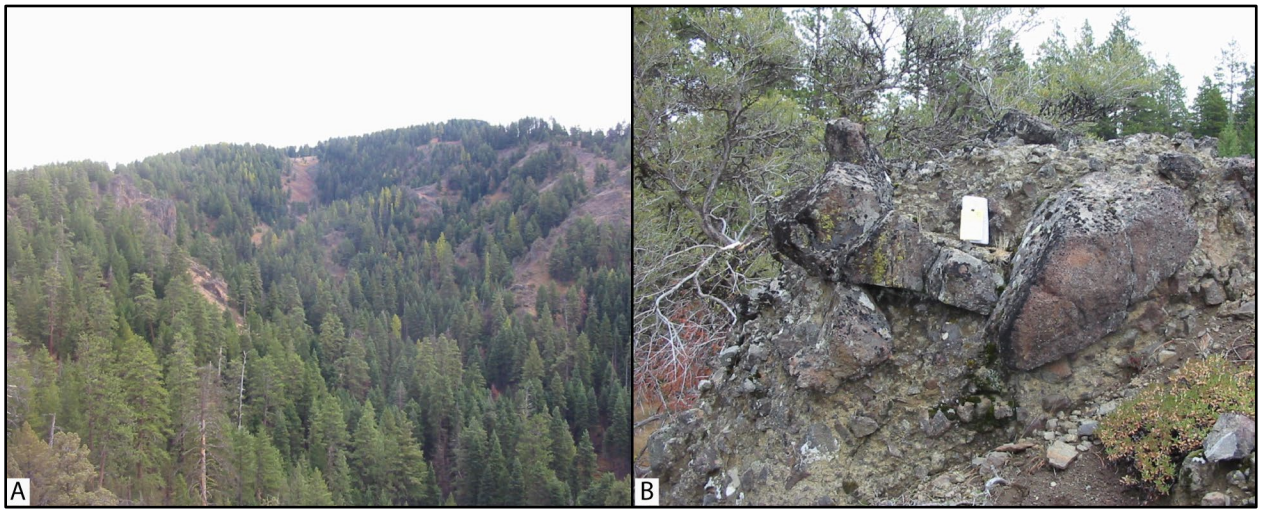

Tchp **plagioclase- and hornblende-phyric andesite and dacite (middle Eocene)—**Plagioclase- and hornblende-phyric andesite and dacite domes and smaller intrusions (SiO_2 = 60.93 to 70.61 weight percent; Zr = 146 to 233 ppm; Nb = 10.1 to 14.1 ppm; *n* = 10 analyses) mapped intruding aphyric andesite (**Tcal**) and porphyritic rocks (**Tcdp**) in the northeast part of the map area (**Figure 5-5**, **Table 6-9**; plate; appendix). Outcrops are typically massive to platy jointed (**Figure 6-92**). The unit (**Tchp**) typically weathers to form rounded slopes armored by angular rock fragments and chips. At Cougar Rock along Allen Creek, the unit (**Tchp**) forms prominent spires. Typical hand samples are medium light gray (N6) to dark gray (N3) and porphyritic, containing 5 to 7 percent (vol.) phenocrysts of seriate plagioclase, hornblende, and alkali feldspar ≤5 mm (0.2 in) across, distributed within a fine-grained equigranular hypocrystalline groundmass of plagioclase, hornblende, and variably devitrified glass. Minor constituents include rounded quartz phenocrysts and glomerocrysts of plagioclase and hornblende more than 1 cm (0.4 in) in diameter. Occasional hand samples contain plagioclase and hornblende glomerocrysts up to 5 cm (2 in) across and euhedral hornblende phenocrysts up to 1.5 cm (0.6 in) long. Unit (**Tchp**) is assigned a middle Eocene age on the basis of stratigraphic position (**Figure 6-1**; plate).

Figure 6-92. Plagioclase- and hornblende-phyric andesite and dacite (Tchp) exposed south of Polly Creek at the east end of Ochoco Reservoir (44.329234, -120.637348). Arrow points to 40 cm (15.7 in) long hammer for scale. Photo credit: Jason McClaughry, 2007.

Tcih **hornblende-phyric andesite (middle Eocene)—**Chiefly vertical, east-west-striking dikes and plugs intruding aphyric andesite lava flows (**Tcal**) near the intersection of McKay and Allen Creeks, in the north-central part of the map area (**Figure 5-5**; plate). The dike cropping out near Cougar Rock along Allen Creek, is up to 97 m (320 ft) wide and can be mapped discontinuously for ~2.5 km (1.6 mi). It is characterized by well-developed horizontal columnar jointing (plate). Bingert (1984) interpreted this outcrop as a possible feeder to an autobrecciated plagioclase- and hornblende-phyric dacite lava flow cropping out directly above the plug. Unit (**Tcih**) is assigned a middle Eocene age on the basis of stratigraphic position (**Figure 6-1**; plate).

Tcal **basalt, basaltic andesite, andesite, and dacite lava flows (middle Eocene)—**Andesite and dacite lava flows (SiO_2 = 58.4 to 65.18 weight percent; TiO_2 = 0.73 to 1.28 weight percent; FeOTotal = 4.52 to 7.64 weight percent; *n* = 15 analyses) mapped over a wide area (~364 km^2 [140 mi^2]) in the Ochoco Mountains (**Figure 5-5**, **Figure 6-93**; **Table 6-9**; plate; appendix). North of Kings Gap, in the Gray Butte area, unit **Tcal** includes a flow-on-flow series of basalt and basaltic andesite lava flows (SiO_2 = 50.34 to 58.20 weight percent; TiO_2 = 0.83 to 1.82 weight percent; FeOTotal = 6.87 to 9.83 weight percent; *n* = 6 analyses) (**Table 6-9**; plate; appendix). Unit **Tcal** chiefly consists of complexly interbedded sequences of platy to columnar-jointed lava flows (**Figure 6-93a-b**). Lava flows are locally separated by pale red purple (5RP 6/2) to very dusky red purple (5RP 2/2) flow breccia (**Figure 6-93c-d**). Topographic breaks between individual lava flows are commonly marked by moderate brown (5YR 3/4) to light brown (5YR 5/6) clay-rich soils. Lithologic and chemical similarity of lava flows across these breaks precludes the mapping of individual flow units. Unit (**Tcal**) weathers to form steep slopes armored by angular rock fragments and chips. Unit **Tcal** also includes a mass of iron-stained, aphyric andesite mapped between Dry Creek and Mill Creek that is interpreted to represent hydrothermally altered basement rocks to the Wildcat Mountain caldera (Ferns and McClaughry, 2007).

Typical hand samples of andesite and dacite lava flows from outcrops in the Ochoco Mountains (plate) are medium light gray (N6), dusky blue (5PB 3/2), and black (N1) and aphyric or very sparsely porphyritic, containing ≤1 percent (vol.), white (N9) to moderate reddish orange (10R 5/4), lath-shaped, euhedral plagioclase phenocrysts ≤2 mm (0.1 in), ≤1 percent (vol.) black (N1) to grayish olive (10Y 4/2), subhedral, blocky clinopyroxene microphenocrysts, and ≤1 percent (vol.) plagioclase-pyroxene glomerocrysts up to 2 mm (0.1 in), distributed in a hypohyaline to hypocrystalline groundmass of plagioclase, clinopyroxene, glass, and pyramidal- to rectangular-shaped iron-oxide minerals. Thin sections occasionally contain embayed, anhedral quartz rimmed by clinopyroxene grains and broken, twinned plagioclase crystals that may be xenocrysts. Typical hand samples of mafic lavas, north of Gray Butte (plate) are dark gray (N3) and porphyritic, with ~15 percent (vol.) phenocrysts of plagioclase, olivine, and rare clinopyroxene ≤3 mm (0.1 in) across, distributed within a fine-grained holocrystalline groundmass of plagioclase, clinopyroxene, and orthopyroxene.

Unit **Tcal** is assigned a middle Eocene age across the Ochoco Mountains on the basis of stratigraphic position, bracketed by the older 43.86 Ma porphyritic dacite of unit **Tcdp** and younger 41.8 Ma tuff of Steins Pillar (**Tcts**). North of Gray Butte, the upper age the unit is constrained by the overlying John Day Formation Member A tuff (**Tjtma**) (**Figure 6-1**; plate).

Figure 6-93. Andesite lava flows of unit Tcal. (a) Platy weathering, aphyric andesite (Tcal) underlying the ridge between Evans Creek and Dry Creek in the northeast part of the map area (44.416227, -120.680290). (b) Columnar-jointed, aphyric andesite (Tcal) exposed north of Johnson Creek Reservoir (44.352171, -120.755176). Hammer for scale is 40 cm (15.7 in) long. (c) Autobrecciated andesite lava flow forming part of unit Tcal along Johnson Creek Road, northeast of Prineville (44.355866, -120.731986). Person for scale is 1.9 m (6.2 ft) tall. (d) Close-up view of rafted, flow-banded andesite fragments in autobreccia shown in C. Yellow notebook for scale is 19 cm (7.5 in) long. Photo credits: Jason McClaughry, 2005.

Tcdp **porphyritic andesite, dacite, and rhyolite lava flows, domes, and intrusions (middle Eocene)—** Chiefly porphyritic andesite and dacite lava flows, domes, and intrusions (SiO_2 = 58.60 to 68.10 weight percent; TiO_2 = 0.68 to 0.95 weight percent; FeOTotal = 4.57 to 7.09 weight percent; *n* = 6 analyses) mapped over an extensive area (~453 km^2 [175 mi^2]) of the Ochoco Mountains (**Figure 5-5**, **Figure 6-94**; **Table 6-9**; plate; appendix). Unit **Tcdp** also locally includes small, granitic intrusions (SiO_2 = 73.81 to 73.96 weight percent; *n* = 2 analyses) (**Table 6-9**; appendix). Outcrops are typically massive to platy jointed with well-developed flow foliations (**Figure 6-94**). Porphyritic rocks in unit **Tcdp** are locally associated with more aphyric varieties. The contact relations between the two textures are typically diffuse and complex. The gradational nature of the porphyritic to aphyric rocks over tens of meters limits the mappable demarcation of distinct textures in the field. Closely spaced vertical bands or dikes of coarse-grained, porphyritic andesite and dacite, with locally abundant granitic xenoliths up to 3 m (9.8 ft) are common. Typical hand samples are medium dark gray (N4), grayish blue (5PB 5/2), and grayish black (N2), containing >20 percent (vol.) clear, lath-shaped to equant, euhedral plagioclase phenocrysts ≤7 mm (0.3 in) across, 3 to 5 percent (vol.) blocky, equant hypersthene and hornblende microphenocrysts ≤0.5 mm (0.02 in), and 1 to 2 percent (vol.) plagioclase-hornblende-pyroxene glomerocrysts ≤5 mm (0.2 in), distributed within a hypocrystalline groundmass.

Unit **Tcdp** is assigned a middle Eocene age on the basis of an $^{40}Ar/^{39}Ar$ plateau age of 43.86 ± 0.89 Ma (plagioclase; sample 279 LCJ 06) obtained from porphyritic andesite cropping out at Harvey Gap on the west flank of the Wildcat Mountain caldera (**Figure 5-5**, **Figure 5-11, Figure 6-1**; **Table 5-1**; plate; appendix; Ferns and McClaughry, 2007). Walker and Robinson (1990) reported a K-Ar age of 53.7 ± 1.0 Ma for andesite, within the unit, from a locality near Cadle Butte, but the date is of uncertain quality, location, and stratigraphic position.

Figure 6-94. Porphyritic andesite (Tcdp) exposed along Marks Creek at the intersection of U.S. Highway 26 and USFS Road 100 (Summit Road) (44.481223, -120.403425). Correlative outcrops at Harvey Gap, along the western edge of the Wildcat Mountain caldera, have returned an $^{40}Ar/^{39}Ar$ age of 43.86 ± 0.89 Ma. Photo credit: Jason McClaughry, 2008.

Unconformity

6.4.3 Rocks of the early Clarno Formation

Tceb **alkali olivine basalt (lower Eocene)—**High-magnesium alkali-olivine basalt lava flows (SiO_2 = 50.95 to 50.97 weight percent; TiO_2 = 0.83 to 0.86 weight percent; MgO = 9.11 to 13.04 weight percent; *n* = 2 analyses) mapped along the north shore of Prineville Reservoir (**Table 6-9**; plate; appendix). Unit **Tceb** may include at least two lava flows, separated by a grayish purple (5P 4/2) weathering interflow zone. Lava flows (**Tceb**) are typically blocky to columnar or platy jointed. Typical hand samples are dark gray (N3) to medium gray (N5), containing 3 to 5 percent (vol.) conspicuous moderate brown-colored (5YR 3/4) subhedral, seriate, embayed, iddingsite-rimmed olivine phenocrysts, and subhedral, chlorite-rimmed clinopyroxene and orthopyroxene phenocrysts ≤2 mm (0.1 in) across, distributed within a fine-grained, equigranular, holocrystalline groundmass.

Unit **Tceb** is assigned an early Eocene age on the basis of stratigraphic position and an $^{40}Ar/^{39}Ar$ plateau age of 46.40 ± 0.12 Ma obtained from a sample collected in Prineville Reservoir State Park (whole rock; 03 LC 06) (**Figure 5-11, Figure 6-1**; **Table 5-1**; plate; appendix).

6.5 Other rocks

Tosz **sheared rock zone (Oligocene)—**Northeast-striking zone of sheared and fragmented volcanic rock mapped west of Kings Gap Spring in the northwest part of the map area (**Figure 5-12**; plate). One occurrence extends ~2 km (1.2 mi), with width ranging from 100 to 250 m (330 to 820 ft). The fault zone is marked by a pervasive, anastomosing subvertical fracture cleavage. Strong deformation and intense alteration precluded mapping stratigraphic units in this zone. The unit is assigned an Oligocene age on the basis of crosscutting stratigraphic relations and is inferred to have initially formed during initial collapse of the Crooked River caldera at ~29.5 Ma (**Figure 6-1**; plate). Whether deformation continued beyond this time is unknown.

Tcc **clay in alteration zones (Oligocene and/or Eocene [?])—**Clay alteration zones occurring along rhyolite intrusions within the Ochoco Creek mercury area of Brooks (1963) (plate). They lie chiefly in a northeast-trending band that covers an area of 1.2 km^2 (0.5 mi^2), ~ 15 km (9.3 mi) northeast of Ochoco Reservoir. Clay zones often contain cinnabar, pyrite, calcite, opal, chalcedonic quartz in veinlets and as discrete particles (Brooks, 1963). Unit **Tcc** is mapped on the basis of work by Swinney and others (1968).

7.0 STRUCTURE

7.1 Introduction

Geologic structure in the lower Crooked River basin is defined by the mapped distribution of geologic units, faults, topographic lineaments, folds, and bedding attitudes (**Figure 7-1**; plate; appendix). Primary structural features (e.g., fault planes, slickensides, or fault breccia) are rarely observed in the field. Where exposed, faults are typically steeply inclined to vertical. The relative amount of offset along most faults is poorly constrained due to an overall lack of distinct marker beds, traceable over a significant distance.

The lower Crooked River basin lies between the southwestern end of the Blue Mountains (Rogers, 1966; Fisher, 1967; Taylor, 1977; Walker and Robinson, 1990), the Klamath–Blue Mountain gravity-anomaly lineament (Riddihough and others, 1986), and the junction of the Brothers and Sisters fault zones (**Figure 5-2**, **Figure 7-1**; plate). A majority of the observed geologic structure in the area is related to the middle Eocene Wildcat Mountain caldera and the Oligocene Crooked River caldera (**Figure 5-5**, **Figure 5-7**, **Figure 5-12**, **Figure 5-14**, **Figure 7-1**; plate). Only minor structure in the way of middle to late Miocene faulting and folding postdates these large Paleogene volcano-tectonic features.

7.2 Wildcat Mountain caldera

The Wildcat Mountain caldera is a discrete eruptive center within the Ochoco volcanic field, a complex of variably exhumed Eocene volcanic and intrusive rocks that lie along the crest of the Ochoco Mountains (**Figure 5-5**; plate). The Ochoco volcanic field lies astride the southwestern end of the Blue Mountains uplift, a northeast-trending topographic high, interpreted by previous workers as an early Paleogene antiform (**Figure 5-2**; Rogers, 1966; Fisher, 1967; Taylor, 1977; Walker and Robinson, 1990). The Eocene tectonic setting for north-central Oregon has been relatively unstudied, but major structural elements have been identified in local depocenters along the axis of the Blue Mountains (**Figure 5-2**, **Figure 5-4**; e.g., Clarno, Painted Hills, Mitchell). These depocenters preserve broadly folded Eocene stratified rocks with northeast-trending fold axes, and west-northwest-striking faults and dikes (Taylor, 1977, 1981; Walker and Robinson, 1990; Bestland and others, 2002). At Wildcat Mountain caldera, west-northwest to east-west-striking dikes, northeast-striking faults, and northeast-trending lineaments predominate (**Figure 5-5**; plate). These combined structural elements are consistent with a regional tectonic stress regime of northwest- to southeast-directed compression and complementary northeast- to southwest-directed extension in north-central Oregon during the Eocene as suggested by Taylor (1977, 1981) and Robyn and Hoover (1982).

A deep level of erosion, pervasive landslides, and central caldera resurgence have removed a substantial amount of the intracaldera fill tuff (**Tcts**) and dismantled the original topographic rim of the Wildcat Mountain caldera (**Figure 5-5**, **Figure 5-6**; plate). The mapped margin of the Wildcat Mountain caldera is considered to be the fault-bounded structural zone along which a majority of caldera subsidence took place; it is identified or inferred on the basis of the spatial distribution of the intracaldera tuff (**Tcts**), location of hydrothermal alteration zones, the distribution of post-collapse intrusions, and topographic expression (**Figure 5-5**, **Figure 5-6**, **Figure 5-7**; plate). The caldera ring fracture is most distinctly exposed between Kidnap Spring and Salmon Creek in the southern part of the caldera, where steep gullies have exposed a near vertical, curvilinear contact between a >425 m thick (1,394 ft) section of intracaldera tuff (**Tcts**) and early to middle Eocene basement rocks (**Tcal**) (**Figure 5-5**, **Figure 6-81**, **Figure 6-82**; plate). Between Kidnap Spring and Strickland Butte, cinnabar-bearing hydrothermal alteration zones, that

are coincident with breccia dikes and large rhyolite intrusions, indicate the proximity of the western caldera margin (**Figure 5-5**; plate). North of Strickland Butte, the caldera margin's location is approximated by prominent rhyolite dikes at Hash Rock and Twin Pillars (**Figure 5-5**; **Figure 6-79**, **Figure 6-83**; plate). The dikes are inferred to have been emplaced along the ring fracture and are interpreted as the main feeders to the large-volume Hash Rock rhyolite flow (**Tcrh**) (**Figure 5-5**; plate). Cinnabar-bearing hydrothermal alteration zones exposed at Whistler Spring and intracaldera tuff (**Tcts**) ponded against basement rocks south of that area mark part of the eastern caldera ring fault zone (**Figure 5-5, Figure 6-84**, **Figure 6-86**; plate). Further south, between Hamilton Creek and Wildcat Creek, the caldera margin is inferred to enclose the southeast end of a northwest-striking pyroclastic dike, interpreted as an eruptive vent for the tuff of Steins Pillar (**Tcts**) (**Figure 5-5**; plate). The inferred margin here may also correspond with hydrothermally altered basement rocks mapped along Wildcat Creek and along U.S. Highway 26 near Buck Spring. Southwest of Wildcat Creek, a series of variably mineralized mafic to silicic intrusions probably follow the trace of the caldera ring fracture (**Figure 5-5**; plate).

Figure 7-1. Map of major geologic structures in central Oregon (*following page*). Fault and fold data outside of the lower Crooked River basin is from Franczyk and others (2020; OGDC-7) and the USGS Quaternary fault and fold database of the United States. The Crooked River caldera is coincident with the northwest-striking Brothers fault zone, the north-northwest-striking Sisters fault zone, and the northeast-striking Klamath-Blue Mountain lineament. Northeast-striking fault zones, including the Cyrus Springs fault zone and the Prineville Reservoir fault zone, define the northwest and southeast margins of the Crooked River caldera.

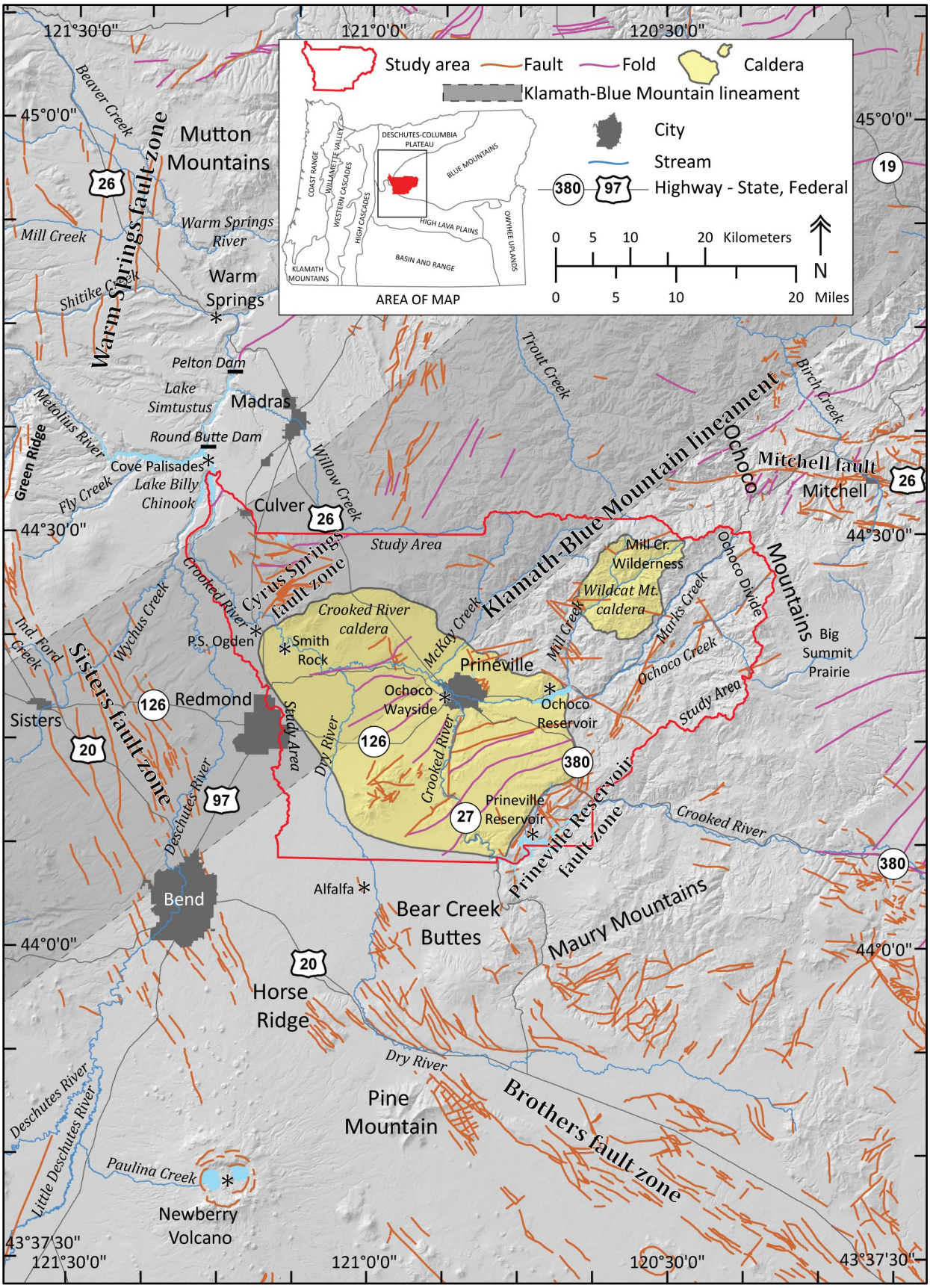
Study area
Fault
Fold
Caldera
Klamath-Blue Mountain lineament
City
Stream
Highway - State, Federal
AREA OF MAP
0 5 10 20 Kilometers
0 5 10 20 Miles
N
DESCHUTES-COLUMBIA PLATEAU
BLUE MOUNTAINS
COAST RANGE
WILLAMETTE VALLEY
WESTERN CASCADES
HIGH CASCADES
HIGH LAVA PLAINS
OWYHEE UPLANDS
KLAMATH MOUNTAINS
BASIN AND RANGE
121°30'0"
121°0'0"
120°30'0"
45°0'0"
44°30'0"
44°0'0"
43°37'30"
Mutton Mountains
Warm Springs fault zone
Beaver Creek
Mill Creek
Warm Springs River
Shitike Creek
Warm Springs
Pelton Dam
Lake Simtustus
Round Butte Dam
Cove Palisades
Lake Billy Chinook
Metolius River
Green Ridge
Fly Creek
Madras
Culver
Willow Creek
Trout Creek
Birch Creek
Ochoco Mitchell fault
Mitchell
Klamath-Blue Mountain lineament
Study Area
Cyrus Springs fault zone
Crooked River
Crooked River caldera
Smith Rock
P.S. Ogden
Wychus Creek
Ind. Ford Creek
Sisters fault zone
Sisters
Redmond
Dry River
McKay Creek
Prineville
Ochoco Wayside
Ochoco Reservoir
Mill Cr. Wilderness
Wildcat Mt. caldera
Mill Creek
Marks Creek
Ochoco Divide
Ochoco Creek
Mountains
Big Summit Prairie
Deschutes River
Bend
Alfalfa
Bear Creek Buttes
Horse Ridge
Maury Mountains
Prineville Reservoir
Prineville Reservoir fault zone
Crooked River
Dry River
Pine Mountain
Brothers fault zone
Paulina Creek
Newberry Volcano
Little Deschutes River
Deschutes River
19
26
97
126
20
27
380

7.3 Crooked River caldera

The Crooked River caldera forms an embayment along the southwest part of the Ochoco Mountains, partially overlapping the older Ochoco volcanic field (**Figure 5-12**, **Figure 5-13**; plate). The boundary of the Crooked River caldera is considered to be the fault-bounded structural zone along which a majority of caldera subsidence took place, as most of the original topographic rim of the caldera has been destroyed by erosion (**Figure 5-12**, **Figure 5-14**). Much of the evidence of this structural margin has further been obliterated by post-caldera intrusions or is buried beneath younger Neogene deposits. It can be inferred on the basis of the spatial distribution of the intra- and extra-caldera tuff, the distribution of post-collapse rhyolite intrusions, location of hydrothermal alteration zones, and topographic expression (**Figure 5-12**, **Figure 5-16**; plate). The ring fracture is only directly exposed on the northeast margin of the caldera, between Grizzly Mountain and Ochoco Reservoir (**Figure 5-12**; plate). A roadcut excavation along Old Dry Creek, ~4 km (2.5 mi) north of Barnes Butte, reveals a complex, vertically dipping contact between faulted andesite basement rock (**Tcal**) and unfaulted massive pumice-lithic intracaldera tuff (**Tjtsi**) (**Figure 6-56**; plate). The wall rock is pervasively cut by a series of regularly spaced, brittle shear-fractures spaced 0.5 to 1 m (1.6 to 3.3 ft) apart that parallel the contact. Faint slickenside lineations are common on the shear fracture planes. This contact is interpreted to represent the caldera margin at this location. To the northwest, the ring fracture zone corresponds to large rhyolite intrusions at Grizzly Mountain (**Tjrgm**) and Gray Butte (**Tjrg**) that follow the ring fault between older basement rocks (**Tcal**) and intracaldera tuff (**Tjtsi**) (**Figure 5-12**; plate). Early Oligocene strata between the Cyrus Springs fault zone and Gray Butte (e.g., **Tjtr**, **Tjtt**, **Tjba**, **Tjta**) strike N. 45° to 60° E. and dip 20° to 35° SE., back into the caldera structure (**Figure 6-67;** plate; appendix). Southwest of Gray Butte, near Terrebonne the caldera margin is inferred to correspond to hydrothermally altered and strongly silicified intracaldera tuff (**Tjtsi**) exposed along U.S. Highway 97 (**Figure 5-12**; plate). Precise continuation of the margin south of Terrebonne is uncertain as it is everywhere buried by Neogene basaltic lavas (**Figure 5-12**; plate). The ring fracture is inferred to extend southeast from this point around the southern end of Powell Buttes. Tuff similar to the intracaldera fill (**Tjtsi**) interstratified with clast-supported breccia and conspicuous basaltic andesite blocks compositionally similar to pre-caldera basement rocks, is preserved as a large roof pendant, nonconformably preserved across post-caldera rhyolite domes at the southern end of Powell Buttes (**Figure 5-12**; plate). Between the south end of Powell Buttes and Ochoco Reservoir to the northeast, the caldera margin is again buried beneath Neogene basaltic lavas, but is inferred to run along Prineville Reservoir. Deformed and altered strata in the Prineville Reservoir fault zone strike N.25°E. to N.56°E., and dip 30° to 55°NW., back into the caldera structure (**Figure 5-12**, **Figure 5-16**, **Figure 6-64a**, **Figure 6-65**; plate). Further to the north, near Ochoco Reservoir, the proximity of the caldera margin is identified by truncated lower Oligocene stratigraphy, hydrothermal alteration zones (±cinnabar), and the distribution of a thickly ponded post-caldera rhyolite lava flow (**Tjro**) and an underlying thick section of sedimentary rocks (**Tjs**) interpreted as moat-fill deposits (**Figure 5-12**; plate).

Two major fault zones that parallel the northeast trend of the Klamath–Blue Mountain gravity-anomaly lineament bracket the Crooked River caldera (**Figure 5-2**, **Figure 5-12**; plate). The Cyrus Springs fault zone (Smith and others, 1998) bounds the northwest margin while the Prineville Reservoir fault zone bounds the southeast margin (**Figure 5-2**). These faults define the northwestern and southeastern ends of a circumferential, peripheral fault zone that mimics the arcuate structural margin of the Crooked River caldera. This peripheral fault zone extends at least 10 km (6 mi) outside the main area of subsidence and is associated with numerous small rhyolite intrusions (**Figure 5-12**, **Figure 7-1**; plate).

The Cyrus Springs fault zone (Smith and others, 1998) is a northeast-striking, 800 m (2,624 ft) wide composite shear zone (**Tosz**), located northwest of Gray Butte (**Figure 5-12**, **Figure 7-1**; plate). The Cyrus Springs fault zone is defined by a stratigraphic contrast across the structure; the fault zone juxtaposes the Member A tuff (**Tjtma**) of the John Day Formation on the south against the 29.57 Ma welded outflow unit of the tuff of Smith Rock (**Tjtso**) on the north. Strata south of the fault zone are capped by the 32.49 Ma tuff of Rodman Spring (Tjtr), dip 20° to 35°S. (**Figure 5-12**, **Figure 6-67**), are cut by numerous basalt to rhyolite dikes within and parallel to the fault zone, and have been hydrothermally altered (Gray Butte mercury prospect; Brooks, 1963; **Figure 5-2**, **Figure 5-12**; plate; appendix). Strata on the north of the fault zone form a broadly folded, north-northwest trending homocline (plate). Intrusions and hydrothermal alteration pervasive on the south of the fault zone are notably absent in strata on the north (Smith and others, 1998). Faults within the zone generally strike N. 45° to 60°E., but some faults in the southeastern part of the zone wrap to east-west orientations (**Figure 5-12**; plate). On the basis of regional lineament mapping, the Cyrus Springs fault zone is now considered to be part of an arcuate set of faults that encircle the Oligocene Crooked River caldera (**Figure 5-12**, ; plate).

The Prineville Reservoir fault zone (McClaughry and others, 2009b, d) is a northeast-striking structural zone on the southeastern margin of the Crooked River caldera (**Figure 5-12**; plate). The main zone of deformation is ~7 km (4 mi) wide and 16 km (10 mi) long and defines a northeast-striking, northwest-dipping homocline pervasively cut by faults with both normal and reverse sense of displacement (plate, cross section A-A'). Within the fault zone, the 29.5 Ma Prineville Reservoir lobe of the tuff of Smith Rock (**Tjtso**, **Tjtsn**) is separated from ~29.7 Ma basaltic andesite lava flows (**Tjba**), the tuff of Antelope Creek (**Tjta**), the tuff of Eagle Rock (**Tjte**), and tuffaceous sedimentary rocks (**Tjtt**) with angular unconformity. Older ~29.7 Ma beds (**Tjba**, **Tjta**, **Tjte**, **Tjtt**) strike N.25°E. to N.56°E., and dip 30° to 55°NW., back into the caldera (**Figure 5-12**, **Figure 6-64a**, **Figure 6-65**; plate). Steep northwest dips, prevalent on the older pre-caldera units (**Tjba**, **Tjta**, **Tjte**, **Tjtt**), are not characteristic of the overlying 29.5 Ma tuff of Smith Rock outflow units (**Tjtso**, **Tjtsn**), which strikes N.51°E. and dips 4°NW at Prineville State Park and strikes N.19°W. and dips 2°SW. on Big Bend Island. Isotopic ages obtained for the outflow unit of the tuff of Smith Rock (**Tjtso**) and the older tuff of Eagle Rock (**Tjte**) at Prineville Reservoir constrain the formation of the angular unconformity between 29.5 and 29.7 Ma (**Figure 6-64a**, **Figure 6-65**). East of Prineville Reservoir, along O'Neil Creek, the 29.5 Ma Smith Rock outflow tuff (**Tjtso**) is ponded against the tilted structural block and is itself faulted and warped with a northwest dip (**Figure 5-12, Figure 7-1**; plate). The welded outflow unit of the tuff of Smith Rock (**Tjtso**) is the youngest unit deformed in the fault zone. Combined isotopic age, stratigraphic, and structural relations within the Prineville Reservoir fault zone indicate that deformation of the Oligocene section of tuff and basaltic andesite (**Tjba**, **Tjta**, **Tjte**, **Tjtt**) occurred synchronously with formation of the Crooked River caldera and deposition of outflow unit of the tuff of Smith Rock (**Tjtso**). Further deformation of the outflow unit of the tuff of Smith Rock (**Tjtso**) in the Prineville reservoir fault zone could be, in part, related to the subsequent development of younger Oligocene and now hidden caldera structures.

7.4 Post middle Miocene faulting and folding

Flows in the Prineville Basalt (**Tcpb**), Simtustus Formation (**Tmos**), and older rocks of the John Day and Clarno Formations are broadly folded into a series of east-northeast-striking (~N.60°E. to N.85°E.) folds in the lower Crooked River basin. Fold limbs generally dip from 3° to 15° but may locally have dips up to 20° to 45° (**Figure 7-1**; plate). Fold structures in the lower Crooked River basin are likely related to deformation occurring near the southern part of the Yakima fold belt, a regional set of asymmetric,

typically southeast-verging, locally overturned and faulted anticlinal ridges separated by broad synclinal valleys (**Figure 5-2**; Swanson and others, 1979, 1981; Anderson, 1987; Watters, 1989; Reidel and others, 1989a, b; Reidel and Campbell, 1989; Tolan and Reidel, 1989). The Yakima fold belt covers much of the western and west-central Columbia Plateau (Tolan and others, 2009) and extends westward beneath the Cascade Range and south to central Oregon (**Figure 5-2**). Folds in the Yakima fold belt are generally east-west-striking across the Columbia Plateau except across the Cascade Range, where fold axes become more northeast in trend (Swanson and others, 1981; Bela, 1982; Reidel and others, 1989b; Reidel and Campbell, 1989; Tolan and others, 2009; McClaughry and others, 2012, 2020a). East-west-striking folds across the Columbia Plateau are inferred by other workers to have formed in response to a general north-south compressional regime during the early to middle Miocene (Reidel and Campbell, 1989; Beeson and Tolan, 1990).

Folding and faulting episodes that broadly deformed the Prineville Basalt (**Tcpb**) are not observed in post-9 Ma Deschutes Formation units. Deschutes-age lava flows and sedimentary units are everywhere flat lying and show little evidence of faulting or folding (plate).

8.0 GEOLOGIC RESOURCES

8.1 Groundwater Resources

A full discussion of the geologic controls on surface and groundwater resources in the lower Crooked River basin is beyond the scope of this report. General geologic investigations do not collect sufficient water data to allow for detailed discussion of the processes that influence groundwater flow, and surface and groundwater interaction. In addition to an assessment of the geologic framework, stream flow measurements, using both long term gaging stations and short-term seepage runs, water well measurements, including aquifer tests and observation wells, estimates of groundwater recharge, and water use analyses are needed before a groundwater flow system can be adequately characterized. The reader is directed to previous reports published by Robinson and Price (1963), Gannett and others (2001), Lite and Gannett (2002), Sherrod and others (2002), and Gannett and Lite (2004) for a more thorough discussion of groundwater resources and hydrogeology in the area.

Movement of groundwater and interactions between groundwater and surface water in the lower Crooked River basin are influenced both by permeability differences between stratigraphic units and geologic structure. For example, the contrasting permeability between Paleogene and Neogene rock units along the lower Crooked River drainage is an important regional boundary to groundwater flow. The Eocene Clarno Formation and the Eocene-Oligocene John Day Formation, exposed near or at the surface over much of the lower Crooked River basin, are considered the lower boundary of the regional groundwater flow system (**Figure 5-3**; plate; Lite and Gannett, 2002; Sherrod and others, 2002). These rocks typically exhibit low permeability due to the abundance of devitrified rhyolite, tuff, and tuffaceous sedimentary rocks that are diagenetically altered to clay and zeolite (Gannett and others, 2001; Lite and Gannett, 2002). Local intense hydrothermal alteration and secondary mineralization around volcanic vents and along fault zones further reduces permeability (McClaughry and others, 2009a, b, d). Most of the water wells that produce out of the John Day and Clarno formations in the lower Crooked River basin have very low yields except where permeability is locally increased by secondary porosity (fractures). Many of the wells open to water bearing zones in the John Day Formation have yields less than 10 gallons per minute (gpm), although local fracture-controlled areas may have larger yields (Lite and Gannett, 2002). The few good aquifers in the John Day Formation are of limited extent, are poorly connected, and

probably have limited long-term water-supply potential. John Day Formation rocks are generally straight forward to identify in well logs, discerned by the predominance of material described by drillers as clay or claystone.

While the low permeability of the Clarno and John Day formations in the lower Crooked River basin limits deep, regional groundwater flow, it results in a high-density of low-discharge springs (Freed and others, 2019). Freed and others (2019) attributed this high density of low-discharge springs in the Clarno and John Day formations to limited infiltration of rain and snowmelt in low-permeability rocks and concentration of short flow path groundwater in the soil and shallow bedrock. These shallow, short flow paths easily intersect the land surface resulting in many springs. Low-discharge springs in the lower Crooked River basin are an important source of water for wildlife, livestock, and biodiversity in general.

The more productive sources for groundwater in the lower Crooked River basin unconformably overlie the John Day and Clarno Formations. These units include the Prineville Basalt (**Tcpb**), Deschutes Formation, and post-Deschutes Formation rocks (**Figure 5-16**; plate). The Simtustus Formation (**Tmos**) is generally fine-grained and thus usually a low-yielding aquifer unit. Lavas of the Prineville Basalt (**Tcpb**) and to an extent the age-equivalent sedimentary rocks of the Simtustus Formation (**Tmos**) are exposed between Lone Pine Flat near Smith Rock and Bowman Dam in the south part of the map area (**Figure 5-16**; plate). The Prineville Basalt (**Tcpb**) is the primary water-producing unit for residential areas north of Powell Buttes and between Stearns Butte and the Crooked River (**Figure 5-16**; plate). Wells constructed into water bearing zones within the Prineville Basalt (**Tcpb**) typically yield amounts (10 to 30 gpm) that are suitable for domestic and stock uses, but are inadequate for irrigation (Gannett and Lite, 2004). The Prineville Basalt (**Tcpb**) is identified in well logs by chemistry where available and is often described in water well logs as broken basalt intermixed with brown clay. Presumably, this description refers to the characteristic burrowing of Prineville Basalt (**Tcpb**) into underlying sedimentary rocks or the pillowed nature of the base of many of the lava flows.

Basaltic lava flows and interbedded sedimentary units in the upper Miocene and Pliocene Deschutes Formation occur at the surface or in the shallow subsurface over much of the western part of the lower Crooked River basin (**Figure 5-16**; plate). These units are the most productive source of groundwater in the western part of the lower Crooked River basin. Permeability in the Deschutes Formation ranges from relatively low in dense lavas, ash-flow tuffs, and fine-grained sedimentary deposits, to relatively high in vesicular and brecciated lavas and coarse-grained, unconsolidated sedimentary deposits (Lite and Gannett, 2002). Smith (1986a, 1987; 1991) subdivided the Deschutes Formation into four depositional environments: proximal volcanic rocks of the High Cascades arc, arc-adjacent alluvial plain, ancestral Deschutes River, and inactive-basin margin (**Figure 5-21**). Numerous basaltic and basaltic andesite lavas were erupted from the Bowman volcanic field, across the southern part of the inactive-basin margin of the Deschutes Basin (**Figure 5-21**). These lava flows are interbedded with fine-grained and generally well-sorted sedimentary units deposited on low gradient alluvial fans and along the thalweg and floodplain of the ancestral Crooked River, which drained uplands composed of the John Day and Clarno Formation. Lite and Gannett (2002), showed well yields within the inactive-basin margin deposits north of Smith Rock are typically less than 30 gpm, but in a few cases may exceed 300 gpm (**Figure 5-21**). Higher yields may locally occur along brecciated interflow zones in lavas and within coarse-grained sedimentary intervals. South and east of Smith Rock in the lower Crooked River basin, Lite and Gannett (2002) included the numerous Bowman volcanic field lavas and locally interbedded sedimentary rocks in their Deschutes Formation proximal facies hydrogeologic unit. Well yields of 300 to 500 gpm are common from Bowman volcanic field lava flow sequences in the Deschutes Formation around Prineville. West of Powell Buttes and along the trace of Dry River Deschutes Formation lavas are interbedded with notably abundant

sedimentary and pyroclastic deposits (Lite and Gannett, 2002). These deposits probably define paleochannels of an ancestral drainage. Similar sections of layered lava flows and sedimentary rocks associated with the proximal High Cascades arc facies in the Bend area can yield 400 gal/min to 2000 gal/min Lite and Gannett (2002) (**Figure 5-21**).

Pleistocene lava flows from Newberry Volcano (**Qbnc**, **Qbn2**, **Qbn4**, **Qbn6**), are mapped broadly across the southwest part of the lower Crooked River basin. These rocks are highly fractured and permeable, serving as conduits for canal leakage and other incidental recharge (Lite and Gannett, 2002). Newberry lava flows often lay above the water table and are only locally saturated north and east of Bend.

Unconsolidated, poorly- to well-sorted deposits of gravel, sand, silt, and clay of late Pleistocene and Holocene age unconformably overlie older strata throughout the lower Crooked River basin (plate). Surficial deposits consist principally of stream alluvium (**Qa**), terrace deposits (**Qto**, **Qty**), alluvial fan and debris fan deposits (**Qoaf**, **Qaf**), and landslide and colluvial deposits (**Qls**, **Qc**) (plate). These surficial units were emplaced by mass wasting of upland areas, alluvial deposition in and adjacent to high-energy streams, and deposition in low-energy streams and lakes. Surficial units are typically less than 100 m (328 ft) thick and their distribution varies both laterally and vertically. Numerous, relatively small, shallow, water bearing zones exist within Quaternary sedimentary units and serve as important aquifers throughout the lower Crooked River basin. Wells producing from Quaternary sedimentary units near Prineville typically have yields that range between 10 and 20 gpm and are mostly suitable for domestic use (Lite and Gannett, 2002). Lower sand and gravel units may be capable of yields of a few hundred gpm.

8.2 Aggregate and Industrial Minerals

Aggregate, in the form of crushed rock and gravel, is the major mineral resource now being mined in the lower Crooked River basin. Locations for aggregate and crushed rock resources in the area can be found in McClaughry and others (2020b) (MILO-3). Much of the basin is underlain by volcanic rocks, but high-quality aggregate-rock, preferred for road construction purposes, is restricted to quarries sited within fine-grained, platy to hackly and columnar jointed lavas of the Prineville Basalt (**Tcpb**) (**Figure 8-1a**). Coarser-grained platy basaltic andesite, andesite, and dacite lavas of the Eocene Clarno Formation are quarried for use on lands administered by the United States Forest Service in the eastern half of the basin (plate). In the western part of the basin, cinder cones in the Deschutes Formation (e.g., Grass Buttes) are good sources of both pit run and crushed rock aggregate (**Figure 5-16**, **Figure 6-20**, **Figure 6-27**; plate). Sand and gravel, suitable for use as aggregate are comparably rare, being restricted to Quaternary terrace deposits (**Qto**) at O'Neil, and local, largely discontinuous sedimentary units (**Tds**; **Tdsg**) in the Deschutes Formation (**Figure 6-4**, **Figure 8-1b**; plate).

Figure 8-1. Aggregate sources in the lower Crooked River basin. (a) Juniper Rock quarry at the intersection of Juniper Canyon Road and Davis Loop, southeast of Prineville (44.265924, -120.822158). The quarry is sited within lavas of the Prineville Basalt (Tcpb). (b) Aggregate quarry at the intersection of the O'Neil Highway and Lone Pine Road, west of Prineville (44.329576, -121.096310). The quarry is sited within unconsolidated sand and gravel that are mapped as terrace deposits (Qto). Photo credits: Jason McClaughry, 2005, 2008.

Rhyolite and tuff in the John Day Formation have been used in the past as a source of local decorative stone. Sawed blocks of grayish yellow green (5GY 7/2) to dusky yellow green (5GY 5/2) tuff (unit **Tjtsi**) were produced for a short time from the Oregon Emerald Tuff quarry north of Prineville (**Figure 8-2**). Pale reddish brown (10R 5/4) tuff (**Tjtsn**) was also mined from the Crooked River tuff quarry near Prineville Reservoir. Large, columnar-jointed blocks of Prineville Basalt (**Tcpb**) from the Juniper Rock quarry south of Prineville are locally used for ornamental purposes (**Figure 8-1a**). Larger basalt columns in the Prineville Basalt (**Tcpb**) and lava flows of the Deschutes Formation also have potential for use as riprap for stabilization and erosion control purposes.

Industrial minerals, such as clay and zeolite, are locally present within the lower Crooked River basin, but have not been mined in the past. Gray and others (1989) reported the occurrence of minor amounts of montmorillonite clay in samples obtained from moderate red (5R 4/6) to very dark red (5R 2/6) volcaniclastic sedimentary units exposed at the top of the Clarno Formation north of Prineville Reservoir and near Ochoco Reservoir (unit **Tces**; plate; appendix). These clay zones, which are marked by a characteristic popcorn-weathering soil, apparently do not contain appreciable amounts of swelling clays that could be used as an industrial mineral product. Kaolinite clay is reported from the northwest flank of Powell Buttes.

Figure 8-2. The Oregon Emerald Tuff quarry, located north of Prineville. (44.416227, -120.680290). Person for scale is 1.9 m (6.2 ft) tall. Photo credit: Jason McClaughry, 2005.

Zeolite minerals have been reported in several areas in the lower Crooked River basin. The zeolite minerals mordenite and clinoptilolite are reported from the intracaldera unit of the tuff of Steins Pillar (**Tcts**) within the Wildcat Mountain caldera at Steins Pillar (Waters, 1966). Mordenite was also found by this study to occur in a ring-fracture rhyolite dike (**Tcrh**) mapped along the northwest margin of the Wildcat Mountain caldera (**Figure 5-5**, **Figure 8-3**; plate). The dike is an aphyric to sparsely plagioclase-phyric rhyolite cored by fresh-appearing, flow-banded vitrophyre and numerous lithophysal cavities up to 3 cm (1.2 in) across. Lithophysae are commonly filled by a white radial fibrous zeolite, identified by X-Ray diffraction as mordenite (**Figure 8-3**; J. Van Tassell, written commun., 2010). These fibrous zeolites are associated with opaline and chalcedonic quartz seams and lenses. Mordenite is a common zeolite widely found in silica-rich rocks; the occurrence of fine euhedral crystals, such as those that fill the cavities in the rhyolite dike, typically indicates a hydrothermal genesis (Ostroumov and Corona-Chávez, 2003).

Gray and others (1989) reported the occurrence of the zeolite mineral clinoptilolite, as well as trace amounts of fluorite and lithium, in tuffs in the John Day Formation near Eagle Rock (sample #55) (**Figure 5-12**, plate).

Figure 8-3. Fibrous zeolite (mordenite) filling lithophysal cavities in a rhyolite dike (Tcrh) along McKay Creek Road, near the western margin of the Wildcat Mountain caldera (44.474131, -120.616029). Outcrop corresponds to alteration geochemical sample 115 LCJ 06 (appendix). Hammer head for scale is 12 cm (4.7 in) tall. Photo credit: Jason McClaughry, 2006.

8.3 Semi-precious Gemstones

Semi-precious gemstones in the form of geodes (thundereggs), agate, jasper, chalcedony, and opal occur locally in rhyolite domes, near the base of prominent ash-flow tuffs, and in sites that hosted siliceous hot-spring pools both within and marginal to the middle Eocene Wildcat Mountain and Oligocene Crooked River calderas (**Figure 5-5**, **Figure 5-12**; plate). The arcuate ring-fractures of these calderas and associated peripheral faults that allowed for the emplacement of rhyolite intrusions, also served as conduits for upward movement of silica-rich hydrothermal fluids after the main caldera subsidence phases.

Strongly welded ash-flow tuffs and rhyolite lava flows locally have lithophysal zones characterized by large open cavities up to 20 cm (7.9 in) across. Where filled by agate, jasper, or opal, the lithophysae form geodes, which are found primarily in areas where silica-rich fluids have circulated along secondary fault structures. Many of the areas in which geodes are found also contain narrow veins filled by agate, jasper, or opal. The most productive sites for geode collection in the lower Crooked River basin are associated

with the Wildcat Mountain caldera (**Figure 5-5**; plate). Notable prospects include those located along the margins of rhyolite lava flows and domes at Whistler Spring, Wildcat Mountain, White Fir Spring, and Strickland Butte on the Ochoco National Forest (**Figure 5-5**; plate). The Lucky Strike Mine, located in the northeast part of the map area, is a mining claim that produces agate-filled geodes derived from a lithophysal zone at the base of the rhyolite of Hash Rock (**Tcrh**) (**Figure 5-5**, **Figure 8-4a**; McClaughry and others, 2009a, d). At the time of publication, geodes can be collected here by the public, with a fee for collection, based on the weight of mined products, charged by the mine operators. Additional information can be obtained at the mine office.

Figure 8-4. Geode and picture jasper. (a) Butterfly wing, agate-filled geode (thunderegg) from the Lucky Strike Mine along the northern rim of the Wildcat Mountain caldera (44.517639, -120.497229). Scale bar is 5 cm (2 in) long. (b) Picture jasper cabochon made from a sample of laminated, silicified mudstone found along the margin of the Crooked River caldera. Scale bar is 2 cm (0.8 in) long. Photo credits: Jason McClaughry, 2008.

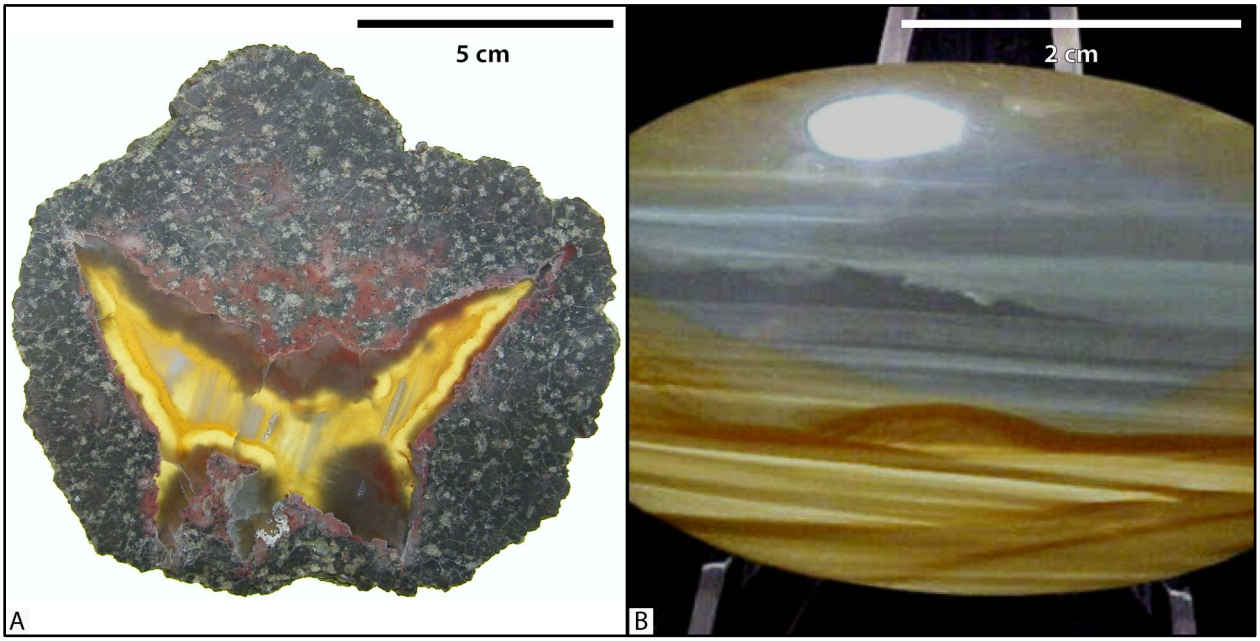

Numerous locations along the ring fracture zone of the Crooked River caldera display evidence of quartz and calcite veining, siliceous sinter, well-laminated, silicified mudstone, and hydrothermal explosion breccias (**Figure 5-12**; plate). Chalcedonic quartz, in the form of jasper and agate, fills fractures in rhyolites and tuffs of the John Day Formation along the caldera margin and along faults cutting the Clarno Formation peripheral to the caldera (**Figure 8-5**). Jaspers occur in a variety of colors including pale reddish brown (10R 5/4), dark yellowish orange (10YR 6/6), white (N9), and grayish black (N2). Locally thin seams of pale reddish brown (10R 5/4) to dark yellowish orange (10YR 6/6), opaline to opaque quartz is associated with the jaspers. Many localities have been prospected in the past and have been variably excavated; several of the sites occur on public land and are open to recreational prospecting. Notable public localities are located on the north shore of Ochoco Reservoir and west of Eagle Rock (**Figure 5-12**, **Figure 8-5c**; plate). The locality north of Ochoco Reservoir occurs near the base of the rhyolite of Ochoco Reservoir (**Tjro**) near the southeast margin of the Crooked River caldera. This site is a popular public collection site for colorful agate and jasper that can be found on the ground surface below the cliffs overlooking the site. Many specimens have cavities filled with drusy quartz. At the Bureau of

Land Management collecting locality, west of Eagle Rock, the base of the outflow sheet to the tuff of Smith Rock (**Tjtso**) is crosscut by massive to fragmented and brecciated seams of grayish black (N2) jasper that are as much as 12 cm (4.8 in) thick (**Figure 5-12**, **Figure 8-5c**; plate). Smaller seams of medium gray (N5) to grayish yellow (5Y 8/4) agate, as well as moss and dendritic agate, also occur locally within the tuff at this location.

Laminated silicified mudstone and siltstone is found within moat-fill sedimentary rocks exposed at several localities along the northern margin of the Crooked River caldera between Smith Rock and Barnes Butte (**Figure 5-12**, **Figure 8-4b**, **Figure 8-5a**, **Figure 8-6a**; plate). These fine-grained sedimentary rocks are often spatially associated with massive, laterally discontinuous pods of breccia containing clasts of heavily silicified mudstone and siltstone (**Figure 8-5a**, **Figure 8-6b**). The silicified character and spatial association of these rocks within and peripheral to the caldera suggests their formation as siliceous sinter and pool deposits and as hydrothermal explosion breccias within geyser and mud pot fields. These deposits were likely the surface manifestation of ancient hot springs, analogous to those now residing within the modern Yellowstone caldera in western Wyoming. Oxidation of microscopic sulfides within the silicified siltstones produced an attractive variety of picture jasper that is marked by thin bands of various shades of moderate reddish brown (10R 6/6), dark yellowish orange (10YR 6/6), and grayish blue (5PB 5/2) (**Figure 8-4b**). Thormahlen (1984) and Gray and Baxter (1986) found detectable amounts of gold (Au), silver (Ag), and arsenic (As) in these deposits (appendix).

Figure 8-5. Examples of cryptocrystalline quartz. (a) Massive to locally brecciated, hydrothermal hot spring-type sinter deposit along the northern margin of the Crooked River caldera, south of Sumner Spring (44.410679, -121.115971). Hammer for scale is 40 cm (15.7 in) long. Outcrop corresponds to alteration geochemical sample 313 LCJ 06. (b) Silicified tuff (Tjtb) with slickensides near the Barnes Butte mercury prospect (44.323619, -120.814809). The tuff is altered and silicified along the intrusive contact with the younger rhyolite of Barnes Butte (Tjrb). Compass for scale is 15 cm (5.9 in) long. (c) Rheomorphic tuff (Tjtso) with fractures and cavities filled by black, cryptocrystalline quartz (44.185576, -120.668216). Hammer for scale is 40 cm (15.7 in) long. Outcrop corresponds to alteration geochemical sample 15 LCJ 06. (d) Very dark red (5R 2/6) and dark yellowish orange (10YR 6/6) jasper exposed along a 6-m-wide (20 ft), N. 70° E.-striking fault zone mapped north of Barnes Butte (44.352863, -120.785261). Hammer for scale is 40 cm long (15.7 in). Photo credits: Jason McClaughry 2005, 2006, 2008.

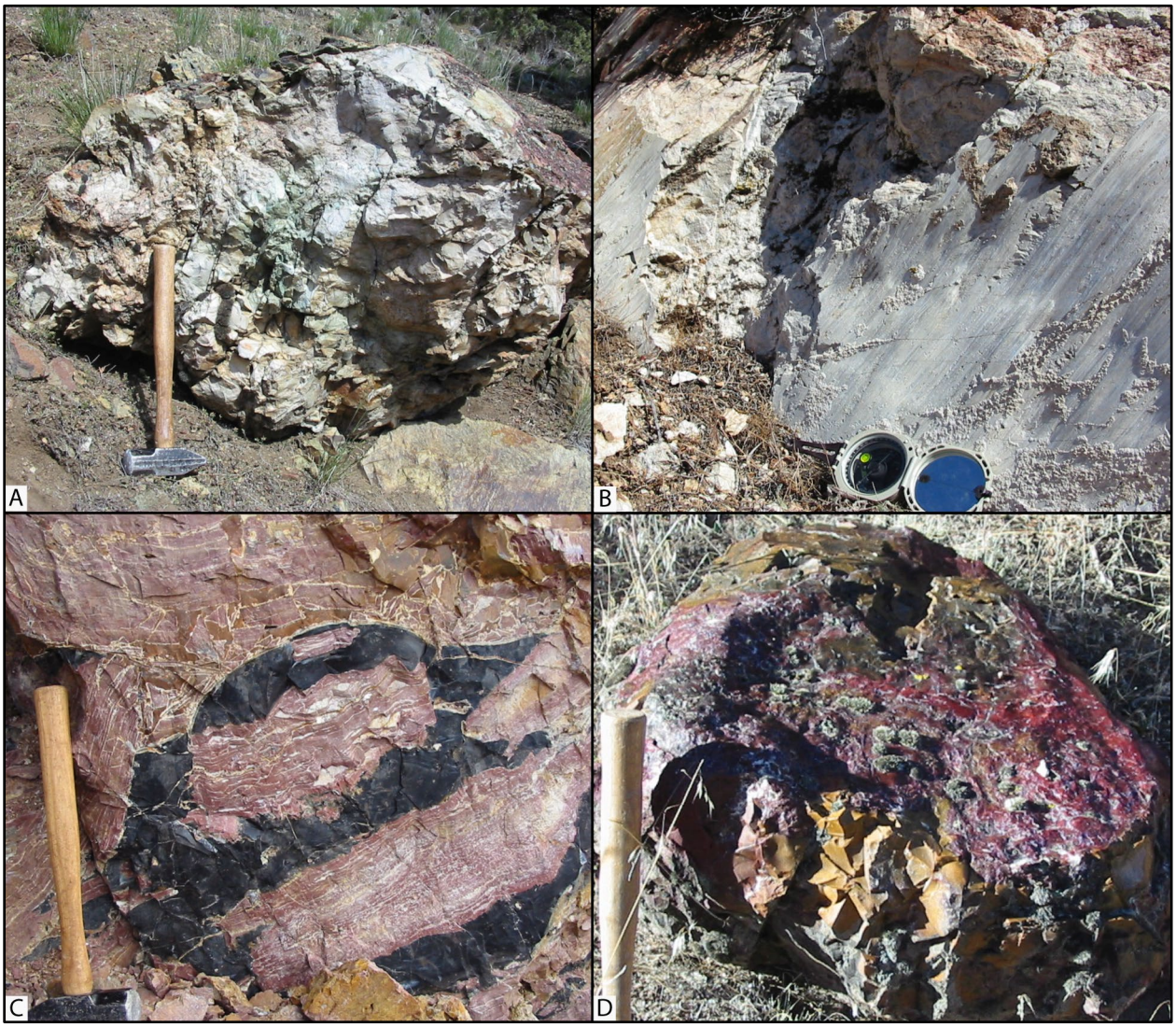

Figure 8-6. Laminated silicified mudstone and silicified breccia.(a) Laminated silicified mudstone found south of Grizzly Mountain (44.403186, -120.923903). Pencil for scale. Outcrop location corresponds approximately to alteration geochemical sample DT-61. (b) Breccia containing clasts of heavily silicified mudstone and siltstone southeast of Grizzly Mountain (44.385699, -120.887300). Pencil for scale is 15 cm (5.9 in) long. Outcrop corresponds to alteration geochemical sample 337 LCJ 07. Photo credits: Jason McClaughry, 2007.

8.4 Metallic Minerals

Metallic minerals, including gold, silver, and mercury have been produced in the past from a number of mines in the lower Crooked River basin (Brooks and Ramp, 1968). Mineralized zones are typically associated with fault zones and, large-scale volcanic centers of middle Eocene and Oligocene age, including the Wildcat Mountain and Crooked River calderas, and smaller volcanoes that were situated in the area of Round Mountain in the eastern part of the map area (**Figure 5-5**, **Figure 5-12**; plate). The most extreme areas of alteration, typically occur in association with post-subsidence rhyolite domes and other intrusive igneous bodies associated with volcanic centers.

8.4.1 Gold and silver

Gold was reportedly first discovered in the eastern part of the map area on Ochoco Creek in 1871 (Champion, 1938) in what would become the Howard mining district (plate). By 1883 the stream placers on Scissors and Ochoco Creeks and the gulch placers between Scissors Creek and Stevensons Gulch had largely been exhausted (plate). Based on where the placer tailings are found, much of the placer gold appears to have come from gulch or residual placers on the west flanks of Gold Hill and Red Bird Hill

(Willis, 1992). The cumulative area mined covered less than 700 acres and the total amount of placer gold produced is unknown. Based on mint reports, Gilluly and others (1933) reported that 537 ounces of placer gold were produced between 1902 and 1923. According to Champion (1938) perhaps as much as 14,000 ounces of gold had been produced by the placer mines in the Ochoco Creek area before 1902 (plate).

Gilluly and others (1933) reported that 2,478 ounces of gold, 442 ounces of silver, and 2,662 pounds of lead were produced from the Ophir-Mayflower Mine at Gold Hill between 1902 and 1923 (plate). The most extensive workings on the Ophir-Mayflower followed a pipe-shaped mineralized zone measuring between 0.3 to 1.8 m (1 to 6 ft) in thickness that was mined over a horizontal distance of 21 m (70 ft) and a vertical distance of 70 m (230 ft) (Gilluly and others, 1933). Mineralized zones are marked by narrow calcite and sulfide veinlets as much as 3 cm (1.2 in) in width that form sheets wherein numerous paralleling calcite and sulfide veinlets are separated by 1- to 5-cm-thick (0.4 to 2 in) bands of rock (Willis, 1992). Gold Hill itself is a subvolcanic intrusive complex (**Tcdp**) characterized by hornblende porphyry flows and intrusives and breccias. The breccias include both clast- and matrix-supported breccias, some of which are described as "tuff" by Willis (1992). The Gold Hill complex is marked by extensive propylitic alteration, characterized by partial to complete replacement of hornblende and plagioclase phenocrysts by a mixture of chlorite and calcite. Greenish propylitic alteration zones at Gold Hill also contain disseminated pyrite in the groundmass and in calcite veinlets. Weak argillic (clay) alteration zones typically weather to shades of yellow and are marked by the nearly complete replacement of plagioclase crystals by sericite and calcite and groundmass minerals by pyrite, calcite, and silica. Weakly altered argillic zones form envelopes around narrow zones of advanced argillic alteration and are confined to vertical fractures and the margins of breccia pipes (Willis, 1992), some of which may lie nearly horizontal. Although the mineralized fractures and cross faults strike in nearly all directions (Gilluly and others, 1933), the predominant strike is N. 40° E. to N. 60° E. (Willis, 1992). Advanced argillic alteration zones are no more than several meters in width and are marked by nearly complete replacement of rock by clay and sulfide minerals. Calcite and sulfide veinlets are apparently confined to the advanced argillic alteration zones (Willis, 1992). Much of the early gold production came from rich surficial "pockets" situated above mineralized fractures. These pockets, which formed by secondary enrichment processes (Gilluly and others, 1933) are honeycombed vein material that is stained brown and black by sooty manganese and iron oxide minerals. Primary metallic minerals include gold and silver in the form of pyrite, sphalerite, galena, arsenopyrite, chalcopyrite and tetrahedrite (Gilluly and others, 1933; Willis, 1992) while secondary minerals include iron and manganese oxides, and chalcocite, (Gilluly and others, 1933). Calcite is the main vein mineral, with quartz being rare and generally readily apparent in the pockets.

Elongate breccia dikes and pipes are also found within and along the west margin of the Wildcat Mountain caldera near Kidnap Spring (**Figure 5-5**, **Figure 5-12**, **Figure 6-73**, **Figure 6-74**; plate). Although gold and silver have not been reported from the Kidnap Spring area, the breccias are characterized by weak argillic alteration wherein feldspars are partially altered to chlorite, calcite, and sericite. Groundmass in some breccia dikes is silicified and locally contains disseminated pyrite. Disseminated pyrite occurs also as streaks in massive bodies of silicified rhyolite and dacite that appear to be cut by the breccia dikes.

8.4.2 Mercury

Mercury mineralization, associated with middle Eocene and Oligocene volcanic centers and related faults and fractures, is widely distributed across the lower Crooked River basin (**Figure 5-5**, **Figure 5-12**; plate). The most productive mercury mines in the lower Crooked River basin were located in the Ochoco Creek

and Johnson Creek mercury areas, while lesser production occurred in the vicinity of Marks Creek, Kidnap Spring, Barnes Butte, and north of Gray Butte (plate; Brooks, 1963).

According to Brooks (1963) mercury was first discovered in the area, about 9 km (5.6 mi) south of the Ophir-Mayflower at the Mother Lode mine in 1900. The Mother Lode, also known as American Almaden, was initially a gold and copper prospect, located on the north side of Lookout Mountain near the head of Canyon Creek, at the extreme southwest end of the Johnson Creek mercury area. The area is marked by a series of andesite lava flows that are cut by N.60°E.-striking diabase dikes and mineralized faults. Mercury mineralization occurs as thin, knife-edge coatings of cinnabar along fractures with higher grade zones forming narrow veinlets as much as 6 mm (0.2 in) thick that branch in all directions (Gilluly and others, 1933). According to Brooks (1963), mercury mineralization is concentrated along cross faults with strikes of N.40°W. to N.45°W., N.10°W. to N.15°W., and N.5°E. to N.10°E. Chloritic stringers within the lava flows are cut by cinnabar-bearing fractures that are locally encrusted with opal, chalcedony, quartz, dolomite, calcite, and asphalt (Gilluly and others, 1933). Total recorded production from the Mother Lode, was 347 flasks (1 flask = 76 pounds).

The Ochoco Creek mercury area consists of a series of mines and prospects that work a broad zone of faulting, intrusions, hydrothermal alteration, and mineralization that extends northeasterly over a distance of ~25 km (15.5 mi). The area extends from the eastern margin of the Crooked River caldera at Ochoco Reservoir to the Ophir-Mayflower (**Figure 5-12**; plate). Mercury was first discovered on Ochoco Creek at the Staley Mine in 1927, which produced at least 448 flasks of mercury (Brooks, 1963). Other notably productive mercury mines in the area included the Byram-Oscar, Champion, and Taylor Ranch mines, which together produced more than 338 flasks. Mines and prospects in the area explored a series of N. 55° E.- to N. 75° E.-striking shear zones that parallel the course of Ochoco Creek and, in places, contain calcite or chalcedonic quartz veinlets with cinnabar and calcite. Cinnabar ore bodies generally occur in extensively crushed, hydrothermally altered fault breccia that is pervasively altered to a clay-rich gouge; gouge is crosscut by discontinuous veinlets and narrow seams of veinlets of calcite and chalcedonic quartz. Although individual fault zones can be altered to a width as much as 6 m (20 ft), the clay gouge zones are discontinuous and are usually less than 1.5 m (5 ft) in width (Brooks, 1963). Alteration appears to be most intense in areas where the northeast trending fault zones are cut by cross faults (Stephenson, 1943). According to Gilluly and others (1933) iron-rich montmorillonite is the most abundant clay mineral in the alteration zones; other clay minerals include kaolinite and nontronite. Additional alteration minerals include iron oxides, pyrite, opal, and a black lustrous hydrocarbon (Brooks, 1963).

A series of northeast-striking fractures in the Marks Creek mercury area, located to the northeast of the Ophir-Mayflower have been explored for mercury (Brooks, 1963). Mercury mineralization in that area was reportedly associated with narrow chalcedonic quartz veins as much as 10 cm (4 in) in width. Country rock includes olivine basalt flows and andesite. The shear zones within which the quartz veins occur are narrow, no more than 1.2 m (4 ft) in width and are marked by clay, iron oxides, and small stringers and seams of chalcedonic quartz. Open spaces in some of the chalcedonic quartz veins contain a black, sooty hydrocarbon (Gilluly and others, 1933).

The Kidnap Spring mercury area is situated along the crest of the ridge between Lemon and Dry Creeks, along the western margin of the Wildcat Mountain caldera (**Figure 5-5**; plate). Brooks (1963) indicated that mercury was first discovered in this area in about 1930 and that about 19 flasks of mercury were produced from small mines. Most of the mercury was produced from the Strickland Butte Mine, which was developed on narrow fractures along the northern, locally perlitic margin of a ring fracture rhyolite dome that forms Strickland Butte proper (**Figure 5-5**, **Figure 8-7**; plate). Cinnabar reportedly occurred as thin fracture fillings and fine disseminations above a dark red clay zone. Other mercury prospects in

the area include the Kidnap Spring, Allison, and Watson prospects, which explored narrow fractures in clay altered andesite.

Figure 8-7. Hydrothermal alteration associated with the Wildcat Mountain caldera. (a) Silicified, spherulitic rhyolite, near Whistler Spring, with surfaces encrusted by manganese (44.496047, -120.485906). Pencil for scale is 15 cm long (5.9 in). Outcrop corresponds to alteration geochemical sample 370 LCJ 07. (b) An abandoned 1940s retort at the Strickland Butte prospect (44.441622, -120.652328). Person for scale is 1.9 m (6.2 ft) tall. Photo credits: Jason McClaughry, 2006, 2007.

Several mercury prospects are located within or marginal to the Crooked River caldera (**Figure 5-12**; plate). The largest mineralized zones are exposed near Gray Butte, where a series of east-west-striking, mineralized fault zones, paralleling the north caldera ring fracture crop out (**Figure 5-12**, **Figure 8-8**; plate). The Gray Butte mercury prospect (Brooks, 1963), located north of Kings Gap Spring, consists of Clarno andesite lava flows (**Tcal**) that are cut by an east-west-striking fault zone and intruded by a series of vertically foliated rhyolite dikes (**Figure 5-12**, **Figure 8-8**). According to Brooks (1963), the fault zone can be traced for a distance of at least 305 m (1,000 ft). The prospect explored a vertically standing rib of silicified rhyolite and tuff that stands as much as 2.4 m (8 ft) above the land surface. The rhyolite dike has a 1 m (3.3 ft) wide margin of moderately silicified breccia and is pervasively cut by stockwork quartz and clay veining (**Figure 8-8a-c**). Fractures are locally coated by cinnabar. Chalcedonic quartz ribs are also exposed along the northern ring fracture west of Gray Butte. Similarly striking calcite veins and pebble dikes are reported northwest of Nichols Spring (**Figure 5-12**; plate; Gray and Baxter, 1986).

A small amount of mercury (29 flasks) was also mined from the Barnes Butte mine, which is situated along a rhyolite dome within the Crooked River caldera (**Figure 5-12**; plate). The mine explored a rib of massive white opaline quartz exposed along a N.65°E.-striking fault that marks the south margin of the rhyolite of Barnes Butte (**Tjrb**; **Figure 6-38**, **Figure 8-5b**). Cinnabar reportedly occurs within seams and

small lenses of opalite along small fractures branching from the main fault. Additional small occurrence of mercury were noted during the course of mapping near the eastern margin of the Crooked River caldera at Ochoco Reservoir (**Figure 5-12**, **Figure 8-9**; plate). Mineralization in this area occurs as small pods and lenses of hydrocarbons and more massive area of white opaline quartz distributed along fracture zones (**Figure 8-9**). Cinnabar is locally encrusted on fracture surfaces.

Figure 8-8. Gray Butte mercury prospect.(a) The Gray Butte mercury prospect consists of andesite cut by an east-west-striking fault zone and intruded by a series of vertically foliated rhyolite dikes (44.437361, -121.116935). View is looking east. Arrow points to silver notebook for scale, which is 30 cm (11.8 in) long. (b) Vertically foliated rhyolite dike intruding brecciated andesite along the east-west-striking fault zone. The dike has a 1 m (3.3 ft) wide margin of moderately silicified breccia. Silver notebook for scale is 30 cm (11.8 in) long. (c) Stockwork quartz and clay veining in the rhyolite dike shown in B. Fractures are locally coated by cinnabar. Pencil for scale is 15 cm (5.9 in) long.

Figure 8-9. Halo of hydrocarbon hosted within an intrusive complex of dacite (Tcdp) dikes along the north shore of Ochoco Reservoir (44.310203, -120.688995). The black hydrocarbon includes more massive areas of white opaline quartz. Cinnabar is locally encrusted on fracture surfaces. Scale bar is 10 cm (3.9 in) long. The outcrop corresponds to alteration geochemical sample 1.28VI.05. Photo credit: Jason McClaughry, 2005.

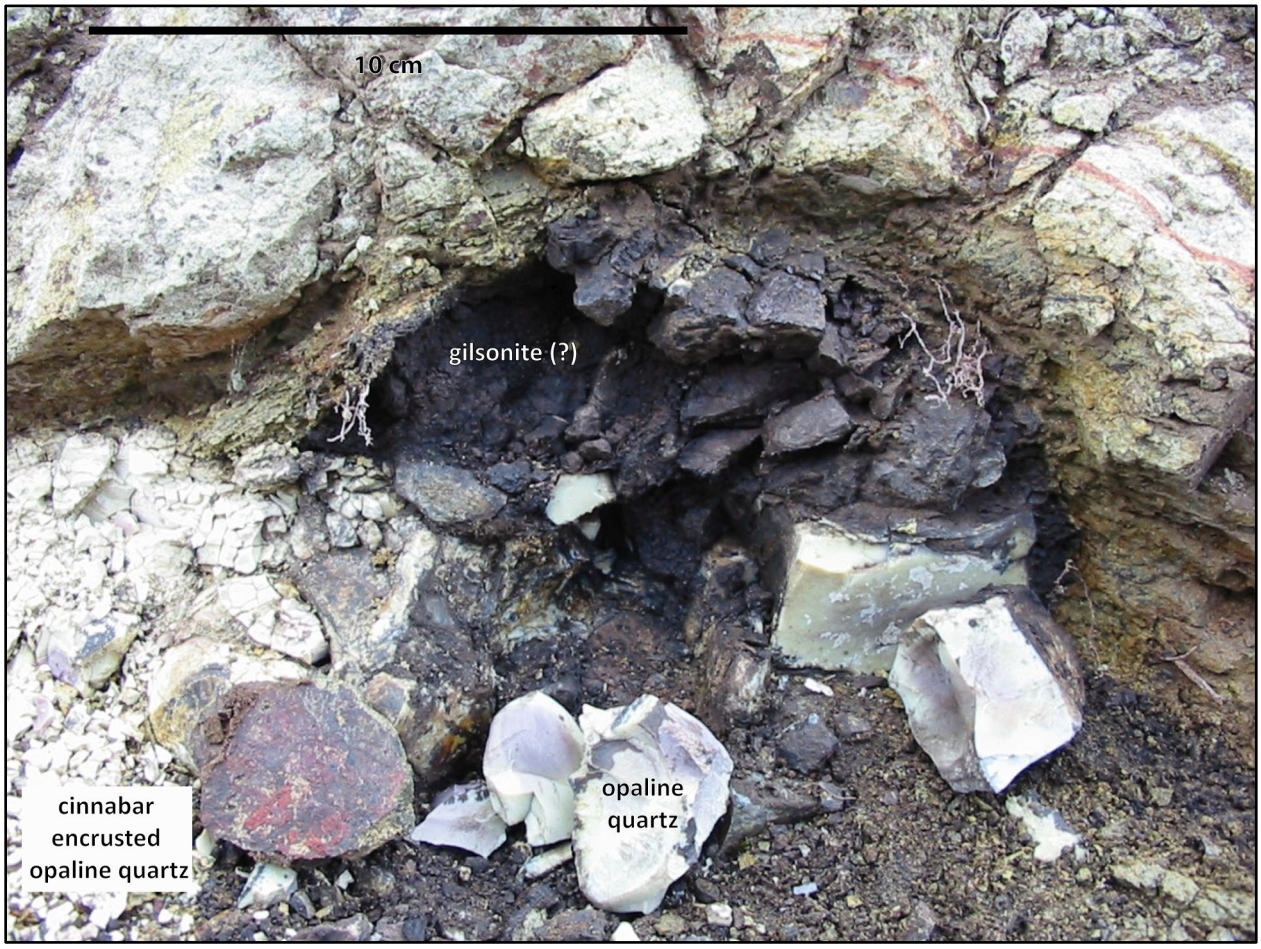

8.5 Energy Resources

8.5.1 Geothermal resources

Abnormally warm waters, with temperatures of at least 27°C (80°F), have been encountered in more than 20 water wells drilled within the Crooked River caldera (**Figure 5-12**; plate; appendix). The highest temperature wells, with water temperatures as high as 42°C (110°F), extend along the northwest end of Powell Buttes (**Figure 5-12**; plate). Wells with water temperatures as high as 29°C (84°F) also occur at Grizzly Mountain (**Figure 5-12**; plate). The highest water temperature, 57°C (135°F), was reported from a depth of 460 m (1,509 ft) in a geothermal gradient well drilled off the west flank of Powell Buttes by DOGAMI in 1980 (**Figure 5-12**; plate). A series of gradient holes drilled on the northwest flank of Powell Buttes identified an abnormally high geothermal gradient (>100°C/km [212°F/km]) over an elongated area of 20 km^2 (7.7 mi^2) (Brown and others, 1980).

8.5.2 Uranium

Indications of uranium mineralization have been found in rhyolite domes and ash-flow tuffs associated with the Crooked River caldera (**Figure 5-12**; plate). The area was extensively prospected for uranium in

the late 1950s and early 1960s, after radioactive material was first discovered on the west side of Powell Buttes in 1955 (**Figure 5-12**, plate; Schafer, 1956). According to Schafer (1956) the rhyolite at Powell Buttes gave an unusually high background reading on a Geiger counter, with the highest readings associated with iron-oxide stained joints and coatings of hyaline opal that fluoresce greenish-yellow (Schafer, 1956). Small amounts of cinnabar have also been found at Powell Buttes (**Figure 5-12**; plate). Schafer (1956) also reported samples of tuff from the Game Guides prospect, near the head of Owl Creek, on the north side of Prineville Reservoir that contain autunite (**Figure 5-12**; plate). Residents have also reported areas of elevated radioactivity, as determined by hand-held Geiger counters, from the Smith Rock area. While rhyolites and tuffs have been prospected in the past for uranium, there are no records of ore-grade uranium deposits. A small amount of uranium was mined from rhyolite-hosted deposits located at Bear Creek Buttes, south of the map area (**Figure 1-1**; Peterson, 1969).

9.0 GEOLOGIC HAZARDS

9.1 Landslide Hazards

Landslides may present a significant geologic hazard to residents, infrastructure, and transportation corridors in the lower Crooked River basin. At least four general types of landslide deposits are present in the map area. They include: 1) rock fall and debris-flows; 2) composite landslides involving slow-moving unstable masses of rock and colluvium; 3) simple landslides involving terrace, cutbank, and cliff collapses; and 4) colluvium-derived landslides and slumps. Differentiation is based on the speed and manner in which the rock and soil move and is defined by geologic setting and triggering mechanisms.

Landslide deposits (**Qls**) cover approximately 189 km^2 (73 mi^2) in the lower Crooked River basin and range in age from late Pleistocene to those that are currently active or those that have been active in recent times. Bedrock landslide deposits occur in at least 3 distinct domains in the lower Crooked River basin, including those fringing Oligocene rhyolite flow and dome complexes, landslides along the length of the Crooked River canyon, and landslides lining upland drainages in the Ochoco Mountains (plate).

9.1.1 Rock fall and landslide-generated debris flows

Rock fall and landslide-generated debris-flows may pose a significant geologic hazard in the lower Crooked River basin where very steep slopes are present, especially along the basalt-lined Crooked River canyon and in stream-carved valleys and smaller draws in the Ochoco Mountains (plate). Periodic rock fall poses hazards in areas adjacent to steeply inclined to vertical cliff faces. Such hazards are especially prevalent along Oregon Highways 27 and 380, extending south and west of the City of Prineville, where Deschutes Formation Basalt is exposed in near vertical cliffs (**Figure 5-16**; plate). Similar hazards exist from Smith Rock and Peter Skene Ogden State Parks downstream to the mouth of the Crooked River (plate). A combination of localized fault and joint sets, and differential weathering between intraflow breccias, hackly entablatures and colonnades in the basalt all contribute to an increased probability for rockfall events in the Crooked River canyon (plate). Potential natural triggering mechanisms for rock fall events may include freeze/thaw conditions, heavy rainfall, earthquakes, or extensive devegetation due to fire.

Many small- to moderate-sized alluvial fans (**Qaf**) in the lower Crooked River basin have been mapped on the basis of field observations, 2009 to 2018 National Agriculture Imagery Program orthophotos, and analysis of 1-m lidar DEMs where available (plate). Rapidly moving landslides in the form of debris flows may be expected on alluvial fans (**Qaf**) that lie at the mouth of steep-sided, colluvium-filled canyons and

upland drainages. Debris flow deposits are also common within small drainages within the Ochoco Mountains, resulting from soil erosion and remobilization of unconsolidated sediment following devegetation by frequently recurring fires and local human activities (plate). The potential for inundation of alluvial fan (**Qaf**) areas by rapidly moving debris flows is increased during episodes of intense rainfall that occur after soils have been saturated by fall and early winter rainfall. Redirected drainage and poor construction and logging practices are human activities that could initiate debris flows. Debris flows have the potential to threaten life and may cause extensive damage to property and public infrastructure.

9.1.2 Composite landslides

Composite landslides (**Qls**) are developed through the progressive emplacement of successive landslide lobes over time, where individual parts of the complex may be active at different times. These types of landslide deposits (**Qls**) may involve coherent blocks of bedrock as large as 0.5 km^2 (0.2 mi^2) and are defined by multiple generations of landslide lobes, with terrain characterized by irregular hummocks, closed depressions, springs, wet seeps, internal head-scarps, and cracks and crevices. Toes to more recent deposits retain convex-up, fan-shaped morphologies. Recent deposits within composite landslide complexes (**Qls**) typically bury and disrupt roads and may pose engineering problems for homes and infrastructure. In the lower Crooked River basin, the distribution of composite landslide complexes is controlled by: 1) bedding plane contact relations; 2) unconformities between geologic units of varying age and lithology; 3) the distribution of major fault and joint structures; 4) high relief; and 5) steep slopes. Large composite landslides (**Qls**) are common fringing Oligocene rhyolite flow and dome complexes, along the length of the Crooked River canyon, and lining upland drainages in the Ochoco Mountains (plate). Composite landslide deposits (**Qls**), mapped in the lower Crooked River basin, range in size from ~0.4 to 19.7 km^2 (0.2 to 7.6 mi^2).

The largest composite landslide complexes (**Qls**) in the map area are mapped adjacent to Oligocene rhyolite flow and dome complexes near Pilot Butte and at Ochoco Reservoir (**Figure 5-12**, **Figure 6-2**, **Figure 9-1**; plate). The Pilot Butte complex covers ~20 km^2 (7.7 mi^2) occurring along intrusive margins with older, west dipping ash-flow tuffs (plate). Hydrothermal alteration and silicification along the contact are also contributing to instability of the land surface in this area. The Ochoco Reservoir landslide complex covers ~7 km^2 (2.7 mi^2) and originates along a south-dipping contact (towards the reservoir) where dense rhyolite lavas (**Tjro**) overlie friable and relatively incompetent sedimentary rocks (**Tjs**) (**Figure 9-1**). The landslide deposit can be traced upslope to prominent cliff-forming head scarps that are regularly segmented by cliff-parallel, tension cracks up to 100 m (328 ft) long (**Figure 6-2**, **Figure 9-1b**). The right abutment of Ochoco Dam, completed in 1920 for irrigation and flood control as part of the United States Bureau of Reclamation Crooked River Project, is founded upon landslide deposits in the Ochoco Reservoir complex (Carter, 1998; Kunzer, 1998; McClaughry and others, 2009c). Since its completion, the dam has suffered from persistent seepage problems beneath the right abutment (north side). Deteriorating site conditions since construction resulted in the temporary emptying of the reservoir in 1993 (Carter, 1998). Water storage resumed in 1995 after modifications to increase bank stability and decrease seepage along the right abutment had been completed. Additional flood protection was provided through modifications to the left abutment spillway (Carter, 1998; Kunzer, 1998). Operational problems at the Ochoco Reservoir dam site are intimately linked to site geology, with persistent seepage beneath the right abutment likely linked to sinkholes developed in poorly sorted landslide deposits that have variable permeability and material strength (Carter, 1998; McClaughry and others, 2009c).

Figure 9-1. Ochoco Reservoir landslide complex (Qls). (a) View north across Ochoco Creek to south-dipping, cliff-forming outcrops of the rhyolite of Ochoco Reservoir (Tjro) (44.297369, -120.726064). The right abutment of the dam and spillway visible in the photo is founded upon a flanking, large active landslide complex (Qls) that is sourced in the rhyolite (Tjro). White arrows indicate general direction of transport of material in the landslide complex (Qls). The flow of Ochoco Creek is to the left (west) in the photograph. X marks the location of photograph in B. (b) Inset photograph is a 3 m (9.8 ft) wide tension crack in the head scarp of the Ochoco Reservoir landslide complex (44.308123, -120.711498). Scale bar is 3 m (9.8 ft) long. Photo credits: Jason McClaughry, 2005.

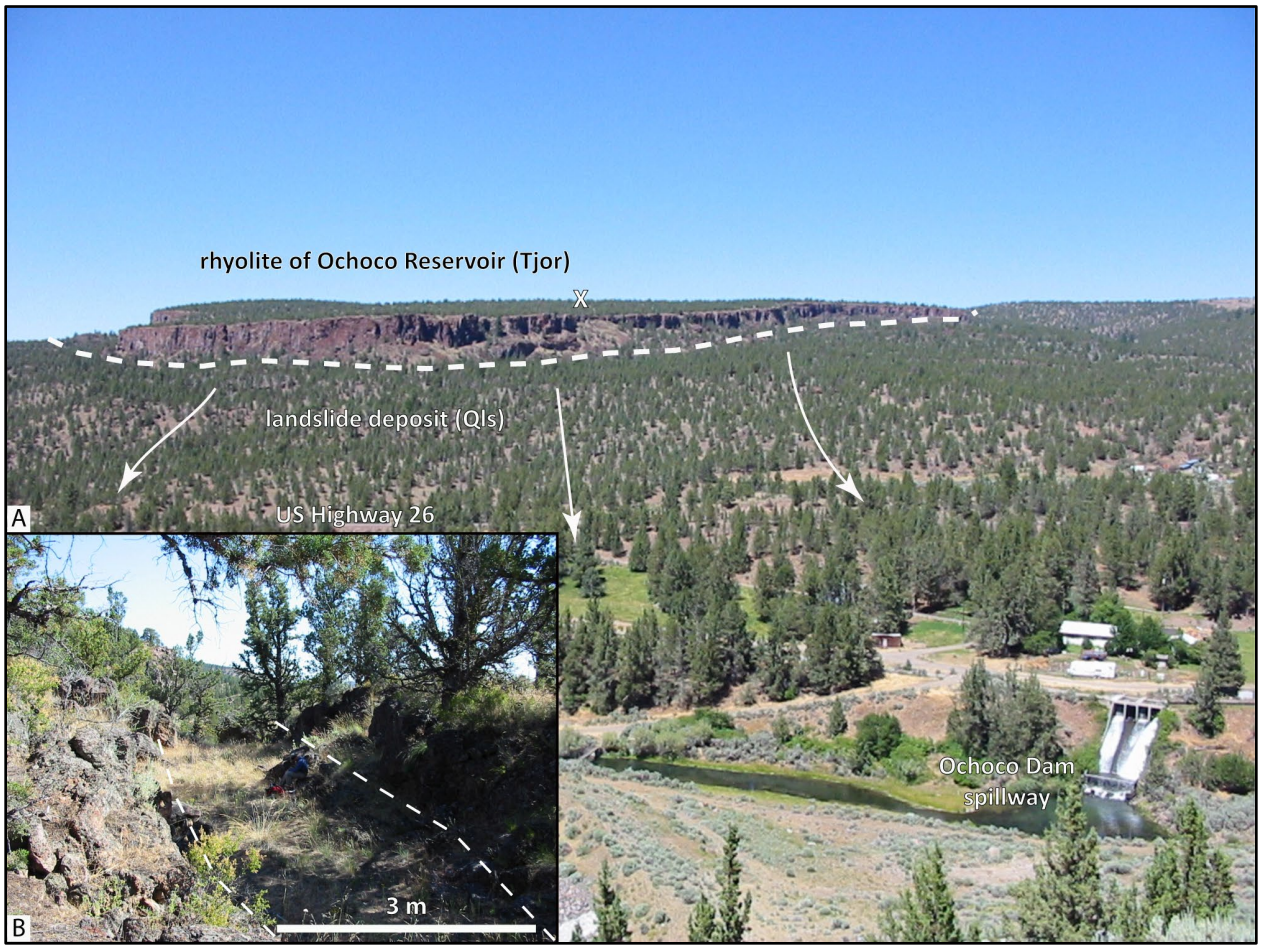

Along the length of the Crooked River canyon, landslide deposits (**Qls**) mantle subvertical to vertical slopes, obscuring the underlying stratigraphy (**Figure 9-2**; plate). These landslide deposits (**Qls**) consist largely of unconsolidated angular basalt blocks derived from over-steepened, tension-cracked cliff-faces, where late Miocene and Pliocene plateau-capping basalts overlie semi-consolidated sections of sedimentary rock or tuff. Basalt lava flows commonly calve and topple or rotate listrically along fractured columnar joint margins (**Figure 9-2a**). Older basalt slides have vegetated and soil-mantled upper surfaces; more recent deposits lack vegetation and soil and in places may be confused for tumuli capped intracanyon flows. Clast-size in the deposits averages 1 to 3 m (3.3 to 9.8 ft) across; the maximum intact landslide blocks may exceed 300 m (984 ft) across (**Figure 9-2b**). Crackle- and jigsaw-breccia fabrics are common in clasts.

Figure 9-2. Examples of landslides sourced in Deschutes Formation basaltic lavas. (a) Lavas of the Deschutes Formation typically break apart into large blocks that calve and topple or rotate listrically along fractured columnar joint margins and cascade downward from over-steepened, tension-cracked cliff-faces. Arrow shows direction of downslope transport. The example in A is located north of the Paulina Highway (OR Highway 380) near the west end of Combs Flat (44.280377, -120.763312). (b) Landslide deposits (Qls) are common along the length of the Crooked River canyon, south of Prineville. Locally, landslide (Qls) blocks may exceed 300 m across (985 ft). View is looking north along the Crooked River (44.213842, -120.876757). Photo credits: Jason McClaughry, 2006.

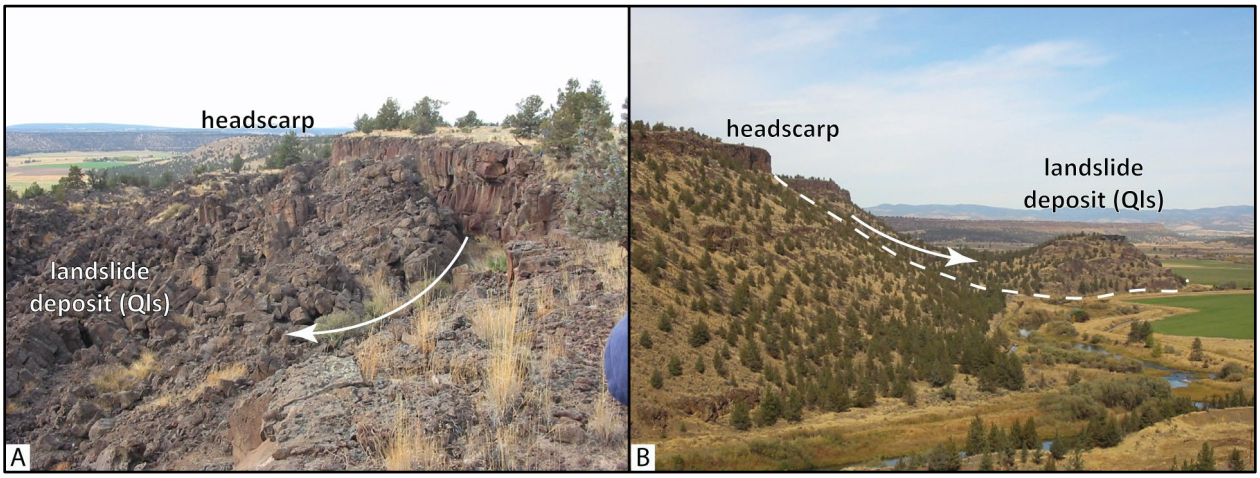

Composite landslides (**Qls**) in the Ochoco Mountains typically form large complexes, consisting of individual slides of different ages, that form coalescing masses that mantle topography in over steepened drainages (**Figure 5-5**; plate). Landslide complexes (**Qls**) have periodically flowed downslope and dammed reaches of both Mill Creek and McKay Creek (**Figure 5-5**; plate). The formation of slide complexes (**Qls**) in the Ochoco Mountains is controlled by a combination of factors including: 1) depositional contacts where thick lava flows (e.g., **Tcrh**, **Tcrm**, **Tjob**, **Tjoa**) disconformably overlie an older, deeply eroded surface of middle Eocene Clarno Formation intermediate composition lava flows and domes (e.g., **Tcal** and **Tcdp**); 2) depositional contacts where thick lava flows (e.g., **Tcrh**, **Tcrm**, **Tjob**, **Tjoa**) disconformably overlie the tuff of Steins Pillar (**Tcts**); 3) steeply dipping intrusive contacts; and 4) over steepened, variably faulted and hydrothermally altered sections of the ring fracture zone of the Eocene Wildcat Mountain caldera (**Figure 5-5**; plate).

Part of a composite landslide complex (**Qls**) along Doe Creek, a small drainage tributary to the main stem of Mill Creek in the Ochoco National Forest, reactivated during the fall of 2000 and has been recurrently active since that time (**Figure 5-5**, **Figure 9-3**, **Figure 9-4**; plate). The active landslide (**Qls**) is marked by an earthflow covering an area of ~0.09 km^2 (0.03 mi^2) with an estimated volume of ~76,455 m^3 (~100,000 yd^3). Initial slope-failure of the active landslide (**Qls**) occurred following a long dry summer, as landslide terrain, previously considered to be dormant, reactivated. Downslope movement of the slide-mass created a distinct head scarp cut into middle Eocene andesite lavas (**Tcal**) that form part of the basement rock of the Wildcat Mountain caldera (**Figure 5-5**; plate). Distal portions of the slide-mass engulfed standing trees and overran USFS Road 3300-450 (**Figure 9-3**, **Figure 9-4**). Unlike most active landslides (**Qls**), the movement was constant (~15 m [50 ft]/year) through the first 5 years with no apparent hiatus. A small flowing spring developed at the terminus of the slide deposit during the summer of 2005. Advent of spring development in 2005 corresponded with the end of large-scale movement in the slide-mass, with the exception of periodic minor adjustments.

The Doe Creek earthflow is part of a larger landslide complex (**Qls**) covering ~0.7 km^2 (~0.3 mi^2, 172 acres). The landslide complex occurs within pre-caldera basement rocks composed of early to middle Eocene platy andesite lavas (**Tcal**) crosscut by post-caldera rhyolite intrusions (**Tcrk**) (**Figure 5-5**; plate). Oligocene basaltic andesite lavas (**Tjob**) disconformably overlie platy andesite lava flows (**Tcal**) in head scarp areas on the north along Squirrel Ridge (**Figure 5-5**, **Figure 9-3**, **Figure 9-4**; plate).

A slope stability investigation was initiated by the USFS on the Doe Creek earthflow in August of 2001 in order to understand the mechanics and potential reactivation of similar terrain within the Ochoco National Forest. The study on Doe Creek included three auger holes and the installation of piezometers to monitor groundwater levels and to serve as simple slope movement indicators. Radiometric age-date testing of charcoal collected from auger holes indicated that the most recent historic movement in the landslide complex was ~9240 BP. The presence of undisturbed in-situ Mazama tephra recovered from one of the drill holes suggests that no landslide movement had occurred at this location since at least ~6850 BP (L. Chitwood to C. Gordon, written commun., 2001).

The reactivation of dormant landslide terrain on the east side of the Cascade Range is directly related to rain-on-snow events beneath the 1,372 m (4,500 ft) elevation band. The Doe Creek landslide originates on a south-facing slope in an area that receives minor average annual precipitation (~49.0 cm [19.3 in]). The landslide occurred independently of extraordinary precipitation events. Following its discovery, the slide moved 25 m (80 ft), even with very little precipitation for a year (Mathisen and Gordon, 2006). In the case of the Doe Creek earthflow, a number of geologic factors played a role in slide reactivation including: 1) failure of incompetent interflow zones within early to middle Eocene platy andesite lava flows (**Tcal**) that form the basement of the Wildcat Mountain caldera; 2) alteration zones associated with the post-caldera rhyolite intrusions; and 3) disconformable contacts between early Eocene platy andesite lava flows (**Tcal**) that pre-date the caldera and overlying Oligocene basaltic andesite lava flows (**Tjob**) that post-date the caldera.

Figure 9-3. The Doe Creek earthflow. (a) Photo looking southeast from the landslide head scarp (44.431072, -120.604041). Black arrows show the direction of slide movement. Dashed white line denotes the boundary of the slide mass. Note the irregular, hummocky topography and subvertical orientation of trees on the landslide surface. Steins Pillar is visible in the background. (b) View of the landslide toe looking northwest toward the head scarp area (44.429201, -120.605222). The landslide toe has engulfed standing trees and blocked USFS Road 3300-450 at this location. The arrow points to the area where a small spring developed in 2005. Photo credits: Jason McClaughry, 2006.

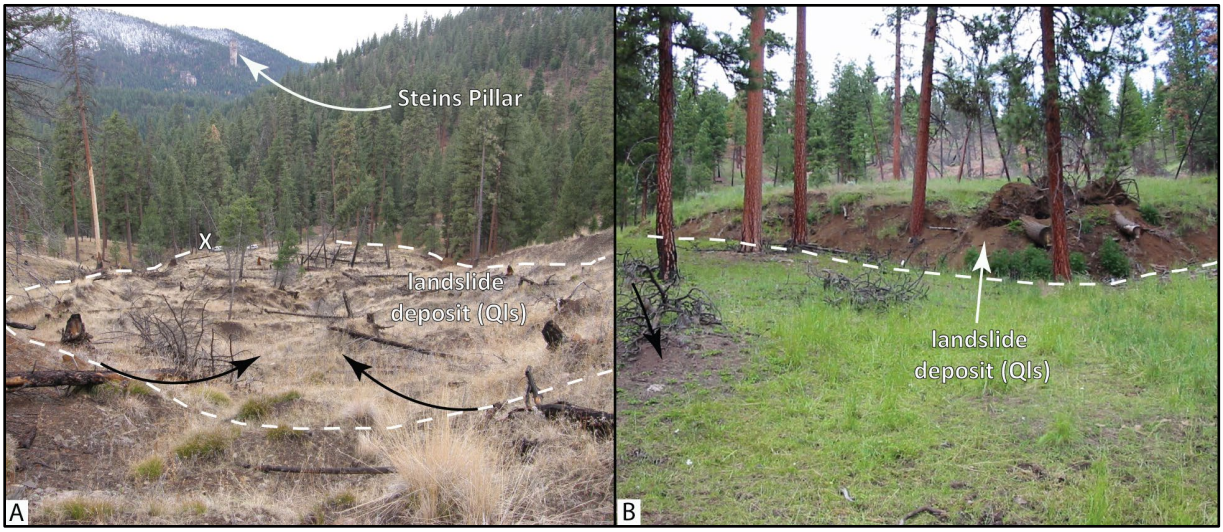

Figure 9-4. The Doe Creek earthflow as visible in a high resolution 1-m lidar DEM. Dashed red line is the mapped extent of the active landslide deposit. Dashed white line is the upper extent of the head scarp area. Yellow dashed arrow indicates direction of landslide movement.

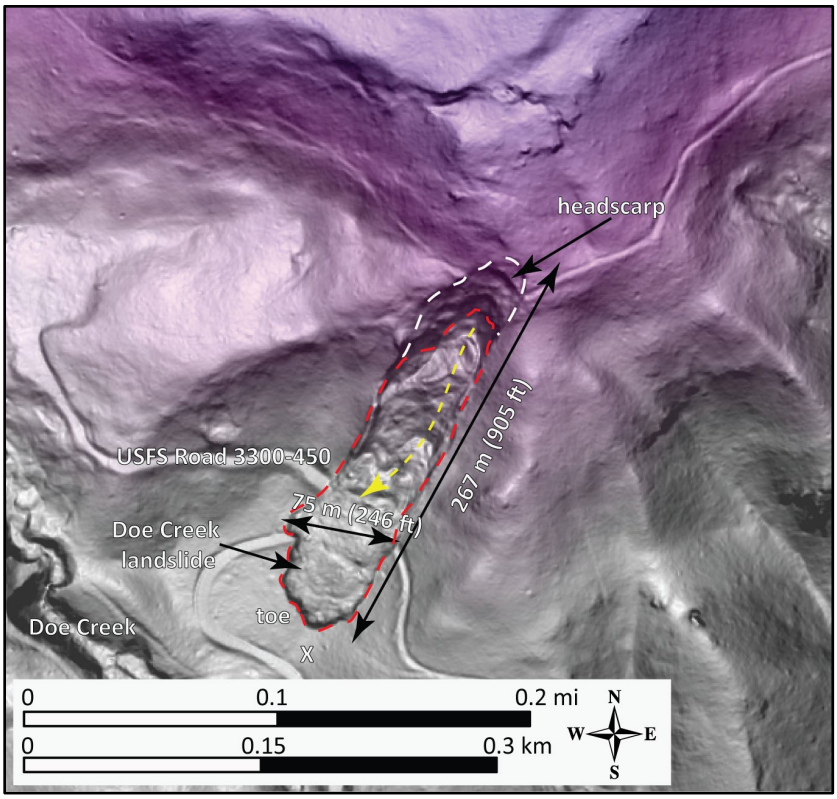

9.1.3 Simple and colluvial Landslides

Simple landslides and rockfall (**Qls**) are typically small and occur where cliffs and gravel terraces have been over steepened due to construction or stream erosion (plate). These types of deposits typically represent singular, isolated events. Deposits usually cover areas less than 200 m^2 (2,152 ft^2). Many other slopes in the lower Crooked River basin are mantled by unstable colluvial wedges of soil and rock. These deposits, mapped as colluvium (**Qc**), typically form when weathered rock particles, ranging in size from clay to boulders, accumulate along a hillside contact (plate). When the mass of the accumulated material reaches a critical size, a triggering event such as heavy rainfall or earthquake may initiate the rapid down slope movement of this mass. Areas denuded by fire or other human vegetative removal can especially be at risk for simple landslides and remobilization of colluvial wedges.

9.2 Earthquake Hazards

9.2.1 Introduction

Numerous studies in the Pacific Northwest have found evidence indicating the recent occurrence of large, regional earthquakes and the possibility of significant local events (e.g., Atwater, 1987; McCaffrey and Goldfinger, 1995; Atwater and Hemphill-Haley, 1997; Clague, 1997; McCaffrey and others, 2007, Frankel and Petersen, 2008). There has been very little in the way of historic seismic activity in the lower Crooked River basin (Niewendorp and Neuhaus, 2003), with much of the recorded seismicity concentrated around local quarry sites. Historic (1896 to 2008) earthquake epicenters in the area show events generally

ranging in magnitude from 1 to 2.9 (Richter scale) along the western edge of the lower Crooked River basin (Niewendorp and Neuhaus, 2003). Communities in the lower Crooked River basin may be at risk from three different types of earthquakes: 1) Cascadia subduction zone earthquakes; 2) crustal fault earthquakes; and 3) deeper intraplate earthquakes occurring within the region (**Figure 9-5**).

Ground shaking, soil liquefaction, landslides, surface ruptures, and seiches are all possible causes of damage during an earthquake in the lower Crooked River basin. The damaging effects of earthquakes can be enhanced by proximity to epicenters, amplification of shaking in soft soils, by liquefaction, or by induced landslides. Relative hazard maps that incorporate all of these hazards into single risk categories have not been yet compiled for the lower Crooked River basin. Liquefaction hazards occur where the shaking of a water-saturated soil causes its material properties to change from a solid to a liquid. Soils that liquefy tend to be loose, granular soils that are saturated with water. Unsaturated soils will not liquefy but may settle. Moderate liquefaction susceptibility may exist in areas underlain by Quaternary surficial units. Areas of modern fill and construction material (**Qf**) may also have a high liquefaction susceptibility. Where bedrock (volcanic rock or lithified sedimentary rock) is exposed at the surface, such as in uplands or in the bottoms of incised drainages, the liquefaction hazard is negligible. Earthquake-induced landslide hazard in the area is probably generally low. Cliffs underlain by basalt along the length of the Crooked River canyon pose a moderate hazard. A high hazard for earthquake-induced landslide and rockfall is expected in areas with over steepened bluffs and in areas of preexisting landslide deposits (plate).

9.2.2 Subduction zone earthquakes

Subduction zone earthquakes occur where one crustal plate overrides an adjacent plate along a dipping interface, commonly known as a subduction zone (**Figure 9-5**). The lower Crooked River basin area sits ~300 km (186 mi) east of the Cascadia subduction zone, which marks the plate boundary between the North American plate on the east and the underlying, smaller Juan de Fuca plate on the west (**Figure 5-1**, **Figure 9-5**). Beneath the Earth's surface, this zone extends eastward from the base of the continental slope, beneath western Oregon, and as the lower plate continues to slide deeper into the Earth, it drives the processes that result in the eruption of volcanoes in the Cascade Range (**Figure 5-1**). The Cascadia subduction zone is generally considered to be at high risk from large subduction zone earthquakes. Goldfinger and others (2003) and Nelson and others (2006) indicated evidence of a number of great Cascadia subduction zone earthquakes, with the most recent occurring in 1700 A.D. (Satake and others, 1996). The Cascadia subduction zone is thought to produce earthquakes as a large as M9.0 every 400 to 500 years (Frankel and Petersen, 2008). More recent work by Goldfinger and others (2012) indicated more frequent intervals of ~240 years, with a 10 to 15 percent chance of a Cascadia event in the next 50 years. Priest and others (2009) reported that at least 20 great subduction zone earthquakes have occurred on the Cascadia subduction zone during the last ~10,000 years. These events, with magnitudes in the range of M8.0 to M9.0 would have caused long duration, moderately strong shaking throughout much of the region, with intensity decreasing eastward from the epicenter. Site effects from such an event, including earthquake induced liquefaction, landsliding, and amplification of shaking by low-velocity surficial deposits could dramatically enhance damage in the area. The 2018 USGS National Seismic Hazard Model for the conterminous United States estimates that the peak ground acceleration for the area with a 2 percent chance of exceedance in 50 years is 0.14 to 0.20 g (Rukstales and Petersen, 2019; https://www.sciencebase.gov/catalog/item/5d5597d0e4b01d82ce8e3ff1). The probabilistic ground shaking is dominated by local crustal sources.

Figure 9-5. Schematic diagram showing tectonic setting of the Pacific Northwest and idealized locations of the four earthquake types described in the text. Modified from Madin and Wang (2000).

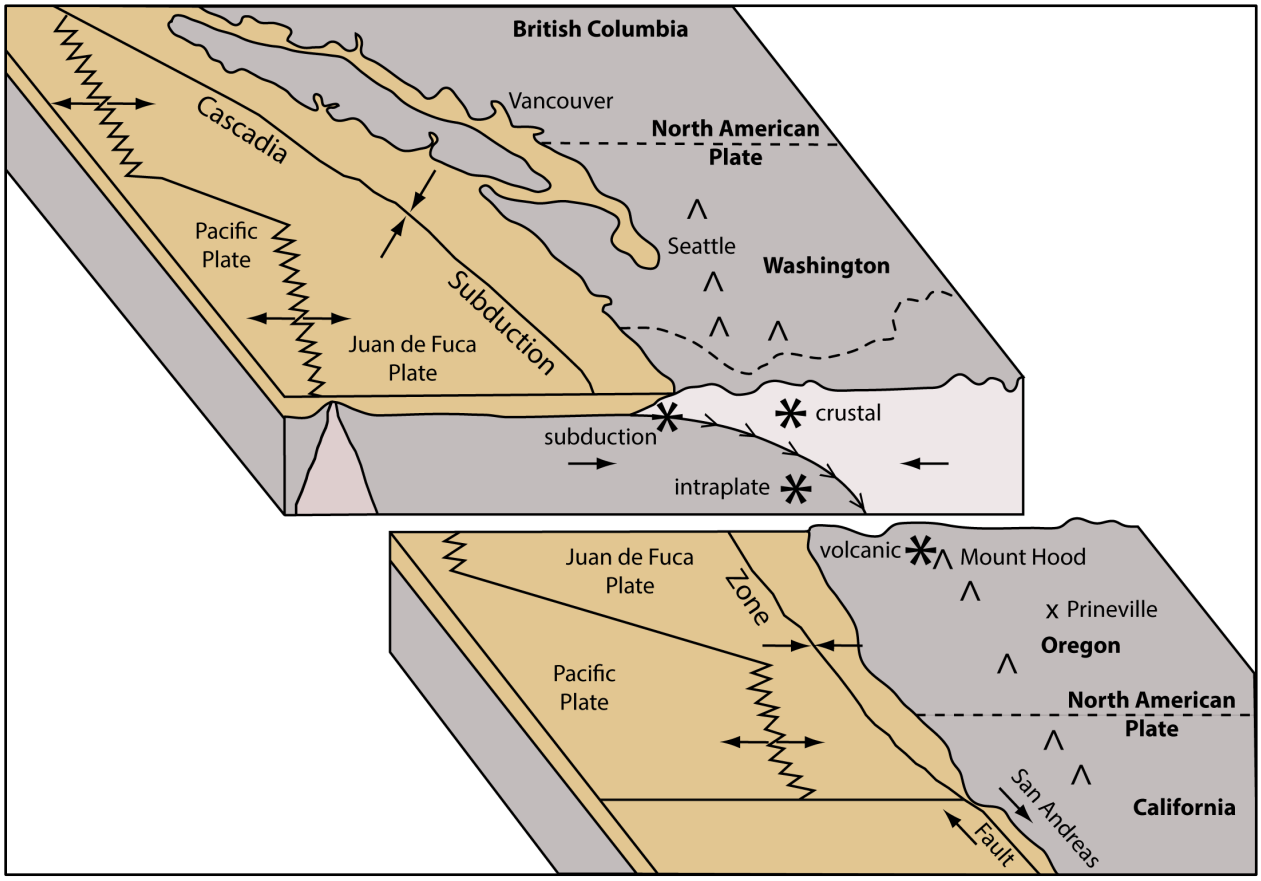

9.2.3 Crustal earthquakes

Crustal earthquakes result from shallow sources within the North American plate at locations above the Cascadia subduction zone (**Figure 9-5**). Epicenters are located at depths of 10 to 20 km (6 to 12 mi) below land surface, much shallower than subduction zone earthquakes. Most of the historic epicenters for earthquakes recorded in the lower Crooked River basin appear to have a crustal origin and are typically spatially associated with rock quarries. Their origin is therefore inferred to be surficial explosive detonations related to work within quarry sites.

9.2.4 Intraplate earthquakes

The lower Crooked River basin area may also experience site effects from deeper intraplate earthquakes, which result from movement within the underlying Juan De Fuca plate (**Figure 9-5**). These earthquakes could occur beneath much of the Pacific Northwest at depths of 40 to 60 km (25 to 37 mi). The M6.7 earthquakes that caused significant damage in the Puget Sound region in 1949 and 1965 are considered to have been deep intraplate earthquakes.

9.3 Volcanic Hazards

Central Oregon is a complex volcanic terrane and volcanic activity within the region can be expected in the future. Unlike other geologic hazards discussed in this report (e.g., earthquakes) which may occur over

several seconds to minutes, a volcanic episode can last days to decades and may include multiple syn- and inter-eruptive events. The City of Prineville in the central part of the lower Crooked River basin is located ~80 km [50 mi] east of the axis of the intermittently active volcanic zone along the Cascade volcanic arc, including the Three Sisters volcanic center (77 km [48 mi] west-southwest) and Mount Jefferson volcano (85 km [53 mi] northwest) (**Figure 5-1**, **Figure 5-2**). Newberry Volcano is located 72 km (45 mi) southwest of the city of Prineville (**Figure 1-1**). Volcanic hazard studies have been published by the USGS for major volcanoes in the region including the Three Sisters volcanic center (Scott and others, 1999), Mount Jefferson (Walder and others, 1999), and Newberry Volcano (Sherrod and others, 1997).

9.3.1 Tephra fall

Tephra (volcanic ash) generated by larger eruptions at Three Sisters, Mount Jefferson, or other nearby Cascade volcanoes like Crater Lake may fall on areas up to several hundred km downwind (**Figure 5-1**, **Figure 5-2**). Hazard probability zones reach farther east from the Cascade Range, because wind blows from west to east most of the time. On the basis of past tephra production in the Cascade Range, it is estimated that communities in the lower Crooked River basin have an annual probability of 1 in 5,000 for the accumulation of ≥1 cm (0.4 in) or more tephra from any of the major Cascade volcanoes. The annual probability of the accumulation of ≥10 cm (4 in) or more of tephra from any of the major Cascade volcanoes is 1 in 10,000 (Sherrod and others, 1997; Scott and others, 1999; Walder and others, 1999). The thickest Holocene tephra fall recognized in the nearby Bend area (47 km [29 mi] southwest) is ~30 cm (12 in) thick. This tephra was deposited downwind (northeast) from Mount Mazama during the cataclysmic eruption that created Crater Lake about 7,700 years ago (Scott and others, 1999). Hazards associated with tephra falls include tens of minutes or more of darkness, paint damage, clogging of engine filters with fine particles, short circuiting of electric transformers and power lines, and disruption of air traffic (e.g., Mount St. Helens eruptions, May 1980). Larger events may include the possibility of roof collapse of structures.

9.3.2 Lava flows

Basaltic lava flows erupted from the northern flanks of Newberry Volcano between 720 and 400 k.y.a advanced and covered a broad plain in the southwestern part of the lower Crooked River basin, reaching 8 km (5 mi) beyond Peter Skene Ogden State Park (**Figure 1-1**, **Figure 5-16**; plate). Renewed eruptive activity on the flanks of Newberry Volcano would probably include fissure vents, cinder cones, and several lava flows (Sherrod and others, 1997). Eruptive periods could range in duration from several weeks to a decade. Hazards associated with lava flow events include tephra falls proximal to vents, lava flows in more distal areas (probably ≥20 km (12.4 mi) from the vent based on topography, and disruption of local stream drainages. Lava flows damming or diverting streams and rivers can form lakes behind lava dams, submerging large areas upstream depending on topography and lava dam height.

The southwestern most part of the lower Crooked River basin, south of Shumway Lake in the upper part of Dry River is included in lava-flow hazard zone LB of Sherrod and others (1997). Lava-flow hazard zone LB includes areas on the lower flanks of Newberry that have relatively few flank vents and those areas downslope that are chiefly covered by large lava flows from vents farther upslope. The distribution of lava flows or site of future eruptions within the hazard zone cannot be predicted. Once eruptive activity begins, scientists can better define areas likely to be affected by approaching lava flows. Sherrod and others (1997) estimate the probability of lava flows erupting from the flanks of Newberry Volcano and inundating areas in lava-flow hazard zone LB at roughly 1 in 100,000 or less, on the basis of geologic mapping of past Newberry lava flows (Sherrod and others, 1997; Sherrod and others, 2004; plate).

9.4 Geochemical Hazards

Mineralized areas with elevated levels of elements such as arsenic and mercury in the lower Crooked River basin may need further evaluation for possible impacts on downstream water quality (Brooks, 1963; Brooks and Ramp, 1968). Assessment and mitigation strategies are needed to determine whether water quality problems can be attributed to point sources such as specific mine workings or to nonpoint sources of naturally weathering outcrops of mineralized rock (appendix). Small mine workings, including dumps, tunnels, and shafts in the basin may be potential point sources. Mineralized zones associated with both the Wildcat Mountain and Crooked River calderas are also possible nonpoint sources for mercury and arsenic (**Figure 5-5**, **Figure 5-12**; plate).

10.0 ACKNOWLEDGMENTS

Geologic mapping in the lower Crooked River basin is dedicated to the memory of our friend and colleague Howard Brooks (1929–2016) whose illustrious career with the Oregon Department of Geology and Mineral Industries spanned parts of five decades between 1957 and 1991. During that time Howard produced dozens of highly sought after and often cited publications, which laid the framework for modern geologic mapping and the understanding of mineralization in eastern Oregon.

Geologic mapping in the lower Crooked River basin was supported in part by grants from the STATEMAP component of the USGS National Cooperative Geologic Mapping Program (05HQAG0037, 06HQAG0027, G20AC00202), and by the Oregon Water Resources Department (OWRD) through Interagency Agreement DOGAMI IAA# DASPS-2542-16/OWRD IAA 16 047 (2016). Additional funds were provided by the State of Oregon through the Oregon Department of Geology and Mineral Industries. Financial support from the U.S. Forest Service Ochoco National Forest for geochemical and geochronological analyses is appreciated.

Geochemical analyses were prepared and analyzed by Dr. Stan Mertzman, Franklin and Marshall College, Lancaster, Pennsylvania, and Dr. Rick Conrey, Washington State University, Pullman, Washington (presently at Hamilton College, Clinton, New York). Radiometric age-date determinations were prepared and analyzed by Dr. John Huard at the College of Oceanic and Atmospheric Sciences, Oregon State University, Dr. Matt Heizler at the New Mexico Geochronological Research Laboratory, and by Dr. Joshua Schwartz at California State University Northridge.

Many colleagues have contributed to our knowledge of the geology of Central Oregon. We are particularly indebted to Karyn Patridge and Angela Seligman, whose graduate studies significantly advanced our understanding of the Wildcat and Crooked River calderas and their origins. Additional key insight came from conversations and data sharing with Paul Hammond, David Sherrod, Ken Lite, Marshall Gannett, Larry Chitwood, Bob Jensen, Julie Donnelly-Nolan, Martin Streck, Rick Conrey, John Wolff, Ilya Bindeman, Bruce Brody-Heine, Greg Retallack, Ted Fremd, and Ellen Bishop. The authors also acknowledge the support of many local residents who recognized the scientific and societal value of geologic mapping and who graciously permitted access to their private lands. Special thanks are extended to John and Lynne Breese of the Dixie Meadows Company, the Crooked River Watershed Council, and the USFS Ochoco National Forest.

Critical and insightful reviews by Marshall Gannett (USGS), Daniele McKay (OSU Cascades), David Sherrod (USGS), Clark Niewendorp (DOGAMI-retired), Carlie Azzopardi (DOGAMI), Matt Williams (DOGAMI), and Bob Houston (DOGAMI) greatly enriched the final manuscript, map plate, and

geodatabase. Geodatabase preparation and report editing by Carlie Azzopardi and Heather Herinckx and cartography of the map plate by Jon Franczyk are sincerely appreciated.

Judy and Dennis McClaughry merit distinguished recognition for a lifetime of steadfast support and encouragement of the geologic adventures of the first author. Together, they kindled a fire for scientific exploration and understanding of the natural world at an early age.

11.0 REFERENCES

Albright III, L.B., Woodburne, M.O., Fremd, T.J., Swisher, C.C., III, MacFadden, B.J., and Scott, G.R., 2008, Revised chronostratigraphy and biostratigraphy of the John Day Formation (Turtle Cove and Kimberly Members), Oregon, with implications for updated calibration of the Arikareean North American Land Mammal Age: The Journal of Geology, v. 116, p. 211–237, doi: 10.1086/587650. https://www.journals.uchicago.edu/doi/10.1086/587650, accessed March 12, 2021.

Allen, J.E., 1966, The Cascade Range volcano-tectonic depression of Oregon, *in* Benson, G.T., ed., Transactions of the Lunar Geological Field Conference, Bend, Oregon, August 1965: Oregon Department of Geology and Mineral Industries Open-File Report O-66-01, p. 21–23. https://www.oregongeology.org/pubs/ofr/O-66-01.pdf, accessed March 12, 2021.

Anderson, J.L., 1987, The structure and ages of deformation of a portion of the southwest Columbia Plateau, Washington and Oregon: Los Angeles, University of Southern California, Ph.D. dissertation, 272 p.

Appel, M., 2001, Alkaline and peraluminous intrusives in the Clarno Formation around Mitchell, Oregon: Ramifications on magma genesis and subduction tectonics: Corvallis, Oregon State University, M.S. thesis, 222 p. https://ir.library.oregonstate.edu/concern/graduate_thesis_or_dissertations/02870z62q?locale=en, accessed March 12, 2021.

Ashwill, M.S., 1983, Seven fossil floras in the rain shadow of the Cascade Mountains, Oregon: Oregon Geology, v. 45, p. 107–111. https://www.oregongeology.org/pubs/og/OGv58n06.pdf, accessed March 12, 2021.

Atwater, B.F., 1987, Evidence for great Holocene earthquakes along the outer coast of Washington State: Science, v. 236, p. 942–944. doi: 10.1126/science.236.4804.942. https://science.sciencemag.org/content/236/4804/942, accessed March 12, 2021.

Atwater, B.F., and Hemphill-Haley, E., 1997, Recurrence intervals for great earthquakes of the past 3,500 years at northeastern Willapa Bay, Washington: U.S. Geological Survey Professional Paper 1576, 108 p. https://pubs.er.usgs.gov/publication/pp1576, accessed March 12, 2021.

Aubin, W., 2000, Ignimbrites of the Deschutes Formation: a record of crustal melting and magma mixing: Pullman, Washington State University, M.S. thesis, 141 p.

Bailey, M.M., 1989, Revisions to the stratigraphic nomenclature of the Picture Gorge Basalt Subgroup, Columbia River Basalt Group *in* Reidel, S. P., and Hooper, P. R., eds., Volcanism and tectonism in the Columbia River Flood-Basalt Province: Geological Society of America Special Paper 239, p. 67–84. doi:10.1130/SPE239-p67. https://specialpapers.gsapubs.org/content/239/67.abstract, accessed March 12, 2021.

Baksi, A.K., 2013, Timing and duration of volcanism in the Columbia River Basalt Group: A review of existing radiometric data and new constraints on the age of the Steens through Wanapum Basalt extrusion, *in* Reidel, S.P., et al., eds., The Columbia River Flood Basalt Province: Geological Society of America Special Paper 497, p. 67–85. https://pubs.geoscienceworld.org/books/book/661/chapter/3807126/Timing-and-duration-of-volcanism-in-the-Columbia, accessed March 12, 2021.

Barry, T.L., Self, S., Kelley, S.P., Reidel, S., Hooper, P., and Widdowson, M., 2010, New $^{40}Ar/^{39}Ar$ dating of the Grande Ronde lavas, Columbia River Basalts, USA: Implications for duration of flood basalt eruption episodes: Lithos, v. 118, p. 213–222. https://www.sciencedirect.com/science/article/abs/pii/S0024493710000897, accessed March 12, 2021.

Barry, T.L., Kelley, S.P., Reidel, S.P., Camp, V.E., Self, S., Jarboe, N.A., Duncan, R.A., and Renne, P.R., 2013, Eruption chronology of the Columbia River Basalt Group, *in* Reidel, S.P., Camp, V.E., Martin, M.E., Ross, M.E., Wolff, J.A., Martin, B.S., Tolan, T.L., and Wells, R.E., eds., Geological Society of America Special Paper 497, p. 45–66. https://pubs.geoscienceworld.org/books/book/661/chapter/3807104/Eruption-chronology-of-the-Columbia-River-Basalt, accessed March 12, 2021.

Beeson, M.H., and Tolan, T.L., 1990, The Columbia River Basalt Group in the Cascade Range: A middle Miocene reference datum for structural analysis: Journal of Geophysical Research, v. 95, p. 19,547–19,559. doi: 10.1029/JB095iB12p19547. https://onlinelibrary.wiley.com/doi/10.1029/JB095iB12p19547/abstract, accessed March 12, 2021.

Bela, J.L., 1982, Geologic and neotectonic evaluation of north-central Oregon: The Dalles 1° × 2° quadrangle: Oregon Department of Geology and Mineral Industries Geologic Map 27, scale 1:250,000. https://www.oregongeology.org/pubs/gms/GMS-027.pdf, accessed March 12, 2021.

Bestland, E.A., 1995, Stratigraphy of the Turtle Cove Member of the John Day Formation at Sheep Rock: U.S. National Park Service Open-File Report, 14 p.

Bestland, E.A., and Retallack, G.J., 1994a, Geology and paleoenvironments of the Clarno Unit, John Day Fossil Beds National Monument, Oregon (1:7,300 scale): Final report, National Park Service contract CX-9000-1-10009, 241 p. https://irma.nps.gov/DataStore/DownloadFile/493483, accessed March 12, 2021.

Bestland, E.A., and Retallack, G.J., 1994b, Geology and paleoenvironments of the Painted Hills Unit, John Day Fossil Beds National Monument, Oregon: National Park Service contract CX-9000-1-10009, final report, scale 1:7,300.

Bestland, E.A., Hammond, P.E., Blackwell, D.L.S., Kays, M.A., Retallack, G.J., and Stimac, J.,1999, Geologic framework of the Clarno Unit, John Day Fossil Beds National Monument, Central Oregon: Oregon Geology, v. 61, p. 3–19. https://www.oregongeology.org/pubs/OG/OGv61n01.pdf, accessed March 12, 2021.

Bestland, E.A., Hammond, P.E., Blackwell, D.L.S., Kays, M.A., Retallack, G.J., and Stimac, J., 2002, Geologic framework of the Clarno Unit, John Day Fossil Beds National Monument, Central Oregon: Oregon Department of Geology and Mineral Industries Open-File Report O-02-03, 39 p. https://www.oregongeology.org/pubs/ofr/O-02-03.pdf, accessed March 12, 2021.

Bestland, E.A., Forbes, M.S., Krull, E.S., Retallack, G.J., and Fremd, T., 2008, Stratigraphy, paleopedology, and geochemistry of the middle Miocene Mascall Formation (type area, central Oregon, USA): PaleoBios, v. 28, no. 2, p. 41. https://cpbuse1.wpmucdn.com/blogs.uoregon.edu/dist/d/3735/files/2013/07/paleobios2008bestland_et_al-o6r2ga.pdf, accessed March 12, 2021.

Bingert, N.J., 1984, Geology of the northeast one-quarter of the Prineville Quadrangle, North-Central Oregon: Corvallis, Oregon State University, M.S. thesis, 141 p. https://ir.library.oregonstate.edu/xmlui/handle/1957/21920, accessed March 12, 2021.

Bishop, E.M., and Smith, G.A., 1990, A field guide to the geology of Cove Palisades State Park and Deschutes Basin in central Oregon: Oregon Geology, v. 52, no. 1, p. 3–12. https://www.oregongeology.org/pubs/OG/OGv52n01.pdf, accessed April 22, 2021.

Black, L.P., Kamo, S.L., Allen, C.M., Aleinikoff, J.N., Davis, D.W., Korsch, R.J., and Foudoulis, C., 2003, TEMORA 1: a new zircon standard for Phanerozoic U-Pb geochronology. Chemical Geology, v. 2000, p. 155–170.

Boyd, F.R., and Mertzman, S.A., 1987, Composition of structure of the Kaapvaal lithosphere, southern Africa: *in* Mysen, B.O., ed., Magmatic processes: physicochemical principles: The Geochemical Society, Special Publication 1, p. 13–24. https://www.geochemsoc.org/files/8214/1258/3689/SP-1_013-024_Boyd.pdf, accessed March 12, 2021.

Bromley, S.A., 2011, Evolution and inheritance of Cascadia sub-arc mantle reservoirs: Corvallis, Oregon State University, M.S. thesis, 210 p. https://ir.library.oregonstate.edu/concern/graduate_thesis_or_dissertations/gt54kq90n, accessed March 12, 2021.

Brooks, H.C., 1963, Quicksilver in Oregon: Oregon Department of Geology and Mineral Industries Bulletin 55, 223 p. https://www.oregongeology.org/pubs/B/B-055.pdf, accessed March 12, 2021.

Brooks, H.C., and Ramp, L., 1968, Gold and silver in Oregon: Oregon Department of Geology and Mineral Industries Bulletin 61, 337 p. https://www.oregongeology.org/pubs/B/B-061.pdf, accessed March 12, 2021.

Brown, C.E., and Thayer, T.P., 1966, Geologic map of the Canyon City quadrangle, northeastern Oregon: U.S. Geological Survey Miscellaneous Geologic Investigations Map I-447, scale 1:250,000. https://ngmdb.usgs.gov/Prodesc/proddesc_1302.htm, accessed March 12, 2021.

Brown, D.E., Black, G.L., McLean, G.D., and Petros, J.R., 1980, Preliminary geology and geothermal resource potential of the Powell Buttes area, Oregon: Oregon Department of Geology and Mineral Industries Open-File Report O-80-8, 117 p. https://www.oregongeology.org/pubs/ofr/O-80-08.pdf, accessed March 12, 2021.

Brown, E.A., 2017, Rhyolite petrogenesis at Tower Mountain caldera, OR: Portland, Oreg., Portland State University, M.S. thesis, 313 p. https://doi.org/10.15760/etd.5881, accessed March 12, 2021.

Butler, R.F., 1992, Origins of natural remanent magnetism, Chap. 3 *in* Butler, R.F., ed., Paleomagnetism: magnetic domains to geologic terranes: Blackwell Scientific Publications, p. 31–63. https://www.geo.arizona.edu/Paleomag/chap03.pdf, accessed June 7, 2021.

Cahoon, E.B., Streck, M.J., Koppers, A.A.P., and Miggins, D.P., 2020, Reshuffling the Columbia River Basalt chronology—Picture Gorge Basalt, the earliest- and longest-erupting formation: Geology, v. 48, p. 348–352. https://doi.org/10.1130/G47122.1, accessed March 12, 2021.

Cande, S.C., and Kent, D.V., 1992, A new geomagnetic polarity time scale for the Late Cretaceous and Cenozoic: Journal of Geophysical Research, v. 97, no. B10, 13,917–13,951. https://doi.org/10.1029/92JB01202, accessed March 12, 2021.

Cannon, D.M., 1985, The stratigraphy, geochemistry, and mineralogy of two ash-flow tuffs in the Deschutes Formation, central Oregon: Corvallis, Oregon State University, M.S. thesis, 142 p., https://ir.library.oregonstate.edu/concern/graduate_thesis_or_dissertations/k643b566p?locale=en, accessed March 12, 2021.

Carter, B.H., 1998, Safety of dams modifications to Ochoco Dam Crooked River Project, Oregon, *in* Schultz, R. A., and Siddharthan, R., eds., Proceedings of the 33rd Symposium of Engineering Geology and Geotechnical Engineering, University of Nevada, Reno. https://scholarsmine.mst.edu/cgi/viewcontent.cgi?article=1786&context=icchge, accessed March 12, 2021.

Champion, A.J., 1938, History of the Mayflower mine: Prineville, Oreg., Central Oregonian, October 27, 1938. Available at: Oregon Historical Mining Information website, https://www.oregongeology.org/milo/index.htm, accessed March 12, 2021.

Champion, D.E., J. Donnelly-Nolan, J.M., and Lanphere, M.A., 2002, Mapping Newberry Volcano's extensive north flank basalts: Geological Society of America Abstracts with Programs, v. 34, https://gsa.confex.com/gsa/2002CD/webprogram/Paper34405.html, accessed March 12, 2021.

Champion, D.E., J. Donnelly-Nolan, J.M., Lanphere, M.A., and Ramsey, D.W., 2004, Magnetic excursion recorded in basalt at Newberry Volcano, central Oregon: Eos (Transactions, American Geophysical Union), v. 85, no. 47, abstract GP43B-0861.

Chang, Z., Vervoort, J.D., McClelland, W.C., and Knaack, C., 2006, U-Pb dating of zircon by LA-ICP-MS: Geochemistry, Geophysics, Geosystems, v. 7, no. 5, p. 1–14. doi: 10.1029/2005GC001100. https://onlinelibrary.wiley.com/doi/10.1029/2005GC001100/full, accessed March 12, 2021.

Clague, J.J., 1997, Evidence for large earthquakes at the Cascadia subduction zone: Reviews in Geophysics, v. 35, p. 439–460. doi: 8755-1209/97/97R G-00222 https://onlinelibrary.wiley.com/doi/10.1029/97RG00222/epdf, accessed March 12, 2021.

Cohen, K.M., Finney, S.C., Gibbard, P.L., and Fan, J.-X., 2013 (updated 2015), The ICS International Chronostratigraphic Chart: Episodes 36, p. 199–204. https://stratigraphy.org/ICSchart/Cohen2013_Episodes.pdf, accessed March 12, 2021.

Conrey, R.C., 1985, Volcanic stratigraphy of the Deschutes Formation, Green Ridge to Fly Creek, north-central Oregon: Corvallis, Oregon State University, M.S. thesis, 328 p. https://ir.library.oregonstate.edu/xmlui/handle/1957/8406, accessed March 12, 2021.

Conrey, R.M., Sherrod, D.R., Hooper, P.R., Swanson, D.A., 1997, Diverse primitive magmas in the Cascade Arc, northern Oregon and southern Washington: The Canadian Mineralogist, v. 35, p. 367–396. https://pubs.geoscienceworld.org/canmin/article-abstract/35/2/367/12854/Diverse-primitive-magmas-in-the-Cascade-Arc?redirectedFrom=fulltext, accessed March 12, 2021.

Conrey, R.M., Taylor, E.M., Donnelly-Nolan, J.M., and Sherrod, D.R., 2002, North-central Oregon Cascades: Exploring petrologic and tectonic intimacy in a propagating intra-arc rift, *in* Moore, G. W., ed., Field guide to geologic processes in Cascadia: Oregon Department of Geology and Mineral Industries Special Paper 36, p. 47–90. https://www.oregongeology.org/pubs/sp/p-SP.htm, accessed March 12, 2021.

Conrey, R.M., Sherrod, D.R., and McClaughry, J.D., 2019, Reconnaissance summary of High Cascades graben structures in central and northern Oregon: Geological Society of America Abstracts with Programs, vol. 51, no. 4. https://gsa.confex.com/gsa/2019CD/webprogram/Paper329797.html, accessed March 12, 2021.

Cox, K. G., Bell, J. D., and Pankhurst, R. J., 1979, The interpretation of igneous rocks: London, George Allen and Unwin, 450 p.

Davenport, R.E., 1971, geology of the Rattlesnake and older ignimbrites in the Paulina basin and adjacent area, central Oregon: Corvallis, Oregon State University, Ph.D. dissertation, 132 p. https://ir.library.oregonstate.edu/xmlui/handle/1957/21967, accessed March 12, 2021.

Dicken, S.N., 1965, Oregon geography: the people, the place, and the time, 4th ed: Ann Arbor, Mich., Edwards Brothers, 147 p.

Dill, T.E., 1992, Stratigraphy of the Neogene volcanic rocks along the lower Metolius River, Jefferson County, central Oregon: Corvallis, Oregon State University, M.S. thesis, 343 p. https://ir.library.oregonstate.edu/xmlui/handle/1957/20681, accessed March 12, 2021.

du Bray, E.A., and John, D.A., 2011, Petrologic, tectonic, and metallogenic evolution of the Ancestral Cascades magmatic arc, Washington, Oregon, and northern California: Geosphere, v. 7, no. 5, p. 1102–1133. https://pubs.geoscienceworld.org/gsa/geosphere/article/7/5/1102/132471/Petrologic-tectonic-and-metallogenic-evolution-of, accessed March 12, 2021.

Duda, C.J.M., McClaughry, J.D., Houston, R.A., and Niewendorp, C.A., 2018, Lidar and Structure from Motion-enhanced geologic mapping, examples from Oregon, *in* Thorleifson, L. H., ed., 2018, Geologic Mapping Forum 2018 Abstracts: Minnesota Geological Survey Open File Report OFR-18-1, 107 p. https://conservancy.umn.edu/handle/11299/194852, accessed March 12, 2021.

Duda, C.J.M., McClaughry, J.D., and Madin, I.P., 2019, Building the modern geologic map in Oregon: a multi-faceted field- and technology-based approach: Geological Society of America Abstracts with Programs. v. 51, no. 4. https://gsa.confex.com/gsa/2019CD/meetingapp.cgi/Paper/329552, accessed March 12, 2021.

Dunbar, E., and Perkins, R., 2015, Hydrostratigraphy of the Prineville Municipal Airport wells field: report to the City of Prineville, 83 p.

Duncan, R.A. and Keller, R.A., 2004, Radiometric ages for basement rocks from the Emperor Seamounts, ODP Leg 197: Geochemistry, Geophysics, Geosystems, v. 5. p. 1–13. https://agupubs.onlinelibrary.wiley.com/doi/full/10.1029/2004GC000704, accessed March 12, 2021.

Enlows, H.E., and Parker, D.J., 1972, Geochronology of the Clarno igneous activity in the Mitchell quadrangle, Wheeler County, Oregon: Ore Bin, v. 34, p. 104–110. https://www.oregongeology.org/pubs/OG/OBv34n06.pdf, accessed March 12, 2021.

Evans, S.H., and Brown, F.H., 1981, Summary of potassium/argon dating —1981: U.S. Department of Energy, Division of Geothermal Energy DE-AC07-80-ID-12079-45, 29 p. https://digital.library.unt.edu/ark:/67531/metadc1067283/, accessed March 12, 2021.

Evernden, J.F., and James, G.T., 1964, Potassium-argon dates and the Tertiary floras of North America: American Journal of Science, v. 262, p. 145–198. https://www.ajsonline.org/content/262/8/945, accessed March 12, 2021.

Farooqui, S.M., Beaulieu, J.D., Bunker, R.C., Stensland, D.E., and Thomas, R.E., 1981, Dalles Group: Neogene formations overlying the Columbia River Basalt Group in north-central Oregon: Oregon Geology, v. 43, no. 10, p. 131–140. https://www.oregongeology.org/pubs/OG/OGv43n10.pdf, accessed March 12, 2021.

Ferns, M.L., and McClaughry, J.D., 2006a, Preliminary geologic map of the Houston Lake 7.5′ quadrangle, Crook County, Oregon: Oregon Department of Geology and Mineral Industries Open-File Report O-06-21, scale 1:24,000. https://www.oregongeology.org/pubs/ofr/O-06-21.zip, accessed March 12, 2021.

Ferns, M.L., and McClaughry, J.D., 2006b, Preliminary geologic map of the Powell Buttes 7.5′ quadrangle, Crook County, Oregon: Oregon Department of Geology and Mineral Industries Open-File Report O-06-24, scale 1:24,000. https://www.oregongeology.org/pubs/ofr/O-06-24.zip, accessed March 12, 2021.

Ferns, M.L., and McClaughry, J.D., 2007, Preliminary geologic map of the Hensley Butte and Salt Butte 7.5′ quadrangles, Crook County, Oregon, Oregon Department of Geology and Mineral Industries Open-File Report O-07-11, scale 1:24,000. https://www.oregongeology.org/pubs/ofr/O-07-11.pdf, accessed March 12, 2021.

Ferns, M.L., and McClaughry, J.D., 2013, Stratigraphy and volcanic evolution of the middle Miocene La Grande—Owyhee eruptive axis in eastern Oregon, *in* Reidel, S.P., Camp, V., Ross, M.E., Wolff, J.A., Martin, B.E., Tolan, T.L., and Wells, R.E., eds., The Columbia River Flood Basalt Province: Geological Society of America Special Paper 497, p. 401–427. https://specialpapers.gsapubs.org/content/497/401.abstract, accessed March 12, 2021.

Ferns, M.L., Stensland, D.L., and Smith, G.A., 1996, Geologic map of the Steelhead Falls quadrangle, Deschutes and Jefferson counties, Oregon: Oregon Department of Geology and Mineral Industries Geologic Map 101, 52 p., scale 1:24,000. https://www.oregongeology.org/pubs/gms/GMS-101.zip, accessed March 12, 2021.

Ferns, M.L., Streck, M.J., and McClaughry, J.D., 2017, Field-trip guide to Columbia River flood basalts, associated rhyolites, and diverse post-plume volcanism in eastern Oregon: U.S. Geological Survey Scientific Investigations Report 2017–5022–O, 71 p. https://doi.org/10.3133/sir20175022O, accessed March 12, 2021.

Fiebelkorn, R.B., Walker, G.W., MacLeod, N.S., McKee, E.H., and Smith, J.G., 1982, Index to K-Ar age determinations for the state of Oregon: U.S. Geological Survey Open File Report 82-596, 42 p., 1 pl. https://doi.org/10.3133/ofr82596, accessed June 7, 2021.

Fiebelkorn, R.B., Walker, G.W., MacLeod, N.S., McKee, E.H., and Smith, J.G., 1983, Index to K-Ar age determinations for the state of Oregon: Isochron/West, no. 37, p. 3–60. https://geoinfo.nmt.edu/publications/periodicals/isochronwest/37/iw_v37_p03.pdf, accessed June 7, 2021.

Fisher, R.V., 1967, Early Tertiary deformation in north-central Oregon: American Association of Petroleum Geologists Bulletin, v. 51, no. 1, p. 111–123. https://doi.org/10.1306/5D25B797-16C1-11D7-8645000102C1865D, accessed June 7, 2021.

Fisher, R.V., and Rensberger, J.M., 1972, Physical stratigraphy of the John Day Formation, central Oregon: California University Publications in Geological Sciences, v. 101, p. 1–45.

Franczyk, J.J., Madin, I.P., Duda, C.J.M., and McClaughry, J.D., 2020, Oregon geologic data compilation, release 7 [OGDC-7] (statewide): Oregon Department of Geology and Mineral Industries Digital Data Series OGDC-7, Esri™ geodatabase. https://www.oregongeology.org/pubs/dds/p-OGDC-7.htm, accessed March 12, 2021.

Frankel, A.D., and Petersen, M.D., 2008, Cascadia Subduction Zone, Appendix L, *in* the Uniform California Earthquake Rupture Forecast, version 2 (UCERF2): U.S. Geological Survey Open-File Report 2007-1437L and California Geological Survey Special Report 203L, 7 p. https://pubs.usgs.gov/of/2007/1437/of2007-1437_text.pdf, accessed March 12, 2021.

Freed, Z., Aldous, A., and Gannett, M.W., 2019, Landscape controls of the distribution and ecohydrology of central Oregon springs: Ecohydrology, v. 12, no. 2, p. 1–16. https://pubs.er.usgs.gov/publication/70201866, accessed March 12, 2021.

Gannett, M.W., and Lite, K.E., Jr., 2004, Simulation of regional groundwater flow in the upper Deschutes Basin, Oregon: U.S. Geological Survey Water Resources Investigation Report 03-4195, 84 https://pubs.er.usgs.gov/publication/wri034195, accessed March 12, 2021.

Gannett, M.W., Lite, K.E., Jr., Morgan, D.S., and Collins, C.A., 2001, Ground-water hydrology of the upper Deschutes Basin, Oregon: U.S. Geological Survey Water Resources Investigation Report 00-4162, 77 p. https://pubs.usgs.gov/wri/wri004162, accessed March 12, 2021.

Gaylord, D.R., McClaughry, J.D., Felt, K.J., Ferns, M.L., Spall, B.N., and Cahoon, E.B., 2015, Stratigraphic and geochronologic confirmation of the middle Eocene Clarno Formation in NE Oregon: Geological Society of America Abstracts with Programs v. 47, no. 4, p. 56. https://gsa.confex.com/gsa/2015CD/webprogram/Paper254966.html, accessed March 12, 2021.

Geological Society of America Rock-Color Chart Committee, 1991, Rock color chart, 7th printing.

Gillespie, M.R., and Styles, M.T., 1999, BGS rock classification scheme, v. 1, Classification of igneous rocks: British Geological Survey Research Report, 2nd ed., RR99-06, 52 p. https://nora.nerc.ac.uk/id/eprint/3223/1/RR99006.pdf, accessed March 12, 2021.

Gilluly, J.E., Reed, J.C., and Park, C.F., Jr., 1933, Some mining districts of eastern Oregon: U.S. Geological Survey Bulletin 846-A, 140 p. https://pubs.usgs.gov/bul/0846a/report.pdf, accessed March 12, 2021.

Goldfinger, C., Nelson, C. H., Johnson, J.E., and the Shipboard Scientific Party, 2003, Deep-water turbidites as Holocene earthquake proxies: The Cascadia subduction zone and Northern San Andreas Fault systems: Annuals of Geophysics, v. 46, no. 5, p. 1169–1194. https://www.annalsofgeophysics.eu/index.php/annals/article/view/3452, accessed March 12, 2021.

Goldfinger, C., Nelson, C.H., Morey, A.E., Johnson, J.E., Patton, J.R., Karabanov, E., Gutiérrez-Pastor, J., Eriksson, A.T., Gràcia, E., Dunhill, G., Enkin, R.J., Dallimore, A., and Vallier, T., 2012, Turbidite event history—methods and implications for Holocene paleoseismicity of the Cascadia subduction zone: U.S. Geological Survey Professional Paper 1661–F, 170 p. https://pubs.usgs.gov/pp/pp1661f/, accessed March 12, 2021.

Gradstein, F.M., Ogg, J.G., and Smith, A.G., 2004, A geologic time scale 2004, Cambridge University Press, 589 p.

Graham, J.P., 2014, John Day Fossil Beds National Monument: Geologic resources inventory report: Fort Collins, Colo., National Park Service, Natural Resource Report NPS/NRSS/GRD/NRR—2014/846. http://npshistory.com/publications/joda/nrr-2014-846.pdf, accessed March 12, 2021.

Gray, J.J., and Baxter, G., 1986, A reinterpretation of the Gray Butte limestone and arenite exposure as a hydrothermally-derived calcite vein and pebble dike: Oregon Geology, v. 48, no. 4, p. 45–46. https://www.oregongeology.org/pubs/OG/OGv48n04.pdf, accessed March 12, 2021.

Gray, J.J., Geitgey, R.P., and Baxter, G.L., 1989, Bentonite in Oregon: occurrences, analyses, and economic potential: Oregon Department of Geology and Mineral Industries Special Paper 20, 28 p., 1 pl., scale 1:500,000. https://www.oregongeology.org/pubs/sp/SP-20.pdf, accessed March 12, 2021.

Hallsworth, C.R., and Knox, R.W.O'B., 1999, BGS rock classification scheme, v. 3, Classification of sediments and sedimentary rocks: Keyworth, U.K., British Geological Survey Research Report RR 99-03, 44 p. https://nora.nerc.ac.uk/3227/1/RR99003.pdf, accessed March 12, 2021.

Hayman, G. A., 1983, Geology of a part of the Eagle Butte and Gateway quadrangles east of the Deschutes River, Jefferson County, Oregon: Corvallis, Oregon State University, M.S. thesis, 111 p. https://ir.library.oregonstate.edu/concern/graduate_thesis_or_dissertations/6108vd82n, accessed March 12, 2021.

Hodge, E.T., 1942, Geology of north-central Oregon: Corvallis, Oregon, Oregon State College Monograph, Studies in Geology No. 3.

Hooper, P.R., Steele, W.K., Conrey, R.M., Smith, G.A., Anderson, J.L., Bailey, D.G., Beeson, M.H., Tolan, T.L., and Urbanczyk, K.M., 1993, The Prineville basalt, north-central Oregon: Oregon Geology, v. 5, p. 3–12. https://www.oregongeology.org/pubs/OG/OGv55n01.pdf, accessed March 12, 2021.

Hunt, R.M., and Stepleton, E., 2004, Geology and paleontology of the upper John Day beds, John Day River Valley, Oregon: lithostratigraphic and biochronologic revision in the Haystack Valley and Kimberly areas (Kimberly and Mt. Misery quadrangles): Bulletin of the American Museum Natural History, v. 282, p. 1–90. https://core.ac.uk/download/pdf/18223015.pdf, accessed March 12, 2021.

Iademarco, M.J., 2009, Volcanism and faulting along the northern margin of Oregon's High Lava Plains: Hampton Butte to Dry Mountain: Corvallis, Oregon State University, M.S. thesis, 141 p. https://ir.library.oregonstate.edu/xmlui/handle/1957/12620, accessed March 12, 2021.

Iademarco, M.J., and Grunder, A., 2012, Hampton Butte, a 30-Ma rhyodacite basement high bounding the subsiding Miocene to Pliocene High Lava Plains of Oregon: American Geophysical Union, Fall Meeting 2012, abstract id. V33B-2876. https://ui.adsabs.harvard.edu/abs/2012AGUFM.V33B2876I/abstract, accessed March 12, 2021.

Jay, J.B., 1982, The geology and stratigraphy of the Tertiary volcanic and volcaniclastic rocks, with special emphasis on the Deschutes Formation, from Lake Simtustus to Madras in central Oregon: Corvallis, Oregon State University, M.S. thesis, 119 p. https://ir.library.oregonstate.edu/concern/parent/tx31qp34q/graduate_thesis_or_dissertations/6395wc84t, accessed March 12, 2021.

Jensen, R.A., J. Donnelly-Nolan, J.M., and McKay, D., 2009, A field guide to Newberry Volcano, *in* O'Connor, J.E., Dorsey, R.J., and Madin, I.P., eds., Volcanoes to vineyards: Geologic field trips through the dynamic landscape of the Pacific Northwest: Geological Society of America Field Guide 15, p. 53–79, doi: 10.1130/2009.fl d015(03). https://10.0.4.106/2009.fld015(03), accessed March 12, 2021.

Johnson, A.K., 2011, Dextral shear and north-directed crustal shortening defines the transition between extensional and contractional provinces in north-central Oregon: Corvallis, Oregon State University, M.S. thesis, 77 p., 3 pl., scale 1:24,000. https://ir.library.oregonstate.edu/xmlui/handle/1957/20928, accessed March 12, 2021.

Johnson, D.M., Hooper, P.R., and Conrey, R.M., 1999, XRF analysis of rocks and minerals for major and trace elements on a single low dilution Li-tetraborate fused bead: Advances in X-ray Analysis, v. 41, p. 843–867. https://s3.wp.wsu.edu/uploads/sites/2191/2017/06/Johnson-Hooper-and-Conrey.pdf, accessed March 12, 2021.

Jordan, B.T., Grunder, A.L., Duncan, R.A., and Deino, A.L., 2004, Geochronology of age-progressive volcanism of the Oregon High Lava Plains: implications for the plume interpretation of Yellowstone: Journal of Geophysical Research, v. 109, no. B10, B10202, 19 p. https://doi.org/10.1029/2003JB002776, accessed March 12, 2021.

Kasbohm, J., and Schoene, B., 2018, Rapid eruption of the Columbia River flood basalt and correlation with mid-Miocene climate optimum; Science Advances v. 4, no. 9. https://advances.sciencemag.org/content/4/9/eaat8223, accessed March 12, 2021.

Koppers, A., 2002, ArArCALC-software for $^{40}Ar/^{39}Ar$ age calculations: Computers and Geosciences, v. 28, no. 5, p. 605-619. https://earthref.org/ArArCALC/, accessed March 12, 2021.

Koppers, A., Staudigel, H., and Duncan, R., 2003, High-resolution $^{40}Ar/^{39}Ar$ dating of the oldest oceanic basement basalts in the western Pacific basin: Geochemistry, Geophysics, Geosystems, v. 4. https://onlinelibrary.wiley.com/doi/10.1029/2003GC000574/full, accessed March 12, 2021.

Kunzer, A.S., 1998, Spillway modifications: Ochoco Dam, Crooked River Project, Oregon, *in* Schultz, R. A., and Siddharthan, R., eds., Proceedings of the 33rd Symposium of Engineering Geology and Geotechnical Engineering, University of Nevada, Reno.

Kylander-Clark, A.R.C., Hacker, B.R., Cottle, J.M., 2013, Laser-ablation split-stream ICP petrochronology: Chemical Geology, v. 345, p. 99–112. http://www.sciencedirect.com/science/article/pii/S0009254113000788, accessed March 12, 2021.

Lawrence, R.D., 1976, Strike-slip terminates the Basin and Range province in Oregon: Geological Society of America Bulletin, v. 87, no. 6, p. 846–850. https://gsabulletin.gsapubs.org/content/87/6/846.abstract, accessed March 12, 2021.

Le Bas, M.J., and Streckeisen, A.L., 1991, The IUGS systematics of igneous rocks: Journal of the Geological Society, v. 148, p. 825–833. doi:10.1144/gsjgs.148.5.0825. http://jgs.lyellcollection.org/content/148/5/825.abstract, accessed March 12, 2021.

Le Bas, M.J., Le Maitre, R.W., Streckeisen, A., and Zanettin, B., 1986, A chemical classification of volcanic rocks based on the total alkali-silica diagram: Journal of Petrology, v. 27, part 3, p. 745–750. https://doi.org/10.1093/petrology/27.3.745, accessed March 12, 2021.

Le Maitre, R.W., Bateman, P., Dudek, A., Keller, J., Lemeyre, J., Le Bas, M.J., Sabine, P.A., Schmid, R., Sorenson, H., Streckeisen, A., Wooley, A.R., and Zanettin, B., 1989, A classification of igneous rocks and glossary of terms: Oxford, Blackwell, 193 p.

Le Maitre, R.W. (ed.), Streckeisen, A., Zanettin, B., Le Bas, M.J., Bonin, B., Bateman, P., Bellieni, G., Dudek, A., Efremova, S., Keller, J., Lameyre, J., Sabine, P.A., Schmid, R., Sørensen, H., and Woolley, A.R., 2004, Igneous rocks: a classification and glossary of terms: Cambridge University Press, Recommendations of the International Union of Geological Sciences, Subcommission on the Systematics of Igneous Rocks, 236 p.

Lite, K.E., Jr., and Gannett, M.W., 2002, Geologic framework of the regional ground-water flow system in the upper Deschutes Basin, Oregon: U.S. Geological Survey Water Resources Investigation Report 02-4015, 44 p. https://pubs.er.usgs.gov/publication/wri024015, accessed March 12, 2021.

Long, P.E., and Duncan, R.A., 1982, $^{40}Ar/^{39}Ar$ ages of Columbia River Basalt from deep boreholes in south-central Washington [abs.]: Fairbanks, Alaska, Proceedings, 33rd Alaska Science Conference, p. 119.

Ludwig, K.R., 2012, Isoplot 3.75: A geochronological toolkit for Microsoft Excel: Berkeley Geochronology Center Special Publication 5, p. 1–75.

Lux, D. R., 1982, K-Ar and $^{40}Ar/^{39}Ar$ ages of mid-Tertiary volcanic rocks from the West Cascades Range, Oregon: Isochron/West, no. 33, p. 27–32.

Mackenzie, W.S., Donaldson, C.H., and Guilford, C., 1997, Atlas of igneous rocks and their textures, 7th ed.: Addison Wesley Longman Limited, 148 p.

Madin, I.P., and Wang, Z., 2000, Relative earthquake hazard maps for selected areas in western Oregon: Oregon Department of Geology and Mineral Industries Interpretive Map Series IMS-7, scale 1:24,000. https://www.oregongeology.org/pubs/ims/p-ims.htm, accessed March 12, 2021.

Mahood, G.A., and Benson, T.R., 2017, Using $^{40}Ar^{39}Ar$ ages of intercalated silicic tuffs to date flood basalts: Precise ages for Steens Basalt Member of the Columbia River Basalt Group: Earth and Planetary Science Letters, v. 459, p. 340–351. https://www.sciencedirect.com/science/article/abs/pii/S0012821X16306720?via%3Dihub, accessed March 12, 2021.

Manchester, S.R., 1981, Fossil plants of the Eocene Clarno Nut Beds: Oregon Geology, v. 43, no. 6, p. 75–81. https://www.oregongeology.org/pubs/OG/OGv43n06.pdf, accessed March 12, 2021.

Manchester, S.R., 1990, Eocene to Oligocene floristic changes recorded in the Clarno and John Day formations, Oregon, U.S.A., *in* Knobloch, E., and Kvacek, Z., eds., Paleofloristic and paleoclimatic change in the Cretaceous and Tertiary, symposium proceedings: Prague, Czekoslovakian Geological Survey Press, p. 183–187.

Manchester, S.R., 1994, Fruits and seeds of the middle Eocene Nut Beds flora, Clarno Formation, Oregon: Palaeontographica Americana, no. 58, 205 p., 70 pl.

Marsh, O.C., 1875, Ancient lake basins of the Rocky Mountains region: American Journal of Science, v. 9, p. 49–52. https://www.ajsonline.org/content/s3-9/49/49, accessed March 12, 2021.

Mathisen, J., and Gordon, C.L., 2006, Doe Creek landslide: examination and analyses: abstract, USFS National Minerals and Geology Workshop.

McArthur, L.A., and McArthur, L.L., 1992, Oregon geographic names, 6th ed.: Portland, Oregon Historical Society Press, p. 778–779.

McCaffrey, R., and Goldfinger, C., 1995, Forearc deformation and great subduction earthquakes: implications for Cascadia offshore earthquake potential: Science, v. 267, p. 856–859. https://science.sciencemag.org/content/267/5199/856, accessed March 12, 2021.

McCaffrey, R., Qamar, A.I., King, R.W., Wells, R., Khazaradze, G., Williams, C.A., Stevens, C.W., Vollick, J.J., and Zwick, P.C., 2007, Fault locking, block rotation and crustal deformation in the Pacific Northwest: Geophysical Journal International, v. 169, no. 3, p. 1315–1340. https://doi.org/10.1111/j.1365-246X.2007.03371.x, accessed March 12, 2021.

McClaughry, J.D., and Ferns, M.L., 2006a, Preliminary geologic map of the Prineville 7.5′ quadrangle, Crook County, Oregon: Oregon Department of Geology and Mineral Industries Open-File Report O-06-22, scale 1:24,000. https://www.oregongeology.org/pubs/ofr/O-06-22.zip, accessed March 12, 2021.

McClaughry, J.D., and Ferns, M.L., 2006b, Preliminary geologic map of the Ochoco Reservoir 7.5′ quadrangle, Crook County, Oregon: Oregon Department of Geology and Mineral Industries Open-File Report O-06-23, scale 1:24,000. https://www.oregongeology.org/pubs/ofr/O-06-23.zip, accessed March 12, 2021.

McClaughry, J.D., and Ferns, M.L., 2007a, The Crooked River Caldera: identification of an early Oligocene eruptive center in the John Day Formation of central Oregon: Geological Society of America Abstracts with Programs, v. 39, no. 4, p. 10. https://gsa.confex.com/gsa/2007CD/webprogram/Paper120471.html, accessed March 12, 2021.

McClaughry, J.D., and Ferns, M.L., 2007b, Neogene basalt flow stratigraphy near Prineville, Oregon: Interaction with the ancestral Crooked River: Geological Society of America Abstracts with Programs, v. 39, no. 4, p. 72. https://gsa.confex.com/gsa/2007CD/webprogram/Paper120474.html, accessed March 12, 2021.

McClaughry, J.D., and Ferns, M.L., 2007c, Preliminary geologic map of the Eagle Rock 7.5′ quadrangle, Crook County, Oregon: Oregon Department of Geology and Mineral Industries, Open-File Report O-07-11, scale 1:24,000. https://www.oregongeology.org/pubs/ofr/O-07-10.pdf, accessed March 12, 2021.

McClaughry, J.D., and Ferns, M.L., 2007d, Preliminary geologic map of the Stearns Butte 7.5′ quadrangle, Crook County, Oregon: Oregon Department of Geology and Mineral Industries, Open-File Report O-07-12, scale 1:24,000. https://www.oregongeology.org/pubs/ofr/O-07-12.pdf, accessed March 12, 2021.

McClaughry, J.D., and Patton, P.M., 2017, Smith Rock State Park (essay): The Oregon Encyclopedia [online]. https://oregonencyclopedia.org/articles/smith_rock_state_park/#.WZI00VGGOUk, accessed March 12, 2021.

McClaughry, J.D., Gordon, C.L., and Ferns, M.L., 2009a, Field trip guide to the middle Eocene Wildcat Mountain caldera, Ochoco National Forest, Crook County, Oregon: Oregon Geology, v. 69, no. 1, p. 5–24. https://www.oregongeology.org/pubs/og/OGv69n01.pdf, accessed March 12, 2021.

McClaughry, J.D., Ferns, M.L., and Gordon, C.L., 2009b, Field trip guide to the Neogene stratigraphy of the lower Crooked River basin and the ancestral Crooked River, Crook County, Oregon: Oregon Geology, v. 69, no. 1, p. 45–60. https://www.oregongeology.org/pubs/og/OGv69n01.pdf, accessed March 12, 2021.

McClaughry, J.D., Ferns, M.L., and Gordon, C.L., 2014, Geologic evolution of the middle Eocene Wildcat Mountain caldera, central, Oregon, U.S.A.: Geological Society of America Abstracts with Programs, v. 46, no. 5, p. 72. https://gsa.confex.com/gsa/2014RM/webprogram/Paper238515.html, accessed March 12, 2021.

McClaughry, J.D., Ferns, M.L., Gordon, C.L., and Patridge, KA., 2009c, Field trip guide to the Oligocene Crooked River caldera: Central Oregon's supervolcano, Crook, Deschutes, and Jefferson counties, Oregon: Oregon Geology, v. 69, no. 1, p. 25–44. https://www.oregongeology.org/pubs/og/OGv69n01.pdf, accessed March 12, 2021.

McClaughry, J.D., Scott, W.E., Duda, C.J.M., and Conrey, R.M., 2020a, Geologic map of the Dog River and northern part of the Badger Lake 7.5′ quadrangles, Hood River County, Oregon: Oregon Department of Geology and Mineral Industries Geological Map 126, 145 p., 1 pl., scale 1:24,000, Esri™ format geodatabases; shapefiles, metadata; spreadsheet (5 sheets). https://www.oregongeology.org/pubs/gms/p-GMS-127.htm, accessed March 12, 2021.

McClaughry, J.D., Ferns, M.L., Streck, M.J., Patridge, K.A., and Gordon, C.L., 2009d, Paleogene calderas of central and eastern Oregon: Eruptive sources of widespread tuffs in the John Day and Clarno Formations, *in* O'Connor, J.E., Dorsey, R.J., and Madin, I.P., eds., Volcanoes to vineyards: geologic field trips through the dynamic landscape of the Pacific Northwest: Geological Society of America Field Guide 15, p. 407–434, doi: 10.1130/2009.fl d015(20). https://doi.org/10.1130/2009.fld015(20), accessed March 12, 2021.

McClaughry, J.D., Niewendorp, C.A., Franczyk, J.J., Duda, C.J.M., and Madin, I. P., 2020b, Mineral Information Layer for Oregon, release 3 [MILO-3]: Oregon Department of Geology and Mineral Industries Digital Data Series MILO-3, Esri™ geodatabase. https://www.oregongeology.org/milo/index.htm, accessed March 12, 2021.

McClaughry, J.D., Wiley, T.J., Conrey, R.C., Jones, C.B., and Lite, K.E., 2012, Digital geologic map of the Hood River Valley, Hood River and Wasco counties, Oregon: Oregon Department of Geology and Mineral Industries Open-File Report O-12-03, 142 p., scale 1:36,000. https://www.oregongeology.org/pubs/ofr/p-O-12-03.htm, accessed March 12, 2021.

McClaughry, J.D., Gaylord, D.R., Ferns, M.L., Felt, K.J., Spall, B.N., and Cahoon, E.B., 2019, Sedimentary and volcanic evolution of the middle Eocene Clarno Formation, NE Oregon: Geological Society of America Abstracts with Programs. v. 51, no. 4. https://10.0.4.106/abs/2019CD-329538, accessed March 12, 2021.

McIntyre, E.H., Ekren, E.B., and Hardyman, R.F., 1982, Stratigraphic and structural framework of the Challis volcanics in the eastern half of the Challis 1° × 2° quadrangle, Idaho, *in* Bonnichsen, B., and Breckenridge, R.M., eds., Cenozoic geology of Idaho: Idaho Bureau of Mines and Geology Bulletin 26, p. 3-22. https://www.idahogeology.org/product/b-26, accessed March 12, 2021.

McKee, T.M., 1970, Preliminary report on fossil fruits and seeds from the mammal quarry of the Clarno Formation, Oregon: Ore Bin, v. 32, p. 117–132. https://www.oregongeology.org/pubs/OG/OBv32n07.pdf, accessed March 12, 2021.

Merriam, J.C., 1901a, A geological section through the John Day Basin: Journal of Geology, v. 9, p. 71–72. https://www.journals.uchicago.edu/doi/pdfplus/10.1086/620881, accessed March 12, 2021.

Merriam, J.C., 1901b, A contribution to the geology of the John Day Basin: University of California, Department of Geology Bulletin, v. 2, p. 269–314.

Merriam, J.C., Stock, C., and Moody, C.L., 1925, The Pliocene Rattlesnake formation and fauna of eastern Oregon, with notes on the geology of the Rattlesnake and Mascall deposits: Carnegie Institute of Washington Publication 347, paper III, p. 43–92. Available at https://core.ac.uk/download/pdf/232284608.pdf, accessed March 12, 2021.

Mertzman, S.A., 2000, K-Ar results from the southern Oregon – northern California Cascade Range: Oregon Geology, v. 62, p. 99–122. https://www.oregongeology.org/pubs/OG/OGv62n04.pdf, accessed March 12, 2021.

Miyashiro, A., 1974, Volcanic rock series in island arcs and active continental margins: American Journal of Science, v. 274, p. 321-355. https://doi.org/10.2475/ajs.274.4.321, accessed March 12, 2021.

Moore, N.E., Grunder, A.L., and Bohrson, W.A., 2018, The three-stage petrochemical evolution of the Steens Basalt (southeast Oregon, USA) compared to large igneous provinces and layered mafic intrusions: Geosphere, v. 14, p. 2505–2532. https://doi.org/10.1130/GES01665.1, accessed March 12, 2021.

Moye, F.J., Hackett, W.R., Blakley, J.D., and Snider, L.G., 1988, Regional geologic setting and volcanic stratigraphy of the Challis volcanic field, central Idaho, *in* Link, P.K., and Hackett, W.R., eds., Guidebook to the geology of central and southern Idaho: Idaho Geological Survey Bulletin 27, p. 87–98. https://www.idahogeology.org/product/b-27, accessed March 12, 2021.

Nelson, A.R., Kelsey, H. M., and Witter, R. C., 2006, Great earthquakes of variable magnitude at the Cascadia subduction zone: Quaternary Research, v. 65, p. 354–365. https://www.sciencedirect.com/science/article/pii/S0033589406000391, accessed March 12, 2021.

Niewendorp, C.A., and Neuhaus, M. E., 2003, Map of selected earthquakes for Oregon, 1841 through 2002: Oregon Department of Geology and Mineral Industries Open-File Report O-03-02. https://www.oregongeology.org/pubs/ofr/O-03-02.pdf, accessed March 12, 2021.

NOAA National Centers for Environmental Information, 2020, Data Tools: 1981–2010 Climate Normals online dataset: https://www.ncdc.noaa.gov/cdo-web/datatools/normals

Obermiller, W.A., 1987, Geologic, structural, and geochemical features of basaltic and rhyolitic volcanic rocks of the Smith Rock–Gray Butte area, central Oregon: Eugene, University of Oregon, M.S. thesis, 169 p.

Ogg, J.G., Ogg, G., and Gradstein, F. M., 2008, The concise geologic time scale: Cambridge University Press, 177 p.

Ostroumov, M., and Corona-Chávez, P., 2003, Mineralogical study of mordenite from the Sierra Madre del Sur, southwestern Mexico: Revista Mexicana de Ciencias Geológicas, v. 20, p.133–138.

Paces, J.B., and Miller, J.D., 1993, Precise U-Pb ages of Duluth Complex and related mafic intrusions, northeastern Minnesota: Geochronological insights to physical, petrogenetic, paleomagnetic, and tectonomagmatic processes associated with the 1.1 Ga mid-continent rift system. Journal of Geophysical Research, v. 98, p. 13997–14013.

Parker, D.J., 1974, Petrology of selected volcanic rocks of the Harney Basin, Oregon: Corvallis, Oregon State University, Ph.D. dissertation, 153 p. https://ir.library.oregonstate.edu/concern/graduate_thesis_or_dissertations/r494vn606, accessed March 12, 2021.

Paton, C., Woodhead, J., Hellstrom, J. Hergt, J., Greig, A., and Maas, R., 2010, Improved laser ablation U-Pb zircon geochronology through robust downhole fractionation correction: Geochemistry, Geophysics, Geosystems, v. 11, Q0AA06. https://onlinelibrary.wiley.com/doi/10.1029/2009GC002618/full, accessed March 12, 2021.

Patridge, K.A., 2010, Geochemistry and petrogenesis of John Day ash flows near Prineville, Oregon: Pullman, Wash., Washington State University, M.S. thesis, 149 p.

Pearce, J.A., Harris, N.B., and Tindle, A.G., 1984, Trace element discrimination diagrams for the tectonic interpretation of granitic rocks: Journal of Petrology. v. 25, p. 956–983. https://doi.org/10.1093/petrology/25.4.956, accessed March 12, 2021.

Peccerillo, A., and Taylor, S.R., 1976, Geochemistry of Eocene calc-alkaline volcanic rocks from the Kastamonu area, northern Turkey: Contributions to Mineralogy and Petrology, v. 58, p. 63–81. https://link.springer.com/article/10.1007/BF00384745, accessed March 12, 2021.

Peck, D.L., 1964, Geologic reconnaissance of the Antelope-Ashwood area of north-central Oregon, with emphasis on the John Day Formation of late Oligocene and early Miocene age: U.S. Geological Survey Bulletin 1161-D, 26 p. https://pubs.usgs.gov/bul/1161d/report.pdf, accessed March 12, 2021.

Peterson, N.V., 1969, Uranium, *in* Mineral and water resources of Oregon: Oregon Department of Geology and Mineral Industries Bulletin 64, p. 180–184. https://www.oregongeology.org/pubs/B/B-064.pdf, accessed March 12, 2021.

Peterson, N.V., Groh, E.A., Taylor, E.M., and Stensland, D.E., 1976, Geology and mineral resources of Deschutes County, Oregon: Oregon Department of Geology and Mineral Industries Bulletin 89, 66 p. https://www.oregongeology.org/pubs/B/B-089.pdf, accessed March 12, 2021.

Phillips, W.M., Korosec, M.A., Schasse, H.W., Anderson, J.L., and Hagen, R.A., 1986, K-Ar ages of volcanic rocks in southwest Washington: Isochron/West, v. 47, p. 18–24.

Pitcher, B.W., 2017, The Deschutes Formation: Evidence of extension-enhanced explosivity in the early High Cascades: Corvallis, Oregon State University, Ph.D. dissertation, 211 p. https://ir.library.oregonstate.edu/concern/graduate_thesis_or_dissertations/wp988q42j, accessed March 12, 2021.

Pitcher, B.W., Kent, A.J.R., Grunder, A.L., and Duncan, R.A., 2017, Frequency and volumes of ignimbrite eruptions following the late Neogene initiation of the Central Oregon High Cascades: Journal of Volcanology and Geothermal Research, v. 339, p. 1–22. https://dx.doi.org/10.1016/j.jvolgeores.2017.04.019, accessed March 12, 2021.

Pitcher, B.W., Kent, A.J.R., and Grunder, A.L., 2021, Tephrochronology of North America's most recent arc-sourced ignimbrite flare-up: The Deschutes Formation of the central Oregon Cascades: Journal of Volcanology and Geothermal Research, v. 412, p. 1–23. https://www.sciencedirect.com/science/article/abs/pii/S0377027321000226?via%3Dihub, accessed May 24, 2021.

Priest, G.R., 1990, Volcanic and tectonic evolution of the Cascade volcanic arc, central Oregon: Journal of Geophysical Research, v. 95, no. B12, p. 19,583–19,599. https://agupubs.onlinelibrary.wiley.com/doi/abs/10.1029/jb095ib12p19611, accessed March 12, 2021.

Priest, G.R., Woller, N.M., and Black, G.L., 1983, Overview of the geology of the central Oregon Cascade Range, *in* Priest, G.R., and Vogt, B.V., eds., Geology and geothermal resources of the central Oregon Cascade Range: Oregon Department of Geology and Mineral Industries Special Paper 15, p. 3–28. https://www.oregongeology.org/pubs/sp/SP-15.pdf, accessed March 12, 2021.

Priest, G.R., Goldfinger, C., Wang, K., Witter, R.C., Zhang, Y., and Baptista, A.M., 2009, Tsunami hazard assessment of the northern Oregon coast: a multideterministic approach tested at Cannon Beach, Clatsop County, Oregon: Oregon Department of Geology and Mineral Industries Special Paper 41, 87 p., GIS files, time histories, animations. Web: https://www.oregongeology.org/pubs/sp/p-SP.htm, accessed March 12, 2021.

Reidel, S.P., and Campbell, N.P., 1989, Structure of the Yakima Fold Belt, Central Washington, *in* Joseph, N.L. and others, eds., Geologic guidebook for Washington and adjacent areas: Washington Division of Geology and Earth Resources Information Circular 86, p. 275–303. https://file.dnr.wa.gov/publications/ger_ic86_geol_guide_wa_area.pdf, accessed March 12, 2021.

Reidel, S.P., and Tolan, T.L., 2013, Grande Ronde Basalt, Columbia River Basalt Group, *in* Reidel, S.P., Camp, V.E., Martin, M.E., Ross, M.E., Wolff, J.A., Martin, B.S., Tolan, T.L., and Wells, R.E., eds., Geological Society of America Special Paper 497, p. 117–154. https://pubs.geoscienceworld.org/books/book/661/chapter/3807152/The-Grande-Ronde-Basalt-Columbia-River-Basalt, accessed March 12, 2021.

Reidel, S.P., Fecht, K.R., Hagood, M.C., and Tolan, T.L., 1989a, The geologic evolution of the central Columbia Plateau, *in* Reidel, S.P., and Hooper, P.R., eds., Volcanism and tectonism in the Columbia River Flood-Basalt Province: Geological Society of America Special Paper 239, p. 247–264. doi:10.1130/SPE239-p247 https://specialpapers.gsapubs.org/content/239/247.abstract, accessed March 12, 2021.

Reidel, S.P., Tolan, T.L., Hooper, P.R., Beeson, M.H., Fecht, K.R., Bentley, R.D., and Anderson, J.L., 1989b, The Grande Ronde Basalt, Columbia River Basalt Group; Stratigraphic descriptions and correlations in Washington, Oregon, and Idaho, *in* Reidel, S. P., and Hooper, P. R., eds., Volcanism and tectonism in the Columbia River Flood-Basalt Province: Geological Society of America Special Paper 239, p. 21–54. doi:10.1130/SPE239-p21. https://specialpapers.gsapubs.org/content/239/21.abstract, accessed March 12, 2021.

Reidel, S.P., Johnson, V.G., and Spane, F.A., 2002, Natural gas storage in basalt aquifers of the Columbia Basin, Pacific Northwest USA: a guide to site characterization: Richland, Wash., Pacific Northwest National Laboratory, 277 p. https://www.pnnl.gov/main/publications/external/technical_reports/PNNL-13962.pdf, accessed March 12, 2021.

Reidel, S.P., Camp, V.E., Tolan, T.L., and Martin, B.S., 2013, The Columbia River flood basalt province: Stratigraphy, areal extent, volume, and physical volcanology, *in* Reidel, S.P., Camp, V.E., Ross, M.E., Wolff, J.A., Martin, B.S., Tolan, T.L., and Wells, R.E., eds., The Columbia River Flood Basalt Province: Geological Society of America Special Paper 497, p. 1–43, doi:10.1130/2013.2497(01). https://specialpapers.gsapubs.org/content/497/1.abstract, accessed March 12, 2021.

Retallack, G.J., Bestland, E.A., and Fremd, T.J., 2000, Eocene and Oligocene paleosols of Central Oregon: Geological Society of America Special Paper 344, 192 p. http://specialpapers.gsapubs.org/content/344, accessed March 12, 2021.

Riddihough, R., Finn, C., and Couch, R., 1986, Klamath–Blue Mountain lineament, Oregon: Geology, v. 14, p. 528–531. https://geology.gsapubs.org/content/14/6/528.abstract, accessed March 12, 2021.

Robertson, S., 1999, BGS rock classification scheme, v. 1, Classification of igneous rocks: British Geological Survey Research Report 99-06, 24 p. https://www.bgs.ac.uk/download/bgs-rock-classification-scheme-igneous/, accessed March 12, 2021.

Robinson, J.W., and Price, D., 1963, Ground water in the Prineville area, Crook County, Oregon: U.S. Geological Survey Water-Supply Paper 1619-P, 49 p. https://pubs.er.usgs.gov/publication/wsp1619P, accessed March 12, 2021.

Robinson, P.T., 1969, High-titania alkali-olivine basalt of north-central Oregon: Contributions to Mineralogy and Petrology, v. 22, p. 349–360. https://link.springer.com/article/10.1007/BF00400129, accessed March 12, 2021.

Robinson, P.T., 1975, Reconnaissance geologic map of the John Day Formation in the southwestern part of the Blue Mountains and adjacent areas, north-central Oregon: U.S. Geological Survey Miscellaneous Investigations Map I-872, scale 1:125,000. https://pubs.er.usgs.gov/publication/i872, accessed March 12, 2021.

Robinson, P.T., and Brem, G.F., 1981, Guide to a geologic field trip between Kimberly and Bend, Oregon with emphasis on the John Day Formation, *in* Johnston, D. A., and J. Donnelly-Nolan, J., eds., Guides to some volcanic terranes in Washington, Idaho, Oregon, and northern California: U.S. Geological Survey Circular 838, p. 41–58. https://pubs.er.usgs.gov/publication/cir838, accessed March 12, 2021.

Robinson, P.T., and Stensland, D., 1979, Geologic map of the Smith Rock area, Oregon: U.S. Geological Survey Miscellaneous Investigations Map I-1142, scale 1:48 000. https://pubs.er.usgs.gov/publication/i1142, accessed March 12, 2021.

Robinson, P.T., Brem, G.F., and McKee, E.H., 1984, John Day Formation of Oregon: a distal record of early Cascade volcanism: Geology, v. 12, p. 229–232. https://geology.gsapubs.org/content/12/4/229.abstract, accessed March 12, 2021.

Robinson, P.T., Walker, G.W., and McKee, E.H., 1990, Eocene(?), Oligocene, and lower Miocene rocks of the Blue Mountains region: *in* Walker, G.W., ed., Geology of the Blue Mountains region of Oregon, Idaho, and Washington: Cenozoic Geology of the Blue Mountains Region: U.S. Geological Survey Professional Paper 1437, p. 29–62. https://doi.org/10.3133/pp1437, accessed March 12, 2021.

Robyn, T.L., and Hoover, J.D., 1982, Late Cenozoic deformation and volcanism in the Blue Mountains of central Oregon: microplate interactions?: Geology, v. 10, p. 572–576. https://geology.gsapubs.org/content/10/11/572.abstract, accessed March 12, 2021.

Rogers, J.W., 1966, Coincidence of structural and topographic highs during post-Clarno time in north central Oregon: American Association of Petroleum Geologists Bulletin, v. 50, p. 390–396.

Rogers, J.W., and Novitsky-Evans, J.M., 1977, The Clarno Formation of central Oregon, U.S.A.—volcanism on a thin continental margin: Earth and Planetary Science Letters, v. 34, no. 1, p. 56–66. http://dx.doi.org/10.1016/0012-821X(77)90105-4, accessed March 12, 2021.

Rukstales, K.S., and Petersen, M.D., 2019, Data release for 2018 Update of the U.S. National Seismic Hazard Model: U.S. Geological Survey data release, https://doi.org/10.5066/P9WT5OVB, accessed March 12, 2021.

Russell, I.C., 1905, A preliminary report on geology and mineral resources of central Oregon: U.S. Geological Survey Bulletin 252, 138 p. https://pubs.er.usgs.gov/publication/b252, accessed March 12, 2021.

Sambridge, M.S., and Compston, W., 1994, Mixture modeling of multi-component datasets with application to ion-probe zircon ages: Earth and Planetary Science Letters, v. 128, no. 3-4, p. 373–390, https://doi.org/10.1016/0012-821X(94)90157-0, accessed March 12, 2021.

Satake, K., Shimazaki, K., Tsuji, Y., and Ueda, K., 1996, Time and size of a giant earthquake in Cascadia inferred from Japanese tsunami records of January 1700: Nature, v. 379, p. 246–249. https://doi.org/10.1038/379246a0, accessed March 12, 2021.

Schafer, M., 1956, Uranium prospecting in Oregon, 1956: Oregon Department of Geology and Mineral Industries, Ore Bin, v. 18, no. 12, p. 101–104. https://www.oregongeology.org/pubs/og/OBv18all.pdf, accessed March 12, 2021.

Scott, W.E., Iverson, R.M., Schilling, S.P., and Fisher, B.J., 1999, Volcano hazards in the Three Sisters region, Oregon: U.S. Geological Survey Open-File Report 99-437, 14 p., 1 map pl., shapefiles. https://pubs.er.usgs.gov/publication/ofr99437, accessed March 12, 2021.

Seligman, A.N., Bindeman, I.N., McClaughry, J.D., Stern, R., and Fisher, C., 2014, The earliest low and high $\delta^{18}O$ caldera-forming eruptions of the Yellowstone plume: implications for the 30–40 Ma Oregon calderas and speculations on plume-triggered delaminations: Frontiers in Earth Science—Volcanology, v. 2, 34. https://doi.org/10.3389/feart.2014.00034, accessed March 12, 2021.

Sherrod, D.R., 2019, Cascade Mountain Range in Oregon: Portland, Oreg., Oregon Historical Society, Oregon Encyclopedia essay, https://oregonencyclopedia.org/articles/cascade_mountain_range/#.XuAE3UVKhaR, accessed March 12, 2021.

Sherrod, D.R., and Smith, J.G., 2000, Geologic map of upper Eocene to Holocene volcanic and related rocks of the Cascade Range, Oregon: U.S. Geological Survey Map I-2569, 17 p., 2 pl., scale 1:500,000. https://pubs.usgs.gov/imap/i-2569/, accessed March 12, 2021.

Sherrod, D.R., Mastin, L.G., Scott, W.E., and Schilling, S.P., 1997, Volcano hazards at Newberry Volcano, Oregon: U.S. Geological Survey Open-File Report 97-513, 14 p., 1 map pl., shapefiles. https://doi.org/10.3133/ofr97513, accessed March 12, 2021.

Sherrod, D.R., Gannett, M.W., and Lite, K.E., Jr., 2002, Hydrogeology of the upper Deschutes Basin, central Oregon: A young basin adjacent to the Cascade volcanic arc, *in* Moore, G.W., Field guide to geologic processes in Cascadia: Oregon Department of Geology and Mineral Industries Special Paper 36, p. 109–144. https://www.oregongeology.org/pubs/sp/SP-36.pdf, accessed March 12, 2021.

Sherrod, D.R., Taylor, E.M., Ferns, M.L., Scott, W.E., Conrey, R.M., and Smith, G.A., 2004, Geologic map of the Bend 30- × 60-minute quadrangle, central Oregon: U.S. Geological Survey Geologic Investigations Series I-2683, 48 p., 2 sheets, scale 1:100,000. https://doi.org/10.3133/i2683, accessed March 12, 2021.

Smith, G.A., 1986a, Stratigraphy, sedimentology, and petrology of Neogene rocks in the Deschutes Basin, central Oregon: a record of continental margin volcanism: Corvallis, Oregon State University, Ph.D. dissertation, 467 p. http://ir.library.oregonstate.edu/xmlui/handle/1957/17932, accessed March 12, 2021.

Smith, G.A., 1986b, Stratigraphy, sedimentology, and the petrology of Neogene rocks in the Deschutes Basin, central Oregon: a record of continental-margin volcanism and its influence on fluvial sedimentation in an arc-adjacent basin: Richland, Wash., Rockwell International Corp., U.S. Department of Energy Basalt Waste Isolation Project, technical report RHO-BW-SA-555-P. https://www.osti.gov/biblio/5216792-stratigraphy-sedimentology-petrology-neogene-rocks-deschutes-basin-central-oregon-record-continental-margin-volcanism-its-influence-fluvial-sedimentation-arc-adjacent-basin, accessed July 7, 2021.

Smith, G.A., 1986c, Simtustus Formation: paleogeographic and stratigraphic significance of a newly defined Miocene unit in the Deschutes Basin, central Oregon: Oregon Geology, v. 48, p. 63–72. https://www.oregongeology.org/pubs/OG/OGv48n06.pdf, accessed March 12, 2021.

Smith, G.A., 1987, The influence of explosive volcanism on fluvial sedimentation: the Deschutes Formation (Neogene) in central Oregon: Journal of Sedimentary Petrology, v. 57, no. 4, p. 613–629. https://doi.org/10.1306/212F8BBB-2B24-11D7-8648000102C1865D, accessed June 8, 2021.

Smith, G.A., 1991, A field guide to depositional processes and unit geometry of Neogene continental volcaniclastic rocks, Deschutes basin, central Oregon: Oregon Geology, v. 53, no. 1, p. 3–20. http://www.oregongeology.org/pubs/OG/OGv53n01.pdf, accessed March 12, 2021.

Smith, G.A., and Snee, L.W., 1984, Revised stratigraphy of the Deschutes basin, Oregon: implications for the Neogene development of the central Oregon Cascades [abstr.]: Eos, (Transactions, American Geophysical Union), v. 65, p. 330.

Smith, G.A., and Taylor, E.M., 1983, The central Oregon High Cascade graben: What? Where? When?: Geothermal Resources Council Transactions, v. 7, p. 275–279.

Smith, G.A., Snee, L.W., and Taylor, E.M., 1987, Stratigraphic, sedimentologic, and petrologic record of late Miocene subsidence of the central Oregon High Cascades: Geology, v. 15, p. 389–392. https://geology.gsapubs.org/content/15/5/389.abstract, accessed March 12, 2021.

Smith, G.A., Manchester, S.R., Ashwill, M., McIntosh, W.C., and Conrey, R.M., 1998, Late Eocene-early Oligocene tectonism, volcanism, and floristic change near Gray Butte, central Oregon: Geological Society of America Bulletin, v. 110, p. 759–778. https://gsabulletin.gsapubs.org/content/110/6/759.abstract, accessed March 12, 2021.

Stearns, H.T., 1931, Geology and water resources of the middle Deschutes River Basin, Oregon: U.S. Geological Survey Water-Supply Paper 637-D, 220 p. https://pubs.er.usgs.gov/publication/wsp637D, accessed March 12, 2021.

Stensland, D.A., 1970, Geology of the northern half of the Bend quadrangle, Jefferson, Wasco, and Deschutes Counties, Oregon: Corvallis, Oregon State University, M.S. thesis, 118 p. https://ir.library.oregonstate.edu/concern/graduate_thesis_or_dissertations/j098zg08h?locale=en, accessed March 12, 2021.

Stephenson, E.L., 1943, Geophysical surveys in the Ochoco quicksilver district, Oregon: U.S. Geological Survey Bulletin 940-C, 43 p. https://doi.org/10.3133/b940C, accessed March 12, 2021.

Streck, M. J., 1994, Volcanology and petrology of the Rattlesnake Ash-Flow Tuff, eastern Oregon: Corvallis, Oregon State University, Ph.D. dissertation, 184 p. http://ir.library.oregonstate.edu/xmlui/handle/1957/8357, accessed March 12, 2021.

Streck, M.J., and Grunder A.L., 1995, Crystallization and welding variations in a widespread ignimbrite sheet: the Rattlesnake Tuff, eastern Oregon: Bulletin of Volcanology, v. 57, p. 151–169. https://link.springer.com/article/10.1007/BF00265035, accessed March 12, 2021.

Streck, M.J., Ferns, M.L., and McIntosh, W., 2015, Large, persistent rhyolitic magma reservoirs above Columbia River Basalt storage sites: the Dinner Creek Tuff Eruptive Center, eastern Oregon: Geosphere, v. 11, no. 2, p. 226–235. https://geosphere.gsapubs.org/content/11/2/226.abstract, accessed March 12, 2021.

Stroh, H.R., 1979, Geology of the Clarno Formation in the vicinity of Stephenson Mountain, Jefferson, Crooke, and Wheeler counties, Oregon: Corvallis, Oregon State University, M.S. thesis, 128 p. https://ir.library.oregonstate.edu/concern/graduate_thesis_or_dissertations/9c67ws172?locale=en , accessed March 12, 2021.

Suayah, I.B., and Rogers, J.J.W., 1991, Petrology of the Lower Tertiary Clarno Formation in north central Oregon: the importance of magma mixing: Journal of Geophysical Research Solid Earth, v. 96, p. 13,357-13,371. https://doi.org/10.1029/91JB00221, accessed March 12, 2021.

Swanson, D.A., 1969, Reconnaissance geologic map of the east half of the Bend quadrangle, Crook, Wheeler, Jefferson, Wasco, and Deschutes counties, Oregon: U.S. Geological Survey Miscellaneous Investigations Map I-568, scale 1:250,000. https://doi.org/10.3133/ofr68266, accessed March 12, 2021.

Swanson, D.A., and Robinson, P.T., 1968, Base of the John Day Formation in and near the Horse Heaven mining district, north-central Oregon, *in* Geological Survey research, 1968, Chapter D: U.S. Geological Survey Professional Paper 600-D, p. D154–D161. https://doi.org/10.3133/pp600D, accessed March 12, 2021.

Swanson, D.A., Wright, T.L., Hooper, P.R., and Bentley, R.D., 1979, Revisions in stratigraphic nomenclature of the Columbia River Basalt Group: U.S. Geological Survey Bulletin 1457-G, 59 p. https://doi.org/10.3133/b1457G, accessed March 12, 2021.

Swanson, D.A., Anderson, J.A., Camp, V.E., Hooper, P.R., Taubeneck, W.H., and Wright, T.L., 1981, Reconnaissance geologic map of the Columbia River basalt group, Northern Oregon and Western Idaho: U.S. Geological Survey Open-File Report 81-797, 35 p., 6 pl., scale 1:250,000. https://doi.org/10.3133/ofr81797, accessed March 12, 2021.

Swinney, C.M., Waters, A.C., and Miller, C.P., 1968, Reconnaissance geologic map of the Lookout Mountain quadrangle, Crook and Wheeler Counties, Oregon: U.S. Geological Survey Miscellaneous Geologic Investigations Map I-543, scale 1:62,500. https://doi.org/10.3133/i543, accessed March 12, 2021.

Taylor, E.M., 1977, The Clarno Formation—a record of early Tertiary volcanism in central Oregon: Geological Society of America Abstracts with Programs, v. 9, no. 6, p. 768.

Taylor, E.M., 1981, A mafic-dike system in the vicinity of Mitchell, Oregon, and its bearing on the timing of Clarno-John Day volcanism and early Oligocene deformation in central Oregon: Oregon Geology, v. 43, no. 8, p. 107-112. https://www.oregongeology.org/pubs/OG/OGv43n08.pdf, accessed March 12, 2021.

Taylor, E.M., 1983, Central High Cascade roadside geology—Bend, Sisters, McKenzie Pass, and Santiam Pass, Oregon: *in* Johnston, D. A., and J. Donnelly-Nolan, J., eds., Guides to some volcanic terranes in Washington, Idaho, Oregon, and northern California: U.S. Geological Survey Circular 838, p. 55–83. https://doi.org/10.3133/cir838, accessed March 12, 2021.

Thayer, T.P., 1957, Some relations of later Tertiary volcanology and structure in eastern Oregon: International Geological Congress, 20th, Mexico 1956, section 1: Volcanologia del Cenozoico, v. 1, p. 231–245.

Thayer, T. P., and Brown, C. E., 1966, Geologic map of the Aldrich Mountain quadrangle, Grant County, Oregon: U.S. Geological Survey, Geologic Quadrangle Map GQ-438, scale 1:62,500. https://ngmdb.usgs.gov/Prodesc/proddesc_905.htm, accessed March 12, 2021.

Thompson, M.L., and Wheeler, H.E., 1942, Permian fusulinids from British Columbia, Washington and Oregon: Journal of Paleontology, v. 16, no. 6, p. 700–711. https://jpaleontol.geoscienceworld.org/content/16/6/700, accessed March 12, 2021.

Thormahlen, D., 1984, Geology of the northwest quarter of the Prineville quadrangle: Corvallis, Oregon State University, M.S. thesis, 116 p. https://ir.library.oregonstate.edu/xmlui/handle/1957/18842, accessed March 12, 2021.

Tolan, T.L., and Reidel, S.P., compilers, 1989, Structure map of a portion the Columbia-River Flood-Basalt Province, *in* Reidel, S. P., and Hooper, P. R., eds., Volcanism and tectonism in the Columbia River Flood-Basalt Province: Geological Society of America Special Paper 239, scale 1:576,000, 1 pl. http://specialpapers.gsapubs.org/content/239/1.abstract, accessed March 12, 2021.

Tolan, T.L., Reidel, S.P., Beeson, M. H., Anderson, J.L., Fecht, K.R., and Swanson, D.A., 1989, Revisions to the estimates of the areal extent and volume of the Columbia River Basalt Group, *in* Reidel, S.P., and Hooper, P.R., eds., Volcanism and tectonism in the Columbia River Flood-Basalt Province: Geological Society of America Special Paper 239, p. 1–20. doi:10.1130/SPE239-p1. http://specialpapers.gsapubs.org/content/239/1.abstract, accessed March 12, 2021.

Tolan, T.L., Martin, B.S., Reidel, S.P., Anderson, J.L., Lindsey, K.A., and Burt, W., 2009, An introduction to the stratigraphy, structural geology, and hydrogeology of the Columbia River flood-basalt province: a primer for the GSA Columbia River Basalt Group field trips, *in* O'Connor, J. E., Dorsey, R. J., and Madin, I. P., eds., Volcanoes to vineyards: geologic field trips through the dynamic landscape of the Pacific Northwest: Geological Society of America Field Guide 15, p. 599-643, doi: 10.1130/2009.fl d015(28). https://fieldguides.gsapubs.org/content/15/599.abstract, accessed March 12, 2021.

Tuttle, O.F., and Bowen, N.L., 1958, Origin of granite in light of experimental studies in the system $NaAlSi_3O_8$–$KAlSi_3O_8$–SiO_2-H_2O: Geological Society of America Memoir 74. https://doi.org/10.1130/MEM74, accessed July 6, 2021.

Uppuluri, V.R., 1974, Prineville chemical type: a new basalt type in the Columbia River group: Geological Society of America Bulletin, v. 85, p. 1315–1318. https://doi.org/10.1130/0016-7606(1974)85%3C1315:PCTANB%3E2.0.CO;2, accessed July 7, 2021.

Urbanczyk, K.M., 1994, Geology of the eastern part of the Clarno Formation, northeast Oregon: Pullman, Washington State University, Ph.D. dissertation, 230 p.

U.S. Geological Survey National Cooperative Geologic Mapping Program, 2020, GeMS (Geologic Map Schema)—A standard format for the digital publication of geologic maps: U.S. Geological Survey Techniques and Methods, book 11, chap. B10, 74 p., https://doi.org//10.3133/tm11B10, accessed March 12, 2021.

Vance, J.A., 1988, New fission track and K-Ar ages from the Clarno Formation, Challis-age volcanic rocks in north-central Oregon: Geological Society of America Abstracts with Programs, v. 20, no. 6, p. 473.

Verplanck, E.P., and Duncan, R.A., 1987, Temporal variations in plate convergence and eruption rates in the Western Cascades Oregon: Tectonics, v. 6, p. 197–209. https://agupubs.onlinelibrary.wiley.com/doi/abs/10.1029/TC006i002p00197, accessed March 12, 2021.

Walder, J.S., Gardner, C.A., Conrey, R.C., Fisher, B.J., and Schilling, S.P., 1999, Volcano hazards in the Mount Jefferson region, Oregon: U.S. Geological Survey Open-File Report 99-24, 14 p., 2 pl. https://pubs.usgs.gov/of/1999/0024/, accessed March 12, 2021.

Walker, G.W., 1990, Overview of the Cenozoic geology of the Blue Mountains region, *in* Walker, G. W., ed., Geology of the Blue Mountains region of Oregon, Idaho, and Washington: U.S. Geological Survey Professional Paper 1437, p. 1–11. https://doi.org/10.3133/pp1437, accessed March 12, 2021.

Walker, G.W., and Robinson, P.T., 1990, Paleocene(?), Eocene, and Oligocene(?) rocks of the Blue Mountains region, *in* Walker, G. W., ed., Geology of the Blue Mountains region of Oregon, Idaho, and Washington: U.S. Geological Survey Professional Paper 1437, p. 29–62. https://doi.org/10.3133/pp1437, accessed March 12, 2021.

Walker, G.W., Peterson, N.V., and Greene, R.C., 1967, Reconnaissance geologic map of the east half of the Crescent quadrangle, Lake, Deschutes, and Crook counties, Oregon: U.S. Geol. Survey Miscellaneous Geologic Investigations Map 1-493, scale 1:250,000. https://doi.org/10.3133/i493, accessed March 12, 2021.

Waters, A.C., 1966, Stein's Pillar area, central Oregon: Ore Bin, v 28, n. 8, p 137–144. https://www.oregongeology.org/pubs/OG/OBv28n08.pdf, accessed March 12, 2021.

Waters, A.C., 1968, Reconnaissance geologic map of the Madras quadrangle, Jefferson and Wasco counties, Oregon: U.S. Geological Survey Miscellaneous Geological Investigations Map I-555, scale 1;125,000. https://doi.org/10.3133/i555, accessed March 12, 2021.

Waters, A.C., and Vaughan, R.H., 1968a, Reconnaissance geologic map of the Ochoco Reservoir quadrangle, Crook County, Oregon: U.S. Geological Survey Miscellaneous Geologic Investigations Map I-541, scale 1;62,500. https://doi.org/10.3133/i541, accessed March 12, 2021.

Waters, A.C., and Vaughan, R.H., 1968b, Reconnaissance geologic map of the Eagle Rock quadrangle, Crook County, Oregon: U.S. Geological Survey Miscellaneous Geologic Investigations Map I-540, scale 1:62,500. https://doi.org/10.3133/i540, accessed March 12, 2021.

Waters, A.C., Brown, R.E., Compton, R.R., Staples, L.W., Walker, G.W., and Williams, H., 1951, Quicksilver deposits of the Horse Heaven mining district, Oregon: U.S. Geological Survey Bulletin 969-E, 149 p, 21 pl. https://doi.org/10.3133/b969E, accessed March 12, 2021.

Watkins, N.D., and Baksi, A.K., 1974, Magnetostratigraphy and oroclinal folding of the Columbia River, Steens and Owyhee basalts in Oregon, Washington, and Idaho: American Journal of Science, v. 274, p. 148–189. https://doi.org/10.2475/ajs.274.2.148, accessed March 12, 2021.

Watters, T.R., 1989, Periodically spaced anticlines of the Columbia Plateau, *in* Reidel, S.P., and Hooper, P.R., eds., Volcanism and tectonism in the Columbia River flood-basalt province: Geological Society of America Special Paper 239, p. 283–292. https://pubs.geoscienceworld.org/books/book/375/chapter/3797045/Periodically-spaced-anticlines-of-the-Columbia, accessed March 12, 2021.

Weidenheim, J.P., 1980, The petrography, structure, and stratigraphy of Powell Buttes, Crook County, central Oregon: Corvallis, Oregon State University, M.S. thesis, 95 p. https://ir.library.oregonstate.edu/concern/graduate_thesis_or_dissertations/0r9678250?locale=en, accessed March 12, 2021.

Wentworth, C.K., 1922, A scale of grade and class terms of clastic sediments: Journal of Geology, v. 30, p. 377–392.

White, J.D.L., and Robinson, P.T., 1992, Intra-arc sedimentation in a low-lying marginal arc, Eocene Clarno Formation, central Oregon: Sedimentary Geology, v. 80, no. 1-2, p. 89–114. http://dx.doi.org/10.1016/0037-0738(92)90034-O, accessed March 12, 2021.

Williams, D.L., Hull, D.A., Ackerman, H.D., and Beeson, M.H., 1982, The Mount Hood region: volcanic history, structure, and geothermal potential: Journal of Geophysical Research, v. 87, p. 2767–2781. https://doi.org/10.1029/JB087iB04p02767, accessed March 12, 2021.

Williams, H., 1957, A geologic map of the Bend quadrangle and a reconnaissance geologic map of the central portion of the High Cascade Mountains: Oregon Department of Geology and Mineral Industries Geologic Quadrangle Map QM-1, scale 1:250,000. https://www.oregongeology.org/pubs/qm/QM-01.pdf, accessed March 12, 2021.

Willis, D.C., 1992, Geology and mineralization of the Ochoco gold prospect, Crook County, Oregon: Corvallis, Oregon State University, M.S. thesis, 97 p. https://ir.library.oregonstate.edu/xmlui/handle/1957/19198, accessed March 12, 2021.

12.0 APPENDIX

This appendix contains a summary of the geodatabase along with a description of analytical and field methods and the list of attribute fields for spreadsheets (see page viii of this report). The appendix is divided into two sections:

- Section 12.1 describes the digital databases included with this publication.
- Section 12.2 contains a summary of analytical and field methods. Accompanying tables explain the fields listed in various spreadsheets.

12.1 Geographic Information Systems (GIS) database

Geodatabase specifications

Digital geologic data created for the lower Crooked River basin are stored in an Esri™ format geodatabase. The geodatabase structure of each follows that outlined by the USGS Geologic Map Schema (GeMS), version 2.7 (U.S. Geological Survey National Cooperative Geologic Mapping Program, 2020). The following information describes the overall database structure, the feature classes, and supplemental tables (**Figure 12-1**, **Figure 12-2**; **Table 12-1**, **Table 12-2**).

The data are stored in a file geodatabase feature dataset (GeologicMap). Accessory file geodatabase tables (DataSources, DescriptionOfMapUnits, GeoMaterialDict, and Glossary) were created by using ArcGIS™ version 10.7 (SP 1). The GeologicMap feature dataset contains all the spatially oriented data (feature classes) (**Figure 12-1**). The file geodatabase tables are used to hold additional geologic attributes (**Figure 12-2**). Each feature class within the GeologicMap feature dataset in the geodatabase contains detailed metadata (**Figure 12-1**). Please see the embedded metadata for detailed information such as process descriptions, accuracy specifications, and entity attribute descriptions. Additional information and complete descriptions of the GeMS — Geologic Map Schema can be found at https://doi.org//10.3133/tm11B10.

All spatial data are stored in the Oregon Statewide Lambert Conformal Conic projection. The datum is NAD83 HARN. The linear unit is international feet. See detailed projection parameters below:

Projection: Lambert_Conformal_Conic
False_Easting: 1312335.958005
False_Northing: 0.0
Central_Meridian: -120.5
Standard_Parallel_1: 43.0
Standard_Parallel_2: 45.5
Latitude_Of_Origin: 41.75
Linear Unit: Foot (0.3048)

Geographic Coordinate System: GCS_North_American_1983_HARN
Angular Unit: Degree (0.0174532925199433)
Prime Meridian: Greenwich (0.0)
Datum: D_North_American_1983_HARN
Spheroid: GRS_1980
Semimajor Axis: 6378137.0
Semiminor Axis: 6356752.314140356
Inverse Flattening: 298.257222101

Figure 12-1. Lower Crooked River basin geodatabase feature datasets.

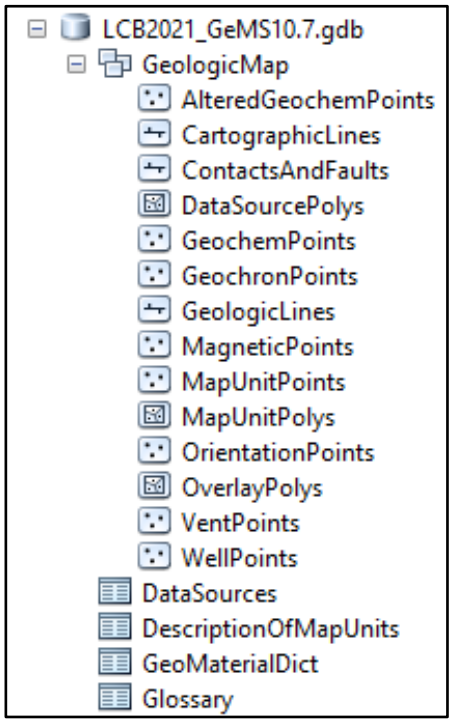

Figure 12-2. Lower Crooked River basin geodatabase data tables.

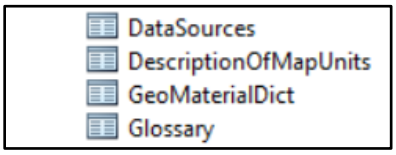

Table 12-1. Feature class description.

Name	Description
AlteredGeochemPoints	This feature class represents point locations where alteration-zone samples have been analyzed by ICP-MS and ICP-AES methods. Includes data collected by the authors during this study or compiled from previous studies. These data are also contained in the alteredgeochempoints spreadsheet.
CartographicLines	Vector lines that have no real-world physical existence and do not participate in map-unit topology. The feature class includes cross section lines used for cartography.
ContactsAndFaults	The vector lines in this feature class contain geologic content including contacts and fault locations used to create the map unit polygon boundaries. The existence and location confidence values for the contacts and faults are provided in the feature class attribute table.
DataSourcePolys	This feature class contains polygons that delineate data sources for all parts of the geologic map. These sources may be a previously published map, new mapping, or mapping with a certain technique. For a map with one data source, for example all new mapping, this feature class contains one polygon that encompasses the map area.
GeochemPoints	This feature class represents point locations where whole-rock samples have been analyzed by X-ray fluorescence (XRF) techniques. Includes data collected by the authors during this study or compiled from previous studies. These data are also contained in the geochemistry spreadsheet.
GeochronPoints	This feature class represents point locations where isotopic ages have been obtained for rock samples in the map area. Data collected by the authors or compiled during the course of this study. These data are also contained in the geochronology spreadsheet.
GeologicLines	These vector lines represent known fold axis locations in the quadrangle. The existence and location confidence for the fold axes are provided in the feature class attribute table.
MagneticPoints	This feature class represents point locations where measurements of natural remanent magnetization have been obtained for strongly magnetized lavas. Includes data collected by the authors during the course of this study. These data are also contained in the magnetic polarity spreadsheet.
MapUnitPoints	This feature class represents points used to generate the MapUnitPolys feature class from the ContactsAndFaults feature class.
MapUnitPolys	This polygon feature class represents the geologic map units as defined by the authors.
OrientationPoints	This feature class represents point locations in the map area where structural measurements were made or were compiled from previous studies. These data are also contained in the bedding (strike and dip) spreadsheet described in more detail below.
OverlayPolys	This feature class holds the reference map outline for each map plate.
WellPoints	This feature class represents point locations of wells in the map area. Includes data obtained by the authors from the Oregon Department of Water Resources (OWRD). These data are also contained in the Wells Points spreadsheet.
VentPoints	This feature class represents point locations of volcanic vents in the map area. These data are also contained in the Vent Points spreadsheet.

Table 12-2. Geodatabase tables.

Name	Description
DataSources	Data table that contains information about data sources used to compile the geology of the area.
DescriptionOfMapUnits	Data table that captures the content of the Description of Map Units (DMU), or equivalent List of Map Units and associated pamphlet text, included in a geologic map.
GeoMaterialDict	Data table providing definitions and hierarchy for GeoMaterial names prescribed by the GeMS database schema.
Glossary	Data table that contains information about the definitions of terms used in the geodatabase.

Geologic map

This report is accompanied by a 1:63,360-scale geologic map (**Figure 12-3**) with six geologic cross sections generated from detailed geologic data (scale of 1:24,000 or better) contained in the accompanying Esri™ format geodatabase.

Figure 12-3. Representation of map plate, Geologic Map of the North Half of the Lower Crooked River Basin, Crook, Deschutes, Jefferson, and Wheeler Counties, Oregon, scale 1:63,360. Plate dimensions are 60 by 60 inches. See digital folder for map plate.

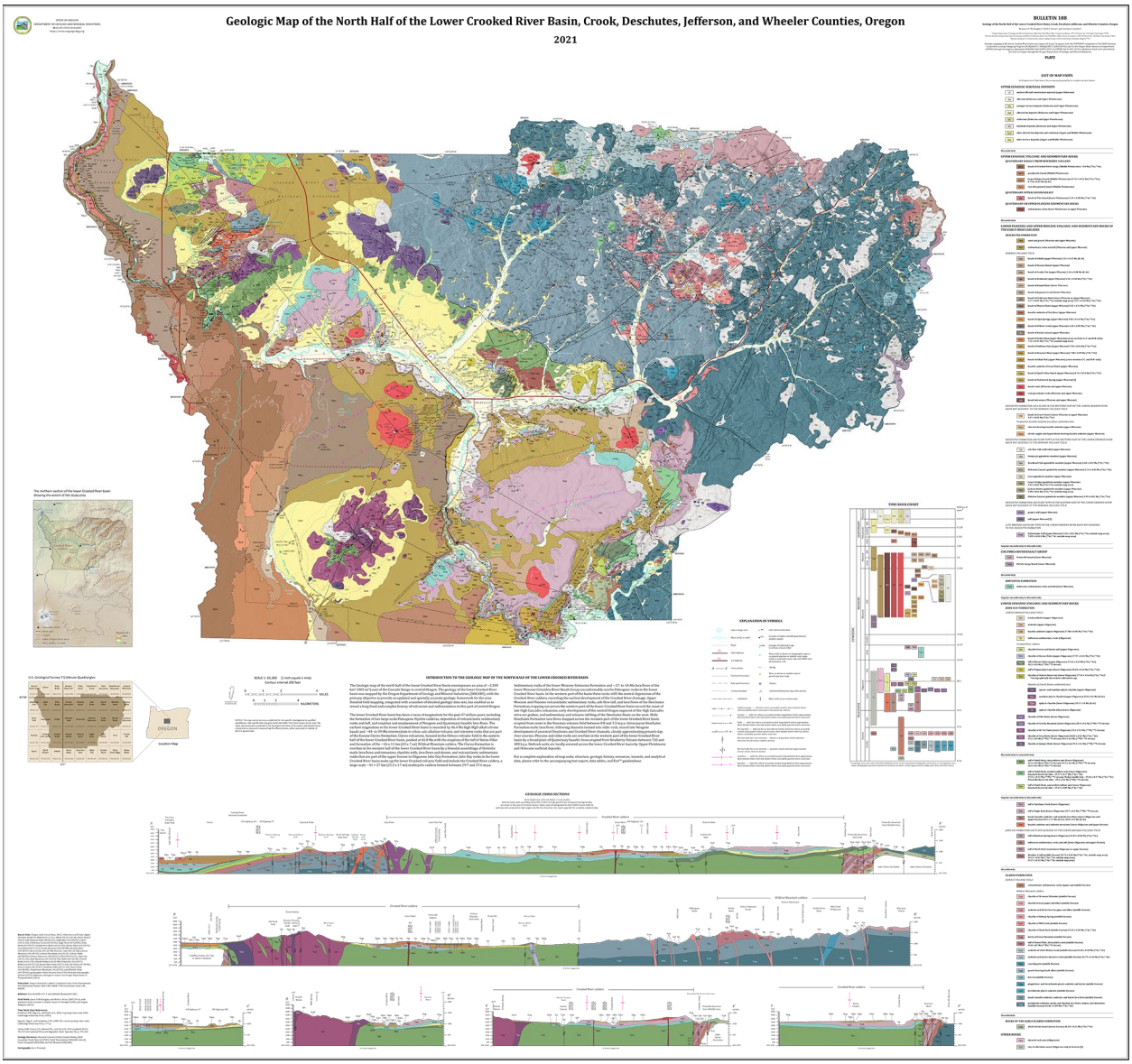

12.2 Methods

12.2.1 Geochemistry

Geologic mapping in the lower Crooked River basin was supported by 548 X-ray fluorescence (XRF) geochemical analyses of whole-rock samples. Whole-rock geochemical samples were prepared and analyzed by XRF at the Franklin and Marshall X-ray laboratory, Lancaster Pennsylvania, and Washington State University GeoAnalytical Lab, Pullman, Washington. Analytical procedures for the Franklin and Marshall X-ray laboratory are described by Boyd and Mertzman (1987) and Mertzman (2000), and are available online at http://www.fandm.edu/earth-environment/laboratory-facilities/xrf-and-xrd-lab; analytical procedures for the Washington State University GeoAnalytical Lab are described by Johnson and others (1999) and are available online at https://environment.wsu.edu/facilities/geoanalytical-lab/technical-notes/. Samples denoted by lab abbreviation FM were analyzed at Franklin and Marshall College; Samples denoted by lab abbreviation WSU were analyzed at the Washington State University; Descriptive rock unit names for igneous rocks are based on normalized major element analyses plotted on the total alkalis ($Na_2O + K_2O$) versus silica (SiO_2) diagram (TAS) of Le Bas and others (1986), Le Bas and Streckeisen (1991), and Le Maitre and others (1989, 2004). New and compiled XRF-geochemical analyses are included the geodatabase (LCB2021_GeMS10.7.gdb), in a separate shapefile (LCB2021_GeochemPoints.shp), and in a Microsoft Excel workbook LCB2021_DATA.xlsx, (sheet LCB2021_GeochemPoints). **Table 12-3** describes the fields listed in the spreadsheets. The locations of all geochemical samples are given in five coordinate systems: UTM Zone 10 (datum = NAD 27, NAD 83, units =meters), Geographic (datum = NAD 27, NAD 83, units = decimal degrees), and Oregon Lambert (datum = NAD 83, HARN, units = international feet). Notes for spreadsheet: -9 equals no data for numerical fields for analytical data; nd equals no data in text fields; na equals information not applicable for text fields; samples shown with an "R" (e.g., 119 LCJ 06R) are a repeat analysis of a single sample.

Table 12-3. Geochemical database spreadsheet columns.

Field	Description
Type	The geochemical method used by laboratory that analyzed the sample – e.g., XRF, ICP-MS
FieldSampleID	Unique alpha-numeric id applied to the sample – e.g., 126 LCJ 06.
AlternateSampleID	Unique alpha-numeric id applied to the sample – e.g., 126 LCJ 06.
Symbol	References a symbol in the GeMS style file – e.g., 31.21.
Label	A unique number assigned to the sample for cartographic purposes – e.g., G1.
LocationConfidenceMeters	Radius in meters of positional uncertainty envelope for the observation locale. Null values not permitted. Recommended value is -9 if value is not otherwise available.
PlotAtScale	Cartographic map scale or larger that the observation or analysis should be plotted at. Value is scale denominator.
Quadrangle	The USGS 7.5' quadrangle in which the sample is located – e.g., Prineville.
Elevation	Elevation of data location in feet – e.g., 22.
MapUnit	Map unit from which the analyzed sample was collected – e.g., Tjtso.
MaterialAnalyzed	Type of material analyzed – e.g., whole rock.
TASLithology	Rock name assigned based on the total alkalis ($Na_2O + K_2O$) versus silica (SiO_2) diagram (TAS) of Le Bas and others (1986), Le Bas and Streckeisen (1991), and Le Maitre and others (1989) – e.g., basalt, rhyolite.
MajorElements	SiO_2, Al_2O_3, TiO_2, FeOTotal, MnO, CaO, MgO, K_2O, Na_2O, P_2O_5. In wt. percent.
TraceElements	Ni, Cr, Sc, V, Ba, Rb, Sr, Zr, Y, Nb, Ga, Cu, Zn, Pb, La, Ce, Th, Nd, U, Cs, Co, Hf, Sm, Eu, Yb, Lu. In ppm.
TotalInitial	Original analytical total as reported by the lab.
LossOnIgnition	Value for loss on ignition as reported by the laboratory.
FE2O3	Iron (III) oxide or ferric oxide reported in original analysis.
FeO	Iron (II) oxide or ferrous oxide reported in original analysis.
UTMNorthingNAD27	Meters north in NAD 27 UTM projection, zone 10.
UTMEastingNAD27	Meters east in NAD 27 UTM projection, zone 10.
LatitudeNAD27	Latitude in NAD 27 geographic coordinates.
LongitudeNAD27	Longitude in NAD 27 geographic coordinates.
UTMNorthingNAD83	Meters north in NAD 83 UTM projection, zone 10.
UTMEastingNAD83	Meters east in NAD 83 UTM projection, zone 10.
LatitudeNAD83	Latitude in NAD 83 geographic coordinates.
LongitudeNAD83	Longitude in NAD 83 geographic coordinates.
Northing83HARN	Feet north in Oregon Lambert NAD 83, HARN, international feet.
Easting83HARN	Feet east in Oregon Lambert NAD 83, HARN, international feet.
LocationSourceID	Unique data source from which the data were obtained – e.g., McClJD2021b.
AnalysisSourceID	Foreign key to DataSources. Identifies source of analytical data for this sample. Null values not permitted – e.g., WSU.
Notes	Special information about certain samples – e.g., alteration.
GeochemPoints_ID	e.g., GCM01

12.2.2 Alteration zone map and alteration zone geochemistry

The distribution of alteration zones in the lower Crooked River basin is defined on the basis of field mapping during the current study, published literature (Brooks, 1963; Waters, 1966; Waters and Vaughan, 1968a, b; Swinney and others, 1968; Swanson, 1969; Gray and Baxter, 1986; Thormahlen, 1984), and unpublished mineral resource reports archived at the Baker City Field Office of DOGAMI. Field data collected from alteration zones were converted into digital format using Esri ArcGIS™ ArcMap™ 10.7 GIS software by on-screen digitizing using georeferenced 1:24,000-scale USGS digital raster images and 2005–2018 National Agriculture Imagery Program digital orthophotos as base maps. Seventeen samples obtained from alteration zones in the lower Crooked River basin were analyzed at ALS Chemex (ALS) in Reno, Nevada by ICP-MS and ICP-AES methods using their ME-MS41 analytical package. Samples were prepared using an aqua regia digestion where samples are treated with a 3:1 mixture of hydrochloric and nitric acids. Nitric acid destroys organic matter and oxidizes sulfide material. It reacts with concentrated hydrochloric acid to generate aqua regia: $3HCl + HNO_3 = 2H_2O + NOCl + Cl_2$. Aqua regia is an effective solvent for most base metal sulphates, sulfides, oxides, and carbonates, but only provides a partial digestion for most rock forming elements of a refractory nature. Therefore, results reported in table LCB_AltChemistry represent only the leachable portion of any analyte. A stronger dissolution technique would recover analytes from more resistive minerals but is not deemed necessary here as the objective was a first pass screening of alteration zones. A table of detection limits for the ME-MS41 analytical package at ALS is shown in **Table 12-4**. The detection limits stated by ALS has an uncertainty of ± 100 percent. Therefore, a detection limit of 1 part per million (ppm) implies an uncertainty of 1 ppm ± 1 ppm. Please note that gold (Au) determinations by the ICP-MS and ICP-AES method are semi-quantitative due to the small sample weight used (0.5 g).

Alteration zone geochemical analyses are included in the geodatabase (LCB2021_GeMS10.7.gdb,), in a separate shapefile named (LCB2021_AlteredGeochemPoints.shp), and in a Microsoft Excel workbook LCB2021_DATA.xlsx (sheet LCB2021_ AlteredGeochemPoints).

Table 12-5 describes the fields listed in the spreadsheet. Elements in ppm except those denoted as weight percent (%); nd = no data. The locations of all alteration zone geochemical samples are given in five coordinate systems: UTM Zone 10 (datum = NAD 27, NAD 83, units =meters), Geographic (datum = NAD 27, NAD 83, units = decimal degrees), and Oregon Lambert (datum = NAD 83, HARN, units = international feet). Notes for spreadsheet: -9 equals no data for numerical fields for analytical data; nd equals no data in text fields; na equals information not applicable for text fields. Please note that samples 09 PJ 05 through 205 LCJ 06 analyzed by ME-MS41 ICP-MS and ICP-AES at ALS Chemex, Reno, Nevada. Samples Gray1 through Gray9 compiled from Gray and Baxter (1986), original analysis by fire assay. Samples DT-28A through DT-110 compiled from Thormahlen (1984); original analysis by fire assay. Elements in ppm except those denoted as weight percent (%); nd = no data. Mapped alteration zones in the lower Crooked River basin are included in the geodatabase (LCB2021_GeMS10.7.gdb,) and as a separate shapefile named (OverlayPolys.shp).

Table 12-4. List of the 41 elements analyzed by ALS Chemex and their detection limits.

Analyte	Range	Analyte	Range	Analyte	Range	Analyte	Range
Ag	0.01–100	Cs	0.05–500	Mo	0.05–10,000	Sr	0.2–10,000
Al%	0.01%–25%	Cu	0.2–10,000	Na%	0.01%–10%	Ta	0.01–500
As	0.1–10,000	Fe%	0.01%–50%	Nb	0.05–500	Te	0.01–500
Au	0.2–25	Ga	0.05–10,000	Ni	0.2–10,000	Th	0.2–10,000
B	10–10,000	Ge	0.05–10,000	P	10–10,000	Ti%	0.005%–10%
Ba	10–10,000	Hf	0.02–500	Pb	0.2–10,000	Tl	0.02–10,000
Be	0.05–1,000	Hg	0.01–10,000	Rb	0.1–10,000	U	0.05–10,000
Bi	0.01–10,000	In	0.005–500	Re	0.001–50	V	1–10,000
Ca%	0.01–25%	K%	0.01%–10%	S%	0.01%–10%	W	0.05–10,000
Cd	0.01–1,000	La	0.2–10,000	Sb	0.05–10,000	Y	0.05–500
Ce	0.02–500	Li	0.1–10,000	Sc	0.1–10,000	Zn	2–10,000
Co	0.1–10,000	Mg%	0.01%–25%	Se	0.2–1,000	Zr	0.5–500
Cr	0.1–10,000	Mn	5–50,000	Sn	0.2–500		

Note: Data reported from an aqua regia leach should be considered as only representing the leachable portion of the particular analyte. ME-MS41 gold determinations by this method are semi-quantitative due to the small sample weight used (0.5 g). Elements reported in parts per million (ppm), except those denoted as weight percent (%).

Table 12-5. Alteration zone geochemical database spreadsheet columns.

Field	Description
Type	The geochemical method used by laboratory that analyzed the sample – e.g., XRD, ICP-MS
FieldSampleID	Unique alpha-numeric id identifying the sample – e.g., 09 PJ 05.
AlternateSampleID	Unique alpha-numeric id identifying the sample – e.g., LCB-5.
Symbol	References a symbol in the GeMS style file – e.g., 31.21.
Label	A unique number assigned to the sample for cartographic purposes – e.g., AG1.
LocationConfidenceMeters	Radius in meters of positional uncertainty envelope for the observation locale. Null values not permitted. Recommended value is -9 if value is not otherwise available.
PlotAtScale	Cartographic map scale that observation or analysis should be plotted at. Value is scale denominator.
Quadrangle	The USGS 7.5' quadrangle in which the sample is located – e.g., Prineville.
Elevation	Elevation of data location in feet – e.g., 3200.
MapUnit	Map unit from which the analyzed sample was collected – e.g., Tjpa.
MaterialAnalyzed	Type of material analyzed – e.g., chalcedonic quartz.
ElementsAnalyzed	Ag, Al (%), As, Au, B, Ba, Be, Bi, Ca (%), Cd, Ce, Co, Cr, Cs, Cu, Fe (%), Ga, Ge, Hf, Hg, In, K (%), La, Li, Mg, Mn, Mo, Na%, Nb, Ni, P, Pb, Rb, Re, S (%), Sb, Sc, Se, Sn, Sr, Ta, Te, Th, Ti (%), Tl, U, V, W, Y, Zn, Zr
UTMNorthingNAD27	Meters north in NAD 27 UTM projection, zone 10.
UTMEastingNAD27	Meters east in NAD 27 UTM projection, zone 10.
LatitudeNAD27	Latitude in NAD 27 geographic coordinates.
LongitudeNAD27	Longitude in NAD 27 geographic coordinates.
UTMNorthingNAD83	Meters north in NAD 83 UTM projection, zone 10.
UTMEastingNAD83	Meters east in NAD 83 UTM projection, zone 10.
LatitudeNAD83	Latitude in NAD 83 geographic coordinates.
LongitudeNAD83	Longitude in NAD 83 geographic coordinates.
Northing83HARN	Feet north in Oregon Lambert NAD 83, HARN, international feet.
Easting83HARN	Feet east in Oregon Lambert NAD 83, HARN, international feet.
LocationSourceID	Unique data source from which the data were obtained – e.g., McClJD2021b.
AnalysisSourceID	Foreign key to DataSources. Identifies source of analytical data for this sample. Null values not permitted – e.g., WSU.
Notes	Special information about certain samples – e.g., alteration.
AltGeochemPoints_ID	e.g., GCM01

12.2.3 Geochronology

Stratigraphic understanding in the lower Crooked River basin has been significantly enhanced by 55 new and previously published K-Ar, $^{40}Ar/^{39}Ar$, and $^{206}Pb/^{238}U$ (zircon) ages reported in this publication. Original data sheets with sample and standard data for new isotopic ages are provided in the appendix. Geochronological data are included in the geodatabase (LCB2021_GeMS10.7.gdb), in a separate shapefile (LCB2021_GeochronPoints.shp), and in Microsoft Excel workbooks LCB2021_DATA.xlsx (sheet LCB2021_GeochronPoints). **Table 12-6** describes the fields listed in the spreadsheet. The location of each radiometric age is given in five coordinate systems: UTM Zone 10 (datum = NAD 27, NAD 83, units = meters), Geographic (datum = NAD 27, NAD 83, units = decimal degrees), and Oregon Lambert (datum = NAD 83, HARN, units = international feet). Notes for spreadsheet: -9 equals no data for numerical fields for analytical data; nd equals no data in text fields; na equals information not applicable for text fields.

Table 12-6. Geochronology database spreadsheet columns.

Field	Description
Type	The geochronological method – e.g., $^{40}Ar^{39}Ar$, K-Ar, U-Pb, radiocarbon used to estimate the age.
FieldSampleID	Unique alpha-numeric id applied to the sample – e.g., 24 LCJ 06.
AlternateSampleID	Unique alpha-numeric id applied to the sample – e.g., 24 LCJ 06.
MapUnit	Map unit from which the analyzed sample was collected.
Symbol	References a symbol in the GeMS style file.
Label	Radiometric age of sample with error – e.g., 29.3 ± 0.02 Ma
LocationConfidenceMeters	Radius in meters of positional uncertainty envelope for the observation locale. Null values not permitted. Recommended value is -9 if value is not otherwise available.
PlotAtScale	Cartographic map scale or larger that the analysis should be plotted. Value is scale denominator.
MaterialAnalyzed	Type of material analyzed – e.g., zircons, amphiboles, plagioclase, groundmass.
NumericAge	Interpreted (preferred) age calculated from geochronological analysis, not necessarily the date calculated from a single set of measurements.
AgePlusError	Plus error in age determination in thousands of years.
AgeMinusError	Minus error in age determination in thousands of years.
AgeUnits	Values = years, Ma, ka, radiocarbon ka, calibrated ka, etc.
UTMNorthingNAD27	Meters north in NAD 27 UTM projection, zone 10.
UTMEastingNAD27	Meters east in NAD 27 UTM projection, zone 10.
LatitudeNAD27	Latitude in NAD 27 geographic coordinates.
LongitudeNAD27	Longitude in NAD 27 geographic coordinates.
UTMNorthingNAD83	Meters north in NAD 83 UTM projection, zone 10.
UTMEastingNAD83	Meters east in NAD 83 UTM projection, zone 10.
LatitudeNAD83	Latitude in NAD 83 geographic coordinates.
LongitudeNAD83	Longitude in NAD 83 geographic coordinates.
Northing83HARN	Feet north in Oregon Lambert NAD 83, HARN, international feet.
Easting83HARN	Feet east in Oregon Lambert NAD 83, HARN, international feet.
StationID	Foreign key to Stations point feature class.
LocationSourceID	Unique data source from which the data were obtained; e.g., McClJD2021b.
AnalysisSourceID	Foreign key to DataSources. Identifies source of analytical data for this sample. Null values not permitted – e.g., OSU.
Notes	Special information about certain samples – e.g., alteration.
GeochronPoints_ID	e.g., GCR1

12.2.3.1 $^{40}Ar/^{39}Ar$ geochronology (OSU)

Ten whole rock or single crystal separates from the rocks in the lower Crooked River basin were dated using $^{40}Ar/^{39}Ar$ incremental heating techniques at the Noble Gas Mass Spectrometry Lab located in the College of Oceanic and Atmospheric Sciences at Oregon State University (OSU) following the methods of Koppers (2002), Koppers and others (2003), and Duncan and Keller (2004) (**Figure 12-4a-l**). The methodology for $^{40}Ar/^{39}Ar$ geochronology at OSU is summarized on the Web at http://geochronology.coas.oregonstate.edu/.

Small hand samples of material from each sample were crushed using a steel hammer and plate. Chips were then fed through a small jaw crusher and sieved to a grain size of ~300 to 500 µm. The resulting material was rinsed and put through an ultrasonic bath in distilled water. Samples were then dried in an oven and put through a Franz magnetic separator to remove magnetic phases. The remaining fraction was cleaned in an ultrasonic bath of 5 percent (by volume) HNO_3 then rinsed thoroughly with deionized water and dried. Fresh single crystal separates or groundmass pieces were then hand-picked under a binocular microscope prior to irradiation and analysis. Approximately 70 mg of each sample was wrapped in Cu-foil and loaded in quartz tubes for irradiation at Oregon State University's TRIGA experimental reactor for 6 hours at 1 MW power. Incremental heating $^{40}Ar/^{39}Ar$ age determinations were performed on single or crystalline groundmass separates using a CO_2 laser probe combined with a MAP-215/50 mass spectrometer. Preferred ages are reported **Figure 12-4a-l** and in the main text body to 2σ.

Figure 12-4. Apparent age (Ma) versus cumulative percent ^{39}Ar gas released (*following pages*). Samples were analyzed at the Noble Gas Mass Spectrometry Lab located in the College of Oceanic and Atmospheric Sciences at Oregon State University. (a) Sample 7.13VII.05. (b) Sample 276 LCJ 06. (c) Sample CROO 53265-435 (Dunbar and Perkins, 2015). (d) Sample CROO 53726-575 (Dunbar and Perkins, 2015). (e) Sample 1.15VII.05. (f) Sample 4b.12VII.05. (g) Sample 1.9.II.06. (h) Sample 448 LCJ 07. (i) Sample 280 LCJ 06. (j). Sample 322 LCJ 07. (k) Sample 45 P 05. (l) Sample 279 LCJ 06.

Figure 12-4. (Apparent age (Ma) versus cumulative percent ^{39}Ar gas released – *caption on previous page)*

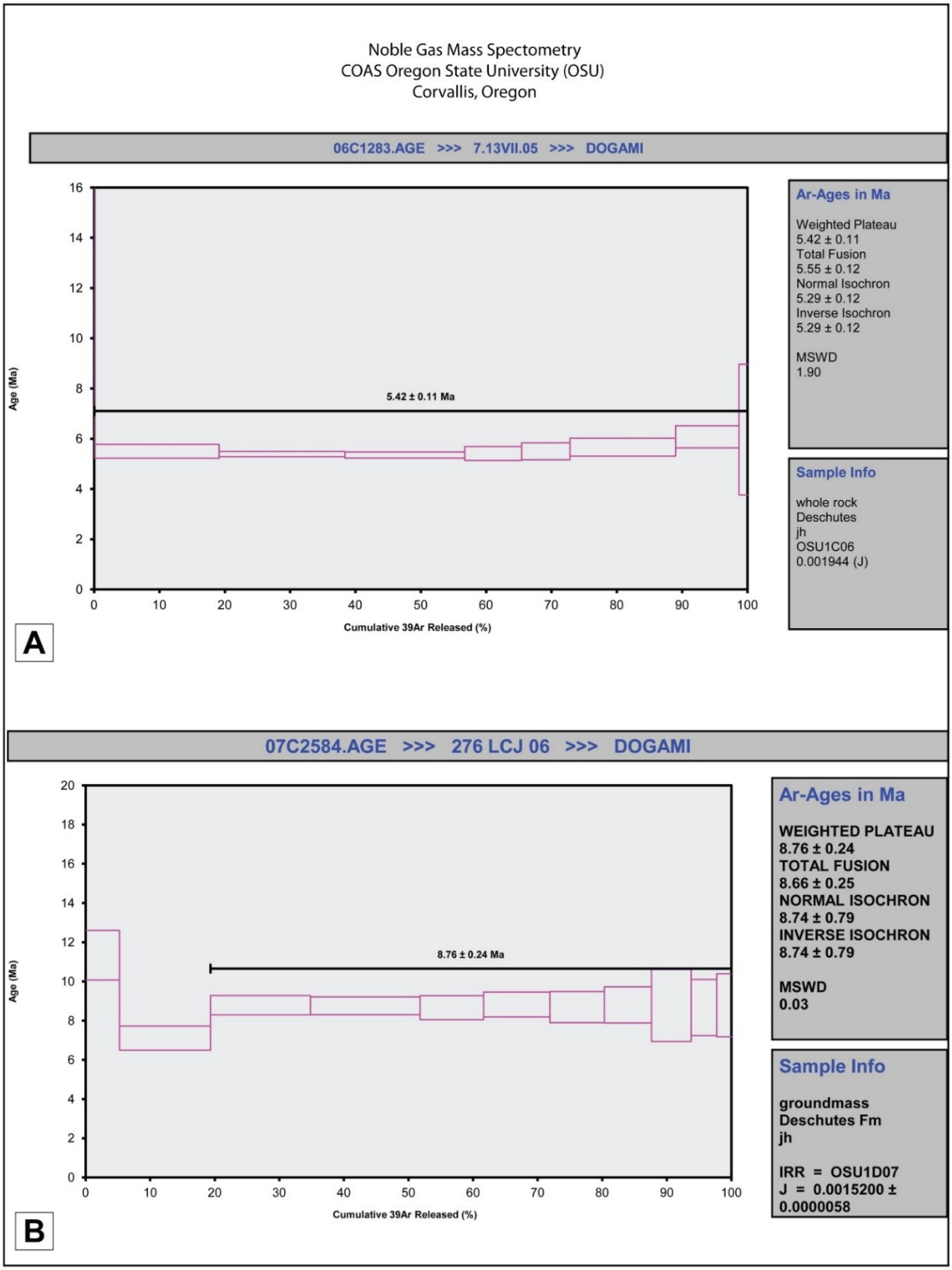

Figure 12-4. (Apparent age (Ma) versus cumulative percent ^{39}Ar gas released – *caption on page 266)*

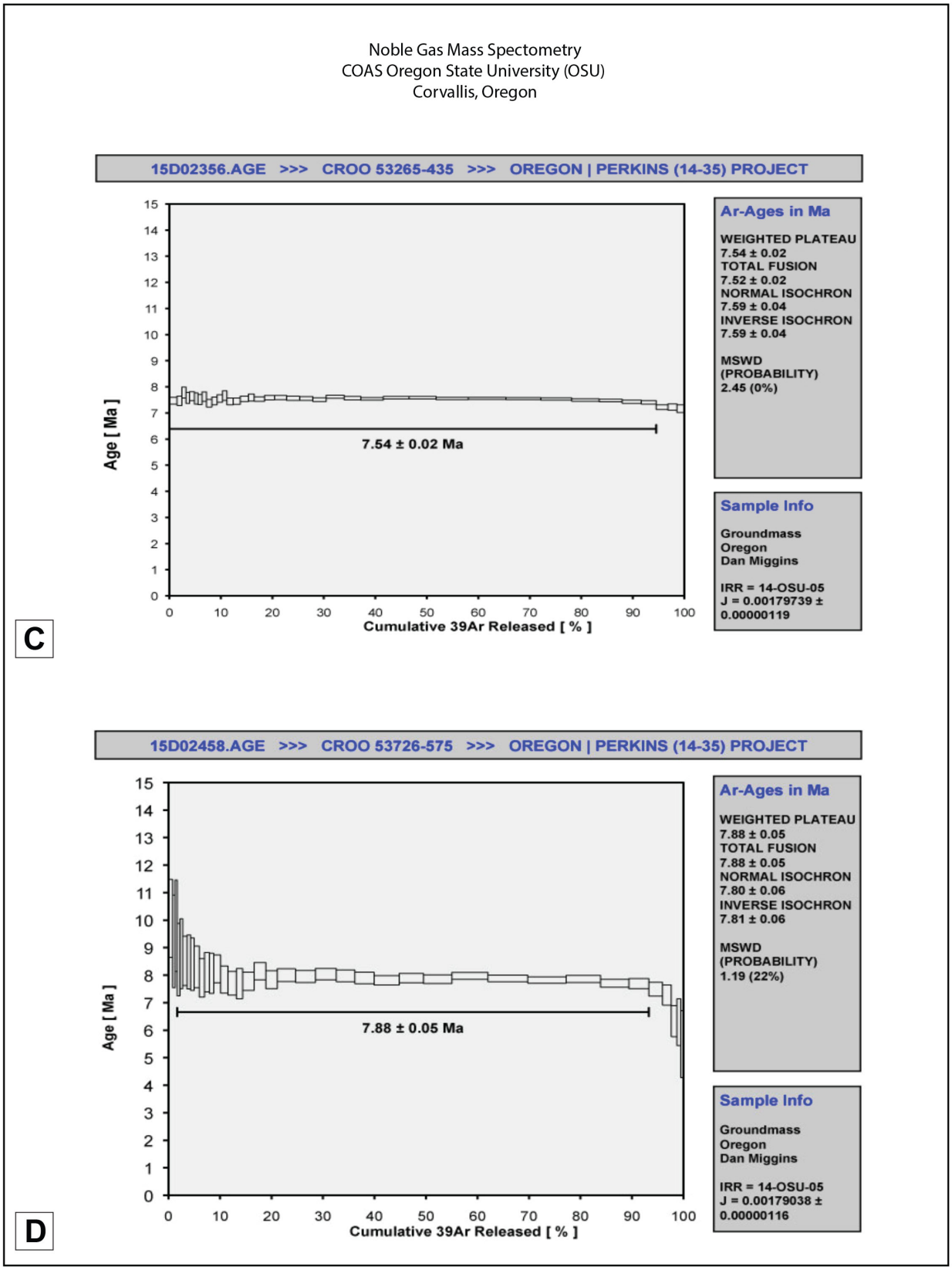

Figure 12-4. (Apparent age (Ma) versus cumulative percent ^{39}Ar gas released – *caption on page 266)*

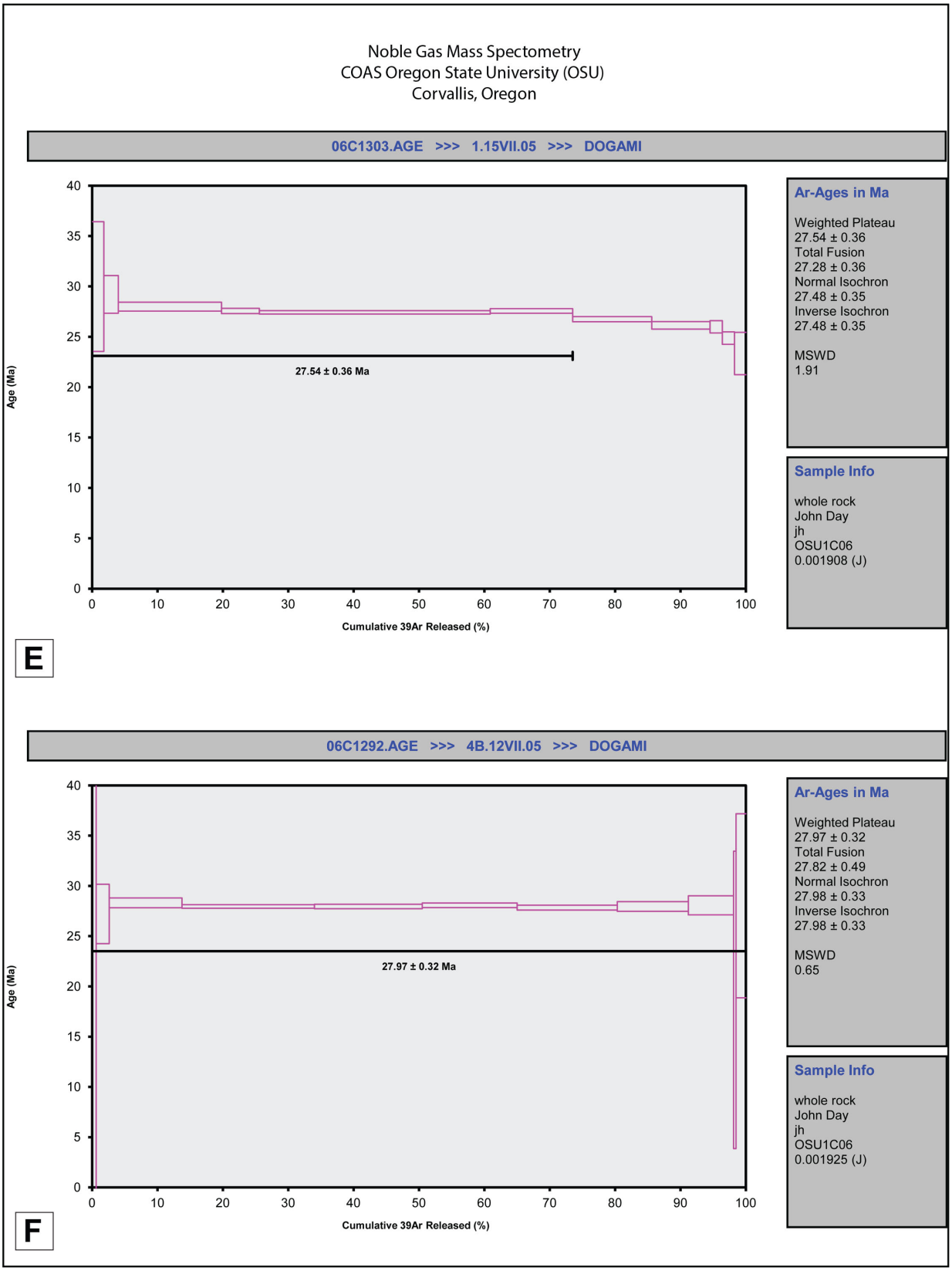

Figure 12-4. (Apparent age (Ma) versus cumulative percent 39Ar gas released – *caption on page 266)*

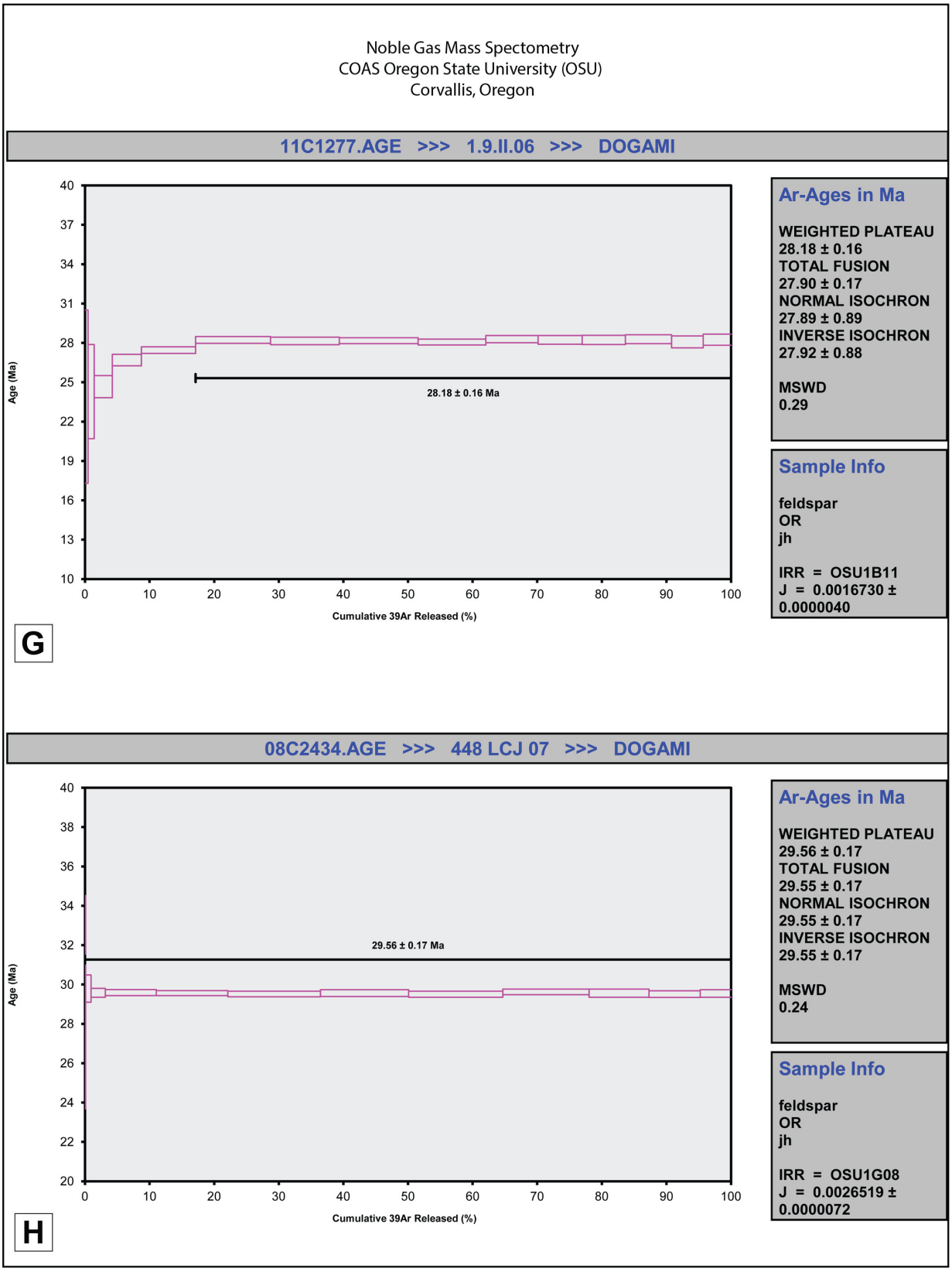

Figure 12-4. (Apparent age (Ma) versus cumulative percent ^{39}Ar gas released – *caption on page 266)*

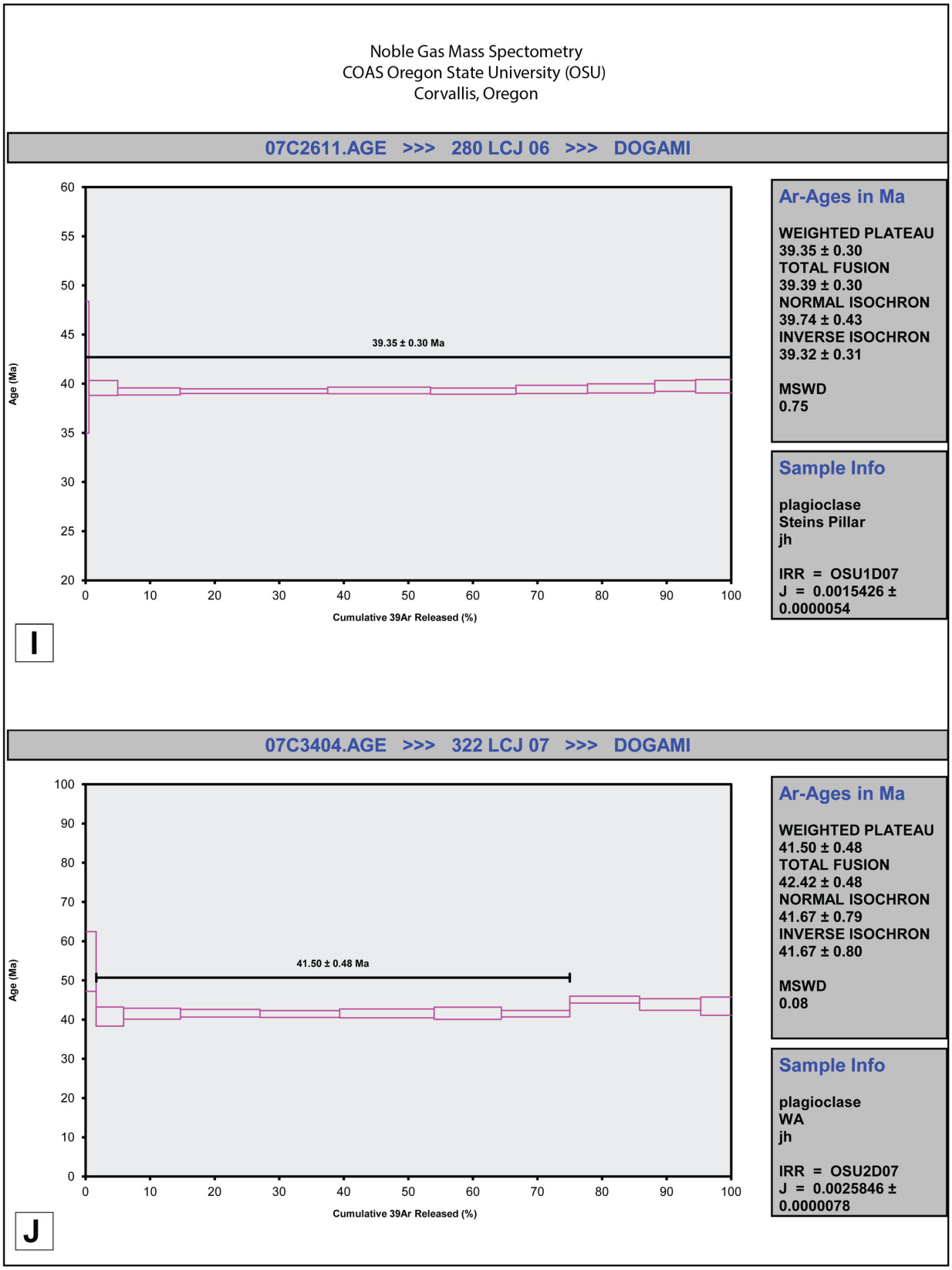

Figure 12-4. (Apparent age (Ma) versus cumulative percent ^{39}Ar gas released – *caption on page 266)*

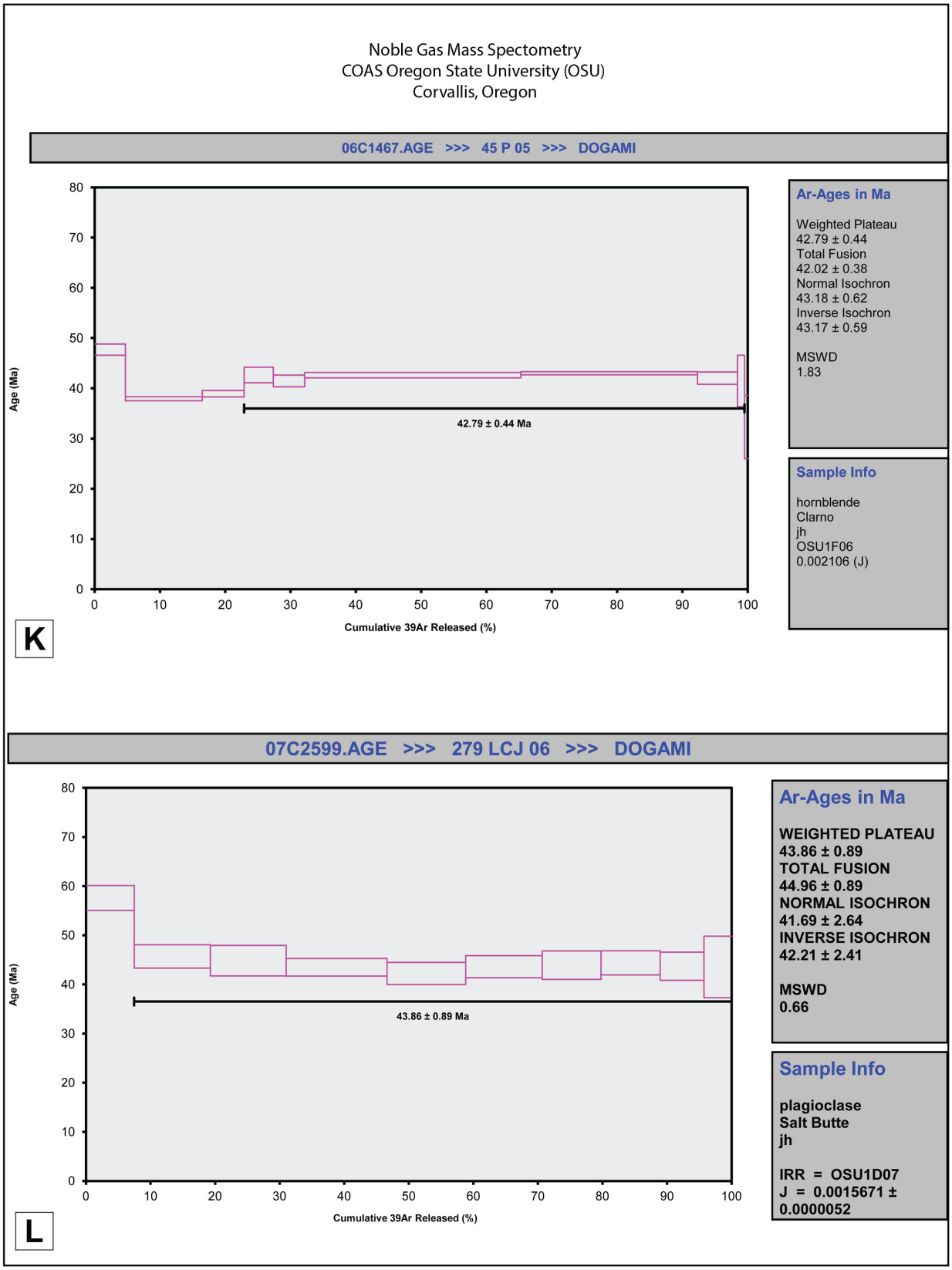

12.2.3.2 $^{40}Ar/^{39}Ar$ geochronology (NMGRL)

Two whole rock samples from the lower Crooked River basin were dated using $^{40}Ar/^{39}Ar$ incremental heating techniques at the New Mexico Geochronological Research Laboratory administered by the New Mexico Bureau of Geology and Mineral Resources at the New Mexico Institute of Mining and Technology in Socorro, New Mexico. Analyses were done under the direction of Drs. Bill McIntosh and Matt Heizler (**Figure 12-5a, b**). The general operational details for the NMGRL can be found at internet site http://geoinfo.nmt.edu/labs/argon/ .

Groundmass concentrates were prepared from the samples by crushing, reaction with dilute HCl, DI water rinse in an ultrasound, and handpicking fragments visibly free of phenocrysts. The prepared samples were loaded into machined Al discs and irradiated for 8 hours in two batches at the USGS TRIGA reactor in Denver, Colorado along with the standard Fish Canyon tuff sanidine as a neutron flux monitor. All samples were analyzed by the step-heating method using a defocused 810 nm diode laser to heat the samples. Samples were analyzed using the incremental heating method using 8 to 15 heating steps. Preferred ages are reported **Figure 12-5** and in the main text body to 2σ.

Figure 12-5. Apparent age (Ma) versus cumulative percent ^{39}Ar gas released for samples analyzed at the New Mexico Geochronological Research Laboratory. (a) Sample JM-SP13-4. (b) Sample 03 LC 06.

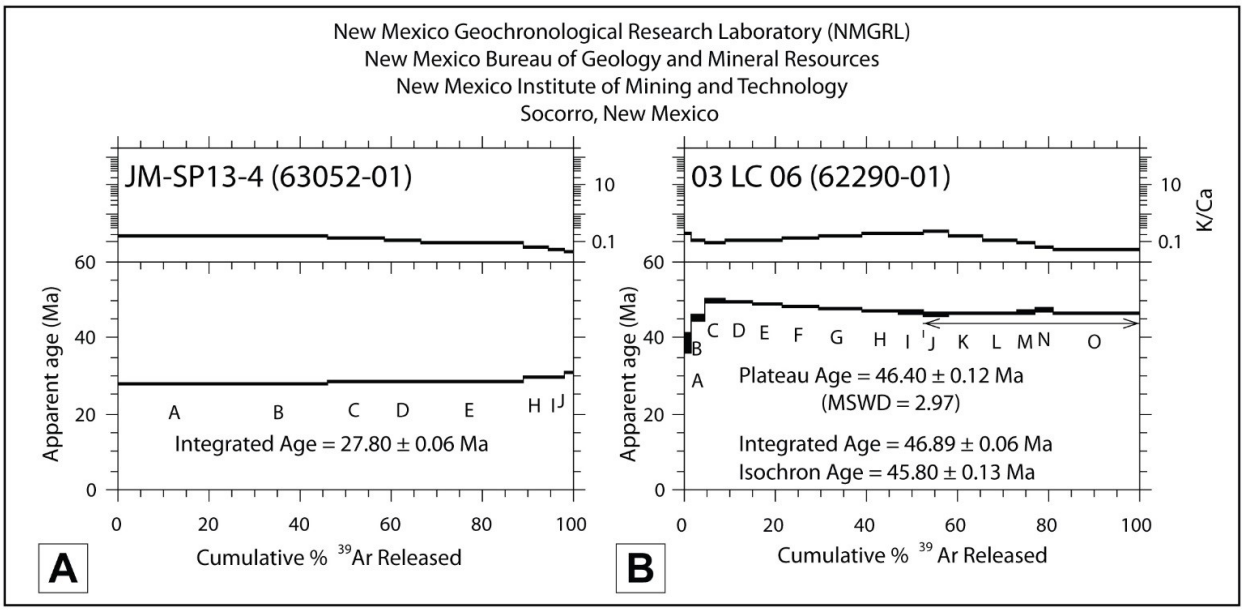

12.2.3.3 $^{206}Pb/^{238}U$ zircon geochronology (CSUN/UCSB)

Ten new $^{206}Pb/^{238}U$ age determinations on individual zircon cores and rims extracted from rhyolites and ash-flow tuffs were prepared and analyzed by Dr. Joshua Schwartz at California State University Northridge, and at the University of California, Santa Barbara (**Figure 12-6a–t**).

Zircons were separated at California State University Northridge following standard methods involving crushing, pulverizing with jaw crusher and disk mill, and density separation on a Wilfley gold table and with heavy liquids. Samples were processed through a Frantz isodynamic separator (side tilt = 5°, front tilt = 20°) at 1.5 amps to remove magnetic (non-zircon) minerals. Zircons were poured onto double sided tape and mounted in epoxy, ground and polished. They were then imaged on a Gatan MiniCL detector attached to a FEI Quanta 600 scanning electron microscope.

Uranium-lead ratios were collected at the University of California Santa Barbara in one analytical session in July 2015 following methods described in Kylander-Clark and others (2013). Analyses were conducted using a Nu Plasma multi-collector inductively coupled plasma mass spectrometer (MC-ICPMS) with a fixed collector array of 12 Faraday cups and four low-mass ion counters. Zircons were ablated using a Photon Machines 193 ArF excimer laser with HelEx cell with a repetition rate of 4 Hz. Spot size for all ablations was ~35 microns. The primary standard, 91500, was analyzed every 10 analyses to correct for in-run fractionation of Pb/U and Pb isotopes. U–Pb isotopic ratios and their uncertainties were calculated using Iolite (Paton and others, 2010). Precision on individual analyses varies by volume and U and Pb concentrations. A typical ablation of 12–26 ng of material yields 1 to 1.5 percent for $^{206}Pb/^{238}U$ ratios and 0.3 to 1 percent on $^{207}Pb/^{206}Pb$ ratios (2SE, using down-hole elemental-fractionation correction; Paton and others 2010).

Three secondary zircon standards, Plesovice, Temora-2, and GJ-1 were analyzed throughout the analytical session to assess reproducibility of the data. U-Pb analysis of the secondary standards yielded concordant results and $^{206}Pb/^{238}U$ error-weighted average ages of 341.0 ± 1.5 (n=23; mswd=0.8), 418.8 ± 2.1 (n=1.2; mswd=0.2), and 604.4 ± 2.5 (n=1.1; mswd=0.4) for Plesovice, Temora-2 and GJ-1, respectively. Error weighted average ages for all secondary standards lie within 1 percent% of the accepted values.

U-Pb isotopic data were plotted using Isoplot 3.75 (Ludwig, 2012). Tuffs and rhyolites commonly yield over dispersed zircon dates in which the mean square weighted deviation (MSWD) is >>2 for zircons from a single sample. Data were deconvolved using the Sambridge and Compston (1994) 'unmix' algorithm in Isoplot assuming Gaussian distributions of two or three age populations. In most cases, the youngest zircon population is reported as the age of eruption/intrusion, and older populations are considered xenocrystic (**Figure 12-6a–t**). The quoted dates in the text and tables are reported at 95 percent confidence interval and are assigned 2 percent total (systematic + analytical) uncertainties, except when comparing analyses within the same sample or grain. Total uncertainties are shown in brackets in the text and tables. $^{206}Pb/^{238}U$ geochronologic data are presented in **Figure 12-6a–t**.

Figure 12-6. Tera-Wasserburg concordia diagrams (left column; $^{207}Pb/^{206}Pb$ versus $^{238}U/^{206}Pb$) and relative probability plots (right column; number of grains versus ^{207}Pb corrected $^{206}Pb/^{238}U$ error-weighted average age) for $^{206}Pb/^{238}U$ zircon age determinations on Oligocene and Eocene tuff and rhyolite samples in the lower Crooked River basin. Data point ellipses in Tera-Wasserburg concordia diagrams are 2 σ . (a, b) Sample 1 OCJ 14. (c, d) Sample SR-RH-2. (e, f) Sample PAT GR 2. (g, h) Sample GSO95-41R. (I, j) Sample 24 LCJ 06. (k, l) Sample SRT-Skull-1. (m, n) Sample JB-JM-01. (o, p) Sample JM ER13-4. (q, r) Sample HS-JM-04. (s, t) 152 LCJ 06.

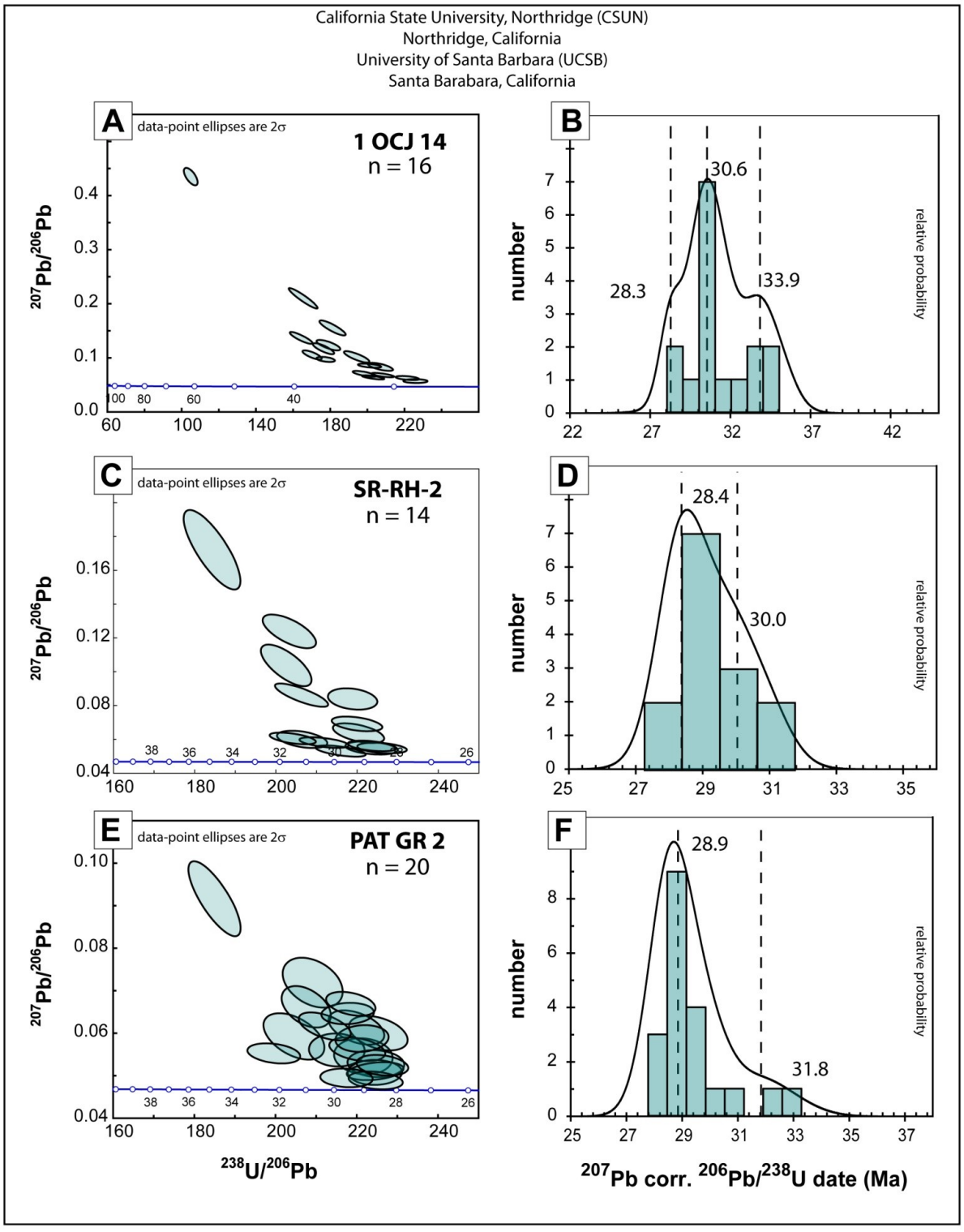

Figure 12-6. (Tera-Wasserburg concordia diagrams and relative probability – *caption on previous page*)

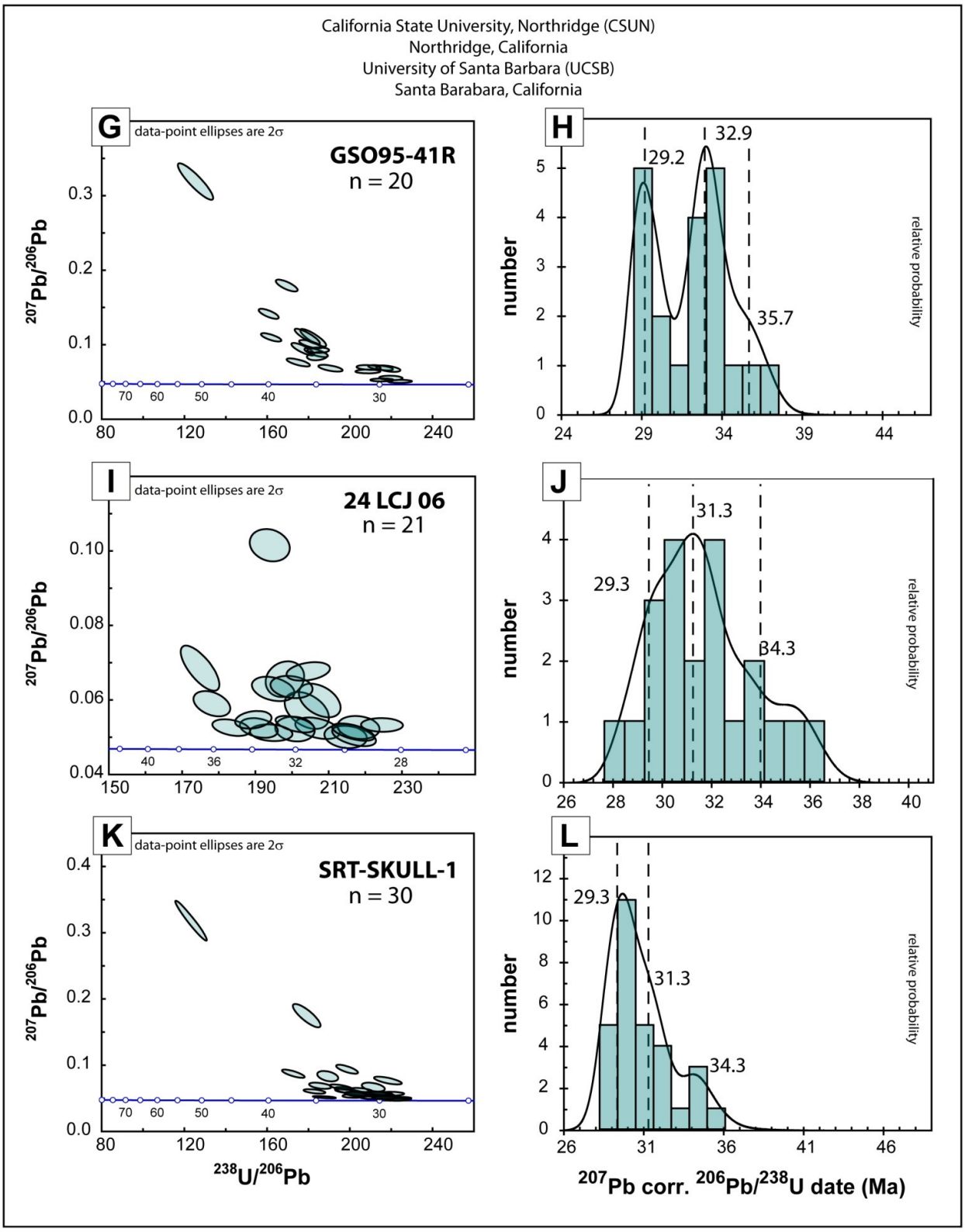

Figure 12-6. (Tera-Wasserburg concordia diagrams and relative probability – *caption on page 275)*

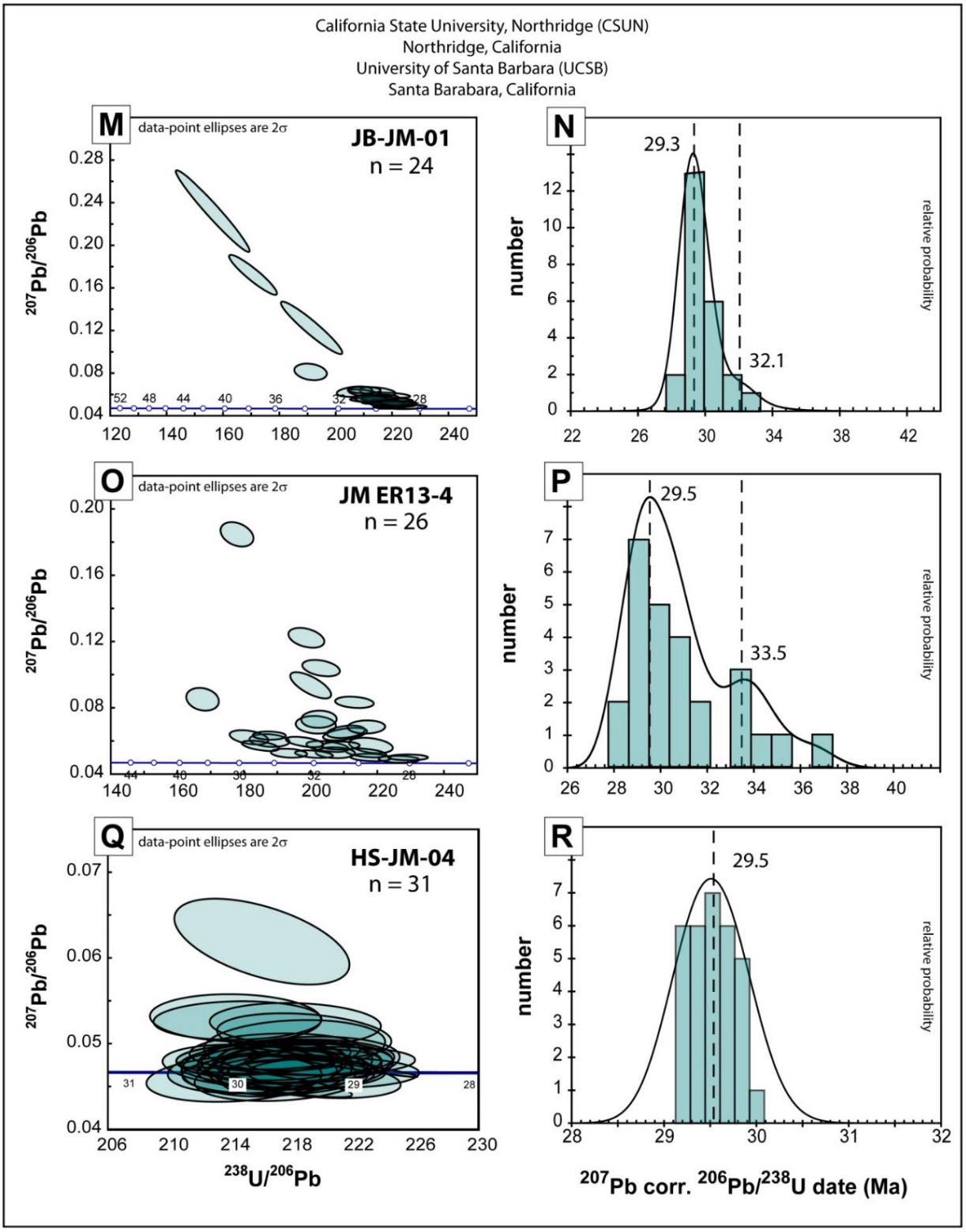

Figure 12-6. (Tera-Wasserburg concordia diagrams and relative probability – *caption on page 275)*

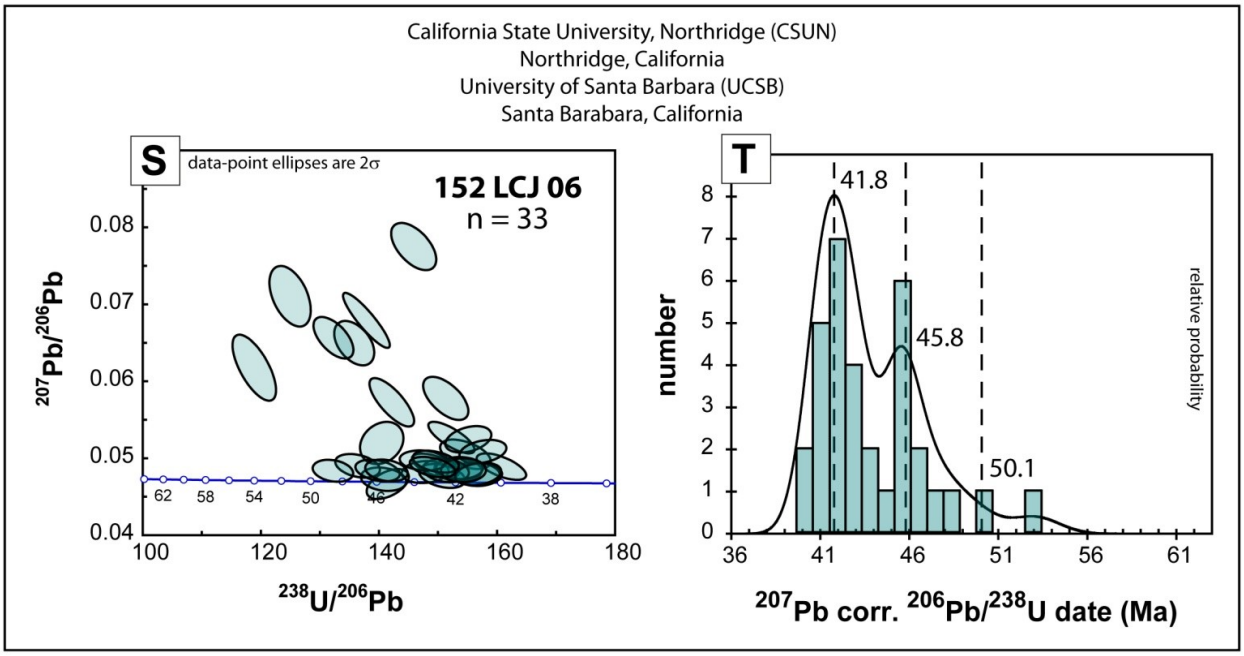

12.2.3.4 $^{206}Pb/^{238}U$ zircon geochronology (UCLA)

Three new $^{206}Pb/^{238}U$ radiometric age-date determinations on individual zircon cores and rims extracted from rhyolites and ash-flow tuffs were prepared and analyzed by Angela Seligman (University of Oregon) at the University of California, Los Angeles. Original data and results were reported in Seligman and others (2014).

$^{206}Pb/^{238}U$ ages of individual zircon cores and rims from Seligman and others (2014) were analyzed at UCLA on a CAMECA IMS 1270 ion microprobe using an $^{16}O^-$ primary beam for analyses. 12 to 15 zircons were analyzed from three units of the Crooked River caldera. Analytical reproducibility was estimated from the standard deviation of replicate analyses of AS3 (1099.1 Ma; Paces and Miller, 1993) and TEM2 (416.8 Ma; Black and others, 2003), which were both used for calibrations of U, Th, and Pb sensitivities. Standards were mounted on the same disk as the unknowns and in close proximity to the unknowns. Standards were analyzed approximately once for every five unknowns. Although the reproducibility between analyses for each unit has standard deviations of ~1 or less, the uncertainty for each analysis is typically high (~5 Ma). These large errors are likely due to a combination of high common Pb and low U content of the zircons (Seligman and others, 2014).

12.2.4 Natural remanent magnetization (magnetic polarity)

Eighty-eight field measurements of natural remanent magnetization (the magnetic field of a sample measured when induced magnetic fields are absent or zeroed out by probe; Butler, 1992) were determined from strongly magnetized lavas cropping out in the lower Crooked River basin during the course of this study in order to distinguish between flow units with normal and reversed magnetic polarity. Magnetic polarity also serves as a check on the permissible age of isotopically-dated samples, when compared to the paleomagnetic time scale of Cande and Kent (1992) (**Figure 5-23**). This method of constraining isotopic ages by magnetic polarity determinations is most effective when the analytical error is less than 0.20 m.y. Large errors reported for isotopic ages may overlap so many polarity subchrons that no constraint is provided by knowing a samples magnetic polarity. Magnetic polarity values reported were determined using a MEDA, Inc. μMag handheld digital fluxgate magnetometer (**Figure 12-7**). The measured point data are included in the geodatabases (LCB2021_GeMS10.7.gdb), in a separate shapefile (LCB2021_MagneticPoints.shp), and in a Microsoft Excel workbook LCB2021_DATA.xlsx (sheet LCB2021_MagneticPoints). **Table 12-7** describes the fields listed in the spreadsheet. The location of magnetics data is given in five coordinate systems: UTM Zone 10 (datum = NAD 27, NAD 83, units = meters), Geographic (datum = NAD 27, NAD 83, units = decimal degrees), and Oregon Lambert (datum = NAD 83, HARN, units = international feet). Notes for spreadsheet: -9 equals no data for numerical fields for analytical data; nd equals no data in text fields; na equals information not applicable for text fields.

The natural remanent magnetization (magnetic polarity) of strongly magnetized lavas was determined using the following method:

- A north-pointing arrow and near horizontal line were drawn on and around (to the extent possible) an approximately fist-sized equidimensional sample that was then removed from the outcrop (**Figure 12-7a**). Next, a line is drawn from the south end of the sample to the north end at an angle approximating the magnetic inclination (approximately equivalent to the latitude). For the study area, a line was drawn inclined at approximately 45° down to the north. This line gives the approximate orientation of the magnetic pole of the sample.
- The magnetometer was placed on the most level ground available in a relatively magnetically clean area (**Figure 12-7b**). The probe was then placed in a fixed position in the horizontal plane and rotated to null the local magnetic field (μMag reads zero). This procedure was done incrementally beginning with minimum range sensitivity (2,000 mG [milliGauss]), increasing the sensitivity (20 mG) and re-rotating the probe until maximum sensitivity was reached. Magnetic polarity was then checked with the north end of a locked compass needle. Total field value will decrease when the compass needle is moved horizontally toward and remains parallel to the probe.
- The polarity of a sample was determined by placing the oriented sample in a path parallel to the probe. The inclined north-directed line drawn to represent the approximate magnetic pole of the sample was held horizontally (approximately) with the north end facing toward the probe at a distance of at least 10 times further than the measurement distance. A reading was then determined with the sample absent from the probe. The sample was then moved to a point (typically within 1 to 2 cm) toward the probe in order to cause a change of at least several times greater than the minimum resolution of the magnetometer (**Figure 12-7b**). A decrease in the total field value indicated normal-polarity (N); an increase in total field value indicated reversed-polarity (R).

- The sample was then rotated backward (top away from the probe) about a horizontal axis approximately 45° to see if field strength increased as the sample's inclined magnetic field was rotated into parallel with the probe.
- The polarity of two to ten representative samples from different portions of an outcrop or from different outcrops was determined to verify the repeatability of results. Erratic results, due to re-magnetization resulting from lighting strikes, obscure post-emplacement alteration, or aberrant declination and inclination are reported as indeterminate (I). Reversed readings should take precedence over normal readings in assigning polarity. Re-magnetization will more likely reset the remanent magnetism to the present-day normal polarity.

Figure 12-7. Procedure for determining natural remanent magnetism of lavas. (a) Ideal sample is selected and oriented in outcrop. North arrow is drawn on upper surface; horizontal lines are drawn around the exposed edges of the sample. Fist-sized sample is then removed. (b) Magnetometer probe is placed in a fixed position in the horizontal plane and rotated to null the local magnetic field. Sample polarity is determined by moving the oriented sample into the path of the probe.

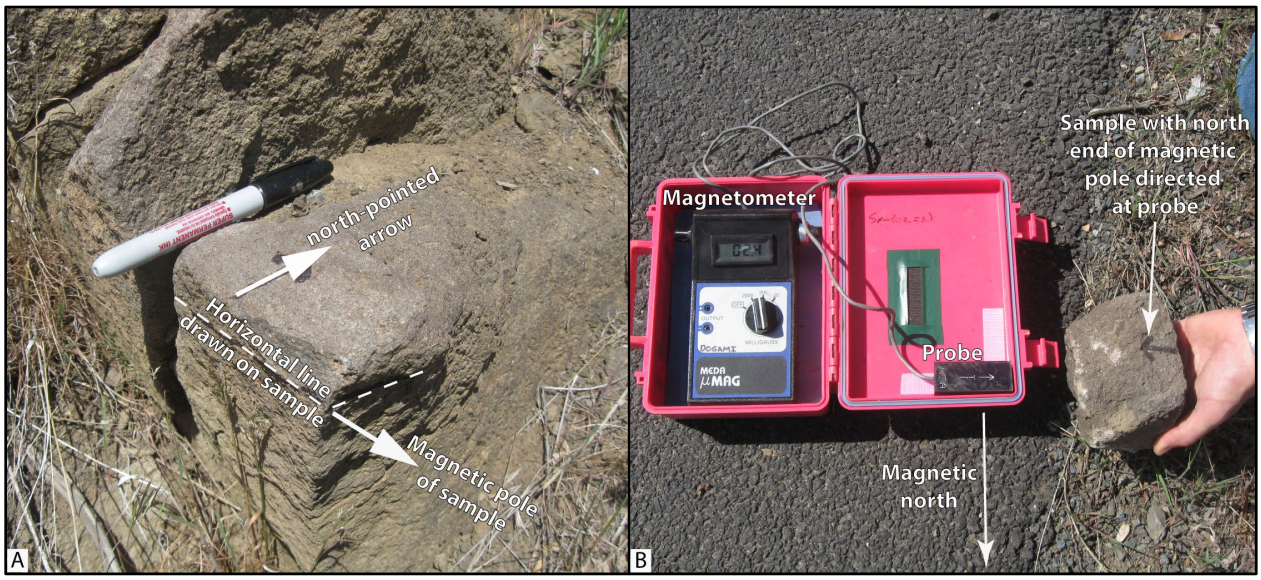

Table 12-7. Magnetic polarity database spreadsheet columns.

Field	Description
Type	The method of measurement – e.g., Digital Portable Fluxgate
FieldSampleID	Unique alpha-numeric id applied to the sample – e.g., 518 LCJ 08.
NaturalRemanentMagnetization	Natural remanent magnetization of sample as determined from a portable fluxgate magnetometer. Normal, reversed, indeterminate.
MapUnit	Map unit from which the analyzed sample was collected.
Symbol	References a symbol in the GeMS style file.
Label	<Null>
LocationConfidenceMeters	Radius in meters of positional uncertainty envelope for the observation locale. Null values not permitted. Recommended value is -9 if value is not otherwise available.
PlotAtScale	Cartographic map scale or larger that the observation or analysis should be plotted at. Value is scale denominator.
Quadrangle	The USGS 7.5' quadrangle in which the sample is located – e.g., Prineville.
Elevation	Elevation of sample location in feet – e.g., 3200.
UTMNorthingNAD27	Meters north in NAD 27 UTM projection, zone 10.
UTMEastingNAD27	Meters east in NAD 27 UTM projection, zone 10.
LatitudeNAD27	Latitude in NAD 27 geographic coordinates.
LongitudeNAD27	Longitude in NAD 27 geographic coordinates.
UTMNorthingNAD83	Meters north in NAD 83 UTM projection, zone 10.
UTMEastingNAD83	Meters east in NAD 83 UTM projection, zone 10.
LatitudeNAD83	Latitude in NAD 83 geographic coordinates.
LongitudeNAD83	Longitude in NAD 83 geographic coordinates.
Northing83HARN	Feet north in Oregon Lambert NAD 83, HARN, international feet.
Easting83HARN	Feet east in Oregon Lambert NAD 83, HARN, international feet.
LocationSourceID	Unique data source from which the data were obtained; e.g., McClJD2021b.
AnalysisSourceID	Foreign key to DataSources. Identifies source of analytical data for this sample. Null values not permitted – e.g., OSU.
Notes	Special information about certain samples – e.g., alteration.
MagneticPoints_ID	e.g., MGP001

12.2.5 Orientation points

Orientation measurements of inclined bedding were taken in the lower Crooked River basin during this study by traditional compass and clinometer methods. Additional measurements have been compiled from previous workers. Orientation points are reported in both quadrant format (e.g., N. 30° W., 15° NE.) and azimuthal format using the right-hand rule (e.g., 330°, 15° NE., American convention); data are coded by the appropriate Federal Geographic Data Committee (FGDC) reference number for geologic map symbolization. The measured point data are included in the geodatabase (LCB2021_GeMS10.7.gdb,), in a separate shapefile (LCB2021_OrientationPoints.shp), and in a Microsoft Excel workbook LCB2021_DATA.xlsx (sheet LCB2021_OrientationPoints). **Table 12-8** describes the fields listed in the spreadsheet. The locations of these point data are given in five coordinate systems: UTM Zone 10 (datum = NAD 27, NAD 83, units = meters), Geographic (datum = NAD 27, NAD 83, units = decimal degrees), and Oregon Lambert (datum = NAD 83, HARN, units = international feet). Strike and dip symbols can be properly drawn by the Esri ArcMap™ product by opening the layer properties, categorizing by type, choosing the appropriate symbol, and rotating the symbol based on the "Azimuth" field. (The Advanced button allows you to select the rotation field.) The rotation style should be set to geographic in order to maintain the right-hand rule property. Azimuths are given in true north; an additional clockwise

correction of about 1.6 degrees is needed to plot strikes and dips properly on the Oregon Lambert conformal conic projection in this area. Notes for spreadsheet: nd, no data.

Table 12-8. Orientation points database spreadsheet columns.

Field	Description
Type	Type of geologic structure from which feature was determined – e.g., Inclined bedding.
Azimuth	Strike or trend, measured in degrees clockwise from geographic North. Values limited to range 0-360. Use right-hand rule (dip is to right of azimuth direction). Horizontal planar features may have any azimuth – e.g., 20.
Inclination	Dip or plunge, measured in degrees down from horizontal. Values limited to range -90 to 90. Types defined as horizontal (e.g., horizontal bedding) have Inclination = 0. Null values not Data type=float – e.g., 45.
StrikeQuadrant	Strike direction of the inclined plane, stated in a north-directed quadrant format – e.g., N35E.
DipQuadrant	Amount of dip, degrees from horizontal, with direction – e.g., 45SE.
Symbol	References a symbol in the GeMS style file – e.g., 6.40.
Label	Amount of dip, degrees from horizontal – e.g., 45.
LocationConfidenceMeters	Radius in meters of positional uncertainty envelope for the observation locale. Null values not permitted. Recommended value is -9 if value is not otherwise available.
IdentityConfidence	Specifies confidence that observed structure is of the type specified; e.g., 'certain', 'questionable', 'unspecified'.
OrientationConfidenceDegrees	Estimated circular error, in degrees – e.g., 20.
PlotAtScale	Cartographic map scale or larger that the observation or analysis should be plotted at. Value is scale denominator.
Quadrangle	The USGS 7.5' quadrangle in which the sample is located – e.g., Prineville.
Elevation	Elevation of data location in feet – e.g., 22.
MapUnit	Map unit from which the analyzed sample was collected.
UTMNorthingNAD27	Meters north in NAD 27 UTM projection, zone 10.
UTMEastingNAD27	Meters east in NAD 27 UTM projection, zone 10.
LatitudeNAD27	Latitude in NAD 27 geographic coordinates.
LongitudeNAD27	Longitude in NAD 27 geographic coordinates.
UTMNorthingNAD83	Meters north in NAD 83 UTM projection, zone 10.
UTMEastingNAD83	Meters east in NAD 83 UTM projection, zone 10.
LatitudeNAD83	Latitude in NAD 83 geographic coordinates.
LongitudeNAD83	Longitude in NAD 83 geographic coordinates.
Northing83HARN	Feet north in Oregon Lambert NAD 83, HARN, international feet.
Easting83HARN	Feet east in Oregon Lambert NAD 83, HARN, international feet.
LocationSourceID	Unique data source from which the data were obtained – e.g., McClJD2021b.
OrientationSourceID	Unique data source from which the data were obtained – e.g., McClJD2021b.
Notes	Special information about the point – e.g., lidar derived.
OrientationPoints_ID	Primary key – e.g., ORP001.
PTTYPE	e.g., Bedding
RuleID1	Rule ID used for cartographic representation – e.g., 6.40.

12.2.6 Well points

The well points spreadsheet is derived from written drillers' logs provided by Oregon Department of Water Resources (OWRD). Well logs vary greatly in completeness and accuracy, so the utility of subsurface interpretations based upon these data can be limited. Water well logs compiled and used for interpretation during this study were not field located. The approximate locations were estimated using tax lot maps, street addresses (coordinates obtained from Google Earth™), and aerial photographs to plot locations on the map. The accuracy of the locations ranges widely, from errors of one-half mile possible for wells located only by section and plotted at the section centroid to a few tens of feet for wells located by address or tax lot number on a city lot with bearing and distance from a corner. At each mapped location the number of the well log is indicated. This number can be combined with the first four letters of the county name (e.g., CROO 5473), to retrieve an image of the well log from the OWRD website.

Well points are included in the geodatabase (LCB2021_GeMS10.7.gdb,), in a separate shapefile (LCB2021_WellPoints.shp), and in a Microsoft Excel workbook LCB2021_DATA.xlsx (sheet LCB2021_WellPoints). **Table 12-9** illustrates the lithologic abbreviations used for lithologies, while **Table 12-10** describes the fields listed in the spreadsheet. The locations of these point data are given in five coordinate systems: UTM Zone 10 (datum = NAD 27, NAD 83, units = meters), Geographic (datum = NAD 27, NAD 83, units = decimal degrees), and Oregon Lambert (datum = NAD 83, HARN, units = international feet).

Lithologies in well intervals listed in the well log spreadsheet can alternate between consolidated and unconsolidated and may be listed as alternating between bedrock and surficial geologic units. This may occur where bedrock units are soft, where paleosols or weak zones lie within bedrock, or where cemented or partly cemented zones alternate with unconsolidated zones in surficial deposits.

Table 12-9. Well point database lithologic abbreviations

Lithologic abbreviations used (alphabetical by group)

UNCONSOLIDATED SURFICIAL UNITS	
Abbreviation	**Description**
a	ash
bd	boulders
c	clay
ch	clay, hard (often logged as claystone but probably not bedrock)
g	gravel
gc	cemented gravel
gs	gravel and sand (also sandy gravel)
m	mud
s	sand
sg	sand and gravel (also gravelly sand)
st	silt
Rock, sedimentary	
bc	breccia
cg	conglomerate
cs	claystone
sh	shale
ss	sandstone
Rock, igneous	
an	andesite
b	basalt
ba	basaltic andesite
cd	cinders
da	dacite
pu	pumice
gr	granite
l	lava
r	rhyolite
sc	scoria
t	tuff
v	volcanic, undivided
vb	volcanic breccia
Other	
af	artificial fill
cl	coal (lignite)
dg	decomposed granite
o	other (drillers unit listed in notes column of spreadsheet)
rk	rock
sl	soil
u	unknown (typically used where a well has been deepened)

Table 12-10. Well point spreadsheet columns.

Field	*Description and Example
Type	Type of well located; e.g., well used for domestic-water supply, well used for irrigation-water supply, drill hole for hydrocarbon exploration or exploitation- Showing name and number.
Symbol	References a symbol in the GeMS style file – e.g., 26.1.25.
Label	A unique label identifying the well, if applicable – e.g., Federal 1-10.
IdentityConfidence	Specifies confidence that observed structure is of the type specified; e.g., 'certain', 'questionable', 'unspecified'.
LocationConfidenceMeters	Radius in meters of positional uncertainty envelope for the observation locale. Null values not permitted. Recommended value is -9 if value is not otherwise available.
PlotAtScale	Cartographic map scale or larger that the observation or analysis should be plotted at. Value is scale denominator.
TownshipRangeSection	Two digits for township, two digits for range, and two for section; negative if township is south of Willamette baseline. Exception for township and range if they contain a decimal – e.g., −2132.503.
County	Hood River County – e.g., CROO
Grid	Well log number for wells. Wells in Crook County preceded by acronym CROO – e.g., CROO53799. Wells in Deschutes County preceded by acronym DESC – e.g., DESC53799. Wells in Jefferson County preceded by acronym JEFF – e.g., JEFF53799. Wells in Wheeler County preceded by acronym WHEE – e.g., CROO53799.
WellElevation	Wellhead elevation in feet as given by Google Earth™ at corresponding WGS 84 location. e.g., 3200.
LocatedBy	Google Earth™ elevation for cursor location at a given address – e.g., Google. Google Earth™ elevation at house in vicinity of given address – e.g., House. Pad identifying approximate well location, visible in air photo – e.g., Pad. Approximate tax lot centroid or other best guess for well location using a combination of tax lot maps and aerial photographs – e.g., Tax lot. Owner name – e.g., Owner. Address of well listed on Oregon Water Resources Department (OWRD) Start card. Wells located by Oregon Water Resources Department (OWRD) using handheld GPS – e.g., OWRD. GPS coordinates of wellhead included with well log – e.g., GPS. Approximate quarter-quarter-quarter section centroid – e.g., QQQ. Approximate quarter-quarter-section centroid – e.g., QQ. Approximate quarter-section centroid – e.g., Q. Approximate fit to sketch map included with well log – e.g., map.
Lithology	Best interpretation of driller's log using abbreviations above – e.g., g.
Base	Record base of driller's interval or, if lithology abbreviation would not change, similar intervals, in feet below wellhead – e.g., 17.
Top	Calculated top of driller's interval or similar intervals, in feet below wellhead – e.g., 14.
TopElevation	Calculated elevation at top of driller's interval, or similar intervals, in feet above sea level – e.g., 86.
BaseElevation	Calculated elevation at base of driller's interval, or similar intervals, in feet above sea level – e.g., 83.
BedrockLithology	Lists bedrock lithologies, when encountered, abbreviations listed above – e.g., b.
BedrockElevation	Calculated elevation at which bedrock or soil over bedrock was first encountered, in feet above sea level – e.g., 1924.
TaxLot	Tax lot number. Where it is determined that a tax lot number is used more than once in the section then the appropriate subdivision of the section is indicated in the notes field – e.g., 800.
Color	Color of interval as reported by the well driller – e.g., green.
MapUnit	Geologic unit interpreted in subsurface based on drillers log and designated by map unit label used in accompanying geodatabase. Intervals labeled "suna" (surface unit not applicable) are those where the lithology as interpreted by the original drillers' log do not correspond; also denotes intervals in the subsurface where a precise unit label cannot be applied – e.g., Tb.
Quadrangle	The USGS 7.5' quadrangle in which the sample is located – e.g., Prineville.
UTMNorthingWGS84	Meters north in WGS84 UTM projection, zone 10.
UTMEastingWGS84	Meters east in WGS84 UTM projection, zone 10.
UTMNorthingNAD27	Meters north in NAD 27 UTM projection, zone 10.
UTMEastingNAD27	Meters east in NAD 27 UTM projection, zone 10.
LatitudeNAD27	Latitude in NAD 27 geographic coordinates.
LongitudeNAD27	Longitude in NAD 27 geographic coordinates.

UTMNorthingNAD83	Meters north in NAD 83 UTM projection, zone 10.
UTMEastingNAD83	Meters east in NAD 83 UTM projection, zone 10.
LatitudeNAD83	Latitude in NAD 83 geographic coordinates.
LongitudeNAD83	Longitude in NAD 83 geographic coordinates.
Northing83HARN	Feet north in Oregon Lambert NAD 83, HARN, international feet.
Easting83HARN	Feet east in Oregon Lambert NAD 83, HARN, international feet.
LocationSourceID	Unique data source from which the data were obtained – e.g., OWRD2020.
WellSourceID	Unique data source from which the data were obtained – e.g., OWRD2020.
Notes	Notes about the stratigraphic interval as originally described by the well driller or observer.
WellPoints_ID	Primary key – e.g., WLP593
PTTYPE	e.g., Water Well, Oil and Gas.

*Well location given in six coordinate systems calculated by reprojecting original WGS 84 UTM, zone 10 locations.

12.2.7 Volcanic vents

Eighteen late Miocene and Pliocene volcanic vents were mapped in and adjacent to the lower Crooked River basin during the course of mapping individual lava flows in the Deschutes Formation. Vent points are included in the geodatabase (LCB2021_GeMS10.7.gdb), in a separate shapefile (LCB2021_VentPoints.shp), and in a Microsoft Excel workbook LCB2021_DATA.xlsx (sheet LCB2021_VentPoints). **Table 12-11** describes the fields listed in the spreadsheet. The locations of these point data are given in five coordinate systems: UTM Zone 10 (datum = NAD 27, NAD 83, units = meters), Geographic (datum = NAD 27, NAD 83, units = decimal degrees), and Oregon Lambert (datum = NAD 83, HARN, units = international feet).

Table 12-11. Volcanic vent point spreadsheet columns.

Field	Description
Type	Classifier that specifies what kind of geologic feature is represented by a database element.
MapUnit	Map unit from which the analyzed sample was collected.
Symbol	FGDC reference code assigned to the feature.
Label	Null, and free text
LocationConfidenceMeters	Radius in meters of positional uncertainty envelope.
PlotAtScale	The denominator of the scale that this observation or analysis should be plotted.
Quadrangle	The USGS 7.5' quadrangle in which the sample is located – e.g., Prineville.
Elevation	Elevation of sample location in feet – e.g., 3200.
UTMNorthingNAD27	Meters north in NAD 27 UTM projection, zone 10.
UTMEastingNAD27	Meters east in NAD 27 UTM projection, zone 10.
LatitudeNAD27	Latitude in NAD 27 geographic coordinates.
LongitudeNAD27	Longitude in NAD 27 geographic coordinates.
UTMNorthingNAD83	Meters north in NAD 83 UTM projection, zone 10.
UTMEastingNAD83	Meters east in NAD 83 UTM projection, zone 10.
LatitudeNAD83	Latitude in NAD 83 geographic coordinates.
LongitudeNAD83	Longitude in NAD 83 geographic coordinates.
Northing83HARN	Feet north in Oregon Lambert NAD 83, HARN, international feet.
Easting83HARN	Feet east in Oregon Lambert NAD 83, HARN, international feet.
LocationSourceID	Foreign key to DataSources feature class. Identifies source of point location.; e.g., McClJD2021c.
Notes	Free text for additional information specific to this feature.
VentPoints_ID	Primary key. Values= VTP1, VTP2, VTP3, ... Null values not permitted e.g., VTP01